MODELLING AND CONTROL OF SEGMENTED LONG-STATOR PERMANENT-MAGNET LINEAR SYNCHRONOUS MOTORS

Christopher Roger Lines

A thesis submitted to the Faculty of Engineering and the Built Environment, University of the Witwatersrand, Johannesburg, in fulfilment of the requirements for the degree of Doctor of Philosophy.

Johannesburg, 2013

Declaration

I declare that this thesis is my own, unaided work, other than where specifically acknowledged. It is being submitted for the degree of Doctor of Philosophy in the University of the Witwatersrand, Johannesburg. It has not been submitted before for any degree or examination in any other university.

Signed this _____ day of _____ 2013

_____

Christopher Roger Lines

Abstract

A novel control strategy for segmented long-stator permanent magnet linear synchronous motors is presented that is particularly suited to ropeless hoisting. The stator (primary) is segmented into modular sections that are shorter than the moving reaction plate (secondary) and a single voltage source inverter per conveyance is used to power the energised sections. Efficient partial excitation of the stator is achieved with an intermediate switching layer placed between the stator sections and the inverter. The common voltage supplied to the sections is controlled with any standard motor vector control technique. Computer simulation and a purpose-built laboratory prototype show the strategy to be effective. There is scope for future research into full sensorless control of the proposed arrangement and a method of further modulating the supply voltage for those stator sections that are only partially covered by the reaction plate, particularly when operating at higher speeds.

Stemming from initial efforts to mathematically model the linear motor, a novel electromagnetic modelling approach was formulated. This hybrid magnetic-equivalent-circuit (MEC) and finite element method (FEM) approach is suited to efficient dynamic simulation and is explicated with a worked example. The method yields accurate results when compared with pure FEM. An MEC formulation is used for highly-permeable polygonal regions, whereas the magnetic field outside these regions is solved, by superposition, as the combined effect of boundary conditions that interface with those MEC regions and any magnetic sources. The required parameter sets for solving the field outside the regions represented as MECs are purely dependent on the geometry of the problem space and are thus precomputed. The force acting on a chosen group of moving components is calculated using an approximation of the Maxwell Stress Tensor method. Future research could address the present limitation that the highly-permeable regions are meshed using exclusively-rectangular flux tube elements.

A dynamic simulation model that caters for the discontinuities of a segmented stator was ultimately derived using an extended space-vector approach and its implementation as a generic Simulink® blockset is detailed. The motor parameters are determined from static FEM solutions over the range of reaction plate displacement, assuming no magnetic saturation.

To Mom and Dad

Thank you for your love and support

Acknowledgements

I greatly appreciate the guidance and sage advice generously offered throughout my studies by my supervisors, Prof. Willie Cronjé and Prof. Brian Wigdorowitz. I also owe much gratitude to Rupert Cruise, founder and director of Texchange Ltd, for funding some of the equipment and materials used for the laboratory prototype and for his continual encouragement and infectious passion for linear motor technology. My thanks also go to Harry Fellows, Mark Goossens, the late Karl Holm and other GENMIN Laboratories staff for their assistance with my laboratory work.

Furthermore, I formally acknowledge the funding that I received from the following establishments over the years:

- The National Research Foundation (NRF) (*opinions expressed and conclusions arrived at in this thesis are my own and should not necessarily be attributed to the NRF*)
- University Council Postgraduate Scholarship
- EP Bradlow / John Lemmer Scholarship
- Hennen Jennings Scholarship
- University Postgraduate Merit Award

Ultimately, I am *most* thankful for the prevailing support, encouragement and patience of my family and friends.

Contents

Declaration i

Abstract ii

Acknowledgements v

Contents vi

List of Figures xii

List of Tables xix

Code Listings xx

List of Symbols xxiii

Nomenclature xxviii

1 Introduction 1

1.1 Problem statement 1

1.1.1 Permanent magnet linear synchronous motors 1

1.1.2 Ropeless hoisting 2

1.1.3 Partial excitation with a segmented stator 3

1.2 Limitations of the prior art 4

1.3 Contributions 6

1.4 Publications 8

1.5 Mathematical notation 8

1.6 Thesis outline 10

2 Background 11

2.1 Mathematical modelling of electromagnetic systems 11
2.1.1 Magnetic Equivalent Circuit approach 11
2.1.2 Finite Element Method 13
2.1.3 Boundary Element Method 14
2.1.4 Finite Integration Technique 14
2.1.5 Magnetic Cell Method 15
2.1.6 Surface Current Method 16
2.2 Control of permanent magnet synchronous motors 17
2.2.1 Scalar control 17
2.2.2 Vector control 18
2.3 Feeding of segmented long-stator linear motors 22
2.3.1 Stator sections longer than the reaction plate 23
2.3.2 Stator sections shorter than the reaction plate 26

3 Hybrid Magnetic-Equivalent-Circuit and Finite Element Method 27
3.1 Methodology 27
3.1.1 Flux tube elements 29
3.1.2 Mutual permeances 33
3.1.3 Source flux 35
3.1.4 Flux linkage with coils 35
3.1.5 Electromagnetic force 35
3.1.6 Dynamic simulation 38
3.2 Worked example 39
3.2.1 Materials 40
3.2.2 Flux tube elements and sources 41
3.2.3 Precomputation of parameter sets 44
3.2.4 Comparison of static results to pure FEM solutions 46

4 Motor Dynamic Model 51
4.1 Power-invariant $\alpha/\beta/0$ transformation 51
4.2 Transformation between α/β and d/q frames 54
4.3 d/q Motor equations 55
4.3.1 Electrical 55
4.3.2 Flux linkage 56

4.3.3 Power and electromagnetic force 57
4.4 Reaction plate mechanical dynamics 58

5 Control Strategy **59**
5.1 Methodology 59
5.1.1 Energising fully-covered sections 60
5.1.2 Representative sections 61
5.1.3 Energising partially-covered sections 65
5.1.4 Multiple independent conveyances 66
5.1.5 Multiple stator blocks 66
5.1.6 Three-phase contactor arrangement 68
5.1.7 Sensorless control 69
5.2 Feeding efficiency and reaction plate utilisation 69

6 Laboratory Prototype **72**
6.1 Construction 72
6.1.1 Stator sections 73
6.1.2 Reaction plate 76
6.1.3 Complete motor assembly 76
6.2 Characterisation 77
6.2.1 Electromagnetic force 79
6.2.2 Position of α-axis 80
6.2.3 Flux linkages and inductances 81
6.2.4 Feeding efficiency and reaction plate utilisation 84
6.2.5 Solid-state contactors 84
6.2.6 Reaction plate position measurement 84
6.3 Simulation model 85
6.4 Controller 86
6.5 Simulation and experimental results 92

7 Conclusion **117**
7.1 Hybrid magnetic-equivalent-circuit and finite element method 117
7.1.1 Recommendations for further work 118
7.2 Motor dynamic model 119

7.2.1 Recommendations for further work 119
7.3 Linear motor feeding and control strategy 119
7.3.1 Recommendations for further work 120

A Hybrid Magnetic-Equivalent-Circuit and Finite Element Method 122
A.1 Implementation in MATLAB® and FEMM 122
A.1.1 Overview 122
A.1.2 Problem specification 122
A.1.3 Calculation of element properties 124
A.1.4 Assignment of boundary indices 125
A.1.5 Calculation of reluctances 128
A.1.6 Interfacing to FEMM 129
A.1.7 Precomputation of parameter sets 142
A.1.8 Reluctance-network graph representation 144
A.1.9 Finding independent MEC loops 145
A.1.10 Force calculation 149
A.1.11 Solver 149
A.1.12 Comparison of static results to full FEM solutions 156
A.2 Worked example 160
A.2.1 Problem specification 160
A.2.2 Assign boundary indices 164
A.2.3 Calculate flux tube reluctances 164
A.2.4 Precompute parameter sets 165
A.2.5 Initialise solver 165
A.2.6 Solve over a range of discrete positions and phase currents . . 165
A.2.7 Results 166
A.3 Schwarz-Christoffel conformal mapping 195
A.3.1 Overview 195
A.3.2 Mutual permeances 197
A.3.3 Source boundary flux 206

B Motor Dynamic Model 216
B.1 Power-invariant $\alpha/\beta/0$ transformation 216
B.2 Transformation between α/β and d/q frames 221

B.3 d/q Motor equations . . . 222
B.3.1 Electrical . . . 222
B.3.2 Inductances and flux linkages . . . 225
B.3.3 Power and electromagnetic force . . . 228
B.3.4 Complete d/q motor model . . . 228
B.4 Relative displacements . . . 231
B.5 Stator section model . . . 231
B.5.1 Interpolation of inductances and flux linkages . . . 234
B.5.2 Wrapping of angular displacement, θ . . . 235
B.6 Reaction plate model . . . 235
B.6.1 Load force . . . 237

C Prototype Construction 238
C.1 Motor . . . 238
C.1.1 Stator sections . . . 238
C.1.2 Stator assembly . . . 245
C.1.3 Reaction plate . . . 257
C.2 Inverter and interfacing circuitry . . . 270
C.2.1 Inverter . . . 270
C.2.2 Interfacing circuitry . . . 271
C.3 Solid-state contactors and interfacing circuitry . . . 273
C.3.1 Contactors . . . 273
C.3.2 Interfacing circuitry . . . 275
C.4 Auxiliary switchgear and wiring . . . 278
C.5 Measurement . . . 281
C.5.1 Inverter DC bus voltage . . . 281
C.5.2 Stator currents . . . 281
C.5.3 Reaction plate position . . . 286
C.6 Overall setup and interconnections . . . 288

D Prototype Characterisation and Modelling 292
D.1 Motor . . . 293
D.1.1 FEMM model . . . 293
D.1.2 Electromagnetic force . . . 294

D.1.3 Position of α-axis 295
D.1.4 Flux linkage and inductances 296
D.2 Feeding efficiency and reaction plate utilisation 303
D.3 Inverter 303
D.4 Solid state contactors 304
D.5 Stator current measurement 306
D.6 Reaction plate position measurement 308

E Prototype Controller **309**
E.1 Controller blocks 310
E.1.1 Background tasks 310
E.1.2 DC bus voltage control 310
E.1.3 Solid-state contactor actuation 311
E.1.4 Stator current measurement 312
E.1.5 Reaction plate position measurement 315
E.1.6 Position trajectory generator 317
E.1.7 Force feedforward compensation 320
E.1.8 Motor vector controller 320
E.1.9 Force the solid-state contactors to turn on 321
E.2 Design of feedback control loops 322

References **325**

List of Figures

1.1 Linear motor arrangement 2
1.2 Segmented-stator linear motor 4
3.1 Primary flux paths for a flux tube element 30
3.2 2D flux tube element 30
3.3 Flux tube region lengths and cross-sectional areas 31
3.4 Assignment of global boundaries for flux tube elements 32
3.5 Concentration of interior boundary current sheets as point currents . 34
3.6 Orientation of vectors for surface magnetic force density 36
3.7 Example—3D representation 39
3.8 Example—B-H curves of materials 40
3.9 Example—geometry 42
3.10 Example—assignment of materials 42
3.11 Example—magnetic equivalent circuit 43
3.12 Example—$\boldsymbol{\mathcal{G}}_{\underset{\sim}{\epsilon}\underset{\sim}{\mathrm{e}}_{24}\underset{\sim}{\kappa}_3}$, $\boldsymbol{\mathcal{G}}_{\underset{\sim}{\zeta}\underset{\sim}{\mathrm{e}}_{24}\underset{\sim}{\kappa}_3}$,$\boldsymbol{H}_{\underset{\sim}{\zeta}\underset{\sim}{\mathrm{e}}_{24}\underset{\sim}{\kappa}_3}$ and $\boldsymbol{\lambda}_{(\underset{\sim}{\mathrm{ph}})\underset{\sim}{\mathrm{e}}_{24}\underset{\sim}{\kappa}_3}$ for $x = 0$ 44
3.13 Example—$\boldsymbol{\mathcal{G}}_{\underset{\sim}{\epsilon}\underset{\sim}{\mathrm{e}}_{29}\underset{\sim}{\kappa}_1}$, $\boldsymbol{\mathcal{G}}_{\underset{\sim}{\zeta}\underset{\sim}{\mathrm{e}}_{29}\underset{\sim}{\kappa}_1}$,$\boldsymbol{H}_{\underset{\sim}{\zeta}\underset{\sim}{\mathrm{e}}_{29}\underset{\sim}{\kappa}_1}$ and $\boldsymbol{\lambda}_{(\underset{\sim}{\mathrm{ph}})\underset{\sim}{\mathrm{e}}_{29}\underset{\sim}{\kappa}_1}$ for $x = 0$ 45
3.14 Example—$\boldsymbol{\Phi}_{\underset{\sim}{\epsilon}(\underset{\sim}{\mathcal{F}}0)_1}$, $\boldsymbol{\Phi}_{\underset{\sim}{\zeta}(\underset{\sim}{\mathcal{F}}0)_1}$,$\boldsymbol{H}_{\underset{\sim}{\zeta}(\underset{\sim}{\mathcal{F}}0)_1}$ and $\boldsymbol{\lambda}_{(\underset{\sim}{\mathrm{ph}})(\underset{\sim}{\mathcal{F}}0)_1}$ for $x = 0$ 45
3.15 Example—$\boldsymbol{\Phi}_{\underset{\sim}{\epsilon}(\underset{\sim}{\mathcal{F}}0)_7}$, $\boldsymbol{\Phi}_{\underset{\sim}{\zeta}(\underset{\sim}{\mathcal{F}}0)_7}$,$\boldsymbol{H}_{\underset{\sim}{\zeta}(\underset{\sim}{\mathcal{F}}0)_7}$ and $\boldsymbol{\lambda}_{(\underset{\sim}{\mathrm{ph}})(\underset{\sim}{\mathcal{F}}0)_7}$ for $x = 0$ 46
3.16 Example—field solution by hybrid method versus a pure FEM solution 47
3.17 Example—geometry with a refined grid for the magnets 49
4.1 Spatial distribution of three-phase stator winding 52
4.2 α/β axes in relation to a/b/c axes 52
4.3 d/q axes in relation to α/β axes 54
5.1 Energising only the stator sections that are fully covered 61
5.2 Handover of active representative stator section 62
5.3 Improved handover of active representative stator section 64

5.4 General arrangement of the feeding strategy 65
5.5 Handover between stator blocks 67
5.6 Three-phase contactor arrangement 68
6.1 Multilayer linear motor 73
6.2 Cross-section of prototype motor 73
6.3 Stator section assembly 74
6.4 Stator section winding arrangement 75
6.5 Reaction plate assembly 76
6.6 Photograph of linear synchronous motor prototype 77
6.7 Propulsion force variation with reaction plate position 79
6.8 Normal force variation with reaction plate position 80
6.9 α-axis offset for stator section 81
6.10 $L_{(\mathrm{dd})}$ versus relative position of reaction plate 82
6.11 $L_{(\mathrm{qq})}$ versus relative position of reaction plate 82
6.12 λ_{md} versus relative position of reaction plate 83
6.13 λ_{mq} versus relative position of reaction plate 83
6.14 Full Simulink® model of prototype system 85
6.15 Complete prototype controller (`lsmDSPACE`) 86
6.16 Cascaded control arrangement (`lsmController`) 87
6.17 Subsystem `lsmController/Modular-Stator Control` 88
6.21 Subsystem `lsmController/Position Feedback Control` 89
6.18 Subsystem `lsmController/Motor Drive/FOC` 90
6.19 Subsystem `lsmController/Motor Drive` 91
6.20 Subsystem `lsmController/Motor Drive/FOC/d,q Current Control` 91
6.22 Position trajectory generated by controller 93
6.23 Simulated reaction plate movement 94
6.24 Measured reaction plate movement 94
6.25 Simulated phase currents for stator section 1 95
6.26 Measured phase currents for stator section 1 96
6.27 Simulated phase currents for stator section 2 97
6.28 Measured phase currents for stator section 2 98
6.29 Simulated phase currents for stator section 3 99
6.30 Measured phase currents for stator section 3 100

6.31 Simulated phase currents for stator section 4 101
6.32 Measured phase currents for stator section 4 102
6.33 Simulated phase currents for stator section 5 103
6.34 Measured phase currents for stator section 5 104
6.35 Measured inverter phase currents 105
6.36 Simulated d-axis current for representative section 107
6.37 Measured d-axis current for representative section 108
6.38 Simulated q-axis current for representative section 109
6.39 Measured q-axis current for representative section 110
6.40 Switch active representative section from section 3 to section 2 . . . 111
6.41 Switch active representative section from section 2 to section 3 . . . 112
6.42 Energising stator section 1 113
6.43 Energising stator section 5 114
6.44 De-energising stator section 1 115
6.45 De-energising stator section 5 116
A.1 Dependency graph for custom MATLAB® functions 123
A.2 Example—*B*-*H* curves for materials (zoomed in on initial slopes) . . 162
A.3 Geometry of the highly-permeable regions in the complex plane . . . 196
A.4 Truncation of open boundary with a rectangular outer boundary . . 196
A.5 Mutual permeances—geometry in the complex plane 199
A.6 Mutual permeances—prevertices in the complex plane 201
A.7 Mutual permeances—contour plot showing flux lines for $\mathcal{F}_{\underset{\sim}{e}_{24}\underset{\sim}{\kappa}_3}$ . . . 202
A.8 Mutual permeances—region used to calculate $\mathcal{G}_{\underset{\sim}{\epsilon}_{30}\underset{\sim}{e}_{24}\underset{\sim}{\kappa}_3}$ 203
A.9 Mutual permeances—region used to calculate $\mathcal{G}_{\underset{\sim}{\epsilon}_{36}\underset{\sim}{e}_{24}\underset{\sim}{\kappa}_3}$ 204
A.10 Mutual permeances—region used to calculate $\mathcal{G}_{\underset{\sim}{\epsilon}_{46}\underset{\sim}{e}_{24}\underset{\sim}{\kappa}_3}$ 205
A.11 Source boundary flux—geometry in the complex plane 208
A.12 Source boundary flux—prevertices in the complex plane 210
A.13 Source boundary flux—contour plot showing flux lines for $\mathcal{F}_{(\underset{\sim}{\mathcal{F}}0)_7}$ . . 211
A.14 Source boundary flux—region used to calculate $\Phi_{\underset{\sim}{\epsilon}_{36}(\underset{\sim}{\mathcal{F}}0)_7}$ 212
A.15 Source boundary flux—region used to calculate $\Phi_{\underset{\sim}{\epsilon}_{41}(\underset{\sim}{\mathcal{F}}0)_7}$ 213
A.16 Source boundary flux—region used to calculate $\Phi_{\underset{\sim}{\epsilon}_{47}(\underset{\sim}{\mathcal{F}}0)_7}$ 214
B.1 Subsystem `lsm/dq/Transforms/inv T_32` 219
B.2 Subsystem `lsm/dq/Transforms/T_22` 221

B.3 Subsystem lsm/dq/Transforms/inv T_22 . . . 221
B.4 Subsystem lsm/dq/Transforms/T_2r . . . 221
B.5 Subsystem lsm/dq/Transforms/inv T_2r . . . 222
B.6 Subsystem lsm/dq/Electrical . . . 225
B.7 Subsystem lsm/dq/Motor Model/Flux Linkage . . . 227
B.8 Subsystem lsm/dq/Motor Model (reduced)/Flux Linkage . . . 227
B.9 Subsystem lsm/dq/EM Force . . . 228
B.10 Subsystem lsm/dq/Motor Model . . . 229
B.11 Subsystem lsm/dq/Motor Model (reduced) . . . 230
B.12 Relative displacement of reaction plate to stator . . . 231
B.13 Subsystem lsm/Stator Section/Full . . . 232
B.14 Subsystem lsm/Stator Section/Reduced . . . 233
B.15 Subsystem lsm/Stator Section/Full/Interpolator . . . 234
B.16 Subsystem lsm/Stator Section/Reduced/Interpolator . . . 235
B.17 Subsystem lsm/dq/Wrap Angle . . . 235
B.18 Subsystem lsm/Reaction Plate/Viscous Friction . . . 236
B.19 Subsystem lsm/Reaction Plate/Stribeck Friction . . . 236
B.20 Subsystem lsm/Reaction Plate/Output . . . 237
B.21 Subsystem lsm/Load . . . 237
C.1 Drawing of LSM stator section lamination stack . . . 239
C.2 Drawing of LSM stator section end cap 1 . . . 241
C.3 Drawing of LSM stator section end cap 2 . . . 242
C.4 Drawing of LSM stator section winding overhang cover 1 . . . 243
C.5 Drawing of LSM stator section winding overhang cover 2 . . . 244
C.6 Photographs of VPI-insulated stator section after cleaning . . . 246
C.7 Drawing of LSM rail 1 . . . 249
C.8 Drawing of LSM rail 2 . . . 250
C.9 Drawing of LSM base plates . . . 251
C.10 Photographs of aligning the stator sections against the first rail . . . 252
C.11 Photographs of fastening the stator sections between the two rails . 253
C.12 Photographs of stator section terminal boxes . . . 254
C.13 Photograph of stator track with end-stops in place . . . 255
C.15 Photograph of stator in position to be bolted to the test bed . . . 255

C.14 Drawing of LSM end brackets 256
C.16 Drawing of LSM reaction plate back-iron 258
C.17 Drawing of LSM reaction plate permanent magnets 259
C.18 Drawing of LSM reaction plate spacers 260
C.19 Drawing of LSM reaction plate side covers 261
C.20 Drawing of LSM reaction plate end covers 262
C.21 Photograph of back-iron with side covers and two spacers 263
C.22 Photograph of back-iron with protective pieces of wood 264
C.23 Photograph of back-iron with first row of magnets 264
C.24 Photographs of procedure to add each subsequent row of magnets . . 265
C.25 Photographs of how each magnet was tapped towards the back-iron and then along to its final position 266
C.26 Photograph of back-iron with all magnets in place 266
C.27 Photograph of fully-assembled reaction plate 267
C.28 Photographs of reaction plate being placed on the track using a crane 268
C.29 Drawing of LSM assembly (end view) 269
C.30 Photographs of SEMIKRON® SEMISTACK inverter unit 270
C.31 Photograph of three-phase variac and brake resistor 271
C.32 Schematic of SEMISTACK / dSPACE interface circuit 272
C.33 Photograph of SEMISTACK / dSPACE interface circuit 273
C.34 Photograph of POWER-IO™ DDA-6V75 solid-state contactor 274
C.35 Photograph of solid-state contactors housed within cabinet 274
C.36 Schematic of solid-state contactor wiring 275
C.37 Schematic of solid-state contactor interface circuit 276
C.38 Veroboard layout of solid-state contactor interface circuit 277
C.39 Photograph of solid-state contactor interface circuit 277
C.41 Photographs of auxiliary switchgear 278
C.40 Schematic of auxiliary switchgear and wiring 279
C.42 Photograph of back of cabinet door 280
C.43 Photograph of cabinet terminals 280
C.44 Schematic of current measurement and multiplexer circuit 283
C.45 Veroboard layout for current measurement and multiplexer circuit . 284
C.46 Photographs of current measurement and multiplexing circuit 285

C.47 Photograph of Stahltronic WCS2 reading head and coded rail 287
C.48 Schematic of Stahltronic WCS2 position encoder wiring 287
C.49 Photograph of dSPACE break-out connection box 288
C.50 Schematic of component interconnections 289
C.51 Photographs of complete linear synchronous motor 290
C.52 Photograph of pulley arrangement used to load motor 291
C.53 Photograph of LSM control setup 291
D.1 FEMM model geometry `lsm.fem` 293
D.2 $L_{(aa)}$ versus relative position of reaction plate 298
D.3 $L_{(bb)}$ versus relative position of reaction plate 298
D.4 $L_{(cc)}$ versus relative position of reaction plate 299
D.5 $L_{(ab)}$ versus relative position of reaction plate 299
D.6 $L_{(bc)}$ versus relative position of reaction plate 300
D.7 $L_{(ca)}$ versus relative position of reaction plate 300
D.8 λ_{ma} versus relative position of reaction plate 301
D.9 λ_{mb} versus relative position of reaction plate 301
D.10 λ_{mc} versus relative position of reaction plate 302
D.11 Subsystem `lsmProto/Inverter` 304
D.12 Subsystem `lsmProto/Contactor/Ideal Switch` 304
D.13 Subsystem `lsmProto/Contactor/Breaker` 304
D.14 Subsystem `lsmProto/Contactor/AP SCC` 305
D.15 Subsystem `lsmProto/Contactor/AP SCC 2` 305
D.16 Subsystem `lsmProto/Current Sensors/Unlimited Bandwidth` 306
D.17 Subsystem `lsmProto/Current Sensors/Limited Bandwidth` 307
D.18 Subsystem `lsmProto/Position Sensor/Simple` 308
D.19 Subsystem `lsmProto/Position Sensor/Quantisation` 308
D.20 Subsystem `lsmProto/Position Sensor/Quantisation and Delay` 308
E.1 Subsystem `lsmDSPACE/Monitor` 310
E.2 Subsystem `lsmProtoHw/DC Bus Control` 310
E.3 Subsystem `lsmProtoHw/Solid-state Contactors` 311
E.4 Subsystem `lsmProtoHw/Current Sensors` 312
E.5 Subsystem `lsmProtoHw/Current Sensors/Check LEM Voltage` 313
E.6 Subsystem `lsmProtoHw/Current Sensors/A2D Conversion` 313

E.7 Subsystem `lsmProtoHw/Current Sensors/Bank 0` 314
E.8 Subsystem `lsmProtoHw/Current Sensors/Bank 1` 314
E.9 Subsystem `lsmProtoHw/Stahl WCS2` 315
E.10 Subsystem `lsmProtoHw/Stahl WCS2/Decode Response` 316
E.11 Subsystem `lsmProtoHw/Stahl WCS2/Convert and Request Next` 316
E.12 Subsystem `lsmController/Trajectory Generator` 317
E.13 Subsystem `lsmController/Trajectory Generator/Plan Trajectory` 318
E.14 Subsystem `lsmController/Trajectory Generator/Generate Trajectory` . . 319
E.15 Subsystem `lsmController/Force Feedforward` 320
E.16 Subsystem `lsmController/Motor Drive/FOC/mod-arg to SVM` 320
E.17 Subsystem `lsmController/Ensure SSRs turn on` 321

List of Tables

3.1 Example—material properties 41
3.2 Example—percentage rms errors for reaction plate positioned where exact precomputed parameters are used 48
3.3 Example—percentage rms errors for reaction plate positioned where the precomputed parameters are interpolated 48
3.4 Example—percentage rms errors for reaction plate positioned where exact precomputed parameters are used (reduced-size mesh) 50
3.5 Example—percentage rms errors for reaction plate positioned where the precomputed parameters are interpolated (reduced-size mesh) . . 50
6.1 Prototype motor parameters and dimensions 77
6.2 Measured stator section electrical parameters 78
6.3 Material properties for FEMM model 78
6.4 Stator section switching events for experimental results 106
A.1 Example—flux tube element outputs 166
A.2 Example—source outputs 187
A.3 Example—flux linkages 189
A.4 Example—force 189
A.5 Example—percentage rms errors 190
A.6 Comparison of mutual permeances calculated by FEM and the conformal mapping method 206
A.7 Comparison of source boundary fluxes calculated by FEM and the conformal mapping method 215
C.1 Measured magnetic field strength over portion of reaction plate . . . 267
C.2 Measured LEM shunt resistances 286
C.3 Mapping of measured current signals from LEMs to dSPACE 286
D.1 Measured SSC turn-on threshold voltages 305

Code Listings

A.1 Calculate element region cross-sectional areas (calc_A_e_kappa.m) . . . 125
A.2 Calculate boundary orientations (calcBoundaryOrientations.m) 125
A.3 Calculate element region lengths (calc_l_e_kappa.m) 125
A.4 Assign global element boundary indices (assign_nu_e_kappa.m) 126
A.5 Assign exterior element boundary indices (assign_epsilon_e_kappa.m) . 127
A.6 Assign moving source boundary indices (assign_zeta_calF_kappa.m) . . 128
A.7 Calculate element reluctances (calc_calR_e_kappa.m) 129
A.8 Define new magnetics problem in FEMM (femSetup.m) 130
A.9 Draw elements / sources in FEMM (femDraw.m) 130
A.10 Create surrounding infinite domain in FEMM (femDrawInfDomain.m) . 132
A.11 Set element boundary conditions in FEMM (femSetBoundaries.m) . . . 134
A.12 Define materials in FEMM (femDefineMaterials.m) 136
A.13 Remove energy from sources in FEMM (femRemoveEnergySources.m) . . 137
A.14 Define unity source materials for calculations in FEMM (femDefineUnitySourceMaterials.m) 137
A.15 Assign source materials in FEMM (femAssignSources.m) 138
A.16 Assign element materials in FEMM (femAssignElements.m) 139
A.17 Obtain exterior boundary fluxes in FEMM (fem_Phi_epsilon.m) 140
A.18 Obtain moving source boundary fluxes in FEMM (fem_Phi_zeta.m) . . 140
A.19 Obtain moving source boundary average field intensities in FEMM (fem_Phi_zeta.m) 141
A.20 Obtain flux linkages in FEMM (fem_lambda_ph.m) 141
A.21 Precompute parameter sets in FEMM (femUpFrontCalcs.m) 142
A.22 Construct reluctance element graph (graph_C_n_n.m) 145
A.23 Find independent MEC loops (find_Lambda_Lambda.m) 146
A.24 Calculate force (calc_F.m) 149
A.25 Initialise solver (solveMECinit.m) 150
A.26 Solver (solveMEC.m) 152

A.27 Solve for magnetic fields in FEMM using sources and element boundary conditions calculated by the hybrid method (femResult.m) 156
A.28 Solve problem purely in FEMM (femFull.m) 156
A.29 Obtain static solutions over a range of phase currents and displacements and compare to full FEM solutions (solveMECstatic.m) 158
A.30 Example—define basic problem parameters (exampleMEC.m) 160
A.31 Example—define materials (exampleMEC.m) 160
A.32 Example—flux tube elements (exampleMEC.m) 162
A.33 Example—sources (exampleMEC.m) 163
A.34 Example—assign boundary indices (exampleMEC.m) 164
A.35 Example—calculate flux tube reluctances (exampleMEC.m) 164
A.36 Example—precompute parameter sets (exampleMEC.m) 165
A.37 Example—initialise solver (exampleMEC.m) 165
A.38 Example—solve at discrete positions and currents (exampleMEC.m) . . 165
A.39 Mutual permeances—define geometry (exampleSCpermeances.m) 198
A.40 Mutual permeances—calculate mapping (exampleSCpermeances.m) . . . 200
A.41 Mutual permeances—prevertices (exampleSCpermeances.m) 201
A.42 Mutual permeances—flux distribution (exampleSCpermeances.m) 202
A.43 Mutual permeances—calculate $\mathcal{G}_{\underset{\sim}{\epsilon}_{30}\underset{\sim}{e}_{24}\underset{\sim}{\kappa}_3}$ (exampleSCpermeances.m) . . . 203
A.44 Mutual permeances—calculate $\mathcal{G}_{\underset{\sim}{\epsilon}_{36}\underset{\sim}{e}_{24}\underset{\sim}{\kappa}_3}$ (exampleSCpermeances.m) . . . 204
A.45 Mutual permeances—calculate $\mathcal{G}_{\underset{\sim}{\epsilon}_{46}\underset{\sim}{e}_{24}\underset{\sim}{\kappa}_3}$ (exampleSCpermeances.m) . . . 205
A.46 Source boundary flux—define geometry (exampleSCsourcePM.m) 207
A.47 Source boundary flux—calculate mapping (exampleSCsourcePM.m) . . . 209
A.48 Source boundary flux—prevertices (exampleSCsourcePM.m) 210
A.49 Source boundary flux—flux distribution (exampleSCsourcePM.m) 211
A.50 Source boundary flux—calculate $\Phi_{\underset{\sim}{\epsilon}_{36}(\underset{\sim}{\mathcal{F}}0)_7}$ (exampleSCsourcePM.m) . . . 212
A.51 Source boundary flux—calculate $\Phi_{\underset{\sim}{\epsilon}_{41}(\underset{\sim}{\mathcal{F}}0)_7}$ (exampleSCsourcePM.m) . . . 213
A.52 Source boundary flux—calculate $\Phi_{\underset{\sim}{\epsilon}_{47}(\underset{\sim}{\mathcal{F}}0)_7}$ (exampleSCsourcePM.m) . . . 214
B.1 Transform from a/b/c to α/β (T_32.m) 219
B.2 Transform from a/b/c to $\alpha/\beta/0$ (T_33.m) 219
B.3 Transform from ab/bc to α/β (T_22.m) 220
B.4 Transform from $\alpha/\beta/0$ to d/q/0 (T_3r.m) 221
B.5 Calculate set of angular displacements (calc_theta_x.m) 225
B.6 Calculate set of d/q/0 inductances (calc_L_dq0_x.m) 226
B.7 Calculate set of d/q/0 PM flux linkages (calc_lambda_m_dq0_x.m) 227

D.1 Obtain $\hat{\boldsymbol{x}}$ and $\hat{\boldsymbol{y}}$ forces using FEMM (`fem_F_xy_x.m`) 294
D.2 Calculate α-axis offset using FEMM (`fem_x_alpha.m`) 295
D.3 Obtain a/b/c inductances using FEMM (`fem_L_abc_x.m`) 296
D.4 Obtain a/b/c PM flux linkage using FEMM (`fem_lambda_m_abc_x.m`) . . 297
D.5 Calculate θ for a set of reaction plate positions (`calc_theta_x.m`) . . . 302
D.6 Calculate d/q/0 inductances (`calc_L_dq0_x.m`) 302
D.7 Calculate d/q/0 flux linkages (`calc_lambda_m_dq0_x.m`) 303
D.8 Calculate reaction plate utilisation (`calc_eta_r.m`) 303
D.9 Calculate stator feeding efficiency (`calc_eta_s.m`) 303
E.1 Design of feedback control loops (`lsmControlDesign.m`) 322

List of Symbols

Constants

μ_0 `(mu0)`	magnetic permeability of free space = $4\pi \cdot 10^{-7}$ H/m
π `(pi)`	pi $\approx$ 3,14
g	gravitational acceleration $\approx 9{,}81\,\mathrm{m/s^2}$
j	$\sqrt{-1}$

Physical quantities

ϵ `(epsilon)`	exterior boundary index
ζ `(zeta)`	source boundary index
η `(eta)`	efficiency (percent) [%]
θ `(theta)`	angular displacement (electrical radians) [rad]
Λ `(Lambda)`	graph loop, as a list of nodes
λ `(lambda)`	magnetic flux linkage (weber-turns) [Wb]
μr `(mur)`	relative magnetic permeability
μ `(mu)`	magnetic permeability (henries per metre) [H/m]
ν `(nu)`	global boundary index
ξ `(xi)`	graph component index (group of connected nodes)
σ `(sigma)`	stress (pascal) [Pa]
τ `(tau)`	pole pitch (metres) [m]
Φ `(Phi)`	magnetic flux (webers) [Wb]
χ `(chi)`	material type index
Ψ `(Psi)`	magnetic scalar potential (ampere-turns) [A]
ω `(omega)`	angular frequency (radians per second) [rad/s]
$\vec{\boldsymbol{A}}$	magnetic vector potential (webers per metre) [Wb/m]
A	cross-sectional area (square metres) [$\mathrm{m^2}$]
a	acceleration (metres per second squared) [$\mathrm{m/s^2}$]

$\vec{\boldsymbol{B}}$	magnetic induction field (tesla) [T]
B	magnetic flux density (normal) (tesla) [T]
b	viscous friction coefficient (newton metre seconds) [N·m·s]
d	depth (metres) [m]
$\mathcal{E}$ `(calE)`	electromotive force (emf) (volts) [V]
$\vec{\boldsymbol{E}}$	electric field (volts per metre) [V/m]
E	Young's modulus (pascals) [Pa]
$\mathcal{F}$ `(calF)`	magneto-motive force (mmf) (ampere-turns) [A]
F	force (newtons) [N]
$\mathcal{G}$ `(calG)`	magnetic permeance (webers per ampere-turns) [Wb/A]
G	signal gain
$\vec{\boldsymbol{H}}$	magnetic intensity field (amperes per metre) [A/m]
H	magnetic intensity (tangential) (amperes per metre) [A/m]
Hc	magnetic coercivity (amperes per metre) [A/m]
$\mathcal{I}$ `(calI)`	area moment of inertia [m^4]
I	electric current (amperes) [A]
J	electric current density (amperes per square metre) [A/m^2]
L	inductance (henries) [H]
l	length (metres) [m]
M	mass (kilograms) [kg]
$\hat{\boldsymbol{n}}$ `(hatn)`	unit normal vector
N	number of
P	power (watts) [W]
p	point in the complex plane
$\mathcal{R}$ `(calR)`	magnetic reluctance (ampere-turns per weber) [A/Wb]
R	electrical resistance (ohms) [Ω]
S	surface
s	Laplace Transform variable
$\hat{\boldsymbol{t}}$ `(hatt)`	unit tangent vector
T	sampling time period (seconds) [s]
t	time (seconds) [s]
$\mathcal{V}$ `(calV)`	volume (cubic metre) [m^3]
V	electric potential difference (volts) [V]

v	velocity (metres per second) [m/s]
W	energy (joules) [J]
w	width (metres) [m]
$\hat{\boldsymbol{x}}$ `(hatx)`	unit vector in the x-direction
$\hat{\boldsymbol{y}}$ `(haty)`	unit vector in the y-direction
x	displacement (metres) [m]
$\hat{\boldsymbol{z}}$ `(hatz)`	unit vector in the z-direction
z	z-Transform variable

Labels / Indices

α `(alpha)`	α-axis of $\alpha/\beta/0$ reference frame
$\alpha\beta0$	$\alpha/\beta/0$ reference frame
β `(beta)`	β-axis of $\alpha/\beta/0$ reference frame
δ `(delta)`	movement
ϵ `(epsilon)`	exterior boundary
ζ `(zeta)`	source boundary
ι `(iota)`	interior boundary
κ `(kappa)`	element region
Λ `(Lambda)`	loop
ν `(nu)`	global boundary
ξ `(xi)`	graph component
χ `(chi)`	material
0	zero-sequence component
a	phase ‘a’
abc	a/b/c reference frame
ang	angle
B	bandwidth
b	phase ‘b’
c	phase ‘c’
d	direct axis of d/q/0 reference frame
dc	dc bus
dq0	d/q/0 reference frame
e	element

em	electromagnetic
$\mathcal{F}0$ `(calF0)`	normalised/unity magneto-motive force (mmf) source
$\mathcal{F}$ `(calF)`	magneto-motive force (mmf) source
f	friction
fb	breakaway friction
fc	Coulomb friction
g	air-gap
I	electric current
int	interval
L	load
m	permanent magnet
mag	magnitude
max	maximum
Mg	weight
min	minimum
N	noise
n	node
p	magnetic pole
ph	phase
pv	pre-vertex
q	quadrature axis of d/q/0 reference frame
r	reaction plate
s	stator section
t0	initial value ($t = 0$)
v	vertex
x	discrete position

Special matrices

$\mathbf{I}$	identity matrix
$\mathbf{C}$	adjacency matrix (graph representation)
$\mathbb{T}$	Maxwell Stress Tensor
$\mathbf{T}$	transformation matrix
$\mathbf{M}$	boolean array/matrix

Mathematical notation

$\vec{\square}$	vector field
$\hat{\square}$	direction unit vector
$\square^{\mathrm{T}}$	transpose
$\dot{\square}$	first derivative with respect to time
$\ddot{\square}$	second derivative with respect to time
$\lfloor\square\rfloor$	floor operator
$\boldsymbol{a}_{\underset{\sim}{\mathrm{b}}\ldots\underset{\sim}{\mathrm{n}}}$	multi-dimensional array with its number of dimensions denoted by the number of index arrays $\underset{\sim}{\mathrm{b}}\ldots\underset{\sim}{\mathrm{n}}$
$*$	element-by-element multiplication
$\triangleq$	corresponds to
$\forall$	for all
$\Im$	imaginary
$\Re$	real

Nomenclature

2D	2-dimensional
3D	3-dimensional
ADC	analogue-to-digital converter
BEM	Boundary Element Method
CMOS	complementary metal-oxide semiconductor
DTC	Direct Torque Control
emf	electromotive force
FEM	Finite Element Method
FFT	Fast Fourier Transform
FIT	Finite Integration Technique
FOC	Field-Orientated Control
IC	integrated circuit
IGBT	insulated-gate bipolar transistor
LSM	linear synchronous motor

maglev magnetically-levitated

MEC magnetic equivalent circuit

mmf magneto-motive force

NdFeB neodymium-iron-boron

PM permanent magnet

PWM pulse-width modulated

rms root-mean-squared

SVM space-vector modulation

TTL transistor-transistor logic

variac variable ac autotransformer

VPI vacuum pressure impregnation

Chapter 1

Introduction

Hypothesis. *The electromagnetic propulsion force, and consequently position, of a segmented long-stator permanent magnet linear synchronous motor, with stator sections shorter than the reaction plate (mover), can be controlled using a single voltage source inverter with an intermediate switching layer that achieves partial excitation of the stator.*

1.1 Problem statement

1.1.1 Permanent magnet linear synchronous motors

Figure 1.1 depicts a single-sided linear motor. It comprises a stationary stator (primary) that houses the windings and a moving reaction plate (secondary) that has an array of permanent magnets. The reaction plate is mechanically guided to only translate in the $\hat{\boldsymbol{x}}$ direction. The thrust force is in the direction of motion but there is also a strong normal force attracting the reaction plate to the stator in the $\hat{\boldsymbol{y}}$ direction and a weak stabilising force keeping the reaction plate centred to the stator in the $\hat{\boldsymbol{z}}$ direction. A symmetrical double-sided linear motor typology is often used so that the strong normal force components cancel, ideally resulting in zero nett normal force on the moving reaction plates.

A three-phase linear synchronous motor (LSM) stator is designed to produce a sinusoidal flux distribution along the length of the air-gap. When three-phase currents flow in the windings (varying sinusoidally in time), the spatial flux distribution is

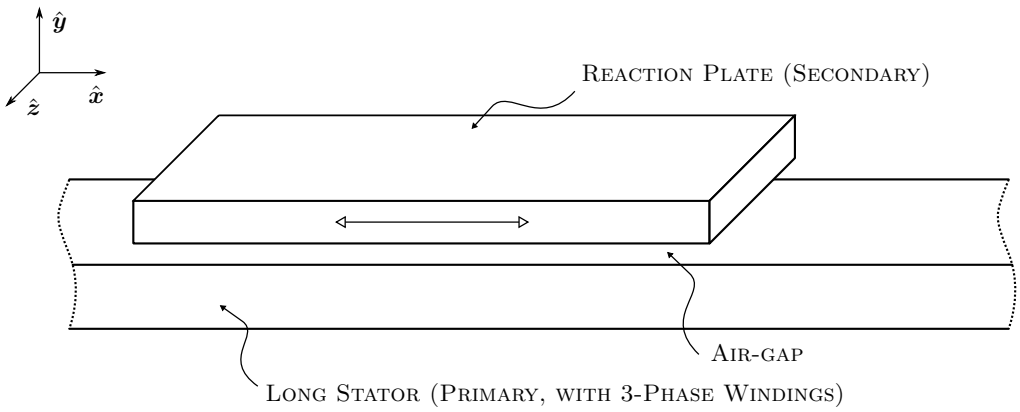

Figure 1.1: Linear motor arrangement

a travelling wave moving at a speed corresponding to the supply frequency. The alternating-polarity array of permanent magnets (constituting the reaction plate) "surfs" this travelling wave of flux. The maximum propulsion force occurs when the travelling wave of flux is 90° out of phase with the permanent magnet flux.

1.1.2 Ropeless hoisting

Permanent magnet (PM) linear synchronous motor (LSM) technology has significant potential for application to ropeless hoisting [1–7] and the work presented in this thesis was carried out with this specific application in mind. In particular, a long-stator configuration with the array of permanent magnets placed on the mover is attractive, as there is then no need to supply power to the conveyance. A ropeless hoist for a deep-level mine would overcome the current depth limitation for a shaft owing to the rope not being able to support its own weight beyond a certain depth [3]. Also, as highlighted by Ishii [1] and Kim et al. [2], the significant advantage of a ropeless elevator system, particularly for use in future super skyscrapers, is that many conveyances can inherently occupy the same shaft. Furthermore, horizontal LSMs can be used to dock conveyances out of the main shaft when stopping at a level and to link several vertical shafts together to form a network of shafts, where conveyances can then all move in the same direction within a particular shaft. Lastly, in the case of a power failure, if the stator windings of a PM LSM are short-circuited, there is a regenerative braking effect that causes the conveyance to have a slow downward terminal velocity. The slow-moving conveyance can then be stopped and held with a mechanical brake or come to rest at the bottom of the shaft with a shock-absorbing

hydraulic buffer. The terminal velocity of the conveyance can be varied by shorting the windings through an external resistance, whose value dictates the amount of braking force as a function of the reaction plate's speed [8].

For a ropeless hoist, the linear motor needs enough thrust force to counter the weight of the conveyance, as well as to accelerate it and overcome the mechanical losses of friction and air resistance. So, typically, a larger motor is required than for a similar-sized conveyance moving horizontally. Also, it is preferable from a capital cost perspective to have longer reaction plates that interact with a narrower stator to achieve the required air-gap surface area and, hence, force capability for each conveyance. Thus, relatively long reaction plates are desirable and are feasible in this application because the exclusively straight-line motion allows the air-gap to be accurately maintained along the full length of the reaction plate.

Several linear motors may be used to move a conveyor/platform. Then, the mechanical arrangement can be designed to either 'loosely' or 'tightly' couple the motors. If the motors are loosely coupled, independent control over each motor's position is necessary so that they all track a common position reference trajectory. In this case, each motor must provide the correct proportion of the total force needed to move the platform whilst keeping it level. If, alternatively, the motors are mechanically tightly coupled, the control system needs to provide a force reference for each motor in the correct proportion to the total force required. Either approach is achievable when the force produced by each linear motor can be controlled.

1.1.3 Partial excitation with a segmented stator

It is not efficient to energise the entire length of stator for a long-stator linear motor. This is because only the currents flowing in the stator coils in the vicinity of the reaction plate interact with it and contribute to the propulsion force [9, 10]. Any currents flowing in stator sections that aren't interacting with the reaction plate only result in additional power loss. Also, it is often necessary to have independent control over several conveyances sharing the same length of stator. Hence, a segmented-stator design is desirable, whereby discrete sections along the length of the stator can be powered independently [11]. If the sections of stator are designed to be identical and modular there are additional advantages in terms of the ease and cost of manufacture, as well as maintenance (e.g. a faulty section can be replaced with a backup unit).

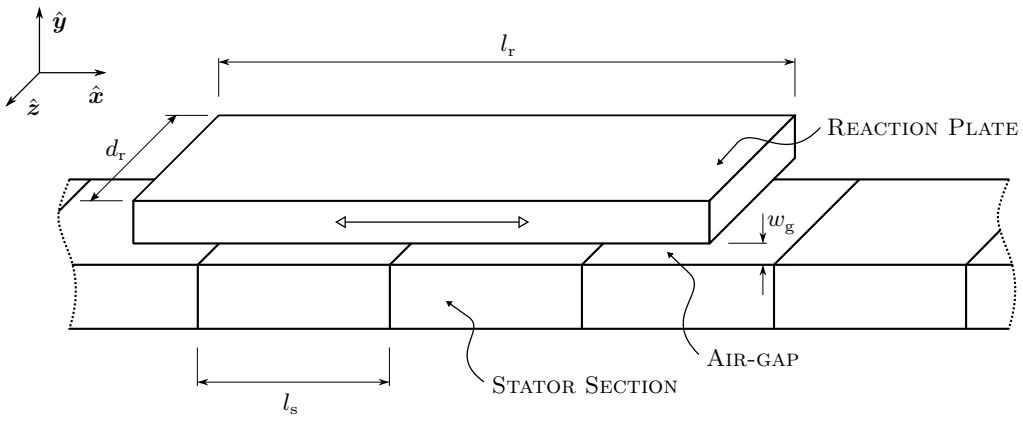

Figure 1.2: Segmented-stator linear motor

Figure 1.2 shows the proposed arrangement of a partially-excited long-stator LSM. The stator is divided into sections of length l_s, each shorter than the reaction plate.

1.2 Limitations of the prior art

The feeding and control of partially-excited LSMs has received limited attention in the literature. In most work presented on the control of LSMs, in contrast to rotating synchronous motors, scaling factors are merely introduced to account for force as opposed to torque [12]. Consequently, these methods do not make provision for a segmented stator with discontinuities. Moreover, although Toida et al. [7], Torii et al. [13], Hu et al. [14] and Sakamoto and Noma [15] all propose controllers for LSM ropeless elevators, they also do not consider a segmented stator.

In the case of using open-loop scalar motor control, it is possible to simply use proximity switches (e.g. Hall sensors) to connect those stator sections in the vicinity of the reaction plate to a common supply. This is problematic, though, because the electrical characteristics of each section change as the reaction plate enters and then leaves. If an independent position sensor is used it is possible to supply power to adjacent stator sections using vector current control with a shared current reference [16, 17]. However, in the case of using a modern sensorless control technique, such as Direct Torque Control, significant modifications are required to facilitate smooth crossing of stator section boundaries [18].

Typically, stator sections that are longer than the reaction plate are used, so that

a maximum of two stator sections need to be energised simultaneously (when the reaction plate is crossing the boundary between two adjacent sections) [2, 19, 20]. However, as the length of the stator section increases relative to the reaction plate length, the time-average length of unnecessarily energised stator increases (for the reaction plate moving at constant velocity). Kim et al. [2] and Perreault [21] discuss the concept of feeding efficiency, which is a useful measure for determining an appropriate section length for this arrangement.

With this conventional configuration, at least two inverters must be used to feed alternate stator sections [17] so that the currents in each section are independently controlled to have the same magnitude and phase when the reaction plate is crossing the section boundary [22]. Alternatively, as proposed in this thesis, stator sections that are shorter than the reaction plate may be used. This configuration has previously not received any notable attention in the literature, except for the extreme case of independently exciting single poles or pole pairs—e.g. Batelaan [23] describe an 'individual pole excitation linear motor' (IPELM) and Gamble et al. [24] refer to a 'locally commutated' LSM for a superconducting magnetically-levitated (maglev) train. Although the high-level concept of feeding sections of coils shorter than the vehicle is described by Fujie and Shibakawa [25] for ground coils shorter than the length of a maglev train, their method is intended for direct-online operation and not vector control. Lastly, the 'discontinuous stator' PM LSM, introduced by Kim et al. [26] for material handling, is an arrangement where there are physical gaps between the stator sections along the length of travel.

To simulate and design the proposed feeding strategy and control system, a dynamic mathematical model of the motor arrangement was required. A full transient Finite Element Method (FEM) model was deemed to be too computationally expensive for this task. Miller et al. [27], Bodika [8] and Wang et al. [28] only consider a space-vector model for non-segmented long-stator permanent magnet motors with no discontinuities and, although Gentile et al. [29] consider end effects, their model is developed for a short-stator motor (finite length of moving armature winding, rather than a moving reaction plate). Similarly, the magnetic equivalent circuit (MEC) based model presented by Polinder et al. [30] for a short-stator configuration considers saturation and end effects but can not cater for the effects of a reaction plate transitioning from one stator section to the next. Enhanced versions of this model proposed by Vaez-Zadeh and Hassanpour Isfahani [31] and Sheikh-Ghalavand

et al. [32], which use an air-gap flux density distribution function to better model the air-gap flux, still suffer from the same limitation. Kazan and Onat [33] also use an MEC approach with flux density distribution functions but for an air-core stator with concentrated coils. Hence, again, there are no discontinuities along the length of stator. Mostly, MECs have been used to study localised effects in synchronous motors, such as zig-zag and slot leakage fluxes [34] or the effect of skewing surface-mounted permanent magnets [35].

The work of Leidhold and Mutschler et al. [19, 36–38], published subsequent to the initial mathematical modelling undertaken for this thesis, details two control-orientated modelling methods that are conceptually similar to the approaches ultimately taken in this work. Specifically, they present a model based on lookup tables, generated offline with FEM, and, alternatively, a model derived using a pure MEC formulation.

1.3 Contributions

A linear motor feeding and control strategy is presented that enables any advanced motor vector control technique originally developed for rotary motors to be directly applied. This is achieved through careful segmentation of the stator and by having an intermediate switching layer between the inverter and stator sections. Provided that the stator sections are shorter than half of the reaction plate length, there is at least one stator section that fully interacts with the magnetic field of the reaction plate at any point in time. That is, every magnetic pole formed by that stator section interacts with a corresponding magnetic pole formed by the reaction plate. A "fully-covered" stator section is therefore electrically indistinguishable from the stator of a rotary machine and one of these sections is designated to be representative of the whole motor. The inverter output voltage, common to all energised stator sections, is thus controlled using only a measurement of the currents flowing within the active representative section. The choice of which representative stator section is active depends on the position of the reaction plate at a particular moment in time. If the underlying motor vector control technique estimates or infers the "angular position" of the "rotor", sensorless control of the linear motor should also be possible.

An advantage of the novel feeding and control approach with shorter stator sections is that the linear motor is fed from a single inverter per reaction plate, as opposed

to at least two inverters with other schemes. Also, a very short headway can be achieved when there are multiple conveyances.

If a relatively long reaction plate is used, such as for ropeless hoisting, it is usually preferable to only energise the stator sections that are fully covered by the reaction plate so that the inductance and induced back-emf are the same for all of the active sections fed in parallel. The compromise, however, is that only a portion of the reaction plate's length is utilised at any time. Formulae for the reaction plate utilisation and stator feeding efficiency are also contributed.

In order to explore suitable feeding and control approaches, it was necessary to devise a suitably complex, generalised, dynamic model of a segmented-stator PM LSM. Initially, it was assumed that a space-vector modelling approach would be unable to cater for a discontinuous stator and so a magnetic equivalent circuit (MEC) approach was pursued. Subsequently, though, it was found that a space-vector model with precomputed tables of parameters relating to the reaction plate's relative position is sufficient for the design and validation of the control method. However, in attempting to address the shortcomings of a pure MEC formulation, a hybrid MEC and FEM approach for dynamic simulation evolved that is included as a separate contribution.

The presented hybrid method uses a magnetic equivalent circuit formulation in the highly-permeable regions of the problem space and then accounts for flux flowing from those boundaries into surrounding constant-permeability regions by the superposition of a plurality of representative magneto-motive force (mmf) sources. This approach capitalises on the computational efficiency of a lumped-parameter MEC formulation where the flux is well-channelled. Crucially, the required mutual permeances and boundary flux components due to the magnetic sources are only dependent on the geometry of the problem and can be calculated upfront. Although ultimately these upfront parameter sets were obtained using FEM, the initial approach of calculating these values using Schwarz-Christoffel conformal mapping process is also documented, since it makes a contribution as a means of using rectified maps of non-trivial geometries for the calculation of magnetic reluctances.

In summary, this thesis primarily contributes:

- An efficient, hybrid magnetic equivalent circuit and finite-element modelling approach for the dynamic simulation of simple electromagnetic systems.
- A generic space-vector dynamic model of a segmented long-stator permanent magnet linear synchronous motor.
- A novel feeding and control strategy for segmented long-stator linear synchronous motors.
- Verification of the proposed control strategy with a purpose-built laboratory prototype.

1.4 Publications

- C.R. Lines, W.A. Cronjé, and B. Wigdorowitz, "Extended 2D magnetic equivalent circuit method," COMPEL: The International Journal for Computation and Mathematics in Electrical and Electronic Engineering, vol. 29, 2010, pp. 1435 - 1443. [39]
- C. Lines, R. Cruise, B. Wigdorowitz, and C. Pritchard, "Suitability of various force control techniques for a modular-stator linear synchronous motor," in proceedings of the *Fifth International Symposium on Linear Drives for Industry Applications (LDIA)*, Kobe-Awaji, Japan, 2005. [11]
- C.R. Lines, W.A. Cronjé, and B. Wigdorowitz, "Extended magnetic equivalent circuit method that accounts for leakage flux using Schwarz-Christoffel mapping and the separation of mmf sources," in proceedings of the *Eighth International Symposium on Electric and Magnetic Fields (EMF)*, Mondovì, Italy, 2009. [40]

1.5 Mathematical notation

A comprehensive list of all physical quantities, labels/indices, symbols and operators is included in the List of Symbols. Care was taken to devise a mathematical notation that could be used consistently throughout this work. Each variable is denoted by an italic, case-sensitive symbol (both Latin and Greek alphabets) uniquely corresponding

to the physical quantity that it represents (F for force, Φ for magnetic flux, etc.), together with subscript label(s) that identify it unambiguously. Subscript labels that are longer than a single letter are enclosed in brackets to avoid confusion (e.g. $F_{(\mathrm{em})}$ for electromagnetic force but F_{fr} for the reaction plate friction force). The labels also act as index arrays for multi-dimensional arrays or matrices, in which case each index is typeset with an under-tilde. The number of dimensions of a non-scalar variable is therefore equal to how many indices it has. To reference a specific item or range of items within an array or matrix, second-level subscripts are used on the indices. Brackets following variables are used to explicitly declare dependency on other variables (e.g. $x_{\mathrm{r}}(t)$ denotes the reaction plate position as a function of time). Vector fields are denoted with an over-arrow and direction unit vectors with a caret/hat symbol. All non-scalar variables are typeset in bold where possible.

To facilitate mathematical matrix operations on higher-dimensional arrays, a "flattening" operator '$:$' is defined to reduce dimensionality, as necessary. The operator denotes that entries in the dimension(s) following it are to be incorporated into the dimension preceding it. For example, $\boldsymbol{M}_{\underset{\sim}{\mathrm{a}}_{1:5}\underset{\sim}{\mathrm{b}}_{1:3}}$ is a 5×3 matrix but $\boldsymbol{M}_{\underset{\sim}{\mathrm{a}}_{1:5}:\underset{\sim}{\mathrm{b}}_{1:3}}$ is a 15×1 column vector with the three columns of $\boldsymbol{M}_{\underset{\sim}{\mathrm{a}}_{1:5}\underset{\sim}{\mathrm{b}}_{1:3}}$ stacked beneath each other, in order. Likewise, $\boldsymbol{M}_{\underset{\sim}{\mathrm{a}}\underset{\sim}{\mathrm{b}}:\underset{\sim}{\mathrm{c}}}$ is a 2-dimensional matrix with each of the c layers stacked in the column dimension and $\boldsymbol{M}_{\underset{\sim}{\mathrm{a}}:\underset{\sim}{\mathrm{b}}\underset{\sim}{\mathrm{c}}}$ is a 1-dimensional column vector with all of the columns of $\boldsymbol{M}_{\underset{\sim}{\mathrm{a}}\underset{\sim}{\mathrm{b}}:\underset{\sim}{\mathrm{c}}}$ stacked beneath each other. This is illustrated in (1.1) and (1.2).

$$\boldsymbol{M}_{\underset{\sim}{\mathrm{a}}\underset{\sim}{\mathrm{b}}:\underset{\sim}{\mathrm{c}}} = \begin{bmatrix} M_{\underset{\sim}{\mathrm{a}}_1\underset{\sim}{\mathrm{b}}_1\underset{\sim}{\mathrm{c}}_1} M_{\underset{\sim}{\mathrm{a}}_1\underset{\sim}{\mathrm{b}}_2\underset{\sim}{\mathrm{c}}_1} M_{\underset{\sim}{\mathrm{a}}_1\underset{\sim}{\mathrm{b}}_1\underset{\sim}{\mathrm{c}}_2} M_{\underset{\sim}{\mathrm{a}}_1\underset{\sim}{\mathrm{b}}_2\underset{\sim}{\mathrm{c}}_2} \\ M_{\underset{\sim}{\mathrm{a}}_2\underset{\sim}{\mathrm{b}}_1\underset{\sim}{\mathrm{c}}_1} M_{\underset{\sim}{\mathrm{a}}_2\underset{\sim}{\mathrm{b}}_2\underset{\sim}{\mathrm{c}}_1} M_{\underset{\sim}{\mathrm{a}}_2\underset{\sim}{\mathrm{b}}_1\underset{\sim}{\mathrm{c}}_2} M_{\underset{\sim}{\mathrm{a}}_2\underset{\sim}{\mathrm{b}}_2\underset{\sim}{\mathrm{c}}_2} \end{bmatrix} \tag{1.1}$$

$$\boldsymbol{M}_{\underset{\sim}{\mathrm{a}}:\underset{\sim}{\mathrm{b}}\underset{\sim}{\mathrm{c}}} = \begin{bmatrix} M_{\underset{\sim}{\mathrm{a}}_1\underset{\sim}{\mathrm{b}}_1\underset{\sim}{\mathrm{c}}_1} M_{\underset{\sim}{\mathrm{a}}_2\underset{\sim}{\mathrm{b}}_1\underset{\sim}{\mathrm{c}}_1} M_{\underset{\sim}{\mathrm{a}}_1\underset{\sim}{\mathrm{b}}_2\underset{\sim}{\mathrm{c}}_1} M_{\underset{\sim}{\mathrm{a}}_2\underset{\sim}{\mathrm{b}}_2\underset{\sim}{\mathrm{c}}_1} M_{\underset{\sim}{\mathrm{a}}_1\underset{\sim}{\mathrm{b}}_1\underset{\sim}{\mathrm{c}}_2} M_{\underset{\sim}{\mathrm{a}}_2\underset{\sim}{\mathrm{b}}_1\underset{\sim}{\mathrm{c}}_2} M_{\underset{\sim}{\mathrm{a}}_1\underset{\sim}{\mathrm{b}}_2\underset{\sim}{\mathrm{c}}_2} M_{\underset{\sim}{\mathrm{a}}_2\underset{\sim}{\mathrm{b}}_2\underset{\sim}{\mathrm{c}}_2} \end{bmatrix}^{\mathrm{T}} \tag{1.2}$$

Where typesetting capability is limited, such as for MATLAB® functions and Simulink® block diagrams, Greek letters are spelled out, calligraphic letters are prefixed with 'cal' and direction vectors are prefixed with 'hat'. Furthermore, each subscript label/index is individually designated using an underscore (thus brackets are not needed for subscript labels consisting of several letters). A double underscore is used to denote the "flatten" operator '$:$'.

1.6 Thesis outline

Chapter 2 *Background*—an overview of the state-of-the-art in the modelling of electromagnetic systems, the control of permanent-magnet synchronous motors and feeding strategies for segmented long-stator linear synchronous motors.

Chapter 3 *Hybrid magnetic-equivalent-circuit and finite element method*—formulation of a 2D extended magnetic-equivalent-circuit approach for the dynamic simulation of a class of electromagnetic systems.

Chapter 4 *Motor dynamic model*—derivation of a generic space-vector dynamic simulation model for segmented long-stator linear synchronous motors.

Chapter 5 *Control strategy*—description of a novel feeding and control strategy for segmented long-stator linear motors.

Chapter 6 *Laboratory prototype*—validation of the feeding and control strategy with a laboratory prototype system.

Chapter 7 *Conclusion*—summary of the outcomes and identification of scope for future research.

Appendix A *Hybrid magnetic-equivalent-circuit and finite element method*—implementation of the magnetic modelling approach as MATLAB® functions, detailed implementation and full solutions for the worked example and examples of how to use a Schwarz-Christoffel conformal mapping approach to obtain mutual permeances and source boundary fluxes.

Appendix B *Motor dynamic model*—detailed space-vector mathematical derivations and implementation of the model in MATLAB® and Simulink®.

Appendix C *Prototype construction*—details of the construction of the motor, custom circuitry and associated control and measurement systems.

Appendix D *Prototype characterisation and modelling*—mathematical modelling of the prototype system's components and the determination of the appropriate parameters for simulation and control design.

Appendix E *Prototype controller*—design and implementation of the controller.

Chapter 2

Background

This chapter provides an overview of the literature that was researched in depth and provides a background to the modelling of electromagnetic systems, the control of permanent-magnet synchronous motors and feeding strategies for segmented long-stator linear synchronous motors.

2.1 Mathematical modelling of electromagnetic systems

2.1.1 Magnetic Equivalent Circuit approach

The basis for a magnetic equivalent circuit (MEC) formulation is that regions containing a quasi-stationary magnetic field (changing slowly enough to not exhibit wave phenomena) may be partitioned into 'flux tubes' [41, 42]. These flux tubes are geometric constructs in which all lines of magnetic flux are perpendicular to their bases and no lines of flux cut their sides. The magnetic scalar potential difference along a flux tube is equal to its magneto-motive force (mmf) and the flux tubes are arranged to form a closed magnetic circuit.

Also referred to as Permeance Network Models or Reluctance Network Models, magnetic equivalent circuits yield good accuracy for a very coarse meshing of the problem space and their solution requires little computing effort [43]. Traditional electrical circuit solution methods such as nodal or loop current analysis are directly applicable to MECs, where permeance is the inverse of reluctance like conductance is the inverse of resistance for electric circuits [41, 44].

When applied to the modelling of electric machines, the air-gap is represented with a network of reluctances/permeances linking the stator teeth to the rotor. These elements are functions of the relative position of the rotor to the stator [45, 46]. Ostović [41] uses an element to connect every stator tooth to every part of the rotor, whereas Perho [47] and Bekkouche et al. [48] only connect adjacent parts of the stator and rotor. Even so, bidirectional elements are used in the teeth (allowing flux to flow in the radial and tangential directions), resulting in a similar level of overall complexity. Rasmussen and Ritchie [49] propose an improved tooth top model that provides for pole-tip leakage flux, comprising two adjacent bidirectional flux tube elements. However, the method of refining the air-gap mesh proposed by Perho [47] is superior since the flux components flowing to the surrounding regions are unchanged with each successive refinement.

Calculating reluctances/permeances

For a rectangular flux tube, it is trivial to calculate the permeance per unit depth, since it equals the ratio of width to length of the element multiplied by the permeability of the medium [41]. It is more challenging, though, to represent complex geometries or regions where the flux is not uniformly channelled. For an air-gap, where fringing of the flux occurs, the cross-sectional area of the tube is typically increased as a function of the air-gap length as an empirical means to account for this [44, 50]. Also, for non-rectangular regions, 'effective' lengths and cross-sectional areas are often empirically approximated [50]. An accurate way to represent the actual geometry is to mathematically transform the region to an equivalent rectangular region.

The Schwarz-Christoffel transformation is a suitable conformal mapping. For example, Cividjian et al. [51, 52] use this approach to calculate constriction and corner permeances for 2D finite domains and Balakrishnan et al. [53] and Marković et al. [54] use it to devise formulae for tooth-to-tooth permeance across an air-gap. Also, Krop et al. [55] show how the transformation can be used to simplify the solution of Poisson's Equation within a motor's air-gap under the assumption that the back-iron and stator core are infinitely permeable and Marković et al. [56] use it to optimise for the lowest attainable cogging force when designing brushless-DC motors.

The Schwarz-Christoffel toolbox for MATLAB® by Driscoll [57] is freely available and can calculate the requisite rectified maps. This toolbox also incorporates the CRDT algorithm (developed by Driscoll and Vavasis) which avoids a type of numerical ill-

conditioning referred to as the "crowding phenomenon" [58]. This greatly extends the technique's usefulness as it allows for the stable and fast solution of polygons with, in principle, arbitrary elongations (e.g. 'T' or 'E' shapes) and not only singly-elongated regions (e.g. 'L' or 'Z' shapes).

2.1.2 Finite Element Method

The Finite Element Method (FEM) is well-documented and has become the standard numerical tool for electromagnetic field analysis because it is able to solve for the field within complex geometrical structures with non-trivial materials exhibiting nonlinear or even hysteretic characteristics. Also, from a numerical solution perspective, FEM yields a system of linear equations with sparse matrices that can be solved efficiently [59]. In contrast to the Finite Difference Method, where the governing partial differential equation is directly approximated with finite differences over a grid, with FEM the solution of an equivalent 'weak' or 'variational' form of the boundary value problem is approximated [60]. The basis functions chosen for the finite element formulation can either be node-based or edge-based [61, 62].

The FEMM software package by Meeker [63] uses first-order triangle elements that are derived using a variational formulation based on energy minimisation rather than a method of weighted residuals [64].

Demenko and Sykulski [65] demonstrate the equivalence between finite element formulations and reluctance/permeance network representations. They show that the description of a magnetic field with nodal finite elements with scalar potentials can be considered equivalent to nodal analysis in circuit theory and that formulations with edge elements, involving vector potentials, are equivalent to circuit loop analysis [65, 66]. This intrinsic link between field descriptions and network equivalent representations is expected because they are merely different discretisations of Maxwell's Equations. On one hand, magnetic equivalent circuits provide useful physical insight and rely on well-understood analogies to Kirchhoff's and Ohm's Laws for electric circuits and are thus generally considered by engineers to be simpler and more intuitive than finite element formulations [65]. However, finite element formulations are generally solved with a much finer mesh over the problem space and therefore yield solutions that are more accurate but take longer to compute.

2.1.3 Boundary Element Method

The Boundary Element Method (BEM), also known as the Boundary Integral Equation Method or Method of Moments, is an integral formulation of Maxwell's Equations as opposed to the usual differential formulation and thus requires only surface discretisation rather than volume discretisation for numerical solution [67, 68]. Like other integral approaches, Boundary Element Method (BEM) has characteristics that are generally complementary to FEM. For example, open boundary problems pose no difficulty with BEM but the method can only be applied to domains where Green's Functions can be calculated, necessitating linear homogeneous media [67, 69]. There are means of including nonlinearities in the formulation, although these approaches generally introduce volume integrals which, in turn, require volume discretisation of the ferromagnetic regions anyway. The dual-reciprocity method for nonlinear media is a useful technique that avoids volume discretisation but yields a very large system of equations that is memory intensive to solve [70]. This prompted Lobry [70] to propose a recurrent formulation of Poisson's equation, where the change in material property between the domains is modelled as a single layer along the interfaces so that the non-homogeneity appears rather as a source term. The underlying principle is that of the transmission-line modelling method, where the nonlinear elements are separated from the rest of the network by substituting the changes in material properties with fictitious excitations.

With regard to its numerical solution, a BEM formulation typically yields full matrices, which means that the required memory and computation time scale as the square of the problem size, as opposed to FEM where the resulting matrices are typically sparse and so the required memory and computation time tend to scale linearly with the mesh size. The complementarity between BEM and FEM has resulted in the formulation of many hybrid methods for solving practical problems [71]. In particular, Bill [72] present a hybrid method for computing the field of an induction motor.

2.1.4 Finite Integration Technique

The Finite Integration Technique (FIT), developed by Weiland in 1977, is a discrete reformulation of Maxwell's Equations in integral form suitable for numerical solution [73, 74]. As described in detail by Clemens and Weiland [73], FIT is a

volume-discretisation scheme that uses integral balances and thus allows stability and conservation properties of the discrete fields to be proven without numerical calculation and spurious modes can be naturally avoided when solving.

Over a bounded domain, a computational grid is formed using simple cells (e.g. tetra- or hexahedra shaped) under the premise that all cells fit exactly to each other. All of the cell edges and facets have an associated direction and applying Faraday's Law in integral form to each discrete cell volume yields a set of ordinary differential equations, relating the edge voltages to the magnetic flux through each face. It is important to note that this is an exact expression for the relationship of the surface quantities of the cell [73]. Applied over the whole domain, this yields a matrix equation with a discrete curl operator over the grid. Secondly, formulating that the sum of surface fluxes must be zero for each cell, gives an expression with a discrete divergence matrix that also only depends on the grid topology. Discretising the last two of Maxwell's Equations, requires a second cell complex to be defined that is the dual of the primal cell complex (constituting a grid doublet) [75]. In Cartesian space, the primal cell foci form the grid for the dual cell complex. In this dual cell complex, edge magneto-motive forces (mmfs) are expressed in terms of the surface dielectric fluxes and electric currents, which is a discretisation of Ampere's Law (analogous to Faraday's Law for the primal cell complex). Lastly, Gauss' Law in integral form is applied to the dual cell grid to complete the set of discrete Maxwell Grid Equations. Since these equations are exact and contain only topological information, discretisation error is only introduced with the discrete constitutive material equations that couple the integral voltage and flux state-variables on the two cell complexes [73, 74].

Demenko et al. [76] show how the resulting FIT equations can, in fact, be considered a special case of the FEM formulation and explain the equivalence of the two methods using circuit theory terminology. This insight motivates a way to reduce FEM formulated equations and benefit from the computational advantages of the diagonalisation of the FIT matrix [76].

2.1.5 Magnetic Cell Method

The Cell Method, proposed by Tonti [77], is a volume-discretisation approach based on an algebraic formulation of the electromagnetic field and thus has a close affinity with the Finite Integration Technique. The formulation is based on the systematic

use of global variables rather than field functions, a distinction between 'source', 'configuration' and 'energy' variables, the use of space-time elements endowed with inner and outer orientations and the use of two cell complexes - a primal one endowed with inner orientation and a dual one endowed with outer orientation [77].

Tonti [77] argues that physical measurements deal mainly with global/integral variables such as voltages, fluxes and currents, not field vectors, and so global variables, which are domain functions, are the natural tool for a direct algebraic finite formulation. This is in contrast to field functions that are linked to points and time instants.

Source variables are defined to be those variables that cause the electromagnet field to exist (e.g. currents), whereas configuration variables are those that describe the configuration of the field and its potentials (e.g. flux density). The configuration variables are linked to the source variables by constitutive equations and the energy variables are all products of one source variable and one configuration variable.

As with FIT, cell complexes (orientated vertices, edges, faces/facets and volumes) rather than coordinate systems are used for the finite formulation of space-time elements. It is useful that when the configuration quantities are defined on the primal cell complex with vertices, edges, faces and volumes endowed with inner orientation, the corresponding domains in the dual cell are all endowed with outer orientation. The source variables are associated with the dual cell complex. The dual relationship implies that each primal cell volume is related to a dual node, whereas each primal face is related to a dual edge [78]. The solution is calculated such that there is no nett current flowing on closed surfaces (Kirchhoff's Current Law) and that Faraday's Law is satisfied for the set of fundamental closed loops [78].

2.1.6 Surface Current Method

As noted by Arehpanahi and Milimonfared [79], the Surface Current Method was introduced in the 1970s by Klepka from the USSR and was originally referred to as the 'Secondary Source Method'. The concept of this method is to replace magnetic discontinuity (boundaries between materials of differing permeability) with uniform surface current sheets in a homogeneous region, such that the magnetic flux distribution is unchanged. Then, because the resulting space is homogeneous, the

Biot-Savart Law can be applied to solve for the magnetic flux density due to each current sheet [80–82].

The point coordinates and vector quantities are represented in the complex plane and transformed from each segment's local reference frame to the global reference frame using reference frame translations and rotations. Conveniently, the shape functions, which dictate the i^{th} segment's flux density due to the j^{th} segment, depend only on the boundary geometry and thus the values can be stored for subsequent calculations of the field for any configuration of the sources.

The total flux density at any point in the domain is found by summing up the contributions from the surface currents and the magnetic sources. Although originally formulated for domains with materials exhibiting constant permeabilities, Andriollo et al. [80] describe an iterative approach to cater for saturating materials with nonlinear B-H curves. Andriollo et al. [80] also described an automated contour refinement process to choose an appropriate subdivision of the boundaries into segments, based on local errors with respect to metrics of the solution accuracy over the whole domain.

Berlec [83] extends the method to solve 3D problems and highlights that the main advantages of the method are that the calculation of the magnetic field density does not involve any potentials and, since there is no need to know boundary conditions, open boundary problems are naturally accommodated.

The Surface Current Method is applied to the analysis of rotating magnetic devices by Arehpanahi and Milimonfared [79], who show that an advantage of using the method for dynamic simulation is that no re-meshing is required as the geometry changes with movement. Furthermore, they formulate a method of coupling electric circuit models to the magnetic circuit formulation [82].

2.2 Control of permanent magnet synchronous motors

2.2.1 Scalar control

Scalar control is a primitive open-loop means of achieving variable speed control of an electric motor. The motor drive acts as a variable-frequency, variable-magnitude

three-phase voltage supply (typically using a pulse-width modulation scheme) [84–86]. For induction motors, a set ratio of voltage to frequency is usually maintained, except for when operating at lower frequencies where the supply voltage is often boosted to compensate for the voltage drop across the winding resistance. This keeps the magnitude of the air-gap flux reasonably constant. When applied to a synchronous motor, however, the rotor speed must match the speed of the travelling air-gap mmf wave for torque to be produced. Within a pole-pair, the rotor will "slip" until the load angle is large enough for the electromagnetic torque to sustain the required rotor speed. However, if at any point the maximum electromagnetic torque is insufficient to keep the rotor synchronised with the travelling mmf wave, the motor will stall. For example, when running a synchronous motor up from standstill using scalar control, care must be taken to increase the supply frequency slowly enough so that the motor maintains synchronism. If done too quickly, the required acceleration force can be too high.

This simple power supply technique is also not efficient for synchronous motors because only a component of the current flowing in the windings contributes to the torque (the component of mmf in space-quadrature with the rotor flux). To achieve maximum torque/force per current, the load angle must be maintained at 90° (assuming no saliency).

An advantage, though, of using a scalar control approach is that the waveforms are effectively sinusoidal and so filters can be used extensively to suppress time harmonics and therefore minimise both conducted and radiated electromagnetic interference. Also, it is cost effective strategy for a linear motor propulsion system with several movers because a single motor drive can be used for multiple movers, as the supply is not being adjusted to control for the load angle of any one particular reaction plate. However, ancillary measures must be implemented to cater for a loss in synchronism for any of the movers.

2.2.2 Vector control

In contrast to scalar control, 'vector control' refers to controlling the magnitude and phase of the stator currents so that spatial orientation of the stator mmf and rotor flux is achieved in the air-gap [84, 86, 87]. This is conceptually similar to the behaviour of a dc motor, where the torque and flux are decoupled and can be

controlled independently [85]. For a PM synchronous motor, the orientation of the spatial air-gap flux wave produced by the permanent magnets is directly dictated by the rotor's shaft position [88]. Thus, to control the orientation of the stator mmf relative to this rotor flux, the rotor's position mostly needs to be measured or estimated. Vector control without an independent measurement of the rotor position is referred to as 'sensorless' control.

Field-Orientated Control

The term Field-Orientated Control (FOC) applies when the stator current is directly controlled to be in space-quadrature with the magnetic flux produced by the rotor (making use of a common rotating reference frame). For a synchronous motor, the reference frame is attached to the rotor and termed the 'd/q reference frame' [84–86]. The direct (d) axis is aligned with the rotor flux and the quadrature (q) axis is in space-quadrature (displaced by 90°). If the motor does not have significant saliency and so there is no reluctance force component, the propulsion force is directly proportional to the amount of quadrature current [88]. Correspondingly, the d-axis current is the flux linkage component. For a PM synchronous machine, the flux is produced by the permanent magnets and so the d-axis current is kept at zero. The d-axis and q-axis currents are regulated using feedback control loops and FOC relies on an accurate measurement or estimate of the rotor position for the Clarke and Park transformations that are used to convert between three-phase and d/q quantities. A pulse-width modulated (PWM) scheme is typically used to generate the appropriate voltage vector at each instant. With a hysteresis current controller, the current for each phase is independently controlled to be within a band surrounding the desired current reference by actuating the corresponding "leg" of a three-phase inverter to either increase or decrease the current for that particular phase [88]. A space-vector modulation (SVM) scheme may also be used to effect the desired voltage vector at each time instant by switching at a fixed rate between several discrete voltage vectors in the appropriate proportions (including zero voltage states) to effect the desired magnitude and angle in the stator reference frame [89]. The discrete voltage vectors used are a function of the inverter topology—for a three-phase voltage source inverter, there are six non-zero voltage vectors and two zero voltage vectors that can be applied to the motor terminals [89].

For sensorless operation, rotor speed and position estimation techniques can be

broadly categorised as back-emf based, observer or stochastic filtering based, model reference adaptive based or saliency based [90–94]. For back-emf based methods, the stator flux linkage waveform is estimated by integrating the back-emf. Thus, these estimators are sensitive to drift and fail for low speeds or at standstill when the back-emf is low or zero [95]. Secondly, with observer theory, an augmented state-space model of the motor is used to provide an estimate of the speed and position [92, 96]. Stochastic filtering methods such as Kalman or Extended Kalman Filtering are also popular [92]. Thirdly, model reference adaptive techniques estimate the speed by forcing the error between two motor models to zero—a speed dependent model and a speed independent model [93, 97]. Lastly, the saliency-based techniques mostly use high-frequency signal injection to detect a position-dependent incremental inductance [91, 92, 98–100]. Evidently, these saliency-based methods only work for motors exhibiting sufficient magnetic anisotropy (difference in d-axis and q-axis inductance) over the full range of operating conditions [101]. They also tend to struggle with ambiguity in the sensed position because the inductance variation usually repeats twice over a single pole pitch. However, this is typically addressed by considering the effect of magnetic saturation on the incremental inductance [91]. In fact, Schmidt et al. [95] and Linke et al. [102] present initial rotor angle detection techniques for non-salient PM motors that exclusively use the effect of localised magnetic saturation in the stator. Alternatively, Acarnley and Watson [91] cite various suggested rotor modifications to increase the variation in inductance with position. With a carefully designed injection sequence, such as that which results from the method proposed by Paulus et al. [100], saliency-based position sensing produces low audible noise and need not require motor parameter information.

When FOC is applied to linear synchronous motors, the d/q reference frame is simply attached to the reaction plate's linear position rather than the rotor's angular position for a rotating machine [103].

Direct Torque Control

In contrast to traditional Field-Orientated Control, Direct Torque Control (DTC) controls the stator flux linkage and motor torque directly (i.e. not via controlling transformed stator currents) [88, 89, 104]. Also, the control of the inverter is performed at the same time level as the torque control and so there is no need for a separate modulator. Thus, the inverter's state is only changed when necessary (based

on the electromagnetic state of the motor at each time step). DTC, however, relies on an accurate estimation of the flux linkage and torque in order to perform the hysteresis control of these two variables using an optimum switching table. At each sample time, the inverter switching state is chosen to best reduce the instantaneous flux and torque errors [104]. Typically, the flux comparator is a 2-level comparator and the torque comparator is a 3-level comparator. Depending on how the switching sectors are selected, two different schemes are possible—Takahashi and Noguchi proposed a circular stator flux vector path and Depenbrock proposed a hexagonal stator flux vector path [104]. Generally, a fixed flux linkage magnitude is used. However, a varying flux linkage reference is suggested by Faiz and Mohseni-Zonoozi [105] as a way to achieve 'maximum torque per flux'.

The flux linkage is estimated by integrating the electromotive force (emf) in vector space and adding the result to the initial flux linkage, which is a function of the initial relative positions of the stator and rotor poles [104]. Since this estimation is an integral estimation, a suitable stabilisation algorithm is often required[106]. The second control variable, the torque, is then estimated using the components of the estimated flux linkage and a measurement of the currents in the stationary stator reference frame [104]. Significantly, DTC relies on only a good estimate of the initial flux linkage and a single motor parameter—the stator resistance [104, 107]. Also, because no reference frame transformations are used, there is no dependence on the rotor position. Hence, DTC is an inherently sensorless motor control method.

To start reliably under sensorless DTC (i.e. for the drive to be able to determine the initial flux linkage), the motor must have sufficient saliency and some degree of magnetic saturation in the direct axis [106]. The saliency-based estimation schemes outlined in the previous section are applicable for detecting this initial rotor position.

In general, compared to FOC, DTC has excellent dynamic torque response yet is prone to higher torque ripple [88, 104]. This torque ripple can be reduced by increasing the number of inverter switching states [108]. Also, the motor's winding inductance should be high enough relative to its winding resistance and the controller's sampling period [104]. Alternatively, to lower the torque ripple and have a more consistent switching frequency, Tang et al. [107] and Rafa et al. [109] propose replacing the hysteresis controller with PI linear controllers and using a SVM scheme. Conversely, Vaez-Zadeh and Jalali [87] use traditional FOC feedback loops on the direct and

quadrature currents but use a DTC style voltage vector switching table based on a comparison between the measured and desired d/q currents.

Jiefan et al. [12], Cui et al. [110, 111], Faiz et al. [112] and Lirong et al. [113] present versions of DTC adapted for linear motors. Although end effects are accounted for, these methods do not apply to a segmented stator with a reaction plate moving from one section to the next.

2.3 Feeding of segmented long-stator linear motors

A short-stator linear motor system uses active vehicles/conveyances, where the power supply is controlled on-board each vehicle [114]. Thus, there is an inverter and control unit per vehicle. This can be a cost effective option for a long track with very different force requirements along the length of travel because some sections of the track can have permanent magnets for synchronous operation and other sections, with a lower force requirement, can just use an induction rail [114]. However, with all short-stator motor arrangements, the energy must either be stored on-board (in batteries) or transferred to the vehicle. Power transfer can either be with a sliding contact (like a pantograph) or by a contact-less means such as inductive coupling [114]. Owing to the inefficiency and cost of providing power to the vehicles, this arrangement is best suited to systems with few vehicles and low force requirements. Moreover, the controller on-board the vehicle needs to communicate with a high-level controller to receive command signals and return status information.

In contrast to a short-stator configuration, a long-stator linear motor has passive movers. For example, a long-stator PM LSM uses a reaction plate (comprising an array of permanent magnets) that is attached to the vehicle and power is supplied only to the stationary stator. In order to have independent control over the motion of several vehicles and for efficient energising of the stator, the stator must be segmented into sections that can be fed independently [20, 114, 115]. Each stator section can be fed with a dedicated inverter [2, 116] or a multiplexing scheme can be used to lower the number of inverters required. Large maglev train systems typically use mechanical vacuum switches [117, 118] but solid-state contactors are preferable for lower power systems and where a higher number of switching cycles is required (e.g. with shorter sections). However, care must be taken when using solid-state contactors with blocking triacs or antiparallel thyristors because they need to withstand the

high $\frac{dV}{dt}$ from the inverters [20, 114]. Snubber circuitry can be used to counter this but additional stress on the inverter insulated-gate bipolar transistors (IGBTs) must be considered [119].

Even if an inverter is dedicated to each stator section, only one controller is needed per vehicle. Furthermore, these controllers would typically be implemented on a single computing device. Thus, both Benavides and Mutschler [116] and Mutschler [114] use an inverter signal bus between the controller(s) and the inverters. However, the bandwidth of the inverter bus limits the total number of vehicles and stator sections. Alternatively, for very low power applications such as lightweight material handling, Intelligent Power Modules (IPMs) can be used to drive sections that require less than about 3 kVA with shunt resistors to measure the currents [20, 114, 120].

The Neue Bahntechnik Paderborn (NBP) project at the University of Paderborn uses a doubly-fed long-stator linear motor arrangement [121]. This configuration is conceptually a hybrid between a short-stator and a long-stator motor, as both the stator and mover have three-phase windings. It is therefore possible to operate the vehicles in synchronous or asynchronous mode [121]. This implies that the relative positions of two vehicles can be controlled even though they share a common stator. On-board energy storage is required since power is only transferred to the vehicles via the linear motor when it is operating in asynchronous generator mode [121].

2.3.1 Stator sections longer than the reaction plate

As an example of a system where the stator sections are considerably longer than the vehicle is the Transrapid maglev train, where the section lengths are in the order one or two kilometres [117, 118]. Many of these stator sections collectively constitute a track segment that extends for many kilometres. Each of these long segments is typically supplied from both ends with large substations and normally only a single vehicle may occupy one of these segments at a time [122]. Engel and Nothhaft [123] do, however, describe an improved strategy whereby the segments overlap at stations and the vehicle is handed over from one segment to the other when stationary. Fischperer [124] also claims further improvements to this scheme with multiplexing of the substations so that a variable headway between vehicles can be accommodated and further reduced. Notwithstanding, only a single vehicle occupies each shorter stator section at once and only those sections that are occupied are connected to

the power supply [125]. Hellinger et al. [117] and Henning et al. [118] describe the two strategies usually employed for this shorter section switching, both of which rely on having a left-hand and a right-hand stator track whose section boundaries are staggered. (The vehicle never crosses a section boundary on both track sides simultaneously.) For the 'step-by-step' or 'two-step' method, the vehicle experiences a significant thrust disturbance when crossing each section boundary that cannot be fully compensated for by the other side of the track. This is because the current must be reduced to zero when switching an inverter from feeding the one section to feeding the next. For improved performance but with added cost, the 'three-step' method uses an extra inverter and feeding cable so that two adjacent stator sections are always fed from different inverters for smooth section crossing [126]. For the Yamanashi maglev system, which also uses two interlaced side-by-side segmented stators, Shigeeda et al. [127] propose a variable section length duplex strategy as an alternative to the original triplex arrangement [128]. However, this approach requires the switchgear to interrupt non-zero currents.

In contrast, Zhang et al. [129] propose a non-interlaced section arrangement for maglev vehicles. By using a staggered arrangement of switches between the stator winding and inverter, and switches that can form star-connected neutral points in the winding, the length of energised stator is made to follow the vehicle by simultaneously switching over these sets of switches in succession. Thus, the feed and neutral points of the winding are moved at the same time and the length of energised stator remains constant. Onuki et al. [130] effectively propose the same technique for a small scale linear induction motor. In fact, they shift the energised length of stator on a pole-by-pole basis, with only single energised pole-pairs at each end that are not covered by the secondary. When switching over, the number of energised poles is briefly decreased by one but the resulting force disturbance is found to be insignificant [130].

Although the optimal stator section/block length is highly dependent on the application, Perreault [21] show that, for a people carrier application, throughput and efficiency taper off gently with an increase in block length yet the required inverter capacity (and thus cost) per unit length decreases dramatically. Thus, the suggestion is that blocks similar in length to the vehicle length be used in and around stations to improve throughput and efficiency but that, from a cost and maintenance perspective, blocks several vehicle lengths long are used for the cruising regions where the stopping distance governs the vehicle spacing [21].

With a FOC motor drive strategy, the stator currents in the two adjacent stator sections must be synchronised as the mover crosses their boundary [21, 115, 116]. A 'master' and 'slave' arrangement with a successive handover procedure is appropriate [131]. Patterson et al. [16] describe this hierarchical modular control approach for an aircraft launching system with two inverters. Each inverter is multiplexed and can power alternate sections of the stator [17, 114, 132]. Patel et al. [120] motivate that this two-stage approach, with a power stage (the two inverters) and local section switches, is best for redundancy. For the aircraft launching system, the sections increase in length along the track, corresponding to the increasing speed of the shuttle, and the active section(s) are determined by a top-level controller based on the shuttle position. FOC is performed for each section to cause constant acceleration or deceleration of the shuttle using its relative position [17, 133]. A similar strategy for an electromagnetic launcher is presented by Li-Yi et al. [22].

When using FOC to synchronise the current for two adjacent sections when crossing boundaries, Benavides and Mutschler [134, 135] additionally propose using feed-forward compensation to reduce force disturbances. The required compensation as a function of reaction plate position can be precomputed with FEM to minimise disturbances caused by a reduction in mmf at the stator section ends (where a double-layer winding typically goes to a single layer winding for modularity) and the sudden increase in back-emf in the previously unoccupied section. Similarly, Perreault [131] proposes using feed-forward compensation that is calculated analytically to compensate for when the back-emf for a particular section changes as its coverage by the reaction plate changes. Furthermore, in the case of there being short gaps in the stator, for fire doors or thermal expansion joints, etc., Perreault [21] suggests that the force command be scaled inversely by the fraction of the reaction plate that interacts with the stator.

Furthermore, Perreault [21] presents an interesting energy optimisation approach when crossing stator section boundaries. For the same magnitude of stator current, two adjacent sections have identical copper losses (I^2R). However, the section that is more covered by the reaction plate contributes more to the propulsion force. He shows that to minimise the total losses for a constant force the section with higher coverage should be driven harder than the other. The optimal case equates to when the power per unit thrust is equal for the energised sections [21].

As with FOC, separate inverters are required to drive each active section of a segmented long-stator LSM using DTC. However, DTC does not use the stator current as a control variable and hence there is no direct way of imposing the same current in adjacent stator sections while the reaction plate is crossing. Rather, as described by Yoshida et al. [18, 136], adjacent sections (each longer than the vehicle length) can be mathematically "connected in series" to form a virtual, longer section as a means of achieving smooth section crossing under sensorless control [18].

To achieve sensorless FOC control with a segmented stator, Leidhold and Mutschler [19, 137] present two approaches—evaluating magnetic saliencies using high frequency signal injection and, alternatively (at speed), a specialised back-emf observer for each active section.

2.3.2 Stator sections shorter than the reaction plate

With respect to superconducting maglev train systems, Fujie and Shibakawa [25] claim a propulsion method with stator sections that are shorter than the train. However, this is for open-loop scalar control, where those sections covered by train are each energised by a separate inverter. Also, in the extreme case, Gamble et al. [24] refer to a 'locally commutated' LSM where each stator pole is separately excited using power electronics. In a similar vain, Batelaan [23] describes an 'individual pole excitation linear motor' for a smaller scale transit system. Also, Kwak and Sul [10] and Jung et al. [9] use triacs to individually switch each stator coil of a linear synchronous motor with concentrated/modular windings.

Although Kim et al. [26], Seki et al. [138], Suzuki et al. [139, 140] propose a linear motor arrangement for material handling that may have stator sections that are shorter than the reaction plate, the discontinuous stator has physical gaps between the sections. The intermittent stator accelerates or decelerates the carriers at specific locations along its travel.

Chapter 3

Hybrid Magnetic-Equivalent-Circuit and Finite Element Method

This chapter presents a novel electromagnetic modelling approach that stemmed from efforts to mathematically model a segmented-stator LSM in detail. Although it ultimately proved unnecessary to apply this electromagnetic modelling method with regard to verifying the motor control strategy, it is presented as a contribution in its own right.

3.1 Methodology

The drawback of a classical MEC approach, such as proposed by Ostović [41], is that the air-gap flux is not accurately represented. This is because, in general, the path of the air-gap flux is not consistent for differing distributions of mmf, as is the case for the more permeable stator core or the reaction plate back-iron. Hence, it is not typically appropriate to imply that this air-gap flux flows through well-defined flux tubes. This shortcoming is addressed in the proposed method by restricting the MEC formulation to the highly-permeable regions and accounting for flux flowing from those boundaries into surrounding constant-permeability regions by the superposition of a plurality of representative magneto-motive force (mmf) sources. This approach capitalises on the computational efficiency of a lumped MEC formulation in the highly-permeable regions (where the flux is channelled reasonably uniformly). Furthermore, any magnetic nonlinearity due to saturation occurs within these more permeable regions and so this computational complexity is restricted to the magnetic equivalent circuits.

In a similar vein to the surface-current method [80], as described in section 2.1.6, the highly permeable regions (represented as interconnected flux tubes) are considered equivalent to infinitely-permeable (zero reluctance) regions with appropriate surface currents on their boundaries. The surface currents mimic their actual finite and, in the case of saturation, flux-dependent reluctances (nonlinear B-H curves). Thus, a pair of uniform surface current sheets represent the mmf drop of each reluctance-network branch. This insight corroborates the use of the superposition principle to determine the total flux through each exterior element boundary because the permeability of the air (and the sources such as permanent magnets and coils) is low and constant, and the flux tubes are effectively seen to have zero reluctance by each isolated component of flux. So, the normal component of flux flowing through a particular boundary is equal to the sum of all the flux components resulting from the plurality of mmf sources, where each flux component is the product of a specific mmf source and its corresponding 'mutual permeance' for that boundary. Contemporary permeance-network models derived from finite element formulations with edge elements, such as the method described by Demenko and Sykulski [65], also contain mutual permeances. In addition to the flux components due to the mmf drops for all of the reluctance branches, each magnetic source (coil or permanent magnet) also contributes flux that flows through the element boundaries. The important assumption is that the flux enters or leaves perpendicularly to each exterior element boundary (i.e. no tangential component). This proves to be a valid approximation so long as the relative permeability of the elements is significantly higher than their surroundings. The interface between the MEC formulation and the exterior flux thus occurs at the exterior element boundaries. In order to calculate the electromagnetic force on moving sources using Maxwell's Stress Tensor, the exterior source boundary fluxes as well as the tangential field intensities are also calculated by superposition. For analysis in two dimensions, it is assumed that the geometry extends sufficiently far into the page so that any end-effects (into or out of the page) are negligible and the resulting field quantities are per unit depth.

The mutual permeances and boundary flux components due to the magnetic sources are only dependent on the geometry of the problem and thus can be pre-calculated. To accommodate a continuous range of movement for a subset of the elements and/or sources, these parameters are obtained for a range of closely-spaced discrete positions and, when solving, values are found for an arbitrary position by interpolation.

The key to the method's suitability for efficient dynamic simulation is that the computation required at each time step is dramatically reduced at the expense of having to first precompute sets of parameters. At each time step, for an input of the current flowing in each phase winding, the method returns the flux linkage for each winding phase and the electromagnetic force acting on the group of moving components. Hence, the magnetic model can be combined with electric circuit and mechanical-interaction models that, at each time step, return the currents flowing in each phase and the displacement of the moving components, respectively.

3.1.1 Flux tube elements

The concept of a 'flux tube', as described in section 2.1.1, is extended here to cater for a generic region of space, where flux could be flowing in one of the six primary paths shown in figure 3.1. This insight motivates the use of a generic 2D flux tube element, as shown in figure 3.2. It takes the same form as a 'facet edge element' [65] or a 'bidirectional flux tube element' [47] and allows flux to flow internally from each boundary to every other boundary. Unfortunately, because there are six possible flux paths and only four reluctance components, the reluctances for all six paths cannot be independently specified and so a trade-off between the accuracy for cornering flux and straight flux must be made. Although conformal mapping techniques can be used to calculate the reluctances of the corner paths [52], for the purpose of this work, the reluctances are simply calculated for the straight flux paths, resulting in approximate reluctances for any cornering flux.

It could be argued that it is more appropriate to refer to the proposed 2D flux tube element as a 'quadrilateral finite element' or 'magnetic cell element' [77], since the flux can also be distributed uniformly along the face/boundary of each element with these magnetic modelling constructs. However, primarily due to the intention that with the proposed method an intuitive, large-scale grid is used for these elements, the MEC-inspired terminology of a 'flux tube' is retained.

All regions with a high relative permeability are partitioned into a network of adjoining 2D flux tubes, each of which have the parameters shown in figure 3.2. Hence, from an MEC perspective, the i^{th} flux tube element is represented by four reluctance branches, $\boldsymbol{\mathcal{R}}_{\underline{\varrho}_i \underline{\kappa}_{1:4}}$. These reluctances are a function of the element's dimensions and the permeability of the medium (they may be a nonlinear function of the flux

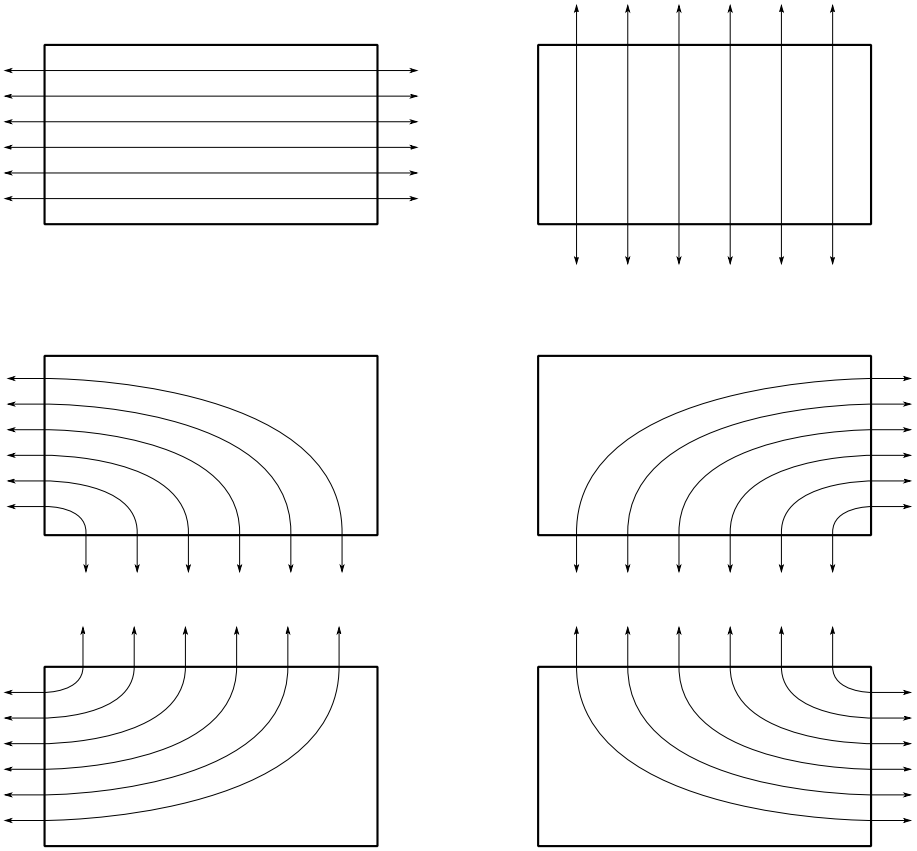

Figure 3.1: Primary flux paths for a flux tube element

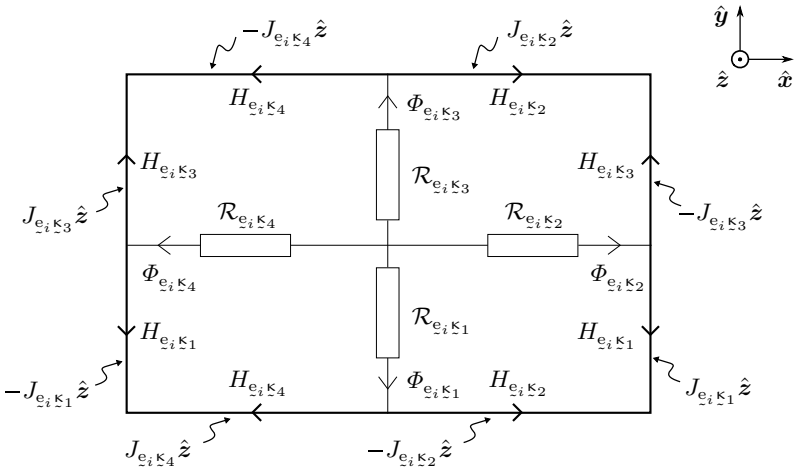

Figure 3.2: 2D flux tube element

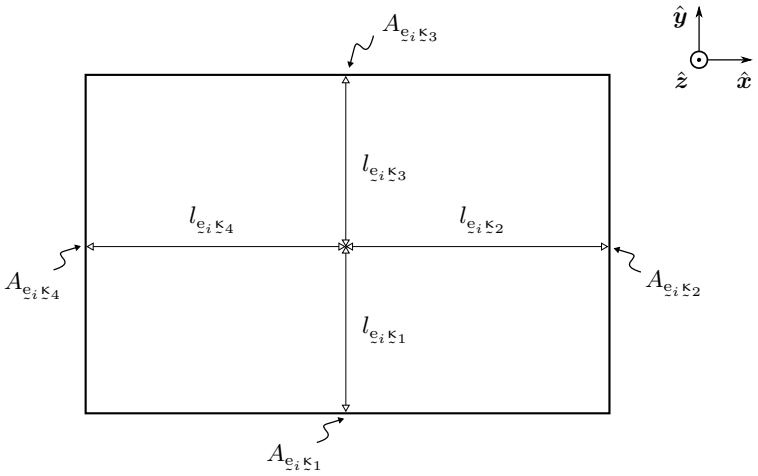

Figure 3.3: Flux tube region lengths and cross-sectional areas

to represent saturation). Analogously to Ohm's Law for electric circuits, the mmf drop across each reluctance (voltage) is equal to the flux (current) multiplied by the reluctance (resistance). This relationship is expressed in (3.1).

$$\boldsymbol{\mathcal{F}}_{\underset{\sim}{e}\underset{\sim}{\kappa}} = \boldsymbol{\Phi}_{\underset{\sim}{e}\underset{\sim}{\kappa}} * \boldsymbol{\mathcal{R}}_{\underset{\sim}{e}\underset{\sim}{\kappa}} \tag{3.1}$$

For a material with a constant permeability, μ, each constant reluctance is given by (3.2), where $\boldsymbol{l}_{\underset{\sim}{e}\underset{\sim}{\kappa}}$ are the element region lengths and $\boldsymbol{A}_{\underset{\sim}{e_i}\underset{\sim}{\kappa}_j}$ are their cross-sectional areas (as depicted in figure 3.3).

$$\mathcal{R}_{\underset{\sim}{e_i}\underset{\sim}{\kappa}_j} = \frac{l_{\underset{\sim}{e_i}\underset{\sim}{\kappa}_j}}{\mu A_{\underset{\sim}{e_i}\underset{\sim}{\kappa}_j}} \tag{3.2}$$

Correspondingly, for materials susceptible to magnetic saturation and hence exhibiting varying permeability, each reluctance is given by (3.3).

$$\mathcal{R}_{\underset{\sim}{e_i}\underset{\sim}{\kappa}_j} = \frac{\mathcal{F}_{\underset{\sim}{e_i}\underset{\sim}{\kappa}_j}(\Phi_{\underset{\sim}{e_i}\underset{\sim}{\kappa}_j})}{\Phi_{\underset{\sim}{e_i}\underset{\sim}{\kappa}_j}} \tag{3.3}$$

As shown in figure 3.2, each mmf drop across a reluctance can be considered equivalent

to an antiparallel pair of current sheets on the relevant portions of the element boundary ($\boldsymbol{J}_{\underset{\sim}{\mathrm{e}}_i \underset{\sim}{\kappa}_{1:4}}$). Further, although current sheets on the boundaries may be easier to conceptualise, it is equivalent to imposing uniform tangential field intensity boundary conditions ($\boldsymbol{H}_{\underset{\sim}{\mathrm{e}}_i \underset{\sim}{\kappa}_{1:4}}$). The magnitude of the corresponding boundary field intensity is related to the mmfs by (3.4).

$$\boldsymbol{\mathcal{F}}_{\underset{\sim}{\mathrm{e}}\underset{\sim}{\kappa}} = \boldsymbol{H}_{\underset{\sim}{\mathrm{e}}\underset{\sim}{\kappa}} * \boldsymbol{l}_{\underset{\sim}{\mathrm{e}}\underset{\sim}{\kappa}} \tag{3.4}$$

By the conservation of flux (analogous to Kirchhoff's Current Law for electric circuits), the sum of flux components meeting at each element's central node must be zero, as expressed by (3.5). Note that, for every cluster of connected elements, Gauss' Law need only be applied to all-but-one of the elements to yield sufficient simultaneous equations.

$$\sum_k \Phi_{\underset{\sim}{\mathrm{e}}_i \underset{\sim}{\kappa}_k} = 0 \qquad \forall\ i \tag{3.5}$$

Similarly, since the four flux components for each element get expressed as global and exterior boundary fluxes ($\boldsymbol{\Phi}_{\underset{\sim}{\nu}}$ and $\boldsymbol{\Phi}_{\underset{\sim}{\epsilon}}$, respectively), flux continuity across the boundaries of adjoining flux tubes is inherent. For example, the assignment of $\Phi_{\underset{\sim}{\mathrm{e}}_1 \underset{\sim}{\kappa}_4} = \Phi_{\underset{\sim}{\iota}_1}$ and $\Phi_{\underset{\sim}{\mathrm{e}}_2 \underset{\sim}{\kappa}_3} = -\Phi_{\underset{\sim}{\iota}_1}$ in figure 3.4. Because of this reassignment of boundaries, it is required that adjoining elements fully share a single common boundary.

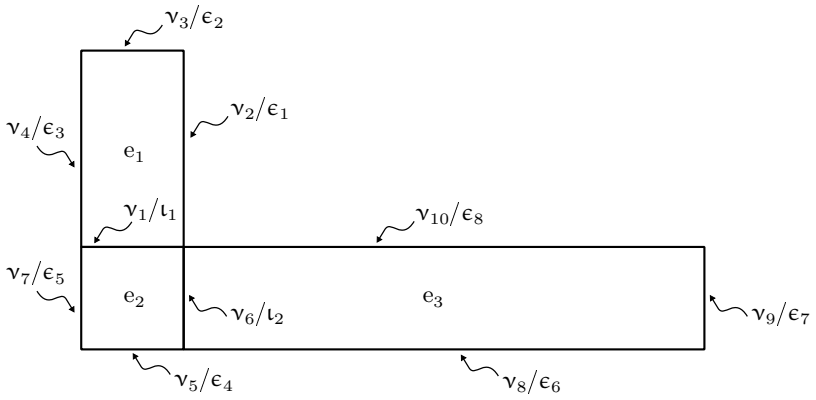

Figure 3.4: Assignment of global boundaries for flux tube elements

By Ampere's Law, mmf drops around any closed loop must sum to the amount of current enclosed by that loop. However, since the regions represented by MECs never contain any current (representative surface current sheets are only along the external boundaries of these regions), the sum of the mmf drops around any closed loop formed by the reluctances must be zero. This is analogous to Kirchhoff's Voltage Law for electric circuits. To obtain the requisite number of independent simultaneous equations, a zero sum must be formulated for every independent loop (a loop that does not contain any other loops).

3.1.2 Mutual permeances

For each mmf drop (corresponding to each flux tube element region), a mutual permeance is calculated for every exterior boundary ϵ_k, so that the normal component of flux through the boundary is equal to the magnitude of the mmf multiplied by that permeance $\mathcal{G}_{\underset{\sim}{\epsilon}_k \underset{\sim}{e}_i \underset{\sim}{\kappa}_j}$. This relationship is expressed in (3.6). $\Phi_{\underset{\sim}{\epsilon}_k \underset{\sim}{e}_i \underset{\sim}{\kappa}_j}$ is the flux component through the k^{th} exterior boundary due to the mmf of the j^{th} region of the i^{th} element. By superposition, the total normal flux through an exterior boundary is the sum of all of these components.

$$\boldsymbol{\Phi}_{\underset{\sim}{\epsilon} \underset{\sim}{e}_i \underset{\sim}{\kappa}_j} = \boldsymbol{\mathcal{G}}_{\underset{\sim}{\epsilon} \underset{\sim}{e}_i \underset{\sim}{\kappa}_j} \mathcal{F}_{\underset{\sim}{e}_i \underset{\sim}{\kappa}_j} \tag{3.6}$$

If movement occurs between different parts of the geometry (e.g. a linear motor's reaction plate moves relative to its stator) the mutual permeances are then functions of that displacement.

The initial approach taken, was to obtain each set of mutual permeances by calculating a rectified Schwarz-Christoffel map that transforms a simple rectangle to the geometry of the relevant physical region (refer to background section 2.1.1). Crucially, the boundary flux due to the mmf of a particular element intersects perpendicularly with all of the flux tube boundaries because the flux tubes are considered infinitely permeable with current sheets on their boundaries to represent their actual finite permeances. In the rectified domain, each exterior permeance could then be approximated as the ratio of the width to length of the relevant rectangular region, multiplied by the permeability of free space, μ_0. For the worked example that follows,

examples of how to approximate the mutual permeances using a Schwarz-Christoffel mapping approach are provided in appendix A.3.

After pursuing the conformal mapping approach, it became evident that, since the merit of this extended MEC method is in the use of pre-calculated parameter sets for efficient transient simulations, any error in the upfront calculation of the parameter values should be minimised. Thus, rather than introducing error because of approximations due to the constraints of an analytical approach, the Finite Element Method is a preferable way to obtain the upfront parameter sets. Moreover, FEM easily caters for distributed current sources and arbitrarily-shaped permanent magnets. Importantly, though, solving for each separate mutual permeance using FEM is far less computationally expensive than obtaining an overall solution by FEM because of the simple boundary conditions and the fact that the problem is always linear. This use of FEM to calculate the parameter sets is why the presented modelling approach is referred to as a hybrid MEC/FEM method.

As shown in figure 3.2, each element's mmf is represented as current sheets on its boundaries. When the current sheet is on an exterior boundary, an equivalent tangential field intensity boundary condition can be imposed. If, however, the current sheet is not on an exterior boundary but is adjacent to an exterior boundary, the total current in the current sheet is concentrated as a point current source on the exterior boundary. This concentration of interior current sheets to point currents is illustrated in figure 3.5.

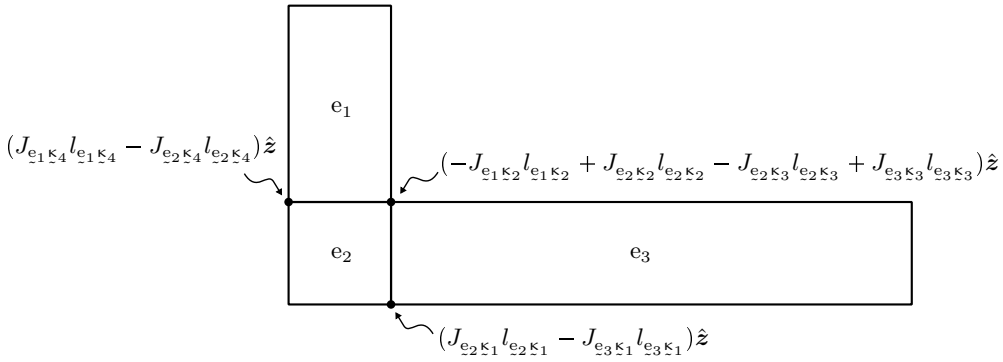

Figure 3.5: Concentration of interior boundary current sheets as point currents

3.1.3 Source flux

Since permanent magnets and conductors are assumed to have a constant relative permeabilities (typically close to unity), superposition can be applied at the exterior element boundaries for each component of source flux. Moreover, also because superposition applies, the boundary flux components due to conductors (coils) can be calculated for unity currents and then simply scaled by the actual currents, at each time step. Thus, as with the mutual permeances, the normalised flux through each exterior element boundary due to each magnetic source $\boldsymbol{\Phi}_{\underset{\sim}{\epsilon}(\underset{\sim}{\mathcal{F}0})}$, is precomputed by FEM as a function of displacement.

No restriction on the geometry of the sources is required, since the calculations to determine their influence are carried out using FEM. However, in this thesis, the sources are assumed to be rectangular to simplify the example and solver implementation.

3.1.4 Flux linkage with coils

If the electromagnetic problem includes coils, it is useful to calculate the flux linkage with the conductors at each time step. This is because the back-emf induced in the coils is given by the rate of change of the flux linkage with time. Again, because superposition holds outside of the regions represented by MECs, a flux linkage component for each source and each flux tube element can be calculated upfront for unity mmfs . The total flux linkage with each coil or winding phase at each time step is then given by the sum of these components, each scaled by the actual mmf or source current.

3.1.5 Electromagnetic force

Maxwell's Magnetic Stress Tensor method can be used to find the force acting on a finite body. Assuming that the field is only magnetic, the volumetric force density is the divergence of the so-called stress tensor, $\mathbb{T}$. Thus, the force on a finite body is given by the integral of this force density over its volume, as expressed in (3.7) [141].

$$F = \int_{\mathcal{V}} \nabla \cdot \mathbb{T} \, \mathrm{d}\mathcal{V} \tag{3.7}$$

The Divergence Theorem can be used to express this volumetric integral as an integral over the field on a bounding surface. Thus, as expressed in (3.8), for a bounding surface S, this results in the closed integral of the inner product of the stress tensor and a unit normal vector, $\hat{\boldsymbol{n}}$, facing outwards from the surface [44, 141].

$$F = \oint_S \mathbb{T} \cdot \hat{\boldsymbol{n}} \, \mathrm{d}S \tag{3.8}$$

For linear homogeneous materials, the scalar components of the stress tensor in terms of magnetic field intensity are expressed in matrix form as (3.9) [44].

$$\mathbb{T} = \mu \begin{bmatrix} \frac{1}{2}(H_\mathrm{x}^2 - H_\mathrm{y}^2 - H_\mathrm{z}^2) & H_\mathrm{x}H_\mathrm{y} & H_\mathrm{x}H_\mathrm{z} \\ H_\mathrm{x}H_\mathrm{y} & \frac{1}{2}(H_\mathrm{y}^2 - H_\mathrm{z}^2 - H_\mathrm{x}^2) & H_\mathrm{y}H_\mathrm{z} \\ H_\mathrm{x}H_\mathrm{z} & H_\mathrm{y}H_\mathrm{z} & \frac{1}{2}(H_\mathrm{z}^2 - H_\mathrm{x}^2 - H_\mathrm{y}^2) \end{bmatrix} \tag{3.9}$$

Considering a point on the surface for a 2D problem where it is assumed that there is no field component in the $\hat{\boldsymbol{z}}$ direction, the x-y plane can be aligned with the normal and tangent unit vectors as shown in figure 3.6. The surface magnetic force density can then be resolved into normal and tangential components, giving the force expression (3.10).

$$\begin{aligned} F &= \mu \oint_S \left(\frac{1}{2} \left(H_\mathrm{x}^2 - H_\mathrm{y}^2 \right) \hat{\boldsymbol{x}} + \left(H_\mathrm{x} H_\mathrm{y} \right) \hat{\boldsymbol{y}} \right) \mathrm{d}S \\ \therefore F &= \mu \oint_S \left(\frac{1}{2} \left[(\vec{\boldsymbol{H}} \cdot \hat{\boldsymbol{n}})^2 - (\vec{\boldsymbol{H}} \cdot \hat{\boldsymbol{t}})^2 \right] \hat{\boldsymbol{n}} - \left[(\vec{\boldsymbol{H}} \cdot \hat{\boldsymbol{n}})(\vec{\boldsymbol{H}} \cdot \hat{\boldsymbol{t}}) \right] \hat{\boldsymbol{t}} \right) \mathrm{d}S \end{aligned} \tag{3.10}$$

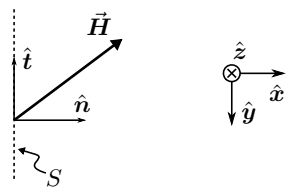

Figure 3.6: Orientation of vectors for surface magnetic force density

For the flux tube elements with relatively high permeability, the tangential component of the field intensity ($\vec{\boldsymbol{H}} \cdot \hat{\boldsymbol{t}}$) can be assumed to be negligible and the resulting force is entirely in the direction of the outward normal, $\hat{\boldsymbol{n}}$. However, this is generally not the case for the sources (e.g. permanent magnets).

Choosing a surface immediately surrounding the body so that the integration takes place within the air, where the constitutive relationship $\vec{\boldsymbol{B}} = \mu_0 \vec{\boldsymbol{H}}$ holds because air is a linear homogeneous material with a constant permeability of μ_0 [141], yields (3.11).

$$F = \oint_S \left(\left[\frac{1}{2\mu_0} (\vec{\boldsymbol{B}} \cdot \hat{\boldsymbol{n}})^2 - \frac{\mu_0}{2} (\vec{\boldsymbol{H}} \cdot \hat{\boldsymbol{t}})^2 \right] \hat{\boldsymbol{n}} - \left[(\vec{\boldsymbol{B}} \cdot \hat{\boldsymbol{n}})(\vec{\boldsymbol{H}} \cdot \hat{\boldsymbol{t}}) \right] \hat{\boldsymbol{t}} \right) \mathrm{d}S \tag{3.11}$$

Lastly, if the surrounding surface is divided into a discrete number of regions, $\boldsymbol{A}_{\underset{\sim}{\mathrm{k}}}$, where the field quantities are constant for each region, k_i, the closed integral can be expressed as a sum, given by (3.12).

$$F = \sum_i \left(\frac{1}{2\mu_0} (\vec{\boldsymbol{B}}_{\underset{\sim}{\mathrm{k}}_i} \cdot \hat{\boldsymbol{n}}_{\underset{\sim}{\mathrm{k}}_i})^2 - \frac{\mu_0}{2} (\vec{\boldsymbol{H}}_{\underset{\sim}{\mathrm{k}}_i} \cdot \hat{\boldsymbol{t}}_{\underset{\sim}{\mathrm{k}}_i})^2 \right) A_{\underset{\sim}{\mathrm{k}}_i} \hat{\boldsymbol{n}}_{\underset{\sim}{\mathrm{k}}_i} - (\vec{\boldsymbol{B}}_{\underset{\sim}{\mathrm{k}}_i} \cdot \hat{\boldsymbol{n}}_{\underset{\sim}{\mathrm{k}}_i})(\vec{\boldsymbol{H}}_{\underset{\sim}{\mathrm{k}}_i} \cdot \hat{\boldsymbol{t}}_{\underset{\sim}{\mathrm{k}}_i}) A_{\underset{\sim}{\mathrm{k}}_i} \hat{\boldsymbol{t}}_{\underset{\sim}{\mathrm{k}}_i} \tag{3.12}$$

In order to calculate the resulting force by this approach, it is thus necessary to assume that the field quantities are constant along the exterior boundaries. The validity of this assumption is what determines the accuracy of the force calculation. Note that this approximation improves with an increase in the number of elements used to represent a region (i.e. a reduction in the grid size for the moving elements and sources).

Considering every moving exterior flux tube element boundary, ϵ_i, where $B_{\underset{\sim}{\epsilon}_i}$ are the average outward normal flux densities and $H_{\underset{\sim}{\epsilon}_i}$ are the average tangential field intensities, and every moving exterior source boundary, ζ_j, where $B_{\underset{\sim}{\zeta}_j}$ are the average outward normal flux densities and $H_{\underset{\sim}{\zeta}_j}$ are the average tangential field intensities, (3.12) can be expressed as (3.13).

$$\begin{aligned} F = &\sum_i \left(\left[\frac{1}{2\mu_0} B_{\underset{\sim}{\epsilon}_i}^2 - \frac{\mu_0}{2} H_{\underset{\sim}{\epsilon}_i}^2 \right] \hat{\boldsymbol{n}}_{\underset{\sim}{\epsilon}_i} - \left[B_{\underset{\sim}{\epsilon}_i} H_{\underset{\sim}{\epsilon}_i} \right] \hat{\boldsymbol{t}}_{\underset{\sim}{\epsilon}_i} \right) A_{\underset{\sim}{\epsilon}_i} \\ &+ \sum_j \left(\left[\frac{1}{2\mu_0} B_{\underset{\sim}{\zeta}_j}^2 - \frac{\mu_0}{2} H_{\underset{\sim}{\zeta}_j}^2 \right] \hat{\boldsymbol{n}}_{\underset{\sim}{\epsilon}_i} - \left[B_{\underset{\sim}{\zeta}_j} H_{\underset{\sim}{\zeta}_j} \right] \hat{\boldsymbol{t}}_{\underset{\sim}{\epsilon}_i} \right) A_{\underset{\sim}{\zeta}_j} \end{aligned} \tag{3.13}$$

Finally, because the average flux density is equal to the total boundary flux divided by the boundary's surface area, the electromagnetic force is given by (3.14).

$$\begin{aligned} F = &\sum_i \left[\frac{1}{2\mu_0} \Phi_{\underset{\sim}{\epsilon}_i}^2 / A_{\underset{\sim}{\epsilon}_i} - \frac{\mu_0}{2} H_{\underset{\sim}{\epsilon}_i}^2 A_{\underset{\sim}{\epsilon}_i} \right] \hat{\boldsymbol{n}}_{\underset{\sim}{\epsilon}_i} - \left[\Phi_{\underset{\sim}{\epsilon}_i} H_{\underset{\sim}{\epsilon}_i} \right] \hat{\boldsymbol{t}}_{\underset{\sim}{\epsilon}_i} \\ &+ \sum_j \left[\frac{1}{2\mu_0} \Phi_{\underset{\sim}{\zeta}_j}^2 / A_{\underset{\sim}{\zeta}_j} - \frac{\mu_0}{2} H_{\underset{\sim}{\zeta}_j}^2 A_{\underset{\sim}{\zeta}_j} \right] \hat{\boldsymbol{n}}_{\underset{\sim}{\epsilon}_i} - \left[\Phi_{\underset{\sim}{\zeta}_j} H_{\underset{\sim}{\zeta}_j} \right] \hat{\boldsymbol{t}}_{\underset{\sim}{\epsilon}_i} \end{aligned} \tag{3.14}$$

As with the flux linkages, because superposition holds outside of the MEC formulation, the normal flux and average tangential field intensity for each exterior boundary that moves are calculated by scaling the values obtained upfront for unity sources.

3.1.6 Dynamic simulation

To perform a dynamic simulation, the described hybrid solver can be coupled with dynamic mechanical and electric circuit models, as appropriate. Since the solver is intended for applications where the magnetic field is quasi-stationary, the field solution can be solved at each time step as if all of the magnetic sources are constant. In fact, the proposed hybrid solver is best suited to dynamic simulation problems.

For coils that are connected to a voltage source, an appropriate simple electric circuit model for each coil is given by (3.15). By Ohm's Law, the current that flows in the winding, $I_{(\mathrm{ph})}$, is related to the applied voltage, $V_{(\mathrm{ph})}$, and back-emf, $\dot{\lambda}_{(\mathrm{ph})}$, by the resistance of the circuit, $R_{(\mathrm{ph})}$. The flux linkage for each phase is returned by the electromagnetic solver and the circuit model provides the resulting phase currents back to the hybrid electromagnetic solver for the next time step.

$$V_{(\mathrm{ph})} - \dot{\lambda}_{(\mathrm{ph})} = I_{(\mathrm{ph})} R_{(\mathrm{ph})} \tag{3.15}$$

Furthermore, the motion of the moving elements and sources relative to the stationary elements and sources is governed by Newton's second law of motion, which states that an object's rate of change of momentum is equal to the net force applied to it. Their acceleration, $\ddot{x}$, is equal to the net applied force multiplied by their combined mass, M. As shown in (3.16), the electromagnetic force, $F_{(\mathrm{em})}$, is typically opposed by a friction force, F_{f}, and a load force, F_{L}. The electromagnetic force is an output of the electromagnetic solver and the resulting displacement of the moving components is then provided by the dynamic mechanical model for the solution at the next time step.

$$F_{(\mathrm{em})} - F_{\mathrm{f}} - F_{\mathrm{L}} = M\ddot{x} \tag{3.16}$$

3.2 Worked example

The presented modelling methodology is applied here to a simple example chosen to be representative of a three-phase segmented linear synchronous motor (an adaptation of the prototype motor detailed in appendix C). To keep this example as straightforward as possible, the reaction plate only consists of a single pole pair (formed by surface mount PMs) and the double-layer three-phase modular stator winding only has a single coil per phase. Figure 3.7 is a 3D representation of this device.

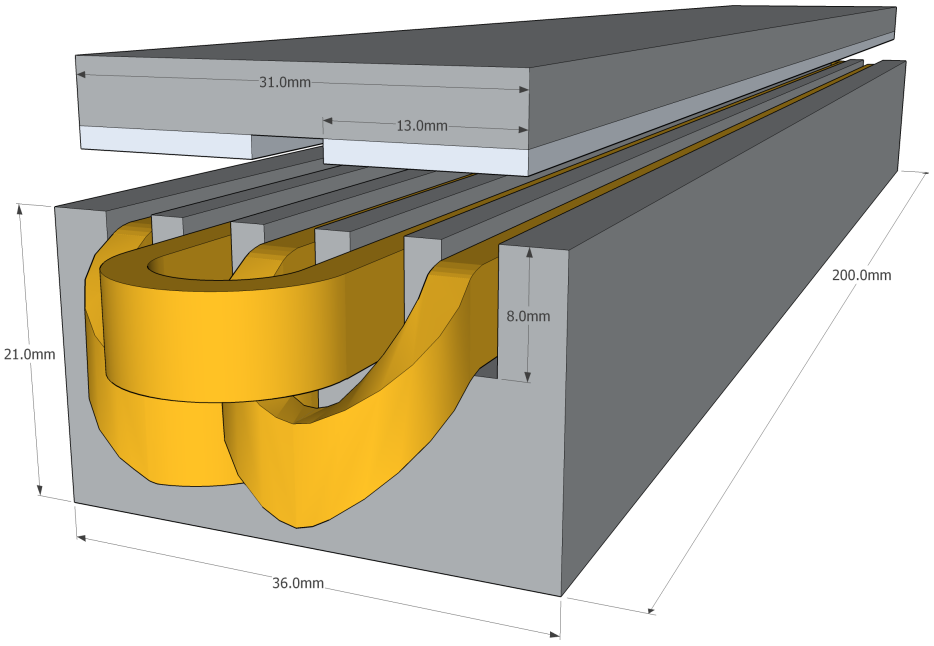

Figure 3.7: 3D representation of example problem

To quantify the accuracy of the hybrid solver, its outputs are compared with those obtained with a pure FEM solver for a range of discrete phase currents and reaction plate positions.

The implementation of the hybrid method using MATLAB® and FEMM [63] is detailed in appendix A.1 and the source code and solver outputs for this worked example are provided in appendix A.2.

3.2.1 Materials

The stator core is chosen to be a stack of SURA® M250-50A electric motor steel laminations and the reaction plate back-iron is chosen to be '1010 Steel'. These materials exhibit the nonlinear *B-H* curves plotted in figure 3.8. (A zoomed-in plot of the initial slopes of these curves is provided as figure A.2 in appendix A.) To also demonstrate the hybrid method's effectiveness when assuming constant material permeabilities, the example is solved with the material permeabilities set at their maximum values (maximum slopes of their respective *B-H* curves). Furthermore, to show how the method's accuracy reduces as the permeability of the flux tubes decreases, the problem is solved for the flux tubes having lower relative permeabilities of 100, 50 and 10.

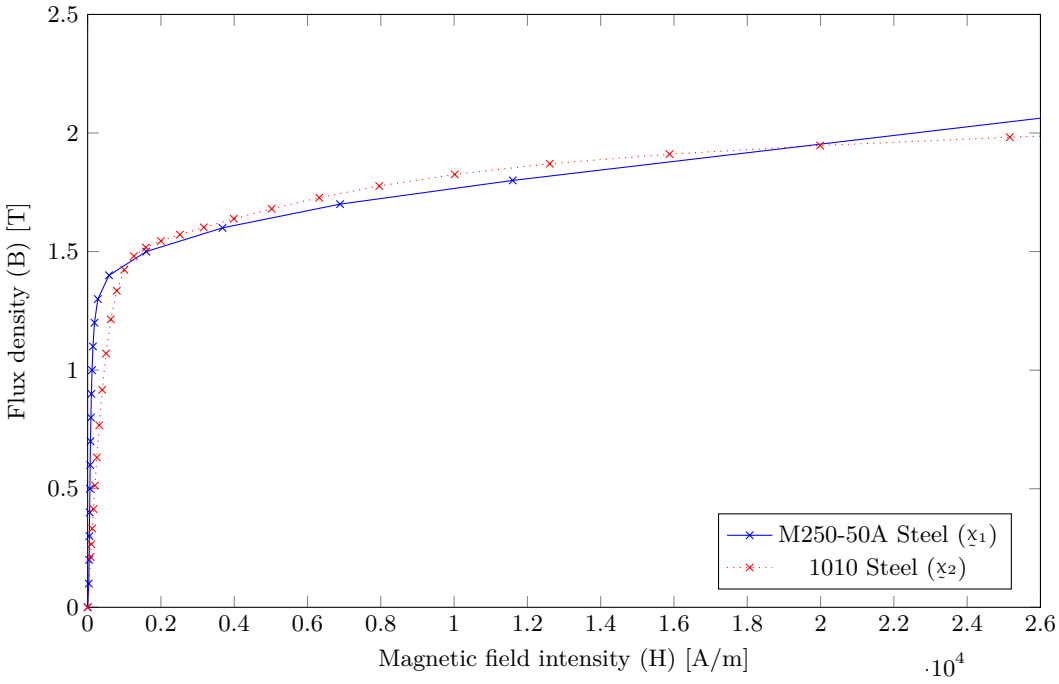

Figure 3.8: *B-H* curves of materials

The magnets are chosen to be Grade 45H neodymium-iron-boron (NdFeB), with a magnetic coercivity, Hc, of 979 kA/m and relative permeability of 1,049. The coils, one for each phase, have 15 turns each and have the permeability of free space, μ_0. In summary, the material properties are provided in table 3.1.

Table 3.1: Material properties

Material (χ)	Description	μr	Hc [kA/m]	Phase	Turns
1	M250-50 lamination steel	7185	0	–	–
2	1010 steel	2119	0	–	–
3	NdFeB-45H	1,049	979	–	–
4	Phase 'A' coil	1	0	1	15
5	Phase 'B' coil	1	0	2	15
6	Phase 'C' coil	1	0	3	15

3.2.2 Flux tube elements and sources

Geometry and assignment of materials

The highly-permeable regions of the example problem (stator core and reaction plate back-iron) are divided into 30 rectangular flux tube elements and 8 rectangular sources. This layout in the complex plane is shown in figure 3.9, where the problem depth is chosen to be 200 mm into the page. The moving components, which are the back-iron (elements 1–26) and permanent magnets (sources 7 & 8), are specified to move parallel to the real axis ($\hat{\boldsymbol{x}} = 1$), with a displacement x.

Figure 3.10 gives the assignment of the specified materials to the elements and sources. The permanent magnet regions are defined with an angle corresponding to their orientation and the sign of each coil region specifies whether the current flows out of the page (positive) or into the page (negative).

MEC representation

The resulting magnetic equivalent circuit representation for the highly-permeable regions is shown in figure 3.11. Also annotated, are the eight independent loops for which the sum of mmfs must be zero.

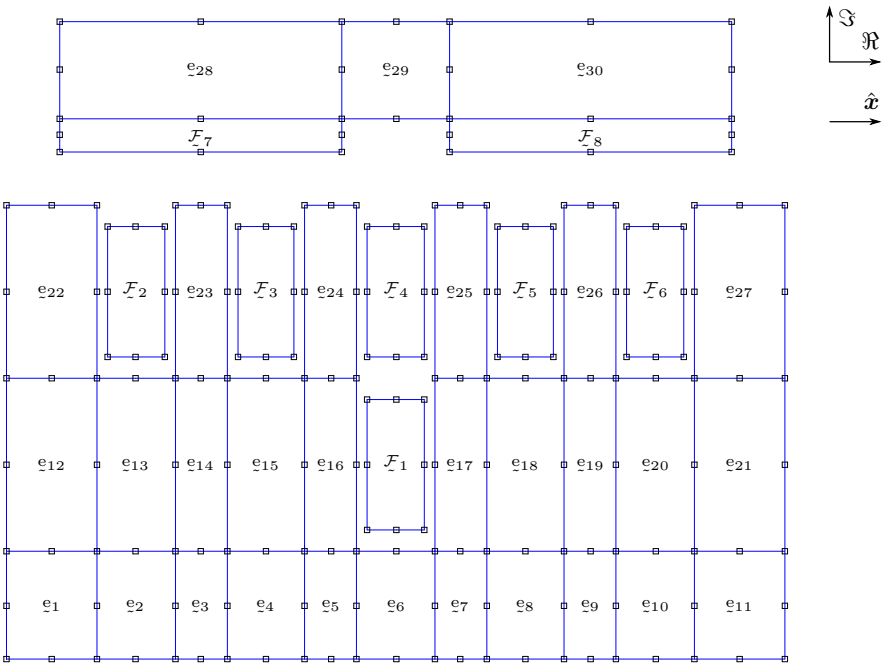

Figure 3.9: Geometry

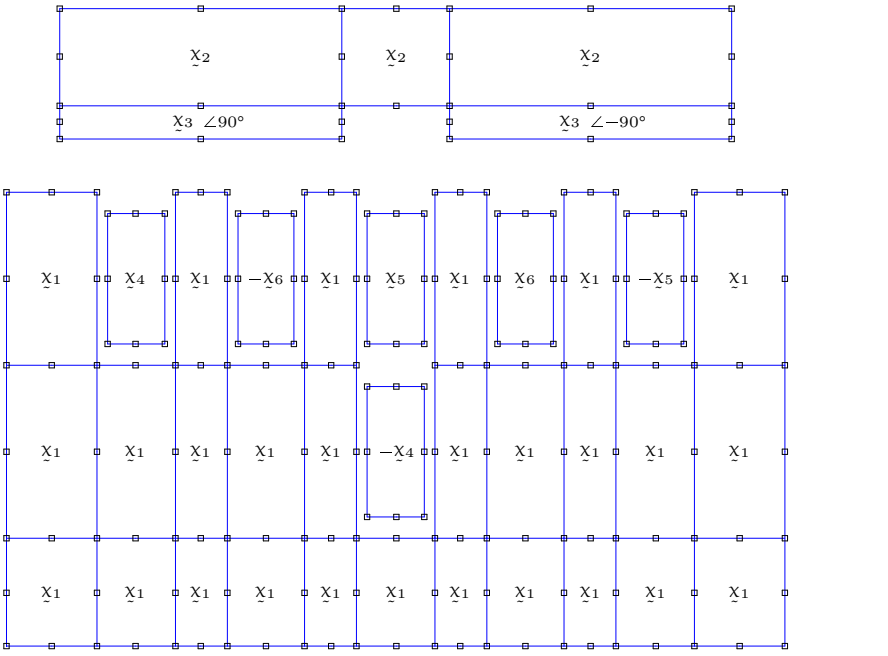

Figure 3.10: Assignment of materials

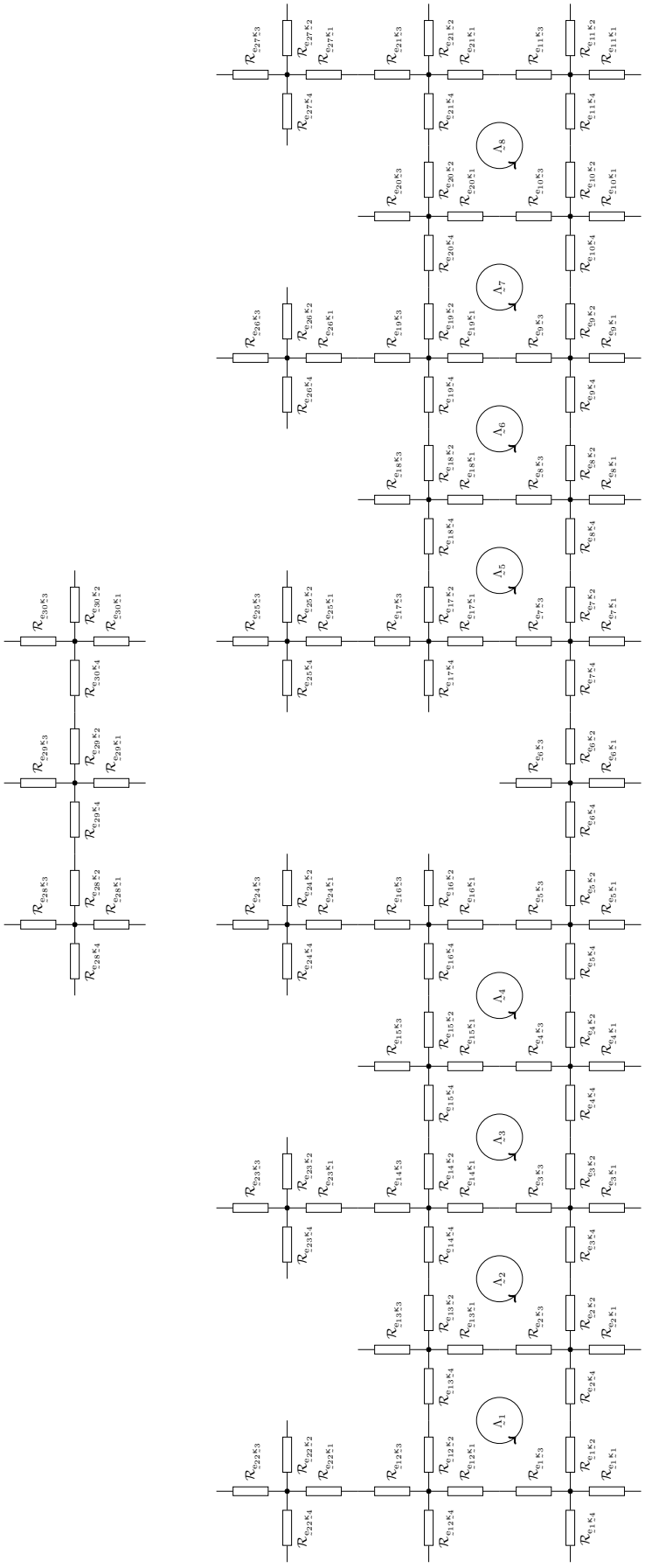

Figure 3.11: Magnetic equivalent circuit

3.2.3 Precomputation of parameter sets

The mutual permeances, normalized source boundary fluxes, normalized source boundary field intensities and normalized flux linkages are calculated upfront for all of the element regions, with the reaction plate positioned at 2 mm increments. To illustrate how the separate mutual permeances are obtained, figure 3.12 shows the flux distribution for element 24, region 3 acting as a unity mmf source ($x = 0$). In addition, figure 3.13 shows the flux distribution for element 29, region 1, where its mmf needs to be modelled as two point current sources because the equivalent current sheets do not lie along exterior boundaries.

Also, for each source, the normalized exterior element fluxes, normalized source boundary fluxes and field intensities, as well as the normalized flux linkages, are precomputed. To illustrate, figure 3.14 shows the flux due to the first coil region and figure 3.15 shows the flux due to the left-hand permanent magnet.

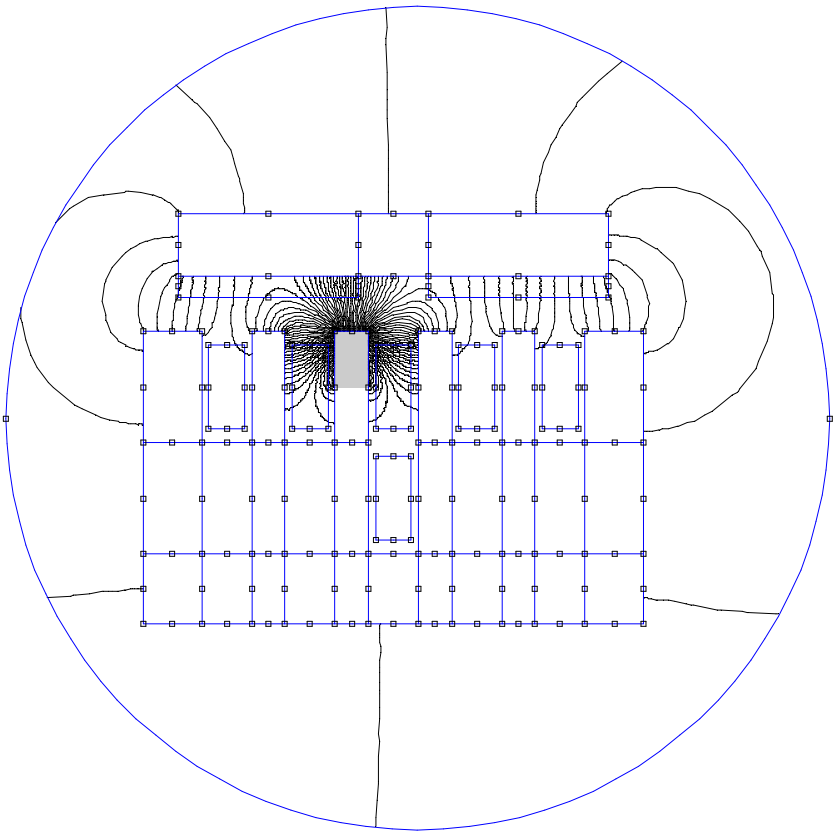

Figure 3.12: Computing $\boldsymbol{\mathcal{G}}_{\underset{\sim}{\epsilon}\underset{\sim}{e}_{24}\underset{\sim}{\kappa}_3}$, $\boldsymbol{\mathcal{G}}_{\underset{\sim}{\zeta}\underset{\sim}{e}_{24}\underset{\sim}{\kappa}_3}$,$\boldsymbol{H}_{\underset{\sim}{\zeta}\underset{\sim}{e}_{24}\underset{\sim}{\kappa}_3}$ and $\boldsymbol{\lambda}_{(\mathrm{ph})\underset{\sim}{e}_{24}\underset{\sim}{\kappa}_3}$ for $x = 0$

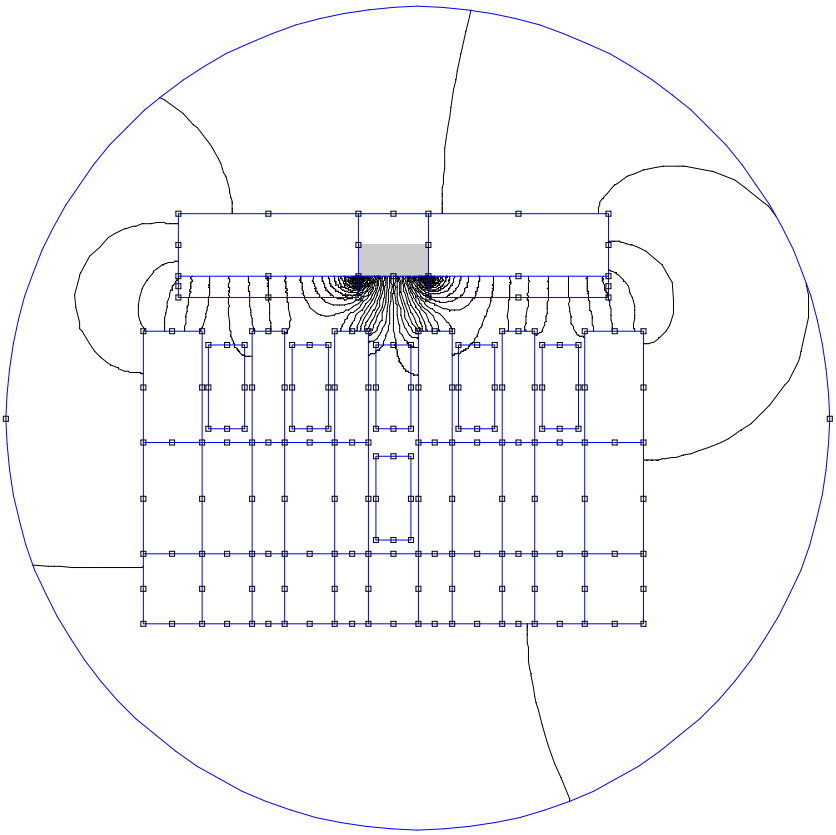

Figure 3.13: Computing $\boldsymbol{\mathcal{G}}_{\underset{\sim}{\epsilon}\underset{\sim}{\mathrm{e}}_{29}\underset{\sim}{\kappa}_1}$, $\boldsymbol{\mathcal{G}}_{\underset{\sim}{\zeta}\underset{\sim}{\mathrm{e}}_{29}\underset{\sim}{\kappa}_1}$,$\boldsymbol{H}_{\underset{\sim}{\zeta}\underset{\sim}{\mathrm{e}}_{29}\underset{\sim}{\kappa}_1}$ and $\boldsymbol{\lambda}_{(\underset{\sim}{\mathrm{ph}})\underset{\sim}{\mathrm{e}}_{29}\underset{\sim}{\kappa}_1}$ for $x = 0$

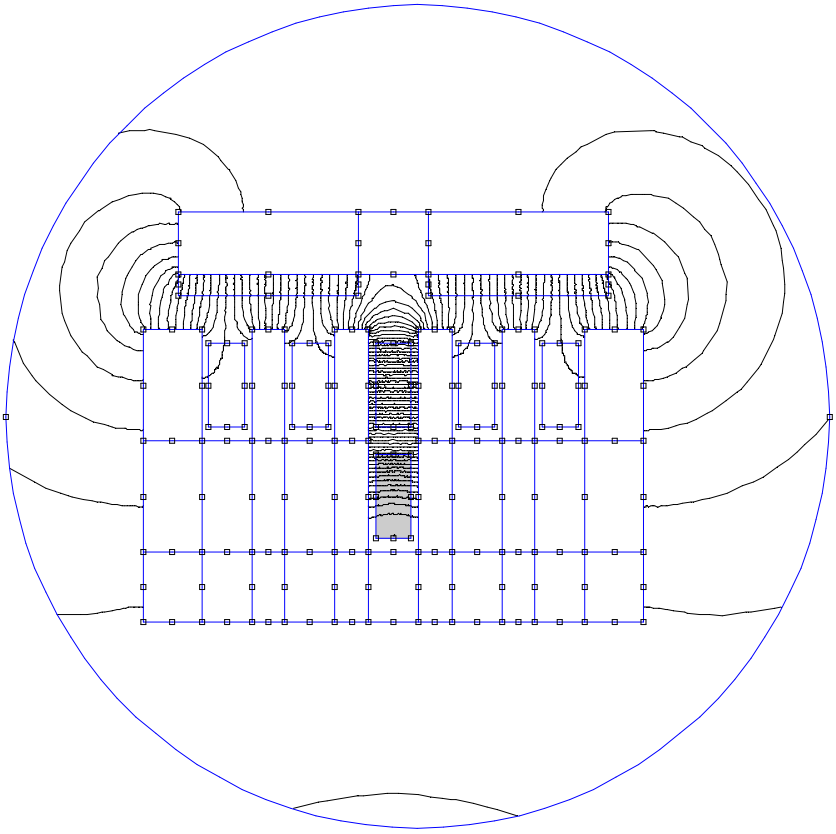

Figure 3.14: Computing $\boldsymbol{\Phi}_{\underset{\sim}{\epsilon}(\underset{\sim}{\mathcal{F}}0)_1}$, $\boldsymbol{\Phi}_{\underset{\sim}{\zeta}(\underset{\sim}{\mathcal{F}}0)_1}$,$\boldsymbol{H}_{\underset{\sim}{\zeta}(\underset{\sim}{\mathcal{F}}0)_1}$ and $\boldsymbol{\lambda}_{(\underset{\sim}{\mathrm{ph}})(\underset{\sim}{\mathcal{F}}0)_1}$ for $x = 0$

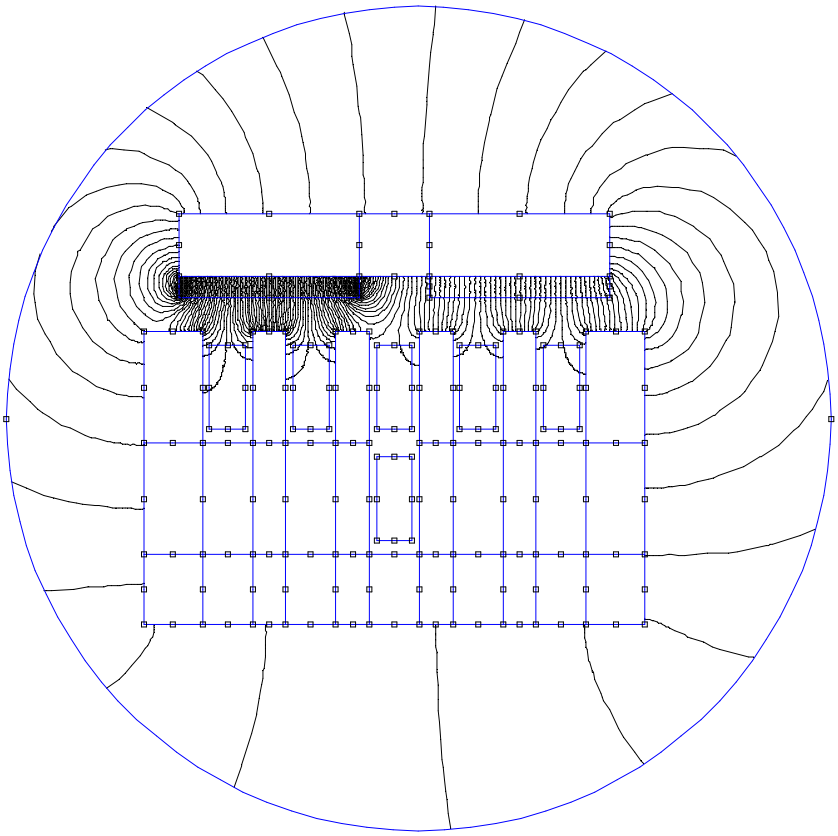

Figure 3.15: Computing $\boldsymbol{\Phi}_{\underset{\sim}{\xi}(\underset{\sim}{\mathcal{F}0})_7}$, $\boldsymbol{\Phi}_{\underset{\sim}{\zeta}(\underset{\sim}{\mathcal{F}0})_7}$,$\boldsymbol{H}_{\underset{\sim}{\zeta}(\underset{\sim}{\mathcal{F}0})_7}$ and $\boldsymbol{\lambda}_{(\mathrm{ph})(\underset{\sim}{\mathcal{F}0})_7}$ for $x = 0$

3.2.4 Comparison of static results to pure FEM solutions

The example problem was solved using the hybrid method over a range of discrete reaction plate positions and phase currents, and each result was then compared with a full FEM solution. Figure 3.16 illustrates how well the flux distributions in the air-gap for boundary conditions found by the hybrid method match pure FEM solutions. In addition to solving the nonlinear equations for the specified B-H curves, the linear problem was solved for the materials just exhibiting their maximum relative permeability, as well as for them having constant relative permeabilities of 100, 50 and 10 (to determine the reduction in accuracy with a decrease in the flux tubes' relative permeability).

To measure the hybrid method's accuracy, normalised root-mean-squared (rms) error values are calculated using pure FEM solution results as a reference. All of the error results are tabulated in appendix A.1.12 but tables 3.2 and 3.3 are included here as representative results.

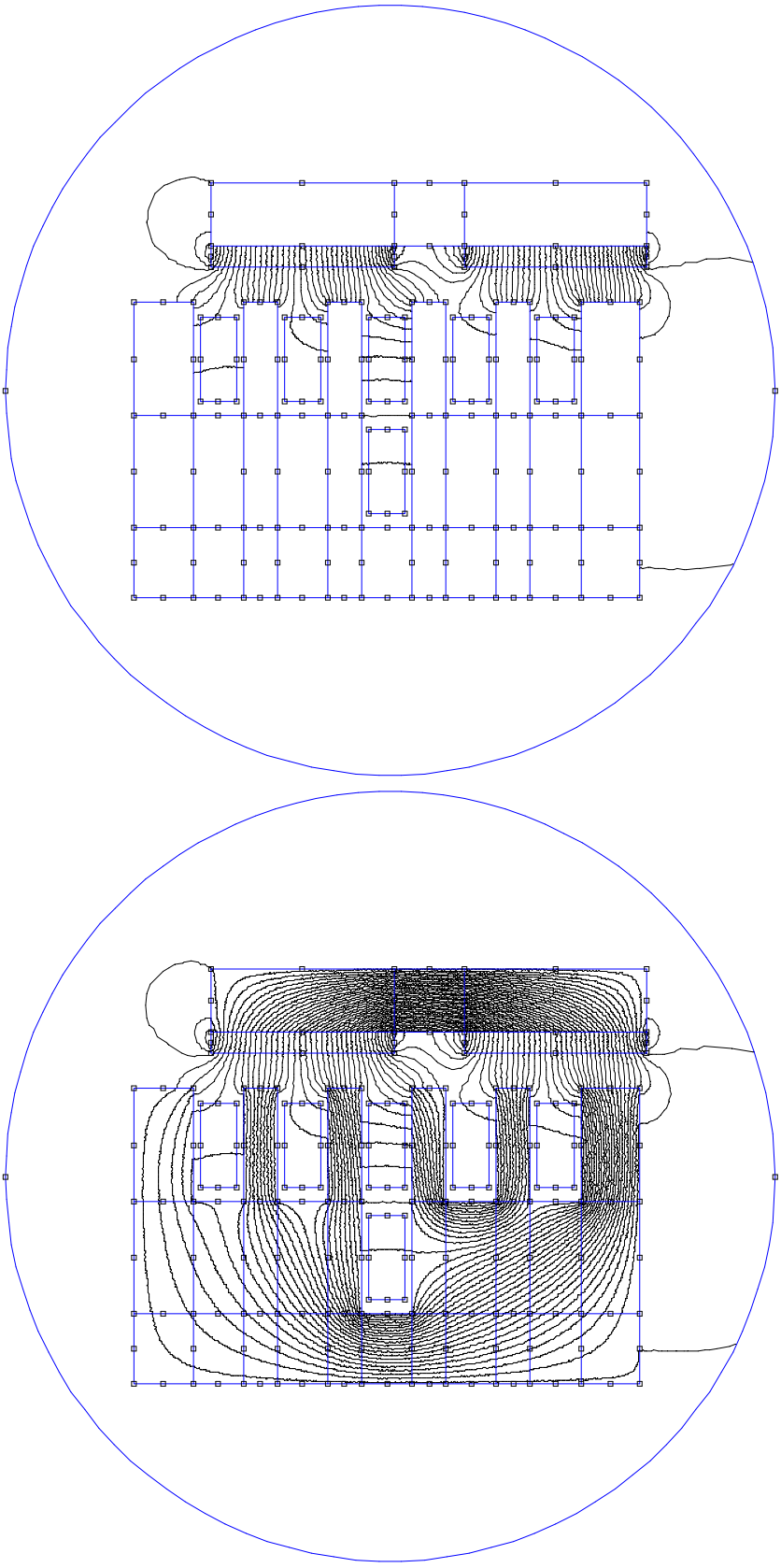

Figure 3.16: Field solution by hybrid method versus pure FEM solution with $\underset{\sim}{\boldsymbol{I}}_{(\mathrm{ph})} = \begin{bmatrix} 20 & -10 & -10 \end{bmatrix}^{\mathrm{T}}$ A, $x = 3\,\mathrm{mm}$

Table 3.2: Percentage rms errors for reaction plate positioned where exact precomputed parameters are used

% rms Error	$\underset{\sim}{I}_{(\mathrm{ph})} = [20\ -10\ -10]^{\mathrm{T}}$ A, $x = 4$ mm					
	$\underset{\sim}{\Phi}_{\epsilon}$	$\underset{\sim}{\Phi}_{\zeta}$	$\underset{\sim}{H}_{\zeta}$	$\underset{\sim}{\lambda}_{(\mathrm{ph})}$	F(tangent)	F(normal)
B-H curves	1,26	0,88	1,10	1,89	36,41	6,24
$\mu r_{\underset{\sim}{\chi}_1} = 7185$, $\mu r_{\underset{\sim}{\chi}_2} = 2119$	0,14	0,10	0,56	0,03	29,84	8,27
$\mu r_{\underset{\sim}{\chi}_1}, \mu r_{\underset{\sim}{\chi}_2} = 100$	1,93	0,23	1,91	2,52	41,42	11,09
$\mu r_{\underset{\sim}{\chi}_1}, \mu r_{\underset{\sim}{\chi}_2} = 50$	3,31	0,43	2,91	4,44	61,23	13,08
$\mu r_{\underset{\sim}{\chi}_1}, \mu r_{\underset{\sim}{\chi}_2} = 10$	8,28	2,94	6,38	10,51	849,02	21,33

Table 3.3: Percentage rms errors for reaction plate positioned where the precomputed parameters are interpolated

% rms Error	$\underset{\sim}{I}_{(\mathrm{ph})} = [20\ -10\ -10]^{\mathrm{T}}$ A, $x = 5$ mm					
	$\underset{\sim}{\Phi}_{\epsilon}$	$\underset{\sim}{\Phi}_{\zeta}$	$\underset{\sim}{H}_{\zeta}$	$\underset{\sim}{\lambda}_{(\mathrm{ph})}$	F(tangent)	F(normal)
B-H curves	1,23	0,65	2,03	1,87	34,17	6,86
$\mu r_{\underset{\sim}{\chi}_1} = 7185$, $\mu r_{\underset{\sim}{\chi}_2} = 2119$	0,36	0,15	1,05	0,25	29,67	8,84
$\mu r_{\underset{\sim}{\chi}_1}, \mu r_{\underset{\sim}{\chi}_2} = 100$	2,06	0,47	1,41	2,83	33,28	11,91
$\mu r_{\underset{\sim}{\chi}_1}, \mu r_{\underset{\sim}{\chi}_2} = 50$	3,44	0,61	2,44	4,80	37,44	14,05
$\mu r_{\underset{\sim}{\chi}_1}, \mu r_{\underset{\sim}{\chi}_2} = 10$	8,45	2,62	6,09	11,05	71,54	22,43

It is evident that the hybrid method is highly accurate for the boundary fluxes and winding flux linkages, so long as the relative flux tube permeabilities are sufficiently high. The results are slightly less accurate for the reaction plate positioned at $x = 5$ mm than for it positioned at $x = 4$ mm because the precomputed parameters need to be interpolated for $x = 5$ mm from those obtained at $x = 4$ mm and $x = 6$ mm.

The calculation of the two force components (tangential to and normal to the direction of movement) is less accurate than the other outputs, owing to the assumption that the normal flux density and tangential field intensity are uniform along each moving exterior boundary. Thus, the accuracy of the calculated force improves with a reduction in the relevant exterior boundary lengths. That is, the accuracy of the calculated force improves with a smaller "mesh" size over the moving regions for which the force is calculated. This is particularly the case for moving sources, where the variation in the tangential field intensity along their boundaries can be significant.

To demonstrate this point, the permanent magnet regions are each subdivided into four source regions, as shown in figure 3.17. The results for this refined grid are

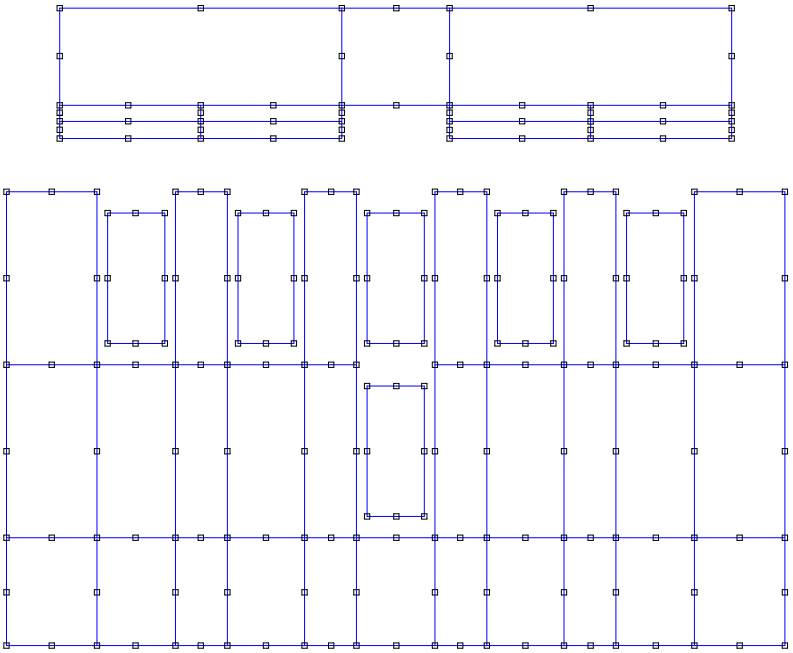

Figure 3.17: Geometry with a refined grid for the magnets

provided in tables 3.4 and 3.5. It can be seen that the finer grid does improve the force calculation, as expected, given the primary assumption that the relative permeability of the flux tubes is sufficiently high.

Although it would be valuable to contrast both the set-up and calculation times for the hybrid method against a pure FEM approach, it is, unfortunately, not possible to draw a meaningful comparison. Considering that the hybrid method has been derived with the intention that it be used for transient simulations, it is not efficient in terms of solution time for the presented example. This is because the precomputation of the required parameter sets adds significantly to the problem set-up time but, in this particular case, the precomputed values are only used for relatively few solution points. One method of comparing the solution times would be to time how long it takes to solve for the first solution point in contrast to subsequent points. However, these relative times are highly contingent on the size of the problem, the chosen FEM mesh size and type, how re-meshing is achieved between solution points for the FEM transient simulation, as well as on the element sizes chosen for the hybrid method. Furthermore, the hybrid method is currently implemented using MATLAB® scripts with function calls to FEMM [63] for the necessary FEM solutions. Thus, it does not run as fast as it would do if it were fully-compiled and optimised code.

Table 3.4: Percentage rms errors for reaction plate positioned where exact precomputed parameters are used (reduced-size mesh for magnets)

% rms Error	$\underset{\sim}{I}_{(\mathrm{ph})} = [20\ -10\ -10]^{\mathrm{T}}$ A					
	$x = 4$ mm					
	$\underset{\sim}{\Phi}_{\epsilon}$	$\underset{\sim}{\Phi}_{\zeta}$	$\underset{\sim}{H}_{\zeta}$	$\underset{\sim}{\lambda}_{(\mathrm{ph})}$	F(tangent)	F(normal)
B-H curves	1,11	0,62	1,24	1,71	29,18	4,88
$\underset{\sim}{\chi}_1 = 7185$, $\underset{\sim}{\chi}_2 = 2119$	0,13	0,10	1,01	0,13	22,70	6,67
$\underset{\sim}{\chi}_1, \underset{\sim}{\chi}_2 = 100$	2,53	1,74	1,46	3,70	35,21	12,33
$\underset{\sim}{\chi}_1, \underset{\sim}{\chi}_2 = 50$	4,13	2,84	1,90	6,45	59,20	16,53
$\underset{\sim}{\chi}_1, \underset{\sim}{\chi}_2 = 10$	7,83	5,48	3,40	15,75	488,82	30,65

Table 3.5: Percentage rms errors for reaction plate positioned where the precomputed parameters are interpolated (reduced-size mesh for magnets)

% rms Error	$\underset{\sim}{I}_{(\mathrm{ph})} = [20\ -10\ -10]^{\mathrm{T}}$ A					
	$x = 5$ mm					
	$\underset{\sim}{\Phi}_{\epsilon}$	$\underset{\sim}{\Phi}_{\zeta}$	$\underset{\sim}{H}_{\zeta}$	$\underset{\sim}{\lambda}_{(\mathrm{ph})}$	F(tangent)	F(normal)
B-H curves	1,18	0,62	1,95	1,78	24,65	5,91
$\underset{\sim}{\chi}_1 = 7185$, $\underset{\sim}{\chi}_2 = 2119$	0,24	0,20	1,59	0,28	19,95	7,70
$\underset{\sim}{\chi}_1, \underset{\sim}{\chi}_2 = 100$	2,70	1,93	1,54	4,07	21,12	13,87
$\underset{\sim}{\chi}_1, \underset{\sim}{\chi}_2 = 50$	4,40	3,14	1,89	7,02	23,76	18,46
$\underset{\sim}{\chi}_1, \underset{\sim}{\chi}_2 = 10$	8,39	6,37	3,54	17,22	48,43	33,77

Chapter 4

Motor Dynamic Model

This chapter describes the derivation of the motor equations for each stator section using a space-vector approach, under the assumption that there is no significant saturation of the magnetic materials. Since each segment of the linear motor stator is fed independently, each stator section can be treated as a separate "motor" with describing equations that depend on the relative position of the reaction plate to it. The resulting force on the reaction plate is therefore the sum of the forces produced by all of the sections. Clearly, when the reaction plate is not in the vicinity of a particular section, that section's contribution to the force is zero.

4.1 Power-invariant $\alpha/\beta/0$ transformation

In a three-phase 'sinusoidal flux' motor, the windings are spatially arranged to produce a sinusoidal travelling wave of flux along the air-gap when fed by sinusoidal phase currents that are out-of-phase by $2\pi/3$ rad *in time*. Thus, neglecting harmonics, the magneto-motive force (mmf) distributions along the air-gap, due to each of the three-phase currents, must be *spatially* displaced by $2\pi/3$ rad (π rad corresponds to the motor's pole pitch, τ). This arrangement is depicted in figure 4.1.

It is convenient to resolve the mmf distributions into two quadrature components in space with corresponding stator and reaction plate quantities [85, 142, 143]. For a purely sinusoidal flux distribution along the air-gap, this approach eliminates the mutual magnetic coupling of the three-phase windings. This standard space-vector modelling approach may not seem appropriate for a segmented stator with

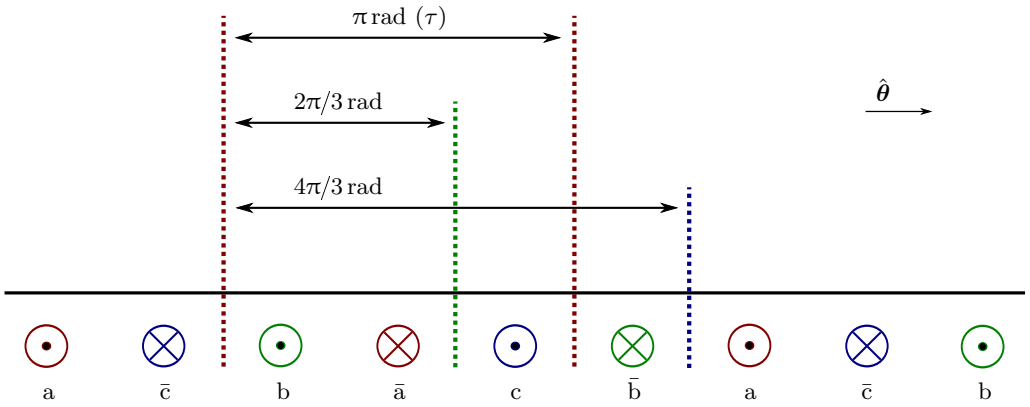

Figure 4.1: Spatial distribution of three-phase stator winding

discontinuities at the section boundaries and a finite-length reaction plate (causing significant spacial harmonics). However, in deriving the motor equations, it is not necessary to assume that the mutual coupling in the two-axis frame is actually zero or, in fact, that the mmf distributions are purely sinusoidal. It is merely convenient because it minimises the cross-coupling effects and thus allows the full motor model, as derived here, to be easily simplified when appropriate.

As is customary, a stationary reference frame is defined, with an α-axis that aligns with the mmf of phase 'a' and a β-axis that is in space quadrature with the α-axis. This is portrayed in figure 4.2. The chosen power-invariant form of the transformation to this α/β reference frame is derived in appendix B.

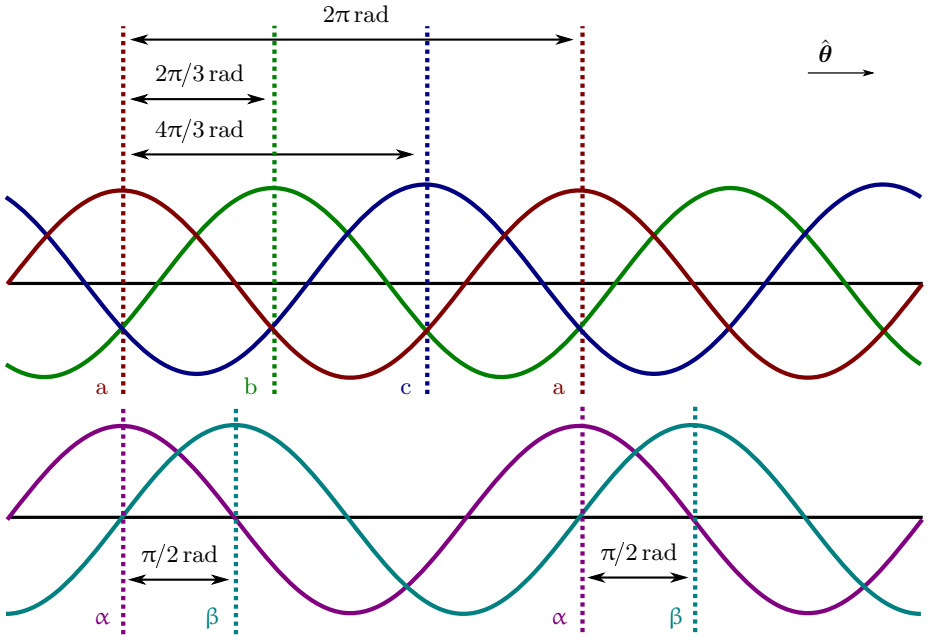

Figure 4.2: α/β axes in relation to a/b/c axes

A third component, termed the zero-sequence component, is required for an invertible transformation when the three-phase quantities do not sum to zero. In matrix form, the full transformation from three-phase voltages to $\alpha/\beta/0$ components is given by (4.1), where $\mathbf{T}_{(33)}$ is defined in (4.2) and the inverse transformation is $\mathbf{T}_{(33)}^{-1}$. Note that, to be a power-invariant transformation, $\mathbf{T}_{(33)}$ is an orthogonal matrix and so $\mathbf{T}_{(33)}^{-1} = \mathbf{T}_{(33)}^{\mathrm{T}}$. Under the assumption that the neutral point of each three-phase stator segment is isolated, and hence that the three-phase currents sum to zero, the transformation from three-phase currents to α/β quantities is given by (4.3), where $\mathbf{T}_{(32)}$ is defined in (4.4). Similarly, the transformation between line-to-line voltages and α/β components is given by (4.5), where $\mathbf{T}_{(22)}$ is defined in (4.6).

$$\begin{bmatrix} V_\alpha \\ V_\beta \\ V_0 \end{bmatrix} = \mathbf{T}_{(33)} \begin{bmatrix} V_\mathrm{a} \\ V_\mathrm{b} \\ V_\mathrm{c} \end{bmatrix} \tag{4.1}$$

where

$$\mathbf{T}_{(33)} = \sqrt{\frac{2}{3}} \begin{bmatrix} 1 & -\frac{1}{2} & -\frac{1}{2} \\ 0 & \frac{\sqrt{3}}{2} & -\frac{\sqrt{3}}{2} \\ \frac{1}{\sqrt{2}} & \frac{1}{\sqrt{2}} & \frac{1}{\sqrt{2}} \end{bmatrix} \tag{4.2}$$

$$\begin{bmatrix} I_\alpha \\ I_\beta \end{bmatrix} = \mathbf{T}_{(32)} \begin{bmatrix} I_\mathrm{a} \\ I_\mathrm{b} \end{bmatrix} \tag{4.3}$$

where

$$\mathbf{T}_{(32)} = \begin{bmatrix} \sqrt{\frac{3}{2}} & 0 \\ \frac{1}{\sqrt{2}} & \sqrt{2} \end{bmatrix} \tag{4.4}$$

$$\begin{bmatrix} V_\alpha \\ V_\beta \end{bmatrix} = \mathbf{T}_{(22)} \begin{bmatrix} V_{(\mathrm{ab})} \\ V_{(\mathrm{bc})} \end{bmatrix} \tag{4.5}$$

where

$$\mathbf{T}_{(22)} = \begin{bmatrix} \sqrt{\frac{2}{3}} & \frac{1}{\sqrt{6}} \\ 0 & \frac{1}{\sqrt{2}} \end{bmatrix} \tag{4.6}$$

4.2 Transformation between α/β and d/q frames

Stator quantities in the stationary α/β reference frame can be subsequently transformed to a d/q reference frame that is fixed to and moves with the reaction plate [85, 142, 143]. This approach was first introduced by Park in the late 1920s and is common practice. Transforming all reaction plate and stator quantities to this shared reaction plate reference frame results in simpler equations to describe the dynamic behaviour of the motor.

The well-known rotation matrix, that performs a rotation in Euclidean space, is used to transform quantities between the stationary frame and the d/q frame (as a function of the space angle, θ, between the two frames). Since the positive $\hat{\boldsymbol{x}}$ and $\hat{\boldsymbol{\theta}}$ directions are chosen to be from left to right (as shown in figure 4.3) but the rotation matrix is defined for an anti-clockwise rotation, the transformation from the stationary α/β frame to the moving d/q frame is given by (4.7).

$$\begin{aligned}\mathbf{T}_{(2r)}(\theta) &= \begin{bmatrix} \cos(-\theta) & -\sin(-\theta) \\ \sin(-\theta) & \cos(-\theta) \end{bmatrix} \\ &= \begin{bmatrix} \cos(\theta) & \sin(\theta) \\ -\sin(\theta) & \cos(\theta) \end{bmatrix}\end{aligned} \tag{4.7}$$

Any zero-sequence component remains unchanged in transforming to the d/q frame and so the full transformation is given by (4.8).

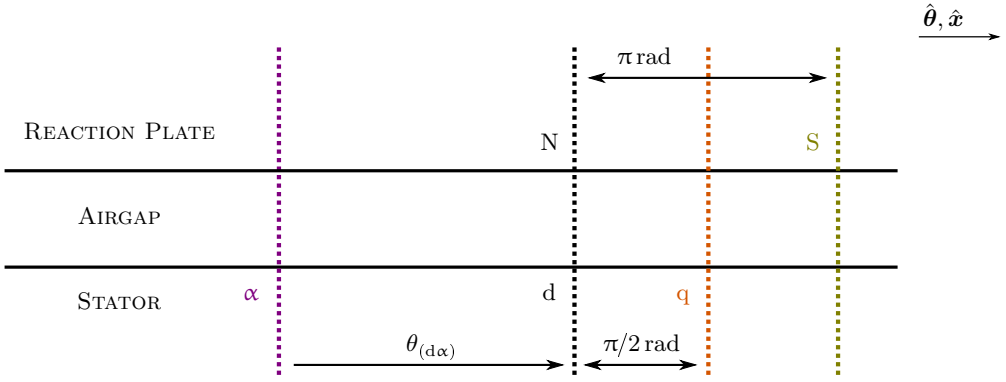

Figure 4.3: d/q axes in relation to α/β axes

$$\mathbf{T}_{(3r)}(\theta) = \begin{bmatrix} \cos(\theta) & \sin(\theta) & 0 \\ -\sin(\theta) & \cos(\theta) & 0 \\ 0 & 0 & 1 \end{bmatrix} \tag{4.8}$$

The angular displacement, $\theta \equiv \theta_{(\mathrm{d}\alpha)}$, is calculated from the actual displacement between the stationary frame and d/q moving frame, $x_{(\mathrm{d}\alpha)}$ according to (4.9). (π rad corresponds to one pole pitch, τ.)

$$\theta = \frac{\pi}{\tau} x_{(\mathrm{d}\alpha)} \tag{4.9}$$

MATLAB® and Simulink® implementations of the d/q transformation are provided in appendix B.2.

4.3 d/q Motor equations

4.3.1 Electrical

For each phase of each stator section, the resulting voltage across the winding resistance equals the supply voltage minus the emf caused by the change in magnetic flux linking with the coils with time (according to Faraday's Law). This relationship is expressed in (4.10). It is common practice to express each flux linkage as the product of current and inductance before transforming to the d/q axes. However, transforming the flux linkages directly is less restrictive because it is valid even for asymmetrical or nonlinear magnetic systems, where the inductances can be functions of the reaction plate position [85]. The stator voltage equations introduced here are thus universal and only the current-to-flux relationship needs to be adapted in the case of asymmetry or nonlinearity.

$$\begin{bmatrix} R_\mathrm{a} & 0 & 0 \\ 0 & R_\mathrm{b} & 0 \\ 0 & 0 & R_\mathrm{c} \end{bmatrix} \begin{bmatrix} I_\mathrm{a} \\ I_\mathrm{b} \\ I_\mathrm{c} \end{bmatrix} = \begin{bmatrix} V_\mathrm{a} \\ V_\mathrm{b} \\ V_\mathrm{c} \end{bmatrix} - \begin{bmatrix} \dot{\lambda}_\mathrm{a} \\ \dot{\lambda}_\mathrm{b} \\ \dot{\lambda}_\mathrm{c} \end{bmatrix} \tag{4.10}$$

As derived in appendix B.3, the electrical matrix equation for the motor in the d/q frame is given by (4.11), under the assumption that all three phase resistances are equal. This is a valid assumption, even for a modular stator design, so long as the phase windings have an equal number of turns (i.e. same length of wire).

$$R\begin{bmatrix} I_\mathrm{d} \\ I_\mathrm{q} \\ 0 \end{bmatrix} = \begin{bmatrix} V_\mathrm{d} \\ V_\mathrm{q} \\ V_0 \end{bmatrix} - \begin{bmatrix} \dot{\lambda}_\mathrm{d} \\ \dot{\lambda}_\mathrm{q} \\ \dot{\lambda}_0 \end{bmatrix} - \omega \begin{bmatrix} 0 & -1 & 0 \\ 1 & 0 & 0 \\ 0 & 0 & 0 \end{bmatrix} \begin{bmatrix} \lambda_\mathrm{d} \\ \lambda_\mathrm{q} \\ \lambda_0 \end{bmatrix} \tag{4.11}$$

4.3.2 Flux linkage

If it is assumed that magnetic saturation of the stator does not occur, the principle of superposition can be applied to the flux linkages and any variations in the self and mutual inductances are only a function of the reaction plate position (and not the magnitude of the currents). Similarly, the flux that links with each phase of the windings due to the permanent magnets is only a function of the reaction plate position, x. This is expressed in (4.12).

$$\begin{bmatrix} \lambda_\mathrm{a} \\ \lambda_\mathrm{b} \\ \lambda_\mathrm{c} \end{bmatrix} = \begin{bmatrix} L_{(\mathrm{aa})}(x) & L_{(\mathrm{ab})}(x) & L_{(\mathrm{ac})}(x) \\ L_{(\mathrm{ba})}(x) & L_{(\mathrm{bb})}(x) & L_{(\mathrm{bc})}(x) \\ L_{(\mathrm{ca})}(x) & L_{(\mathrm{cb})}(x) & L_{(\mathrm{cc})}(x) \end{bmatrix} \begin{bmatrix} I_\mathrm{a} \\ I_\mathrm{b} \\ I_\mathrm{c} \end{bmatrix} + \begin{bmatrix} \lambda_\mathrm{ma}(x) \\ \lambda_\mathrm{mb}(x) \\ \lambda_\mathrm{mc}(x) \end{bmatrix}$$

$$\therefore \quad \begin{bmatrix} \lambda_\mathrm{a} \\ \lambda_\mathrm{b} \\ \lambda_\mathrm{c} \end{bmatrix} = \boldsymbol{L}_{(\mathrm{abc})}(x) \begin{bmatrix} I_\mathrm{a} \\ I_\mathrm{b} \\ I_\mathrm{c} \end{bmatrix} + \begin{bmatrix} \lambda_\mathrm{ma}(x) \\ \lambda_\mathrm{mb}(x) \\ \lambda_\mathrm{mc}(x) \end{bmatrix} \tag{4.12}$$

As derived in appendix B.3.2, the corresponding inductance matrix and permanent magnet flux linkages in the d/q/0 reference frame are given by (4.13) and (4.14), respectively.

$$\boldsymbol{L}_{(\mathrm{dq0})}(x) = \begin{bmatrix} L_{(\mathrm{dd})}(x) & L_{(\mathrm{dq})}(x) & L_{(\mathrm{d0})}(x) \\ L_{(\mathrm{qd})}(x) & L_{(\mathrm{qq})}(x) & L_{(\mathrm{q0})}(x) \\ L_{(\mathrm{0d})}(x) & L_{(\mathrm{0q})}(x) & L_{(00)}(x) \end{bmatrix} = \mathbf{T}_{(3\mathrm{r})}\mathbf{T}_{(33)}\boldsymbol{L}_{(\mathrm{abc})}(x)\mathbf{T}_{(33)}^{-1}\mathbf{T}_{(3\mathrm{r})}^{-1} \tag{4.13}$$

$$\boldsymbol{\lambda}_{\mathrm{m(dq0)}}(x) = \begin{bmatrix} \lambda_{\mathrm{md}}(x) \\ \lambda_{\mathrm{mq}}(x) \\ \lambda_{\mathrm{m0}}(x) \end{bmatrix} = \mathbf{T}_{(3\mathrm{r})}\mathbf{T}_{(33)} \begin{bmatrix} \lambda_{\mathrm{ma}}(x) \\ \lambda_{\mathrm{mb}}(x) \\ \lambda_{\mathrm{mc}}(x) \end{bmatrix} \tag{4.14}$$

Therefore, the matrix equation for the d/q/0 flux linkages is (4.15). The implementation of the flux linkage relationships in Simulink® is provided in appendix B.3.2.

$$\begin{bmatrix} \lambda_{\mathrm{d}} \\ \lambda_{\mathrm{q}} \\ \lambda_{0} \end{bmatrix} = \boldsymbol{L}_{(\mathrm{dq0})}(x) \begin{bmatrix} I_{\mathrm{d}} \\ I_{\mathrm{q}} \\ 0 \end{bmatrix} + \boldsymbol{\lambda}_{\mathrm{m(dq0)}}(x) \tag{4.15}$$

The MATLAB® function to perform the inductance and PM flux linkage transformations is also provided in appendix B.3.2.

4.3.3 Power and electromagnetic force

Although the d/q voltages, currents and flux linkages are dependent on the angular velocity of the moving reference frame, the electrical input power to the motor, $P_{(\mathrm{in})}$, is shown in appendix B.3.3 to be invariant. Thus, substituting for the d-axis and q-axis voltages from (4.11) in the expression for the input power yields (4.16).

$$\begin{aligned} P_{(\mathrm{in})} &= V_{\mathrm{d}}I_{\mathrm{d}} + V_{\mathrm{q}}I_{\mathrm{q}} \\ &= \left(RI_{\mathrm{d}} + \dot{\lambda}_{\mathrm{d}} - \lambda_{\mathrm{q}}\omega\right)I_{\mathrm{d}} + \left(RI_{\mathrm{q}} + \dot{\lambda}_{\mathrm{q}} + \lambda_{\mathrm{d}}\omega\right)I_{\mathrm{q}} \\ &= \left(RI_{\mathrm{d}}^2 + RI_{\mathrm{q}}^2\right) + \left(I_{\mathrm{d}}\dot{\lambda}_{\mathrm{d}} + I_{\mathrm{q}}\dot{\lambda}_{\mathrm{q}}\right) + \omega\left(I_{\mathrm{q}}\lambda_{\mathrm{d}} - I_{\mathrm{d}}\lambda_{\mathrm{q}}\right) \\ &= P_{(\mathrm{loss})} + P_{(\mathrm{field})} + P_{(\mathrm{mech})} \end{aligned} \tag{4.16}$$

As shown in (4.16), the resistive losses (I^2R) and stored magnetic field components ($I\dot{\lambda}$) of the power are apparent, where the remaining term can only correspond to the mechanical power output, $P_{(\text{mech})}$. Note that, friction, iron and windage losses are thus grouped under the mechanical power.

The mechanical power can also be expressed as (4.17) in terms of linear velocity and force. Therefore, by equating (4.16) and (4.17), as shown in (4.18), the electromagnetic force, $F_{(\text{em})}$, is obtained.

$$P_{(\text{mech})} = vF_{(\text{em})} = \left(\frac{\tau}{\pi}\omega\right) F_{(\text{em})} \tag{4.17}$$

$$\begin{aligned} P_{(\text{mech})} &= \omega \left(I_{\text{q}}\lambda_{\text{d}} - I_{\text{d}}\lambda_{\text{q}}\right) = \frac{\tau}{\pi}\omega F_{(\text{em})} \\ \therefore \qquad F_{(\text{em})} &= \frac{\pi}{\tau}\left(I_{\text{q}}\lambda_{\text{d}} - I_{\text{d}}\lambda_{\text{q}}\right) \end{aligned} \tag{4.18}$$

4.4 Reaction plate mechanical dynamics

The movement of the reaction plate relative to the stator is governed by Newton's Second Law of Motion. As given by (4.19), the sum of electromagnetic force contributions from all the stator sections, minus the frictional force, F_{f}, and any additional load force, F_{L}, causes an acceleration of the reaction plate, $a_{\text{r}} = \ddot{x}_{\text{r}}$, that is inversely proportional to the moving mass, M. For a vertical hoisting arrangement, F_{L} includes the weight of the reaction plate and conveyance.

$$\sum_i F_{(\text{em})\underset{\sim}{\text{S}}_i} - F_{\text{f}} - F_{\text{L}} = M\ddot{x}_{\text{r}} \tag{4.19}$$

Chapter 5

Control Strategy

This chapter describes a novel feeding and control strategy for segmented long-stator linear motors, with stator sections that are much shorter than the reaction plate.

5.1 Methodology

The crux of the presented control strategy is that, for each reaction plate, measurements of the currents flowing within the windings of a single representative stator section are used to control the power supply to all of the sections that interact with it. Since the chosen representative stator section is always "fully-covered" by the reaction plate, it is electrically indistinguishable from a rotating machine. This is because the spatial air-gap flux quantities are periodic over the length of the section, as each section has an integral number of magnetic poles. Therefore, vector motor control techniques originally developed for traditional rotating machines can be applied to a segmented long-stator LSM with the inclusion of an additional switching and control layer. The force reference provided to the vector motor controller is scaled by the ratio of the section length to the actual active air-gap length.

The requirement that the active representative stator section is always covered by the reaction plate necessitates that the stator is segmented into sections that are shorter than half of the reaction plate length. Nevertheless, the strategy is for a three-phase winding and each stator section comprises several magnetic poles. Clearly, segmentation need not necessarily be with physically-distinct stator modules but could merely entail the provision of connections to different sections of the winding.

Furthermore, the motor sections must be of equal length and must interact consistently with the reaction plate (e.g. maintain a constant air-gap). Evidently, the proposed arrangement is best suited to a high-force application such as ropeless hoisting, where relatively long reaction plates are appropriate and can be accommodated.

5.1.1 Energising fully-covered sections

In the ordinary case, only those stator sections that fully interact with the reaction plate are energised, as shown in figure 5.1. These fully-covered sections are connected in parallel to the supply using electrical contactors (solid-state or mechanical). Note that, although depicted with a single switch per section and a single supply line, in reality these are three-phase contactors that connect to a three-phase supply from the inverter. The sections are supplied with the same three-phase terminal voltage and, considering that they are electrically identical, their resulting phase currents are the same in steady-state. Consequently, the energised sections contribute equally to the propulsion force of the motor. The compromise is that the full length of the reaction plate is not utilised to produce thrust.

The force reference supplied to the motor controller must be inversely scaled by the number of energised sections. This is because the number of fully-covered sections varies by one section when the reaction plate length is not an exact multiple of the section length. The number of energised sections could be kept constant by delaying the switching in of the front unenergised section until the back energised section is switched out. However, this reduces the average reaction plate utilisation and, for the same propulsion force, increases the average demand on the stator sections.

When a new section is switched in, the rise time for the currents to be established in that section are expected to closely match the fall time for the currents in the other energised sections. (The magnitude of the current per energised section reduces owing to the lower force reference supplied to the motor controller.) Likewise, when a section is switched out, its currents die down (through the path provided by the contactor snubber circuit) with a fall time that is similar to the rise time for the currents in the sections that remain energised. This is because these time constants are governed by the winding inductance and resistance, which are closely matched for all of the covered sections. Hence, the force disturbance that the outer-loop position or speed controller needs to reject should be minimal if the change in force

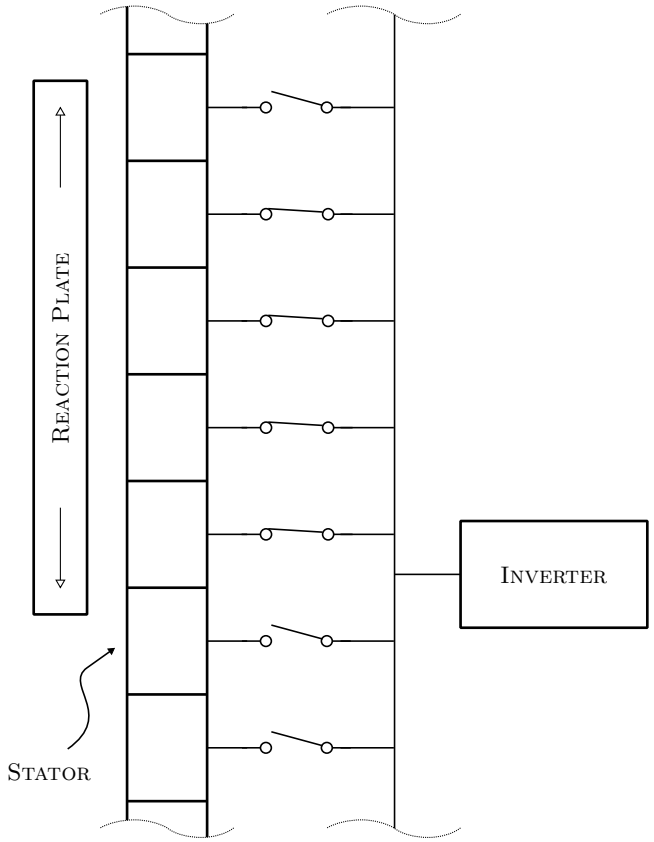

Figure 5.1: Energising only the stator sections that are fully covered

reference to the motor controller is closely synchronised with the actual switching-in or switching-out of a section. The characteristics of the type of contactors that are used should be considered in order to achieve this switching synchronisation (e.g. thyristor-based solid-state contactors naturally commutate until a zero-current crossing). Clearly, the greater the number of stator sections per reaction plate length, the higher the reaction plate utilisation and the lower the potential force disturbance to the system when energising and de-energising sections.

5.1.2 Representative sections

Vector control of the motor requires feedback of the motor's state in the form of a measurement of the stator currents. Since the currents in the covered sections should be equal, only measurements of the currents flowing in a designated representative stator section are used by the motor vector control scheme to control the supply voltage at each instant. Additionally, a measurement of the reaction plate position is provided to the motor controller, unless a 'sensorless' technique is used.

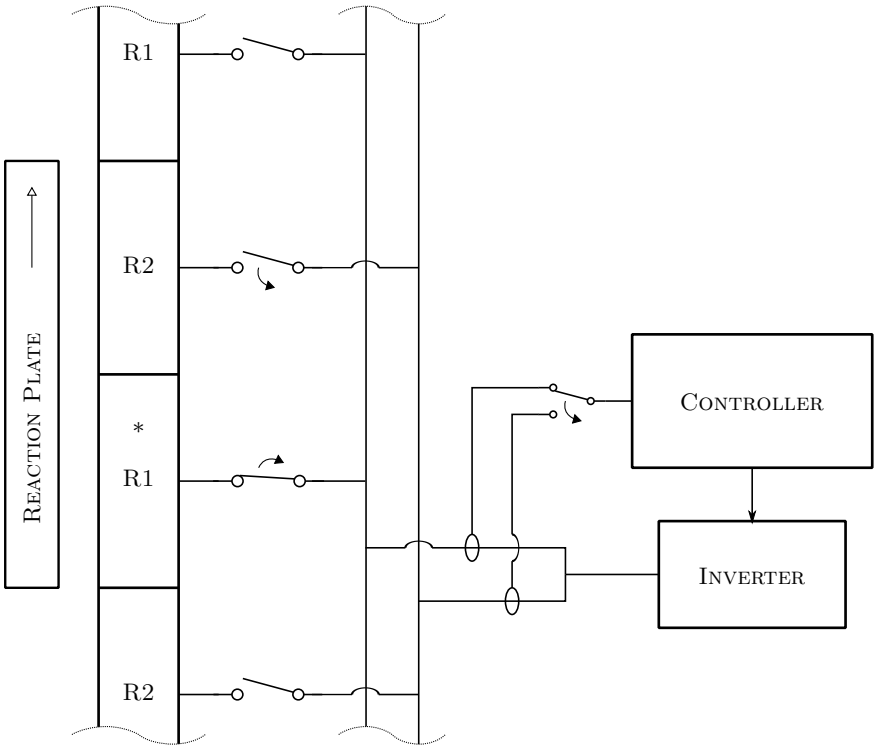

Figure 5.2: Handover of active representative stator section

The simplest manifestation of this strategy is depicted in figure 5.2. The stator sections are half of the reaction plate length and only a single section is energised at a time. All of the sections are designated to be representative sections and these representative sections are divided into two sets (R1 and R2). The active representative section is denoted in the diagrams with *. Alternate representative sections are grouped into the same set and share a supply bus from the inverter. With the reaction plate moving upwards and in the position shown, only the active representative section is energised and the motor controller is using the currents flowing in this section to control the inverter and hence the voltage supply. To continue upwards, R1 must be de-energised and R2 must be energised simultaneously. Moreover, the motor controller must then use the measurement of current flowing in R2 to control the inverter. Thus, at the same time, the current measurement must also change from the R1 bus to the R2 bus. Clearly, the multiplexing between the current sensors may be performed in software.

This simple arrangement is not recommended in practice, however, because a representative section should only be selected once any switching transients have diminished. Otherwise, the motor controller is likely to detect and attempt to

counter a significant disturbance. Furthermore, only half of the reaction plate length is utilised.

A better arrangement is thus shown in figure 5.3. In this case, the sections are a third of the length of the reaction plate and, again, are all designated to be representative sections (allocated alternately to the two supply buses). The handover from one representative section to the next now occurs while both energised representative sections are in an identical state (figure 5.3a). In addition, the handover occurs when none of the sections are being energised or de-energised, as that only happens when the reaction plate reaches the position shown in figure 5.3b.

The same segmentation strategy applies for a reaction plate spanning up to four sections. However, the number of energised sections could then alternate between two and three sections, since the front and back sections need not be energised and de-energised simultaneously. So, care must be taken not to switch to a representative measurement for a bus that is feeding more than one section. To overcome this limitation, and accommodate reaction plates that span more than four sections, the general arrangement shown in figure 5.4 is proposed.

As depicted, there may be any fixed number of ordinary sections between the representative sections. All of these non-representative sections connect to a third bus powered by the inverter. The currents flowing in this third bus are never used by the motor vector controller as feedback. However, a high-level controller should still monitor all of the bus currents in order to detect a fault condition (using knowledge of how many sections are meant to be energised off each bus at a particular point in time).

The two extremes of reaction plate length relative to section length are shown. Operation with the minimum reaction plate length requires changing to a new active representative section at the moment when it is energised. As previously discussed, this is not recommended. The maximum length is restricted by the requirement that only a single section belonging to the active representative set may be energised. However, it is also not recommended to operate with this maximum reaction plate length because there may be switching transients from the simultaneous de-energising of a section on the newly-selected active representative bus.

Significantly, with the proposed scheme, the reaction plate can transition across the

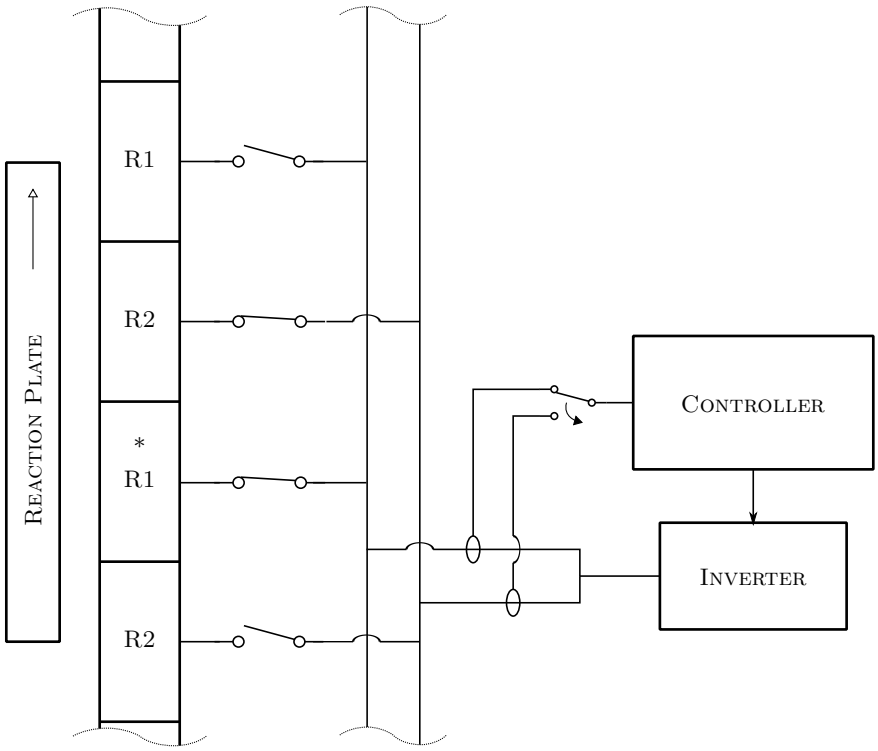

(a) handover of active representative section

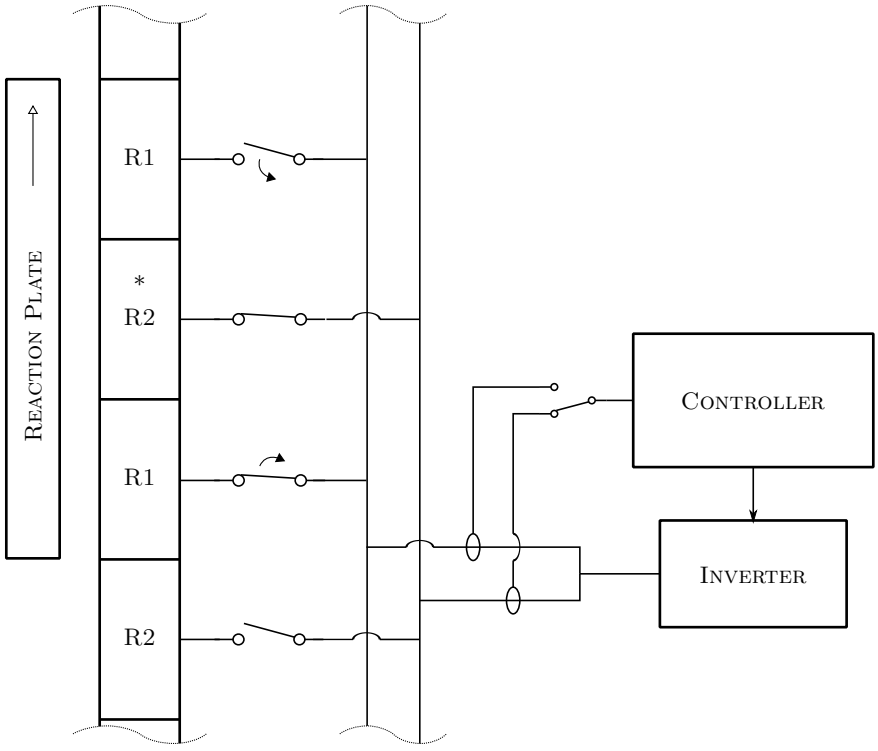

(b) switching in front section and switching out back section

Figure 5.3: Improved handover of active representative stator section

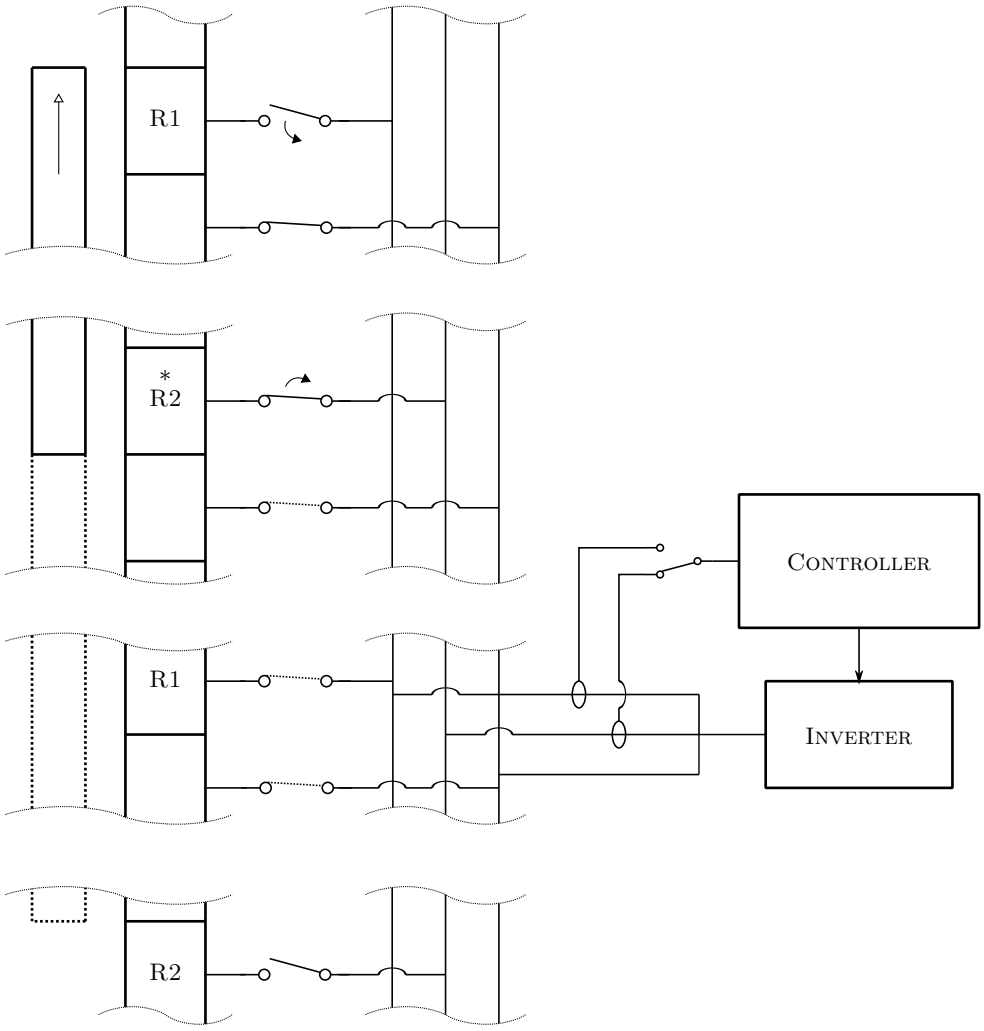

Figure 5.4: General arrangement of the feeding strategy

sections of a segmented long-stator LSM with only a single inverter.

5.1.3 Energising partially-covered sections

To utilise the full length of the reaction plate, it may be desirable to energise those sections at the front and back that are only partially covered. However, with the presented strategy of feeding the stator sections in parallel, this is only feasible for slow speed operation (low back-emf) and with motors that have a relatively large air-gap (small difference in covered versus uncovered winding inductance). Otherwise, much higher currents flow in the partially-covered sections than the covered sections. This is undesirable because it results in a force disturbance, high copper losses and a varying distribution of thrust along the reaction plate. Investigation into a means

of possibly further modulating the voltage to these outer partially-covered sections using the stator-side solid-state contactors is left as a topic for further research. Such a method would need to lower the effective voltage to these partially-covered sections in proportion to their coverage.

If, however, the partially-covered sections are energised, the maximum length for the reaction plate shown in figure 5.4 is reduced by one section. Also, the force reference for the motor vector controller must be scaled by the length of a section in proportion to the full reaction plate length.

5.1.4 Multiple independent conveyances

Several conveyances can be independently controlled along the length of stator by designating a separate inverter and associated motor controller to each reaction plate. Thus, several stator-side switches are then used to connect each section to the relevant output bus of each inverter. A high-level controller is required, though, to ensure that the conveyances never collide. A significant benefit with the presented strategy is that the conveyances can be operated with zero headway when only energising fully-covered sections. If partially-covered sections are also energised, this minimum headway only increases to the length of a single short section.

5.1.5 Multiple stator blocks

For very long lengths of stator, it can be advantageous to demarcate several stator 'blocks', where each block comprises many stator sections. The described feeding strategy is then applied to each stator block separately. This both limits how long the inverter supply buses need to be and reduces the number of required stator-side switches (corresponding to the maximum number of conveyances allowed within the block as opposed to the whole stator).

Handover of a conveyance from one stator block to the next is straightforward and occurs with a 'master' and 'slave' arrangement, as shown in figure 5.5. When approaching a block boundary, an available controller and inverter set must be allocated to the incoming conveyance. Clearly, the conveyance may not enter a block unless there is an unused set available. When the conveyance enters the new block, the slave controller simply mimics the master controller's output so that the two

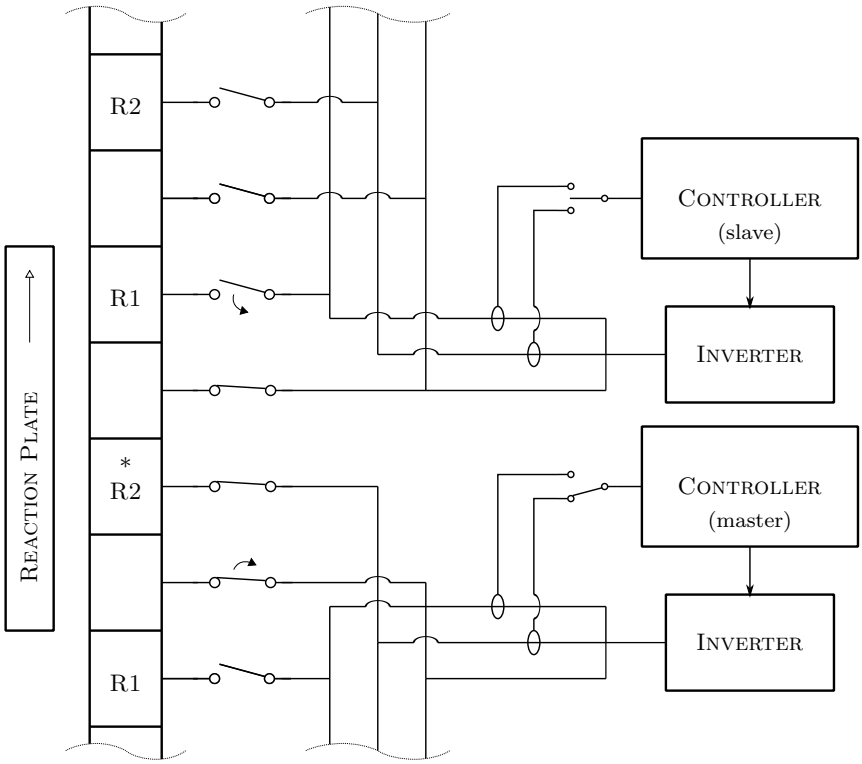

(a) top controller is the slave

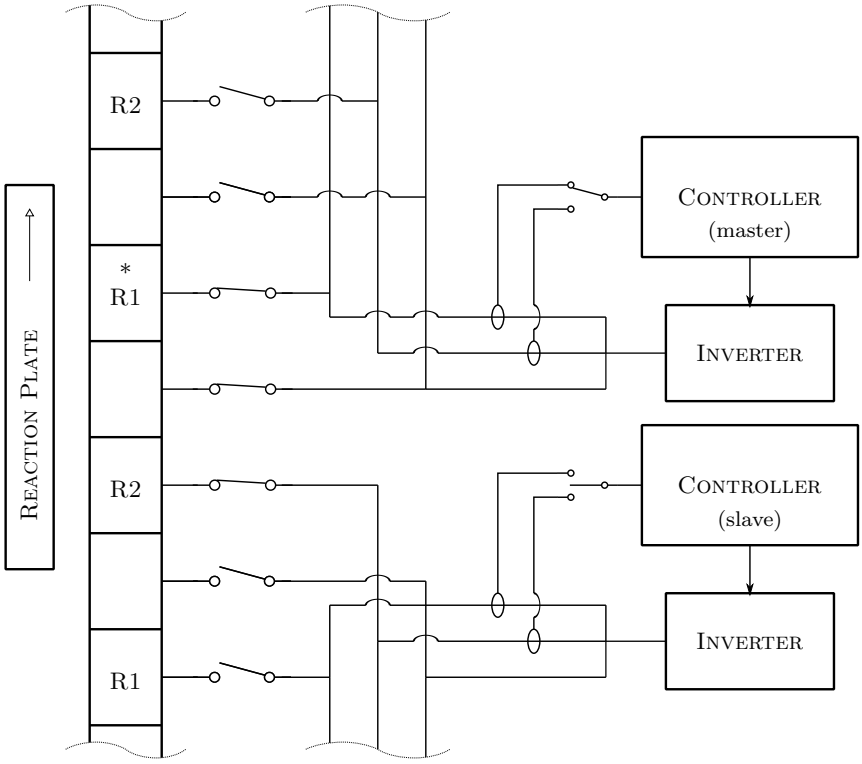

(b) top controller is the master

Figure 5.5: Handover between stator blocks

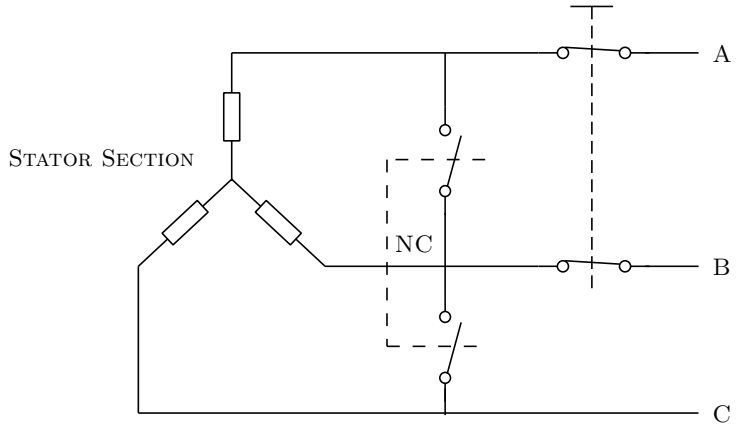

Figure 5.6: Three-phase contactor arrangement

inverter outputs are the same. This is depicted in figure 5.5a. When the reaction plate has moved far enough into the new block and the active representative section changes to a representative section in this new block, the 'master' and 'slave' roles are reversed, as shown in 5.5b.

5.1.6 Three-phase contactor arrangement

If only a single reaction plate is allowed per block and hence there is only one inverter per block, only two of the three phases need to be connected or disconnected from the inverter. Also, when the motor is used for ropeless hoisting or for an inclined track, a failsafe mechanism can be incorporated to cater for a power failure. By using normally-closed electromechanical contactors to short the section windings when power is lost, the motor defaults to a passive regenerative braking mode. This significantly reduces a free-falling conveyance's terminal velocity since currents are induced in the windings and energy is dissipated in their internal resistance. A mechanical brake or shock-absorbing hydraulic buffer can then be used to stop the slow-moving conveyance.

The typical contactor configuration for three-phase windings is shown in figure 5.6. As explained, a contactor is not needed for the third phase if there is only one inverter for the stator block.

5.1.7 Sensorless control

To achieve sensorless control, a sensorless motor vector control technique can be used. However, it is necessary to detect the approximate initial position of the reaction plate within the stator block to determine the active representative section and which other sections are also energised. Evidently, for multiple conveyances within a stator block, the initial position estimator would need to detect the approximate positions of all of the conveyances. Thereafter, an incremental position estimate from the sensorless motor control technique can be used by the high-level controller. It is proposed that a binary search based on winding inductance can be used to find the approximate initial position because the inductance of each winding is dependent on how much of it is covered by the reaction plate. The inductance of a portion of the winding can be effectively measured by timing the current decay after the relevant section of stator is briefly energised. The time-constant for this decay is directly proportional to the inductance since the winding resistance is constant. After the approximate position is determined, a method such as the one proposed by Kim et al. [144] may be applied using the representative section to obtain the precise position of the conveyance within a single magnetic pole-pitch. However, the testing of a full sensorless approach remains a topic for further research.

5.2 Feeding efficiency and reaction plate utilisation

For traditional long-stator systems, where the stator sections are longer than the reaction plate, Kim et al. [2] derive an appropriate measure of stator feeding efficiency, given by (5.1). This expression is derived as the ratio of the time taken for the reaction plate to travel a distance equal to its length, divided by the time that the stator section is energised.

$$\begin{aligned} \eta_{\mathrm{s}} &= \frac{\frac{l_{\mathrm{r}}}{\dot{x}}}{\frac{l_{\mathrm{s}}}{\dot{x}} + \frac{l_{\mathrm{r}}}{\dot{x}}} \\ &= \frac{l_{\mathrm{r}}}{l_{\mathrm{r}} + l_{\mathrm{s}}} \end{aligned} \tag{5.1}$$

For the proposed control strategy, where the stator sections are shorter than the reaction plate, there are two scenarios in terms of feeding efficiency depending on

whether or not those stator sections that are only partially covered by the reaction plate are energised. If only fully-covered stator sections are energised, the entire length of energised stator contributes to the motor's force production. However, the full length of the reaction plate is not utilised. Conversely, if partially-covered stator sections are energised, the entire length of reaction plate is utilised but there are portions of energised stator that don't contribute to the propulsion force.

The stator feeding efficiency, η_{s}, is thus defined as an average measure of the length of active air-gap (contributing to force production) compared to the length of energised stator, with the reaction plate moving at constant velocity. Similarly, the reaction plate utilisation, η_{r}, is the average portion of the reaction plate that contributes to force production, when it is moving at constant velocity. Both the feeding efficiency and reaction plate utilisation are functions of the number of magnetic poles per stator section compared to the number of poles on the reaction plate.

If only fully-covered stator sections are energised, the reaction plate utilisation can be calculated by considering the number of stator sections that are fully-covered (and thus, energised) as the leading edge of the reaction plate moves over one complete stator section. Since the reaction plate is moving at constant velocity, the average number of stator sections energised with *time* is equal to the average number of stator section energised with the reaction plate's *displacement* over one stator section. The maximum number of stator sections that the reaction plate can fully cover is found by dividing the number of reaction plate poles, N_{pr}, by the number of poles per stator section, N_{ps}, and rounding down to the nearest integer (written using the 'floor' operator as $\left\lfloor \frac{N_{\mathrm{pr}}}{N_{\mathrm{ps}}} \right\rfloor$). The number of reaction plate poles for which the reaction plate can overlap the next stator section whilst still fully covering this maximum number of stator sections, is given by N_{pr} modulo N_{ps} (the remainder of $\frac{N_{\mathrm{pr}}}{N_{\mathrm{ps}}}$, calculated as $N_{\mathrm{pr}} - \left\lfloor \frac{N_{\mathrm{pr}}}{N_{\mathrm{ps}}} \right\rfloor N_{\mathrm{ps}}$). For the reaction plate's displacement over the remaining poles of the stator section, one fewer stator sections is energised. Therefore, the reaction plate utilisation is given by (5.2).

$$\begin{aligned}\eta_{\mathrm{r}} &= \left(\frac{N_{\mathrm{pr}} - \left\lfloor \frac{N_{\mathrm{pr}}}{N_{\mathrm{ps}}} \right\rfloor N_{\mathrm{ps}}}{N_{\mathrm{ps}}}\right) \frac{\left\lfloor \frac{N_{\mathrm{pr}}}{N_{\mathrm{ps}}} \right\rfloor N_{\mathrm{ps}}}{N_{\mathrm{pr}}} \\ &\quad + \left(\frac{N_{\mathrm{ps}} - \left(N_{\mathrm{pr}} - \left\lfloor \frac{N_{\mathrm{pr}}}{N_{\mathrm{ps}}} \right\rfloor N_{\mathrm{ps}}\right)}{N_{\mathrm{ps}}}\right) \frac{\left(\left\lfloor \frac{N_{\mathrm{pr}}}{N_{\mathrm{ps}}} \right\rfloor - 1\right) N_{\mathrm{ps}}}{N_{\mathrm{pr}}} \\ &= \frac{\left(N_{\mathrm{pr}} - \left\lfloor \frac{N_{\mathrm{pr}}}{N_{\mathrm{ps}}} \right\rfloor N_{\mathrm{ps}}\right) \left\lfloor \frac{N_{\mathrm{pr}}}{N_{\mathrm{ps}}} \right\rfloor + \left(N_{\mathrm{ps}} - \left(N_{\mathrm{pr}} - \left\lfloor \frac{N_{\mathrm{pr}}}{N_{\mathrm{ps}}} \right\rfloor N_{\mathrm{ps}}\right)\right) \left(\left\lfloor \frac{N_{\mathrm{pr}}}{N_{\mathrm{ps}}} \right\rfloor - 1\right)}{N_{\mathrm{pr}}}\end{aligned} \tag{5.2}$$

Similarly, for the case where partially-covered sections are energised, the stator feeding efficiency can be calculated according to (5.3).

$$\begin{aligned}\eta_{\mathrm{s}} &= \left(\frac{N_{\mathrm{pr}} - \left\lfloor \frac{N_{\mathrm{pr}}}{N_{\mathrm{ps}}} \right\rfloor N_{\mathrm{ps}}}{N_{\mathrm{ps}}}\right) \frac{N_{\mathrm{pr}}}{\left(\left\lfloor \frac{N_{\mathrm{pr}}}{N_{\mathrm{ps}}} \right\rfloor + 2\right) N_{\mathrm{ps}}} \\ &\quad + \left(\frac{N_{\mathrm{ps}} - \left(N_{\mathrm{pr}} - \left\lfloor \frac{N_{\mathrm{pr}}}{N_{\mathrm{ps}}} \right\rfloor N_{\mathrm{ps}}\right)}{N_{\mathrm{ps}}}\right) \frac{N_{\mathrm{pr}}}{\left(\left\lfloor \frac{N_{\mathrm{pr}}}{N_{\mathrm{ps}}} \right\rfloor + 1\right) N_{\mathrm{ps}}} \\ &= \frac{\left(N_{\mathrm{pr}} - \left\lfloor \frac{N_{\mathrm{pr}}}{N_{\mathrm{ps}}} \right\rfloor N_{\mathrm{ps}}\right) N_{\mathrm{pr}}}{\left(\left\lfloor \frac{N_{\mathrm{pr}}}{N_{\mathrm{ps}}} \right\rfloor + 2\right) N_{\mathrm{ps}}^2} + \frac{\left(N_{\mathrm{ps}} - \left(N_{\mathrm{pr}} - \left\lfloor \frac{N_{\mathrm{pr}}}{N_{\mathrm{ps}}} \right\rfloor N_{\mathrm{ps}}\right)\right) N_{\mathrm{pr}}}{\left(\left\lfloor \frac{N_{\mathrm{pr}}}{N_{\mathrm{ps}}} \right\rfloor + 1\right) N_{\mathrm{ps}}^2}\end{aligned} \tag{5.3}$$

Clearly, maximum feeding efficiency and reaction plate utilisation is achieved with the minimum number of poles per stator section (a single pole-pair). Thus, this feeding efficiency or reaction plate utilisation metric must be linked to other costs and used within the context of a system-level optimisation. The MATLAB® function implementations of (5.2) and (5.3) are provided in appendix D.2.

Chapter 6

Laboratory Prototype

This chapter provides details of the construction, characterisation, simulation and control of a laboratory prototype system used to demonstrate the linear motor feeding and control strategy.

6.1 Construction

Texchange Ltd generously donated five linear motor stator sections to form the basis for a laboratory prototype. The stator sections were originally designed for a prototype advanced weapons elevator for a next-generation United States Navy aircraft carrier. This elevator was designed with a linear motor for each corner of the load carrier, moving in unison. As shown in figure 6.1, the stator sections are intended to be used in a multilayer configuration (several mounted side-by-side, interacting with a corresponding number of reaction plate fins). This multilayer arrangement, with double-sided stator sections, provides for a high force density owing to a large air-gap surface area per volume. Also, with a symmetrical double-sided configuration there is ideally no resultant normal force on the reaction plates, which places significantly less strain on the mechanical guidance system.

For the purpose of demonstrating the proposed control strategy, however, a single-sided motor suffices. There is also adequate core material in the centre of the stator sections to provide return paths for the flux in this arrangement. Furthermore, it was unnecessary to incur the mechanical complexity of guiding the linear motor vertically and so the prototype is built with a horizontal track. A cross-sectional view of the prototype motor, showing the length of the reaction plate relative to the five stator

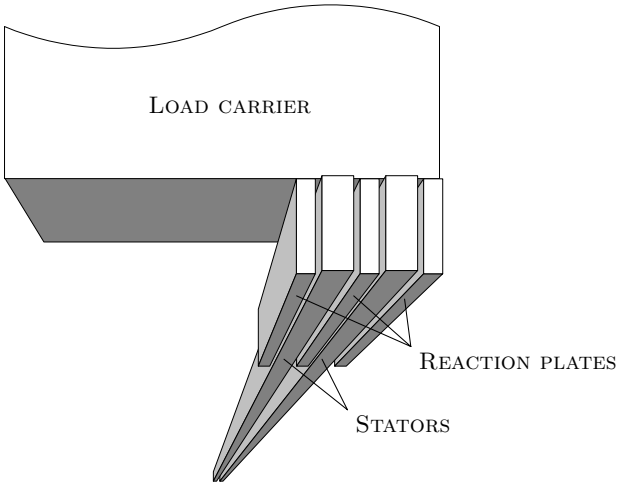

Figure 6.1: Multilayer linear motor

sections, is provided in figure 6.2. The motor is loaded using a suspended weight, connected to the one end of the reaction plate via two pulleys.

The dSPACE RTI1104 realtime control platform is used to implement all control and to interface with the inverter, measurement devices and solid-state contactors. The contactors independently connect each of the stator sections to the inverter output.

Appendix C details the construction of the prototype system and includes a complete set of engineering drawings of the motor.

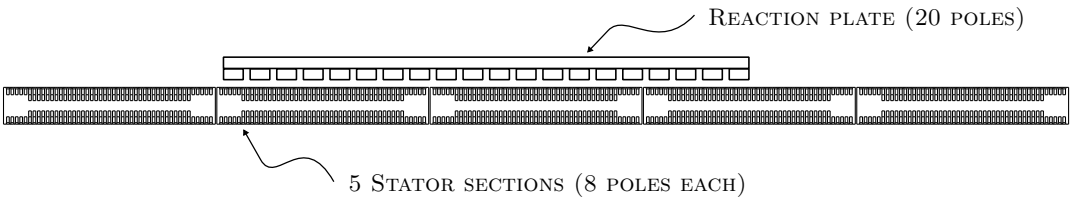

Figure 6.2: Cross-section of prototype motor

6.1.1 Stator sections

Each stator section winding spans 8 poles and is based on a double-layer, short-corded, three-phase winding (2 slots per pole per phase, short-corded by 1 slot). The pole pitch is 36 mm, with a slot width to tooth width ratio of 3:2. Figure 6.4a shows the portion of this double layer winding that can be self-contained within 48 slots

(corresponding to 8 poles). Since the stator section is modular, the winding must start and end as a single layer. With this winding arrangement, however, there is an unused slot at the end of the section and the end teeth are very thin and thus mechanically weak. Therefore, the actual winding design is as shown in figure 6.4b, where the unused slot is left uncut and the stator section boundary is shifted so that this additional thickness is distributed equally between the end teeth. From a mechanical perspective, the extra core thickness at the two ends of the section provides structural strength and space for through-rods to clamp the lamination stack and provide mounting points. There are 21 turns of 0,95 mm diameter wire per coil. Figure 6.3 shows how the lamination stack, end caps and winding overhang covers are assembled to form each section. The track is only five stator sections long owing to their high cost.

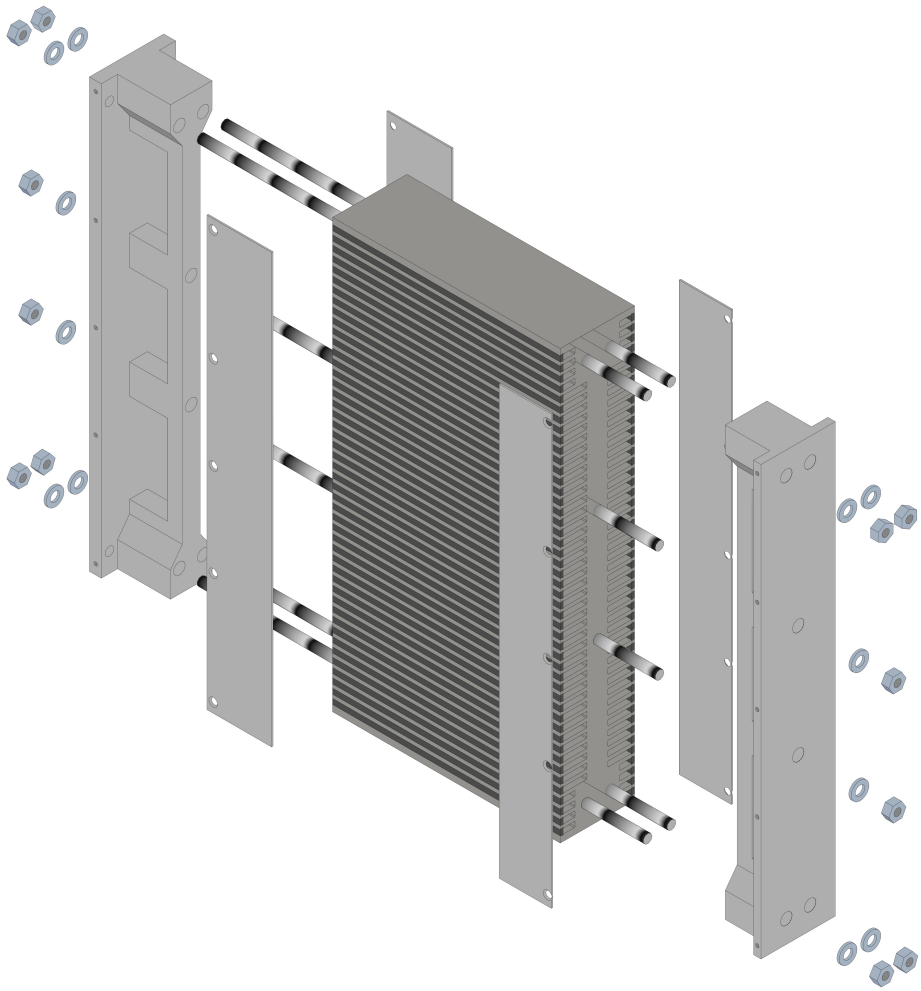

Figure 6.3: Stator section assembly

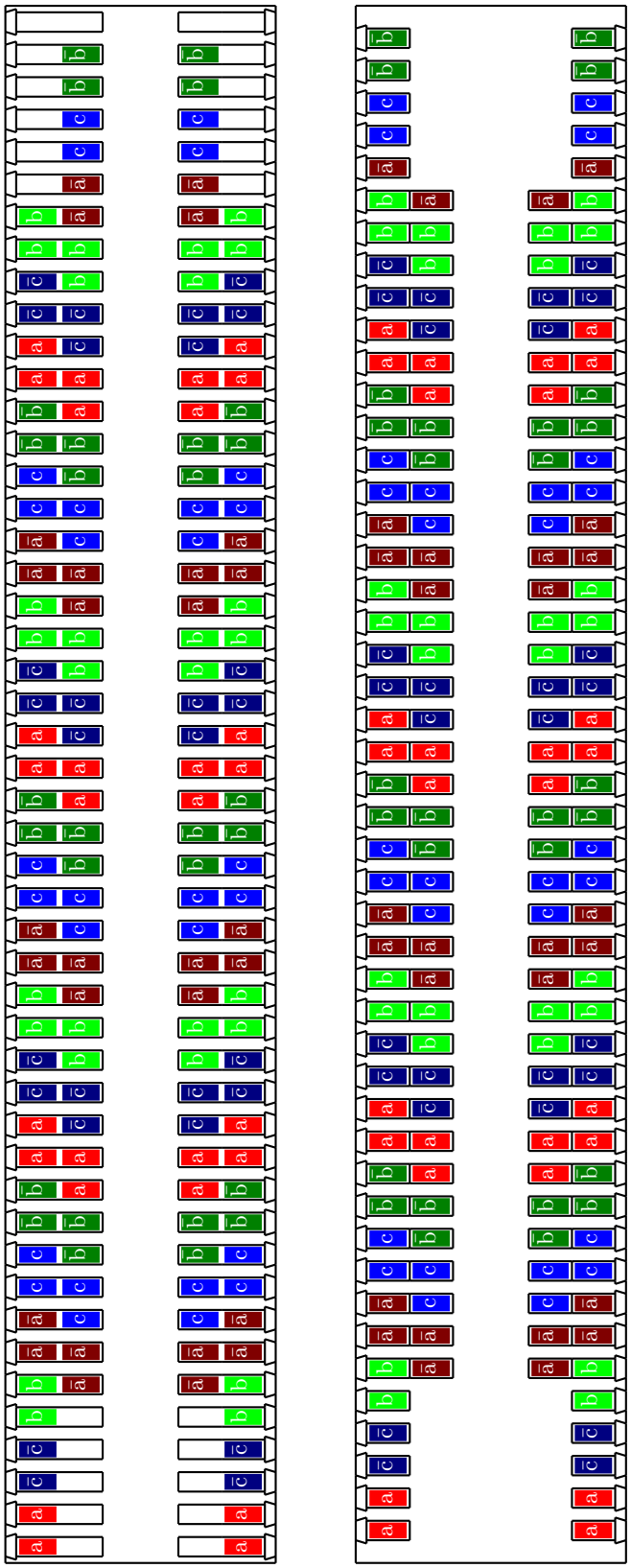

(a) Base winding pattern **(b)** Implemented winding

Figure 6.4: Stator section winding arrangement

6.1.2 Reaction plate

A straightforward surface-mount reaction plate was constructed using NdFeB-45H permanent magnets. The magnet span is 135° (27 mm) and nylon spacers and end covers are used to keep the magnets in position. The reaction plate was chosen to be 20 poles long as a compromise between the motor's stroke length and the number of covered stator sections. Thus, the reaction plate covers $2\frac{1}{2}$ stator sections. Figure 6.5 shows the reaction plate assembly.

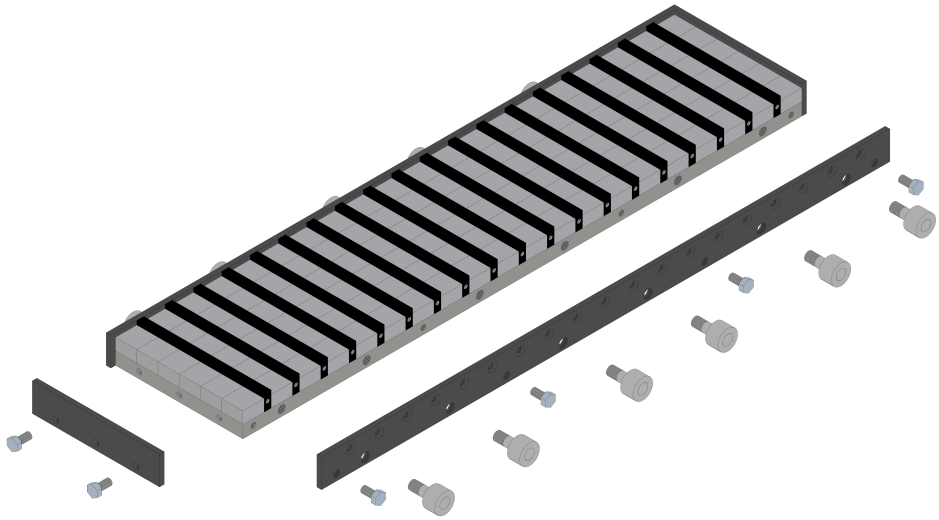

Figure 6.5: Reaction plate assembly

6.1.3 Complete motor assembly

Figure 6.6 is a photograph of the complete linear motor. The five independently-fed stator sections form a 1,44 m track and a linear absolute position encoder attached to the top of the reaction plate provides a measurement of its position. The physical air-gap between the reaction plate and stator sections is 4,7 mm, with an effective air-gap (from stator core to back-iron) of 24,7 mm. Table 6.1 provides a summary of the prototype motor's key parameters and dimensions.

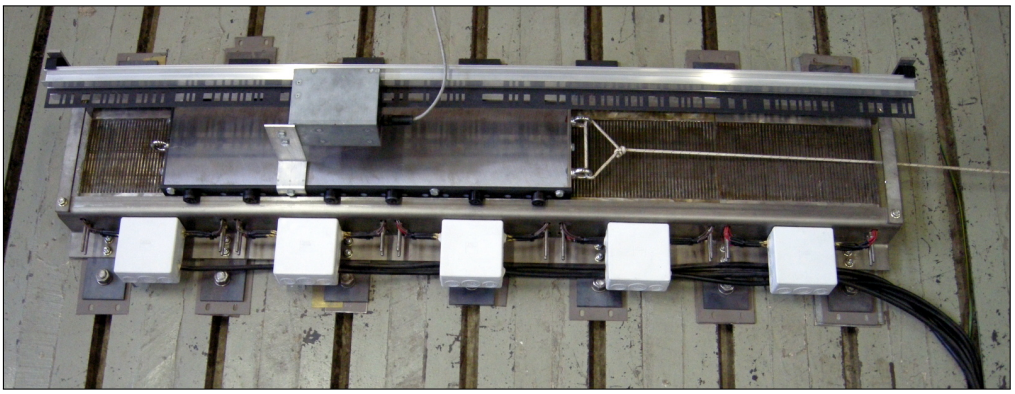

Figure 6.6: Linear synchronous motor prototype

Table 6.1: Prototype motor parameters and dimensions

Pole pitch	36 mm
Physical air-gap	4,7 mm
Effective air-gap (stator teeth to reaction plate back-iron)	24,7 mm
Air-gap width	162 mm
Air-gap / reaction plate length	711 mm (20 poles)
Stator section length	288 mm (8 poles)
Slots per pole per phase	2
Tooth width	2,4 mm
Slot width	3,6 mm
Slot pitch	6 mm
Slot depth (double-layer regions)	18 mm
Slot depth (single-layer regions)	10 mm
Wire diameter	0,95 mm
Turns per coil	21
Coil span	30 mm (5 slots)
Coil overhang	30 mm
Yoke height	14 mm
Magnet height	15 mm
Magnet span	27 mm (135°)
Back-iron height	15,8 mm

6.2 Characterisation

The measured phase resistances and uncovered phase inductances for the stator sections are provided in table 6.2. A FEM model is used to obtain the other motor parameter sets for the space-vector simulation model. The required magnetostatic solutions are obtained with the free Finite Element Method Magnetics (FEMM) package written by Meeker [63]. Table 6.3 lists the material properties used in

Table 6.2: Measured stator section electrical parameters (with no reaction plate and with an ambient temperature of 21 °C)

Section	Serial no.	Resistance [Ω]			Inductance [mH]		
		R_{a}	R_{b}	R_{c}	$L_{(\mathrm{aa})}$	$L_{(\mathrm{bb})}$	$L_{(\mathrm{cc})}$
1	16870-13	4.9	5.0	4.9	16.3	16.3	16.3
2	16870-14	5.1	5.0	5.0	17.4	17.0	17.3
3	16870-16	5.0	5.0	5.0	17.3	17.2	17.1
4	16870-15	4.9	4.9	4.9	17.1	17.1	17.2
5	16870-12	4.9	4.8	4.8	16.0	15.9	15.9

the model of the prototype motor. Since the space-vector dynamic model does not account for magnetic saturation, all of the materials are defined with constant permeabilities. It is therefore assumed that the field intensities in the core and back-iron remain within the linear regions of their B-H curves. This is reasonable owing to the motor's large air-gap and low electrical loading.

Table 6.3: Material properties for FEMM model

Description	μr	Hc [kA/m]
M250-50 lamination steel	7185	0
Back-iron	2119	0
NdFeB-45H permanent magnets	1,049	979
Coils	1	0
Slot wedges	4	0

The FEM model comprises three adjacent stator sections and the reaction plate. This arrangement allows the parameters for the stator sections to be obtained using the centre stator section in the model, which does not have erroneous leakage flux either side of it. The solution domain is truncated with a rectangular magnetic isolation boundary that runs along the top of the reaction plate's back-iron, extending far enough out to the sides to accommodate the reaction plate movement, and then through the stator core, excluding the unused bottom winding. Hence it is assumed that no flux leaks out from the top of the reaction plate or flows across the unused bottom slots. The model's geometry is included as figure D.1 in appendix D, together with the MATLAB® scripts used to obtain the parameters described in the sections that follow.

6.2.1 Electromagnetic force

To show the variation in propulsion and normal force with load angle, the FEMM model is used to calculate the force over a range of reaction plate positions for the same winding currents. Only the centre stator section is energised and the current vector is aligned with the α-axis. The reaction plate is then moved over a full pole pair, symmetrically about the centre, in 2 mm increments. For an α-axis current of 7,35 A (corresponding to $I_a = 6\,\text{A}$, $I_b = -3\,\text{A}$ and $I_c = -3\,\text{A}$), figures 6.7 and 6.8 are plots of the obtained propulsion and normal forces, respectively. Although the corresponding conductor current density of $6\,\text{A/mm}^2$ would be considered high for a rotary machine, the stator sections are not rated for continuous operation.

The propulsion and normal forces vary sinusoidally with load angle and are periodic over a pole pair, as expected. It may be surprising that no significant cogging force is evident for this permanent-magnet machine with relatively few slots per pole. However, this is owing to the large air-gap (especially with respect to the short pole-pitch), the use of magnetic slot wedges and careful optimisation of the magnet span. Testament to this is that there is no perceivable force ripple when moving the reaction plate along the stator by hand.

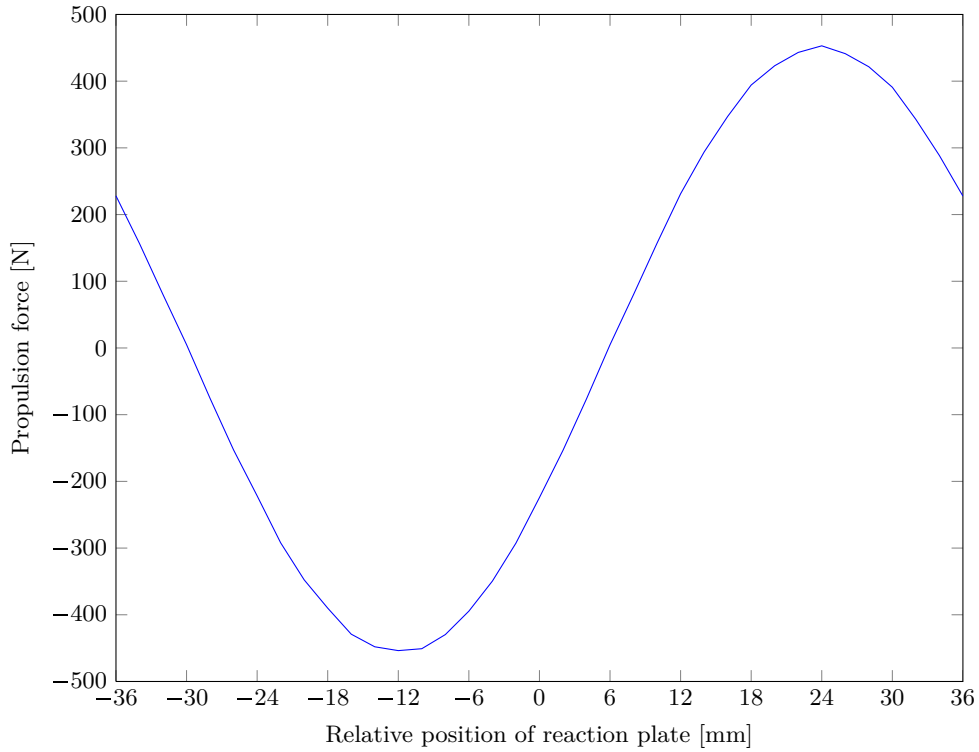

Figure 6.7: Propulsion force variation with reaction plate position for $I_\alpha = 7{,}35\,\text{A}$

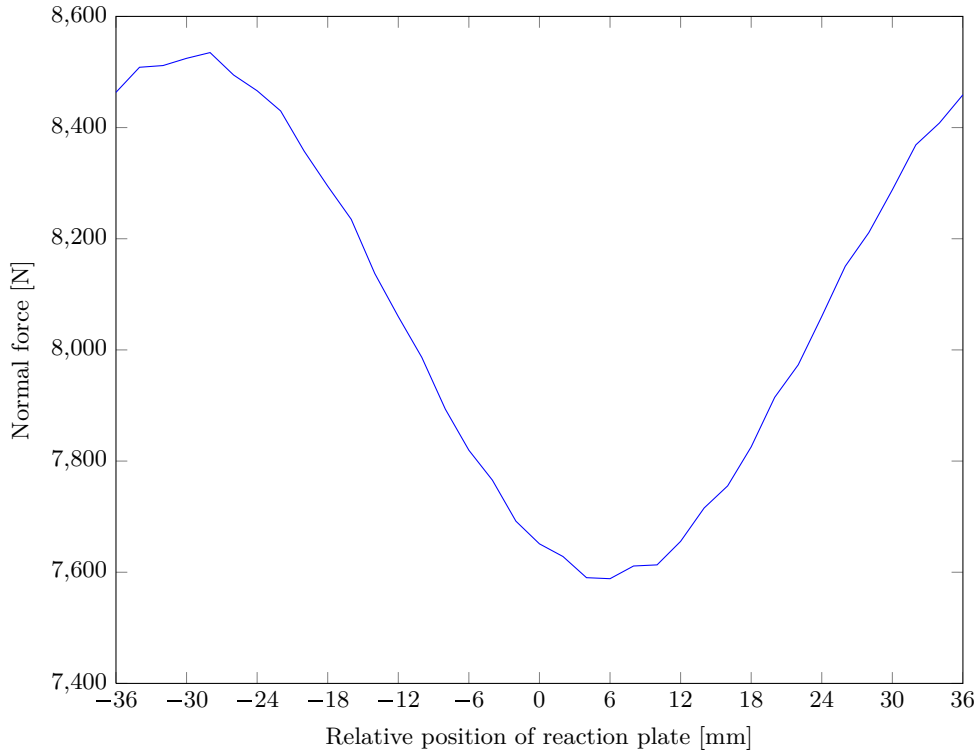

Figure 6.8: Normal force variation with reaction plate position for $I_\alpha = 7{,}35\,\text{A}$

Note that the large average normal force ($\approx 8\,\text{kN}$) is due to all of the reaction plate poles being attracted to the stator and not only those interacting with the centre section. As shown, the maximum expected normal force is approximately $8{,}5\,\text{kN}$.

6.2.2 Position of α-axis

It is necessary to determine the α-axis offset for the stator sections in order to relate the reaction plate position to the angular displacement, θ, between the d and α axes. This is achieved by solving for the normal component of the flux density along the air-gap, with only an α-axis component of current flowing in the winding. The energy of the permanent magnets is removed so that the winding flux is isolated and a unity current vector is chosen since the magnitude of the current is irrelevant owing to the model being linear. A Fast Fourier Transform (FFT) is then calculated for the resulting spatial flux distribution and the phase angle of the α-axis is obtained corresponding to the fundamental period of the space wave (one pole pair). This phase angle is then scaled by the pole-pitch to obtain the offset position. The α-axis offset is calculated to be $60\,\text{mm}$ and is shown in figure 6.9.

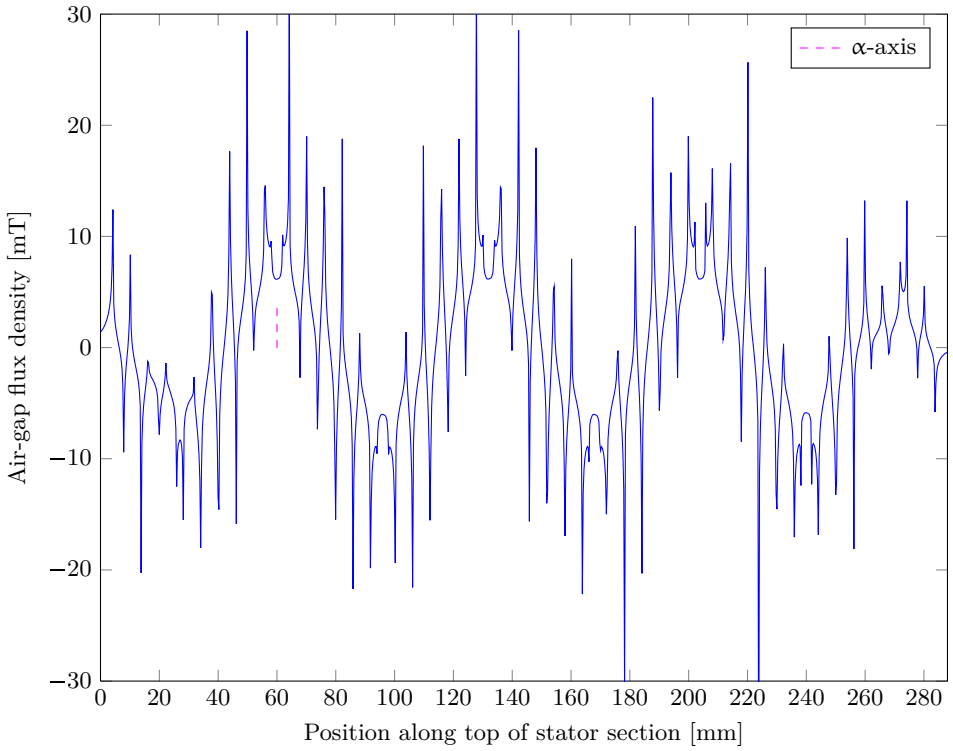

Figure 6.9: α-axis offset for stator section

6.2.3 Flux linkages and inductances

The permanent-magnet flux linkage and winding inductances are obtained over the full range of reaction plate displacement relative to a stator section. That is, the FEM model is solved with the reaction plate incrementally moved along, from completely not covering the centre section on the left-hand side, to fully covering the section, to then completely uncovering the section again on the right-hand side. Plots of the permanent-magnet flux linkage per phase and the self and mutual inductances per phase are provided in appendix D.1.4. The calculated uncovered self-inductances correlate closely with the measured values in table 6.2. Also, there is only a small difference between the covered and uncovered inductances, owing to the large air-gap.

To transform the values to the d/q/0 reference frame, θ (the angular displacement between the d-axis and the α-axis) is calculated at each reaction plate position. Figures 6.10 and 6.10 show the calculated d-axis and q-axis self-inductances, respectively. $L_{(00)}$ remains approximately constant at 10 mH and the d/q mutual inductances fluctuate about zero within 0,15 mH. So, for this particular motor, there is negligible cross-coupling between the d and q axes. The d-axis and q-axis permanent-magnet flux linkages are shown in figures 6.12 and 6.13, respectively.

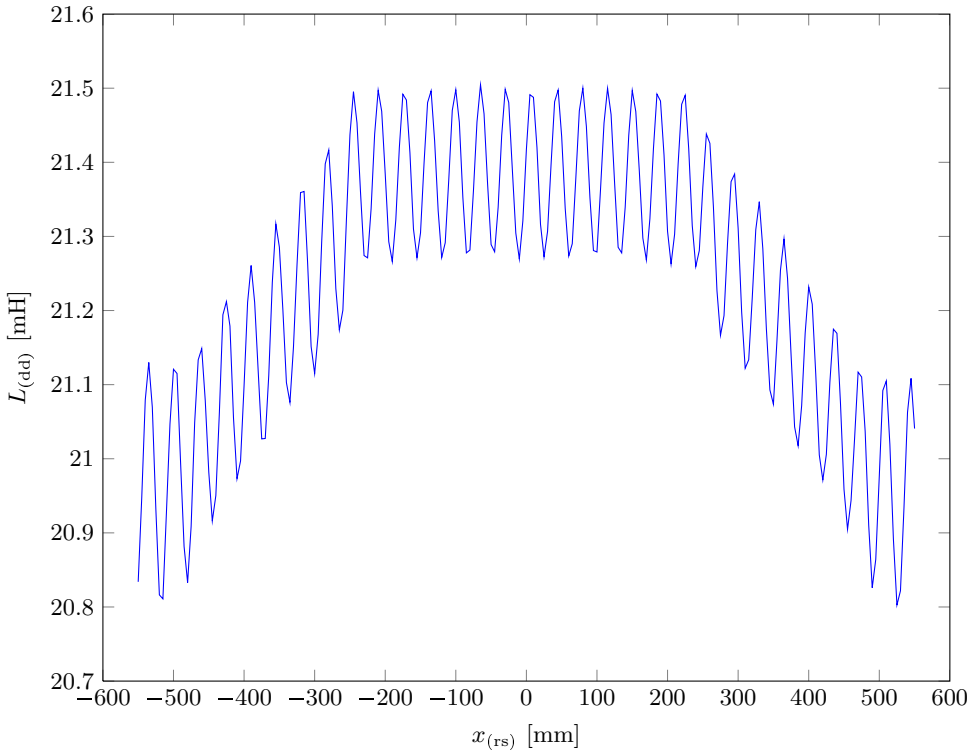

Figure 6.10: $L_{(\mathrm{dd})}$ versus relative position of reaction plate

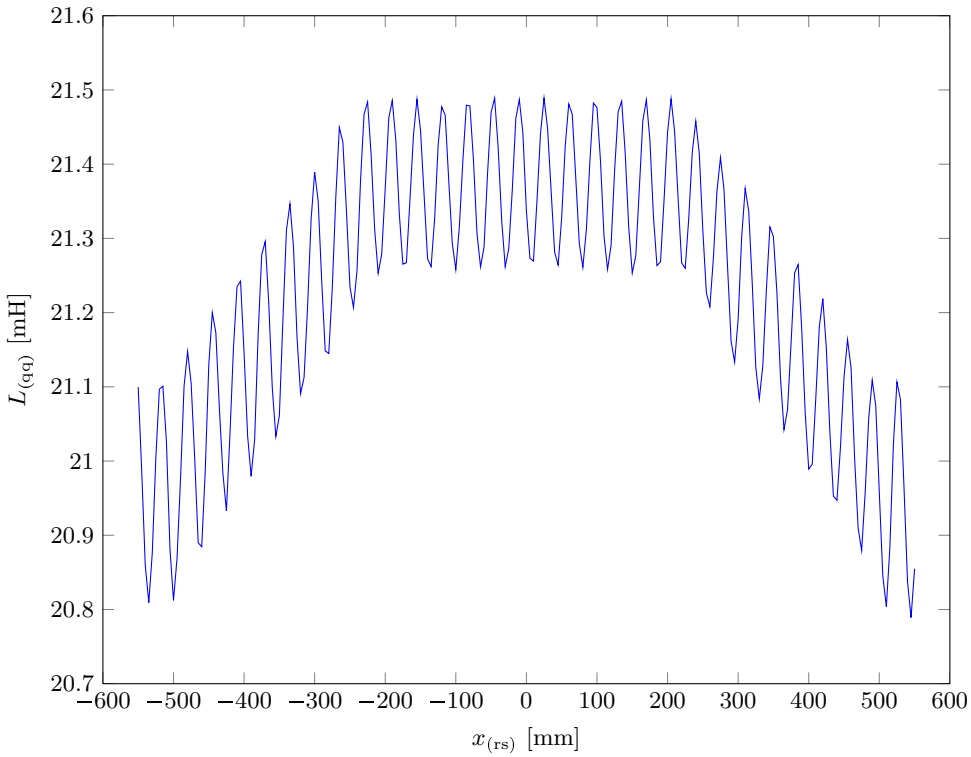

Figure 6.11: $L_{(\mathrm{qq})}$ versus relative position of reaction plate

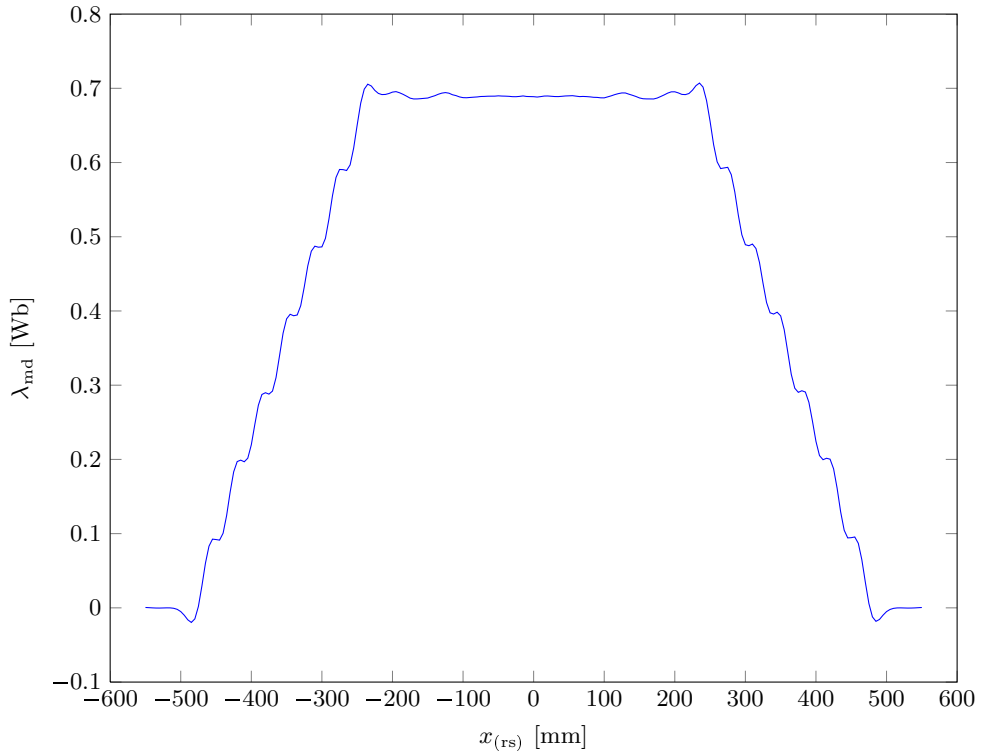

Figure 6.12: λ_{md} versus relative position of reaction plate

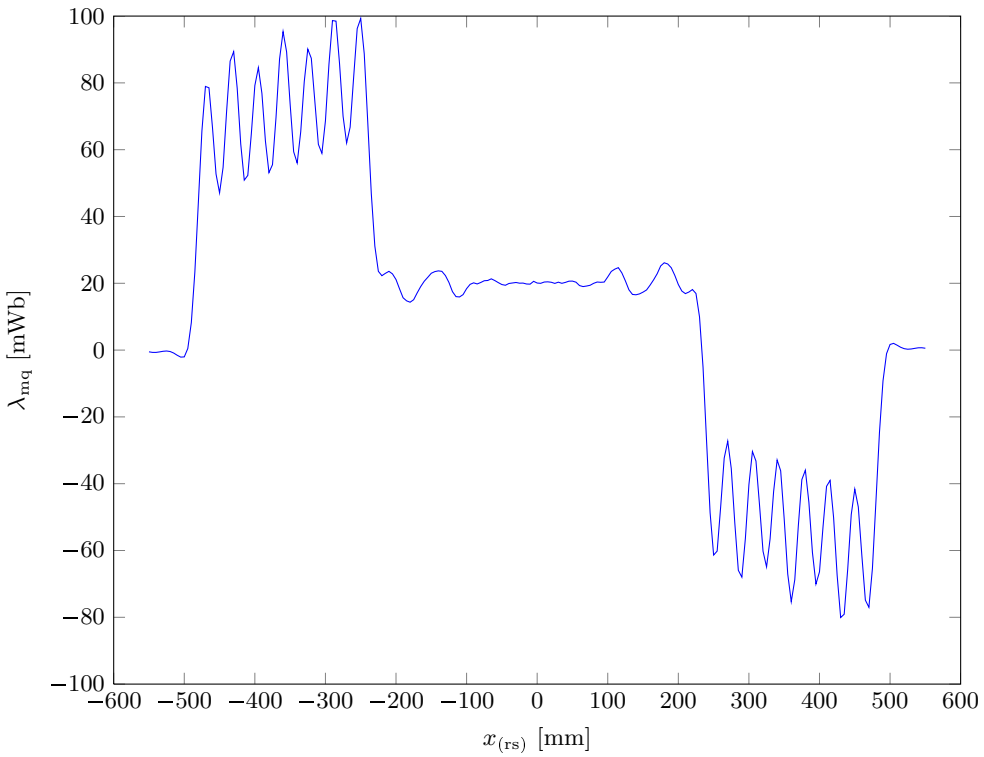

Figure 6.13: λ_{mq} versus relative position of reaction plate

As predicted for a non-salient machine, the d and q inductances are closely matched. Their increase with reaction plate coverage, though, would be more pronounced for a motor with a smaller air-gap. The permanent-magnet flux linkage is predominantly in the d-axis, as expected, and increases linearly with reaction plate coverage. The component of flux in the q-axis, when entering or leaving the section, is due to the reaction plate's end-effects. Clearly, there is zero flux linkage when the section is fully uncovered. λ_{m0} is calculated to be effectively zero (less than 25 mWb).

6.2.4 Feeding efficiency and reaction plate utilisation

If only fully-covered stator sections are energised, the reaction plate utilisation for the prototype system is 60 %, as calculated using (5.2). Correspondingly, when also energising partially-covered sections, the feeding efficiency is 73 %, as calculated using (5.3).

6.2.5 Solid-state contactors

The solid-state contactors were reused from another application and are vastly overrated for the prototype system. (They are rated for 75 A but the phase currents for the stator sections remain below 8 A.) Unfortunately, they are also designed with resistive loads in mind and so implement zero voltage crossing turn-on logic. Initially, this was thought not to be a problem because the inverter output is consistently switched to zero in order to effect an output voltage that is less than the dc bus voltage. However, because the contactors expect a sinusoidal voltage waveform, they only trigger to turn on subsequent to the voltage being zero, once it rises above a particular threshold. The measured threshold voltages for the contactors are included in appendix D as table D.1.

6.2.6 Reaction plate position measurement

The linear absolute position encoder used to track the position of the reaction plate operates with a coded rail. Hence, it is a discrete measurement and has a resolution of $0.8\overline{3}$ mm (1200 codes per metre).

6.3 Simulation model

The complete simulation model of the prototype system is shown in figure 6.14. It uses the generic space-vector model derived in chapter 4 and full details of the subsystems are provided in appendices B and D. Configurable subsystems are used for the components so that one of several variants can be selected depending on the desired level of complexity.

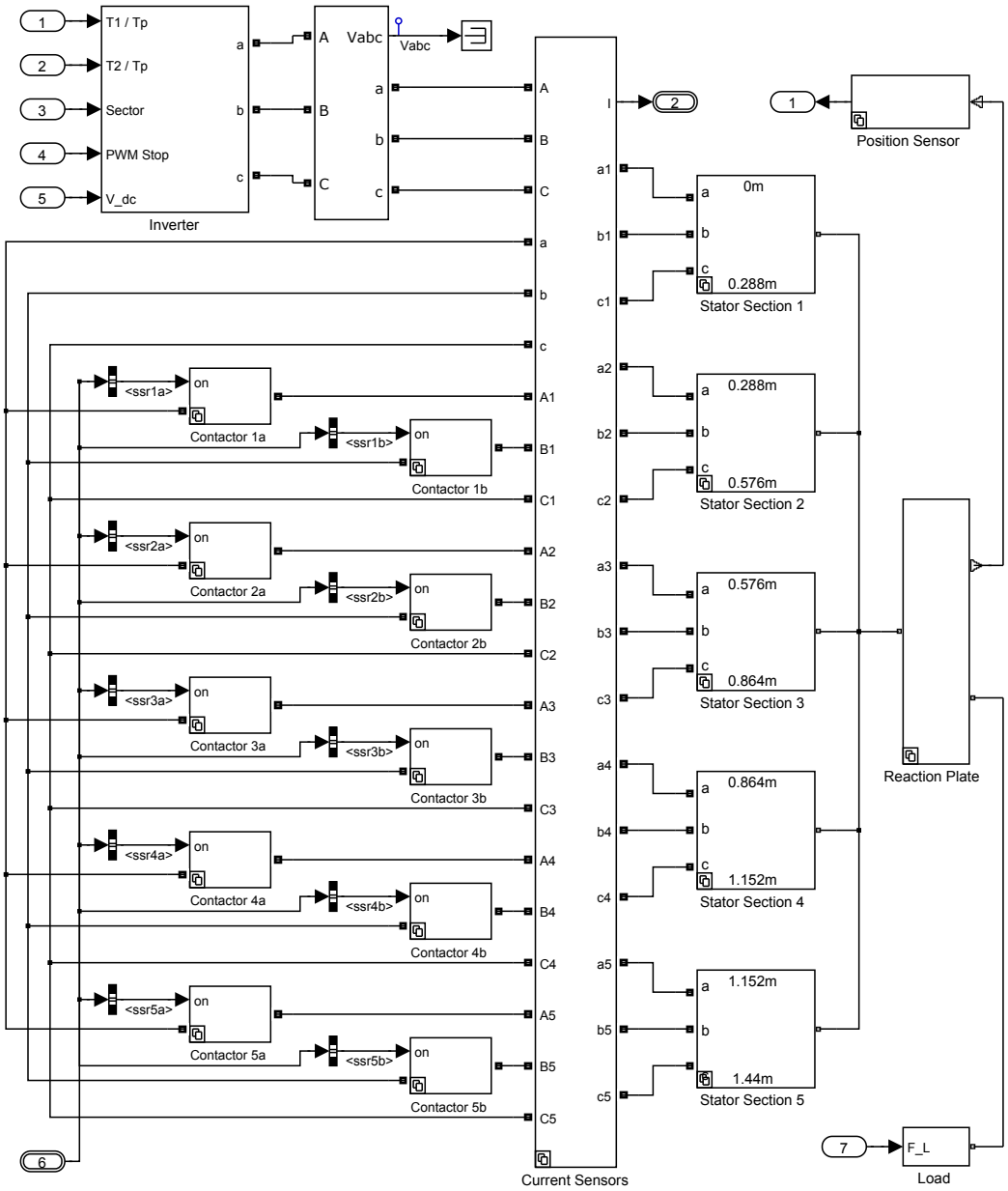

Figure 6.14: Full Simulink® model of prototype system

6.4 Controller

A multi-rate, cascaded controller was implemented for the prototype system using dSPACE. The Simulink® model shown in figure 6.15 is compiled by dSPACE to run on the embedded realtime controller. The controller blocks that are not included in this section are provided in appendix E.

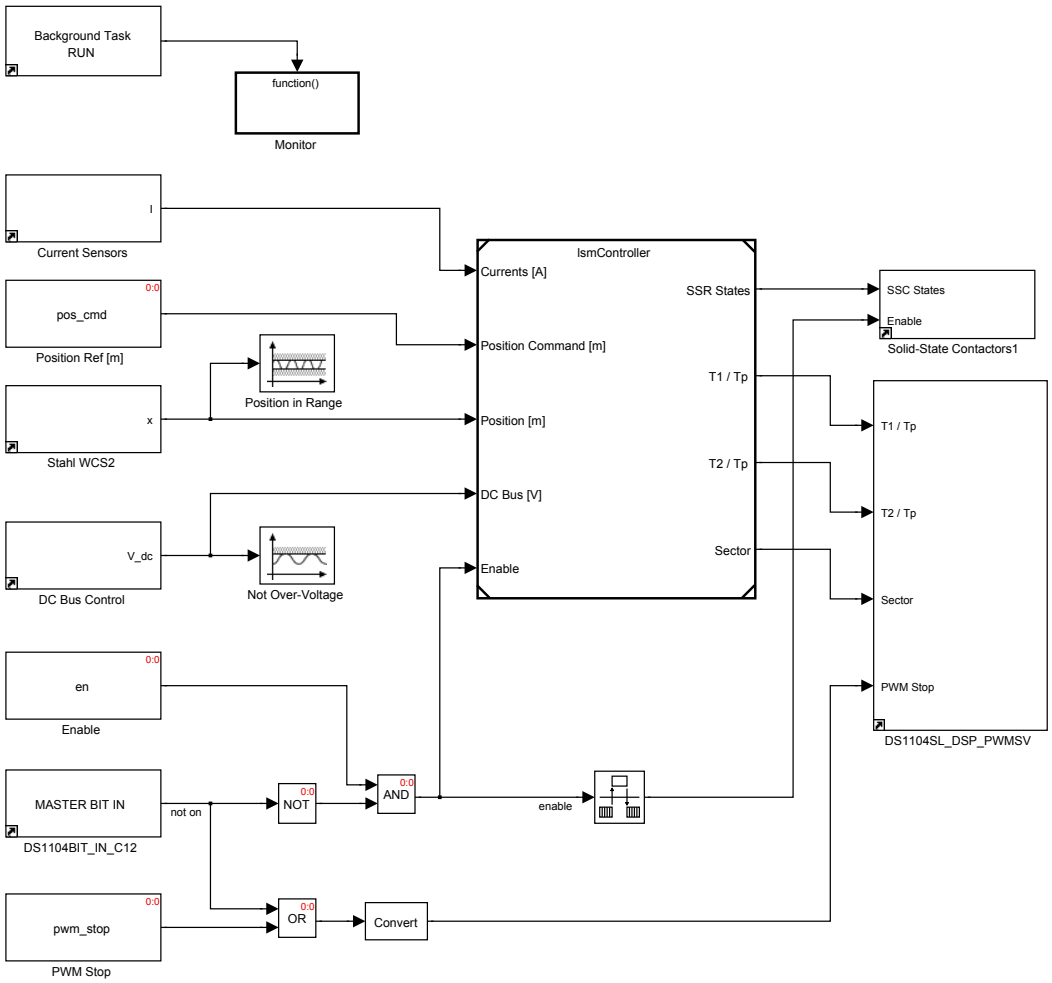

Figure 6.15: Complete prototype controller (`lsmDSPACE`)

Figure 6.16 shows the overall cascaded control scheme. The determination of which stator sections are energised, and which is the representative section, is performed by the subsystem shown in figure 6.17.

The feedback control loops were designed in the frequency domain and a robust control design process was followed, accounting for parametric uncertainty.

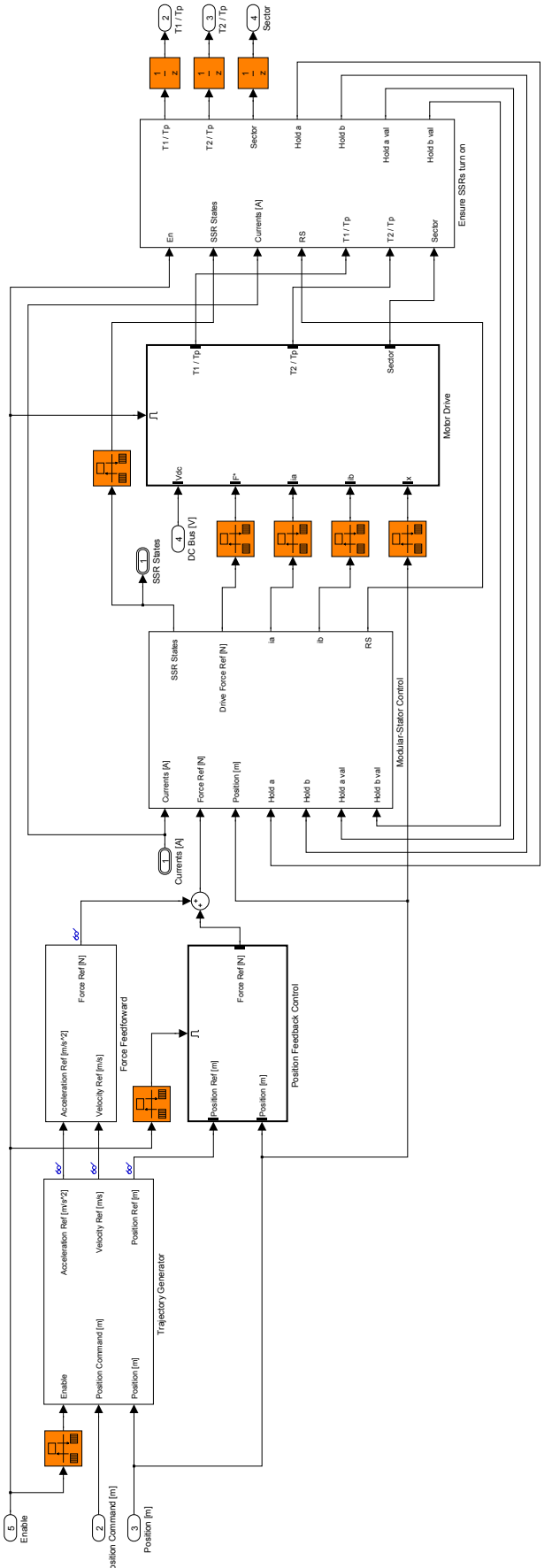

Figure 6.16: Cascaded control arrangement (`lsmController`)

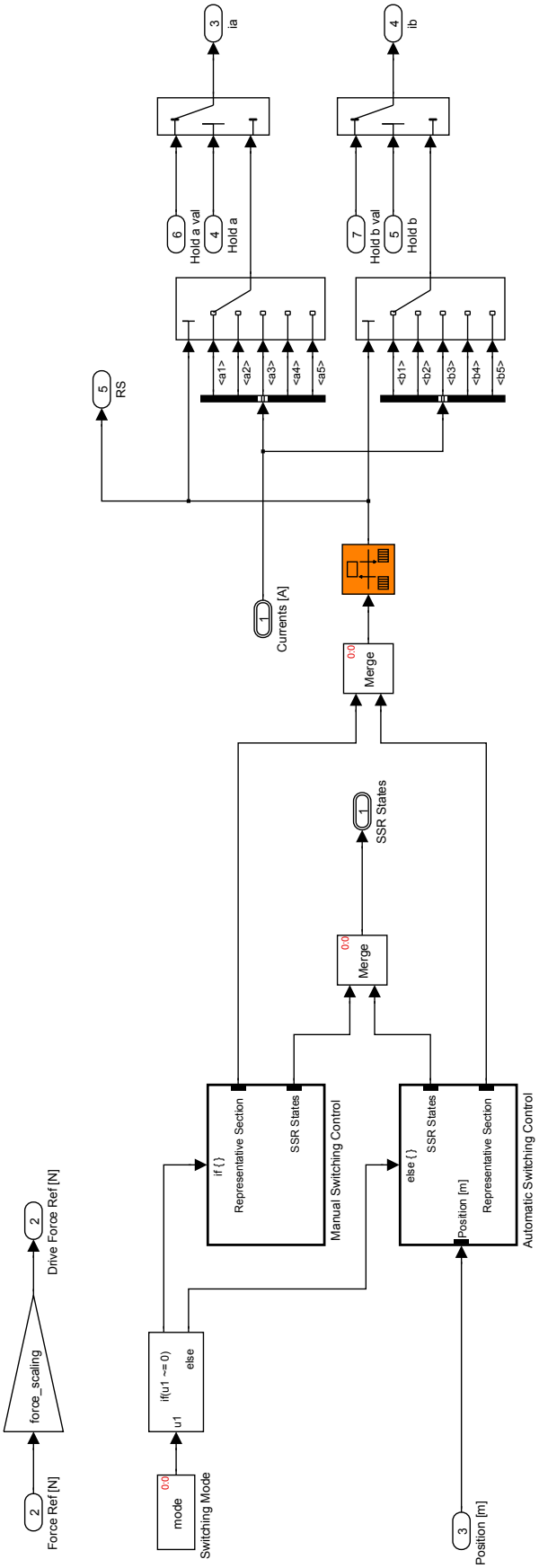

Figure 6.17: Subsystem `lsmController/Modular-Stator Control`

Field-Orientated Control is used for the motor vector control scheme since an accurate measurement of the reaction plate position is available. This controller is shown in figure 6.18 and the scaling of the torque reference and conversion from linear position to angular position for the vector controller is shown in figure 6.19. As shown in figure 6.20, two independent linear feedback loops are used to control the d-axis and q-axis currents. Anti-windup is effected by a saturation signal, which temporarily breaks the positive-feedback integration loops when the voltage output is saturated.

The inverter voltage is controlled with SVM and a brake resistor with a chopper is used to keep the dc bus voltage at 90 V. Operation at this reduced voltage improves the quality of the modulation for the low voltages required.

Owing to the zero voltage turn-on characteristics of the contactors, a mechanism was needed to force a particular contactor to turn on if it did not trigger correctly. This was successfully achieved with a system that briefly overrides the control output to the inverter to satisfy the necessary voltage threshold for the relevant contactor.

The outer-loop position feedback controller, shown in figure 6.21, is used in conjunction with a position trajectory generator to provide the necessary force reference to the inner control loop. This allows for good dynamic performance and disturbance rejection without demanding a very high acceleration for the reaction plate when there is a large change in the position reference.

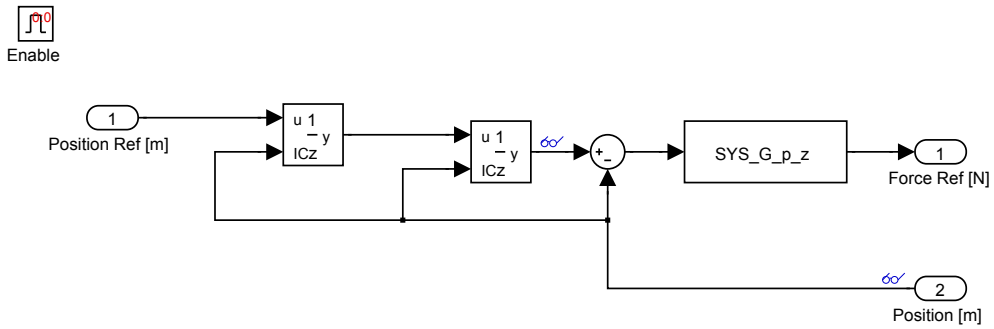

Figure 6.21: Subsystem `lsmController/Position Feedback Control`

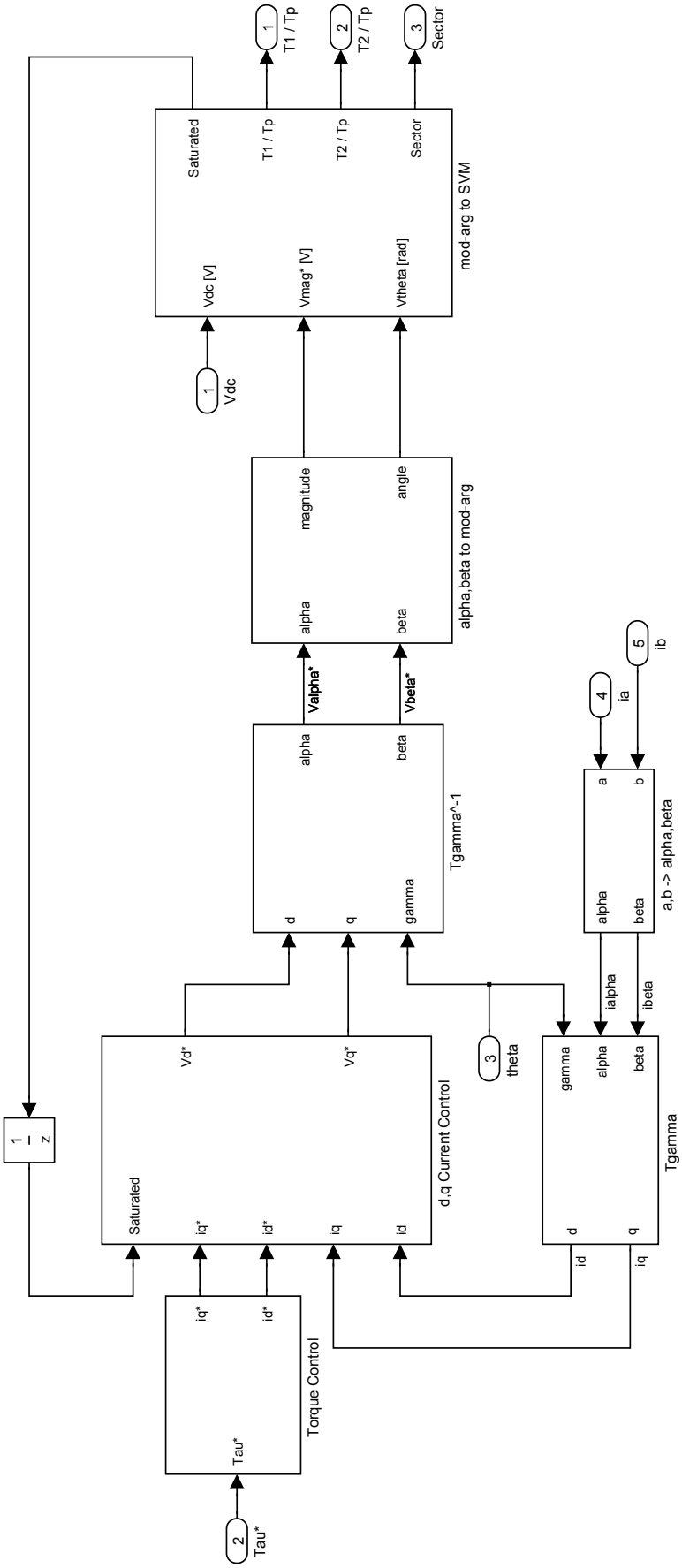

Figure 6.18: Subsystem `lsmController/Motor Drive/FOC`

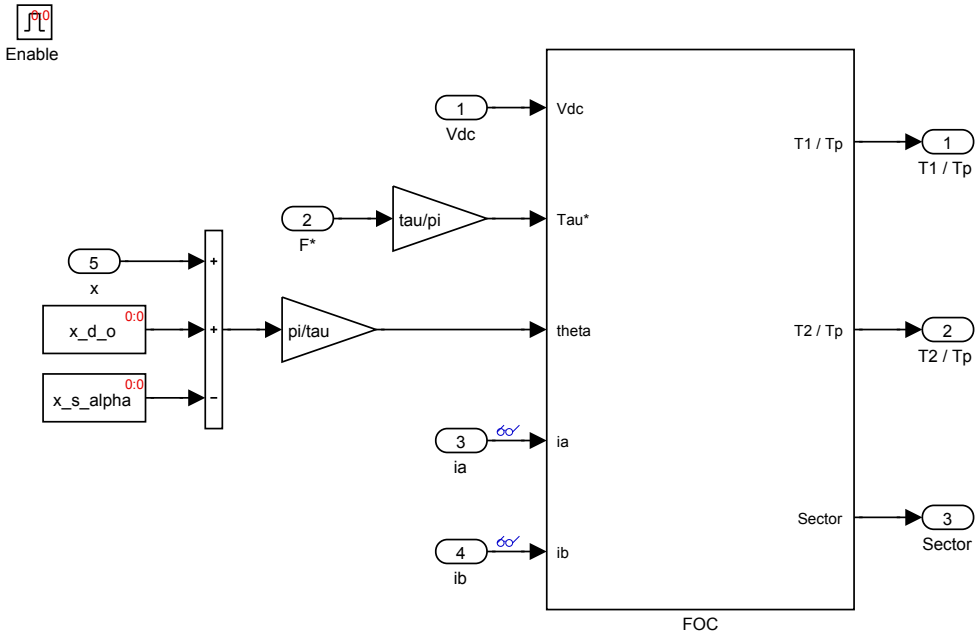

Figure 6.19: Subsystem `lsmController/Motor Drive`

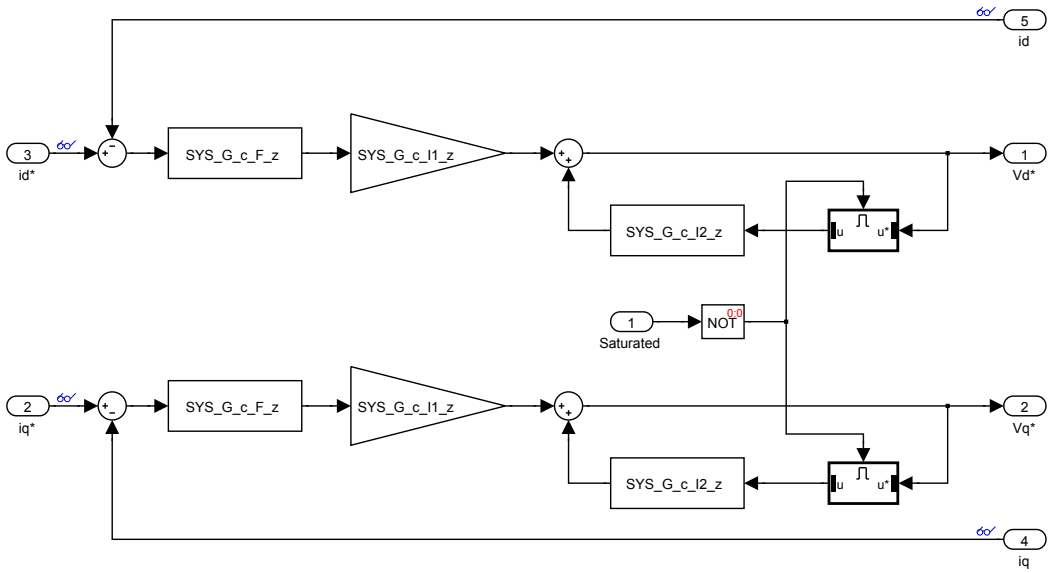

Figure 6.20: Subsystem `lsmController/Motor Drive/FOC/d,q Current Control`

6.5 Simulation and experimental results

A sandbag weighing approximately 50 kg was used to load the motor. Otherwise, without a load, it requires very little force to move the reaction plate along the lubricated track. The rope and pulleys are arranged so that, with the reaction plate almost at the extreme right-hand stop, the sandbag is resting on the floor. As the reaction plate moves to the left, it lifts the sandbag into the air and experiences a constant load force to the right (equal to the bag's weight).

The motor is operated according to the control strategy described in chapter 5 and both fully and partially-covered sections are energised. This is feasible because the reaction plate's speed is low due to the limited travel and there is also minimal difference between the covered and uncovered inductances for this particular motor (as shown in section 6.2.3). As the reaction plate moves along the track, the active representative section is selected to be one of the three middle sections.

When the system is powered on, the position reference is initialised to be slightly left of the reaction plate's resting position. This causes the reaction plate to immediately lift the sandbag and then hold its position by countering the sandbag's weight with an electromagnetic force to the left. Once in this steady initial state, the position reference can then be changed to command the reaction plate to move backwards and forwards along the track.

Results are provided here for the reaction plate being commanded to move from $x_\mathrm{r} = 900\,\mathrm{mm}$ to $x_\mathrm{r} = 500\,\mathrm{mm}$ and then back again to $x_\mathrm{r} = 900\,\mathrm{mm}$. The reference position trajectory generated by the controller in response to these two step changes is shown in figure 6.22.

Figure 6.23 shows the corresponding reaction plate movement predicted by the simulation model and figure 6.24 shows the plate's actual measured movement. For easier comparison, the captured measurements were time-shifted so that they are synchronised with the simulation results. It is evident that the simulated and measured results correlate well and that the controller is successful in accurately positioning the reaction plate, under loaded conditions, with no significant oscillation or overshoot. The small steady-state errors in position are owing to static friction and the lack of integral action in the outer position feedback control loop, which

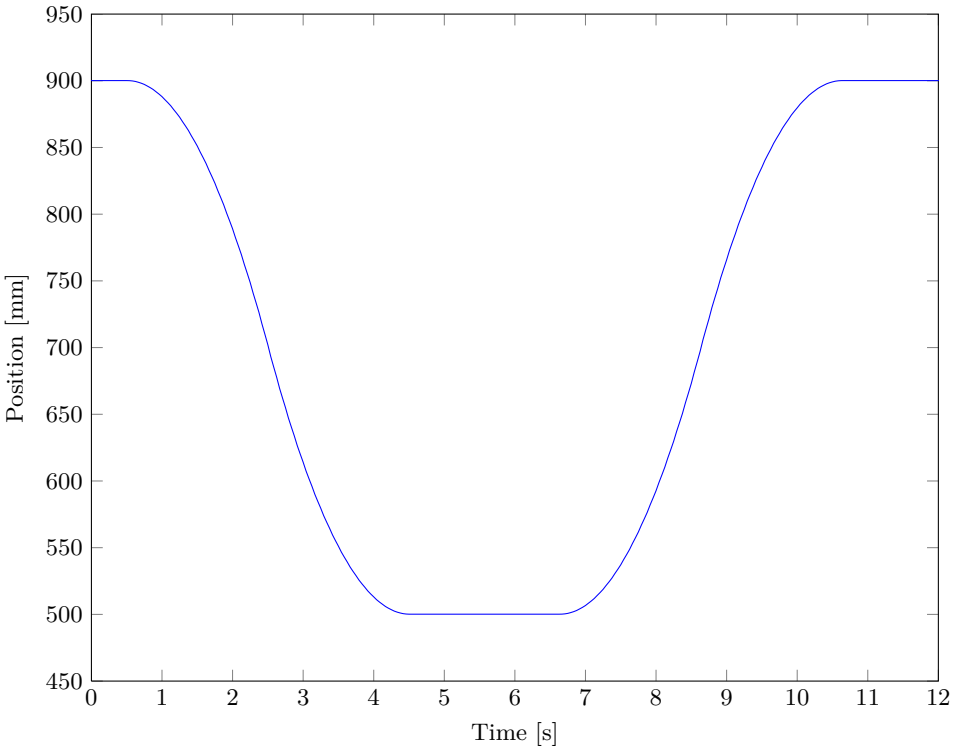

Figure 6.22: Position trajectory generated by controller

allows a high stability margin to be maintained.

The corresponding simulated and measured phase 'a' and phase 'b' currents for the five stator sections are provided in figures 6.25 through to 6.34. In addition, the measured combined phase currents, supplied by the inverter to the motor as a whole, are shown in figure 6.35. As discussed in appendix C.5.2, the electrical bandwidth of the stator sections is only approximately 50 Hz. Hence, considering that the space-vector pulse-width-modulation of the inverter output voltage occurs at a rate that is significantly higher than this (10 kHz), it is unsurprising that no significant inverter switching harmonics are evident in the current waveforms because these high-frequency harmonics are filtered out by the stator winding itself.

As is evident from the current waveforms, the controller only energises section 1 and section 5 when they are at least partially covered by the reaction plate. Also, note that the observed phase differences between the measured and simulated stator section currents are because of only small differences in the simulated and measured reaction plate positions over time and that this is exaggerated by the motor's small pole pitch. The waveform envelopes do, however, correspond closely.

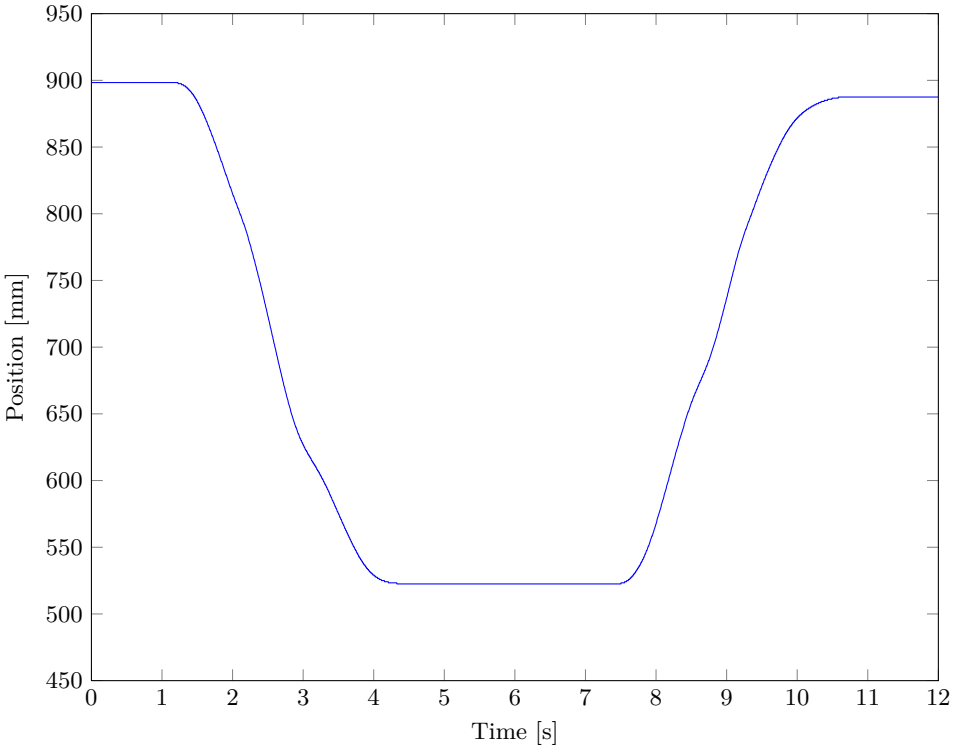

Figure 6.23: Simulated reaction plate movement

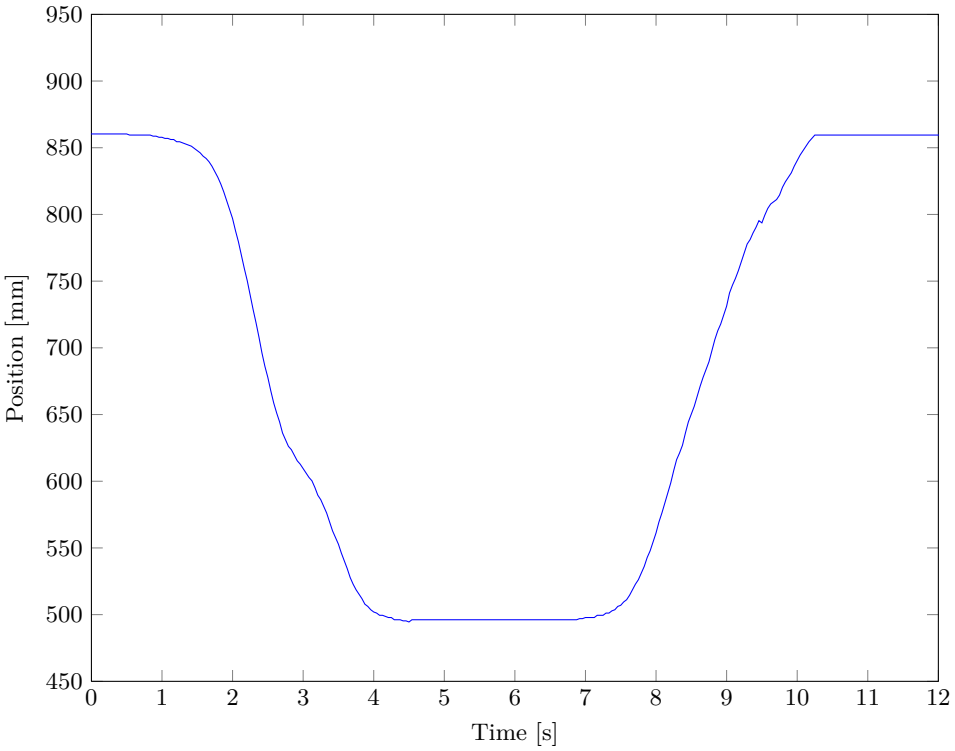

Figure 6.24: Measured reaction plate movement

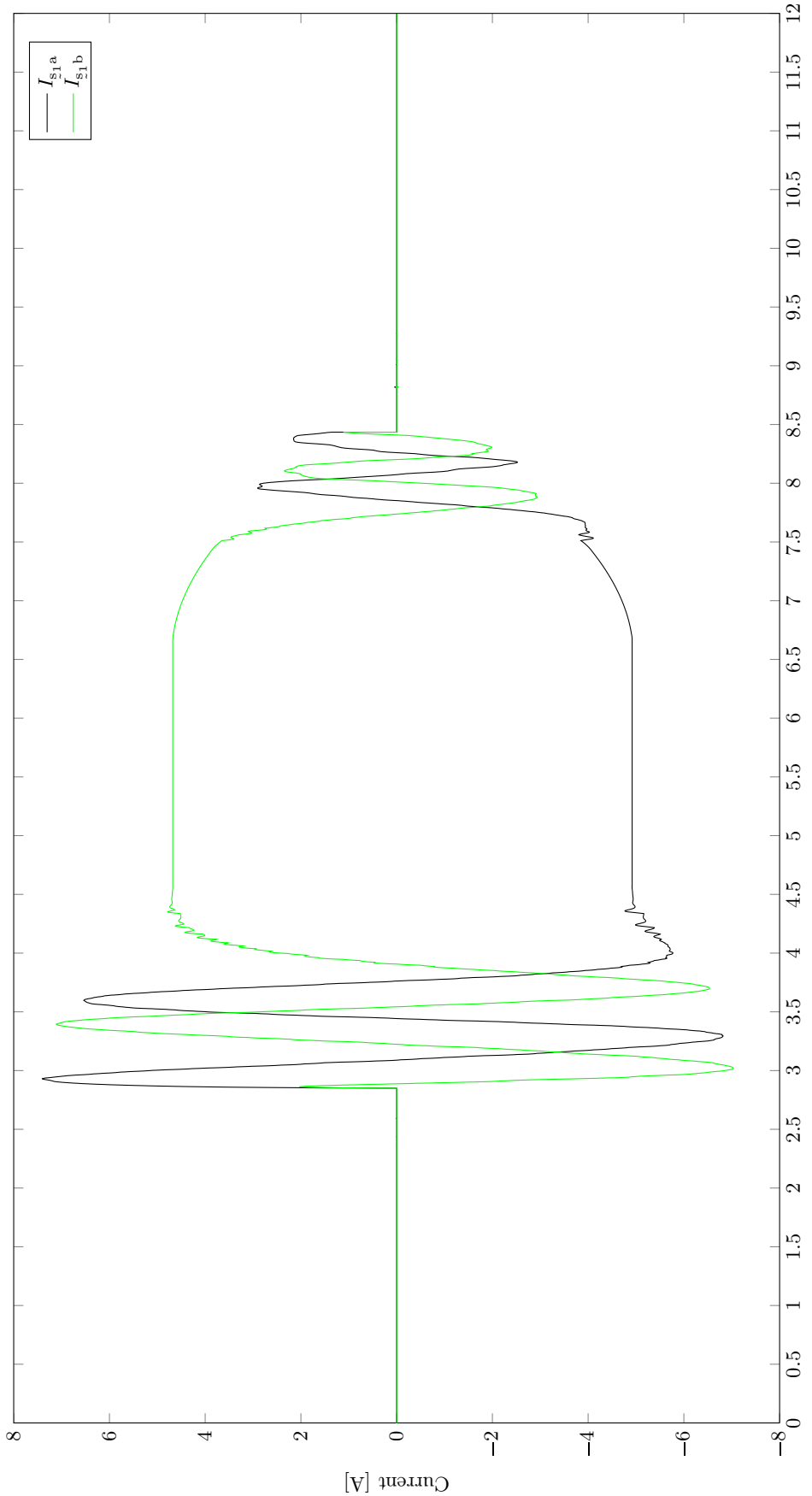

Figure 6.25: Simulated phase currents for stator section 1

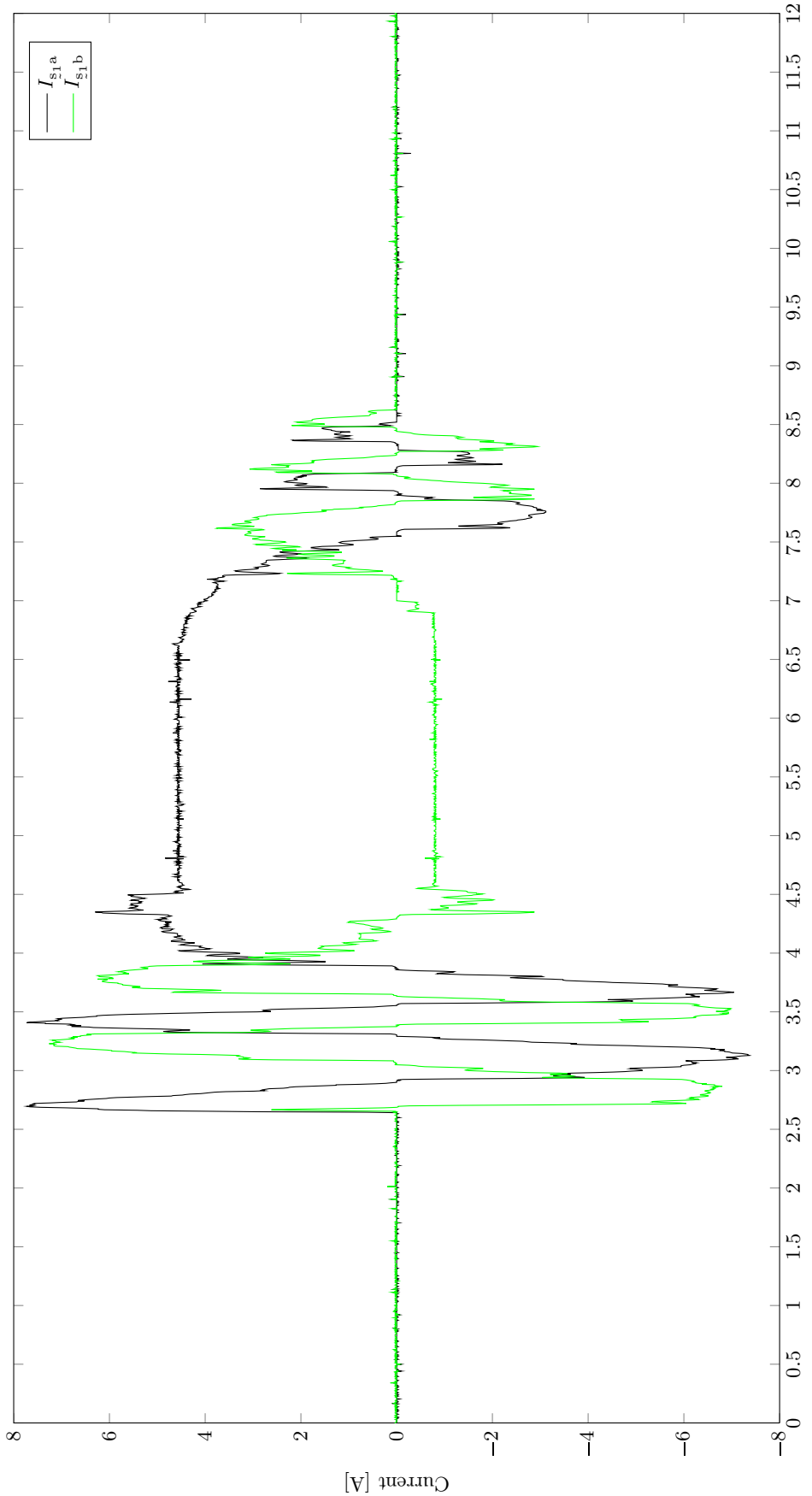

Figure 6.26: Measured phase currents for stator section 1

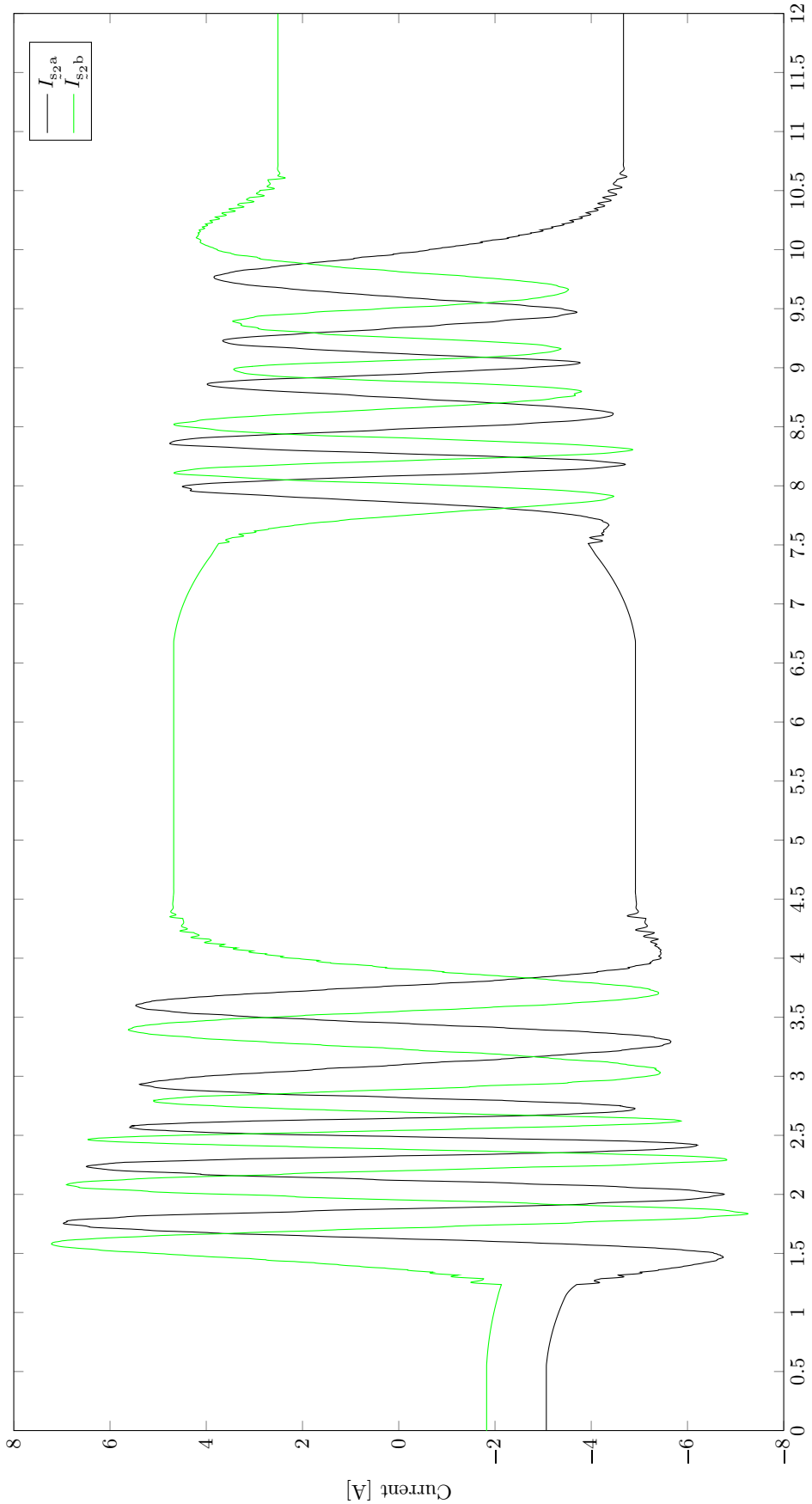

Figure 6.27: Simulated phase currents for stator section 2

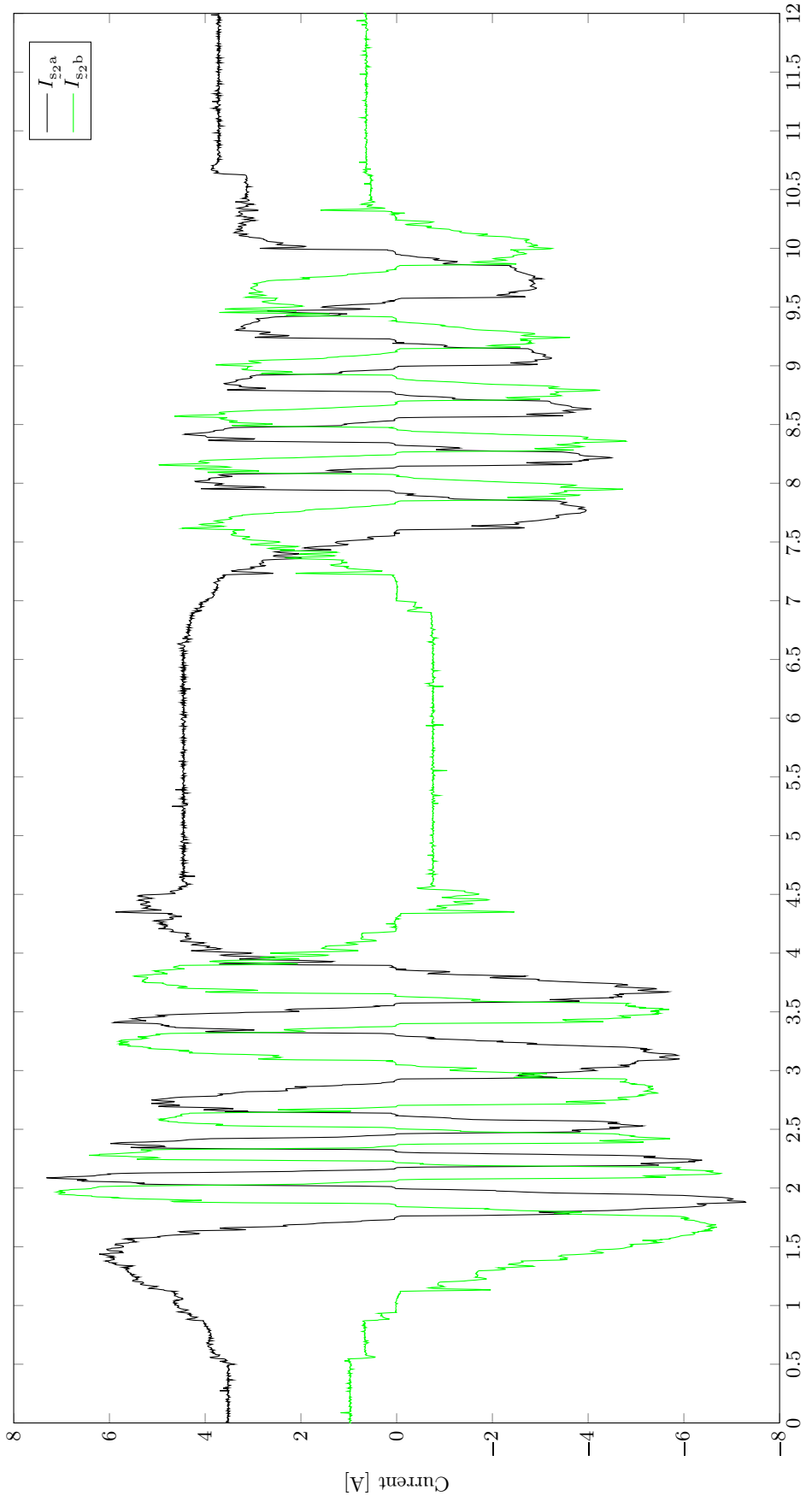

Figure 6.28: Measured phase currents for stator section 2

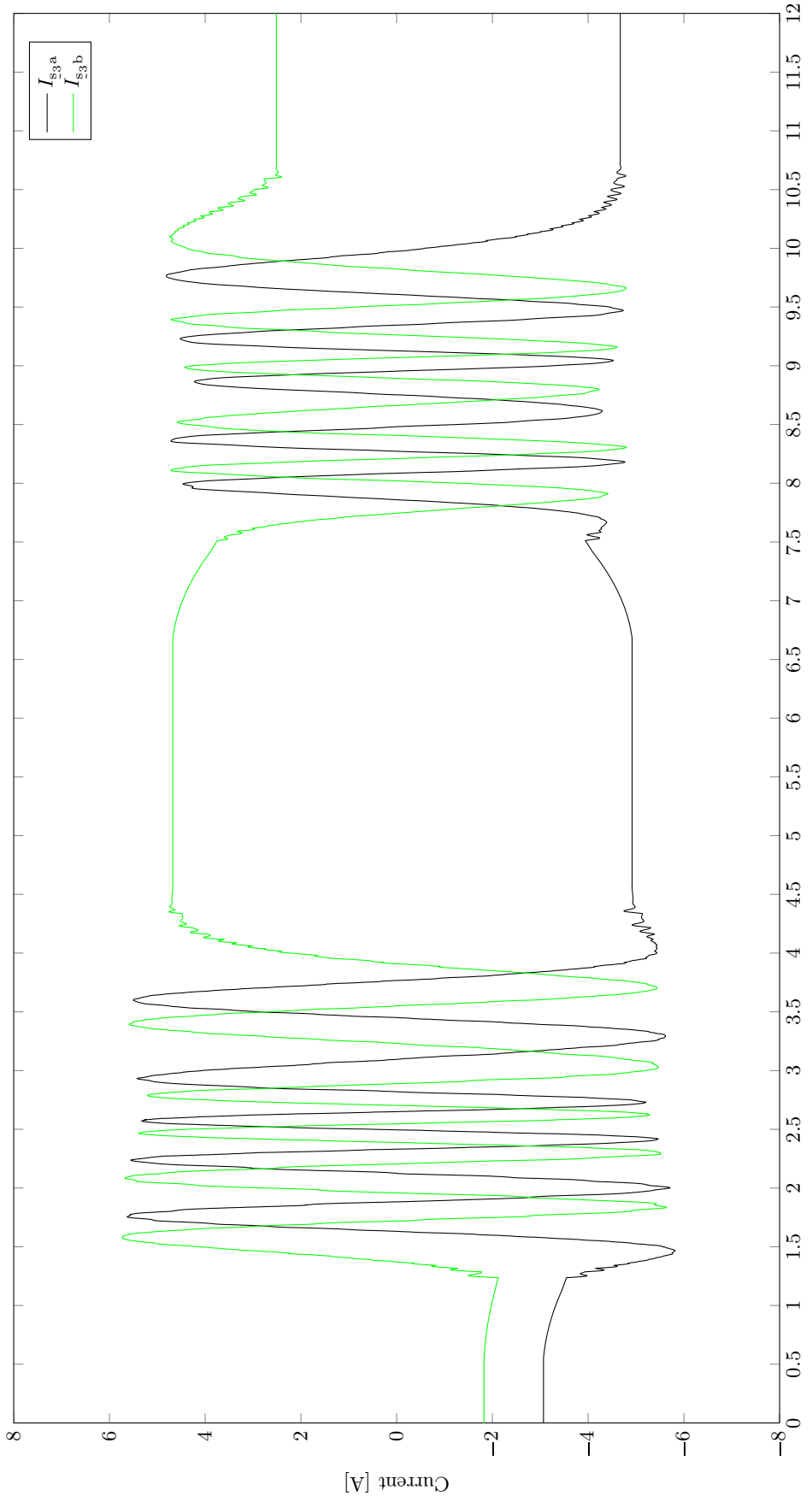

Figure 6.29: Simulated phase currents for stator section 3

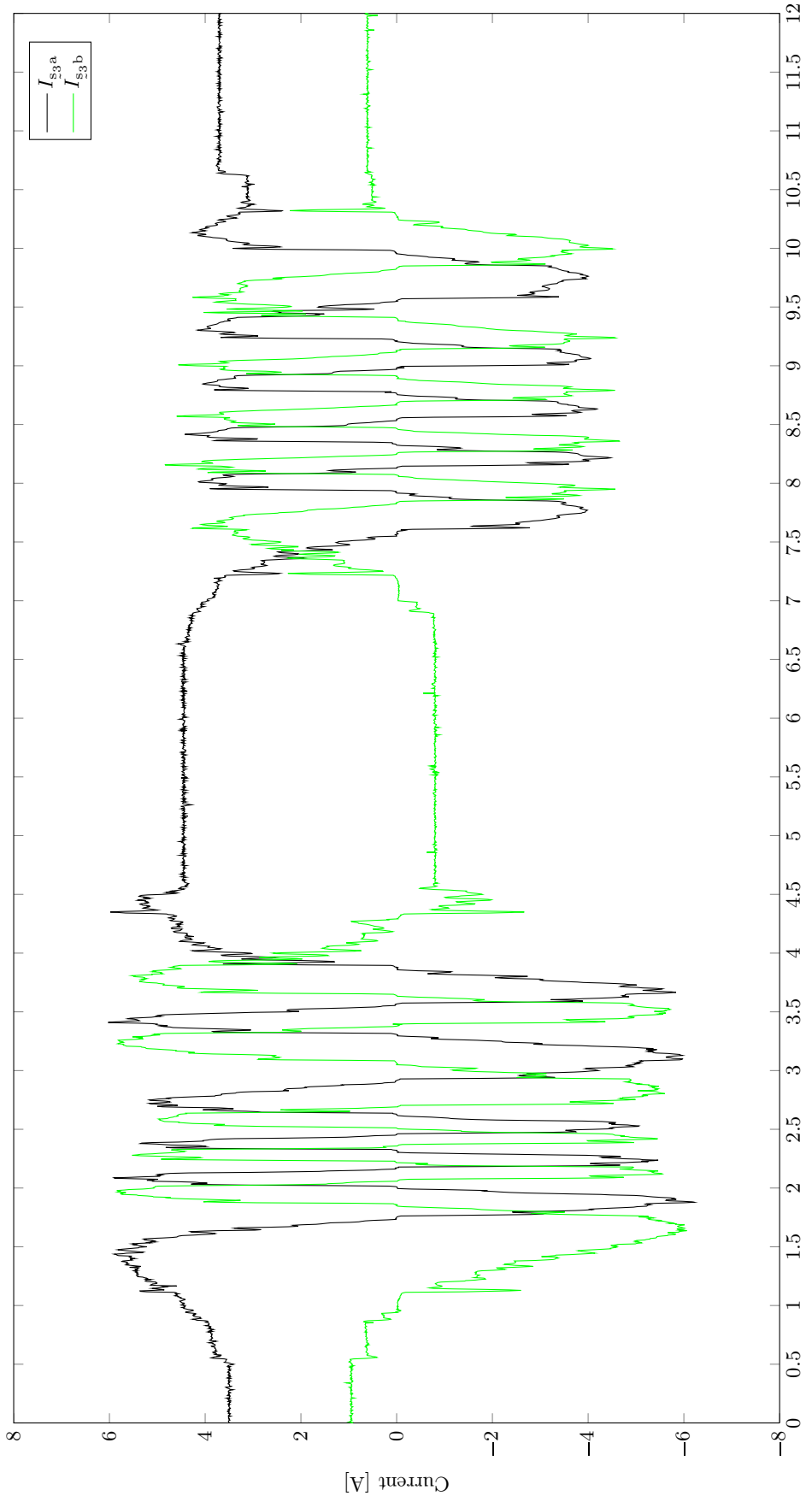

Figure 6.30: Measured phase currents for stator section 3

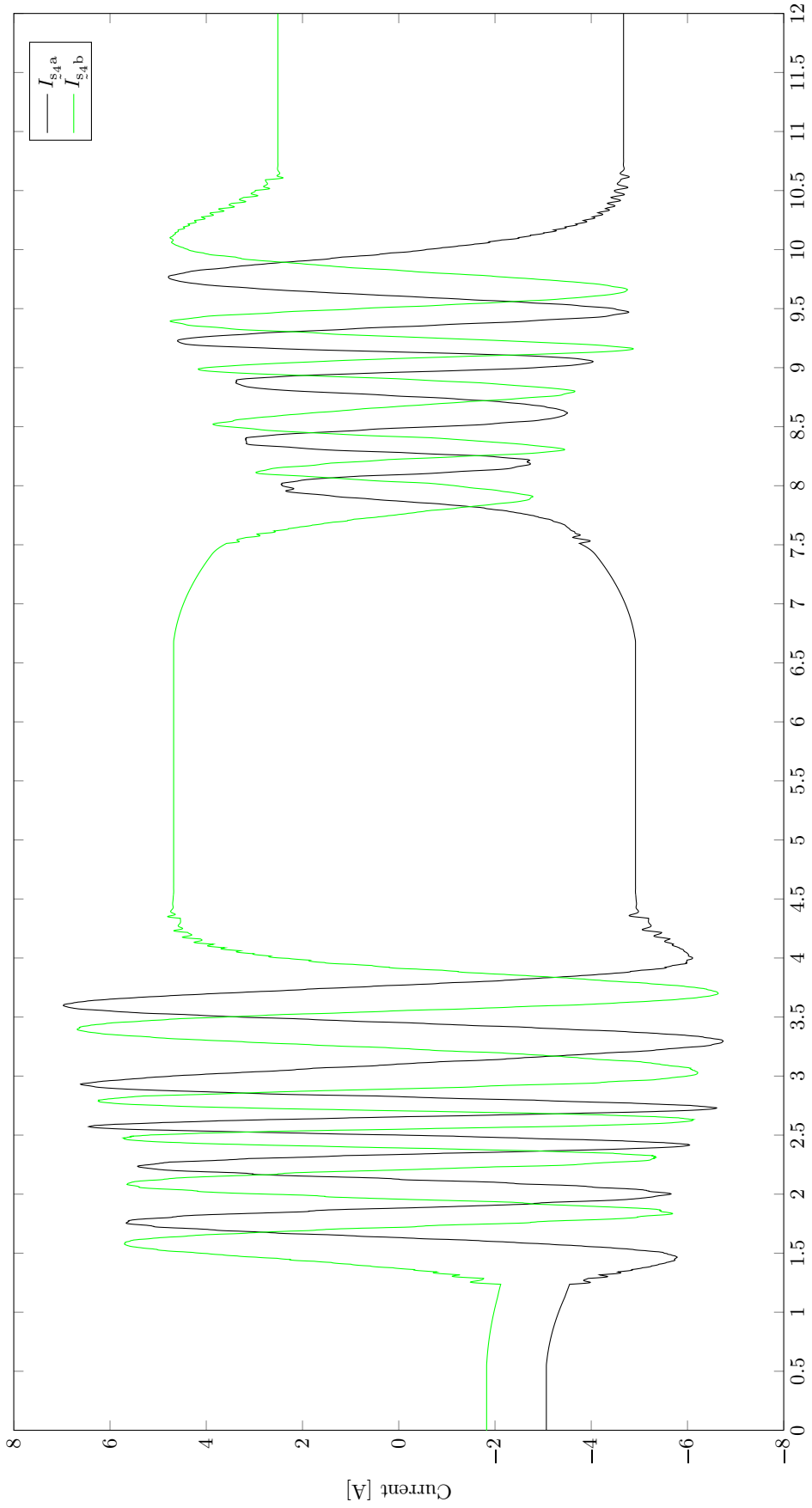

Figure 6.31: Simulated phase currents for stator section 4

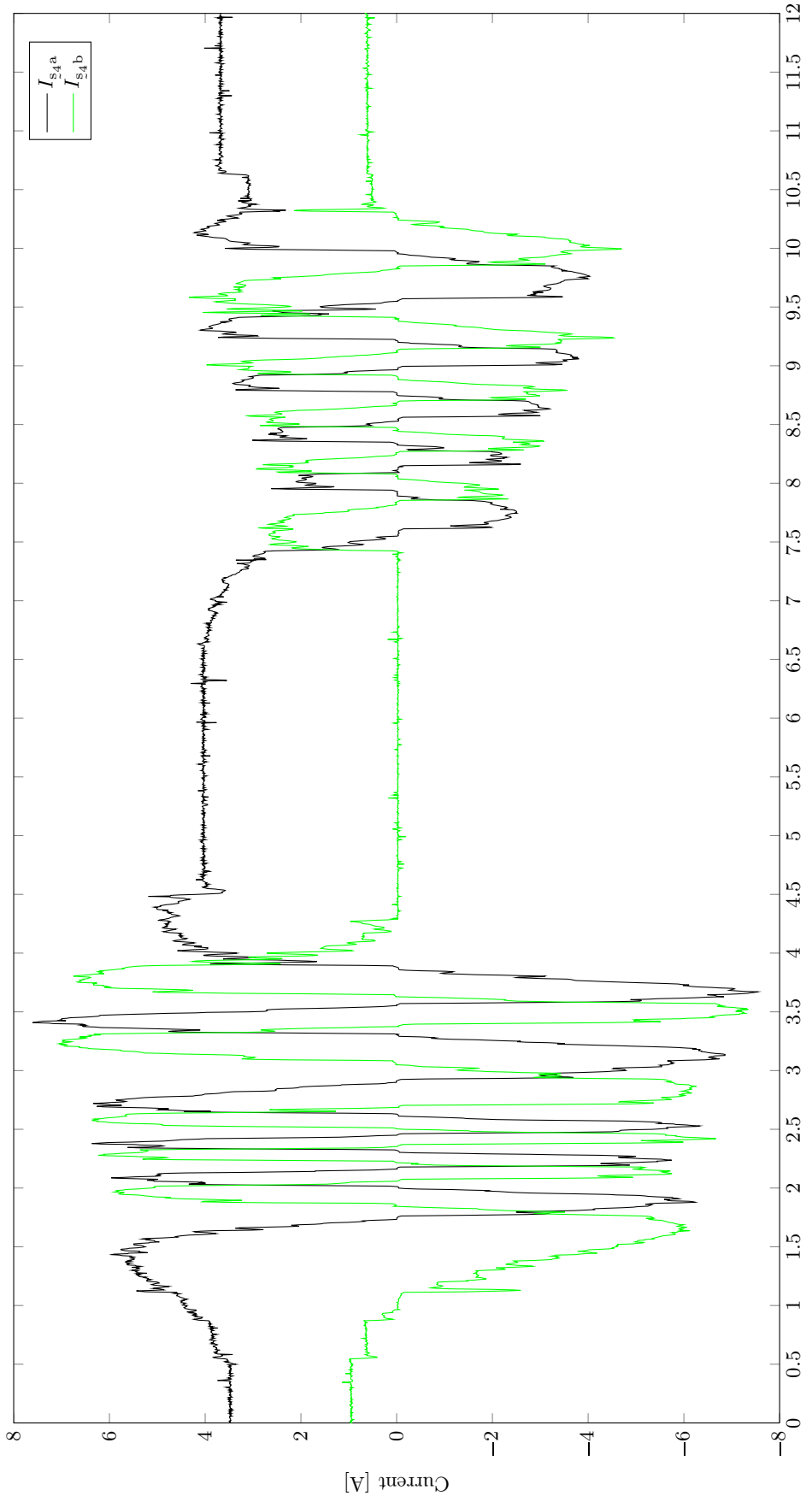

Figure 6.32: Measured phase currents for stator section 4

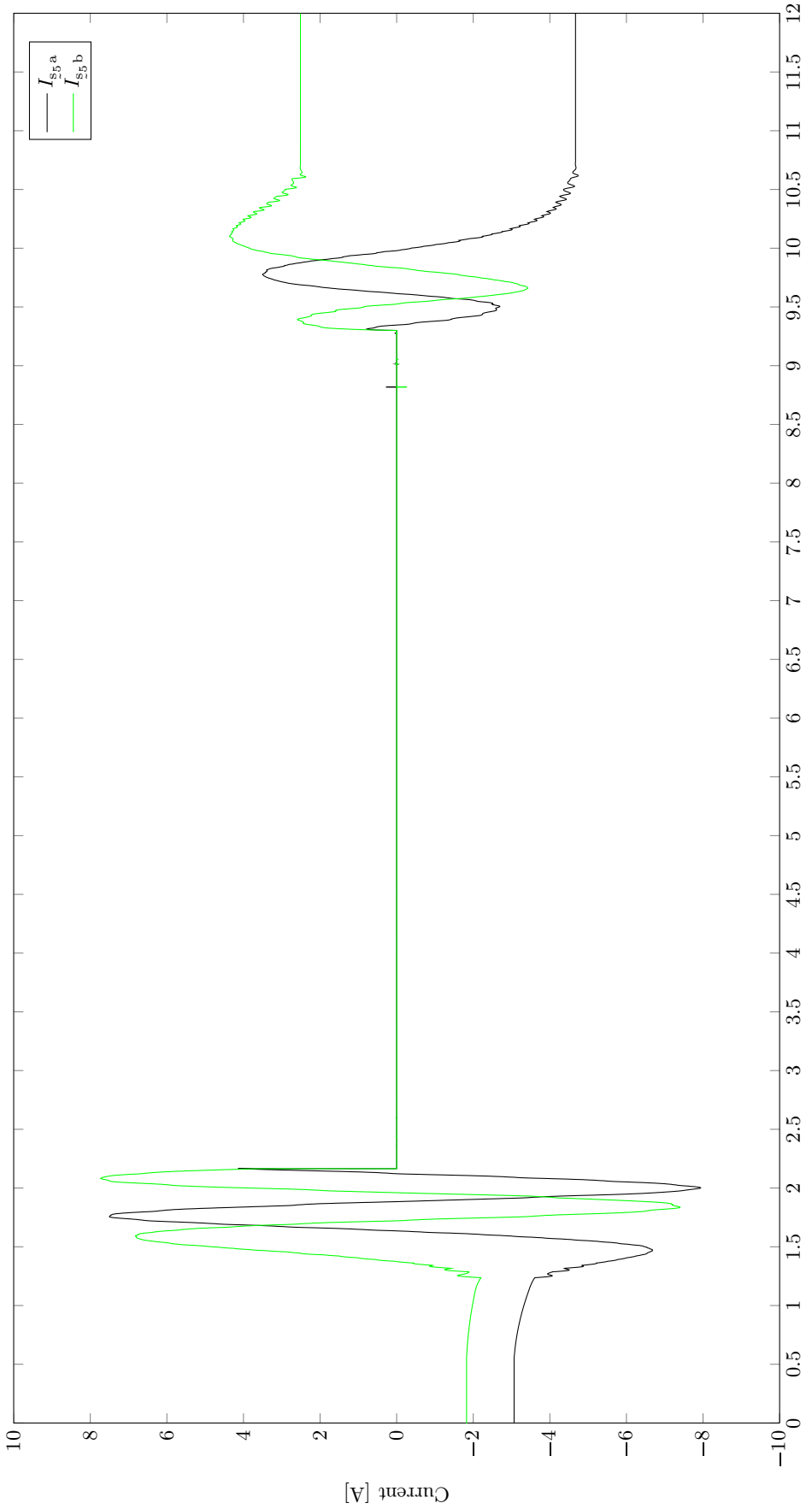

Figure 6.33: Simulated phase currents for stator section 5

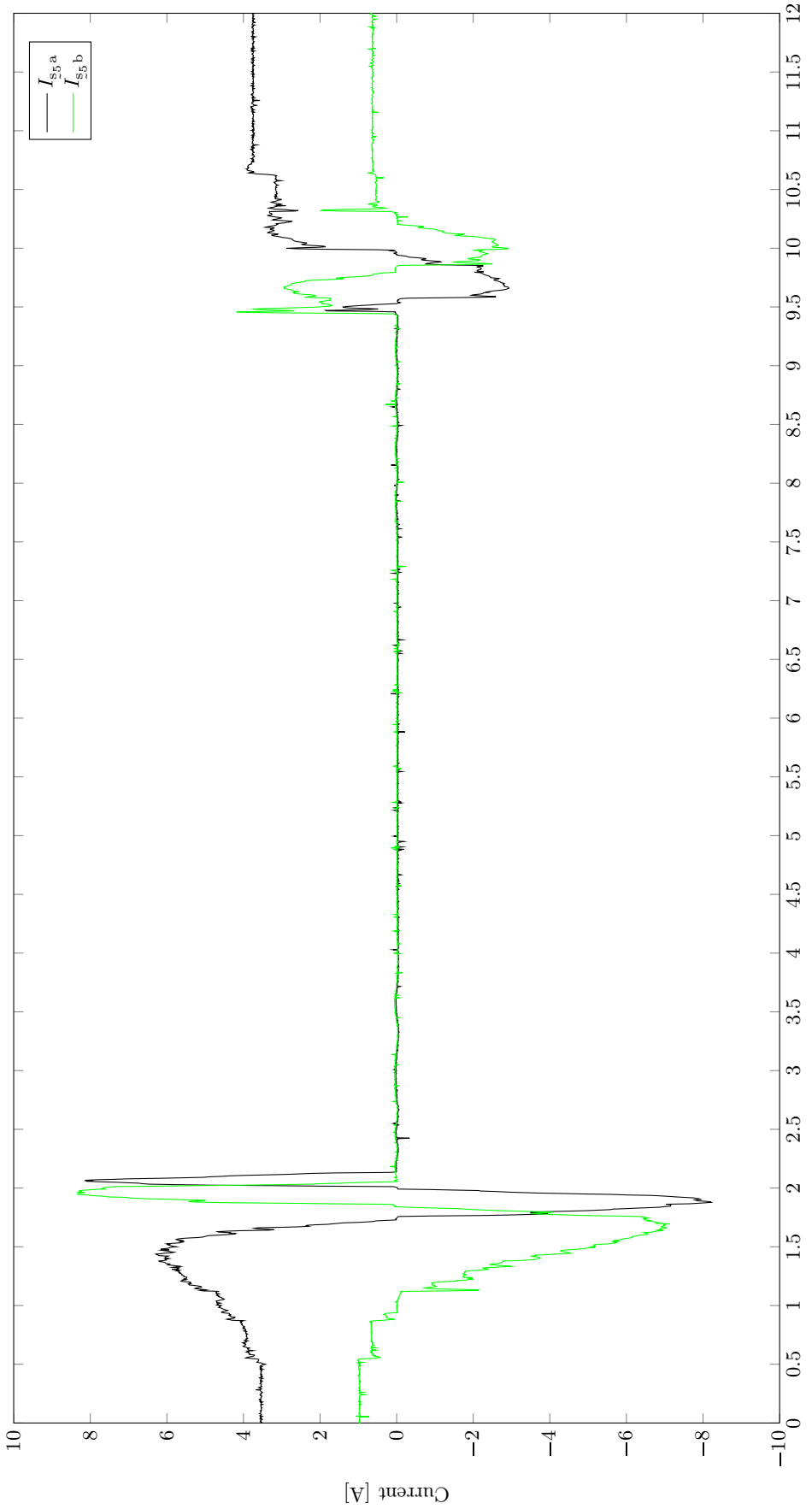

Figure 6.34: Measured phase currents for stator section 5

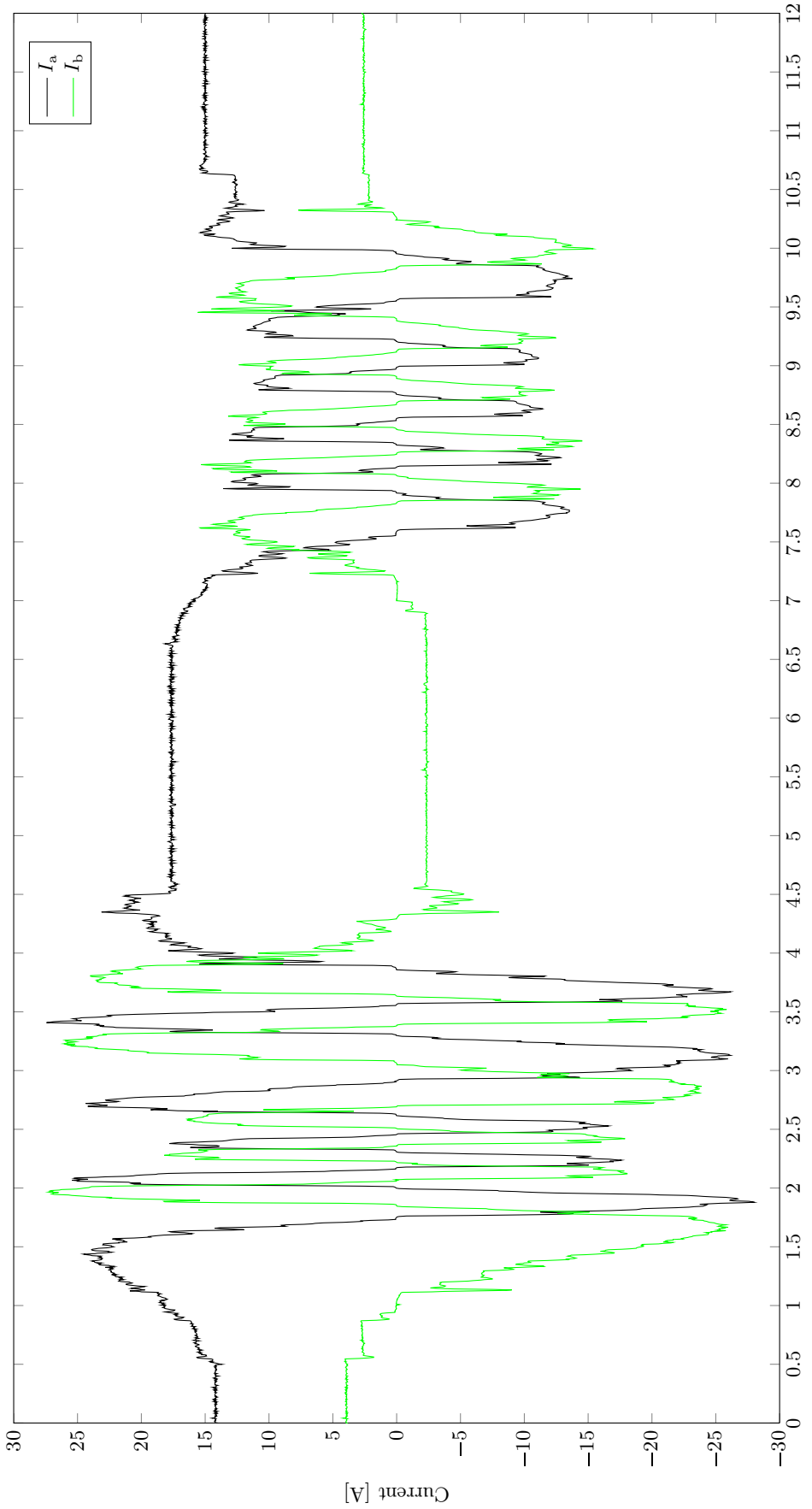

Figure 6.35: Measured inverter phase currents

The simulated and measured d-axis current waveforms are provided in figure 6.36 and figure 6.37, respectively. The motor controller exhibits good disturbance rejection whilst keeping the d-axis component of the current close to zero. Also, the simulated and measured waveforms of the q-axis current are provided in figure 6.38 and figure 6.39. Likewise, the motor controller is shown to be effective at tracking the q-axis current reference, which is proportional to the force reference.

In accordance with the segmented-stator control strategy, section-switching events occur as the reaction plate moves along the stator. They are triggered by the reaction plate's position. Table 6.4 summarises these events and provides the corresponding reaction plate positions and timings for the experimental results.

Table 6.4: Stator section switching events for experimental results

	Switch active representative section	Energise/de-energise section 1	Energise/de-energise section 5
Reaction plate position	576 mm	648 mm	792 mm
Time of crossing (moving in negative direction)	3,33 s	2,64 s	2,02 s
Time of crossing (moving in positive direction)	8,08 s	8,48 s	9,43 s

The zoomed-in plots of the phase currents for section 2 and section 3, provided in figure 6.40 and figure 6.41, show that they are closely matched when the role of active representative section is changed from the one to the other. This validates the assumption that the currents flowing in two identical, fully-covered stator sections are equal in steady-state.

Figure 6.42 and figure 6.43 provide zoomed-in views of the section 1 and section 5 phase currents when they are each energised (as the reaction plate starts to cover them). The phase currents for section 3, the active representative section, are also shown for reference. It can be seen that the latching of the solid-state contactors is sometimes delayed (due to their internal zero-voltage-crossing turn-on logic).

Lastly, figures 6.44 and 6.45 show the phase currents for section 1 and section 5 when they are de-energised. Since the contactors are thyristor-based, they continue to conduct until a zero-current crossing occurs. This does not cause a disturbance, however, because the reaction plate is no longer interacting with that section.

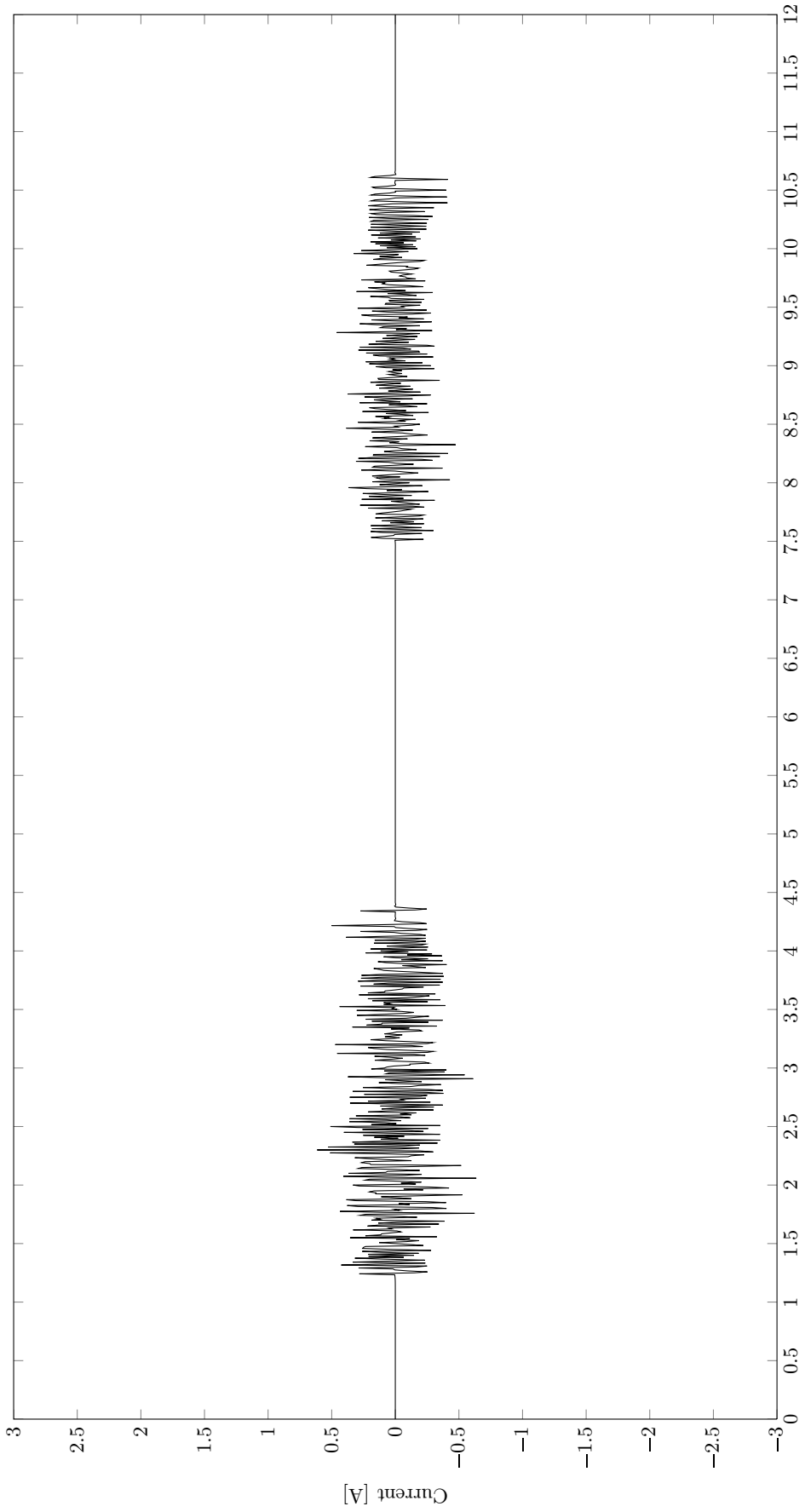

Figure 6.36: Simulated d-axis current for representative section

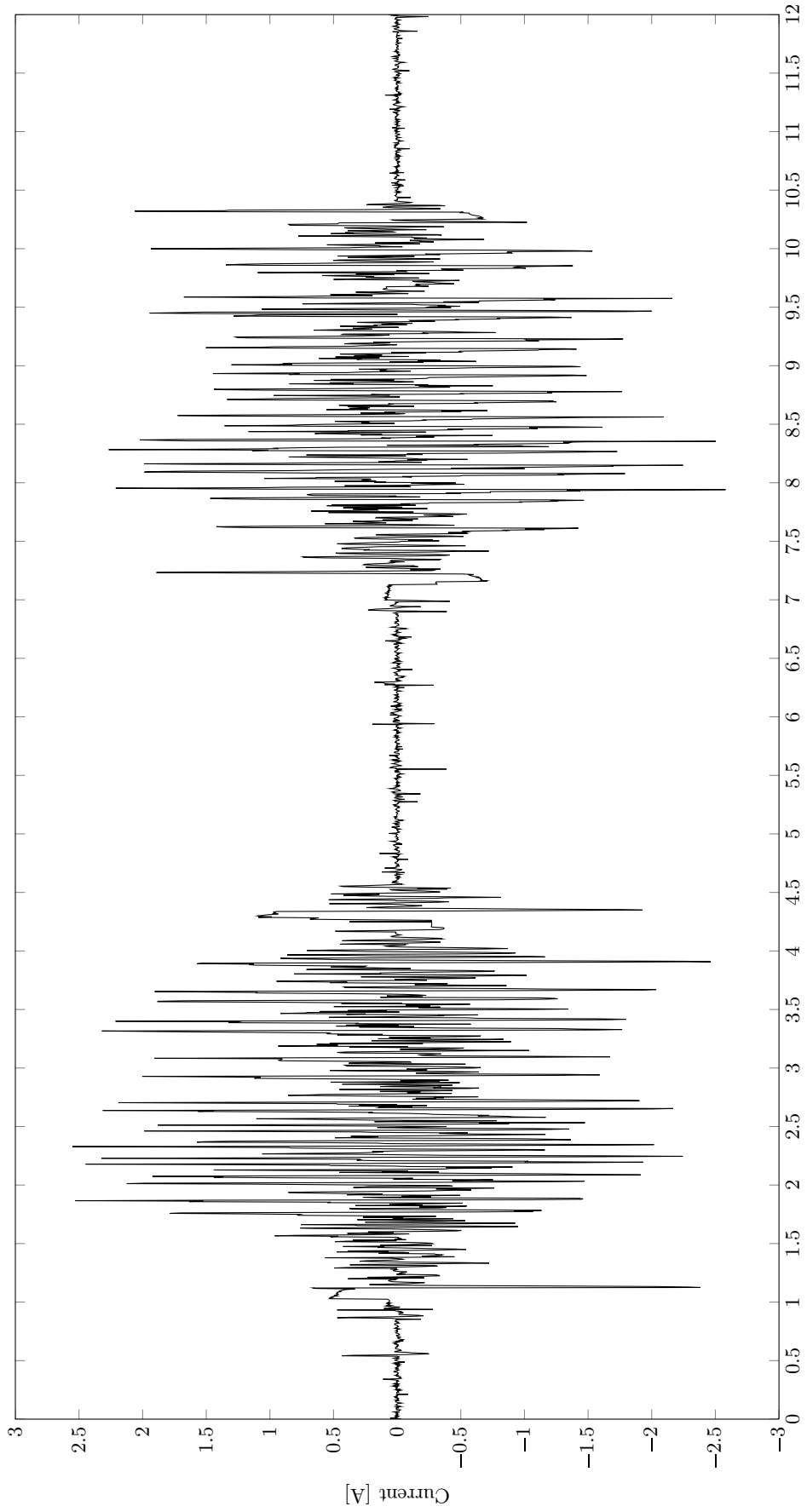

Figure 6.37: Measured d-axis current for representative section

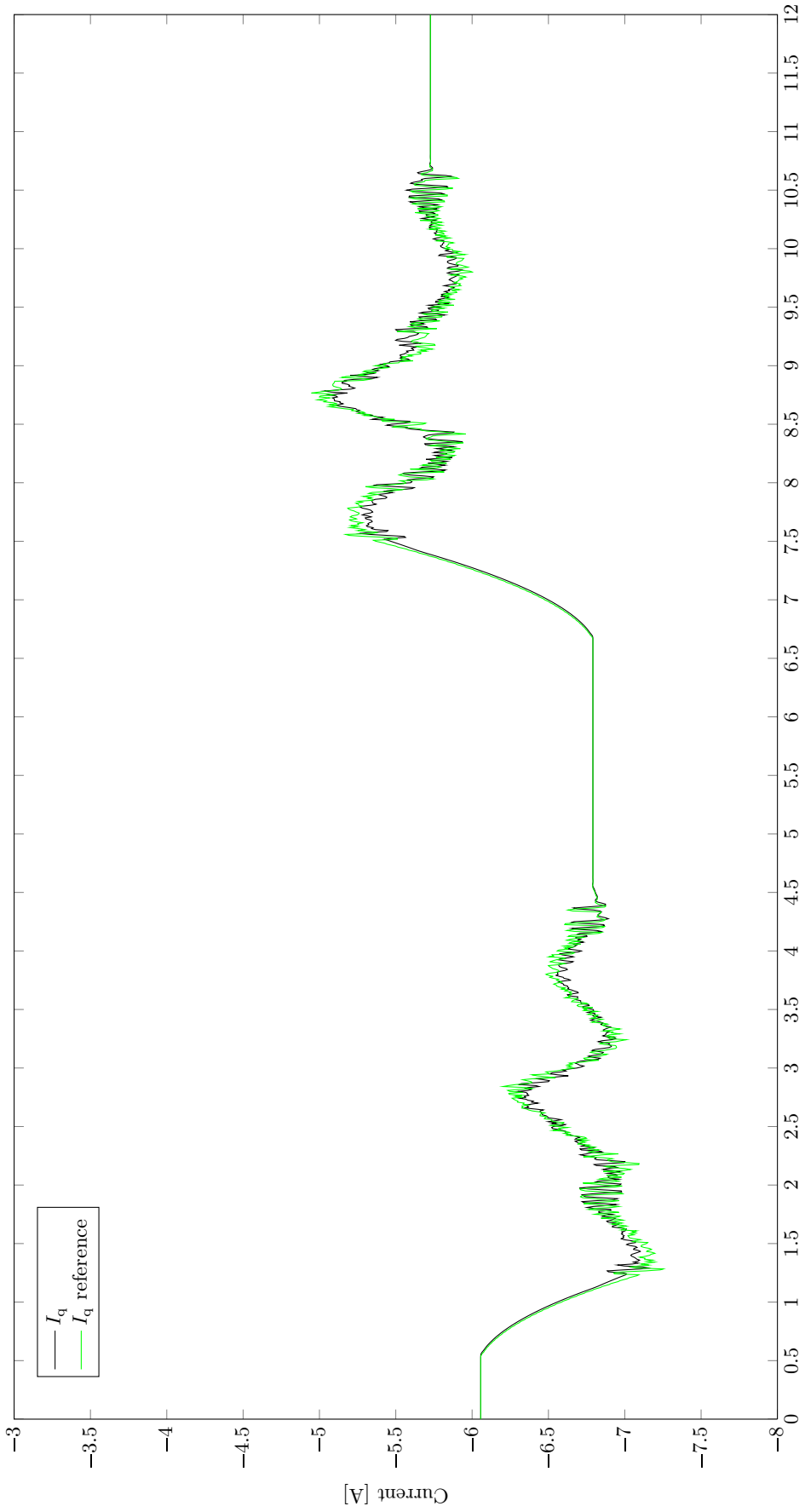

Figure 6.38: Simulated q-axis current for representative section, compared to the controller reference

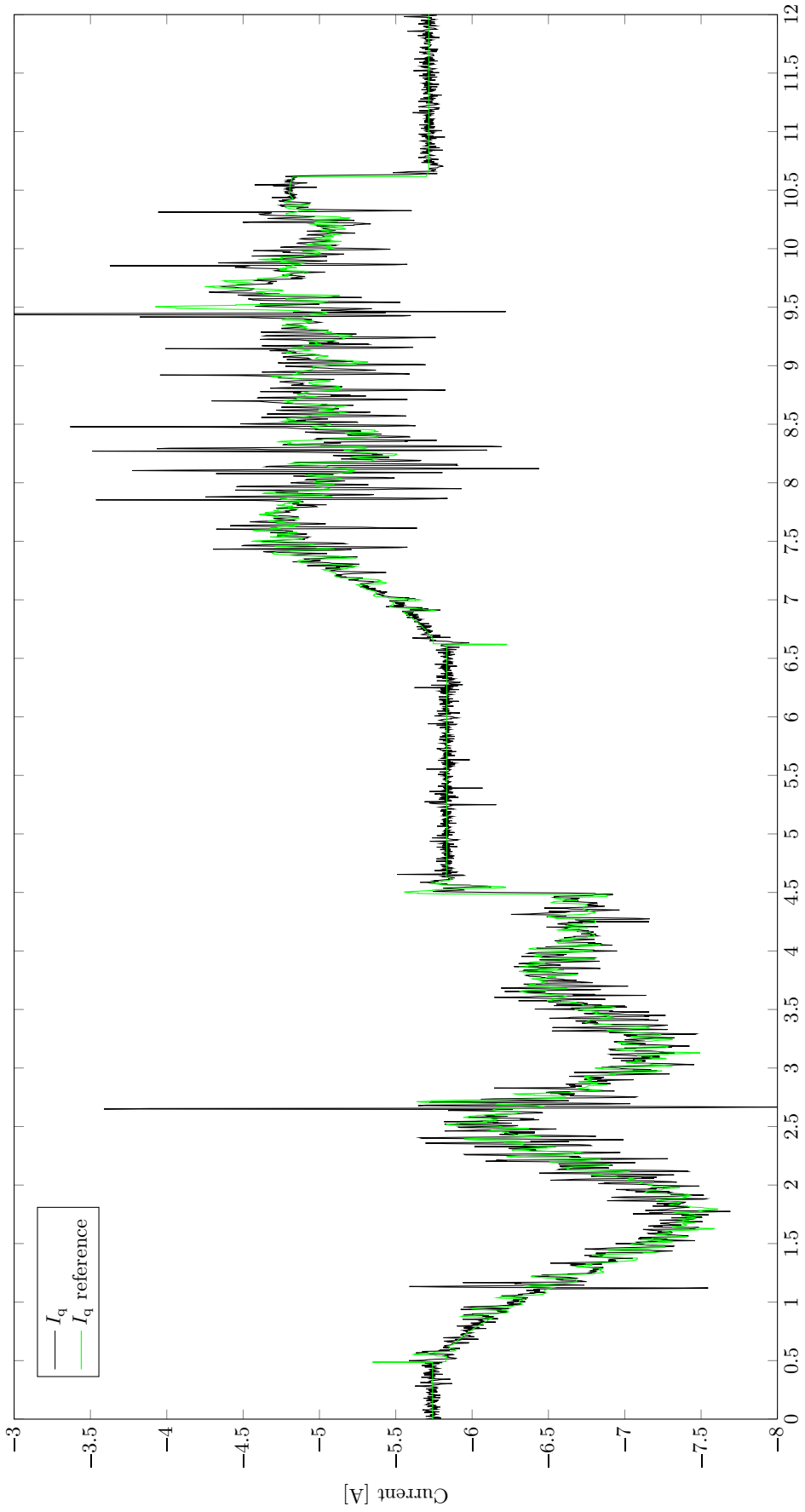

Figure 6.39: Measured q-axis current for representative section, compared to the controller reference

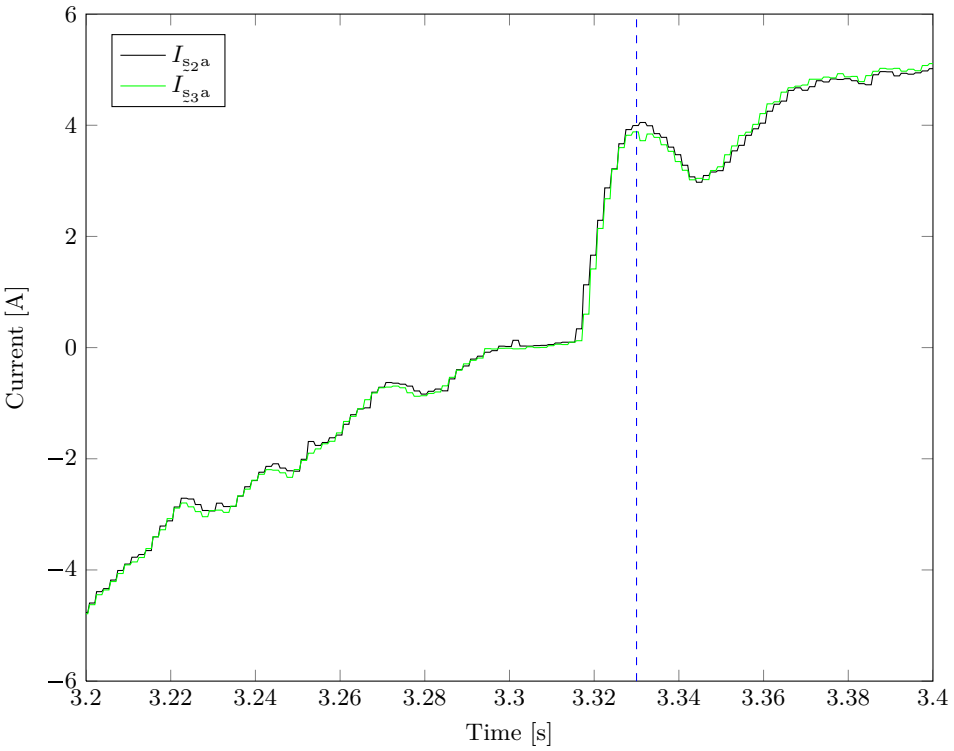

(a) Phase 'a' currents

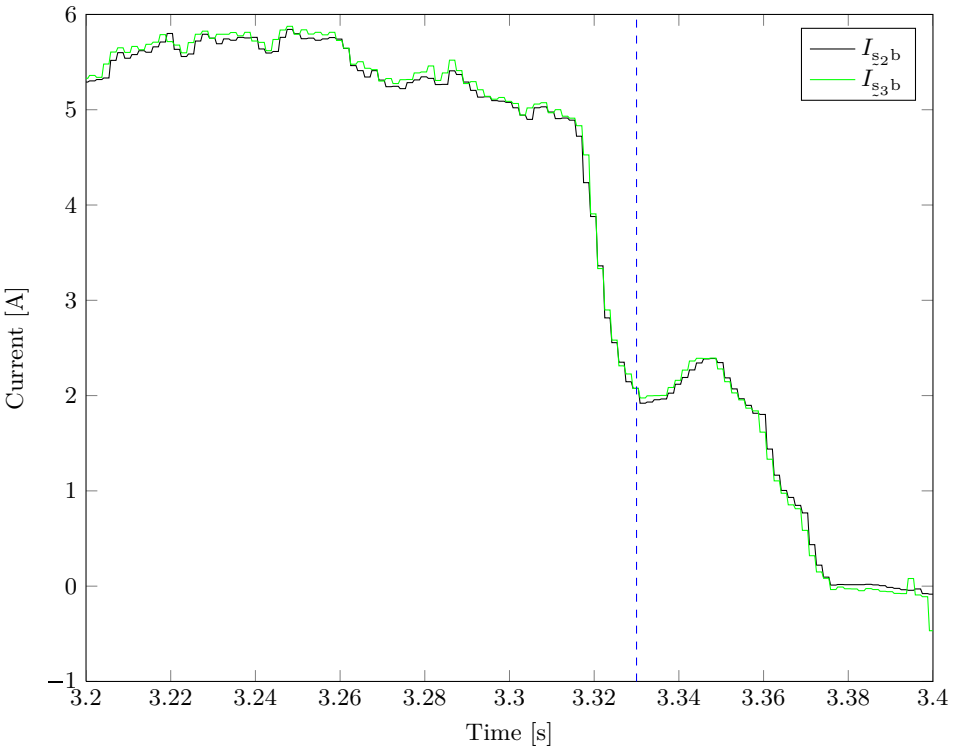

(b) Phase 'b' currents

Figure 6.40: Switch active representative section from section 3 to section 2

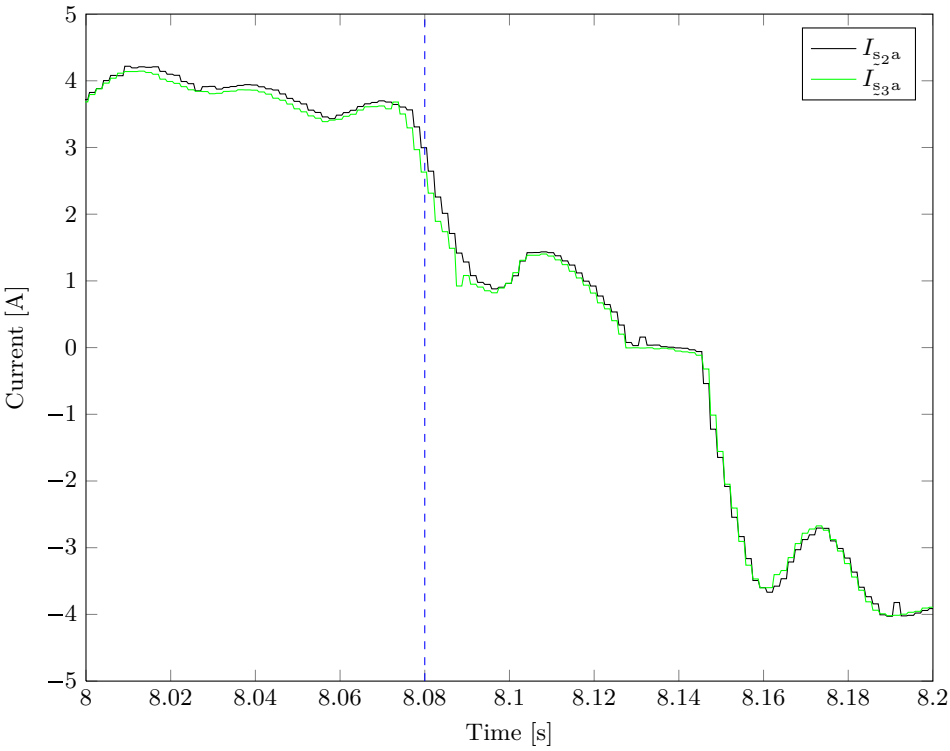

(a) Phase 'a' currents

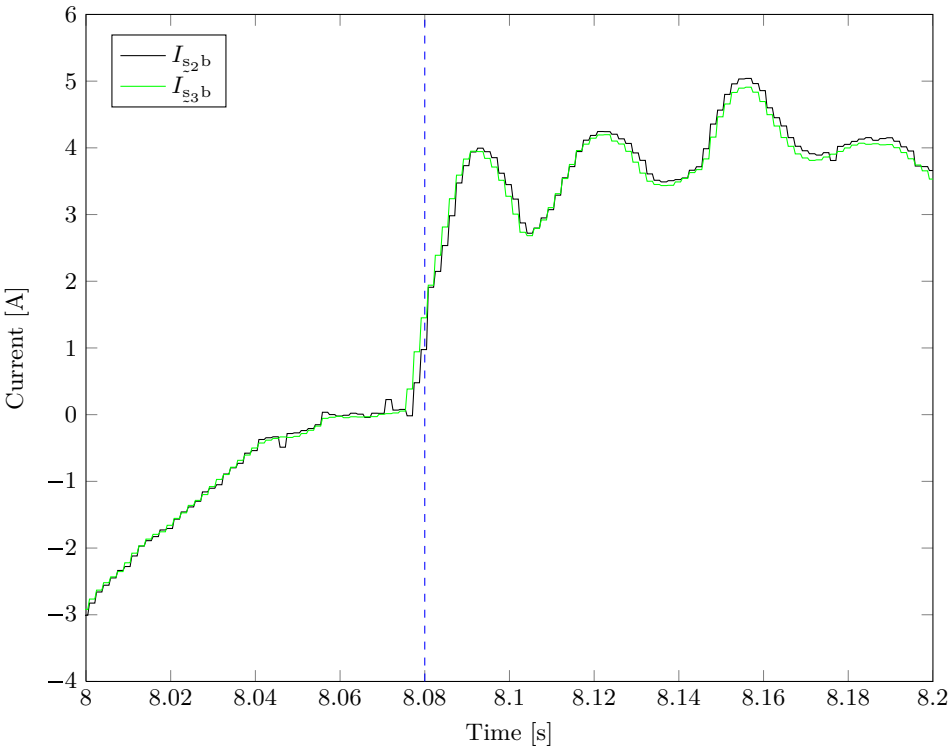

(b) Phase 'b' currents

Figure 6.41: Switch active representative section from section 2 to section 3

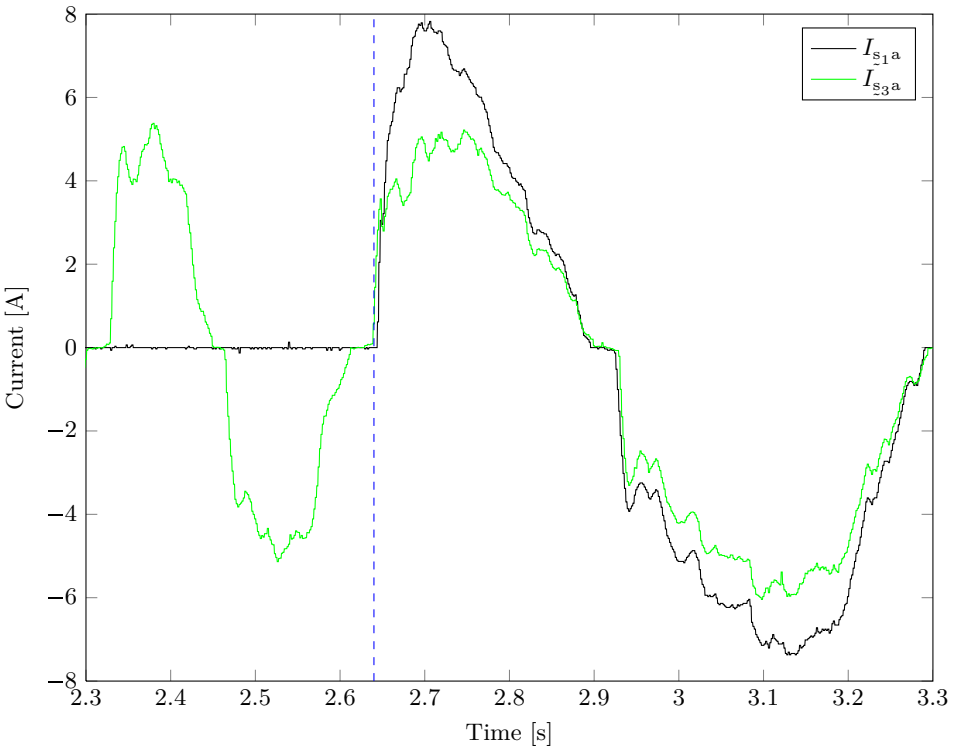

(a) Phase 'a' currents

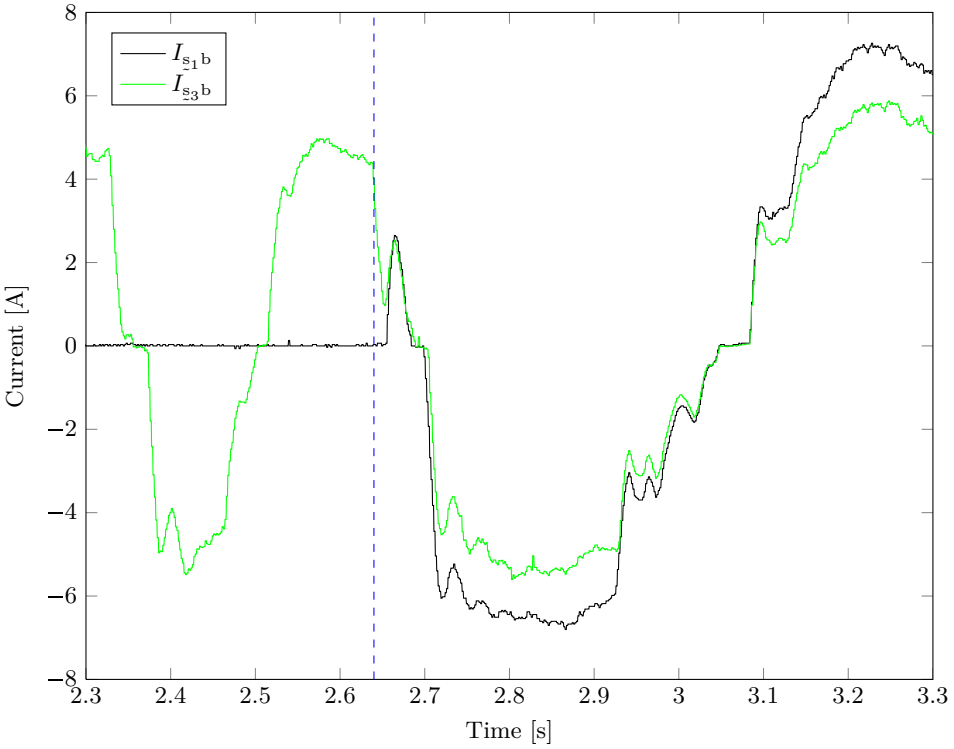

(b) Phase 'b' currents

Figure 6.42: Energising stator section 1

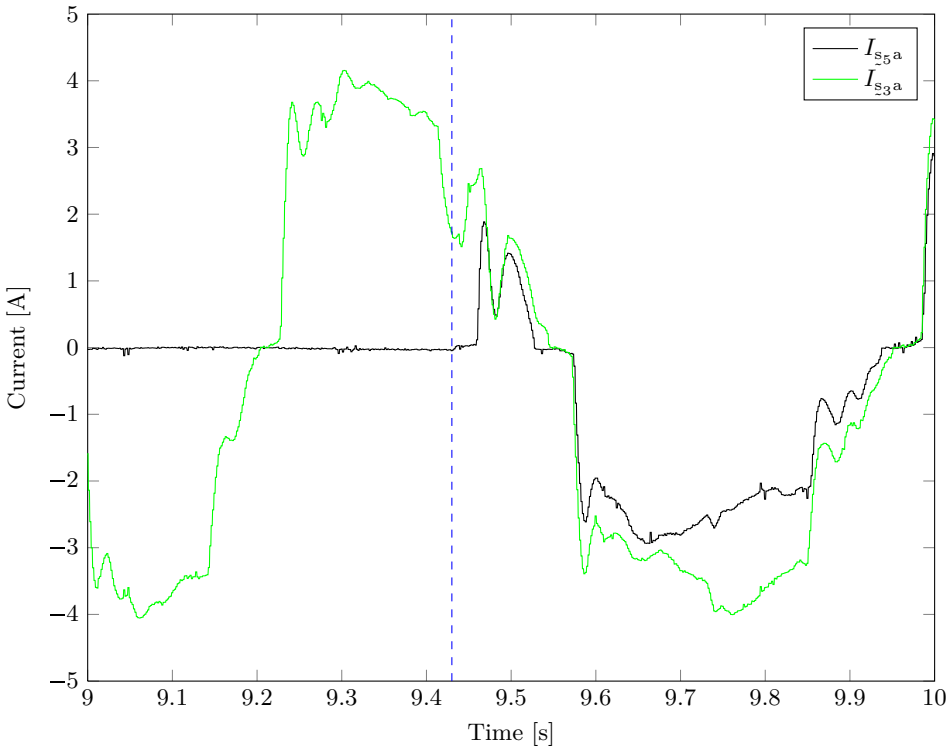

(a) Phase 'a' currents

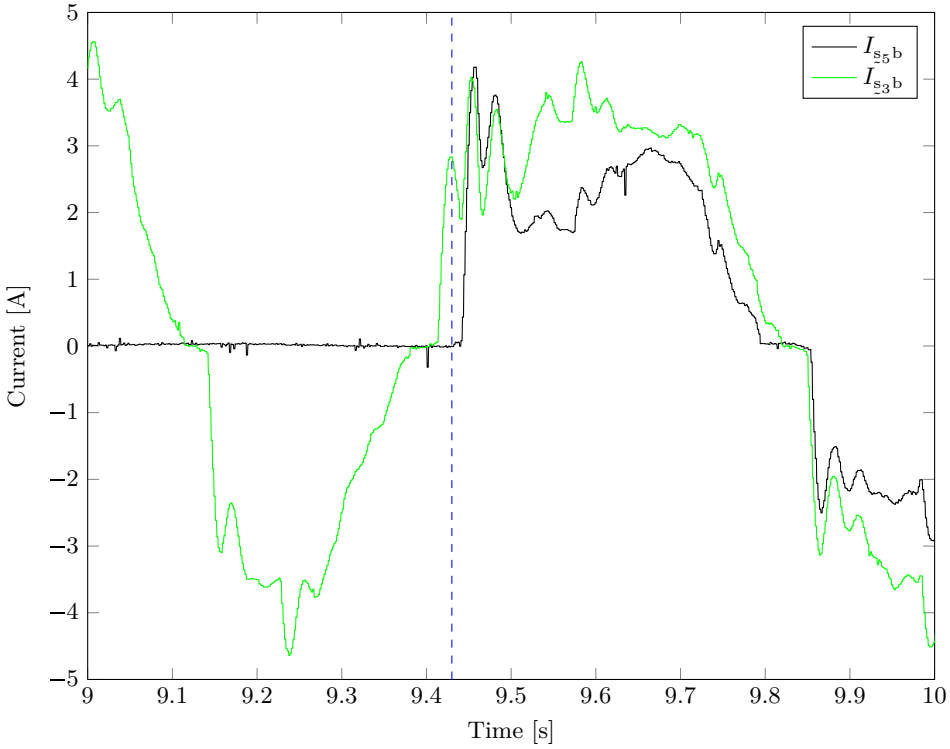

(b) Phase 'b' currents

Figure 6.43: Energising stator section 5

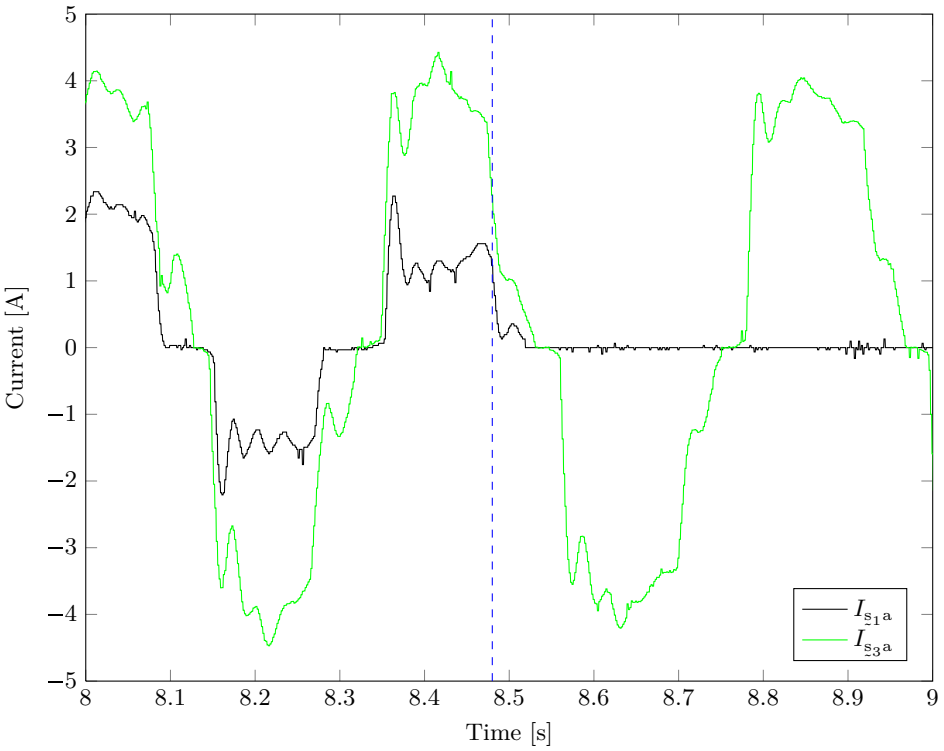

(a) Phase 'a' currents

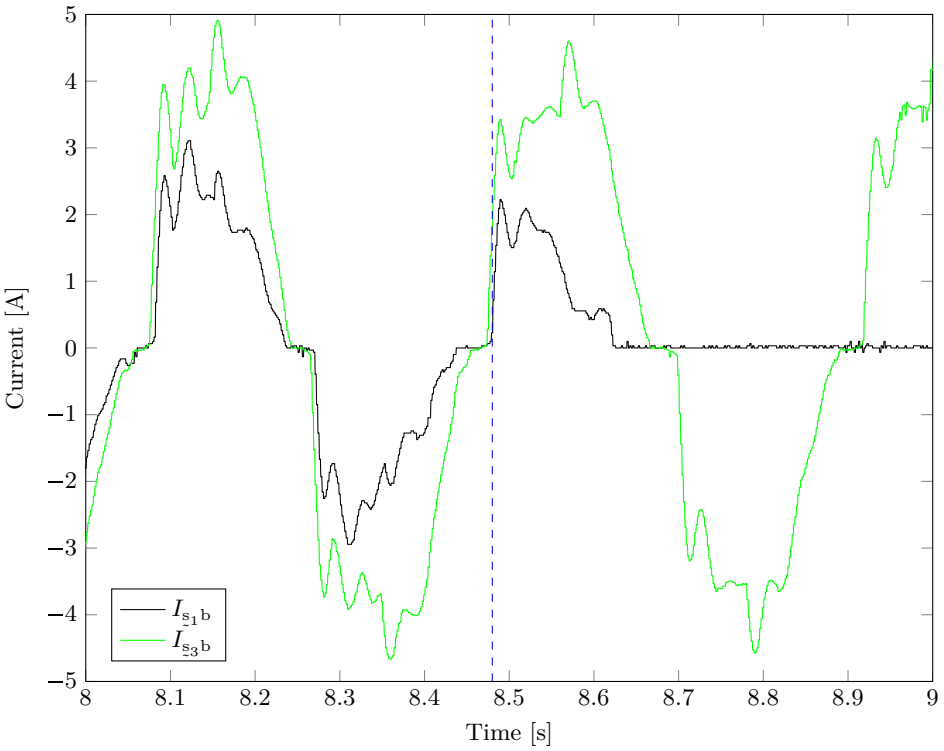

(b) Phase 'b' currents

Figure 6.44: De-energising stator section 1

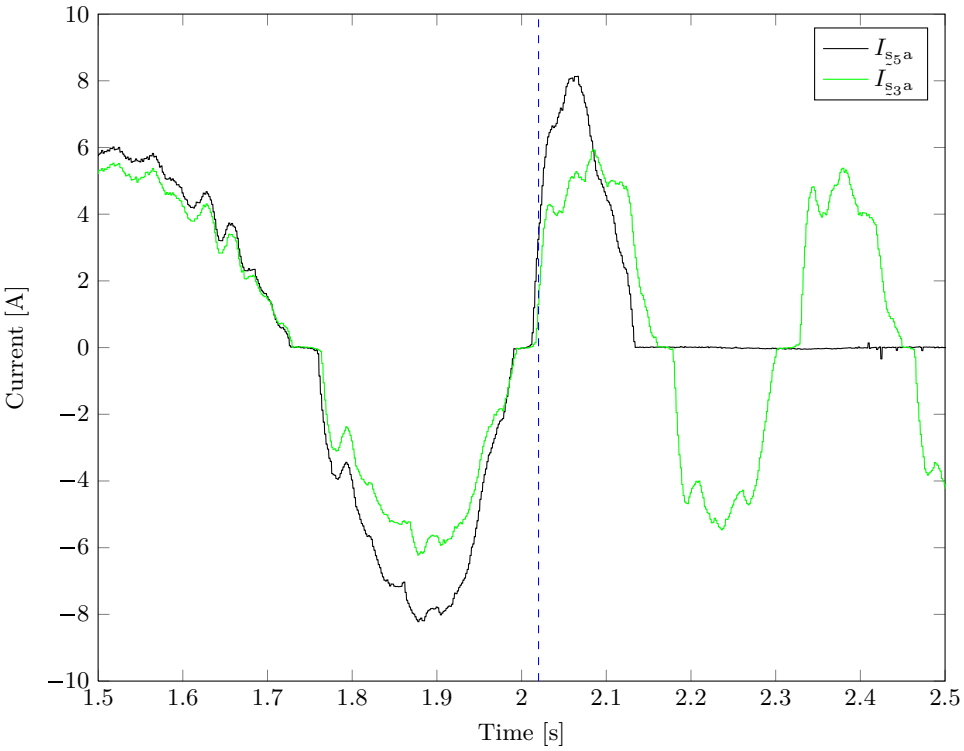

(a) Phase 'a' currents

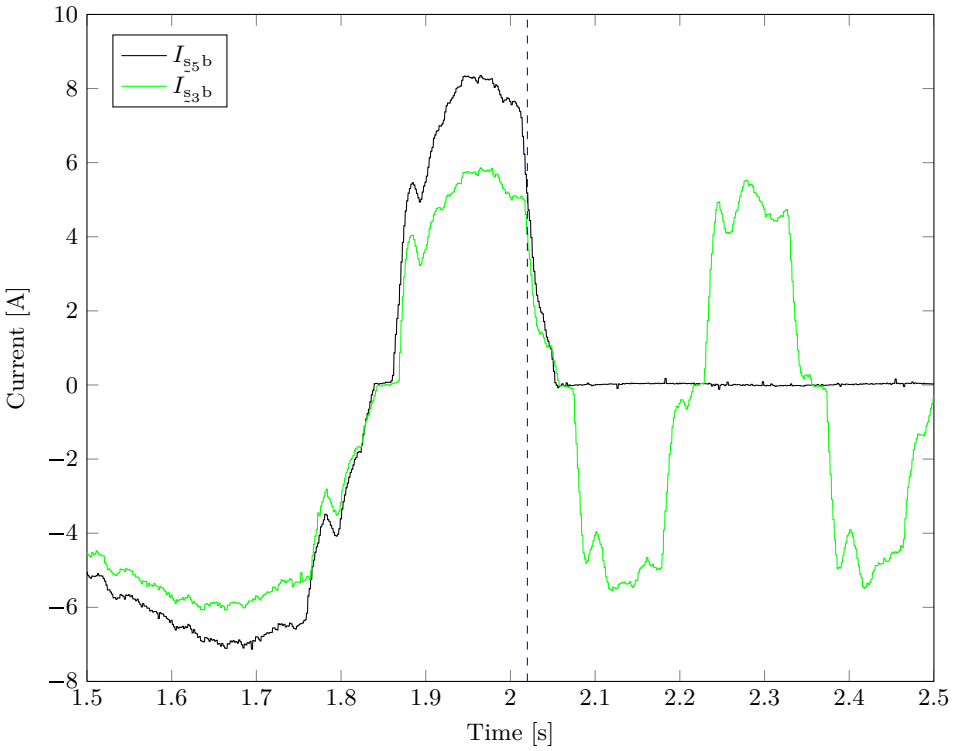

(b) Phase 'b' currents

Figure 6.45: De-energising stator section 5

Chapter 7

Conclusion

7.1 Hybrid magnetic-equivalent-circuit and finite element method

An extended magnetic-equivalent-circuit approach for the dynamic simulation of electromagnetic systems has been presented. This method leverages off the computational efficiency of a large-scale lumped-parameter MEC formulation, with networks of interconnected flux tubes for highly-permeable polygonal regions where the magnetic flux is well-channelled, and accounts for the flux flowing from those boundaries into surrounding constant-permeability regions by the superposition of a plurality of representative mmf sources. The method is intended for dynamic simulation because the computation required at each time step is dramatically reduced at the expense of having to precompute sets of parameters. Furthermore, any magnetic nonlinearity due to saturation occurs within these more permeable regions and so this computational complexity is restricted to the large-scale grid formulation.

At each time step, for an input of the current flowing in each phase winding, the electromagnetic force acting on the selected group of moving components is calculated using an approximation of the Maxwell Stress Tensor method and the winding flux linkages are obtained by superposition. Hence, to model a full electromagnetic system, this magnetic model can be combined with electric circuit and mechanical-interaction models that, at each time step, return the currents flowing in each phase and the displacement of the moving components, respectively.

Some of the work's initial limitations and shortcomings were addressed, primarily by extending the concept of a traditional flux tube element to a 2-dimensional flux tube element and by using the Finite Element Method to precompute the required parameter sets rather than using a Schwarz-Christoffel conformal mapping approach. Examples of the conformal mapping approach have been included, though, to demonstrate how rectified mapping can be used to obtain magnetic field solutions for non-trivial geometries.

The detailed worked example demonstrates the methodology and the results obtained are shown to be accurate compared to pure FEM solutions, so long as the relative permeability of the MEC regions is high compared to the surrounding regions. The normalised percentage errors for the obtained boundary flux values and flux linkages are less than 5 % for the example problem when using the nonlinear B-H curves of the materials or a constant relative permeability of at least 100. It may be argued that the MEC grid should be refined to the point where the solution accuracy is, in fact, comparable to a pure FEM solution. However, the very intention of the presented hybrid method is that an intuitive large-scale meshing of the high-permeability regions provides sufficient accuracy given the gain in computation speed for dynamic simulation problems. Should a vastly smaller grid be used for the MEC regions, it would be more efficient to just use the Magnetic Cell Method, Finite Integration Technique or FEM over the entire problem space. The demonstrated decline in accuracy with a drop in the relative permeability of the MEC-represented regions to their surroundings, provides a useful gauge for deciding whether it is appropriate to apply the presented method to a particular electromagnetic problem.

7.1.1 Recommendations for further work

It is suggested that an improved method to obtain the mutual permeances and normalised source boundary fluxes be pursued. Specifically, it is anticipated that these values can be expressed as closed-form boundary integral equations rather than having to be calculated by FEM [71]. Furthermore, although the presented hybrid method yields relatively accurate results for the boundary fluxes and flux linkages, a way to meliorate the accuracy of the force calculation should be further investigated. The relative inaccuracy with the presented approach is as a consequence of the force being calculated using the average field intensity along each moving boundary, rather than being sensitive to the often-significant variation in field intensity along the

boundaries. Also, research into the use of a more generic quadrilateral flux tube element would be valuable because such elements could cater for a broader range of geometries than the rectangular flux tube elements.

Lastly, to obtain an objective measure of the method's performance for dynamic simulation, the computation time for a benchmark dynamic problem solved by the hybrid method should be compared to those for other magnetic modelling methods implemented on the same computing platform.

7.2 Motor dynamic model

A fully parametrised and generic dynamic model of a segmented-stator permanent magnet linear synchronous motor has been devised and implemented as a custom blockset for Simulink®. For detailed simulations, lookup tables are populated with motor parameters that are precomputed using FEM, as a function of reaction plate position. A reduced version of the model can also be selected, which omits any cross-coupling between the d and q axes. This simplified model is appropriate for designing and tuning the control loops in the motor vector controller.

7.2.1 Recommendations for further work

To better model motors that exhibit significant magnetic saturation in the stator, it is anticipated that the presented model can be extended to account for magnetic saturation effects by using precomputed parameter lookup tables that depend on the magnitude of the currents as well as the relative position of the reaction plate.

7.3 Linear motor feeding and control strategy

A linear motor feeding and control strategy has been presented that enables any motor control method originally developed for rotary motors to be applied to linear synchronous motors. This is achieved through careful segmentation of the linear motor stator and the addition of an intermediate switching layer between the inverter and stator segments. The inverter output voltage, which is common to all energised stator sections, is controlled with a standard motor vector control technique using a measurement of only the currents that are flowing within the active representative

stator section. The currents flowing within the other energised stator sections need only be monitored to detect fault conditions. The choice of which stator sections are energised and which of these is the active representative section depends on the position of the reaction plate at each point in time. A significant advantage of the novel approach over other segmentation and control strategies is that over a stator block (comprising many sections), the linear motor can be fed with a single inverter per conveyance rather than at least two inverters per conveyance. Also, if only fully-covered stator sections are energised, maximum electrical efficiency is achieved as all of the energised stator length contributes to the propulsion force. Furthermore, very short headway is required between independently-controlled conveyances.

The strategy is best suited to high-force, straight-line-motion applications such as ropeless hoisting, with a low number of conveyances per block length. For a long-distance track with many vehicles and variable or low force requirements, however, it is preferable to use stator sections that are much longer than the vehicles with an inverter dedicated to each stator section. This is owing to the cost of the high number of section-side switches needed when several vehicles occupy a stator block.

The underlying principle of the control strategy is demonstrated to be effective with a purpose-built laboratory prototype system, despite complications due to the behaviour of the particular solid-state contactors used.

7.3.1 Recommendations for further work

The solid-state contactors used to implement the prototype system are not ideal for this application as they do not trigger reliably with the non-sinusoidal inverter output voltage. Thus, it is suggested that solid-state or electromechanical contactors that are better-suited to these atypical operating conditions be designed or sourced.

A proposed improvement to the control strategy is to further modulate the supply voltage to the outer stator sections that are only partially covered by the reaction plate. This is because the winding inductance of a partially-covered section is lower than that of a fully-covered section and there is less back-emf induced in the windings. It is anticipated that improved efficiency can be achieved by reducing the effective supply voltage to these partially-covered sections so that their currents more closely match the currents flowing in the fully-covered sections.

Lastly, it would be desirable to achieve full sensorless control of the conveyance(s). In order to do this, it is necessary to detect the initial position of each reaction plate within a stator block. Thereafter, the incremental position estimates from a sensorless motor vector control technique can be used to track its position. It is proposed that a binary search based on winding inductance measurement be used to find the approximate initial position because the inductance of each winding is dependent on how much of it is covered by the reaction plate. However, having several reaction plates within a stator block complicates this procedure.

Appendix A

Hybrid Magnetic-Equivalent-Circuit and Finite Element Method

This appendix details the implementation of the hybrid magnetic modelling method using MATLAB® and FEMM. Additionally, it contains the detailed inputs and outputs for the worked example, as well as a section demonstrating the use of Schwarz-Christoffel rectified mapping to obtain magnetic field solutions for non-trivial geometries.

A.1 Implementation in Matlab® and FEMM

A.1.1 Overview

Figure A.1 serves as an overview of the custom MATLAB® functions that implement the hybrid magnetic modelling method, as well as those functions to solve the example problem and compare the method's outputs to pure FEM solutions.

A.1.2 Problem specification

Materials

A MATLAB® structure array, '`material_chi`', is used to store all of the parameters for the materials used in a particular problem. The material's '`type`' field must be set to 'Linear', 'Nonlinear', 'Magnet' or 'Coil'. 'Linear' implies that the material has a constant relative permeability, specified by the '`params.mur`' field, and 'Nonlinear'

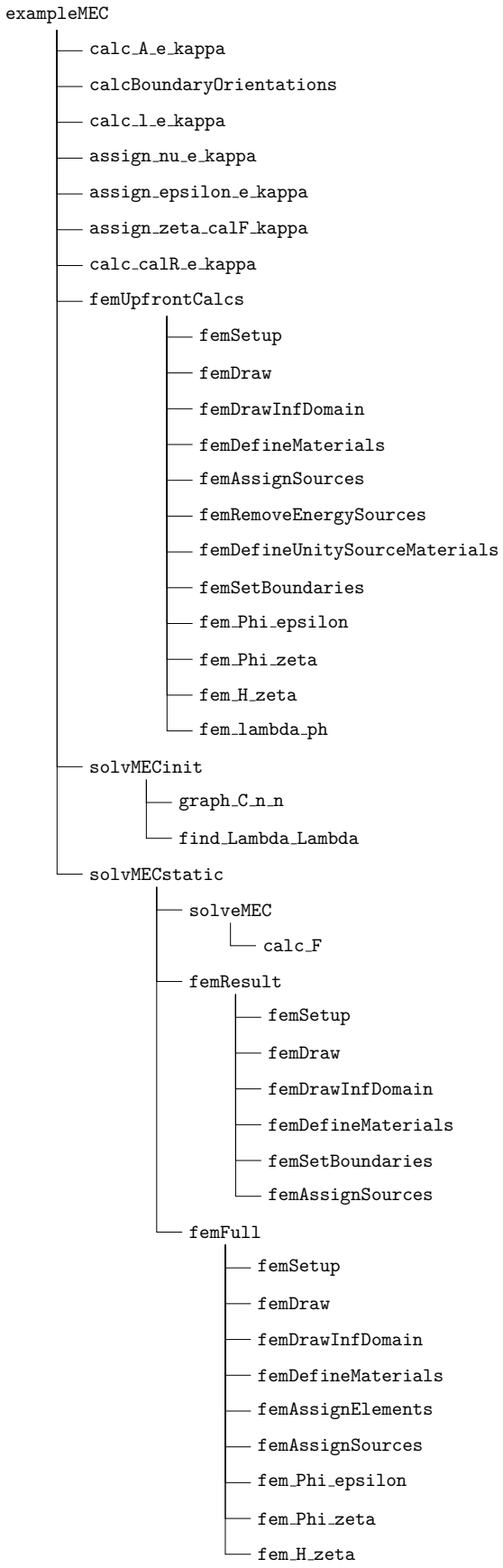

Figure A.1: Dependency graph for custom MATLAB® functions

means that the B-H curve, specified by the points in the '`params.B`' and '`params.H`' arrays, should be used. Each unique permanent magnet material has a specified magnetic coercivity, Hc, set with the '`params.Hc`' field, and a relative permeability, μr set by the '`params.mur`' field. Lastly, each coil is specified by its relative permeability, '`params.mur`', the winding phase it belongs to, '`params.ph`', and its number of turns, '`params.turns`'.

Geometry

The vertices for each flux tube element, $\boldsymbol{p}_{\underset{\sim}{e}\underset{\sim}{v}}$, are specified in the complex plane as the array '`p_e_v`'. Note that the vertices are assumed to be stored in anti-clockwise order. The boolean array $\mathbf{M}_{\delta\underset{\sim}{e}}$ ('`M_delta_e`') specifies which of the flux tube elements move and each element is assigned a material-type index, χ, with the array '`chi_e`'. Since the sources are also assumed to be rectangular in this implementation of the method, they are correspondingly defined by $\boldsymbol{p}_{\underset{\sim}{\mathcal{F}}\underset{\sim}{v}}$ ('`p_calF_v`'), $\mathbf{M}_{\delta\underset{\sim}{\mathcal{F}}}$ ('M_delta_calF') and $\boldsymbol{\chi}_{\underset{\sim}{\mathcal{F}}}$ ('`chi_calF`').

The problem depth, d, is common to all elements and sources and the direction of movement, $\hat{\boldsymbol{x}}$, is specified as a unit vector in the complex plane ('`hatx`').

A.1.3 Calculation of element properties

Code listing A.1 is a function that returns the four boundary surface areas for each element, given the problem space depth, d and the element vertices. The outward-facing boundary normal vectors, $\hat{\boldsymbol{n}}_{\underset{\sim}{e}\underset{\sim}{\kappa}}$ ('`hatn_e_kappa`'), and corresponding tangential unit vectors, $\hat{\boldsymbol{t}}_{\underset{\sim}{e}\underset{\sim}{\kappa}}$ ('`hatt_e_kappa`'), are calculated by function A.2. Additionally, the element region lengths, $\boldsymbol{l}_{\underset{\sim}{e}\underset{\sim}{\kappa}}$ ('`l_e_kappa`'), are calculated by the function A.3.

Code listing A.1: Calculate element region cross-sectional areas (`calc_A_e_kappa.m`)

```
function A_e_kappa = calc_A_e_kappa(p_e_v,d)
%  Calculate element boundary surface areas

[N_e,N_v] = size(p_e_v);
N_kappa = N_v;
A_e_kappa = zeros(N_e,N_kappa); %Preallocate output
wrapIdx = @(idx,N_idx) (1+mod(idx-1,N_idx));
for idx_v = 1:N_v
  A_e_kappa(:,idx_v) = d*abs(p_e_v(:,wrapIdx(idx_v+1,N_v))-...
    p_e_v(:,idx_v));
end
```

Code listing A.2: Calculate boundary orientations (`calcBoundaryOrientations.m`)

```
function [hatn_e_kappa,hatt_e_kappa] = calcBoundaryOrientations(p_e_v)
%  Calculate boundary unit normal and tangent vectors

[N_e,N_v] = size(p_e_v);
N_kappa = N_v;
hatt_e_kappa = zeros(N_e,N_kappa); %Preallocate output
wrapIdx = @(idx,N_idx) (1+mod(idx-1,N_idx));
for idx_v = 1:N_v
  hatt_e_kappa(:,idx_v) = (p_e_v(:,wrapIdx(idx_v+1,N_v))-...
    p_e_v(:,idx_v))./abs(p_e_v(:,wrapIdx(idx_v+1,N_v))-...
    p_e_v(:,idx_v));
end
hatn_e_kappa = imag(hatt_e_kappa) - 1j*real(hatt_e_kappa);
```

Code listing A.3: Calculate element region lengths (`calc_l_e_kappa.m`)

```
function l_e_kappa = calc_l_e_kappa(p_e_v)
%  Calculate flux tube element region lengths

[N_e,N_kappa] = size(p_e_v);
l_e_kappa = zeros(N_e,N_kappa); %Preallocate output
l_e_kappa(:,[1,3]) = repmat((abs(p_e_v(:,1)-p_e_v(:,4))/2 + ...
    abs(p_e_v(:,2)-p_e_v(:,3))/2)/2,1,2);
l_e_kappa(:,[2,4]) = repmat((abs(p_e_v(:,2)-p_e_v(:,1))/2 + ...
    abs(p_e_v(:,3)-p_e_v(:,4))/2)/2,1,2);
```

A.1.4 Assignment of boundary indices

All flux tube element boundaries in the problem space are assigned a global boundary index, ν. If the boundary is an interior boundary, and thus shared between two

elements, the boundary index assigned for the second element is the negative of the boundary index for the first element. This is a convenient way to represent that the flux (always defined to flow outwards from an element region) is the negative of the flux returned by the solver for the corresponding global element boundary. Using global boundaries is a natural approach to markedly reduce the number of simultaneous equations that need to be solved.

Code listing A.4: Assign global element boundary indices (`assign_nu_e_kappa.m`)

```
function nu_e_kappa = assign_nu_e_kappa(p_e_v)
%  Assign global element boundary indices across the problem space

[N_e,N_v] = size(p_e_v);
N_kappa = N_v;
nu_e_kappa = zeros(N_e,N_kappa); %Preallocate output
nu_nu = [];
wrapIdx = @(idx,N_idx) (1+mod(idx-1,N_idx));
for idx_e = 1:N_e
  for idx_kappa = 1:N_kappa
    idx_v_1 = idx_kappa;
    idx_v_2 = wrapIdx(idx_v_1+1,N_v); %Choose adjacent vertex
    if ~isempty(nu_nu) %Boundary already assigned?
      idx_nu = -find(...
        (abs([nu_nu(:).p_1]-p_e_v(idx_e,idx_v_2)) < eps) & ...
        (abs([nu_nu(:).p_2]-p_e_v(idx_e,idx_v_1)) < eps),1);
    else
      idx_nu = [];
    end
    if isempty(idx_nu) %New boundary?
      nu_nu(end+1).p_1 = p_e_v(idx_e,idx_v_1); %#ok<AGROW>
      nu_nu(end).p_2 = p_e_v(idx_e,idx_v_2); %#ok<AGROW>
      idx_nu = numel(nu_nu);
    end
    nu_e_kappa(idx_e,idx_kappa) = idx_nu; %Assign boundary index
  end
end
```

An element boundary is determined to be an interior boundary by the presence of a matching negative global boundary index. All boundaries that are not in the set of interior boundaries are then sequentially allocated an exterior boundary index, forming the array $\underset{\sim}{\underset{\sim}{\epsilon}}_{e\kappa}$ (‘`epsilon_e_kappa`’). The exterior boundary index for all interior boundaries is set to zero. The function that performs this allocation is included as code listing A.5 and additionally returns $\underset{\sim}{\nu}_{\epsilon}$ (‘`nu_epsilon`’), the mapping of exterior element boundaries to global element boundaries.

Code listing A.5: Assign exterior element boundary indices (`assign_epsilon_e_kappa.m`)

```
function [epsilon_e_kappa nu_epsilon] = ...
  assign_epsilon_e_kappa(nu_e_kappa)
%  Assign global exterior boundary indices across flux tube elements

[N_e,N_kappa] = size(nu_e_kappa);
N_nu = max(nu_e_kappa(:));
```

Code listing A.5: Assign exterior element boundary indices (`assign_epsilon_e_kappa.m`) *... cont*

```
nu_iota = abs(nu_e_kappa(nu_e_kappa<0)); %Set of interior boundaries
N_iota = numel(nu_iota);
epsilon_e_kappa = zeros(N_e,N_kappa); %Preallocate output
nu_epsilon = zeros(N_nu-N_iota,1); %Preallocate output
idx_epsilon = 0;
for idx_e = 1:N_e
  for idx_kappa = 1:N_kappa
    if ~ismember(abs(nu_e_kappa(idx_e,idx_kappa)),nu_iota)
      idx_epsilon = idx_epsilon + 1;
      %Assign exterior boundary index
      epsilon_e_kappa(idx_e,idx_kappa) = idx_epsilon;
      %Update mapping from exterior boundary to global boundary
      nu_epsilon(idx_epsilon) = nu_e_kappa(idx_e,idx_kappa);
    end
  end
end
```

For the calculation of the electromagnetic force acting on the moving magnetic sources, it is necessary to calculate the flux flowing through every exterior boundary of each moving source region. Consequently, a global source boundary index, ζ, is assigned to each of these boundaries by the function included here as code listing A.6.

Code listing A.6: Assign moving source boundary indices (`assign_zeta_calF_kappa.m`)

```
function zeta_calF_kappa = assign_zeta_calF_kappa(p_calF_v,...
  M_delta_calF)
%  Assign source boundary indices for all moving sources

[N_calF,N_v] = size(p_calF_v);
N_kappa = N_v;
zeta_calF_kappa = zeros(N_calF,N_kappa); %Preallocate output
idx_zeta = 0;
for idx_calF = 1:N_calF
  if M_delta_calF(idx_calF) %Moving source?
    for idx_kappa = 1:N_kappa
      idx_zeta = idx_zeta + 1;
      %Assign source boundary index
      zeta_calF_kappa(idx_calF,idx_kappa) = idx_zeta;
    end
  end
end
```

A.1.5 Calculation of reluctances

Code listing A.7 calculates the element reluctances using their dimensions and assigned material properties. For a 'Linear' material type, the reluctance is given by that region's ratio of length to cross-sectional area, divided by its magnetic permeability. For a 'Nonlinear' material, the reluctance must be found as a function of flux. That is, for a particular value of flux, Φ, the reluctance, $\mathcal{R}(\Phi)$ is given by the mmf drop caused by the flux, $\mathcal{F}$, divided by Φ. These reluctances are stored as spline representations, with 'knots' at the specific fluxes resulting from the flux densities corresponding to the points in the B-H curve specification. Furthermore, a knot at $\Phi = 0$ is created with a reluctance value equal to the reluctance at the first non-zero flux value. This prevents a discontinuity that would be troublesome for the nonlinear solver.

Code listing A.7: Calculate element reluctances (`calc_calR_e_kappa.m`)

```
function calR_e_kappa = calc_calR_e_kappa(p_e_v,l_e_kappa,...
  A_e_kappa,chi_e,material_chi)
%  Calculate element reluctances

[~,N_kappa] = size(p_e_v);
params_e = [material_chi(chi_e).params].';
switch material_chi(chi_e(1)).type
  case 'Linear'
    mur_e = [params_e.mur].';
    mur_e_kappa = repmat(mur_e,[1 N_kappa]);
    calR_e_kappa = l_e_kappa./(4e-7*pi*mur_e_kappa.*A_e_kappa);
  case 'Nonlinear'
    B_e = {params_e.B}.';
    H_e = {params_e.H}.';
    B_e_kappa = repmat(B_e,[1 N_kappa]);
    H_e_kappa = repmat(H_e,[1 N_kappa]);
    Phi_e_kappa = cellfun(@(B,A) B*A,...
      B_e_kappa,num2cell(A_e_kappa),'UniformOutput',false);
    calF_e_kappa = cellfun(@(H,l) H*l,...
      H_e_kappa,num2cell(l_e_kappa),'UniformOutput',false);
    calR_e_kappa = cellfun(@(calF,Phi) calF./Phi,...
      calF_e_kappa,Phi_e_kappa,'UniformOutput',false);
    %Construct calR splines as functions of Phi
    calR_e_kappa = cellfun(@(Phi,calR) ...
      spline([0; Phi],[calR(1); calR]),Phi_e_kappa,calR_e_kappa);
end
```

A.1.6 Interfacing to FEMM

The FEM solutions are obtained using the free Finite Element Method Magnetics (FEMM) software written by Meeker [63]. Convenient MATLAB® functions are provided by Meeker [63] for interfacing directly to FEMM.

Function A.8 creates a new planar magnetics problem of depth d in FEMM. The solver accuracy (maximum rms of the residual) and the minimum angle restraint for the mesh generator are specified with the '`femm`' structure.

Code listing A.8: Define new magnetics problem in FEMM (`femSetup.m`)

```
function femSetup(d,femm)
%  Open new problem in FEMM

openfemm;
main_maximize;
newdocument(0);
mi_probdef(0,'meters','planar',femm.accuracy,d,femm.minMeshDeg);
mi_saveas('tmp.fem');
```

Problem geometry

The elements are drawn in FEMM and assigned default properties using function A.9. This function is also used to draw the sources because, in this work, they are also rectangular. Any moving components are assigned to a separate 'group' in FEMM so that they can be positioned collectively.

Code listing A.9: Draw elements / sources in FEMM (`femDraw.m`)

```
function femDraw(p_e_v,M_delta_e,femm)
%  Draw elements in FEMM

[N_e,N_v] = size(p_e_v);
wrapIdx = @(idx,N_idx) (1+mod(idx-1,N_idx));
for idx_e = 1:N_e
  for idx_v = 1:N_v % Add nodes
    mi_addnode(real(p_e_v(idx_e,idx_v)),imag(p_e_v(idx_e,idx_v)));
    mi_selectnode(real(p_e_v(idx_e,idx_v)),imag(p_e_v(idx_e,idx_v)));
    mi_setnodeprop('<None>', M_delta_e(idx_e));
  end
  mi_clearselected;
```

Code listing A.9: Draw elements / sources in FEMM (`femDraw.m`) *... cont*

```
13    for idx_v = 1:N_v % Add segments
14      mi_addsegment(real(p_e_v(idx_e,idx_v)),...
15        imag(p_e_v(idx_e,idx_v)),...
16        real(p_e_v(idx_e,wrapIdx(idx_v+1,N_v))),...
17        imag(p_e_v(idx_e,wrapIdx(idx_v+1,N_v))));
18      mi_selectsegment(real(p_e_v(idx_e,idx_v)+...
19        p_e_v(idx_e,wrapIdx(idx_v+1,N_v)))/2,...
20        imag(p_e_v(idx_e,idx_v)+...
21        p_e_v(idx_e,wrapIdx(idx_v+1,N_v)))/2);
22      mi_setsegmentprop('<None>',femm.meshSize,0,0,M_delta_e(idx_e));
23    end
24    mi_clearselected;
25    for idx_v = 1:N_v % Add intermediate nodes
26      mi_addnode(real(p_e_v(idx_e,idx_v)+...
27        p_e_v(idx_e,wrapIdx(idx_v+1,N_v)))/2,...
28        imag(p_e_v(idx_e,idx_v)+...
29        p_e_v(idx_e,wrapIdx(idx_v+1,N_v)))/2);
30      mi_selectnode(real(p_e_v(idx_e,idx_v)+...
31        p_e_v(idx_e,wrapIdx(idx_v+1,N_v)))/2,...
32        imag(p_e_v(idx_e,idx_v)+...
33        p_e_v(idx_e,wrapIdx(idx_v+1,N_v)))/2);
34      mi_setnodeprop('<None>',M_delta_e(idx_e));
35    end
36    mi_clearselected;
37    % Set default properties
38    mi_addblocklabel(real(sum(p_e_v(idx_e,:)))/N_v,...
39      imag(sum(p_e_v(idx_e,:)))/N_v);
40    mi_selectlabel(real(sum(p_e_v(idx_e,:)))/N_v,...
41      imag(sum(p_e_v(idx_e,:)))/N_v);
42    mi_setblockprop('<No Mesh>',1,0,'<None>',0,M_delta_e(idx_e),1);
43    mi_clearselected;
44  end
```

FEM formulations are best suited to problems with well-defined, closed solution regions [64]. This poses a problem when there is no natural outer boundary. To overcome this issue, a Kelvin Transformation approach [64, 145] is followed in this work using periodic boundary conditions. Code listing A.10 is a function that draws a circular boundary around the problem region and creates a second identical-size circular region to represent the "far field". By applying matching periodic boundary conditions to these two circular boundaries, infinity maps to the point at the centre of the far-field circular region and thus $\vec{\boldsymbol{A}}$ can be set to zero at this single reference point.

Code listing A.10: Create surrounding infinite domain in FEMM (`femDrawInfDomain.m`)

```
function femDrawInfDomain(p_e_v,M_delta_e,x_x,femm)
%  Create infinite domain in FEMM

[~,N_v] = size(p_e_v);
x_delta_x = diff([0; x_x]);
x_min = inf;
y_min = inf;
x_max = -inf;
y_max = -inf;
G = 0.75; %Scaling factor for width of problem to boundary width
% Find total range of element and source positions
for x_delta = x_delta_x.'
  p_e_v(repmat(M_delta_e,[1 N_v])==true) = ...
    p_e_v(repmat(M_delta_e,[1 N_v])==true) + x_delta;
  x_min = min(x_min,min(real(p_e_v(:))));
  y_min = min(y_min,min(imag(p_e_v(:))));
  x_max = max(x_max,max(real(p_e_v(:))));
  y_max = max(y_max,max(imag(p_e_v(:))));
end
w = x_max - x_min;
x_mid = (x_min + x_max)/2;
h = y_max - y_min;
y_mid = (y_min + y_max)/2;
mi_addboundprop('periodic A',0,0,0,0,0,0,0,0,4);
mi_addboundprop('periodic B',0,0,0,0,0,0,0,0,4);
% Create circular boundary around problem space
mi_addnode(x_mid-G*max(w,h),y_mid);
mi_addnode(x_mid+G*max(w,h),y_mid);
mi_addarc(x_mid-G*max(w,h),y_mid,...
  x_mid+G*max(w,h),y_mid,180,femm.arcSegDeg);
mi_addarc(x_mid+G*max(w,h),y_mid,...
  x_mid-G*max(w,h),y_mid,180,femm.arcSegDeg);
% Create matching second empty circular region
mi_addnode(x_mid-G*max(w,h),y_mid-2.5*max(w,h));
mi_addnode(x_mid+G*max(w,h),y_mid-2.5*max(w,h));
mi_addarc(x_mid-G*max(w,h),y_mid-2.5*max(w,h),...
  x_mid+G*max(w,h),y_mid-2.5*max(w,h),180,1);
mi_addarc(x_mid+G*max(w,h),y_mid-2.5*max(w,h),...
  x_mid-G*max(w,h),y_mid-2.5*max(w,h),180,1);
% Set periodic boundary conditions to map outer region of problem
% space to inner region of empty circular area
mi_selectarcsegment(x_mid,y_mid+G*max(w,h));
mi_selectarcsegment(x_mid,y_mid-(2.5-G)*max(w,h));
mi_setarcsegmentprop(femm.arcSegDeg,'periodic A',0,0);
mi_clearselected;
mi_selectarcsegment(x_mid,y_mid-G*max(w,h));
mi_selectarcsegment(x_mid,y_mid-(2.5+G)*max(w,h));
mi_setarcsegmentprop(femm.arcSegDeg,'periodic B',0,0);
mi_clearselected;
% Create point that maps to infinity
mi_addpointprop('infinity',0,0);
mi_addnode(x_mid,y_mid-2.5*max(w,h));
```

Code listing A.10: Create surrounding infinite domain in FEMM (`femDrawInfDomain.m`)

... cont

```
53 mi_selectnode(x_mid,y_mid-2.5*max(w,h));
54 mi_setnodeprop('infinity',0);
55 mi_clearselected;
56 % Set surrounding material to 'air' with unity relative permeability
57 mi_addmaterial('air',1,1);
58 mi_addblocklabel(x_mid,y_mid-0.8*G*max(w,h));
59 mi_addblocklabel(x_mid,y_mid-0.8*(2.5+G)*max(w,h));
60 mi_selectlabel(x_mid,y_mid-0.8*G*max(w,h));
61 mi_selectlabel(x_mid,y_mid-0.8*(2.5+G)*max(w,h));
62 mi_setblockprop('air',1,0,'<None>',0,0,1);
63 mi_clearselected;
64 %Zoom view to problem extents
65 mi_zoom(x_mid-G*max(w,h),y_mid-G*max(w,h),...
66   x_mid+G*max(w,h),y_mid+G*max(w,h));
```

Boundary conditions

FEMM supports 'mixed' boundary conditions of the form (A.1), which allows the field intensity parallel to a boundary to be stipulated [64]. This is achieved by setting c_0 to zero and c_1 to the required value of H. Note, however, that it is not necessary to prescribe $\frac{\partial \vec{\boldsymbol{A}}}{\partial \hat{\boldsymbol{n}}} = 0$ for the boundaries of infinitely permeable regions because the first-order triangle elements used by FEMM imply this condition by default [64].

$$\frac{1}{\mu}\frac{\partial \vec{\boldsymbol{A}}}{\partial \hat{\boldsymbol{n}}} + c_0 \vec{\boldsymbol{A}} + c_1 = 0 \tag{A.1}$$

The field intensity parallel to each element boundary is equal to its corresponding mmf, divided by its length (i.e. $H = \mathcal{F}/l$). For a positive current sheet (flowing in the $\hat{\boldsymbol{z}}$ direction), c_1 is set with the opposite sign to the mmf, whereas for a negative current sheet, $c_1 = H$ has the same sign as $\mathcal{F}$. For an interior boundary that is adjacent to an exterior boundary, the current sheet needs to be concentrated as a point current on the exterior boundary. Boundary conditions are irrelevant for elements with no exterior boundaries.

Function A.11 sets the relevant element boundary conditions in FEMM.

Code listing A.11: Set element boundary conditions in FEMM (`femSetBoundaries.m`)

```
function femSetBoundaries(p_e_v,M_delta_e,epsilon_e_kappa,...
  calF_e_kappa,femm)
%  Set exterior element boundary conditions in FEMM preprocesor

[N_e,N_kappa] = size(epsilon_e_kappa);
N_v = N_kappa;
l_e_kappa = calc_l_e_kappa(p_e_v);
p_n = [];
wrapIdx = @(idx,N_idx) (1+mod(idx-1,N_idx));
for idx_e = 1:N_e
  for idx_kappa = 1:N_kappa
    % Set negative field intensity along boundary / point source
    idx_v = wrapIdx(idx_kappa+1,N_v);
    if ... %Adjacent exterior boundary?
        epsilon_e_kappa(idx_e,wrapIdx(idx_kappa+1,N_kappa))
      mi_selectsegment(real((p_e_v(idx_e,idx_v)+...
        (p_e_v(idx_e,idx_v)+p_e_v(idx_e,wrapIdx(idx_v+1,N_v)))/...
        2)/2),imag((p_e_v(idx_e,idx_v)+...
        (p_e_v(idx_e,idx_v)+p_e_v(idx_e,wrapIdx(idx_v+1,N_v)))/...
        2)/2));
      mi_deleteboundprop(... %Delete existing if already defined
        ['-H ' num2str(idx_e) ' ' num2str(idx_kappa)]);
      if (calF_e_kappa(idx_e,idx_kappa)~=0) %Nonzero mmf?
        mi_addboundprop(...
          ['-H ' num2str(idx_e) ' ' num2str(idx_kappa)],...
          0,0,0,0,0,0,-calF_e_kappa(idx_e,idx_kappa)/...
          l_e_kappa(idx_e,idx_kappa),2);
        mi_setsegmentprop(...
          ['-H ' num2str(idx_e) ' ' num2str(idx_kappa)],...
          femm.meshSize,0,0,M_delta_e(idx_e));
      else %Zero mmf
        mi_setsegmentprop('<None>',...
          femm.meshSize,0,0,M_delta_e(idx_e));
      end
      mi_clearselected;
    elseif ... %Exterior boundary but adjacent interior boundary?
        epsilon_e_kappa(idx_e,idx_kappa)
      idx_n = find(abs(p_n-p_e_v(idx_e,idx_v))<eps,1);
      if isempty(idx_n) %No point current already defined?
        mi_selectnode(real(p_e_v(idx_e,idx_v)),...
          imag(p_e_v(idx_e,idx_v)));
        if (calF_e_kappa(idx_e,idx_kappa)~=0) %Nonzero mmf?
          p_n(end+1) = p_e_v(idx_e,idx_v); %#ok<AGROW>
          idx_n = numel(p_n);
          I_n(idx_n) = calF_e_kappa(idx_e,idx_kappa); %#ok<AGROW>
          %Delete existing point current if already defined
          mi_deletepointprop(['I ' num2str(idx_n)]);
          mi_addpointprop(['I ' num2str(idx_n)],0,I_n(idx_n));
          mi_setnodeprop(['I ' num2str(idx_n)],M_delta_e(idx_e));
        else %Zero mmf
          mi_setnodeprop('<None>',M_delta_e(idx_e));
        end
        mi_clearselected;
```

Code listing A.11: Set element boundary conditions in FEMM (`femSetBoundaries.m`)

... cont

```
54        else %Point current already defined
55          %Add point current to existing value
56          I_n(idx_n) = I_n(idx_n) + ....
57            calF_e_kappa(idx_e,idx_kappa); %#ok<AGROW>
58          if (I_n(idx_n)~=0) %Resulting point current nonzero?
59            mi_modifypointprop(['I ' num2str(idx_n)],2,I_n(idx_n));
60          else
61            mi_deletepointprop(['I ' num2str(idx_n)]);
62          end
63        end
64      end
65      % Set positive field intensity along boundary / point source
66      idx_v = idx_kappa;
67      if ... %Adjacent exterior boundary?
68          epsilon_e_kappa(idx_e,wrapIdx(idx_kappa-1,N_kappa))
69        mi_selectsegment(real((p_e_v(idx_e,idx_v)+...
70          (p_e_v(idx_e,idx_v)+p_e_v(idx_e,wrapIdx(idx_v-1,N_v)))/...
71          2)/2),imag((p_e_v(idx_e,idx_v)+...
72          (p_e_v(idx_e,idx_v)+p_e_v(idx_e,wrapIdx(idx_v-1,N_v)))/...
73          2)/2));
74        mi_deleteboundprop(... %Delete existing if already defined
75          ['+H ' num2str(idx_e) ' ' num2str(idx_kappa)]);
76        if (calF_e_kappa(idx_e,idx_kappa)~=0) %Nonzero mmf?
77          mi_addboundprop(...
78            ['+H ' num2str(idx_e) ' ' num2str(idx_kappa)],...
79            0,0,0,0,0,0,0,calF_e_kappa(idx_e,idx_kappa)/...
80            l_e_kappa(idx_e,idx_kappa),2);
81          mi_setsegmentprop(...
82            ['+H ' num2str(idx_e) ' ' num2str(idx_kappa)],...
83            femm.meshSize,0,0,M_delta_e(idx_e));
84        else %Zero mmf
85          mi_setsegmentprop('<None>',...
86            femm.meshSize,0,0,M_delta_e(idx_e));
87        end
88        mi_clearselected;
89      elseif ... %Exterior boundary but adjacent interior boundary?
90          epsilon_e_kappa(idx_e,idx_kappa)
91        idx_n = find(abs(p_n-p_e_v(idx_e,idx_v))<eps,1);
92        if isempty(idx_n) %No point current already defined?
93          mi_selectnode(real(p_e_v(idx_e,idx_v)),...
94            imag(p_e_v(idx_e,idx_v)));
95          if (calF_e_kappa(idx_e,idx_kappa)~=0) %Nonzero mmf?
96            p_n(end+1) = p_e_v(idx_e,idx_v); %#ok<AGROW>
97            idx_n = numel(p_n);
98            I_n(idx_n) = -calF_e_kappa(idx_e,idx_kappa); %#ok<AGROW>
99            %Delete existing point current if already defined
100           mi_deletepointprop(['I ' num2str(idx_n)]);
101           mi_addpointprop(['I ' num2str(idx_n)],0,I_n(idx_n));
102           mi_setnodeprop(['I ' num2str(idx_n)],M_delta_e(idx_e));
103         else %Zero mmf
104           mi_setnodeprop('<None>',M_delta_e(idx_e));
105         end
106         mi_clearselected;
```

Code listing A.11: Set element boundary conditions in FEMM (`femSetBoundaries.m`)

... cont

```
107       else %Point current already defined
108         %Add point current to existing value
109         I_n(idx_n) = I_n(idx_n) - ....
110           calF_e_kappa(idx_e,idx_kappa); %#ok<AGROW>
111         if (I_n(idx_n)~=0) %Resulting point current nonzero?
112           mi_modifypointprop(['I ' num2str(idx_n)],2,I_n(idx_n));
113         else
114           mi_deletepointprop(['I ' num2str(idx_n)]);
115         end
116       end
117     end
118   end
119 end
```

Materials

Function A.12 defines the relevant materials in the FEMM workspace using their definitions in the structure array '`material_chi`'. A 'circuit' definition in FEMM is also added for each phase winding.

Code listing A.12: Define materials in FEMM (`femDefineMaterials.m`)

```
1  function femDefineMaterials(material_chi,I_ph)
2  %  Define list of materials in FEMM
3
4  % Add a circuit for each phase
5  N_ph = numel(I_ph);
6  for idx_ph = 1:N_ph
7    mi_addcircprop(num2str(idx_ph),I_ph(idx_ph),1);
8  end
9  % Add element and source materials
10 N_chi = numel(material_chi);
11 for idx_chi = 1:N_chi
12   switch material_chi(idx_chi).type
13     case 'Linear'
14       if ~isinf(material_chi(idx_chi).params.mur)
15         mi_addmaterial([num2str(idx_chi) 'L'],...
16           material_chi(idx_chi).params.mur,...
17           material_chi(idx_chi).params.mur,0,0);
18       end
19     case 'Nonlinear'
20       mi_addmaterial([num2str(idx_chi) 'N'],0,0,0,0);
21       for idx = 1:numel(material_chi(idx_chi).params.B)
22         mi_addbhpoint([num2str(idx_chi) 'N'],...
23           material_chi(idx_chi).params.B(idx),...
24           material_chi(idx_chi).params.H(idx))
25       end
```

Code listing A.12: Define materials in FEMM (`femDefineMaterials.m`) *... cont*

```
26      case 'Coil'
27        mi_addmaterial([num2str(idx_chi) 'C'],...
28          material_chi(idx_chi).params.mur,...
29          material_chi(idx_chi).params.mur,0,0);
30      case 'Magnet'
31        mi_addmaterial([num2str(idx_chi) 'M'],...
32          material_chi(idx_chi).params.mur,...
33          material_chi(idx_chi).params.mur,...
34          material_chi(idx_chi).params.Hc,0);
35    end
36  end
```

When calculating the influence of sources in isolation (e.g. precomputing exterior boundary flux components for each unity source), it is necessary to remove the energy from the other sources (zero current for coils and zero magnetic coercivity for magnets). The removal of all of the energy sources is performed by function A.13. Function A.14 defines special unity source materials that are then assigned one-at-a-time to each source in succession.

Code listing A.13: Remove energy from sources in FEMM (`femRemoveEnergySources.m`)

```
1  function femRemoveEnergySources(material_chi,N_ph)
2  %  Remove energy sources (currents and permanent magnets) in FEMM
3
4  % Set all phase current to zero
5  for idx_ph = 1:N_ph
6    mi_modifycircprop(num2str(idx_ph),1,0);
7  end
8  % Set Hc to zero for all magnets
9  N_chi = numel(material_chi);
10 for idx_chi = 1:N_chi
11   if strcmp(material_chi(idx_chi).type,'Magnet')
12     mi_modifymaterial([num2str(idx_chi) 'M'],3,0);
13   end
14 end
```

Code listing A.14: Define unity source materials for calculations in FEMM (`femDefineUnitySourceMaterials.m`)

```
1  function femDefineUnitySourceMaterials(material_chi)
2  %  Create materials for when using unity sources in FEMM
3
4  %Add circuit with 1 A current
5  mi_addcircprop('0',1,1);
```

Code listing A.14: Define unity source materials for calculations in FEMM (`femDefineUnitySourceMaterials.m`) *... cont*

```
% Add magnet materials with correct Hc
N_chi = numel(material_chi);
for idx_chi = 1:N_chi
  if strcmp(material_chi(idx_chi).type,'Magnet')
    mi_addmaterial([num2str(idx_chi) 'M0'],...
      material_chi(idx_chi).params.mur,...
      material_chi(idx_chi).params.mur,...
      material_chi(idx_chi).params.Hc,0);
  end
end
```

The source regions are assigned to materials by function A.15. If a unity source is required, that source is assigned one of the special unity source materials defined by function A.14. When performing a full FEM analysis for comparison purposes, function A.16 is also used to assign materials to the flux tube elements.

Code listing A.15: Assign source materials in FEMM (`femAssignSources.m`)

```
function femAssignSources(p_calF_v,M_delta_calF,chi_calF,...
  material_chi,femm,varargin)
%  Assign source materials in FEMM

% Provide option to set a unity source
if isempty(varargin)
  setUnitySource = false;
else
  setUnitySource = varargin{1};
end
[N_calF,N_v] = size(p_calF_v);
for idx_calF = 1:N_calF
  idx_chi = abs(chi_calF(idx_calF));
  mi_selectlabel(real(sum(p_calF_v(idx_calF,:)))/N_v,...
    imag(sum(p_calF_v(idx_calF,:)))/N_v);
  switch material_chi(idx_chi).type
    case 'Coil'
      if setUnitySource
        mi_setblockprop([num2str(idx_chi) 'C'],0,femm.meshSize,'0',...
          0,M_delta_calF(idx_calF),sign(chi_calF(idx_calF))*...
          material_chi(idx_chi).params.turns);
      else
        mi_setblockprop([num2str(idx_chi) 'C'],0,femm.meshSize,...
          num2str(material_chi(idx_chi).params.ph),...
          0,M_delta_calF(idx_calF),sign(chi_calF(idx_calF))*...
          material_chi(idx_chi).params.turns);
      end
```

Code listing A.15: Assign source materials in FEMM (`femAssignSources.m`)

```
28      case 'Magnet'
29        if setUnitySource
30          mi_setblockprop([num2str(idx_chi) 'M0'],0,femm.meshSize,...
31            '<None>',angle(chi_calF(idx_calF))*180/pi,...
32            M_delta_calF(idx_calF),0);
33        else
34          mi_setblockprop([num2str(idx_chi) 'M'],0,femm.meshSize,...
35            '<None>',angle(chi_calF(idx_calF))*180/pi,...
36            M_delta_calF(idx_calF),0);
37        end
38    end
39    mi_clearselected;
40  end
```

Code listing A.16: Assign element materials in FEMM (`femAssignElements.m`)

```
1  function femAssignElements(p_e_v,M_delta_e,chi_e,material_chi,femm)
2  %  Assign element materials in FEMM
3
4  [N_e,N_v] = size(p_e_v);
5  for idx_e = 1:N_e
6    idx_chi = abs(chi_e(idx_e));
7    mi_selectlabel(real(sum(p_e_v(idx_e,:)))/N_v,...
8      imag(sum(p_e_v(idx_e,:)))/N_v);
9    switch material_chi(idx_chi).type
10     case 'Linear'
11       if ~isinf(material_chi(idx_chi).params.mur)
12         mi_setblockprop([num2str(idx_chi) 'L'],0,femm.meshSize,...
13           '<None>',0,M_delta_e(idx_e),0);
14       end
15     case 'Nonlinear'
16       mi_setblockprop([num2str(idx_chi) 'N'],0,femm.meshSize,...
17         '<None>',0,M_delta_e(idx_e),0);
18   end
19   mi_clearselected;
20 end
```

Obtaining boundary quantities

The FEMM post-processor is used to obtain each exterior boundary's normal flux (integration of the normal flux density along the boundary) by function A.17. Similarly, for each moving source boundary, the normal flux is obtained from the post-processor with function A.18 and the average tangential field intensity with function A.19.

Code listing A.17: Obtain exterior boundary fluxes in FEMM (`fem_Phi_epsilon.m`)

```
function Phi_epsilon = fem_Phi_epsilon(p_e_v,epsilon_e_kappa)
%  Get element exterior boundary fluxes in FEMM postprocessor

[N_e,N_kappa] = size(p_e_v);
N_epsilon = max(epsilon_e_kappa(:));
Phi_epsilon = zeros(N_epsilon,1); %Preallocate output
wrapIdx = @(idx,N_idx) (1+mod(idx-1,N_idx));
mo_seteditmode('contour');
for idx_e = 1:N_e
  for idx_kappa = 1:N_kappa
    if epsilon_e_kappa(idx_e,idx_kappa) %Exterior boundary?
      mo_addcontour(...
        real(p_e_v(idx_e,wrapIdx(idx_kappa+1,N_kappa))),...
        imag(p_e_v(idx_e,wrapIdx(idx_kappa+1,N_kappa))));
      mo_addcontour(...
        real(p_e_v(idx_e,idx_kappa)),...
        imag(p_e_v(idx_e,idx_kappa)));
      Phi = mo_lineintegral(0);
      Phi_epsilon(epsilon_e_kappa(idx_e,idx_kappa)) = Phi(1); %Flux
      mo_clearcontour;
    end
  end
end
```

Code listing A.18: Obtain moving source boundary fluxes in FEMM (`fem_Phi_zeta.m`)

```
function Phi_zeta = fem_Phi_zeta(p_calF_v,zeta_calF_kappa)
%  Get source boundary fluxes in FEMM postprocessor

[N_calF,N_kappa] = size(zeta_calF_kappa);
N_zeta = max(zeta_calF_kappa(:));
Phi_zeta = zeros(N_zeta,1); %Preallocate output
wrapIdx = @(idx,N_idx) (1+mod(idx-1,N_idx));
mo_seteditmode('contour');
for idx_calF = 1:N_calF
  for idx_kappa = 1:N_kappa
    if zeta_calF_kappa(idx_calF,idx_kappa) %Moving source boundary?
      mo_addcontour(...
        real(p_calF_v(idx_calF,wrapIdx(idx_kappa+1,N_kappa))),...
        imag(p_calF_v(idx_calF,wrapIdx(idx_kappa+1,N_kappa))));
      mo_addcontour(...
        real(p_calF_v(idx_calF,idx_kappa)),...
        imag(p_calF_v(idx_calF,idx_kappa)));
      Phi = mo_lineintegral(0);
      Phi_zeta(zeta_calF_kappa(idx_calF,idx_kappa)) = Phi(1); %Flux
      mo_clearcontour;
    end
  end
end
```

Code listing A.19: Obtain moving source boundary average field intensities in FEMM (`fem_Phi_zeta.m`)

```
function H_zeta = fem_H_zeta(p_calF_v,zeta_calF_kappa)
%  Get source boundary tangential field intensities in FEMM
%  postprocessor

[N_calF,N_kappa] = size(zeta_calF_kappa);
N_zeta = max(zeta_calF_kappa(:));
H_zeta = zeros(N_zeta,1); %Preallocate output
wrapIdx = @(idx,N_idx) (1+mod(idx-1,N_idx));
mo_seteditmode('contour');
for idx_calF = 1:N_calF
  for idx_kappa = 1:N_kappa
    if zeta_calF_kappa(idx_calF,idx_kappa) %Moving source boundary?
      mo_addcontour(...
        real(p_calF_v(idx_calF,wrapIdx(idx_kappa+1,N_kappa))),...
        imag(p_calF_v(idx_calF,wrapIdx(idx_kappa+1,N_kappa))));
      mo_addcontour(...
        real(p_calF_v(idx_calF,idx_kappa)),...
        imag(p_calF_v(idx_calF,idx_kappa)));
      H = mo_lineintegral(1);
      H_zeta(zeta_calF_kappa(idx_calF,idx_kappa)) = H(2);
      mo_clearcontour;
    end
  end
end
```

Flux linkage

The total flux linking with each phase winding is an output available in the FEMM post-processor. The MATLAB® function to extract these quantities is included as code listing A.20.

Code listing A.20: Obtain flux linkages in FEMM (`fem_lambda_ph.m`)

```
function lambda_ph = fem_lambda_ph(N_ph,varargin)
%  Get flux linkages for each phase from FEMM postprocessor

lambda_ph = zeros(N_ph,1); %Preallocate output
for idx_ph = 1:N_ph
  circProps = mo_getcircuitproperties(num2str(idx_ph));
  lambda_ph(idx_ph) = circProps(3); %Flux linkage
  %Include any additional flux linkage due to a unity source current
  %itself when obtaining components due to isolated unity sources
  if (~isempty(varargin) && (varargin{1}==idx_ph))
    circProps2 = mo_getcircuitproperties('0');
      lambda_ph(idx_ph) = lambda_ph(idx_ph) + circProps2(3);
  end
end
```

A.1.7 Precomputation of parameter sets

The required parameters are calculated over a range of discrete displacements by function A.21. This function returns cubic spline representations of the parameter sets that are later interpolated for an arbitrary displacement of the group of moving components over the same range.

Code listing A.21: Precompute parameter sets in FEMM (`femUpFrontCalcs.m`)

```
function [calG_epsilon_e_kappa,Phi_epsilon_calF0,calG_zeta_e_kappa,...
  H_zeta_e_kappa,Phi_zeta_calF0,H_zeta_calF0,lambda_ph_e_kappa,...
  lambda_ph_calF0] = femUpfrontCalcs(p_e_v,M_delta_e,p_calF_v,...
  M_delta_calF,d,epsilon_e_kappa,zeta_calF_kappa,chi_calF,...
  material_chi,N_ph,x_x,femm)
%  In preparation for dynamic simulation, calculate mutual permeances,
%  boundary flux due to unity sources, flux linkages due to unity
%  elements and sources, as well as force components due to unity
%  elements and sources

[N_e,N_kappa] = size(epsilon_e_kappa);
N_epsilon = max(epsilon_e_kappa(:));
N_zeta = max(zeta_calF_kappa(:));
[N_calF,N_v] = size(p_calF_v);
N_x = numel(x_x);

x_delta_x = diff([0; x_x]);

% Preallocate outputs
calG_epsilon_e_kappa_x = zeros(N_epsilon,N_e,N_kappa,N_x);
Phi_epsilon_calF0_x = zeros(N_epsilon,N_calF,N_x);
calG_zeta_e_kappa_x = zeros(N_zeta,N_e,N_kappa,N_x);
H_zeta_e_kappa_x = zeros(N_zeta,N_e,N_kappa,N_x);
Phi_zeta_calF0_x = zeros(N_zeta,N_calF,N_x);
H_zeta_calF0_x = zeros(N_zeta,N_calF,N_x);
lambda_ph_e_kappa_x = zeros(N_ph,N_e,N_kappa,N_x);
lambda_ph_calF0_x = zeros(N_ph,N_calF,N_x);

% Set up problem in FEMM
femSetup(d,femm);
femDraw(p_e_v,M_delta_e,femm);
femDraw(p_calF_v,M_delta_calF,femm);
femDrawInfDomain([p_e_v; p_calF_v],[M_delta_e; M_delta_calF],...
  x_x,femm);
femDefineMaterials(material_chi,zeros(N_ph,1));
femAssignSources(p_calF_v,M_delta_calF,chi_calF,material_chi,femm);
femRemoveEnergySources(material_chi,N_ph);
femDefineUnitySourceMaterials(material_chi);

for idx_x = 1:N_x
  % Move elements and sources to correct position
  mi_selectgroup(1);
```

Code listing A.21: Precompute parameter sets in FEMM (`femUpFrontCalcs.m`) *... cont*

```
43  mi_movetranslate(real(x_delta_x(idx_x)),imag(x_delta_x(idx_x)));
44  mi_clearselected;
45  p_e_v(repmat(M_delta_e,[1 N_v])==true) = ...
46    p_e_v(repmat(M_delta_e,[1 N_v])==true) + x_delta_x(idx_x);
47  p_calF_v(repmat(M_delta_calF,[1 N_v])==true) = ...
48    p_calF_v(repmat(M_delta_calF,[1 N_v])==true) + x_delta_x(idx_x);
49
50  % Obtain solutions for unity element mmfs
51  for idx_e = 1:N_e
52    for idx_kappa = 1:N_kappa
53      % Set unity boundary current sheets
54      calF_kappa = zeros(N_kappa,1);
55      calF_kappa(idx_kappa) = 1;
56      femSetBoundaries(p_e_v(idx_e,:),M_delta_e(idx_e),...
57        epsilon_e_kappa(idx_e,:),calF_kappa.',femm);
58
59      mi_analyze;
60      mi_loadsolution;
61
62      %Get resulting element boundary flux
63      calG_epsilon_e_kappa_x(:,idx_e,idx_kappa,idx_x) = ...
64        fem_Phi_epsilon(p_e_v,epsilon_e_kappa);
65
66      %Get resulting source boundary flux
67      calG_zeta_e_kappa_x(:,idx_e,idx_kappa,idx_x) = ...
68        fem_Phi_zeta(p_calF_v,zeta_calF_kappa);
69
70      %Get resulting source boundary field intensities
71      H_zeta_e_kappa_x(:,idx_e,idx_kappa,idx_x) = ...
72        fem_H_zeta(p_calF_v,zeta_calF_kappa);
73
74      %Get resulting flux linkages with coils
75      lambda_ph_e_kappa_x(:,idx_e,idx_kappa,idx_x) = ...
76        fem_lambda_ph(N_ph);
77
78      mo_close;
79
80      %Remove boundary current sheets
81      femSetBoundaries(p_e_v(idx_e,:),M_delta_e(idx_e),...
82        epsilon_e_kappa(idx_e,:),zeros(1,N_kappa),femm);
83    end
84  end
85
86  % Obtain solutions for unity sources
87  for idx_calF = 1:N_calF
88    %Set unity source
89    femAssignSources(p_calF_v(idx_calF,:),M_delta_calF(idx_calF),...
90      chi_calF(idx_calF),material_chi,femm,true);
91
92    mi_analyze;
93    mi_loadsolution;
```

Code listing A.21: Precompute parameter sets in FEMM (`femUpFrontCalcs.m`) *... cont*

```
94      %Get resulting element boundary flux
95      Phi_epsilon_calF0_x(:,idx_calF,idx_x) = ...
96        fem_Phi_epsilon(p_e_v,epsilon_e_kappa);
97
98      %Get resulting source boundary flux
99      Phi_zeta_calF0_x(:,idx_calF,idx_x) = ...
100       fem_Phi_zeta(p_calF_v,zeta_calF_kappa);
101
102     %Get resulting source boundary field intensities
103     H_zeta_calF0_x(:,idx_calF,idx_x) = ...
104       fem_H_zeta(p_calF_v,zeta_calF_kappa);
105
106     %Get resulting flux linkages with coils
107     if strcmp(material_chi(abs(chi_calF(idx_calF))).type,'Coil')
108       lambda_ph_calF0_x(:,idx_calF,idx_x) = fem_lambda_ph(N_ph,...
109         material_chi(abs(chi_calF(idx_calF))).params.ph);
110     else
111       lambda_ph_calF0_x(:,idx_calF,idx_x) = fem_lambda_ph(N_ph);
112     end
113     pause;
114     mo_close;
115     %Revert to orginal source material (with no energy)
116     femAssignSources(p_calF_v(idx_calF,:),M_delta_calF(idx_calF),...
117       chi_calF(idx_calF),material_chi,femm,false);
118   end
119 end
120 closefemm;
121
122 % Construct splines over x
123 calG_epsilon_e_kappa = spline(abs(x_x),calG_epsilon_e_kappa_x);
124 Phi_epsilon_calF0 = spline(abs(x_x),Phi_epsilon_calF0_x);
125 if (N_zeta~=0)
126   calG_zeta_e_kappa = spline(abs(x_x),calG_zeta_e_kappa_x);
127   H_zeta_e_kappa = spline(abs(x_x),H_zeta_e_kappa_x);
128   Phi_zeta_calF0 = spline(abs(x_x),Phi_zeta_calF0_x);
129   H_zeta_calF0 = spline(abs(x_x),H_zeta_calF0_x);
130 else
131   calG_zeta_e_kappa = [];
132   Phi_zeta_calF0 = [];
133 end
134 lambda_ph_e_kappa = spline(abs(x_x),lambda_ph_e_kappa_x);
135 lambda_ph_calF0 = spline(abs(x_x),lambda_ph_calF0_x);
```

A.1.8 Reluctance-network graph representation

Since graph theory is used to determine the clusters of flux tube elements and to find the independent MEC loops within each cluster, a directed graph representation of the MEC components is required. This graph representation is in the form of

an adjacency matrix, $\mathbf{C}_{\underset{\sim}{n}\underset{\sim}{n}}$, which is returned by function A.22. The nodes at the centre of each element are numbered with the element index and the nodes on each boundary are numbered by the total number of elements plus the corresponding global boundary index. Each graph edge stores the corresponding reluctance element as a complex number, where the real part is the element index and the imaginary part is the region index.

Code listing A.22: Construct reluctance element graph (`graph_C_n_n.m`)

```
function C_n_n = graph_C_n_n(nu_e_kappa)
%  Create directed graph representation of magnetic equivalent circuit
%  from element global boundary assignment
%  Edges are complex numbers with real part equal to the element index
%  and complex part equal to the element region

[N_e,N_kappa] = size(nu_e_kappa);
N_nu = max(abs(nu_e_kappa(:)));
N_n = N_e + N_nu;
n_from = [];
n_to = [];
edges = [];
for idx_e = 1:N_e
  for idx_kappa = 1:N_kappa
    if (nu_e_kappa(idx_e,idx_kappa)>0)
      n_from(end+1) = idx_e; %#ok<AGROW>
      n_to(end+1) = N_e+abs(nu_e_kappa(idx_e,idx_kappa)); %#ok<AGROW>
    else
      n_from(end+1) = N_e+...
        abs(nu_e_kappa(idx_e,idx_kappa)); %#ok<AGROW>
      n_to(end+1) = idx_e; %#ok<AGROW>
    end
    edges(end+1) = idx_e + 1j*idx_kappa; %#ok<AGROW>
  end
end
C_n_n = sparse(n_from,n_to,edges,N_n,N_n);
```

A.1.9 Finding independent MEC loops

Code listing A.23, a MATLAB® function to find the independent loops for a single connected graph of MEC nodes, is based on code written by Kirk [146] that counts the number of loops within an undirected graph using the 'Iterative Loop Counting Algorithm'. Considering that the algorithm only works for connected graphs, it is necessary to find the loops for each graph component separately. Amendments to the original code by Kirk [146] are indicated by 'CRL' tags within the code comments.

Code listing A.23: Find independent MEC loops (`find_Lambda_Lambda.m`)

```
function Lambda_Lambda = find_Lambda_Lambda(C_e_e)
%  Find essential loops (loops not containing other loops) for a
%  connected, directed flux tube element graph

% Based on code by Joseph Kirk.  New code is annotated with 'CRL'.
%
% Copyright (c) 2006, Joseph Kirk
% All rights reserved.
%
% Redistribution and use in source and binary forms, with or without
% modification, are permitted provided that the following conditions
% are met:
%
%     * Redistributions of source code must retain the above copyright
%       notice, this list of conditions and the following disclaimer.
%     * Redistributions in binary form must reproduce the above
%       copyright notice, this list of conditions and the following
%       disclaimer in the documentation and/or other materials
%       provided with the distribution
%
% THIS SOFTWARE IS PROVIDED BY THE COPYRIGHT HOLDERS AND CONTRIBUTORS
% "AS IS" AND ANY EXPRESS OR IMPLIED WARRANTIES, INCLUDING, BUT NOT
% LIMITED TO, THE IMPLIED WARRANTIES OF MERCHANTABILITY AND FITNESS
% FOR A PARTICULAR PURPOSE ARE DISCLAIMED. IN NO EVENT SHALL THE
% COPYRIGHT OWNER OR CONTRIBUTORS BE LIABLE FOR ANY DIRECT, INDIRECT,
% INCIDENTAL, SPECIAL, EXEMPLARY, OR CONSEQUENTIAL DAMAGES (INCLUDING,
% BUT NOT LIMITED TO, PROCUREMENT OF SUBSTITUTE GOODS OR SERVICES;
% LOSS OF USE, DATA, OR PROFITS; OR BUSINESS INTERRUPTION) HOWEVER
% CAUSED AND ON ANY THEORY OF LIABILITY, WHETHER IN CONTRACT, STRICT
% LIABILITY, OR TORT (INCLUDING NEGLIGENCE OR OTHERWISE) ARISING IN
% ANY WAY OUT OF THE USE OF THIS SOFTWARE, EVEN IF ADVISED OF THE
% POSSIBILITY OF SUCH DAMAGE.

%% Construct undirected network from directed graph C_e_e  % CRL
[~,N_n] = size(C_e_e);
net = struct('node',num2cell(1:N_n),'edges',...
  cellfun(@(n) sort([find(C_e_e(n,:)) find(C_e_e(:,n).')]),...
  num2cell(1:N_n),'UniformOutput',false));

%% Find loops
n = get_starting_node(net);  %give path nearly optimal starting node
path = net(n).node;  %initialize the path
current_edge = net(n).edges(1);  %initialize the first edge
loop_list = [];  %initialize the loop list

while (length(path)>1 || ~isempty(current_edge))
  [net,path,current_edge,loop_list] = ...
    iterate_tree(net,path,current_edge,loop_list);
end

if isempty(loop_list)
  Lambda_Lambda = [];
```

Code listing A.23: Find independent MEC loops (`find_Lambda_Lambda.m`) *... cont*

```
53 else
54   %Convert loop_list structure to Lambda_Lambda cell array  %CRL
55   Lambda_Lambda = squeeze(struct2cell(loop_list));
56
57   %Complete loops by adding first node to the end of each list  %CRL
58   Lambda_Lambda = cellfun(@(loop) [loop loop(1)],Lambda_Lambda, ...
59     'UniformOutput',false);
60 end
61
62 %-------------------------------------------------------------------------
63 function n = get_starting_node(net)
64 %  Pick the (nearly) optimal starting node
65
66 n = 1;
67 for k = 2:length(net)
68   if (length(net(k).edges) > length(net(n).edges))
69     n = k;
70   end
71 end
72
73 %-------------------------------------------------------------------------
74 function [net,path,current_edge,loop_list] = ...
75   iterate_tree(net,path,current_edge,loop_list)
76 %  Execute the current iterative step in the loop counting algorithm
77
78 path_size = length(path);
79 % DONE - finished searching tree
80 if (path_size == 1 && isempty(current_edge))
81   return
82   % CURRENT EDGE LIST FINISHED - go up tree
83 elseif (isempty(current_edge))
84   current_edge = get_next_edge(net,path(path_size-1),...
85     path(path_size));
86   path(path_size) = [];
87   % CURRENT EDGE IS THE SAME AS PREVIOUS VERTEX - move to next edge
88 elseif (length(path) > 1 && path(path_size-1) == current_edge)
89   current_edge = get_next_edge(net,path(path_size),current_edge);
90 elseif (check_path4loop(path,current_edge)) % LOOP FOUND!
91   loop = loop2std_form(path,current_edge);
92   %CRL -start-
93   new_loop = true;
94   for k = 1:numel(loop_list) % Only keep essential loops
95     if (numel(loop)<=numel(loop_list(k).loop))
96       if (nnz(~ismember(loop,loop_list(k).loop))<=1)
97         loop_list(k).loop = loop; % Replace exisiting loop
98         new_loop = false;
99         break
100      end
101    else
102      if (nnz(~ismember(loop_list(k).loop,loop))<=1)
103        new_loop = false;
104        break
```

Code listing A.23: Find independent MEC loops (`find_Lambda_Lambda.m`) *... cont*

```
105       end
106     end
107   end
108   if new_loop
109     loop_list(end+1).loop = loop;
110   end
111   %CRL —end—
112   current_edge = get_next_edge(net,path(path_size),current_edge);
113 else % NO LOOP FOUND — keep going down tree
114   path = [path current_edge];
115   current_edge = get_next_edge(net,path(path_size+1),[]);
116 end
117
118 %————————————————————————————————————————————————————————————————
119 function status = check_path4loop(path,current_edge)
120 %  Check to see if the current edge is in the path
121
122 status = 0;
123 if find(path == current_edge,1)
124   status = 1;
125 end
126
127 %————————————————————————————————————————————————————————————————
128 function next_edge = get_next_edge(net,current_node,current_edge)
129 %  Find the next edge of the current node in the network
130
131 next_edge = [];
132 for k = 1:length(net)
133   if (current_node == net(k).node)
134     if isempty(current_edge)  % start with first edge of the node
135       next_edge = net(k).edges(1);
136     else    % get the next edge in the list,if there is one
137       kk = find(net(k).edges == current_edge);
138       if kk < length(net(k).edges)
139         next_edge = net(k).edges(kk+1);
140       end
141     end
142     return
143   end
144 end
145
146 %————————————————————————————————————————————————————————————————
147 function loop = loop2std_form(path,current_edge)
148 %  Take a loop found in the path and return the loop vector in
149 %  standard form, where the smallest node ID is at the front of the
150 %  list and the smaller of the two neighbors is listed second
151
152 ii = find(path == current_edge);
153 loopy = path(ii:end); %get the loop from the path
154 n = length(loopy);
155 jj = find(loopy == min(loopy));
156 loop = loopy([(jj:n) (1:jj—1)]); %order loop with the smallest first
```

Code listing A.23: Find independent MEC loops (`find_Lambda_Lambda.m`) *... cont*

```
157 % order the remainder with the smaller of the two neighbors second
158 if loop(2) > loop(n)
159   loop = [loop(1) fliplr(loop(2:n))];
160 end
```

A.1.10 Force calculation

The calculation of the force on the subset of moving elements and sources is performed by the function provided as code listing A.24. This function implements (3.14), an approximation of the Maxwell Stress Tensor method, and outputs the force as a complex number where the real component is in the direction of motion.

Code listing A.24: Calculate force (`calc_F.m`)

```
1  function F = calc_F(Phi_e_kappa,H_e_kappa,A_e_kappa,hatn_e_kappa,...
2    hatt_e_kappa,M_delta_e,epsilon_e_kappa,hatx)
3
4  %Include only external boundaries for moving elements
5  [~,N_kappa] = size(epsilon_e_kappa);
6  M_e_kappa = (epsilon_e_kappa~=0) & repmat(M_delta_e,[1 N_kappa]);
7
8  F = sum((1/(2*4*pi*1e-7)*Phi_e_kappa(M_e_kappa).^2./...
9    A_e_kappa(M_e_kappa) - 4*pi*1e-7/2*H_e_kappa(M_e_kappa).^2.*...
10   A_e_kappa(M_e_kappa)).*hatn_e_kappa(M_e_kappa) - ...
11   Phi_e_kappa(M_e_kappa).*H_e_kappa(M_e_kappa).*...
12   hatt_e_kappa(M_e_kappa));
13
14 %Align real component of force with direction of movement
15 haty = -imag(hatx) + 1j*real(hatx);
16 F = (real(F)*real(hatx) + imag(F)*imag(hatx)) + ...
17   1j*(real(F)*real(haty) + imag(F)*imag(haty));
```

A.1.11 Solver

The solver initialisation function (code listing A.25) assembles the required number of independent simultaneous equations and the solver (code listing A.26) then solves these equations for a specified displacement and set of phase currents. Sparse matrices are used to construct the simultaneous equations as this reduces the computation time for larger-scale problems.

For nonlinear problems, where the reluctances are dependent on the flux values, the

MATLAB® function '`fsolve`' is used to find the solution by optimisation. To minimise the number of iterations required during dynamic simulation, the solution found at the previous time step is used as the starting point for the optimisation at the next time step (if available).

Code listing A.25: Initialise solver (`solveMECinit.m`)

```
function [N_Lambda,N_kcl,matA1,matA2,matA3,matA4,matB1,matB2,...
  matB3] = solveMECinit(nu_e_kappa,nu_epsilon,calR_e_kappa)
%  MEC solver initialisation

nonlinear = ~isnumeric(calR_e_kappa);
N_nu = max(abs(nu_e_kappa(:)));
[N_e,N_kappa] = size(nu_e_kappa);
N_epsilon = numel(nu_epsilon);

%% Construct directed reluctance graph from global boundary assignment
C_n_n = graph_C_n_n(nu_e_kappa);

%% Find separate components of connected elements
xi_n = scomponents(max(C_n_n,C_n_n.'));
N_xi = max(xi_n);

%% Find essential mmf loops
Lambda_Lambda = {};
for idx_xi = 1:N_xi %Find loops in each graph component separately
  C_xi_n_n = C_n_n;
  C_xi_n_n(xi_n~=idx_xi,xi_n~=idx_xi) = 0;
  Lambda_Lambda = [Lambda_Lambda; ...
    find_Lambda_Lambda(C_xi_n_n)]; %#ok<AGROW>
end
N_Lambda = numel(Lambda_Lambda);

%% Find elements that require application of Gauss' Law
e_kcl = [];  % Initialise list of elements for Gauss' Law
xi_e = xi_n(1:N_e);  % Get component info for element nodes
for idx_xi = 1:N_xi  % For each graph component c
  e_xi_e = find(xi_e==idx_xi);  % Get elements comprising component
  % Add all but one element from each component to list
  e_kcl = [e_kcl; e_xi_e(1:end-1)]; %#ok<AGROW>
end
N_kcl = numel(e_kcl);

%% Construct simultaneous equations: matA * matX = matB
% matX = [Phi_nu; calF_kappa__e]

N_unknowns = N_nu + N_kappa*N_e; %Number of unknowns to solve for
```

Code listing A.25: Initialise solver (`solveMECinit.m`) *... cont*

```
41 % KCL
42 % For each element (e_kcl), sum of boundary fluxes (Phi_nu, with
43 % correct signs) must equal zero
44 matA1 = sparse(reshape(repmat(1:N_kcl,[N_kappa 1]).',[],1),...
45   reshape(abs(nu_e_kappa(e_kcl,:)),[],1),...
46   reshape(sign(nu_e_kappa(e_kcl,:)),[],1),...
47   N_kcl,N_unknowns);
48
49 matB1 = sparse(N_kcl,1);
50
51 %------------------------------------------------------------------------%
52 % KVL
53 % For each loop (Lambda), sum of mmfs (calF_e__kappa, with correct
54 % signs) must equal zero
55 matA2 = sparse(N_Lambda,N_unknowns);
56 for idx_Lambda = 1:N_Lambda
57   for idx_n = 1:numel(Lambda_Lambda{idx_Lambda})-1
58     if (C_n_n(Lambda_Lambda{idx_Lambda}(idx_n),...
59         Lambda_Lambda{idx_Lambda}(idx_n+1))~=0)
60       if (Lambda_Lambda{idx_Lambda}(idx_n)<=N_e) %Element node
61         matA2(idx_Lambda,N_nu+...
62           N_kappa*(real(C_n_n(Lambda_Lambda{idx_Lambda}(idx_n),...
63           Lambda_Lambda{idx_Lambda}(idx_n+1)))-1)+...
64           imag(C_n_n(Lambda_Lambda{idx_Lambda}(idx_n),...
65           Lambda_Lambda{idx_Lambda}(idx_n+1)))) = 1; %#ok<SPRIX>
66       else %Boundary node
67         matA2(idx_Lambda,N_nu+...
68           N_kappa*(real(C_n_n(Lambda_Lambda{idx_Lambda}(idx_n),...
69           Lambda_Lambda{idx_Lambda}(idx_n+1)))-1)+...
70           imag(C_n_n(Lambda_Lambda{idx_Lambda}(idx_n),...
71           Lambda_Lambda{idx_Lambda}(idx_n+1)))) = -1; %#ok<SPRIX>
72       end
73     else
74       if (Lambda_Lambda{idx_Lambda}(idx_n)<=N_e) %Element node
75         matA2(idx_Lambda,N_nu+...
76           N_kappa*(real(C_n_n(Lambda_Lambda{idx_Lambda}(idx_n+1),...
77           Lambda_Lambda{idx_Lambda}(idx_n)))-1)+...
78           imag(C_n_n(Lambda_Lambda{idx_Lambda}(idx_n+1),...
79           Lambda_Lambda{idx_Lambda}(idx_n)))) = 1; %#ok<SPRIX>
80       else %Boundary node
81         matA2(idx_Lambda,N_nu+...
82           N_kappa*(real(C_n_n(Lambda_Lambda{idx_Lambda}(idx_n+1),...
83           Lambda_Lambda{idx_Lambda}(idx_n)))-1)+...
84           imag(C_n_n(Lambda_Lambda{idx_Lambda}(idx_n+1),...
85           Lambda_Lambda{idx_Lambda}(idx_n)))) = -1; %#ok<SPRIX>
86       end
87     end
88   end
89 end
90
91 matB2 = sparse(N_Lambda,1);
```

Code listing A.25: Initialise solver (`solveMECinit.m`) *... cont*

```
92 %-------------------------------------------------------------------------%
93 % calF_e_kappa + calR_e_kappa.*Phi_e_kappa = 0
94 matA3 = [sparse(N_kappa*N_e,N_nu) speye(N_kappa*N_e)];
95
96 if nonlinear %Use reluctances at Phi=0 as starting point
97   for idx_e = 1:N_e
98     for idx_kappa = 1:N_kappa
99       matA3((idx_e-1)*N_kappa+idx_kappa,...
100        abs(nu_e_kappa(idx_e,idx_kappa))) = ...
101        sign(nu_e_kappa(idx_e,idx_kappa))*...
102        ppval(calR_e_kappa(idx_e,idx_kappa),0); %#ok<SPRIX>
103    end
104  end
105 else %Reluctances are static
106   for idx_e = 1:N_e
107     for idx_kappa = 1:N_kappa
108       matA3((idx_e-1)*N_kappa+idx_kappa,...
109         abs(nu_e_kappa(idx_e,idx_kappa))) = ...
110         sign(nu_e_kappa(idx_e,idx_kappa))*...
111         calR_e_kappa(idx_e,idx_kappa); %#ok<SPRIX>
112    end
113  end
114 end
115
116 matB3 = sparse(N_kappa*N_e,1);
117
118 %-------------------------------------------------------------------------%
119 % Phi_epsilon - calG_epsilon_kappa__e*calF_kappa__e = Phi_epsilon_calF
120 matA4 = sparse(N_epsilon,N_unknowns);
121 matA4(1:N_epsilon,nu_epsilon) = speye(N_epsilon);
122
123 %matB4 is set within solver on each iteration
```

Code listing A.26: Solver (`solveMEC.m`)

```
1  function [Phi_e_kappa,calF_e_kappa,Phi_zeta,H_zeta,lambda_ph,F,...
2    varargout] = solveMEC(x,I_ph,M_delta_e,M_delta_calF,nu_e_kappa,...
3    epsilon_e_kappa,zeta_calF_kappa,calR_e_kappa,...
4    calG_epsilon_e_kappa,Phi_epsilon_calF0,calG_zeta_e_kappa,...
5    H_zeta_e_kappa,Phi_zeta_calF0,H_zeta_calF0,lambda_ph_e_kappa,...
6    lambda_ph_calF0,A_e_kappa,hatn_e_kappa,hatt_e_kappa,A_calF_kappa,...
7    hatn_calF_kappa,hatt_calF_kappa,hatx,chi_calF,material_chi,...
8    matA1,matA2,matA3,matA4,matB1,matB2,matB3,varargin)
9  %  MEC solver
10
11 [N_e,N_kappa] = size(nu_e_kappa);
12 [N_calF,~] = size(zeta_calF_kappa);
13 N_nu = max(abs(nu_e_kappa(:)));
14 N_epsilon = max(epsilon_e_kappa(:));
```

Code listing A.26: Solver (`solveMEC.m`) *... cont*

```
15 switch numel(varargin)
16   case 2
17     N_kcl = varargin{1};
18     N_Lambda = varargin{2};
19   case 3
20     N_kcl = varargin{1};
21     N_Lambda = varargin{2};
22     matX0 = varargin{3};
23 end
24 nonlinear = ~isnumeric(calR_e_kappa);
25
26 %% Update parameters
27 calG_epsilon_kappa_e = permute(ppval(calG_epsilon_e_kappa,abs(x)),...
28   [1,3,2]);
29 calG_epsilon_kappa__e = reshape(calG_epsilon_kappa_e,N_epsilon,[]);
30 matA4(1:N_epsilon,N_nu+(1:N_e*N_kappa)) = -calG_epsilon_kappa__e;
31
32 Phi_epsilon_calF = ppval(Phi_epsilon_calF0,abs(x));
33 % Scale by phase currents
34 for idx_calF = 1:N_calF
35   idx_chi = abs(chi_calF(idx_calF));
36   if strcmp(material_chi(idx_chi).type,'Coil')
37     Phi_epsilon_calF(:,idx_calF) = Phi_epsilon_calF(:,idx_calF)*...
38       I_ph(material_chi(idx_chi).params.ph);
39   end
40 end
41
42 matB4 = sum(Phi_epsilon_calF,2);
43
44 %% Solve
45 matA = [matA1; matA2; matA3; matA4];
46 matB = [matB1; matB2; matB3; matB4];
47
48 fprintf('Sparsity = %f %%\n',nnz(matA)/numel(matA)*100);
49 fprintf('Solving %i equations for %i unknowns...\n',...
50   numel(matB),numel(matA(1,:)));
51
52 if nonlinear
53   if ~exist('matX0','var')
54     matX0 = full(matA\matB); %Use as starting solution vector
55   end
56   tic; matX = fsolve(@(X) err(X,N_kcl,N_Lambda,N_nu,N_e,N_kappa,...
57     nu_e_kappa,calR_e_kappa,matA,matB),matX0,...
58     optimset('Display','iter'));
59   toc
60   %Pass out solution vector in case needed for next starting point
61   varargout{1} = matX;
62 else
63   tic; matX = matA\matB; toc
64 end
```

Code listing A.26: Solver (`solveMEC.m`) *... cont*

```
% Collate MEC outputs
Phi_nu = matX(1:N_nu);
Phi_e_kappa = full(sign(nu_e_kappa).*Phi_nu(abs(nu_e_kappa)));
calF_kappa_e = reshape(matX(N_nu+1:end),N_kappa,N_e);
calF_e_kappa = full(calF_kappa_e.');

%------------------------------------------------------------------------%
% Calculate flux linkages
lambda_ph_calF = ppval(lambda_ph_calF0,abs(x));
% Scale by phase currents
for idx_calF = 1:N_calF
  idx_chi = abs(chi_calF(idx_calF));
  if strcmp(material_chi(idx_chi).type,'Coil')
    lambda_ph_calF(:,idx_calF) = lambda_ph_calF(:,idx_calF)*...
      I_ph(material_chi(idx_chi).params.ph);
  end
end
%Sum all flux linkage components
lambda_ph = sum(sum(bsxfun(@times,ppval(lambda_ph_e_kappa,abs(x)),...
  shiftdim(calF_e_kappa,-1)),3),2) + sum(lambda_ph_calF,2);

%------------------------------------------------------------------------%
% Calculate moving source boundary fluxes
if ~isempty(Phi_zeta_calF0)
  Phi_zeta_calF = ppval(Phi_zeta_calF0,abs(x));
  % Scale by phase currents
  for idx_calF = 1:N_calF
    idx_chi = abs(chi_calF(idx_calF));
    if strcmp(material_chi(idx_chi).type,'Coil')
      Phi_zeta_calF(:,idx_calF) = Phi_zeta_calF(:,idx_calF)*...
        I_ph(material_chi(idx_chi).params.ph);
    end
  end
  %Sum all flux components
  Phi_zeta = sum(sum(bsxfun(@times,ppval(calG_zeta_e_kappa,abs(x)),...
    shiftdim(calF_e_kappa,-1)),3),2) + sum(Phi_zeta_calF,2);
else
  Phi_zeta = 0;
end

%------------------------------------------------------------------------%
% Calculate moving source boundary field intensities
if ~isempty(H_zeta_calF0)
  H_zeta_calF = ppval(H_zeta_calF0,abs(x));
  % Scale by phase currents
  for idx_calF = 1:N_calF
    idx_chi = abs(chi_calF(idx_calF));
    if strcmp(material_chi(idx_chi).type,'Coil')
      H_zeta_calF(:,idx_calF) = H_zeta_calF(:,idx_calF)*...
        I_ph(material_chi(idx_chi).params.ph);
    end
  end
```

Code listing A.26: Solver (`solveMEC.m`) *... cont*

```
117   %Sum all flux components
118   H_zeta = sum(sum(bsxfun(@times,ppval(H_zeta_e_kappa,abs(x)),...
119     shiftdim(calF_e_kappa,-1)),3),2) + sum(H_zeta_calF,2);
120 else
121   H_zeta = 0;
122 end
123
124 %-------------------------------------------------------------------------%
125 % Calculate electromagnetic force on moving elements and sources
126 Phi_calF_kappa = zeros(N_calF,N_kappa);
127 if ~isempty(Phi_zeta_calF0)
128   Phi_calF_kappa(zeta_calF_kappa~=0) = ...
129     Phi_zeta(zeta_calF_kappa(zeta_calF_kappa~=0));
130 end
131 H_calF_kappa = zeros(N_calF,N_kappa);
132 if ~isempty(H_zeta_calF0)
133   H_calF_kappa(zeta_calF_kappa~=0) = ...
134     H_zeta(zeta_calF_kappa(zeta_calF_kappa~=0));
135 end
136 %Ignore tangential field intensities for flux tube elements
137 H_e_kappa = zeros(N_e,N_kappa);
138
139 F = calc_F(Phi_e_kappa,H_e_kappa,A_e_kappa,hatn_e_kappa,...
140   hatt_e_kappa,M_delta_e,epsilon_e_kappa,hatx) + ...
141   calc_F(Phi_calF_kappa,H_calF_kappa,A_calF_kappa,hatn_calF_kappa,...
142   hatt_calF_kappa,M_delta_calF,zeta_calF_kappa,hatx);
143
144 %-------------------------------------------------------------------------%
145   function output = err(matX_iter,N_kcl,N_Lambda,N_nu,N_e,N_kappa,...
146       nu_e_kappa,calR_e_kappa,matA,matB)
147     %Set calR_e_kappa for calF_e_kappa + calR_e_kappa.*Phi_e_kappa = 0
148     Phi_iter_nu = matX_iter(1:N_nu);
149     Phi_iter_e_kappa = sign(nu_e_kappa).*Phi_iter_nu(abs(nu_e_kappa));
150     matA_iter = matA;
151     for idx_iter_e = 1:N_e
152       for idx_iter_kappa = 1:N_kappa
153         matA_iter(N_kcl+N_Lambda+(idx_iter_e-1)*N_kappa+...
154           idx_iter_kappa,...
155           abs(nu_e_kappa(idx_iter_e,idx_iter_kappa))) = ...
156           sign(nu_e_kappa(idx_iter_e,idx_iter_kappa))*...
157           ppval(calR_e_kappa(idx_iter_e,idx_iter_kappa),...
158           abs(Phi_iter_e_kappa(idx_iter_e,idx_iter_kappa)));
159       end
160     end
161     output = matA_iter*matX_iter - matB;
162   end
163
164 end
```

A.1.12 Comparison of static results to full FEM solutions

For comparison purposes, function A.27 obtains the field solution outside of the flux tube element regions by using the exact boundary conditions returned by the hybrid method solver. This field solution can then be visually compared with a solution obtained with function A.28, which uses FEMM to obtain a pure FEM solution over the entire problem space.

Code listing A.27: Solve for magnetic fields in FEMM using sources and element boundary conditions calculated by the hybrid method (`femResult.m`)

```
function femResult(x,I_ph,calF_e_kappa,p_e_v,M_delta_e,p_calF_v,...
  M_delta_calF,d,epsilon_e_kappa,chi_calF,material_chi,femm)
%  Calculate field solution for boundary mmfs and sources using FEMM

% Set up problem in FEMM
femSetup(d,femm);
femDraw([p_e_v; p_calF_v],[M_delta_e; M_delta_calF],femm);
femDrawInfDomain([p_e_v; p_calF_v],[M_delta_e; M_delta_calF],...
  x,femm);
femDefineMaterials(material_chi,I_ph);
femSetBoundaries(p_e_v,M_delta_e,epsilon_e_kappa,calF_e_kappa,...
  femm);
femAssignSources(p_calF_v,M_delta_calF,chi_calF,material_chi,femm);
% Move elements and sources to specified position
mi_selectgroup(1);
mi_movetranslate(real(x),imag(x));
mi_clearselected;
% Solve
mi_analyze;
mi_loadsolution;
closefemm;
```

Code listing A.28: Solve problem purely in FEMM (`femFull.m`)

```
function [Phi_epsilon_x,Phi_zeta_x,H_zeta_x,lambda_ph_x,F_x] = ...
  femFull(x_x,I_ph,p_e_v,M_delta_e,p_calF_v,M_delta_calF,d,...
  epsilon_e_kappa,zeta_calF_kappa,hatx,chi_e,chi_calF,material_chi,...
  femm)
%  Calculate full solution using FEMM

N_epsilon = max(epsilon_e_kappa(:));
N_zeta = max(zeta_calF_kappa(:));
N_x = numel(x_x);
[~,N_v] = size(p_e_v);
N_ph = numel(I_ph);
```

Code listing A.28: Solve problem purely in FEMM (`femFull.m`) *... cont*

```
% Preallocate outputs
Phi_epsilon_x = zeros(N_epsilon,N_x);
Phi_zeta_x = zeros(N_zeta,N_x);
H_zeta_x = zeros(N_zeta,N_x);
lambda_ph_x = zeros(N_ph,N_x);
F_x = zeros(N_x,1);
%Calculate incremental displacements
x_delta_x = diff([0; x_x]);
% Set up problem in FEMM
femSetup(d,femm);
femDraw([p_e_v; p_calF_v],[M_delta_e; M_delta_calF],femm);
femDrawInfDomain([p_e_v; p_calF_v],[M_delta_e; M_delta_calF],...
  x_x,femm);
femDefineMaterials(material_chi,I_ph);
femAssignElements(p_e_v,M_delta_e,chi_e,material_chi,femm);
femAssignSources(p_calF_v,M_delta_calF,chi_calF,material_chi,femm);
% Solve at each position
for idx_x = 1:N_x
  % Move to next position
  mi_selectgroup(1);
  mi_movetranslate(real(x_delta_x(idx_x)),imag(x_delta_x(idx_x)));
  mi_clearselected;
  p_e_v(repmat(M_delta_e,[1 N_v])==true) = ...
    p_e_v(repmat(M_delta_e,[1 N_v])==true) + x_delta_x(idx_x);
  p_calF_v(repmat(M_delta_calF,[1 N_v])==true) = ...
    p_calF_v(repmat(M_delta_calF,[1 N_v])==true) + x_delta_x(idx_x);
  % Solve
  mi_analyze;
  mi_loadsolution;
  %Get element boundary flux
  Phi_epsilon_x(:,idx_x) = fem_Phi_epsilon(p_e_v,epsilon_e_kappa);
  %Get source boundary flux
  Phi_zeta_x(:,idx_x) = fem_Phi_zeta(p_calF_v,zeta_calF_kappa);
  %Get source boundary tangential field intensities
  H_zeta_x(:,idx_x) = fem_H_zeta(p_calF_v,zeta_calF_kappa);
  % Get flux linkages
  for idx_ph = 1:N_ph
    circProps = mo_getcircuitproperties(num2str(idx_ph));
    lambda_ph_x(idx_ph,idx_x) = circProps(3);
  end
  % Get force on moving parts
  haty = -imag(hatx) + 1j*real(hatx);
  mo_seteditmode('area');
  mo_groupselectblock(1);
  try %#ok<TRYNC>
    F_x(idx_x) = (mo_blockintegral(18)*real(hatx) + ...
      mo_blockintegral(19)*imag(hatx)) + ...
      1j*(mo_blockintegral(18)*real(haty) + ...
      mo_blockintegral(19)*imag(haty));
  end
  mo_close;
end
closefemm;
```

Function A.29 calculates normalised root-mean-squared (rms) errors for the boundary flux, winding flux linkages and electromagnetic force over a specified range of discrete phase currents and displacements. The errors are normalised with respect to the pure FEM solution rms values.

Code listing A.29: Obtain static solutions over a range of phase currents and displacements and compare to full FEM solutions (`solveMECstatic.m`)

```
function [calF_e_kappa_x_I,Phi_e_kappa_x_I,Phi_zeta_x_I,H_zeta_x_I,...
  lambda_ph_x_I,F_x_I,error_Phi_epsilon_x_I,error_Phi_zeta_x_I,...
  error_H_zeta_x_I,error_lambda_ph_x_I,error_F_x_I] = ...
  solveMECstatic(x_x,I_ph_I,p_e_v,M_delta_e,p_calF_v,M_delta_calF,...
  d,nu_e_kappa,epsilon_e_kappa,zeta_calF_kappa,A_e_kappa,...
  hatn_e_kappa,hatt_e_kappa,A_calF_kappa,hatn_calF_kappa,...
  hatt_calF_kappa,calR_e_kappa,calG_epsilon_e_kappa,...
  Phi_epsilon_calF0,calG_zeta_e_kappa,H_zeta_e_kappa,...
  Phi_zeta_calF0,H_zeta_calF0,lambda_ph_e_kappa,lambda_ph_calF0,...
  hatx,chi_e,chi_calF,material_chi,N_kc1,N_Lambda,matA1,matA2,...
  matA3,matA4,matB1,matB2,matB3,femm)
%  Solve problem using hybrid method over a range of discrete
%  phase currents and displacements, and compare to full FEM solutions
%  with rms error analysis

nonlinear = ~isnumeric(calR_e_kappa);
[N_e,N_kappa] = size(nu_e_kappa);
[N_ph,N_I] = size(I_ph_I);
N_x = numel(x_x);
N_epsilon = max(epsilon_e_kappa(:));
N_zeta = max(zeta_calF_kappa(:));

% Preallocate outputs
calF_e_kappa_x_I = zeros(N_e,N_kappa,N_x,N_I);
Phi_e_kappa_x_I = zeros(N_e,N_kappa,N_x,N_I);
Phi_epsilon_x_I = zeros(N_epsilon,N_x,N_I);
Phi_zeta_x_I = zeros(N_zeta,N_x,N_I);
H_zeta_x_I = zeros(N_zeta,N_x,N_I);
lambda_ph_x_I = zeros(N_ph,N_x,N_I);
F_x_I = zeros(N_x,N_I);
Phi_fem_epsilon_x_I = zeros(N_epsilon,N_x,N_I);
Phi_fem_zeta_x_I = zeros(N_zeta,N_x,N_I);
H_fem_zeta_x_I = zeros(N_zeta,N_x,N_I);
lambda_fem_ph_x_I = zeros(N_ph,N_x,N_I);
F_fem_x_I = zeros(N_x,N_I);

for idx_I = 1:N_I
  for idx_x = 1:N_x
```

Code listing A.29: Obtain static solutions over a range of phase currents and displacements and compare to full FEM solutions (`solveMECstatic.m`) *... cont*

```
39      % Solve using hybrid MEC/FEM method
40      if nonlinear
41        [Phi_e_kappa_x_I(:,:,idx_x,idx_I),...
42          calF_e_kappa_x_I(:,:,idx_x,idx_I),...
43          Phi_zeta_x_I(:,idx_x,idx_I),H_zeta_x_I(:,idx_x,idx_I),...
44          lambda_ph_x_I(:,idx_x,idx_I),F_x_I(idx_x,idx_I)] = ...
45          solveMEC(x_x(idx_x),I_ph_I(:,idx_I),M_delta_e,M_delta_calF,...
46          nu_e_kappa,epsilon_e_kappa,zeta_calF_kappa,calR_e_kappa,...
47          calG_epsilon_e_kappa,Phi_epsilon_calF0,calG_zeta_e_kappa,...
48          H_zeta_e_kappa,Phi_zeta_calF0,H_zeta_calF0,...
49          lambda_ph_e_kappa,lambda_ph_calF0,A_e_kappa,hatn_e_kappa,...
50          hatt_e_kappa,A_calF_kappa,hatn_calF_kappa,hatt_calF_kappa,...
51          hatx,chi_calF,material_chi,matA1,matA2,matA3,matA4,matB1,...
52          matB2,matB3,N_kcl,N_Lambda);
53      else
54      [Phi_e_kappa_x_I(:,:,idx_x,idx_I),...
55        calF_e_kappa_x_I(:,:,idx_x,idx_I),...
56        Phi_zeta_x_I(:,idx_x,idx_I),H_zeta_x_I(:,idx_x,idx_I),...
57        lambda_ph_x_I(:,idx_x,idx_I),F_x_I(idx_x,idx_I)] = ...
58        solveMEC(x_x(idx_x),I_ph_I(:,idx_I),M_delta_e,M_delta_calF,...
59        nu_e_kappa,epsilon_e_kappa,zeta_calF_kappa,calR_e_kappa,...
60        calG_epsilon_e_kappa,Phi_epsilon_calF0,calG_zeta_e_kappa,...
61        H_zeta_e_kappa,Phi_zeta_calF0,H_zeta_calF0,lambda_ph_e_kappa,...
62        lambda_ph_calF0,A_e_kappa,hatn_e_kappa,hatt_e_kappa,...
63        A_calF_kappa,hatn_calF_kappa,hatt_calF_kappa,hatx,chi_calF,...
64        material_chi,matA1,matA2,matA3,matA4,matB1,matB2,matB3);
65      end
66      femResult(x_x(idx_x),I_ph_I(:,idx_I),...
67        calF_e_kappa_x_I(:,:,idx_x,idx_I),p_e_v,M_delta_e,p_calF_v,...
68        M_delta_calF,d,epsilon_e_kappa,chi_calF,material_chi,femm);
69    end
70    % Solve using pure FEM for comparison
71    [Phi_fem_epsilon_x_I(:,:,idx_I),Phi_fem_zeta_x_I(:,:,idx_I),...
72      H_fem_zeta_x_I(:,:,idx_I),lambda_fem_ph_x_I(:,:,idx_I),...
73      F_fem_x_I(:,idx_I)] = femFull(x_x,I_ph_I(:,idx_I),p_e_v,...
74      M_delta_e,p_calF_v,M_delta_calF,d,epsilon_e_kappa,...
75      zeta_calF_kappa,hatx,chi_e,chi_calF,material_chi,femm);
76  end
77
78  %% Measure rms errors
79
80  %Isolate exterior element boundary fluxes
81  Phi_epsilon_x_I(epsilon_e_kappa(epsilon_e_kappa(:)~=0),:,:) = ...
82    reshape(...
83    Phi_e_kappa_x_I(repmat(epsilon_e_kappa(:)~=0,[1 N_x N_I])),...
84    [],N_x,N_I);
85
86  error_Phi_epsilon_x_I = ...
87    sqrt(sum((Phi_epsilon_x_I-Phi_fem_epsilon_x_I).^2)/N_epsilon)./...
88    sqrt(sum(Phi_fem_epsilon_x_I.^2)/N_epsilon)*100;
```

Code listing A.29: Obtain static solutions over a range of phase currents and displacements and compare to full FEM solutions (`solveMECstatic.m`) *... cont*

```
89 error_Phi_zeta_x_I = ...
90   sqrt(sum((Phi_zeta_x_I-Phi_fem_zeta_x_I).^2)/N_zeta)./...
91   sqrt(sum(Phi_fem_zeta_x_I.^2)/N_zeta)*100;
92
93 error_H_zeta_x_I = ...
94   sqrt(sum((H_zeta_x_I-H_fem_zeta_x_I).^2)/N_zeta)./...
95   sqrt(sum(H_fem_zeta_x_I.^2)/N_zeta)*100;
96
97 error_lambda_ph_x_I = ...
98   sqrt(sum((lambda_ph_x_I-lambda_fem_ph_x_I).^2)/N_ph)./...
99   sqrt(sum(lambda_fem_ph_x_I.^2)/N_ph)*100;
100
101 error_F_x_I = abs(real(F_x_I-F_fem_x_I)./real(F_fem_x_I))*100 + ...
102   1j*abs(imag(F_x_I-F_fem_x_I)./imag(F_fem_x_I)*100);
```

A.2 Worked example

A.2.1 Problem specification

Code listing A.30: Example—define basic problem parameters (`exampleMEC.m`)

```
1 %% Define problem depth
2 d = 0.2;
3
4 %% Define movement direction
5 hatx = 1;
6
7 %% Set FEMM parameters
8 femm.accuracy = 1e-12;
9 femm.meshSize = 1e-4;
10 femm.minMeshDeg = 30;
11 femm.arcSegDeg = 5;
```

Materials

Code listing A.31: Example—define materials (`exampleMEC.m`)

```
12 %  Stator core and back-iron
13 BH_M250_50A = load('BH_M250-50A.csv');
14 BH_1010 = load('BH_1010.csv');
```

Code listing A.31: Example—define materials (`exampleMEC.m`) *... cont*

```
% Sura 250-50 Steel
material_chi(1,1).name = ...
  'M250-50A Steel ($\raisebox{0.5ex}{\idx[1]{\upchi}}$)';
material_chi(1,1).params.B = BH_M250_50A(:,1);
material_chi(1,1).params.H = BH_M250_50A(:,2);
material_chi(1,1).params.mur = max(material_chi(1).params.B ./ ...
  material_chi(1).params.H) / (4*pi*1e-7);
% 1010 Steel
material_chi(2,1).name = ...
  '1010 Steel ($\raisebox{0.5ex}{\idx[2]{\upchi}}$)';
material_chi(2,1).params.B = BH_1010(:,1);
material_chi(2,1).params.H = BH_1010(:,2);
material_chi(2,1).params.mur = max(material_chi(2).params.B ./ ...
  material_chi(2).params.H) / (4*pi*1e-7);
% Plot BH curves
plot_BH('BH.tikz',material_chi(1:2),2.6e4);
plot_BH('BHzoomed.tikz',material_chi(1:2),1e3);
if nonlinear
  material_chi(1,1).type = 'Nonlinear';
  material_chi(2,1).type = 'Nonlinear';
else
  material_chi(1,1).type = 'Linear';
  material_chi(2,1).type = 'Linear';
end
%  Magnets
material_chi(3,1).type = 'Magnet';
material_chi(3,1).params.mur = 1.049;
material_chi(3,1).params.Hc = 979000;
%  Coils
N_ph = 3;
% Phase 'A'
material_chi(4,1).type = 'Coil';
material_chi(4,1).params.mur = 1;
material_chi(4,1).params.ph = 1;
material_chi(4,1).params.turns = 15;
% Phase 'B'
material_chi(5,1).type = 'Coil';
material_chi(5,1).params.mur = 1;
material_chi(5,1).params.ph = 2;
material_chi(5,1).params.turns = 15;
% Phase 'C'
material_chi(6,1).type = 'Coil';
material_chi(6,1).params.mur = 1;
material_chi(6,1).params.ph = 3;
material_chi(6,1).params.turns = 15;
```

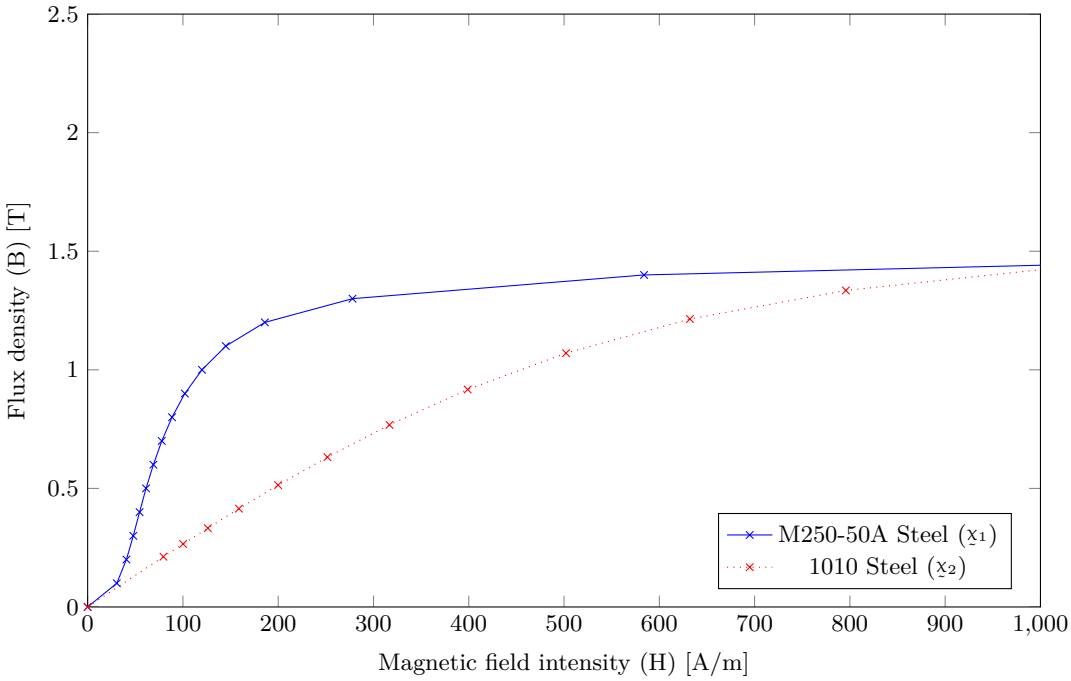

Figure A.2: Example—*B*-*H* curves for materials (zoomed in on initial slopes)

Flux tube elements and sources

Code listing A.32: Example—flux tube elements (`exampleMEC.m`)

```
60 %  Stator
61 % Geometry
62 p_e_v( 1,:) = [0   4.2   4.2+5j   5j];
63 p_e_v( 2,:) = [0   3.6   3.6+5j   5j] + 4.2;
64 p_e_v( 3,:) = [0   2.4   2.4+5j   5j] + 7.8;
65 p_e_v( 4,:) = [0   3.6   3.6+5j   5j] + 4.2 + 6;
66 p_e_v( 5,:) = [0   2.4   2.4+5j   5j] + 7.8 + 6;
67 p_e_v( 6,:) = [0   3.6   3.6+5j   5j] + 4.2 + 2*6;
68 p_e_v( 7,:) = [0   2.4   2.4+5j   5j] + 7.8 + 2*6;
69 p_e_v( 8,:) = [0   3.6   3.6+5j   5j] + 4.2 + 3*6;
70 p_e_v( 9,:) = [0   2.4   2.4+5j   5j] + 7.8 + 3*6;
71 p_e_v(10,:) = [0   3.6   3.6+5j   5j] + 4.2 + 4*6;
72 p_e_v(11,:) = [0   4.2   4.2+5j   5j] + 7.8 + 4*6;
73 p_e_v(12,:) = [0   4.2   4.2+8j   8j] + 5j;
74 p_e_v(13,:) = [0   3.6   3.6+8j   8j] + 5j + 4.2;
75 p_e_v(14,:) = [0   2.4   2.4+8j   8j] + 5j + 7.8;
76 p_e_v(15,:) = [0   3.6   3.6+8j   8j] + 5j + 4.2 + 6;
77 p_e_v(16,:) = [0   2.4   2.4+8j   8j] + 5j + 7.8 + 6;
```

Code listing A.32: Example—flux tube elements (`exampleMEC.m`) *... cont*

```
p_e_v(17,:) = [0   2.4   2.4+8j   8j] + 5j + 7.8 + 2*6;
p_e_v(18,:) = [0   3.6   3.6+8j   8j] + 5j + 4.2 + 3*6;
p_e_v(19,:) = [0   2.4   2.4+8j   8j] + 5j + 7.8 + 3*6;
p_e_v(20,:) = [0   3.6   3.6+8j   8j] + 5j + 4.2 + 4*6;
p_e_v(21,:) = [0   4.2   4.2+8j   8j] + 5j + 7.8 + 4*6;
p_e_v(22,:) = [0   4.2   4.2+8j   8j] + 8j + 5j;
p_e_v(23,:) = [0   2.4   2.4+8j   8j] + 8j + 5j + 7.8;
p_e_v(24,:) = [0   2.4   2.4+8j   8j] + 8j + 5j + 7.8 + 6;
p_e_v(25,:) = [0   2.4   2.4+8j   8j] + 8j + 5j + 7.8 + 2*6;
p_e_v(26,:) = [0   2.4   2.4+8j   8j] + 8j + 5j + 7.8 + 3*6;
p_e_v(27,:) = [0   4.2   4.2+8j   8j] + 8j + 5j + 7.8 + 4*6;
% Movement
M_delta_e(1:27,1) = false;
% Material
chi_e(1:27,1) = 1;

%  Reaction plate
% Geometry
p_e_v(28,:) = [0   13    13+4.5j    4.5j] + 25j + 2.5;
p_e_v(29,:) = [0   5     5+4.5j     4.5j] + 25j + 2.5 + 13;
p_e_v(30,:) = [0   13    13+4.5j    4.5j] + 25j + 2.5 + 18;
% Movement
M_delta_e(28:30,1) = true;
% Material
chi_e(28:30,1) = 2;

p_e_v = p_e_v*1e-3;  %mm -> m

% Calculate surface areas and orientations
A_e_kappa = calc_A_e_kappa(p_e_v,d);
[hatn_e_kappa,hatt_e_kappa] = calcBoundaryOrientations(p_e_v);
```

Code listing A.33: Example—sources (`exampleMEC.m`)

```
%  Coils
% Geometry
p_calF_v(1,:) = [0   2.6   2.6+6j   6j] + 6j + 4.7 + 2*6;
p_calF_v(2,:) = [0   2.6   2.6+6j   6j] + 8j + 6j + 4.7;
p_calF_v(3,:) = [0   2.6   2.6+6j   6j] + 8j + 6j + 4.7 + 6;
p_calF_v(4,:) = [0   2.6   2.6+6j   6j] + 8j + 6j + 4.7 + 2*6;
p_calF_v(5,:) = [0   2.6   2.6+6j   6j] + 8j + 6j + 4.7 + 3*6;
p_calF_v(6,:) = [0   2.6   2.6+6j   6j] + 8j + 6j + 4.7 + 4*6;
% Movement
M_delta_calF(1:6,1) = false;
```

Code listing A.33: Example—sources (`exampleMEC.m`) *... cont*

```
% Materials and polarity
chi_calF(1,1) = -4;
chi_calF(2,1) = 4;
chi_calF(3,1) = -6;
chi_calF(4,1) = 5;
chi_calF(5,1) = 6;
chi_calF(6,1) = -5;

%  Magnets
% Geometry
p_calF_v(7,:) = [0   13    13+1.5j    1.5j] + 23.5j + 2.5;
p_calF_v(8,:) = [0   13    13+1.5j    1.5j] + 23.5j + 2.5 + 18;
% Movement
M_delta_calF(7:8,1) = true;
% Materials and angle
chi_calF(7,1) = 3*exp(1i*pi/2);
chi_calF(8,1) = 3*exp(1i*-pi/2);

p_calF_v = p_calF_v*1e-3;  %mm -> m

% Calculate surface areas, orientations and lengths
A_calF_kappa = calc_A_e_kappa(p_calF_v,d);
[hatn_calF_kappa,hatt_calF_kappa] = ...
  calcBoundaryOrientations(p_calF_v);
l_e_kappa = calc_l_e_kappa(p_e_v);
```

A.2.2 Assign boundary indices

Code listing A.34: Example—assign boundary indices (`exampleMEC.m`)

```
nu_e_kappa = assign_nu_e_kappa(p_e_v);
[epsilon_e_kappa nu_epsilon] = assign_epsilon_e_kappa(nu_e_kappa);
zeta_calF_kappa = assign_zeta_calF_kappa(p_calF_v,M_delta_calF);
```

A.2.3 Calculate flux tube reluctances

Code listing A.35: Example—calculate flux tube reluctances (`exampleMEC.m`)

```
calR_e_kappa = calc_calR_e_kappa(p_e_v,l_e_kappa,A_e_kappa,...
  chi_e,material_chi);
```

A.2.4 Precompute parameter sets

Code listing A.36: Example—precompute parameter sets (`exampleMEC.m`)

```
% Discrete positions to obtain upfront parameters for
x_x = [0; 2; 4; 6]*1e-3;

[calG_epsilon_e_kappa,Phi_epsilon_calF0,calG_zeta_e_kappa,...
  H_zeta_e_kappa,Phi_zeta_calF0,H_zeta_calF0,lambda_ph_e_kappa,...
  lambda_ph_calF0] = femUpfrontCalcs(p_e_v,M_delta_e,p_calF_v,...
  M_delta_calF,d,epsilon_e_kappa,zeta_calF_kappa,chi_calF,...
  material_chi,N_ph,x_x,femm);
```

A.2.5 Initialise solver

Code listing A.37: Example—initialise solver (`exampleMEC.m`)

```
[N_Lambda,N_kcl,matA1,matA2,matA3,matA4,matB1,matB2,matB3] = ...
  solveMECinit(nu_e_kappa,nu_epsilon,calR_e_kappa);
```

A.2.6 Solve over a range of discrete positions and phase currents

Code listing A.38: Example—solve at discrete positions and currents (`exampleMEC.m`)

```
% Positions to solve at
x_x = [0; 1; 2; 3; 4; 5; 6]*1e-3;

% Phase currents to solve for
I_ph_I = [[20; -10; -10] [-10; 20; -10] [-10; -10; 20]];

[calF_e_kappa_x_I,Phi_e_kappa_x_I,Phi_zeta_x_I,H_zeta_x_I,...
  lambda_ph_x_I,F_x_I,error_Phi_epsilon_x_I,error_Phi_zeta_x_I,...
  error_H_zeta_x_I,error_lambda_ph_x_I,error_F_x_I] = ...
  solveMECstatic(x_x,I_ph_I,p_e_v,M_delta_e,p_calF_v,M_delta_calF,...
  d,nu_e_kappa,epsilon_e_kappa,zeta_calF_kappa,A_e_kappa,...
  hatn_e_kappa,hatt_e_kappa,A_calF_kappa,hatn_calF_kappa,...
  hatt_calF_kappa,calR_e_kappa,calG_epsilon_e_kappa,...
  Phi_epsilon_calF0,calG_zeta_e_kappa,H_zeta_e_kappa,...
  Phi_zeta_calF0,H_zeta_calF0,lambda_ph_e_kappa,lambda_ph_calF0,...
  hatx,chi_e,chi_calF,material_chi,N_kcl,N_Lambda,matA1,matA2,...
  matA3,matA4,matB1,matB2,matB3,femm);

% Calculate average flux densities for all boundaries
B_e_kappa_x_I = bsxfun(@rdivide,Phi_e_kappa_x_I,A_e_kappa);
```

A.2.7 Results

Table A.1: Flux tube element outputs

Element Region	$\underline{I}_{(\mathrm{ph})} = \begin{bmatrix} 20 & -10 & -10 \end{bmatrix}^{\mathrm{T}}$					
	$x = 0\,\mathrm{mm}$			$x = 1\,\mathrm{mm}$		
	Φ [Wb]	B [T]	$\mathcal{F}$ [A]	Φ [Wb]	B [T]	$\mathcal{F}$ [A]
$\mathfrak{e}_1\mathfrak{k}_1$	$-1{,}892 \cdot 10^{-6}$	$-2{,}253 \cdot 10^{-3}$	$1{,}739 \cdot 10^{-3}$	$-1{,}916 \cdot 10^{-6}$	$-2{,}281 \cdot 10^{-3}$	$1{,}761 \cdot 10^{-3}$
$\mathfrak{e}_1\mathfrak{k}_2$	$-9{,}654 \cdot 10^{-5}$	$-9{,}654 \cdot 10^{-2}$	$6{,}264 \cdot 10^{-2}$	$-7{,}545 \cdot 10^{-5}$	$-7{,}545 \cdot 10^{-2}$	$5{,}131 \cdot 10^{-2}$
$\mathfrak{e}_1\mathfrak{k}_3$	$1{,}006 \cdot 10^{-4}$	$1{,}197 \cdot 10^{-1}$	$-8{,}592 \cdot 10^{-2}$	$7{,}960 \cdot 10^{-5}$	$9{,}476 \cdot 10^{-2}$	$-7{,}354 \cdot 10^{-2}$
$\mathfrak{e}_1\mathfrak{k}_4$	$-2{,}136 \cdot 10^{-6}$	$-2{,}136 \cdot 10^{-3}$	$1{,}384 \cdot 10^{-3}$	$-2{,}237 \cdot 10^{-6}$	$-2{,}237 \cdot 10^{-3}$	$1{,}450 \cdot 10^{-3}$
$\mathfrak{e}_2\mathfrak{k}_1$	$-1{,}100 \cdot 10^{-6}$	$-1{,}528 \cdot 10^{-3}$	$1{,}176 \cdot 10^{-3}$	$-1{,}096 \cdot 10^{-6}$	$-1{,}522 \cdot 10^{-3}$	$1{,}171 \cdot 10^{-3}$
$\mathfrak{e}_2\mathfrak{k}_2$	$-2{,}433 \cdot 10^{-4}$	$-2{,}433 \cdot 10^{-1}$	$7{,}764 \cdot 10^{-2}$	$-2{,}044 \cdot 10^{-4}$	$-2{,}044 \cdot 10^{-1}$	$7{,}359 \cdot 10^{-2}$
$\mathfrak{e}_2\mathfrak{k}_3$	$1{,}478 \cdot 10^{-4}$	$2{,}053 \cdot 10^{-1}$	$-1{,}023 \cdot 10^{-1}$	$1{,}300 \cdot 10^{-4}$	$1{,}806 \cdot 10^{-1}$	$-9{,}987 \cdot 10^{-2}$
$\mathfrak{e}_2\mathfrak{k}_4$	$9{,}654 \cdot 10^{-5}$	$9{,}654 \cdot 10^{-2}$	$-5{,}369 \cdot 10^{-2}$	$7{,}545 \cdot 10^{-5}$	$7{,}545 \cdot 10^{-2}$	$-4{,}398 \cdot 10^{-2}$
$\mathfrak{e}_3\mathfrak{k}_1$	$-7{,}434 \cdot 10^{-7}$	$-1{,}549 \cdot 10^{-3}$	$1{,}192 \cdot 10^{-3}$	$-7{,}297 \cdot 10^{-7}$	$-1{,}520 \cdot 10^{-3}$	$1{,}170 \cdot 10^{-3}$
$\mathfrak{e}_3\mathfrak{k}_2$	$-5{,}136 \cdot 10^{-4}$	$-5{,}136 \cdot 10^{-1}$	$7{,}477 \cdot 10^{-2}$	$-4{,}853 \cdot 10^{-4}$	$-4{,}853 \cdot 10^{-1}$	$7{,}227 \cdot 10^{-2}$
$\mathfrak{e}_3\mathfrak{k}_3$	$2{,}710 \cdot 10^{-4}$	$5{,}647 \cdot 10^{-1}$	$-1{,}655 \cdot 10^{-1}$	$2{,}817 \cdot 10^{-4}$	$5{,}869 \cdot 10^{-1}$	$-1{,}699 \cdot 10^{-1}$
$\mathfrak{e}_3\mathfrak{k}_4$	$2{,}433 \cdot 10^{-4}$	$2{,}433 \cdot 10^{-1}$	$-5{,}176 \cdot 10^{-2}$	$2{,}044 \cdot 10^{-4}$	$2{,}044 \cdot 10^{-1}$	$-4{,}906 \cdot 10^{-2}$
$\mathfrak{e}_4\mathfrak{k}_1$	$-1{,}351 \cdot 10^{-6}$	$-1{,}876 \cdot 10^{-3}$	$1{,}446 \cdot 10^{-3}$	$-1{,}297 \cdot 10^{-6}$	$-1{,}802 \cdot 10^{-3}$	$1{,}388 \cdot 10^{-3}$
$\mathfrak{e}_4\mathfrak{k}_2$	$-1{,}007 \cdot 10^{-3}$	$-1{,}007$	$2{,}185 \cdot 10^{-1}$	$-9{,}912 \cdot 10^{-4}$	$-9{,}912 \cdot 10^{-1}$	$2{,}127 \cdot 10^{-1}$
$\mathfrak{e}_4\mathfrak{k}_3$	$4{,}944 \cdot 10^{-4}$	$6{,}866 \cdot 10^{-1}$	$-1{,}913 \cdot 10^{-1}$	$5{,}072 \cdot 10^{-4}$	$7{,}044 \cdot 10^{-1}$	$-1{,}956 \cdot 10^{-1}$
$\mathfrak{e}_4\mathfrak{k}_4$	$5{,}136 \cdot 10^{-4}$	$5{,}136 \cdot 10^{-1}$	$-1{,}122 \cdot 10^{-1}$	$4{,}853 \cdot 10^{-4}$	$4{,}853 \cdot 10^{-1}$	$-1{,}084 \cdot 10^{-1}$
$\mathfrak{e}_5\mathfrak{k}_1$	$-1{,}435 \cdot 10^{-6}$	$-2{,}990 \cdot 10^{-3}$	$2{,}314 \cdot 10^{-3}$	$-1{,}336 \cdot 10^{-6}$	$-2{,}784 \cdot 10^{-3}$	$2{,}153 \cdot 10^{-3}$
$\mathfrak{e}_5\mathfrak{k}_2$	$-1{,}539 \cdot 10^{-3}$	$-1{,}539$	$2{,}748$	$-1{,}527 \cdot 10^{-3}$	$-1{,}527$	$2{,}463$
$\mathfrak{e}_5\mathfrak{k}_3$	$5{,}342 \cdot 10^{-4}$	$1{,}113$	$-3{,}726 \cdot 10^{-1}$	$5{,}371 \cdot 10^{-4}$	$1{,}119$	$-3{,}774 \cdot 10^{-1}$
$\mathfrak{e}_5\mathfrak{k}_4$	$1{,}007 \cdot 10^{-3}$	$1{,}007$	$-1{,}457 \cdot 10^{-1}$	$9{,}912 \cdot 10^{-4}$	$9{,}912 \cdot 10^{-1}$	$-1{,}418 \cdot 10^{-1}$
$\mathfrak{e}_6\mathfrak{k}_1$	$-5{,}224 \cdot 10^{-7}$	$-7{,}255 \cdot 10^{-4}$	$5{,}566 \cdot 10^{-4}$	$-5{,}504 \cdot 10^{-7}$	$-7{,}644 \cdot 10^{-4}$	$5{,}866 \cdot 10^{-4}$
$\mathfrak{e}_6\mathfrak{k}_2$	$-1{,}539 \cdot 10^{-3}$	$-1{,}539$	$4{,}103$	$-1{,}526 \cdot 10^{-3}$	$-1{,}526$	$3{,}677$
$\mathfrak{e}_6\mathfrak{k}_3$	$1{,}315 \cdot 10^{-8}$	$1{,}827 \cdot 10^{-5}$	$-1{,}397 \cdot 10^{-5}$	$3{,}416 \cdot 10^{-8}$	$4{,}745 \cdot 10^{-5}$	$-3{,}630 \cdot 10^{-5}$
$\mathfrak{e}_6\mathfrak{k}_4$	$1{,}539 \cdot 10^{-3}$	$1{,}539$	$-4{,}121$	$1{,}527 \cdot 10^{-3}$	$1{,}527$	$-3{,}694$
$\mathfrak{e}_7\mathfrak{k}_1$	$7{,}287 \cdot 10^{-7}$	$1{,}518 \cdot 10^{-3}$	$-1{,}168 \cdot 10^{-3}$	$5{,}921 \cdot 10^{-7}$	$1{,}234 \cdot 10^{-3}$	$-9{,}483 \cdot 10^{-4}$
$\mathfrak{e}_7\mathfrak{k}_2$	$-1{,}029 \cdot 10^{-3}$	$-1{,}029$	$1{,}515 \cdot 10^{-1}$	$-1{,}034 \cdot 10^{-3}$	$-1{,}034$	$1{,}530 \cdot 10^{-1}$
$\mathfrak{e}_7\mathfrak{k}_3$	$-5{,}109 \cdot 10^{-4}$	$-1{,}064$	$3{,}375 \cdot 10^{-1}$	$-4{,}929 \cdot 10^{-4}$	$-1{,}027$	$3{,}147 \cdot 10^{-1}$
$\mathfrak{e}_7\mathfrak{k}_4$	$1{,}539 \cdot 10^{-3}$	$1{,}539$	$-2{,}736$	$1{,}526 \cdot 10^{-3}$	$1{,}526$	$-2{,}451$
$\mathfrak{e}_8\mathfrak{k}_1$	$2{,}399 \cdot 10^{-7}$	$3{,}332 \cdot 10^{-4}$	$-2{,}552 \cdot 10^{-4}$	$1{,}285 \cdot 10^{-7}$	$1{,}784 \cdot 10^{-4}$	$-1{,}366 \cdot 10^{-4}$
$\mathfrak{e}_8\mathfrak{k}_2$	$-5{,}627 \cdot 10^{-4}$	$-5{,}627 \cdot 10^{-1}$	$1{,}189 \cdot 10^{-1}$	$-5{,}901 \cdot 10^{-4}$	$-5{,}901 \cdot 10^{-1}$	$1{,}228 \cdot 10^{-1}$
$\mathfrak{e}_8\mathfrak{k}_3$	$-4{,}663 \cdot 10^{-4}$	$-6{,}476 \cdot 10^{-1}$	$1{,}825 \cdot 10^{-1}$	$-4{,}441 \cdot 10^{-4}$	$-6{,}169 \cdot 10^{-1}$	$1{,}760 \cdot 10^{-1}$
$\mathfrak{e}_8\mathfrak{k}_4$	$1{,}029 \cdot 10^{-3}$	$1{,}029$	$-2{,}273 \cdot 10^{-1}$	$1{,}034 \cdot 10^{-3}$	$1{,}034$	$-2{,}295 \cdot 10^{-1}$
$\mathfrak{e}_9\mathfrak{k}_1$	$-6{,}206 \cdot 10^{-8}$	$-1{,}293 \cdot 10^{-4}$	$9{,}897 \cdot 10^{-5}$	$-1{,}171 \cdot 10^{-7}$	$-2{,}440 \cdot 10^{-4}$	$1{,}869 \cdot 10^{-4}$
$\mathfrak{e}_9\mathfrak{k}_2$	$-3{,}099 \cdot 10^{-4}$	$-3{,}099 \cdot 10^{-1}$	$5{,}845 \cdot 10^{-2}$	$-3{,}519 \cdot 10^{-4}$	$-3{,}519 \cdot 10^{-1}$	$6{,}196 \cdot 10^{-2}$
$\mathfrak{e}_9\mathfrak{k}_3$	$-2{,}527 \cdot 10^{-4}$	$-5{,}265 \cdot 10^{-1}$	$1{,}582 \cdot 10^{-1}$	$-2{,}380 \cdot 10^{-4}$	$-4{,}959 \cdot 10^{-1}$	$1{,}525 \cdot 10^{-1}$
$\mathfrak{e}_9\mathfrak{k}_4$	$5{,}627 \cdot 10^{-4}$	$5{,}627 \cdot 10^{-1}$	$-7{,}925 \cdot 10^{-2}$	$5{,}901 \cdot 10^{-4}$	$5{,}901 \cdot 10^{-1}$	$-8{,}184 \cdot 10^{-2}$
$\mathfrak{e}_{10}\mathfrak{k}_1$	$-3{,}007 \cdot 10^{-7}$	$-4{,}177 \cdot 10^{-4}$	$3{,}201 \cdot 10^{-4}$	$-3{,}806 \cdot 10^{-7}$	$-5{,}286 \cdot 10^{-4}$	$4{,}053 \cdot 10^{-4}$
$\mathfrak{e}_{10}\mathfrak{k}_2$	$-1{,}449 \cdot 10^{-4}$	$-1{,}449 \cdot 10^{-1}$	$6{,}774 \cdot 10^{-2}$	$-1{,}807 \cdot 10^{-4}$	$-1{,}807 \cdot 10^{-1}$	$7{,}192 \cdot 10^{-2}$
$\mathfrak{e}_{10}\mathfrak{k}_3$	$-1{,}648 \cdot 10^{-4}$	$-2{,}288 \cdot 10^{-1}$	$1{,}054 \cdot 10^{-1}$	$-1{,}708 \cdot 10^{-4}$	$-2{,}373 \cdot 10^{-1}$	$1{,}068 \cdot 10^{-1}$
$\mathfrak{e}_{10}\mathfrak{k}_4$	$3{,}099 \cdot 10^{-4}$	$3{,}099 \cdot 10^{-1}$	$-8{,}767 \cdot 10^{-2}$	$3{,}519 \cdot 10^{-4}$	$3{,}519 \cdot 10^{-1}$	$-9{,}294 \cdot 10^{-2}$
$\mathfrak{e}_{11}\mathfrak{k}_1$	$-1{,}044 \cdot 10^{-6}$	$-1{,}243 \cdot 10^{-3}$	$9{,}554 \cdot 10^{-4}$	$-1{,}193 \cdot 10^{-6}$	$-1{,}421 \cdot 10^{-3}$	$1{,}093 \cdot 10^{-3}$
$\mathfrak{e}_{11}\mathfrak{k}_2$	$-2{,}137 \cdot 10^{-6}$	$-2{,}137 \cdot 10^{-3}$	$1{,}385 \cdot 10^{-3}$	$-2{,}402 \cdot 10^{-6}$	$-2{,}402 \cdot 10^{-3}$	$1{,}558 \cdot 10^{-3}$
$\mathfrak{e}_{11}\mathfrak{k}_3$	$-1{,}417 \cdot 10^{-4}$	$-1{,}687 \cdot 10^{-1}$	$9{,}848 \cdot 10^{-2}$	$-1{,}771 \cdot 10^{-4}$	$-2{,}108 \cdot 10^{-1}$	$1{,}029 \cdot 10^{-1}$
$\mathfrak{e}_{11}\mathfrak{k}_4$	$1{,}449 \cdot 10^{-4}$	$1{,}449 \cdot 10^{-1}$	$-7{,}903 \cdot 10^{-2}$	$1{,}807 \cdot 10^{-4}$	$1{,}807 \cdot 10^{-1}$	$-8{,}391 \cdot 10^{-2}$
$\mathfrak{e}_{12}\mathfrak{k}_1$	$-1{,}006 \cdot 10^{-4}$	$-1{,}197 \cdot 10^{-1}$	$1{,}375 \cdot 10^{-1}$	$-7{,}960 \cdot 10^{-5}$	$-9{,}476 \cdot 10^{-2}$	$1{,}177 \cdot 10^{-1}$
$\mathfrak{e}_{12}\mathfrak{k}_2$	$-9{,}131 \cdot 10^{-5}$	$-5{,}707 \cdot 10^{-2}$	$3{,}969 \cdot 10^{-2}$	$-3{,}383 \cdot 10^{-5}$	$-2{,}114 \cdot 10^{-2}$	$1{,}444 \cdot 10^{-2}$
$\mathfrak{e}_{12}\mathfrak{k}_3$	$1{,}943 \cdot 10^{-4}$	$2{,}313 \cdot 10^{-1}$	$-1{,}693 \cdot 10^{-1}$	$1{,}161 \cdot 10^{-4}$	$1{,}382 \cdot 10^{-1}$	$-1{,}477 \cdot 10^{-1}$
$\mathfrak{e}_{12}\mathfrak{k}_4$	$-2{,}380 \cdot 10^{-6}$	$-1{,}488 \cdot 10^{-3}$	$9{,}616 \cdot 10^{-4}$	$-2{,}655 \cdot 10^{-6}$	$-1{,}659 \cdot 10^{-3}$	$1{,}073 \cdot 10^{-3}$
$\mathfrak{e}_{13}\mathfrak{k}_1$	$-1{,}478 \cdot 10^{-4}$	$-2{,}053 \cdot 10^{-1}$	$1{,}637 \cdot 10^{-1}$	$-1{,}300 \cdot 10^{-4}$	$-1{,}806 \cdot 10^{-1}$	$1{,}598 \cdot 10^{-1}$
$\mathfrak{e}_{13}\mathfrak{k}_2$	$5{,}608 \cdot 10^{-5}$	$3{,}505 \cdot 10^{-2}$	$-2{,}089 \cdot 10^{-2}$	$9{,}573 \cdot 10^{-5}$	$5{,}983 \cdot 10^{-2}$	$-3{,}559 \cdot 10^{-2}$
$\mathfrak{e}_{13}\mathfrak{k}_3$	$4{,}619 \cdot 10^{-7}$	$6{,}415 \cdot 10^{-4}$	$-7{,}872 \cdot 10^{-4}$	$4{,}418 \cdot 10^{-7}$	$6{,}136 \cdot 10^{-4}$	$-7{,}529 \cdot 10^{-4}$
$\mathfrak{e}_{13}\mathfrak{k}_4$	$9{,}131 \cdot 10^{-5}$	$5{,}707 \cdot 10^{-2}$	$-3{,}402 \cdot 10^{-2}$	$3{,}383 \cdot 10^{-5}$	$2{,}114 \cdot 10^{-2}$	$-1{,}238 \cdot 10^{-2}$

Table A.1: Flux tube element outputs ... *cont*

Element Region	$I_{(\mathrm{ph})} = \begin{bmatrix} 20 & -10 & -10 \end{bmatrix}^{\mathrm{T}}$					
	$x = 0\,\mathrm{mm}$			$x = 1\,\mathrm{mm}$		
	Φ [Wb]	B [T]	$\mathcal{F}$ [A]	Φ [Wb]	B [T]	$\mathcal{F}$ [A]
$\mathfrak{e}_{14}\mathfrak{k}_1$	$-2{,}710 \cdot 10^{-4}$	$-5{,}647 \cdot 10^{-1}$	$2{,}648 \cdot 10^{-1}$	$-2{,}817 \cdot 10^{-4}$	$-5{,}869 \cdot 10^{-1}$	$2{,}718 \cdot 10^{-1}$
$\mathfrak{e}_{14}\mathfrak{k}_2$	$-2{,}878 \cdot 10^{-4}$	$-1{,}799 \cdot 10^{-1}$	$4{,}790 \cdot 10^{-2}$	$-2{,}370 \cdot 10^{-4}$	$-1{,}481 \cdot 10^{-1}$	$4{,}552 \cdot 10^{-2}$
$\mathfrak{e}_{14}\mathfrak{k}_3$	$6{,}149 \cdot 10^{-4}$	$1{,}281$	$-1{,}013$	$6{,}144 \cdot 10^{-4}$	$1{,}280$	$-1{,}008$
$\mathfrak{e}_{14}\mathfrak{k}_4$	$-5{,}608 \cdot 10^{-5}$	$-3{,}505 \cdot 10^{-2}$	$1{,}393 \cdot 10^{-2}$	$-9{,}573 \cdot 10^{-5}$	$-5{,}983 \cdot 10^{-2}$	$2{,}373 \cdot 10^{-2}$
$\mathfrak{e}_{15}\mathfrak{k}_1$	$-4{,}944 \cdot 10^{-4}$	$-6{,}866 \cdot 10^{-1}$	$3{,}061 \cdot 10^{-1}$	$-5{,}072 \cdot 10^{-4}$	$-7{,}044 \cdot 10^{-1}$	$3{,}129 \cdot 10^{-1}$
$\mathfrak{e}_{15}\mathfrak{k}_2$	$2{,}058 \cdot 10^{-4}$	$1{,}287 \cdot 10^{-1}$	$-6{,}429 \cdot 10^{-2}$	$2{,}689 \cdot 10^{-4}$	$1{,}681 \cdot 10^{-1}$	$-7{,}085 \cdot 10^{-2}$
$\mathfrak{e}_{15}\mathfrak{k}_3$	$7{,}228 \cdot 10^{-7}$	$1{,}004 \cdot 10^{-3}$	$-1{,}234 \cdot 10^{-3}$	$1{,}336 \cdot 10^{-6}$	$1{,}855 \cdot 10^{-3}$	$-2{,}288 \cdot 10^{-3}$
$\mathfrak{e}_{15}\mathfrak{k}_4$	$2{,}878 \cdot 10^{-4}$	$1{,}799 \cdot 10^{-1}$	$-7{,}186 \cdot 10^{-2}$	$2{,}370 \cdot 10^{-4}$	$1{,}481 \cdot 10^{-1}$	$-6{,}828 \cdot 10^{-2}$
$\mathfrak{e}_{16}\mathfrak{k}_1$	$-5{,}342 \cdot 10^{-4}$	$-1{,}113$	$5{,}961 \cdot 10^{-1}$	$-5{,}371 \cdot 10^{-4}$	$-1{,}119$	$6{,}038 \cdot 10^{-1}$
$\mathfrak{e}_{16}\mathfrak{k}_2$	$7{,}842 \cdot 10^{-5}$	$4{,}901 \cdot 10^{-2}$	$-1{,}955 \cdot 10^{-2}$	$7{,}857 \cdot 10^{-5}$	$4{,}911 \cdot 10^{-2}$	$-1{,}959 \cdot 10^{-2}$
$\mathfrak{e}_{16}\mathfrak{k}_3$	$6{,}617 \cdot 10^{-4}$	$1{,}378$	$-1{,}908$	$7{,}274 \cdot 10^{-4}$	$1{,}515$	$-7{,}392$
$\mathfrak{e}_{16}\mathfrak{k}_4$	$-2{,}058 \cdot 10^{-4}$	$-1{,}287 \cdot 10^{-1}$	$4{,}286 \cdot 10^{-2}$	$-2{,}689 \cdot 10^{-4}$	$-1{,}681 \cdot 10^{-1}$	$4{,}723 \cdot 10^{-2}$
$\mathfrak{e}_{17}\mathfrak{k}_1$	$5{,}109 \cdot 10^{-4}$	$1{,}064$	$-5{,}400 \cdot 10^{-1}$	$4{,}929 \cdot 10^{-4}$	$1{,}027$	$-5{,}035 \cdot 10^{-1}$
$\mathfrak{e}_{17}\mathfrak{k}_2$	$3{,}934 \cdot 10^{-5}$	$2{,}459 \cdot 10^{-2}$	$-9{,}655 \cdot 10^{-3}$	$-3{,}586 \cdot 10^{-5}$	$-2{,}241 \cdot 10^{-2}$	$8{,}768 \cdot 10^{-3}$
$\mathfrak{e}_{17}\mathfrak{k}_3$	$-4{,}720 \cdot 10^{-4}$	$-9{,}833 \cdot 10^{-1}$	$4{,}664 \cdot 10^{-1}$	$-3{,}793 \cdot 10^{-4}$	$-7{,}902 \cdot 10^{-1}$	$3{,}498 \cdot 10^{-1}$
$\mathfrak{e}_{17}\mathfrak{k}_4$	$-7{,}826 \cdot 10^{-5}$	$-4{,}891 \cdot 10^{-2}$	$1{,}951 \cdot 10^{-2}$	$-7{,}778 \cdot 10^{-5}$	$-4{,}862 \cdot 10^{-2}$	$1{,}939 \cdot 10^{-2}$
$\mathfrak{e}_{18}\mathfrak{k}_1$	$4{,}663 \cdot 10^{-4}$	$6{,}476 \cdot 10^{-1}$	$-2{,}920 \cdot 10^{-1}$	$4{,}441 \cdot 10^{-4}$	$6{,}169 \cdot 10^{-1}$	$-2{,}815 \cdot 10^{-1}$
$\mathfrak{e}_{18}\mathfrak{k}_2$	$-4{,}263 \cdot 10^{-4}$	$-2{,}664 \cdot 10^{-1}$	$8{,}096 \cdot 10^{-2}$	$-4{,}794 \cdot 10^{-4}$	$-2{,}996 \cdot 10^{-1}$	$8{,}617 \cdot 10^{-2}$
$\mathfrak{e}_{18}\mathfrak{k}_3$	$-6{,}331 \cdot 10^{-7}$	$-8{,}793 \cdot 10^{-4}$	$1{,}080 \cdot 10^{-3}$	$-5{,}804 \cdot 10^{-7}$	$-8{,}061 \cdot 10^{-4}$	$9{,}899 \cdot 10^{-4}$
$\mathfrak{e}_{18}\mathfrak{k}_4$	$-3{,}934 \cdot 10^{-5}$	$-2{,}459 \cdot 10^{-2}$	$1{,}448 \cdot 10^{-2}$	$3{,}586 \cdot 10^{-5}$	$2{,}241 \cdot 10^{-2}$	$-1{,}315 \cdot 10^{-2}$
$\mathfrak{e}_{19}\mathfrak{k}_1$	$2{,}527 \cdot 10^{-4}$	$5{,}265 \cdot 10^{-1}$	$-2{,}531 \cdot 10^{-1}$	$2{,}380 \cdot 10^{-4}$	$4{,}959 \cdot 10^{-1}$	$-2{,}440 \cdot 10^{-1}$
$\mathfrak{e}_{19}\mathfrak{k}_2$	$-1{,}502 \cdot 10^{-5}$	$-9{,}389 \cdot 10^{-3}$	$3{,}563 \cdot 10^{-3}$	$-5{,}793 \cdot 10^{-5}$	$-3{,}620 \cdot 10^{-2}$	$1{,}440 \cdot 10^{-2}$
$\mathfrak{e}_{19}\mathfrak{k}_3$	$-6{,}640 \cdot 10^{-4}$	$-1{,}383$	$1{,}993$	$-6{,}595 \cdot 10^{-4}$	$-1{,}374$	$1{,}834$
$\mathfrak{e}_{19}\mathfrak{k}_4$	$4{,}263 \cdot 10^{-4}$	$2{,}664 \cdot 10^{-1}$	$-5{,}397 \cdot 10^{-2}$	$4{,}794 \cdot 10^{-4}$	$2{,}996 \cdot 10^{-1}$	$-5{,}744 \cdot 10^{-2}$
$\mathfrak{e}_{20}\mathfrak{k}_1$	$1{,}648 \cdot 10^{-4}$	$2{,}288 \cdot 10^{-1}$	$-1{,}686 \cdot 10^{-1}$	$1{,}708 \cdot 10^{-4}$	$2{,}373 \cdot 10^{-1}$	$-1{,}708 \cdot 10^{-1}$
$\mathfrak{e}_{20}\mathfrak{k}_2$	$-1{,}792 \cdot 10^{-4}$	$-1{,}120 \cdot 10^{-1}$	$5{,}943 \cdot 10^{-2}$	$-2{,}281 \cdot 10^{-4}$	$-1{,}426 \cdot 10^{-1}$	$6{,}732 \cdot 10^{-2}$
$\mathfrak{e}_{20}\mathfrak{k}_3$	$-6{,}050 \cdot 10^{-7}$	$-8{,}403 \cdot 10^{-4}$	$1{,}032 \cdot 10^{-3}$	$-5{,}975 \cdot 10^{-7}$	$-8{,}298 \cdot 10^{-4}$	$1{,}019 \cdot 10^{-3}$
$\mathfrak{e}_{20}\mathfrak{k}_4$	$1{,}502 \cdot 10^{-5}$	$9{,}389 \cdot 10^{-3}$	$-5{,}344 \cdot 10^{-3}$	$5{,}793 \cdot 10^{-5}$	$3{,}620 \cdot 10^{-2}$	$-2{,}160 \cdot 10^{-2}$
$\mathfrak{e}_{21}\mathfrak{k}_1$	$1{,}417 \cdot 10^{-4}$	$1{,}687 \cdot 10^{-1}$	$-1{,}576 \cdot 10^{-1}$	$1{,}771 \cdot 10^{-4}$	$2{,}108 \cdot 10^{-1}$	$-1{,}647 \cdot 10^{-1}$
$\mathfrak{e}_{21}\mathfrak{k}_2$	$-4{,}057 \cdot 10^{-6}$	$-2{,}535 \cdot 10^{-3}$	$1{,}645 \cdot 10^{-3}$	$-4{,}710 \cdot 10^{-6}$	$-2{,}944 \cdot 10^{-3}$	$1{,}913 \cdot 10^{-3}$
$\mathfrak{e}_{21}\mathfrak{k}_3$	$-3{,}168 \cdot 10^{-4}$	$-3{,}772 \cdot 10^{-1}$	$2{,}126 \cdot 10^{-1}$	$-4{,}005 \cdot 10^{-4}$	$-4{,}768 \cdot 10^{-1}$	$2{,}384 \cdot 10^{-1}$
$\mathfrak{e}_{21}\mathfrak{k}_4$	$1{,}792 \cdot 10^{-4}$	$1{,}120 \cdot 10^{-1}$	$-6{,}934 \cdot 10^{-2}$	$2{,}281 \cdot 10^{-4}$	$1{,}426 \cdot 10^{-1}$	$-7{,}854 \cdot 10^{-2}$
$\mathfrak{e}_{22}\mathfrak{k}_1$	$-1{,}943 \cdot 10^{-4}$	$-2{,}313 \cdot 10^{-1}$	$1{,}693 \cdot 10^{-1}$	$-1{,}161 \cdot 10^{-4}$	$-1{,}382 \cdot 10^{-1}$	$1{,}477 \cdot 10^{-1}$
$\mathfrak{e}_{22}\mathfrak{k}_2$	$8{,}335 \cdot 10^{-6}$	$5{,}209 \cdot 10^{-3}$	$-3{,}413 \cdot 10^{-3}$	$-2{,}207 \cdot 10^{-7}$	$-1{,}379 \cdot 10^{-4}$	$8{,}868 \cdot 10^{-5}$
$\mathfrak{e}_{22}\mathfrak{k}_3$	$1{,}830 \cdot 10^{-4}$	$2{,}179 \cdot 10^{-1}$	$-1{,}661 \cdot 10^{-1}$	$1{,}173 \cdot 10^{-4}$	$1{,}396 \cdot 10^{-1}$	$-1{,}483 \cdot 10^{-1}$
$\mathfrak{e}_{22}\mathfrak{k}_4$	$2{,}913 \cdot 10^{-6}$	$1{,}820 \cdot 10^{-3}$	$-1{,}178 \cdot 10^{-3}$	$-9{,}958 \cdot 10^{-7}$	$-6{,}224 \cdot 10^{-4}$	$4{,}009 \cdot 10^{-4}$
$\mathfrak{e}_{23}\mathfrak{k}_1$	$-6{,}149 \cdot 10^{-4}$	$-1{,}281$	$1{,}013$	$-6{,}144 \cdot 10^{-4}$	$-1{,}280$	$1{,}008$
$\mathfrak{e}_{23}\mathfrak{k}_2$	$7{,}549 \cdot 10^{-5}$	$4{,}718 \cdot 10^{-2}$	$-1{,}883 \cdot 10^{-2}$	$7{,}959 \cdot 10^{-5}$	$4{,}974 \cdot 10^{-2}$	$-1{,}984 \cdot 10^{-2}$
$\mathfrak{e}_{23}\mathfrak{k}_3$	$3{,}434 \cdot 10^{-4}$	$7{,}155 \cdot 10^{-1}$	$-3{,}173 \cdot 10^{-1}$	$3{,}418 \cdot 10^{-4}$	$7{,}121 \cdot 10^{-1}$	$-3{,}159 \cdot 10^{-1}$
$\mathfrak{e}_{23}\mathfrak{k}_4$	$1{,}960 \cdot 10^{-4}$	$1{,}225 \cdot 10^{-1}$	$-4{,}177 \cdot 10^{-2}$	$1{,}930 \cdot 10^{-4}$	$1{,}206 \cdot 10^{-1}$	$-4{,}142 \cdot 10^{-2}$
$\mathfrak{e}_{24}\mathfrak{k}_1$	$-6{,}617 \cdot 10^{-4}$	$-1{,}378$	$1{,}908$	$-7{,}274 \cdot 10^{-4}$	$-1{,}515$	$7{,}392$
$\mathfrak{e}_{24}\mathfrak{k}_2$	$2{,}345 \cdot 10^{-4}$	$1{,}465 \cdot 10^{-1}$	$-4{,}535 \cdot 10^{-2}$	$2{,}503 \cdot 10^{-4}$	$1{,}564 \cdot 10^{-1}$	$-4{,}634 \cdot 10^{-2}$
$\mathfrak{e}_{24}\mathfrak{k}_3$	$2{,}656 \cdot 10^{-4}$	$5{,}532 \cdot 10^{-1}$	$-2{,}612 \cdot 10^{-1}$	$3{,}140 \cdot 10^{-4}$	$6{,}541 \cdot 10^{-1}$	$-2{,}943 \cdot 10^{-1}$
$\mathfrak{e}_{24}\mathfrak{k}_4$	$1{,}616 \cdot 10^{-4}$	$1{,}010 \cdot 10^{-1}$	$-3{,}699 \cdot 10^{-2}$	$1{,}631 \cdot 10^{-4}$	$1{,}019 \cdot 10^{-1}$	$-3{,}722 \cdot 10^{-2}$
$\mathfrak{e}_{25}\mathfrak{k}_1$	$4{,}720 \cdot 10^{-4}$	$9{,}833 \cdot 10^{-1}$	$-4{,}664 \cdot 10^{-1}$	$3{,}793 \cdot 10^{-4}$	$7{,}902 \cdot 10^{-1}$	$-3{,}498 \cdot 10^{-1}$
$\mathfrak{e}_{25}\mathfrak{k}_2$	$-6{,}140 \cdot 10^{-5}$	$-3{,}838 \cdot 10^{-2}$	$1{,}528 \cdot 10^{-2}$	$-5{,}130 \cdot 10^{-5}$	$-3{,}206 \cdot 10^{-2}$	$1{,}271 \cdot 10^{-2}$
$\mathfrak{e}_{25}\mathfrak{k}_3$	$-1{,}971 \cdot 10^{-4}$	$-4{,}106 \cdot 10^{-1}$	$2{,}206 \cdot 10^{-1}$	$-1{,}359 \cdot 10^{-4}$	$-2{,}831 \cdot 10^{-1}$	$1{,}857 \cdot 10^{-1}$
$\mathfrak{e}_{25}\mathfrak{k}_4$	$-2{,}135 \cdot 10^{-4}$	$-1{,}334 \cdot 10^{-1}$	$4{,}362 \cdot 10^{-2}$	$-1{,}921 \cdot 10^{-4}$	$-1{,}201 \cdot 10^{-1}$	$4{,}131 \cdot 10^{-2}$
$\mathfrak{e}_{26}\mathfrak{k}_1$	$6{,}640 \cdot 10^{-4}$	$1{,}383$	$-1{,}993$	$6{,}595 \cdot 10^{-4}$	$1{,}374$	$-1{,}834$
$\mathfrak{e}_{26}\mathfrak{k}_2$	$-1{,}568 \cdot 10^{-4}$	$-9{,}800 \cdot 10^{-2}$	$3{,}619 \cdot 10^{-2}$	$-1{,}581 \cdot 10^{-4}$	$-9{,}882 \cdot 10^{-2}$	$3{,}641 \cdot 10^{-2}$
$\mathfrak{e}_{26}\mathfrak{k}_3$	$-3{,}502 \cdot 10^{-4}$	$-7{,}296 \cdot 10^{-1}$	$3{,}231 \cdot 10^{-1}$	$-3{,}484 \cdot 10^{-4}$	$-7{,}258 \cdot 10^{-1}$	$3{,}215 \cdot 10^{-1}$
$\mathfrak{e}_{26}\mathfrak{k}_4$	$-1{,}570 \cdot 10^{-4}$	$-9{,}811 \cdot 10^{-2}$	$3{,}622 \cdot 10^{-2}$	$-1{,}530 \cdot 10^{-4}$	$-9{,}564 \cdot 10^{-2}$	$3{,}554 \cdot 10^{-2}$
$\mathfrak{e}_{27}\mathfrak{k}_1$	$3{,}168 \cdot 10^{-4}$	$3{,}772 \cdot 10^{-1}$	$-2{,}126 \cdot 10^{-1}$	$4{,}005 \cdot 10^{-4}$	$4{,}768 \cdot 10^{-1}$	$-2{,}384 \cdot 10^{-1}$
$\mathfrak{e}_{27}\mathfrak{k}_2$	$-2{,}228 \cdot 10^{-5}$	$-1{,}392 \cdot 10^{-2}$	$9{,}361 \cdot 10^{-3}$	$-2{,}963 \cdot 10^{-5}$	$-1{,}852 \cdot 10^{-2}$	$1{,}258 \cdot 10^{-2}$
$\mathfrak{e}_{27}\mathfrak{k}_3$	$-2{,}339 \cdot 10^{-4}$	$-2{,}785 \cdot 10^{-1}$	$1{,}841 \cdot 10^{-1}$	$-3{,}064 \cdot 10^{-4}$	$-3{,}647 \cdot 10^{-1}$	$2{,}097 \cdot 10^{-1}$
$\mathfrak{e}_{27}\mathfrak{k}_4$	$-6{,}063 \cdot 10^{-5}$	$-3{,}790 \cdot 10^{-2}$	$2{,}641 \cdot 10^{-2}$	$-6{,}454 \cdot 10^{-5}$	$-4{,}034 \cdot 10^{-2}$	$2{,}814 \cdot 10^{-2}$

Table A.1: Flux tube element outputs ... *cont*

Element Region	$I_{(\mathrm{ph})} = \begin{bmatrix} 20 & -10 & -10 \end{bmatrix}^{\mathrm{T}}$					
	$x = 0\,\mathrm{mm}$			$x = 1\,\mathrm{mm}$		
	Φ [Wb]	B [T]	$\mathcal{F}$ [A]	Φ [Wb]	B [T]	$\mathcal{F}$ [A]
$\mathfrak{e}_{28}\mathfrak{k}_1$	$-1{,}431 \cdot 10^{-3}$	$-5{,}504 \cdot 10^{-1}$	$4{,}850 \cdot 10^{-1}$	$-1{,}450 \cdot 10^{-3}$	$-5{,}576 \cdot 10^{-1}$	$4{,}920 \cdot 10^{-1}$
$\mathfrak{e}_{28}\mathfrak{k}_2$	$1{,}342 \cdot 10^{-3}$	$1{,}491$	$-8{,}652$	$1{,}359 \cdot 10^{-3}$	$1{,}510$	$-9{,}785$
$\mathfrak{e}_{28}\mathfrak{k}_3$	$1{,}719 \cdot 10^{-5}$	$6{,}612 \cdot 10^{-3}$	$-5{,}585 \cdot 10^{-3}$	$1{,}723 \cdot 10^{-5}$	$6{,}627 \cdot 10^{-3}$	$-5{,}597 \cdot 10^{-3}$
$\mathfrak{e}_{28}\mathfrak{k}_4$	$7{,}238 \cdot 10^{-5}$	$8{,}042 \cdot 10^{-2}$	$-1{,}956 \cdot 10^{-1}$	$7{,}355 \cdot 10^{-5}$	$8{,}173 \cdot 10^{-2}$	$-1{,}988 \cdot 10^{-1}$
$\mathfrak{e}_{29}\mathfrak{k}_1$	$-3{,}786 \cdot 10^{-5}$	$-3{,}786 \cdot 10^{-2}$	$3{,}192 \cdot 10^{-2}$	$-1{,}827 \cdot 10^{-5}$	$-1{,}827 \cdot 10^{-2}$	$1{,}542 \cdot 10^{-2}$
$\mathfrak{e}_{29}\mathfrak{k}_2$	$1{,}377 \cdot 10^{-3}$	$1{,}530$	$-4{,}406$	$1{,}375 \cdot 10^{-3}$	$1{,}528$	$-4{,}329$
$\mathfrak{e}_{29}\mathfrak{k}_3$	$2{,}421 \cdot 10^{-6}$	$2{,}421 \cdot 10^{-3}$	$-2{,}046 \cdot 10^{-3}$	$2{,}114 \cdot 10^{-6}$	$2{,}114 \cdot 10^{-3}$	$-1{,}786 \cdot 10^{-3}$
$\mathfrak{e}_{29}\mathfrak{k}_4$	$-1{,}342 \cdot 10^{-3}$	$-1{,}491$	$3{,}328$	$-1{,}359 \cdot 10^{-3}$	$-1{,}510$	$3{,}763$
$\mathfrak{e}_{30}\mathfrak{k}_1$	$1{,}419 \cdot 10^{-3}$	$5{,}456 \cdot 10^{-1}$	$-4{,}803 \cdot 10^{-1}$	$1{,}421 \cdot 10^{-3}$	$5{,}465 \cdot 10^{-1}$	$-4{,}811 \cdot 10^{-1}$
$\mathfrak{e}_{30}\mathfrak{k}_2$	$-4{,}242 \cdot 10^{-5}$	$-4{,}714 \cdot 10^{-2}$	$1{,}148 \cdot 10^{-1}$	$-4{,}529 \cdot 10^{-5}$	$-5{,}032 \cdot 10^{-2}$	$1{,}225 \cdot 10^{-1}$
$\mathfrak{e}_{30}\mathfrak{k}_3$	$8{,}219 \cdot 10^{-7}$	$3{,}161 \cdot 10^{-4}$	$-2{,}672 \cdot 10^{-4}$	$-3{,}415 \cdot 10^{-7}$	$-1{,}313 \cdot 10^{-4}$	$1{,}110 \cdot 10^{-4}$
$\mathfrak{e}_{30}\mathfrak{k}_4$	$-1{,}377 \cdot 10^{-3}$	$-1{,}530$	$1{,}146 \cdot 10^{1}$	$-1{,}375 \cdot 10^{-3}$	$-1{,}528$	$1{,}126 \cdot 10^{1}$

Table A.1: Flux tube element outputs ... *cont*

Element Region	$I_{(\mathrm{ph})} = \begin{bmatrix} 20 & -10 & -10 \end{bmatrix}^{\mathrm{T}}$					
	$x = 2\,\mathrm{mm}$			$x = 3\,\mathrm{mm}$		
	Φ [Wb]	B [T]	$\mathcal{F}$ [A]	Φ [Wb]	B [T]	$\mathcal{F}$ [A]
$\mathfrak{e}_{1}\mathfrak{k}_1$	$-1{,}914 \cdot 10^{-6}$	$-2{,}278 \cdot 10^{-3}$	$1{,}759 \cdot 10^{-3}$	$-1{,}954 \cdot 10^{-6}$	$-2{,}326 \cdot 10^{-3}$	$1{,}795 \cdot 10^{-3}$
$\mathfrak{e}_{1}\mathfrak{k}_2$	$-5{,}914 \cdot 10^{-5}$	$-5{,}914 \cdot 10^{-2}$	$4{,}107 \cdot 10^{-2}$	$-4{,}497 \cdot 10^{-5}$	$-4{,}497 \cdot 10^{-2}$	$3{,}140 \cdot 10^{-2}$
$\mathfrak{e}_{1}\mathfrak{k}_3$	$6{,}338 \cdot 10^{-5}$	$7{,}545 \cdot 10^{-2}$	$-6{,}108 \cdot 10^{-3}$	$4{,}938 \cdot 10^{-5}$	$5{,}879 \cdot 10^{-2}$	$-4{,}861 \cdot 10^{-2}$
$\mathfrak{e}_{1}\mathfrak{k}_4$	$-2{,}327 \cdot 10^{-6}$	$-2{,}327 \cdot 10^{-3}$	$1{,}509 \cdot 10^{-3}$	$-2{,}458 \cdot 10^{-6}$	$-2{,}458 \cdot 10^{-3}$	$1{,}595 \cdot 10^{-3}$
$\mathfrak{e}_{2}\mathfrak{k}_1$	$-1{,}059 \cdot 10^{-6}$	$-1{,}471 \cdot 10^{-3}$	$1{,}132 \cdot 10^{-3}$	$-1{,}044 \cdot 10^{-6}$	$-1{,}450 \cdot 10^{-3}$	$1{,}116 \cdot 10^{-3}$
$\mathfrak{e}_{2}\mathfrak{k}_2$	$-1{,}674 \cdot 10^{-4}$	$-1{,}674 \cdot 10^{-1}$	$7{,}078 \cdot 10^{-2}$	$-1{,}374 \cdot 10^{-4}$	$-1{,}374 \cdot 10^{-1}$	$6{,}629 \cdot 10^{-2}$
$\mathfrak{e}_{2}\mathfrak{k}_3$	$1{,}093 \cdot 10^{-4}$	$1{,}519 \cdot 10^{-1}$	$-9{,}566 \cdot 10^{-2}$	$9{,}345 \cdot 10^{-5}$	$1{,}298 \cdot 10^{-1}$	$-8{,}968 \cdot 10^{-2}$
$\mathfrak{e}_{2}\mathfrak{k}_4$	$5{,}914 \cdot 10^{-5}$	$5{,}914 \cdot 10^{-2}$	$-3{,}520 \cdot 10^{-2}$	$4{,}497 \cdot 10^{-5}$	$4{,}497 \cdot 10^{-2}$	$-2{,}692 \cdot 10^{-2}$
$\mathfrak{e}_{3}\mathfrak{k}_1$	$-6{,}834 \cdot 10^{-7}$	$-1{,}424 \cdot 10^{-3}$	$1{,}095 \cdot 10^{-3}$	$-6{,}506 \cdot 10^{-7}$	$-1{,}355 \cdot 10^{-3}$	$1{,}042 \cdot 10^{-3}$
$\mathfrak{e}_{3}\mathfrak{k}_2$	$-4{,}497 \cdot 10^{-4}$	$-4{,}497 \cdot 10^{-1}$	$6{,}924 \cdot 10^{-2}$	$-4{,}099 \cdot 10^{-4}$	$-4{,}099 \cdot 10^{-1}$	$6{,}613 \cdot 10^{-2}$
$\mathfrak{e}_{3}\mathfrak{k}_3$	$2{,}830 \cdot 10^{-4}$	$5{,}896 \cdot 10^{-1}$	$-1{,}704 \cdot 10^{-1}$	$2{,}732 \cdot 10^{-4}$	$5{,}692 \cdot 10^{-1}$	$-1{,}664 \cdot 10^{-1}$
$\mathfrak{e}_{3}\mathfrak{k}_4$	$1{,}674 \cdot 10^{-4}$	$1{,}674 \cdot 10^{-1}$	$-4{,}719 \cdot 10^{-2}$	$1{,}374 \cdot 10^{-4}$	$1{,}374 \cdot 10^{-1}$	$-4{,}419 \cdot 10^{-2}$
$\mathfrak{e}_{4}\mathfrak{k}_1$	$-1{,}156 \cdot 10^{-6}$	$-1{,}605 \cdot 10^{-3}$	$1{,}236 \cdot 10^{-3}$	$-1{,}028 \cdot 10^{-6}$	$-1{,}428 \cdot 10^{-3}$	$1{,}099 \cdot 10^{-3}$
$\mathfrak{e}_{4}\mathfrak{k}_2$	$-9{,}599 \cdot 10^{-4}$	$-9{,}599 \cdot 10^{-1}$	$2{,}018 \cdot 10^{-1}$	$-9{,}157 \cdot 10^{-4}$	$-9{,}157 \cdot 10^{-1}$	$1{,}880 \cdot 10^{-1}$
$\mathfrak{e}_{4}\mathfrak{k}_3$	$5{,}113 \cdot 10^{-4}$	$7{,}102 \cdot 10^{-1}$	$-1{,}970 \cdot 10^{-1}$	$5{,}068 \cdot 10^{-4}$	$7{,}039 \cdot 10^{-1}$	$-1{,}954 \cdot 10^{-1}$
$\mathfrak{e}_{4}\mathfrak{k}_4$	$4{,}497 \cdot 10^{-4}$	$4{,}497 \cdot 10^{-1}$	$-1{,}039 \cdot 10^{-1}$	$4{,}099 \cdot 10^{-4}$	$4{,}099 \cdot 10^{-1}$	$-9{,}919 \cdot 10^{-2}$
$\mathfrak{e}_{5}\mathfrak{k}_1$	$-1{,}099 \cdot 10^{-6}$	$-2{,}291 \cdot 10^{-3}$	$1{,}768 \cdot 10^{-3}$	$-8{,}635 \cdot 10^{-7}$	$-1{,}799 \cdot 10^{-3}$	$1{,}386 \cdot 10^{-3}$
$\mathfrak{e}_{5}\mathfrak{k}_2$	$-1{,}493 \cdot 10^{-3}$	$-1{,}493$	$1{,}802$	$-1{,}444 \cdot 10^{-3}$	$-1{,}444$	$1{,}095$
$\mathfrak{e}_{5}\mathfrak{k}_3$	$5{,}346 \cdot 10^{-4}$	$1{,}114$	$-3{,}732 \cdot 10^{-1}$	$5{,}289 \cdot 10^{-4}$	$1{,}102$	$-3{,}639 \cdot 10^{-1}$
$\mathfrak{e}_{5}\mathfrak{k}_4$	$9{,}599 \cdot 10^{-4}$	$9{,}599 \cdot 10^{-1}$	$-1{,}345 \cdot 10^{-1}$	$9{,}157 \cdot 10^{-4}$	$9{,}157 \cdot 10^{-1}$	$-1{,}254 \cdot 10^{-1}$
$\mathfrak{e}_{6}\mathfrak{k}_1$	$-5{,}973 \cdot 10^{-7}$	$-8{,}296 \cdot 10^{-4}$	$6{,}368 \cdot 10^{-4}$	$-6{,}761 \cdot 10^{-7}$	$-9{,}391 \cdot 10^{-4}$	$7{,}211 \cdot 10^{-4}$
$\mathfrak{e}_{6}\mathfrak{k}_2$	$-1{,}493 \cdot 10^{-3}$	$-1{,}493$	$2{,}690$	$-1{,}443 \cdot 10^{-3}$	$-1{,}443$	$1{,}632$
$\mathfrak{e}_{6}\mathfrak{k}_3$	$5{,}986 \cdot 10^{-8}$	$8{,}314 \cdot 10^{-5}$	$-6{,}362 \cdot 10^{-5}$	$8{,}116 \cdot 10^{-8}$	$1{,}127 \cdot 10^{-4}$	$-8{,}627 \cdot 10^{-5}$
$\mathfrak{e}_{6}\mathfrak{k}_4$	$1{,}493 \cdot 10^{-3}$	$1{,}493$	$-2{,}704$	$1{,}444 \cdot 10^{-3}$	$1{,}444$	$-1{,}642$
$\mathfrak{e}_{7}\mathfrak{k}_1$	$2{,}881 \cdot 10^{-7}$	$6{,}002 \cdot 10^{-4}$	$-4{,}602 \cdot 10^{-4}$	$-5{,}713 \cdot 10^{-8}$	$-1{,}190 \cdot 10^{-4}$	$9{,}110 \cdot 10^{-5}$
$\mathfrak{e}_{7}\mathfrak{k}_2$	$-1{,}026 \cdot 10^{-3}$	$-1{,}026$	$1{,}507 \cdot 10^{-1}$	$-1{,}004 \cdot 10^{-3}$	$-1{,}004$	$1{,}449 \cdot 10^{-1}$
$\mathfrak{e}_{7}\mathfrak{k}_3$	$-4{,}676 \cdot 10^{-4}$	$-9{,}741 \cdot 10^{-1}$	$2{,}870 \cdot 10^{-1}$	$-4{,}394 \cdot 10^{-4}$	$-9{,}153 \cdot 10^{-1}$	$2{,}610 \cdot 10^{-1}$
$\mathfrak{e}_{7}\mathfrak{k}_4$	$1{,}493 \cdot 10^{-3}$	$1{,}493$	$-1{,}793$	$1{,}443 \cdot 10^{-3}$	$1{,}443$	$-1{,}088$
$\mathfrak{e}_{8}\mathfrak{k}_1$	$-1{,}144 \cdot 10^{-7}$	$-1{,}589 \cdot 10^{-4}$	$1{,}217 \cdot 10^{-4}$	$-4{,}105 \cdot 10^{-7}$	$-5{,}701 \cdot 10^{-4}$	$4{,}371 \cdot 10^{-4}$
$\mathfrak{e}_{8}\mathfrak{k}_2$	$-6{,}079 \cdot 10^{-4}$	$-6{,}079 \cdot 10^{-1}$	$1{,}254 \cdot 10^{-1}$	$-6{,}147 \cdot 10^{-4}$	$-6{,}147 \cdot 10^{-1}$	$1{,}264 \cdot 10^{-1}$
$\mathfrak{e}_{8}\mathfrak{k}_3$	$-4{,}175 \cdot 10^{-4}$	$-5{,}799 \cdot 10^{-1}$	$1{,}685 \cdot 10^{-1}$	$-3{,}886 \cdot 10^{-4}$	$-5{,}397 \cdot 10^{-1}$	$1{,}607 \cdot 10^{-1}$
$\mathfrak{e}_{8}\mathfrak{k}_4$	$1{,}026 \cdot 10^{-3}$	$1{,}026$	$-2{,}260 \cdot 10^{-1}$	$1{,}004 \cdot 10^{-3}$	$1{,}004$	$-2{,}174 \cdot 10^{-1}$

Table A.1: Flux tube element outputs ... *cont*

Element Region	$I_{(\mathrm{ph})} = \begin{bmatrix} 20 & -10 & -10 \end{bmatrix}^{\mathrm{T}}$					
	$x = 2\,\mathrm{mm}$			$x = 3\,\mathrm{mm}$		
	Φ [Wb]	B [T]	$\mathcal{F}$ [A]	Φ [Wb]	B [T]	$\mathcal{F}$ [A]
$\varrho_9\varkappa_1$	$-2{,}371 \cdot 10^{-7}$	$-4{,}940 \cdot 10^{-4}$	$3{,}787 \cdot 10^{-4}$	$-3{,}946 \cdot 10^{-7}$	$-8{,}220 \cdot 10^{-4}$	$6{,}309 \cdot 10^{-4}$
$\varrho_9\varkappa_2$	$-3{,}868 \cdot 10^{-4}$	$-3{,}868 \cdot 10^{-1}$	$6{,}446 \cdot 10^{-2}$	$-4{,}115 \cdot 10^{-4}$	$-4{,}115 \cdot 10^{-1}$	$6{,}624 \cdot 10^{-2}$
$\varrho_9\varkappa_3$	$-2{,}209 \cdot 10^{-4}$	$-4{,}603 \cdot 10^{-1}$	$1{,}461 \cdot 10^{-1}$	$-2{,}029 \cdot 10^{-4}$	$-4{,}226 \cdot 10^{-1}$	$1{,}398 \cdot 10^{-1}$
$\varrho_9\varkappa_4$	$6{,}079 \cdot 10^{-4}$	$6{,}079 \cdot 10^{-1}$	$-8{,}358 \cdot 10^{-2}$	$6{,}147 \cdot 10^{-4}$	$6{,}147 \cdot 10^{-1}$	$-8{,}425 \cdot 10^{-2}$
$\varrho_{10}\varkappa_1$	$-5{,}513 \cdot 10^{-7}$	$-7{,}657 \cdot 10^{-4}$	$5{,}876 \cdot 10^{-4}$	$-7{,}895 \cdot 10^{-7}$	$-1{,}096 \cdot 10^{-3}$	$8{,}425 \cdot 10^{-4}$
$\varrho_{10}\varkappa_2$	$-2{,}064 \cdot 10^{-4}$	$-2{,}064 \cdot 10^{-1}$	$7{,}375 \cdot 10^{-2}$	$-2{,}228 \cdot 10^{-4}$	$-2{,}228 \cdot 10^{-1}$	$7{,}525 \cdot 10^{-2}$
$\varrho_{10}\varkappa_3$	$-1{,}798 \cdot 10^{-4}$	$-2{,}497 \cdot 10^{-1}$	$1{,}090 \cdot 10^{-1}$	$-1{,}879 \cdot 10^{-4}$	$-2{,}609 \cdot 10^{-1}$	$1{,}113 \cdot 10^{-1}$
$\varrho_{10}\varkappa_4$	$3{,}868 \cdot 10^{-4}$	$3{,}868 \cdot 10^{-1}$	$-9{,}669 \cdot 10^{-2}$	$4{,}115 \cdot 10^{-4}$	$4{,}115 \cdot 10^{-1}$	$-9{,}936 \cdot 10^{-2}$
$\varrho_{11}\varkappa_1$	$-1{,}505 \cdot 10^{-6}$	$-1{,}791 \cdot 10^{-3}$	$1{,}380 \cdot 10^{-3}$	$-1{,}978 \cdot 10^{-6}$	$-2{,}355 \cdot 10^{-3}$	$1{,}818 \cdot 10^{-3}$
$\varrho_{11}\varkappa_2$	$-2{,}913 \cdot 10^{-6}$	$-2{,}913 \cdot 10^{-3}$	$1{,}893 \cdot 10^{-3}$	$-3{,}739 \cdot 10^{-6}$	$-3{,}739 \cdot 10^{-3}$	$2{,}437 \cdot 10^{-3}$
$\varrho_{11}\varkappa_3$	$-2{,}020 \cdot 10^{-4}$	$-2{,}405 \cdot 10^{-1}$	$1{,}073 \cdot 10^{-1}$	$-2{,}171 \cdot 10^{-4}$	$-2{,}585 \cdot 10^{-1}$	$1{,}108 \cdot 10^{-1}$
$\varrho_{11}\varkappa_4$	$2{,}064 \cdot 10^{-4}$	$2{,}064 \cdot 10^{-1}$	$-8{,}604 \cdot 10^{-2}$	$2{,}228 \cdot 10^{-4}$	$2{,}228 \cdot 10^{-1}$	$-8{,}779 \cdot 10^{-2}$
$\varrho_{12}\varkappa_1$	$-6{,}338 \cdot 10^{-5}$	$-7{,}545 \cdot 10^{-2}$	$9{,}773 \cdot 10^{-2}$	$-4{,}938 \cdot 10^{-5}$	$-5{,}879 \cdot 10^{-2}$	$7{,}778 \cdot 10^{-2}$
$\varrho_{12}\varkappa_2$	$1{,}761 \cdot 10^{-5}$	$1{,}101 \cdot 10^{-2}$	$-7{,}344 \cdot 10^{-3}$	$5{,}992 \cdot 10^{-5}$	$3{,}745 \cdot 10^{-2}$	$-2{,}609 \cdot 10^{-2}$
$\varrho_{12}\varkappa_3$	$4{,}867 \cdot 10^{-5}$	$5{,}794 \cdot 10^{-2}$	$-7{,}671 \cdot 10^{-2}$	$-7{,}377 \cdot 10^{-6}$	$-8{,}783 \cdot 10^{-3}$	$1{,}109 \cdot 10^{-2}$
$\varrho_{12}\varkappa_4$	$-2{,}902 \cdot 10^{-6}$	$-1{,}813 \cdot 10^{-3}$	$1{,}174 \cdot 10^{-3}$	$-3{,}163 \cdot 10^{-6}$	$-1{,}977 \cdot 10^{-3}$	$1{,}280 \cdot 10^{-3}$
$\varrho_{13}\varkappa_1$	$-1{,}093 \cdot 10^{-4}$	$-1{,}519 \cdot 10^{-1}$	$1{,}531 \cdot 10^{-1}$	$-9{,}345 \cdot 10^{-5}$	$-1{,}298 \cdot 10^{-1}$	$1{,}435 \cdot 10^{-1}$
$\varrho_{13}\varkappa_2$	$1{,}266 \cdot 10^{-4}$	$7{,}911 \cdot 10^{-2}$	$-4{,}581 \cdot 10^{-2}$	$1{,}531 \cdot 10^{-4}$	$9{,}567 \cdot 10^{-2}$	$-5{,}333 \cdot 10^{-2}$
$\varrho_{13}\varkappa_3$	$3{,}825 \cdot 10^{-7}$	$5{,}313 \cdot 10^{-4}$	$-6{,}517 \cdot 10^{-4}$	$3{,}007 \cdot 10^{-7}$	$4{,}176 \cdot 10^{-4}$	$-5{,}121 \cdot 10^{-4}$
$\varrho_{13}\varkappa_4$	$-1{,}761 \cdot 10^{-5}$	$-1{,}101 \cdot 10^{-2}$	$6{,}295 \cdot 10^{-3}$	$-5{,}992 \cdot 10^{-5}$	$-3{,}745 \cdot 10^{-2}$	$2{,}236 \cdot 10^{-2}$
$\varrho_{14}\varkappa_1$	$-2{,}830 \cdot 10^{-4}$	$-5{,}896 \cdot 10^{-1}$	$2{,}726 \cdot 10^{-1}$	$-2{,}732 \cdot 10^{-4}$	$-5{,}692 \cdot 10^{-1}$	$2{,}662 \cdot 10^{-1}$
$\varrho_{14}\varkappa_2$	$-1{,}944 \cdot 10^{-4}$	$-1{,}215 \cdot 10^{-1}$	$4{,}158 \cdot 10^{-2}$	$-1{,}550 \cdot 10^{-4}$	$-9{,}685 \cdot 10^{-2}$	$3{,}588 \cdot 10^{-2}$
$\varrho_{14}\varkappa_3$	$6{,}039 \cdot 10^{-4}$	$1{,}258$	$-9{,}157 \cdot 10^{-1}$	$5{,}812 \cdot 10^{-4}$	$1{,}211$	$-7{,}699 \cdot 10^{-1}$
$\varrho_{14}\varkappa_4$	$-1{,}266 \cdot 10^{-4}$	$-7{,}911 \cdot 10^{-2}$	$3{,}054 \cdot 10^{-2}$	$-1{,}531 \cdot 10^{-4}$	$-9{,}567 \cdot 10^{-2}$	$3{,}555 \cdot 10^{-2}$
$\varrho_{15}\varkappa_1$	$-5{,}113 \cdot 10^{-4}$	$-7{,}102 \cdot 10^{-1}$	$3{,}152 \cdot 10^{-1}$	$-5{,}068 \cdot 10^{-4}$	$-7{,}039 \cdot 10^{-1}$	$3{,}127 \cdot 10^{-1}$
$\varrho_{15}\varkappa_2$	$3{,}148 \cdot 10^{-4}$	$1{,}967 \cdot 10^{-1}$	$-7{,}303 \cdot 10^{-2}$	$3{,}489 \cdot 10^{-4}$	$2{,}181 \cdot 10^{-1}$	$-7{,}478 \cdot 10^{-2}$
$\varrho_{15}\varkappa_3$	$2{,}188 \cdot 10^{-6}$	$3{,}039 \cdot 10^{-3}$	$-3{,}763 \cdot 10^{-3}$	$2{,}926 \cdot 10^{-6}$	$4{,}065 \cdot 10^{-3}$	$-5{,}052 \cdot 10^{-3}$
$\varrho_{15}\varkappa_4$	$1{,}944 \cdot 10^{-4}$	$1{,}215 \cdot 10^{-1}$	$-6{,}237 \cdot 10^{-2}$	$1{,}550 \cdot 10^{-4}$	$9{,}685 \cdot 10^{-2}$	$-5{,}382 \cdot 10^{-2}$
$\varrho_{16}\varkappa_1$	$-5{,}346 \cdot 10^{-4}$	$-1{,}114$	$5{,}971 \cdot 10^{-1}$	$-5{,}289 \cdot 10^{-4}$	$-1{,}102$	$5{,}823 \cdot 10^{-1}$
$\varrho_{16}\varkappa_2$	$7{,}920 \cdot 10^{-5}$	$4{,}950 \cdot 10^{-2}$	$-1{,}974 \cdot 10^{-2}$	$7{,}997 \cdot 10^{-5}$	$4{,}998 \cdot 10^{-2}$	$-1{,}993 \cdot 10^{-2}$
$\varrho_{16}\varkappa_3$	$7{,}702 \cdot 10^{-4}$	$1{,}605$	$-1{,}519 \cdot 10^{1}$	$7{,}978 \cdot 10^{-4}$	$1{,}662$	$-2{,}207 \cdot 10^{1}$
$\varrho_{16}\varkappa_4$	$-3{,}148 \cdot 10^{-4}$	$-1{,}967 \cdot 10^{-1}$	$4{,}869 \cdot 10^{-2}$	$-3{,}489 \cdot 10^{-4}$	$-2{,}181 \cdot 10^{-1}$	$4{,}985 \cdot 10^{-2}$
$\varrho_{17}\varkappa_1$	$4{,}676 \cdot 10^{-4}$	$9{,}741 \cdot 10^{-1}$	$-4{,}592 \cdot 10^{-1}$	$4{,}394 \cdot 10^{-4}$	$9{,}153 \cdot 10^{-1}$	$-4{,}176 \cdot 10^{-1}$
$\varrho_{17}\varkappa_2$	$-1{,}119 \cdot 10^{-4}$	$-6{,}995 \cdot 10^{-2}$	$2{,}742 \cdot 10^{-2}$	$-1{,}863 \cdot 10^{-4}$	$-1{,}164 \cdot 10^{-1}$	$4{,}058 \cdot 10^{-2}$
$\varrho_{17}\varkappa_3$	$-2{,}781 \cdot 10^{-4}$	$-5{,}794 \cdot 10^{-1}$	$2{,}694 \cdot 10^{-1}$	$-1{,}755 \cdot 10^{-4}$	$-3{,}657 \cdot 10^{-1}$	$2{,}099 \cdot 10^{-1}$
$\varrho_{17}\varkappa_4$	$-7{,}754 \cdot 10^{-5}$	$-4{,}846 \cdot 10^{-2}$	$1{,}933 \cdot 10^{-2}$	$-7{,}753 \cdot 10^{-5}$	$-4{,}846 \cdot 10^{-2}$	$1{,}933 \cdot 10^{-2}$
$\varrho_{18}\varkappa_1$	$4{,}175 \cdot 10^{-4}$	$5{,}799 \cdot 10^{-1}$	$-2{,}696 \cdot 10^{-1}$	$3{,}886 \cdot 10^{-4}$	$5{,}397 \cdot 10^{-1}$	$-2{,}571 \cdot 10^{-1}$
$\varrho_{18}\varkappa_2$	$-5{,}290 \cdot 10^{-4}$	$-3{,}306 \cdot 10^{-1}$	$9{,}042 \cdot 10^{-2}$	$-5{,}745 \cdot 10^{-4}$	$-3{,}591 \cdot 10^{-1}$	$9{,}373 \cdot 10^{-2}$
$\varrho_{18}\varkappa_3$	$-4{,}805 \cdot 10^{-7}$	$-6{,}674 \cdot 10^{-4}$	$8{,}191 \cdot 10^{-4}$	$-3{,}693 \cdot 10^{-7}$	$-5{,}129 \cdot 10^{-4}$	$6{,}290 \cdot 10^{-4}$
$\varrho_{18}\varkappa_4$	$1{,}119 \cdot 10^{-4}$	$6{,}995 \cdot 10^{-2}$	$-4{,}113 \cdot 10^{-2}$	$1{,}863 \cdot 10^{-4}$	$1{,}164 \cdot 10^{-1}$	$-6{,}087 \cdot 10^{-2}$
$\varrho_{19}\varkappa_1$	$2{,}209 \cdot 10^{-4}$	$4{,}603 \cdot 10^{-1}$	$-2{,}337 \cdot 10^{-1}$	$2{,}029 \cdot 10^{-4}$	$4{,}226 \cdot 10^{-1}$	$-2{,}236 \cdot 10^{-1}$
$\varrho_{19}\varkappa_2$	$-1{,}053 \cdot 10^{-4}$	$-6{,}581 \cdot 10^{-2}$	$2{,}594 \cdot 10^{-2}$	$-1{,}594 \cdot 10^{-4}$	$-9{,}961 \cdot 10^{-2}$	$3{,}662 \cdot 10^{-2}$
$\varrho_{19}\varkappa_3$	$-6{,}446 \cdot 10^{-4}$	$-1{,}343$	$1{,}435$	$-6{,}180 \cdot 10^{-4}$	$-1{,}287$	$1{,}045$
$\varrho_{19}\varkappa_4$	$5{,}290 \cdot 10^{-4}$	$3{,}306 \cdot 10^{-1}$	$-6{,}028 \cdot 10^{-2}$	$5{,}745 \cdot 10^{-4}$	$3{,}591 \cdot 10^{-1}$	$-6{,}249 \cdot 10^{-2}$
$\varrho_{20}\varkappa_1$	$1{,}798 \cdot 10^{-4}$	$2{,}497 \cdot 10^{-1}$	$-1{,}745 \cdot 10^{-1}$	$1{,}879 \cdot 10^{-4}$	$2{,}609 \cdot 10^{-1}$	$-1{,}780 \cdot 10^{-1}$
$\varrho_{20}\varkappa_2$	$-2{,}845 \cdot 10^{-4}$	$-1{,}778 \cdot 10^{-1}$	$7{,}170 \cdot 10^{-2}$	$-3{,}467 \cdot 10^{-4}$	$-2{,}167 \cdot 10^{-1}$	$7{,}465 \cdot 10^{-2}$
$\varrho_{20}\varkappa_3$	$-5{,}586 \cdot 10^{-7}$	$-7{,}758 \cdot 10^{-4}$	$9{,}525 \cdot 10^{-4}$	$-5{,}174 \cdot 10^{-7}$	$-7{,}185 \cdot 10^{-4}$	$8{,}820 \cdot 10^{-4}$
$\varrho_{20}\varkappa_4$	$1{,}053 \cdot 10^{-4}$	$6{,}581 \cdot 10^{-2}$	$-3{,}890 \cdot 10^{-2}$	$1{,}594 \cdot 10^{-4}$	$9{,}961 \cdot 10^{-2}$	$-5{,}493 \cdot 10^{-2}$
$\varrho_{21}\varkappa_1$	$2{,}020 \cdot 10^{-4}$	$2{,}405 \cdot 10^{-1}$	$-1{,}717 \cdot 10^{-1}$	$2{,}171 \cdot 10^{-4}$	$2{,}585 \cdot 10^{-1}$	$-1{,}772 \cdot 10^{-1}$
$\varrho_{21}\varkappa_2$	$-5{,}976 \cdot 10^{-6}$	$-3{,}735 \cdot 10^{-3}$	$2{,}434 \cdot 10^{-3}$	$-8{,}049 \cdot 10^{-6}$	$-5{,}031 \cdot 10^{-3}$	$3{,}294 \cdot 10^{-3}$
$\varrho_{21}\varkappa_3$	$-4{,}805 \cdot 10^{-4}$	$-5{,}721 \cdot 10^{-1}$	$2{,}671 \cdot 10^{-1}$	$-5{,}558 \cdot 10^{-4}$	$-6{,}616 \cdot 10^{-1}$	$2{,}969 \cdot 10^{-1}$
$\varrho_{21}\varkappa_4$	$2{,}845 \cdot 10^{-4}$	$1{,}778 \cdot 10^{-1}$	$-8{,}365 \cdot 10^{-2}$	$3{,}467 \cdot 10^{-4}$	$2{,}167 \cdot 10^{-1}$	$-8{,}709 \cdot 10^{-2}$
$\varrho_{22}\varkappa_1$	$-4{,}867 \cdot 10^{-5}$	$-5{,}794 \cdot 10^{-2}$	$7{,}671 \cdot 10^{-2}$	$7{,}377 \cdot 10^{-6}$	$8{,}783 \cdot 10^{-3}$	$-1{,}109 \cdot 10^{-2}$
$\varrho_{22}\varkappa_2$	$-1{,}522 \cdot 10^{-5}$	$-9{,}513 \cdot 10^{-3}$	$6{,}319 \cdot 10^{-3}$	$-3{,}340 \cdot 10^{-5}$	$-2{,}088 \cdot 10^{-2}$	$1{,}425 \cdot 10^{-2}$
$\varrho_{22}\varkappa_3$	$6{,}753 \cdot 10^{-5}$	$8{,}040 \cdot 10^{-2}$	$-1{,}032 \cdot 10^{-1}$	$3{,}143 \cdot 10^{-5}$	$3{,}742 \cdot 10^{-2}$	$-4{,}965 \cdot 10^{-2}$
$\varrho_{22}\varkappa_4$	$-3{,}644 \cdot 10^{-6}$	$-2{,}277 \cdot 10^{-3}$	$1{,}476 \cdot 10^{-3}$	$-5{,}408 \cdot 10^{-6}$	$-3{,}380 \cdot 10^{-3}$	$2{,}200 \cdot 10^{-3}$

Table A.1: Flux tube element outputs ... *cont*

Element Region	$I_{(\mathrm{ph})} = \begin{bmatrix} 20 & -10 & -10 \end{bmatrix}^{\mathrm{T}}$					
	$x = 2\,\mathrm{mm}$			$x = 3\,\mathrm{mm}$		
	Φ [Wb]	B [T]	$\mathcal{F}$ [A]	Φ [Wb]	B [T]	$\mathcal{F}$ [A]
$\mathrm{e}_{23}\mathrm{k}_1$	$-6{,}039 \cdot 10^{-4}$	$-1{,}258$	$9{,}157 \cdot 10^{-1}$	$-5{,}812 \cdot 10^{-4}$	$-1{,}211$	$7{,}699 \cdot 10^{-1}$
$\mathrm{e}_{23}\mathrm{k}_2$	$8{,}378 \cdot 10^{-5}$	$5{,}236 \cdot 10^{-2}$	$-2{,}086 \cdot 10^{-2}$	$8{,}649 \cdot 10^{-5}$	$5{,}406 \cdot 10^{-2}$	$-2{,}152 \cdot 10^{-2}$
$\mathrm{e}_{23}\mathrm{k}_3$	$3{,}365 \cdot 10^{-4}$	$7{,}010 \cdot 10^{-1}$	$-3{,}116 \cdot 10^{-1}$	$3{,}250 \cdot 10^{-4}$	$6{,}770 \cdot 10^{-1}$	$-3{,}025 \cdot 10^{-1}$
$\mathrm{e}_{23}\mathrm{k}_4$	$1{,}837 \cdot 10^{-4}$	$1{,}148 \cdot 10^{-1}$	$-4{,}023 \cdot 10^{-2}$	$1{,}698 \cdot 10^{-4}$	$1{,}061 \cdot 10^{-1}$	$-3{,}826 \cdot 10^{-2}$
$\mathrm{e}_{24}\mathrm{k}_1$	$-7{,}702 \cdot 10^{-4}$	$-1{,}605$	$1{,}519 \cdot 10^{1}$	$-7{,}978 \cdot 10^{-4}$	$-1{,}662$	$2{,}207 \cdot 10^{1}$
$\mathrm{e}_{24}\mathrm{k}_2$	$2{,}639 \cdot 10^{-4}$	$1{,}649 \cdot 10^{-1}$	$-4{,}702 \cdot 10^{-2}$	$2{,}764 \cdot 10^{-4}$	$1{,}728 \cdot 10^{-1}$	$-4{,}752 \cdot 10^{-2}$
$\mathrm{e}_{24}\mathrm{k}_3$	$3{,}450 \cdot 10^{-4}$	$7{,}188 \cdot 10^{-1}$	$-3{,}186 \cdot 10^{-1}$	$3{,}631 \cdot 10^{-4}$	$7{,}565 \cdot 10^{-1}$	$-3{,}345 \cdot 10^{-1}$
$\mathrm{e}_{24}\mathrm{k}_4$	$1{,}613 \cdot 10^{-4}$	$1{,}008 \cdot 10^{-1}$	$-3{,}693 \cdot 10^{-2}$	$1{,}583 \cdot 10^{-4}$	$9{,}893 \cdot 10^{-2}$	$-3{,}644 \cdot 10^{-2}$
$\mathrm{e}_{25}\mathrm{k}_1$	$2{,}781 \cdot 10^{-4}$	$5{,}794 \cdot 10^{-1}$	$-2{,}694 \cdot 10^{-1}$	$1{,}755 \cdot 10^{-4}$	$3{,}657 \cdot 10^{-1}$	$-2{,}099 \cdot 10^{-1}$
$\mathrm{e}_{25}\mathrm{k}_2$	$-3{,}451 \cdot 10^{-5}$	$-2{,}157 \cdot 10^{-2}$	$8{,}426 \cdot 10^{-3}$	$-1{,}391 \cdot 10^{-5}$	$-8{,}692 \cdot 10^{-3}$	$3{,}291 \cdot 10^{-3}$
$\mathrm{e}_{25}\mathrm{k}_3$	$-7{,}838 \cdot 10^{-5}$	$-1{,}633 \cdot 10^{-1}$	$1{,}563 \cdot 10^{-1}$	$-2{,}348 \cdot 10^{-4}$	$-4{,}891 \cdot 10^{-2}$	$6{,}504 \cdot 10^{-2}$
$\mathrm{e}_{25}\mathrm{k}_4$	$-1{,}652 \cdot 10^{-4}$	$-1{,}033 \cdot 10^{-1}$	$3{,}756 \cdot 10^{-2}$	$-1{,}382 \cdot 10^{-4}$	$-8{,}635 \cdot 10^{-2}$	$3{,}283 \cdot 10^{-2}$
$\mathrm{e}_{26}\mathrm{k}_1$	$6{,}446 \cdot 10^{-4}$	$1{,}343$	$-1{,}435$	$6{,}180 \cdot 10^{-4}$	$1{,}287$	$-1{,}045$
$\mathrm{e}_{26}\mathrm{k}_2$	$-1{,}590 \cdot 10^{-4}$	$-9{,}936 \cdot 10^{-2}$	$3{,}655 \cdot 10^{-2}$	$-1{,}591 \cdot 10^{-4}$	$-9{,}945 \cdot 10^{-2}$	$3{,}657 \cdot 10^{-2}$
$\mathrm{e}_{26}\mathrm{k}_3$	$-3{,}430 \cdot 10^{-4}$	$-7{,}145 \cdot 10^{-1}$	$3{,}169 \cdot 10^{-1}$	$-3{,}314 \cdot 10^{-4}$	$-6{,}904 \cdot 10^{-1}$	$3{,}075 \cdot 10^{-1}$
$\mathrm{e}_{26}\mathrm{k}_4$	$-1{,}427 \cdot 10^{-4}$	$-8{,}917 \cdot 10^{-2}$	$3{,}369 \cdot 10^{-2}$	$-1{,}275 \cdot 10^{-4}$	$-7{,}967 \cdot 10^{-2}$	$3{,}072 \cdot 10^{-2}$
$\mathrm{e}_{27}\mathrm{k}_1$	$4{,}805 \cdot 10^{-4}$	$5{,}721 \cdot 10^{-1}$	$-2{,}671 \cdot 10^{-1}$	$5{,}558 \cdot 10^{-4}$	$6{,}616 \cdot 10^{-1}$	$-2{,}969 \cdot 10^{-1}$
$\mathrm{e}_{27}\mathrm{k}_2$	$-4{,}743 \cdot 10^{-5}$	$-2{,}965 \cdot 10^{-2}$	$2{,}051 \cdot 10^{-2}$	$-7{,}339 \cdot 10^{-5}$	$-4{,}587 \cdot 10^{-2}$	$3{,}203 \cdot 10^{-2}$
$\mathrm{e}_{27}\mathrm{k}_3$	$-3{,}666 \cdot 10^{-4}$	$-4{,}365 \cdot 10^{-1}$	$2{,}272 \cdot 10^{-1}$	$-4{,}153 \cdot 10^{-4}$	$-4{,}944 \cdot 10^{-1}$	$2{,}436 \cdot 10^{-1}$
$\mathrm{e}_{27}\mathrm{k}_4$	$-6{,}648 \cdot 10^{-5}$	$-4{,}155 \cdot 10^{-2}$	$2{,}900 \cdot 10^{-2}$	$-6{,}708 \cdot 10^{-5}$	$-4{,}192 \cdot 10^{-2}$	$2{,}926 \cdot 10^{-2}$
$\mathrm{e}_{28}\mathrm{k}_1$	$-1{,}460 \cdot 10^{-3}$	$-5{,}615 \cdot 10^{-1}$	$4{,}958 \cdot 10^{-1}$	$-1{,}463 \cdot 10^{-3}$	$-5{,}627 \cdot 10^{-1}$	$4{,}969 \cdot 10^{-1}$
$\mathrm{e}_{28}\mathrm{k}_2$	$1{,}370 \cdot 10^{-3}$	$1{,}522$	$-1{,}070 \cdot 10^{1}$	$1{,}374 \cdot 10^{-3}$	$1{,}527$	$-1{,}117 \cdot 10^{1}$
$\mathrm{e}_{28}\mathrm{k}_3$	$1{,}723 \cdot 10^{-5}$	$6{,}626 \cdot 10^{-3}$	$-5{,}597 \cdot 10^{-3}$	$1{,}713 \cdot 10^{-5}$	$6{,}589 \cdot 10^{-3}$	$-5{,}566 \cdot 10^{-3}$
$\mathrm{e}_{28}\mathrm{k}_4$	$7{,}318 \cdot 10^{-5}$	$8{,}131 \cdot 10^{-2}$	$-1{,}978 \cdot 10^{-1}$	$7{,}144 \cdot 10^{-5}$	$7{,}938 \cdot 10^{-2}$	$-1{,}931 \cdot 10^{-1}$
$\mathrm{e}_{29}\mathrm{k}_1$	$-3{,}257 \cdot 10^{-6}$	$-3{,}257 \cdot 10^{-3}$	$2{,}752 \cdot 10^{-3}$	$8{,}712 \cdot 10^{-6}$	$8{,}712 \cdot 10^{-3}$	$-7{,}358 \cdot 10^{-3}$
$\mathrm{e}_{29}\mathrm{k}_2$	$1{,}371 \cdot 10^{-3}$	$1{,}523$	$-4{,}169$	$1{,}364 \cdot 10^{-3}$	$1{,}516$	$-3{,}923$
$\mathrm{e}_{29}\mathrm{k}_3$	$1{,}791 \cdot 10^{-6}$	$1{,}791 \cdot 10^{-3}$	$-1{,}514 \cdot 10^{-3}$	$1{,}510 \cdot 10^{-6}$	$1{,}510 \cdot 10^{-3}$	$-1{,}276 \cdot 10^{-3}$
$\mathrm{e}_{29}\mathrm{k}_4$	$-1{,}370 \cdot 10^{-3}$	$-1{,}522$	$4{,}115$	$-1{,}374 \cdot 10^{-3}$	$-1{,}527$	$4{,}296$
$\mathrm{e}_{30}\mathrm{k}_1$	$1{,}423 \cdot 10^{-3}$	$5{,}472 \cdot 10^{-1}$	$-4{,}819 \cdot 10^{-1}$	$1{,}423 \cdot 10^{-3}$	$5{,}473 \cdot 10^{-1}$	$-4{,}820 \cdot 10^{-1}$
$\mathrm{e}_{30}\mathrm{k}_2$	$-5{,}004 \cdot 10^{-5}$	$-5{,}560 \cdot 10^{-2}$	$1{,}353 \cdot 10^{-1}$	$-5{,}588 \cdot 10^{-5}$	$-6{,}208 \cdot 10^{-2}$	$1{,}511 \cdot 10^{-1}$
$\mathrm{e}_{30}\mathrm{k}_3$	$-1{,}733 \cdot 10^{-6}$	$-6{,}665 \cdot 10^{-4}$	$5{,}633 \cdot 10^{-4}$	$-3{,}092 \cdot 10^{-6}$	$-1{,}189 \cdot 10^{-3}$	$1{,}005 \cdot 10^{-3}$
$\mathrm{e}_{30}\mathrm{k}_4$	$-1{,}371 \cdot 10^{-3}$	$-1{,}523$	$1{,}084 \cdot 10^{1}$	$-1{,}364 \cdot 10^{-3}$	$-1{,}516$	$1{,}020 \cdot 10^{1}$

Table A.1: Flux tube element outputs ... *cont*

Element Region	$I_{(\mathrm{ph})} = \begin{bmatrix} 20 & -10 & -10 \end{bmatrix}^{\mathrm{T}}$					
	$x = 4\,\mathrm{mm}$			$x = 5\,\mathrm{mm}$		
	Φ [Wb]	B [T]	$\mathcal{F}$ [A]	Φ [Wb]	B [T]	$\mathcal{F}$ [A]
$\mathrm{e}_{1}\mathrm{k}_1$	$-2{,}095 \cdot 10^{-6}$	$-2{,}494 \cdot 10^{-3}$	$1{,}927 \cdot 10^{-3}$	$-2{,}374 \cdot 10^{-6}$	$-2{,}827 \cdot 10^{-3}$	$2{,}186 \cdot 10^{-3}$
$\mathrm{e}_{1}\mathrm{k}_2$	$-3{,}305 \cdot 10^{-5}$	$-3{,}305 \cdot 10^{-2}$	$2{,}295 \cdot 10^{-2}$	$-2{,}321 \cdot 10^{-5}$	$-2{,}321 \cdot 10^{-2}$	$1{,}591 \cdot 10^{-2}$
$\mathrm{e}_{1}\mathrm{k}_3$	$3{,}784 \cdot 10^{-5}$	$4{,}505 \cdot 10^{-2}$	$-3{,}745 \cdot 10^{-2}$	$2{,}865 \cdot 10^{-5}$	$3{,}411 \cdot 10^{-2}$	$-2{,}822 \cdot 10^{-2}$
$\mathrm{e}_{1}\mathrm{k}_4$	$-2{,}690 \cdot 10^{-6}$	$-2{,}690 \cdot 10^{-3}$	$1{,}747 \cdot 10^{-3}$	$-3{,}065 \cdot 10^{-6}$	$-3{,}065 \cdot 10^{-3}$	$1{,}993 \cdot 10^{-3}$
$\mathrm{e}_{2}\mathrm{k}_1$	$-1{,}095 \cdot 10^{-6}$	$-1{,}521 \cdot 10^{-3}$	$1{,}171 \cdot 10^{-3}$	$-1{,}235 \cdot 10^{-6}$	$-1{,}716 \cdot 10^{-3}$	$1{,}321 \cdot 10^{-3}$
$\mathrm{e}_{2}\mathrm{k}_2$	$-1{,}129 \cdot 10^{-4}$	$-1{,}129 \cdot 10^{-1}$	$5{,}973 \cdot 10^{-2}$	$-9{,}233 \cdot 10^{-5}$	$-9{,}233 \cdot 10^{-2}$	$5{,}191 \cdot 10^{-2}$
$\mathrm{e}_{2}\mathrm{k}_3$	$8{,}092 \cdot 10^{-5}$	$1{,}124 \cdot 10^{-1}$	$-8{,}274 \cdot 10^{-2}$	$7{,}035 \cdot 10^{-5}$	$9{,}771 \cdot 10^{-2}$	$-7{,}523 \cdot 10^{-2}$
$\mathrm{e}_{2}\mathrm{k}_4$	$3{,}305 \cdot 10^{-5}$	$3{,}305 \cdot 10^{-2}$	$-1{,}967 \cdot 10^{-2}$	$2{,}321 \cdot 10^{-5}$	$2{,}321 \cdot 10^{-2}$	$-1{,}364 \cdot 10^{-2}$
$\mathrm{e}_{3}\mathrm{k}_1$	$-6{,}656 \cdot 10^{-7}$	$-1{,}387 \cdot 10^{-3}$	$1{,}067 \cdot 10^{-3}$	$-7{,}449 \cdot 10^{-7}$	$-1{,}552 \cdot 10^{-3}$	$1{,}194 \cdot 10^{-3}$
$\mathrm{e}_{3}\mathrm{k}_2$	$-3{,}655 \cdot 10^{-4}$	$-3{,}655 \cdot 10^{-1}$	$6{,}295 \cdot 10^{-2}$	$-3{,}167 \cdot 10^{-4}$	$-3{,}167 \cdot 10^{-1}$	$5{,}908 \cdot 10^{-2}$
$\mathrm{e}_{3}\mathrm{k}_3$	$2{,}533 \cdot 10^{-4}$	$5{,}276 \cdot 10^{-1}$	$-1{,}584 \cdot 10^{-1}$	$2{,}252 \cdot 10^{-4}$	$4{,}691 \cdot 10^{-1}$	$-1{,}476 \cdot 10^{-1}$
$\mathrm{e}_{3}\mathrm{k}_4$	$1{,}129 \cdot 10^{-4}$	$1{,}129 \cdot 10^{-1}$	$-3{,}982 \cdot 10^{-2}$	$9{,}233 \cdot 10^{-5}$	$9{,}233 \cdot 10^{-2}$	$-3{,}461 \cdot 10^{-2}$

Table A.1: Flux tube element outputs ... *cont*

Element Region	$I_{(\mathrm{ph})} = \begin{bmatrix} 20 & -10 & -10 \end{bmatrix}^{\mathrm{T}}$					
	$x = 4\,\mathrm{mm}$			$x = 5\,\mathrm{mm}$		
	Φ [Wb]	B [T]	$\mathcal{F}$ [A]	Φ [Wb]	B [T]	$\mathcal{F}$ [A]
$\varrho_4\kappa_1$	$-9{,}923 \cdot 10^{-7}$	$-1{,}378 \cdot 10^{-3}$	$1{,}060 \cdot 10^{-3}$	$-1{,}082 \cdot 10^{-6}$	$-1{,}503 \cdot 10^{-3}$	$1{,}156 \cdot 10^{-3}$
$\varrho_4\kappa_2$	$-8{,}592 \cdot 10^{-4}$	$-8{,}592 \cdot 10^{-1}$	$1{,}730 \cdot 10^{-1}$	$-7{,}912 \cdot 10^{-4}$	$-7{,}912 \cdot 10^{-1}$	$1{,}576 \cdot 10^{-1}$
$\varrho_4\kappa_3$	$4{,}947 \cdot 10^{-4}$	$6{,}871 \cdot 10^{-1}$	$-1{,}914 \cdot 10^{-1}$	$4{,}755 \cdot 10^{-4}$	$6{,}605 \cdot 10^{-1}$	$-1{,}853 \cdot 10^{-1}$
$\varrho_4\kappa_4$	$3{,}655 \cdot 10^{-4}$	$3{,}655 \cdot 10^{-1}$	$-9{,}443 \cdot 10^{-2}$	$3{,}167 \cdot 10^{-4}$	$3{,}167 \cdot 10^{-1}$	$-8{,}862 \cdot 10^{-2}$
$\varrho_5\kappa_1$	$-7{,}299 \cdot 10^{-7}$	$-1{,}521 \cdot 10^{-3}$	$1{,}170 \cdot 10^{-3}$	$-7{,}419 \cdot 10^{-7}$	$-1{,}546 \cdot 10^{-3}$	$1{,}190 \cdot 10^{-3}$
$\varrho_5\kappa_2$	$-1{,}379 \cdot 10^{-3}$	$-1{,}379$	$5{,}756 \cdot 10^{-1}$	$-1{,}300 \cdot 10^{-3}$	$-1{,}300$	$3{,}344 \cdot 10^{-1}$
$\varrho_5\kappa_3$	$5{,}207 \cdot 10^{-4}$	$1{,}085$	$-3{,}513 \cdot 10^{-1}$	$5{,}100 \cdot 10^{-4}$	$1{,}062$	$-3{,}363 \cdot 10^{-1}$
$\varrho_5\kappa_4$	$8{,}592 \cdot 10^{-4}$	$8{,}592 \cdot 10^{-1}$	$-1{,}153 \cdot 10^{-1}$	$7{,}912 \cdot 10^{-4}$	$7{,}912 \cdot 10^{-1}$	$-1{,}051 \cdot 10^{-1}$
$\varrho_6\kappa_1$	$-7{,}968 \cdot 10^{-7}$	$-1{,}107 \cdot 10^{-3}$	$8{,}504 \cdot 10^{-4}$	$-9{,}676 \cdot 10^{-7}$	$-1{,}344 \cdot 10^{-3}$	$1{,}034 \cdot 10^{-3}$
$\varrho_6\kappa_2$	$-1{,}378 \cdot 10^{-3}$	$-1{,}378$	$8{,}580 \cdot 10^{-1}$	$-1{,}300 \cdot 10^{-3}$	$-1{,}300$	$4{,}993 \cdot 10^{-1}$
$\varrho_6\kappa_3$	$9{,}524 \cdot 10^{-8}$	$1{,}323 \cdot 10^{-4}$	$-1{,}012 \cdot 10^{-4}$	$1{,}024 \cdot 10^{-7}$	$1{,}422 \cdot 10^{-4}$	$-1{,}089 \cdot 10^{-4}$
$\varrho_6\kappa_4$	$1{,}379 \cdot 10^{-3}$	$1{,}379$	$-8{,}634 \cdot 10^{-1}$	$1{,}300 \cdot 10^{-3}$	$1{,}300$	$-5{,}015 \cdot 10^{-1}$
$\varrho_7\kappa_1$	$-3{,}539 \cdot 10^{-7}$	$-7{,}373 \cdot 10^{-4}$	$5{,}657 \cdot 10^{-4}$	$-5{,}724 \cdot 10^{-7}$	$-1{,}192 \cdot 10^{-3}$	$9{,}165 \cdot 10^{-4}$
$\varrho_7\kappa_2$	$-9{,}678 \cdot 10^{-4}$	$-9{,}678 \cdot 10^{-1}$	$1{,}363 \cdot 10^{-1}$	$-9{,}195 \cdot 10^{-4}$	$-9{,}195 \cdot 10^{-1}$	$1{,}261 \cdot 10^{-1}$
$\varrho_7\kappa_3$	$-4{,}102 \cdot 10^{-4}$	$-8{,}547 \cdot 10^{-1}$	$2{,}387 \cdot 10^{-1}$	$-3{,}795 \cdot 10^{-4}$	$-7{,}906 \cdot 10^{-1}$	$2{,}187 \cdot 10^{-1}$
$\varrho_7\kappa_4$	$1{,}378 \cdot 10^{-3}$	$1{,}378$	$-5{,}720 \cdot 10^{-1}$	$1{,}300 \cdot 10^{-3}$	$1{,}300$	$-3{,}329 \cdot 10^{-1}$
$\varrho_8\kappa_1$	$-7{,}043 \cdot 10^{-7}$	$-9{,}782 \cdot 10^{-4}$	$7{,}513 \cdot 10^{-4}$	$-9{,}813 \cdot 10^{-7}$	$-1{,}363 \cdot 10^{-3}$	$1{,}048 \cdot 10^{-3}$
$\varrho_8\kappa_2$	$-6{,}099 \cdot 10^{-4}$	$-6{,}099 \cdot 10^{-1}$	$1{,}257 \cdot 10^{-1}$	$-5{,}943 \cdot 10^{-4}$	$-5{,}943 \cdot 10^{-1}$	$1{,}234 \cdot 10^{-1}$
$\varrho_8\kappa_3$	$-3{,}572 \cdot 10^{-4}$	$-4{,}962 \cdot 10^{-1}$	$1{,}525 \cdot 10^{-1}$	$-3{,}243 \cdot 10^{-4}$	$-4{,}504 \cdot 10^{-1}$	$1{,}444 \cdot 10^{-1}$
$\varrho_8\kappa_4$	$9{,}678 \cdot 10^{-4}$	$9{,}678 \cdot 10^{-1}$	$-2{,}045 \cdot 10^{-1}$	$9{,}195 \cdot 10^{-4}$	$9{,}195 \cdot 10^{-1}$	$-1{,}892 \cdot 10^{-1}$
$\varrho_9\kappa_1$	$-5{,}701 \cdot 10^{-7}$	$-1{,}188 \cdot 10^{-3}$	$9{,}129 \cdot 10^{-4}$	$-7{,}613 \cdot 10^{-7}$	$-1{,}586 \cdot 10^{-3}$	$1{,}221 \cdot 10^{-3}$
$\varrho_9\kappa_2$	$-4{,}254 \cdot 10^{-4}$	$-4{,}254 \cdot 10^{-1}$	$6{,}730 \cdot 10^{-2}$	$-4{,}271 \cdot 10^{-4}$	$-4{,}271 \cdot 10^{-1}$	$6{,}743 \cdot 10^{-2}$
$\varrho_9\kappa_3$	$-1{,}839 \cdot 10^{-4}$	$-3{,}831 \cdot 10^{-1}$	$1{,}338 \cdot 10^{-1}$	$-1{,}664 \cdot 10^{-4}$	$-3{,}467 \cdot 10^{-1}$	$1{,}283 \cdot 10^{-1}$
$\varrho_9\kappa_4$	$6{,}099 \cdot 10^{-4}$	$6{,}099 \cdot 10^{-1}$	$-8{,}377 \cdot 10^{-2}$	$5{,}943 \cdot 10^{-4}$	$5{,}943 \cdot 10^{-1}$	$-8{,}225 \cdot 10^{-2}$
$\varrho_{10}\kappa_1$	$-1{,}078 \cdot 10^{-6}$	$-1{,}497 \cdot 10^{-3}$	$1{,}152 \cdot 10^{-3}$	$-1{,}419 \cdot 10^{-6}$	$-1{,}971 \cdot 10^{-3}$	$1{,}520 \cdot 10^{-3}$
$\varrho_{10}\kappa_2$	$-2{,}358 \cdot 10^{-4}$	$-2{,}358 \cdot 10^{-1}$	$7{,}670 \cdot 10^{-2}$	$-2{,}446 \cdot 10^{-4}$	$-2{,}446 \cdot 10^{-1}$	$7{,}781 \cdot 10^{-2}$
$\varrho_{10}\kappa_3$	$-1{,}886 \cdot 10^{-4}$	$-2{,}619 \cdot 10^{-1}$	$1{,}115 \cdot 10^{-1}$	$-1{,}811 \cdot 10^{-4}$	$-2{,}516 \cdot 10^{-1}$	$1{,}094 \cdot 10^{-1}$
$\varrho_{10}\kappa_4$	$4{,}254 \cdot 10^{-4}$	$4{,}254 \cdot 10^{-1}$	$-1{,}010 \cdot 10^{-1}$	$4{,}271 \cdot 10^{-4}$	$4{,}271 \cdot 10^{-1}$	$-1{,}011 \cdot 10^{-1}$
$\varrho_{11}\kappa_1$	$-2{,}613 \cdot 10^{-6}$	$-3{,}111 \cdot 10^{-3}$	$2{,}408 \cdot 10^{-3}$	$-3{,}433 \cdot 10^{-6}$	$-4{,}087 \cdot 10^{-3}$	$3{,}176 \cdot 10^{-3}$
$\varrho_{11}\kappa_2$	$-4{,}929 \cdot 10^{-6}$	$-4{,}929 \cdot 10^{-3}$	$3{,}226 \cdot 10^{-3}$	$-6{,}549 \cdot 10^{-6}$	$-6{,}549 \cdot 10^{-3}$	$4{,}310 \cdot 10^{-3}$
$\varrho_{11}\kappa_3$	$-2{,}282 \cdot 10^{-4}$	$-2{,}717 \cdot 10^{-1}$	$1{,}136 \cdot 10^{-1}$	$-2{,}346 \cdot 10^{-4}$	$-2{,}793 \cdot 10^{-1}$	$1{,}152 \cdot 10^{-1}$
$\varrho_{11}\kappa_4$	$2{,}358 \cdot 10^{-4}$	$2{,}358 \cdot 10^{-1}$	$-8{,}948 \cdot 10^{-2}$	$2{,}446 \cdot 10^{-4}$	$2{,}446 \cdot 10^{-1}$	$-9{,}078 \cdot 10^{-2}$
$\varrho_{12}\kappa_1$	$-3{,}784 \cdot 10^{-5}$	$-4{,}505 \cdot 10^{-2}$	$5{,}992 \cdot 10^{-2}$	$-2{,}865 \cdot 10^{-5}$	$-3{,}411 \cdot 10^{-2}$	$4{,}515 \cdot 10^{-2}$
$\varrho_{12}\kappa_2$	$9{,}313 \cdot 10^{-5}$	$5{,}821 \cdot 10^{-2}$	$-4{,}045 \cdot 10^{-2}$	$1{,}170 \cdot 10^{-4}$	$7{,}310 \cdot 10^{-2}$	$-4{,}990 \cdot 10^{-2}$
$\varrho_{12}\kappa_3$	$-5{,}179 \cdot 10^{-5}$	$-6{,}165 \cdot 10^{-2}$	$8{,}136 \cdot 10^{-2}$	$-8{,}433 \cdot 10^{-5}$	$-1{,}004 \cdot 10^{-1}$	$1{,}227 \cdot 10^{-1}$
$\varrho_{12}\kappa_4$	$-3{,}502 \cdot 10^{-6}$	$-2{,}189 \cdot 10^{-3}$	$1{,}419 \cdot 10^{-3}$	$-3{,}979 \cdot 10^{-6}$	$-2{,}487 \cdot 10^{-3}$	$1{,}613 \cdot 10^{-3}$
$\varrho_{13}\kappa_1$	$-8{,}092 \cdot 10^{-5}$	$-1{,}124 \cdot 10^{-1}$	$1{,}324 \cdot 10^{-1}$	$-7{,}035 \cdot 10^{-5}$	$-9{,}771 \cdot 10^{-2}$	$1{,}204 \cdot 10^{-1}$
$\varrho_{13}\kappa_2$	$1{,}738 \cdot 10^{-4}$	$1{,}086 \cdot 10^{-1}$	$-5{,}830 \cdot 10^{-2}$	$1{,}872 \cdot 10^{-4}$	$1{,}170 \cdot 10^{-1}$	$-6{,}104 \cdot 10^{-2}$
$\varrho_{13}\kappa_3$	$2{,}158 \cdot 10^{-7}$	$2{,}997 \cdot 10^{-4}$	$-3{,}673 \cdot 10^{-4}$	$1{,}410 \cdot 10^{-7}$	$1{,}958 \cdot 10^{-4}$	$-2{,}398 \cdot 10^{-4}$
$\varrho_{13}\kappa_4$	$-9{,}313 \cdot 10^{-5}$	$-5{,}821 \cdot 10^{-2}$	$3{,}467 \cdot 10^{-2}$	$-1{,}170 \cdot 10^{-4}$	$-7{,}310 \cdot 10^{-2}$	$4{,}277 \cdot 10^{-2}$
$\varrho_{14}\kappa_1$	$-2{,}533 \cdot 10^{-4}$	$-5{,}276 \cdot 10^{-1}$	$2{,}534 \cdot 10^{-1}$	$-2{,}252 \cdot 10^{-4}$	$-4{,}691 \cdot 10^{-1}$	$2{,}362 \cdot 10^{-1}$
$\varrho_{14}\kappa_2$	$-1{,}174 \cdot 10^{-4}$	$-7{,}336 \cdot 10^{-2}$	$2{,}861 \cdot 10^{-2}$	$-7{,}978 \cdot 10^{-5}$	$-4{,}986 \cdot 10^{-2}$	$1{,}989 \cdot 10^{-2}$
$\varrho_{14}\kappa_3$	$5{,}445 \cdot 10^{-4}$	$1{,}134$	$-6{,}250 \cdot 10^{-1}$	$4{,}921 \cdot 10^{-4}$	$1{,}025$	$-5{,}019 \cdot 10^{-1}$
$\varrho_{14}\kappa_4$	$-1{,}738 \cdot 10^{-4}$	$-1{,}086 \cdot 10^{-1}$	$3{,}886 \cdot 10^{-2}$	$-1{,}872 \cdot 10^{-4}$	$-1{,}170 \cdot 10^{-1}$	$4{,}069 \cdot 10^{-2}$
$\varrho_{15}\kappa_1$	$-4{,}947 \cdot 10^{-4}$	$-6{,}871 \cdot 10^{-1}$	$3{,}063 \cdot 10^{-1}$	$-4{,}755 \cdot 10^{-4}$	$-6{,}605 \cdot 10^{-1}$	$2{,}965 \cdot 10^{-1}$
$\varrho_{15}\kappa_2$	$3{,}739 \cdot 10^{-4}$	$2{,}337 \cdot 10^{-1}$	$-7{,}645 \cdot 10^{-2}$	$3{,}921 \cdot 10^{-4}$	$2{,}450 \cdot 10^{-1}$	$-7{,}787 \cdot 10^{-2}$
$\varrho_{15}\kappa_3$	$3{,}437 \cdot 10^{-6}$	$4{,}773 \cdot 10^{-3}$	$-5{,}948 \cdot 10^{-3}$	$3{,}675 \cdot 10^{-6}$	$5{,}104 \cdot 10^{-3}$	$-6{,}368 \cdot 10^{-3}$
$\varrho_{15}\kappa_4$	$1{,}174 \cdot 10^{-4}$	$7{,}336 \cdot 10^{-2}$	$-4{,}291 \cdot 10^{-2}$	$7{,}978 \cdot 10^{-5}$	$4{,}986 \cdot 10^{-2}$	$-2{,}983 \cdot 10^{-2}$
$\varrho_{16}\kappa_1$	$-5{,}207 \cdot 10^{-4}$	$-1{,}085$	$5{,}621 \cdot 10^{-1}$	$-5{,}100 \cdot 10^{-4}$	$-1{,}062$	$5{,}380 \cdot 10^{-1}$
$\varrho_{16}\kappa_2$	$8{,}055 \cdot 10^{-5}$	$5{,}035 \cdot 10^{-2}$	$-2{,}008 \cdot 10^{-2}$	$8{,}087 \cdot 10^{-5}$	$5{,}054 \cdot 10^{-2}$	$-2{,}015 \cdot 10^{-2}$
$\varrho_{16}\kappa_3$	$8{,}140 \cdot 10^{-4}$	$1{,}696$	$-2{,}691 \cdot 10^{1}$	$8{,}212 \cdot 10^{-4}$	$1{,}711$	$-2{,}930 \cdot 10^{1}$
$\varrho_{16}\kappa_4$	$-3{,}739 \cdot 10^{-4}$	$-2{,}337 \cdot 10^{-1}$	$5{,}097 \cdot 10^{-2}$	$-3{,}921 \cdot 10^{-4}$	$-2{,}450 \cdot 10^{-1}$	$5{,}192 \cdot 10^{-2}$
$\varrho_{17}\kappa_1$	$4{,}102 \cdot 10^{-4}$	$8{,}547 \cdot 10^{-1}$	$-3{,}820 \cdot 10^{-1}$	$3{,}795 \cdot 10^{-4}$	$7{,}906 \cdot 10^{-1}$	$-3{,}499 \cdot 10^{-1}$
$\varrho_{17}\kappa_2$	$-2{,}566 \cdot 10^{-4}$	$-1{,}604 \cdot 10^{-1}$	$4{,}667 \cdot 10^{-2}$	$-3{,}180 \cdot 10^{-4}$	$-1{,}987 \cdot 10^{-1}$	$4{,}878 \cdot 10^{-2}$
$\varrho_{17}\kappa_3$	$-7{,}610 \cdot 10^{-5}$	$-1{,}585 \cdot 10^{-1}$	$1{,}551 \cdot 10^{-1}$	$1{,}607 \cdot 10^{-5}$	$3{,}349 \cdot 10^{-2}$	$-4{,}431 \cdot 10^{-2}$
$\varrho_{17}\kappa_4$	$-7{,}757 \cdot 10^{-5}$	$-4{,}848 \cdot 10^{-2}$	$1{,}934 \cdot 10^{-2}$	$-7{,}758 \cdot 10^{-5}$	$-4{,}849 \cdot 10^{-2}$	$1{,}934 \cdot 10^{-2}$

Table A.1: Flux tube element outputs ... *cont*

Element Region	$I_{(\mathrm{ph})} = \begin{bmatrix} 20 & -10 & -10 \end{bmatrix}^{\mathrm{T}}$					
	$x = 4\,\mathrm{mm}$			$x = 5\,\mathrm{mm}$		
	Φ [Wb]	B [T]	$\mathcal{F}$ [A]	Φ [Wb]	B [T]	$\mathcal{F}$ [A]
$e_{18}s_1$	$3{,}572 \cdot 10^{-4}$	$4{,}962 \cdot 10^{-1}$	$-2{,}441 \cdot 10^{-1}$	$3{,}243 \cdot 10^{-4}$	$4{,}504 \cdot 10^{-1}$	$-2{,}310 \cdot 10^{-1}$
$e_{18}s_2$	$-6{,}135 \cdot 10^{-4}$	$-3{,}835 \cdot 10^{-1}$	$9{,}634 \cdot 10^{-2}$	$-6{,}421 \cdot 10^{-4}$	$-4{,}013 \cdot 10^{-1}$	$9{,}824 \cdot 10^{-2}$
$e_{18}s_3$	$-2{,}640 \cdot 10^{-7}$	$-3{,}667 \cdot 10^{-4}$	$4{,}494 \cdot 10^{-4}$	$-1{,}565 \cdot 10^{-7}$	$-2{,}173 \cdot 10^{-4}$	$2{,}662 \cdot 10^{-4}$
$e_{18}s_4$	$2{,}566 \cdot 10^{-4}$	$1{,}604 \cdot 10^{-1}$	$-7{,}001 \cdot 10^{-2}$	$3{,}180 \cdot 10^{-4}$	$1{,}987 \cdot 10^{-1}$	$-7{,}317 \cdot 10^{-2}$
$e_{19}s_1$	$1{,}839 \cdot 10^{-4}$	$3{,}831 \cdot 10^{-1}$	$-2{,}140 \cdot 10^{-1}$	$1{,}664 \cdot 10^{-4}$	$3{,}467 \cdot 10^{-1}$	$-2{,}052 \cdot 10^{-1}$
$e_{19}s_2$	$-2{,}193 \cdot 10^{-4}$	$-1{,}371 \cdot 10^{-1}$	$4{,}415 \cdot 10^{-2}$	$-2{,}849 \cdot 10^{-4}$	$-1{,}781 \cdot 10^{-1}$	$4{,}781 \cdot 10^{-2}$
$e_{19}s_3$	$-5{,}781 \cdot 10^{-4}$	$-1{,}204$	$7{,}542 \cdot 10^{-1}$	$-5{,}235 \cdot 10^{-4}$	$-1{,}091$	$5{,}690 \cdot 10^{-1}$
$e_{19}s_4$	$6{,}135 \cdot 10^{-4}$	$3{,}835 \cdot 10^{-1}$	$-6{,}423 \cdot 10^{-2}$	$6{,}421 \cdot 10^{-4}$	$4{,}013 \cdot 10^{-1}$	$-6{,}549 \cdot 10^{-2}$
$e_{20}s_1$	$1{,}886 \cdot 10^{-4}$	$2{,}619 \cdot 10^{-1}$	$-1{,}784 \cdot 10^{-1}$	$1{,}811 \cdot 10^{-4}$	$2{,}516 \cdot 10^{-1}$	$-1{,}750 \cdot 10^{-1}$
$e_{20}s_2$	$-4{,}074 \cdot 10^{-4}$	$-2{,}546 \cdot 10^{-1}$	$7{,}920 \cdot 10^{-2}$	$-4{,}656 \cdot 10^{-4}$	$-2{,}910 \cdot 10^{-1}$	$8{,}483 \cdot 10^{-2}$
$e_{20}s_3$	$-4{,}858 \cdot 10^{-7}$	$-6{,}747 \cdot 10^{-4}$	$8{,}281 \cdot 10^{-4}$	$-4{,}650 \cdot 10^{-7}$	$-6{,}459 \cdot 10^{-4}$	$7{,}926 \cdot 10^{-4}$
$e_{20}s_4$	$2{,}193 \cdot 10^{-4}$	$1{,}371 \cdot 10^{-1}$	$-6{,}622 \cdot 10^{-2}$	$2{,}849 \cdot 10^{-4}$	$1{,}781 \cdot 10^{-1}$	$-7{,}172 \cdot 10^{-2}$
$e_{21}s_1$	$2{,}282 \cdot 10^{-4}$	$2{,}717 \cdot 10^{-1}$	$-1{,}817 \cdot 10^{-1}$	$2{,}346 \cdot 10^{-4}$	$2{,}793 \cdot 10^{-1}$	$-1{,}844 \cdot 10^{-1}$
$e_{21}s_2$	$-1{,}109 \cdot 10^{-5}$	$-6{,}929 \cdot 10^{-3}$	$4{,}566 \cdot 10^{-3}$	$-1{,}525 \cdot 10^{-5}$	$-9{,}532 \cdot 10^{-3}$	$6{,}332 \cdot 10^{-3}$
$e_{21}s_3$	$-6{,}245 \cdot 10^{-4}$	$-7{,}435 \cdot 10^{-1}$	$3{,}289 \cdot 10^{-1}$	$-6{,}850 \cdot 10^{-4}$	$-8{,}154 \cdot 10^{-1}$	$3{,}619 \cdot 10^{-1}$
$e_{21}s_4$	$4{,}074 \cdot 10^{-4}$	$2{,}546 \cdot 10^{-1}$	$-9{,}240 \cdot 10^{-2}$	$4{,}656 \cdot 10^{-4}$	$2{,}910 \cdot 10^{-1}$	$-9{,}897 \cdot 10^{-2}$
$e_{22}s_1$	$5{,}179 \cdot 10^{-5}$	$6{,}165 \cdot 10^{-2}$	$-8{,}136 \cdot 10^{-2}$	$8{,}433 \cdot 10^{-5}$	$1{,}004 \cdot 10^{-1}$	$-1{,}227 \cdot 10^{-1}$
$e_{22}s_2$	$-5{,}156 \cdot 10^{-5}$	$-3{,}223 \cdot 10^{-2}$	$2{,}236 \cdot 10^{-2}$	$-6{,}651 \cdot 10^{-5}$	$-4{,}157 \cdot 10^{-2}$	$2{,}901 \cdot 10^{-2}$
$e_{22}s_3$	$6{,}521 \cdot 10^{-6}$	$7{,}763 \cdot 10^{-3}$	$-9{,}770 \cdot 10^{-3}$	$-9{,}704 \cdot 10^{-6}$	$-1{,}155 \cdot 10^{-2}$	$1{,}470 \cdot 10^{-2}$
$e_{22}s_4$	$-6{,}749 \cdot 10^{-6}$	$-4{,}218 \cdot 10^{-3}$	$2{,}754 \cdot 10^{-3}$	$-8{,}113 \cdot 10^{-6}$	$-5{,}071 \cdot 10^{-3}$	$3{,}321 \cdot 10^{-3}$
$e_{23}s_1$	$-5{,}445 \cdot 10^{-4}$	$-1{,}134$	$6{,}250 \cdot 10^{-1}$	$-4{,}921 \cdot 10^{-4}$	$-1{,}025$	$5{,}019 \cdot 10^{-1}$
$e_{23}s_2$	$8{,}692 \cdot 10^{-5}$	$5{,}432 \cdot 10^{-2}$	$-2{,}163 \cdot 10^{-2}$	$8{,}447 \cdot 10^{-5}$	$5{,}280 \cdot 10^{-2}$	$-2{,}103 \cdot 10^{-2}$
$e_{23}s_3$	$3{,}045 \cdot 10^{-4}$	$6{,}344 \cdot 10^{-1}$	$-2{,}874 \cdot 10^{-1}$	$2{,}726 \cdot 10^{-4}$	$5{,}678 \cdot 10^{-1}$	$-2{,}657 \cdot 10^{-1}$
$e_{23}s_4$	$1{,}530 \cdot 10^{-4}$	$9{,}564 \cdot 10^{-2}$	$-3{,}555 \cdot 10^{-2}$	$1{,}351 \cdot 10^{-4}$	$8{,}442 \cdot 10^{-2}$	$-3{,}224 \cdot 10^{-2}$
$e_{24}s_1$	$-8{,}140 \cdot 10^{-4}$	$-1{,}696$	$2{,}691 \cdot 10^{1}$	$-8{,}212 \cdot 10^{-4}$	$-1{,}711$	$2{,}930 \cdot 10^{1}$
$e_{24}s_2$	$2{,}870 \cdot 10^{-4}$	$1{,}794 \cdot 10^{-1}$	$-4{,}788 \cdot 10^{-2}$	$2{,}942 \cdot 10^{-4}$	$1{,}839 \cdot 10^{-1}$	$-4{,}810 \cdot 10^{-2}$
$e_{24}s_3$	$3{,}720 \cdot 10^{-4}$	$7{,}750 \cdot 10^{-1}$	$-3{,}428 \cdot 10^{-1}$	$3{,}751 \cdot 10^{-4}$	$7{,}815 \cdot 10^{-1}$	$-3{,}457 \cdot 10^{-1}$
$e_{24}s_4$	$1{,}550 \cdot 10^{-4}$	$9{,}687 \cdot 10^{-2}$	$-3{,}588 \cdot 10^{-2}$	$1{,}519 \cdot 10^{-4}$	$9{,}491 \cdot 10^{-2}$	$-3{,}534 \cdot 10^{-2}$
$e_{25}s_1$	$7{,}610 \cdot 10^{-5}$	$1{,}585 \cdot 10^{-1}$	$-1{,}551 \cdot 10^{-1}$	$-1{,}607 \cdot 10^{-5}$	$-3{,}349 \cdot 10^{-2}$	$4{,}431 \cdot 10^{-2}$
$e_{25}s_2$	$7{,}800 \cdot 10^{-6}$	$4{,}875 \cdot 10^{-3}$	$-1{,}823 \cdot 10^{-3}$	$2{,}790 \cdot 10^{-5}$	$1{,}744 \cdot 10^{-2}$	$-6{,}756 \cdot 10^{-3}$
$e_{25}s_3$	$3{,}041 \cdot 10^{-5}$	$6{,}336 \cdot 10^{-2}$	$-8{,}347 \cdot 10^{-2}$	$8{,}498 \cdot 10^{-5}$	$1{,}770 \cdot 10^{-1}$	$-1{,}592 \cdot 10^{-1}$
$e_{25}s_4$	$-1{,}143 \cdot 10^{-4}$	$-7{,}145 \cdot 10^{-2}$	$2{,}794 \cdot 10^{-2}$	$-9{,}680 \cdot 10^{-5}$	$-6{,}050 \cdot 10^{-2}$	$2{,}398 \cdot 10^{-2}$
$e_{26}s_1$	$5{,}781 \cdot 10^{-4}$	$1{,}204$	$-7{,}542 \cdot 10^{-1}$	$5{,}235 \cdot 10^{-4}$	$1{,}091$	$-5{,}690 \cdot 10^{-1}$
$e_{26}s_2$	$-1{,}582 \cdot 10^{-4}$	$-9{,}890 \cdot 10^{-2}$	$3{,}643 \cdot 10^{-2}$	$-1{,}561 \cdot 10^{-4}$	$-9{,}755 \cdot 10^{-2}$	$3{,}607 \cdot 10^{-2}$
$e_{26}s_3$	$-3{,}109 \cdot 10^{-4}$	$-6{,}478 \cdot 10^{-1}$	$2{,}920 \cdot 10^{-1}$	$-2{,}788 \cdot 10^{-4}$	$-5{,}808 \cdot 10^{-1}$	$2{,}698 \cdot 10^{-1}$
$e_{26}s_4$	$-1{,}090 \cdot 10^{-4}$	$-6{,}809 \cdot 10^{-2}$	$2{,}676 \cdot 10^{-2}$	$-8{,}866 \cdot 10^{-5}$	$-5{,}541 \cdot 10^{-2}$	$2{,}205 \cdot 10^{-2}$
$e_{27}s_1$	$6{,}245 \cdot 10^{-4}$	$7{,}435 \cdot 10^{-1}$	$-3{,}289 \cdot 10^{-1}$	$6{,}850 \cdot 10^{-4}$	$8{,}154 \cdot 10^{-1}$	$-3{,}619 \cdot 10^{-1}$
$e_{27}s_2$	$-1{,}051 \cdot 10^{-4}$	$-6{,}567 \cdot 10^{-2}$	$4{,}530 \cdot 10^{-2}$	$-1{,}401 \cdot 10^{-4}$	$-8{,}753 \cdot 10^{-2}$	$5{,}809 \cdot 10^{-2}$
$e_{27}s_3$	$-4{,}527 \cdot 10^{-4}$	$-5{,}389 \cdot 10^{-1}$	$2{,}568 \cdot 10^{-1}$	$-4{,}788 \cdot 10^{-4}$	$-5{,}700 \cdot 10^{-1}$	$2{,}664 \cdot 10^{-1}$
$e_{27}s_4$	$-6{,}682 \cdot 10^{-5}$	$-4{,}176 \cdot 10^{-2}$	$2{,}915 \cdot 10^{-2}$	$-6{,}612 \cdot 10^{-5}$	$-4{,}133 \cdot 10^{-2}$	$2{,}884 \cdot 10^{-2}$
$e_{28}s_1$	$-1{,}459 \cdot 10^{-3}$	$-5{,}610 \cdot 10^{-1}$	$4{,}953 \cdot 10^{-1}$	$-1{,}447 \cdot 10^{-3}$	$-5{,}565 \cdot 10^{-1}$	$4{,}909 \cdot 10^{-1}$
$e_{28}s_2$	$1{,}373 \cdot 10^{-3}$	$1{,}526$	$-1{,}104 \cdot 10^{1}$	$1{,}365 \cdot 10^{-3}$	$1{,}517$	$-1{,}028 \cdot 10^{1}$
$e_{28}s_3$	$1{,}692 \cdot 10^{-5}$	$6{,}507 \cdot 10^{-3}$	$-5{,}497 \cdot 10^{-3}$	$1{,}662 \cdot 10^{-5}$	$6{,}393 \cdot 10^{-3}$	$-5{,}400 \cdot 10^{-3}$
$e_{28}s_4$	$6{,}867 \cdot 10^{-5}$	$7{,}630 \cdot 10^{-2}$	$-1{,}856 \cdot 10^{-1}$	$6{,}520 \cdot 10^{-5}$	$7{,}244 \cdot 10^{-2}$	$-1{,}762 \cdot 10^{-1}$
$e_{29}s_1$	$1{,}943 \cdot 10^{-5}$	$1{,}943 \cdot 10^{-2}$	$-1{,}640 \cdot 10^{-2}$	$3{,}061 \cdot 10^{-5}$	$3{,}061 \cdot 10^{-2}$	$-2{,}582 \cdot 10^{-2}$
$e_{29}s_2$	$1{,}352 \cdot 10^{-3}$	$1{,}503$	$-3{,}577$	$1{,}333 \cdot 10^{-3}$	$1{,}481$	$-3{,}165$
$e_{29}s_3$	$1{,}304 \cdot 10^{-6}$	$1{,}304 \cdot 10^{-3}$	$-1{,}102 \cdot 10^{-3}$	$1{,}202 \cdot 10^{-6}$	$1{,}202 \cdot 10^{-3}$	$-1{,}016 \cdot 10^{-3}$
$e_{29}s_4$	$-1{,}373 \cdot 10^{-3}$	$-1{,}526$	$4{,}245$	$-1{,}365 \cdot 10^{-3}$	$-1{,}517$	$3{,}954$
$e_{30}s_1$	$1{,}419 \cdot 10^{-3}$	$5{,}457 \cdot 10^{-1}$	$-4{,}804 \cdot 10^{-1}$	$1{,}407 \cdot 10^{-3}$	$5{,}412 \cdot 10^{-1}$	$-4{,}760 \cdot 10^{-1}$
$e_{30}s_2$	$-6{,}224 \cdot 10^{-5}$	$-6{,}916 \cdot 10^{-2}$	$1{,}683 \cdot 10^{-1}$	$-6{,}867 \cdot 10^{-5}$	$-7{,}630 \cdot 10^{-2}$	$1{,}856 \cdot 10^{-1}$
$e_{30}s_3$	$-4{,}253 \cdot 10^{-6}$	$-1{,}636 \cdot 10^{-3}$	$1{,}382 \cdot 10^{-3}$	$-5{,}127 \cdot 10^{-6}$	$-1{,}972 \cdot 10^{-3}$	$1{,}666 \cdot 10^{-3}$
$e_{30}s_4$	$-1{,}352 \cdot 10^{-3}$	$-1{,}503$	$9{,}300$	$-1{,}333 \cdot 10^{-3}$	$-1{,}481$	$8{,}229$

Table A.1: Flux tube element outputs ... *cont*

Element Region	$I_{(\mathrm{ph})} = \begin{bmatrix} -10 & 20 & -10 \end{bmatrix}^{\mathrm{T}}$					
	$x = 0\,\mathrm{mm}$			$x = 1\,\mathrm{mm}$		
	Φ [Wb]	B [T]	$\mathcal{F}$ [A]	Φ [Wb]	B [T]	$\mathcal{F}$ [A]
$\varrho_1\kappa_1$	$-1{,}313 \cdot 10^{-6}$	$-1{,}563 \cdot 10^{-3}$	$1{,}203 \cdot 10^{-3}$	$-1{,}374 \cdot 10^{-6}$	$-1{,}636 \cdot 10^{-3}$	$1{,}260 \cdot 10^{-3}$
$\varrho_1\kappa_2$	$-1{,}145 \cdot 10^{-4}$	$-1{,}145 \cdot 10^{-1}$	$7{,}029 \cdot 10^{-2}$	$-9{,}356 \cdot 10^{-5}$	$-9{,}356 \cdot 10^{-2}$	$6{,}118 \cdot 10^{-2}$
$\varrho_1\kappa_3$	$1{,}174 \cdot 10^{-4}$	$1{,}397 \cdot 10^{-1}$	$-9{,}273 \cdot 10^{-2}$	$9{,}660 \cdot 10^{-5}$	$1{,}150 \cdot 10^{-1}$	$-8{,}391 \cdot 10^{-2}$
$\varrho_1\kappa_4$	$-1{,}571 \cdot 10^{-6}$	$-1{,}571 \cdot 10^{-3}$	$1{,}016 \cdot 10^{-3}$	$-1{,}673 \cdot 10^{-6}$	$-1{,}673 \cdot 10^{-3}$	$1{,}082 \cdot 10^{-3}$
$\varrho_2\kappa_1$	$-6{,}750 \cdot 10^{-7}$	$-9{,}374 \cdot 10^{-4}$	$7{,}198 \cdot 10^{-4}$	$-7{,}090 \cdot 10^{-7}$	$-9{,}847 \cdot 10^{-4}$	$7{,}562 \cdot 10^{-4}$
$\varrho_2\kappa_2$	$-2{,}030 \cdot 10^{-4}$	$-2{,}030 \cdot 10^{-1}$	$7{,}348 \cdot 10^{-2}$	$-1{,}709 \cdot 10^{-4}$	$-1{,}709 \cdot 10^{-1}$	$7{,}111 \cdot 10^{-2}$
$\varrho_2\kappa_3$	$8{,}920 \cdot 10^{-5}$	$1{,}239 \cdot 10^{-1}$	$-8{,}756 \cdot 10^{-2}$	$7{,}804 \cdot 10^{-5}$	$1{,}084 \cdot 10^{-1}$	$-8{,}084 \cdot 10^{-2}$
$\varrho_2\kappa_4$	$1{,}145 \cdot 10^{-4}$	$1{,}145 \cdot 10^{-1}$	$-6{,}025 \cdot 10^{-2}$	$9{,}356 \cdot 10^{-5}$	$9{,}356 \cdot 10^{-2}$	$-5{,}244 \cdot 10^{-2}$
$\varrho_3\kappa_1$	$-3{,}987 \cdot 10^{-7}$	$-8{,}307 \cdot 10^{-4}$	$6{,}376 \cdot 10^{-4}$	$-4{,}189 \cdot 10^{-7}$	$-8{,}727 \cdot 10^{-4}$	$6{,}700 \cdot 10^{-4}$
$\varrho_3\kappa_2$	$-3{,}085 \cdot 10^{-4}$	$-3{,}085 \cdot 10^{-1}$	$5{,}831 \cdot 10^{-2}$	$-2{,}812 \cdot 10^{-4}$	$-2{,}812 \cdot 10^{-1}$	$5{,}552 \cdot 10^{-2}$
$\varrho_3\kappa_3$	$1{,}059 \cdot 10^{-4}$	$2{,}206 \cdot 10^{-1}$	$-1{,}042 \cdot 10^{-1}$	$1{,}107 \cdot 10^{-4}$	$2{,}307 \cdot 10^{-1}$	$-1{,}057 \cdot 10^{-1}$
$\varrho_3\kappa_4$	$2{,}030 \cdot 10^{-4}$	$2{,}030 \cdot 10^{-1}$	$-4{,}899 \cdot 10^{-2}$	$1{,}709 \cdot 10^{-4}$	$1{,}709 \cdot 10^{-1}$	$-4{,}741 \cdot 10^{-2}$
$\varrho_4\kappa_1$	$-5{,}617 \cdot 10^{-7}$	$-7{,}802 \cdot 10^{-4}$	$5{,}987 \cdot 10^{-4}$	$-5{,}925 \cdot 10^{-7}$	$-8{,}229 \cdot 10^{-4}$	$6{,}315 \cdot 10^{-4}$
$\varrho_4\kappa_2$	$-4{,}995 \cdot 10^{-4}$	$-4{,}995 \cdot 10^{-1}$	$1{,}103 \cdot 10^{-1}$	$-4{,}736 \cdot 10^{-4}$	$-4{,}736 \cdot 10^{-1}$	$1{,}069 \cdot 10^{-1}$
$\varrho_4\kappa_3$	$1{,}916 \cdot 10^{-4}$	$2{,}661 \cdot 10^{-1}$	$-1{,}124 \cdot 10^{-1}$	$1{,}930 \cdot 10^{-4}$	$2{,}680 \cdot 10^{-1}$	$-1{,}128 \cdot 10^{-1}$
$\varrho_4\kappa_4$	$3{,}085 \cdot 10^{-4}$	$3{,}085 \cdot 10^{-1}$	$-8{,}747 \cdot 10^{-2}$	$2{,}812 \cdot 10^{-4}$	$2{,}812 \cdot 10^{-1}$	$-8{,}327 \cdot 10^{-2}$
$\varrho_5\kappa_1$	$-3{,}621 \cdot 10^{-7}$	$-7{,}543 \cdot 10^{-4}$	$5{,}788 \cdot 10^{-4}$	$-3{,}835 \cdot 10^{-7}$	$-7{,}990 \cdot 10^{-4}$	$6{,}132 \cdot 10^{-4}$
$\varrho_5\kappa_2$	$-7{,}260 \cdot 10^{-4}$	$-7{,}260 \cdot 10^{-1}$	$9{,}647 \cdot 10^{-2}$	$-7{,}225 \cdot 10^{-4}$	$-7{,}225 \cdot 10^{-1}$	$9{,}604 \cdot 10^{-2}$
$\varrho_5\kappa_3$	$2{,}268 \cdot 10^{-4}$	$4{,}726 \cdot 10^{-1}$	$-1{,}483 \cdot 10^{-1}$	$2{,}493 \cdot 10^{-4}$	$5{,}193 \cdot 10^{-1}$	$-1{,}568 \cdot 10^{-1}$
$\varrho_5\kappa_4$	$4{,}995 \cdot 10^{-4}$	$4{,}995 \cdot 10^{-1}$	$-7{,}352 \cdot 10^{-2}$	$4{,}736 \cdot 10^{-4}$	$4{,}736 \cdot 10^{-1}$	$-7{,}125 \cdot 10^{-2}$
$\varrho_6\kappa_1$	$-5{,}233 \cdot 10^{-7}$	$-7{,}268 \cdot 10^{-4}$	$5{,}576 \cdot 10^{-4}$	$-5{,}565 \cdot 10^{-7}$	$-7{,}729 \cdot 10^{-4}$	$5{,}931 \cdot 10^{-4}$
$\varrho_6\kappa_2$	$-7{,}255 \cdot 10^{-4}$	$-7{,}255 \cdot 10^{-1}$	$1{,}446 \cdot 10^{-1}$	$-7{,}219 \cdot 10^{-4}$	$-7{,}219 \cdot 10^{-1}$	$1{,}440 \cdot 10^{-1}$
$\varrho_6\kappa_3$	$3{,}507 \cdot 10^{-9}$	$4{,}870 \cdot 10^{-6}$	$-3{,}726 \cdot 10^{-6}$	$5{,}814 \cdot 10^{-9}$	$8{,}074 \cdot 10^{-6}$	$-6{,}177 \cdot 10^{-6}$
$\varrho_6\kappa_4$	$7{,}260 \cdot 10^{-4}$	$7{,}260 \cdot 10^{-1}$	$-1{,}447 \cdot 10^{-1}$	$7{,}225 \cdot 10^{-4}$	$7{,}225 \cdot 10^{-1}$	$-1{,}441 \cdot 10^{-1}$
$\varrho_7\kappa_1$	$-3{,}455 \cdot 10^{-7}$	$-7{,}198 \cdot 10^{-4}$	$5{,}522 \cdot 10^{-4}$	$-3{,}698 \cdot 10^{-7}$	$-7{,}704 \cdot 10^{-4}$	$5{,}912 \cdot 10^{-4}$
$\varrho_7\kappa_2$	$-5{,}365 \cdot 10^{-4}$	$-5{,}365 \cdot 10^{-1}$	$7{,}683 \cdot 10^{-2}$	$-5{,}468 \cdot 10^{-4}$	$-5{,}468 \cdot 10^{-1}$	$7{,}778 \cdot 10^{-2}$
$\varrho_7\kappa_3$	$-1{,}886 \cdot 10^{-4}$	$-3{,}930 \cdot 10^{-1}$	$1{,}352 \cdot 10^{-1}$	$-1{,}747 \cdot 10^{-4}$	$-3{,}639 \cdot 10^{-1}$	$1{,}309 \cdot 10^{-1}$
$\varrho_7\kappa_4$	$7{,}255 \cdot 10^{-4}$	$7{,}255 \cdot 10^{-1}$	$-9{,}641 \cdot 10^{-2}$	$7{,}219 \cdot 10^{-4}$	$7{,}219 \cdot 10^{-1}$	$-9{,}597 \cdot 10^{-2}$
$\varrho_8\kappa_1$	$-5{,}488 \cdot 10^{-7}$	$-7{,}622 \cdot 10^{-4}$	$5{,}848 \cdot 10^{-4}$	$-5{,}900 \cdot 10^{-7}$	$-8{,}194 \cdot 10^{-4}$	$6{,}289 \cdot 10^{-4}$
$\varrho_8\kappa_2$	$-3{,}600 \cdot 10^{-4}$	$-3{,}600 \cdot 10^{-1}$	$9{,}383 \cdot 10^{-2}$	$-3{,}806 \cdot 10^{-4}$	$-3{,}806 \cdot 10^{-1}$	$9{,}604 \cdot 10^{-2}$
$\varrho_8\kappa_3$	$-1{,}759 \cdot 10^{-4}$	$-2{,}443 \cdot 10^{-1}$	$1{,}080 \cdot 10^{-1}$	$-1{,}657 \cdot 10^{-4}$	$-2{,}301 \cdot 10^{-1}$	$1{,}056 \cdot 10^{-1}$
$\varrho_8\kappa_4$	$5{,}365 \cdot 10^{-4}$	$5{,}365 \cdot 10^{-1}$	$-1{,}152 \cdot 10^{-1}$	$5{,}468 \cdot 10^{-4}$	$5{,}468 \cdot 10^{-1}$	$-1{,}167 \cdot 10^{-1}$
$\varrho_9\kappa_1$	$-4{,}056 \cdot 10^{-7}$	$-8{,}450 \cdot 10^{-4}$	$6{,}486 \cdot 10^{-4}$	$-4{,}374 \cdot 10^{-7}$	$-9{,}112 \cdot 10^{-4}$	$6{,}996 \cdot 10^{-4}$
$\varrho_9\kappa_2$	$-2{,}562 \cdot 10^{-4}$	$-2{,}562 \cdot 10^{-1}$	$5{,}295 \cdot 10^{-2}$	$-2{,}789 \cdot 10^{-4}$	$-2{,}789 \cdot 10^{-1}$	$5{,}527 \cdot 10^{-2}$
$\varrho_9\kappa_3$	$-1{,}034 \cdot 10^{-4}$	$-2{,}154 \cdot 10^{-1}$	$1{,}035 \cdot 10^{-1}$	$-1{,}012 \cdot 10^{-4}$	$-2{,}109 \cdot 10^{-1}$	$1{,}030 \cdot 10^{-1}$
$\varrho_9\kappa_4$	$3{,}600 \cdot 10^{-4}$	$3{,}600 \cdot 10^{-1}$	$-6{,}256 \cdot 10^{-2}$	$3{,}806 \cdot 10^{-4}$	$3{,}806 \cdot 10^{-1}$	$-6{,}402 \cdot 10^{-2}$
$\varrho_{10}\kappa_1$	$-7{,}260 \cdot 10^{-7}$	$-1{,}008 \cdot 10^{-3}$	$7{,}745 \cdot 10^{-4}$	$-7{,}852 \cdot 10^{-7}$	$-1{,}091 \cdot 10^{-3}$	$8{,}379 \cdot 10^{-4}$
$\varrho_{10}\kappa_2$	$-1{,}490 \cdot 10^{-4}$	$-1{,}490 \cdot 10^{-1}$	$6{,}843 \cdot 10^{-2}$	$-1{,}688 \cdot 10^{-4}$	$-1{,}688 \cdot 10^{-1}$	$7{,}092 \cdot 10^{-2}$
$\varrho_{10}\kappa_3$	$-1{,}065 \cdot 10^{-4}$	$-1{,}479 \cdot 10^{-1}$	$9{,}480 \cdot 10^{-2}$	$-1{,}093 \cdot 10^{-4}$	$-1{,}518 \cdot 10^{-1}$	$9{,}565 \cdot 10^{-2}$
$\varrho_{10}\kappa_4$	$2{,}562 \cdot 10^{-4}$	$2{,}562 \cdot 10^{-1}$	$-7{,}943 \cdot 10^{-2}$	$2{,}789 \cdot 10^{-4}$	$2{,}789 \cdot 10^{-1}$	$-8{,}291 \cdot 10^{-2}$
$\varrho_{11}\kappa_1$	$-1{,}629 \cdot 10^{-6}$	$-1{,}939 \cdot 10^{-3}$	$1{,}495 \cdot 10^{-3}$	$-1{,}781 \cdot 10^{-6}$	$-2{,}121 \cdot 10^{-3}$	$1{,}636 \cdot 10^{-3}$
$\varrho_{11}\kappa_2$	$-2{,}708 \cdot 10^{-6}$	$-2{,}708 \cdot 10^{-3}$	$1{,}759 \cdot 10^{-3}$	$-3{,}031 \cdot 10^{-6}$	$-3{,}031 \cdot 10^{-3}$	$1{,}971 \cdot 10^{-3}$
$\varrho_{11}\kappa_3$	$-1{,}446 \cdot 10^{-4}$	$-1{,}722 \cdot 10^{-1}$	$9{,}893 \cdot 10^{-2}$	$-1{,}640 \cdot 10^{-4}$	$-1{,}952 \cdot 10^{-1}$	$1{,}013 \cdot 10^{-1}$
$\varrho_{11}\kappa_4$	$1{,}490 \cdot 10^{-4}$	$1{,}490 \cdot 10^{-1}$	$-7{,}983 \cdot 10^{-2}$	$1{,}688 \cdot 10^{-4}$	$1{,}688 \cdot 10^{-1}$	$-8{,}274 \cdot 10^{-2}$
$\varrho_{12}\kappa_1$	$-1{,}174 \cdot 10^{-4}$	$-1{,}397 \cdot 10^{-1}$	$1{,}484 \cdot 10^{-1}$	$-9{,}660 \cdot 10^{-5}$	$-1{,}150 \cdot 10^{-1}$	$1{,}343 \cdot 10^{-1}$
$\varrho_{12}\kappa_2$	$-2{,}211 \cdot 10^{-4}$	$-1{,}382 \cdot 10^{-1}$	$7{,}753 \cdot 10^{-2}$	$-1{,}644 \cdot 10^{-4}$	$-1{,}027 \cdot 10^{-1}$	$6{,}549 \cdot 10^{-2}$
$\varrho_{12}\kappa_3$	$3{,}402 \cdot 10^{-4}$	$4{,}050 \cdot 10^{-1}$	$-2{,}192 \cdot 10^{-1}$	$2{,}629 \cdot 10^{-4}$	$3{,}130 \cdot 10^{-1}$	$-1{,}958 \cdot 10^{-1}$
$\varrho_{12}\kappa_4$	$-1{,}722 \cdot 10^{-6}$	$-1{,}076 \cdot 10^{-3}$	$6{,}944 \cdot 10^{-4}$	$-1{,}956 \cdot 10^{-6}$	$-1{,}222 \cdot 10^{-3}$	$7{,}892 \cdot 10^{-4}$
$\varrho_{13}\kappa_1$	$-8{,}920 \cdot 10^{-5}$	$-1{,}239 \cdot 10^{-1}$	$1{,}401 \cdot 10^{-1}$	$-7{,}804 \cdot 10^{-5}$	$-1{,}084 \cdot 10^{-1}$	$1{,}293 \cdot 10^{-1}$
$\varrho_{13}\kappa_2$	$-1{,}322 \cdot 10^{-4}$	$-8{,}265 \cdot 10^{-2}$	$4{,}752 \cdot 10^{-2}$	$-8{,}665 \cdot 10^{-5}$	$-5{,}416 \cdot 10^{-2}$	$3{,}234 \cdot 10^{-2}$
$\varrho_{13}\kappa_3$	$3{,}539 \cdot 10^{-7}$	$4{,}915 \cdot 10^{-4}$	$-6{,}028 \cdot 10^{-4}$	$3{,}369 \cdot 10^{-7}$	$4{,}679 \cdot 10^{-4}$	$-5{,}737 \cdot 10^{-4}$
$\varrho_{13}\kappa_4$	$2{,}211 \cdot 10^{-4}$	$1{,}382 \cdot 10^{-1}$	$-6{,}646 \cdot 10^{-2}$	$1{,}644 \cdot 10^{-4}$	$1{,}027 \cdot 10^{-1}$	$-5{,}613 \cdot 10^{-2}$
$\varrho_{14}\kappa_1$	$-1{,}059 \cdot 10^{-4}$	$-2{,}206 \cdot 10^{-1}$	$1{,}667 \cdot 10^{-1}$	$-1{,}107 \cdot 10^{-4}$	$-2{,}307 \cdot 10^{-1}$	$1{,}691 \cdot 10^{-1}$
$\varrho_{14}\kappa_2$	$-3{,}481 \cdot 10^{-4}$	$-2{,}175 \cdot 10^{-1}$	$4{,}982 \cdot 10^{-2}$	$-2{,}957 \cdot 10^{-4}$	$-1{,}848 \cdot 10^{-1}$	$4{,}814 \cdot 10^{-2}$
$\varrho_{14}\kappa_3$	$3{,}217 \cdot 10^{-4}$	$6{,}702 \cdot 10^{-1}$	$-3{,}000 \cdot 10^{-1}$	$3{,}198 \cdot 10^{-4}$	$6{,}662 \cdot 10^{-1}$	$-2{,}986 \cdot 10^{-1}$
$\varrho_{14}\kappa_4$	$1{,}322 \cdot 10^{-4}$	$8{,}265 \cdot 10^{-2}$	$-3{,}168 \cdot 10^{-2}$	$8{,}665 \cdot 10^{-5}$	$5{,}416 \cdot 10^{-2}$	$-2{,}156 \cdot 10^{-2}$

Table A.1: Flux tube element outputs ... *cont*

Element Region	$I_{(\mathrm{ph})} = \begin{bmatrix} -10 & 20 & -10 \end{bmatrix}^{\mathrm{T}}$					
	$x = 0\,\mathrm{mm}$			$x = 1\,\mathrm{mm}$		
	Φ [Wb]	B [T]	$\mathcal{F}$ [A]	Φ [Wb]	B [T]	$\mathcal{F}$ [A]
$e_{15}\xi_1$	$-1{,}916 \cdot 10^{-4}$	$-2{,}661 \cdot 10^{-1}$	$1{,}798 \cdot 10^{-1}$	$-1{,}930 \cdot 10^{-4}$	$-2{,}680 \cdot 10^{-1}$	$1{,}804 \cdot 10^{-1}$
$e_{15}\xi_2$	$-1{,}568 \cdot 10^{-4}$	$-9{,}801 \cdot 10^{-2}$	$5{,}429 \cdot 10^{-2}$	$-1{,}031 \cdot 10^{-4}$	$-6{,}443 \cdot 10^{-2}$	$3{,}815 \cdot 10^{-2}$
$e_{15}\xi_3$	$3{,}293 \cdot 10^{-7}$	$4{,}574 \cdot 10^{-4}$	$-5{,}609 \cdot 10^{-4}$	$3{,}470 \cdot 10^{-7}$	$4{,}820 \cdot 10^{-4}$	$-5{,}911 \cdot 10^{-4}$
$e_{15}\xi_4$	$3{,}481 \cdot 10^{-4}$	$2{,}175 \cdot 10^{-1}$	$-7{,}473 \cdot 10^{-2}$	$2{,}957 \cdot 10^{-4}$	$1{,}848 \cdot 10^{-1}$	$-7{,}222 \cdot 10^{-2}$
$e_{16}\xi_1$	$-2{,}268 \cdot 10^{-4}$	$-4{,}726 \cdot 10^{-1}$	$2{,}372 \cdot 10^{-1}$	$-2{,}493 \cdot 10^{-4}$	$-5{,}193 \cdot 10^{-1}$	$2{,}509 \cdot 10^{-1}$
$e_{16}\xi_2$	$-4{,}225 \cdot 10^{-5}$	$-2{,}641 \cdot 10^{-2}$	$1{,}040 \cdot 10^{-2}$	$-4{,}223 \cdot 10^{-5}$	$-2{,}640 \cdot 10^{-2}$	$1{,}039 \cdot 10^{-2}$
$e_{16}\xi_3$	$1{,}123 \cdot 10^{-4}$	$2{,}339 \cdot 10^{-1}$	$-1{,}699 \cdot 10^{-1}$	$1{,}884 \cdot 10^{-4}$	$3{,}925 \cdot 10^{-1}$	$-2{,}162 \cdot 10^{-1}$
$e_{16}\xi_4$	$1{,}568 \cdot 10^{-4}$	$9{,}801 \cdot 10^{-2}$	$-3{,}619 \cdot 10^{-2}$	$1{,}031 \cdot 10^{-4}$	$6{,}443 \cdot 10^{-2}$	$-2{,}543 \cdot 10^{-2}$
$e_{17}\xi_1$	$1{,}886 \cdot 10^{-4}$	$3{,}930 \cdot 10^{-1}$	$-2{,}163 \cdot 10^{-1}$	$1{,}747 \cdot 10^{-4}$	$3{,}639 \cdot 10^{-1}$	$-2{,}095 \cdot 10^{-1}$
$e_{17}\xi_2$	$-3{,}103 \cdot 10^{-4}$	$-1{,}939 \cdot 10^{-1}$	$4{,}856 \cdot 10^{-2}$	$-3{,}833 \cdot 10^{-4}$	$-2{,}396 \cdot 10^{-1}$	$5{,}144 \cdot 10^{-2}$
$e_{17}\xi_3$	$7{,}937 \cdot 10^{-5}$	$1{,}654 \cdot 10^{-1}$	$-1{,}568 \cdot 10^{-1}$	$1{,}663 \cdot 10^{-4}$	$3{,}464 \cdot 10^{-1}$	$-2{,}051 \cdot 10^{-1}$
$e_{17}\xi_4$	$4{,}230 \cdot 10^{-5}$	$2{,}644 \cdot 10^{-2}$	$-1{,}041 \cdot 10^{-2}$	$4{,}232 \cdot 10^{-5}$	$2{,}645 \cdot 10^{-2}$	$-1{,}042 \cdot 10^{-2}$
$e_{18}\xi_1$	$1{,}759 \cdot 10^{-4}$	$2{,}443 \cdot 10^{-1}$	$-1{,}728 \cdot 10^{-1}$	$1{,}657 \cdot 10^{-4}$	$2{,}301 \cdot 10^{-1}$	$-1{,}690 \cdot 10^{-1}$
$e_{18}\xi_2$	$-4{,}860 \cdot 10^{-4}$	$-3{,}037 \cdot 10^{-1}$	$8{,}678 \cdot 10^{-2}$	$-5{,}487 \cdot 10^{-4}$	$-3{,}429 \cdot 10^{-1}$	$9{,}191 \cdot 10^{-2}$
$e_{18}\xi_3$	$-2{,}651 \cdot 10^{-7}$	$-3{,}682 \cdot 10^{-4}$	$4{,}514 \cdot 10^{-4}$	$-2{,}421 \cdot 10^{-7}$	$-3{,}363 \cdot 10^{-4}$	$4{,}122 \cdot 10^{-4}$
$e_{18}\xi_4$	$3{,}103 \cdot 10^{-4}$	$1{,}939 \cdot 10^{-1}$	$-7{,}284 \cdot 10^{-2}$	$3{,}833 \cdot 10^{-4}$	$2{,}396 \cdot 10^{-1}$	$-7{,}716 \cdot 10^{-2}$
$e_{19}\xi_1$	$1{,}034 \cdot 10^{-4}$	$2{,}154 \cdot 10^{-1}$	$-1{,}656 \cdot 10^{-1}$	$1{,}012 \cdot 10^{-4}$	$2{,}109 \cdot 10^{-1}$	$-1{,}647 \cdot 10^{-1}$
$e_{19}\xi_2$	$-2{,}165 \cdot 10^{-4}$	$-1{,}353 \cdot 10^{-1}$	$4{,}390 \cdot 10^{-2}$	$-2{,}809 \cdot 10^{-4}$	$-1{,}755 \cdot 10^{-1}$	$4{,}768 \cdot 10^{-2}$
$e_{19}\xi_3$	$-3{,}728 \cdot 10^{-4}$	$-7{,}767 \cdot 10^{-1}$	$3{,}435 \cdot 10^{-1}$	$-3{,}691 \cdot 10^{-4}$	$-7{,}690 \cdot 10^{-1}$	$3{,}400 \cdot 10^{-1}$
$e_{19}\xi_4$	$4{,}860 \cdot 10^{-4}$	$3{,}037 \cdot 10^{-1}$	$-5{,}785 \cdot 10^{-2}$	$5{,}487 \cdot 10^{-4}$	$3{,}429 \cdot 10^{-1}$	$-6{,}127 \cdot 10^{-2}$
$e_{20}\xi_1$	$1{,}065 \cdot 10^{-4}$	$1{,}479 \cdot 10^{-1}$	$-1{,}517 \cdot 10^{-1}$	$1{,}093 \cdot 10^{-4}$	$1{,}518 \cdot 10^{-1}$	$-1{,}530 \cdot 10^{-1}$
$e_{20}\xi_2$	$-3{,}227 \cdot 10^{-4}$	$-2{,}017 \cdot 10^{-1}$	$7{,}338 \cdot 10^{-2}$	$-3{,}898 \cdot 10^{-4}$	$-2{,}436 \cdot 10^{-1}$	$7{,}768 \cdot 10^{-2}$
$e_{20}\xi_3$	$-3{,}837 \cdot 10^{-7}$	$-5{,}329 \cdot 10^{-4}$	$6{,}536 \cdot 10^{-4}$	$-3{,}950 \cdot 10^{-7}$	$-5{,}487 \cdot 10^{-4}$	$6{,}730 \cdot 10^{-4}$
$e_{20}\xi_4$	$2{,}165 \cdot 10^{-4}$	$1{,}353 \cdot 10^{-1}$	$-6{,}586 \cdot 10^{-2}$	$2{,}809 \cdot 10^{-4}$	$1{,}755 \cdot 10^{-1}$	$-7{,}152 \cdot 10^{-2}$
$e_{21}\xi_1$	$1{,}446 \cdot 10^{-4}$	$1{,}722 \cdot 10^{-1}$	$-1{,}583 \cdot 10^{-1}$	$1{,}640 \cdot 10^{-4}$	$1{,}952 \cdot 10^{-1}$	$-1{,}621 \cdot 10^{-1}$
$e_{21}\xi_2$	$-4{,}730 \cdot 10^{-6}$	$-2{,}956 \cdot 10^{-3}$	$1{,}922 \cdot 10^{-3}$	$-5{,}524 \cdot 10^{-6}$	$-3{,}453 \cdot 10^{-3}$	$2{,}248 \cdot 10^{-3}$
$e_{21}\xi_3$	$-4{,}626 \cdot 10^{-4}$	$-5{,}507 \cdot 10^{-1}$	$2{,}604 \cdot 10^{-1}$	$-5{,}483 \cdot 10^{-4}$	$-6{,}527 \cdot 10^{-1}$	$2{,}938 \cdot 10^{-1}$
$e_{21}\xi_4$	$3{,}227 \cdot 10^{-4}$	$2{,}017 \cdot 10^{-1}$	$-8{,}561 \cdot 10^{-2}$	$3{,}898 \cdot 10^{-4}$	$2{,}436 \cdot 10^{-1}$	$-9{,}063 \cdot 10^{-2}$
$e_{22}\xi_1$	$-3{,}402 \cdot 10^{-4}$	$-4{,}050 \cdot 10^{-1}$	$2{,}192 \cdot 10^{-1}$	$-2{,}629 \cdot 10^{-4}$	$-3{,}130 \cdot 10^{-1}$	$1{,}958 \cdot 10^{-1}$
$e_{22}\xi_2$	$1{,}302 \cdot 10^{-4}$	$8{,}136 \cdot 10^{-2}$	$-5{,}472 \cdot 10^{-2}$	$1{,}216 \cdot 10^{-4}$	$7{,}602 \cdot 10^{-2}$	$-5{,}164 \cdot 10^{-2}$
$e_{22}\xi_3$	$2{,}052 \cdot 10^{-4}$	$2{,}442 \cdot 10^{-1}$	$-1{,}728 \cdot 10^{-1}$	$1{,}401 \cdot 10^{-4}$	$1{,}668 \cdot 10^{-1}$	$-1{,}572 \cdot 10^{-1}$
$e_{22}\xi_4$	$4{,}828 \cdot 10^{-6}$	$3{,}018 \cdot 10^{-3}$	$-1{,}962 \cdot 10^{-3}$	$1{,}138 \cdot 10^{-6}$	$7{,}116 \cdot 10^{-4}$	$-4{,}585 \cdot 10^{-4}$
$e_{23}\xi_1$	$-3{,}217 \cdot 10^{-4}$	$-6{,}702 \cdot 10^{-1}$	$3{,}000 \cdot 10^{-1}$	$-3{,}198 \cdot 10^{-4}$	$-6{,}662 \cdot 10^{-1}$	$2{,}986 \cdot 10^{-1}$
$e_{23}\xi_2$	$4{,}245 \cdot 10^{-5}$	$2{,}653 \cdot 10^{-2}$	$-1{,}045 \cdot 10^{-2}$	$4{,}461 \cdot 10^{-5}$	$2{,}788 \cdot 10^{-2}$	$-1{,}100 \cdot 10^{-2}$
$e_{23}\xi_3$	$2{,}356 \cdot 10^{-4}$	$4{,}908 \cdot 10^{-1}$	$-2{,}425 \cdot 10^{-1}$	$2{,}343 \cdot 10^{-4}$	$4{,}880 \cdot 10^{-1}$	$-2{,}417 \cdot 10^{-1}$
$e_{23}\xi_4$	$4{,}366 \cdot 10^{-5}$	$2{,}729 \cdot 10^{-2}$	$-1{,}076 \cdot 10^{-2}$	$4{,}092 \cdot 10^{-5}$	$2{,}557 \cdot 10^{-2}$	$-1{,}006 \cdot 10^{-2}$
$e_{24}\xi_1$	$-1{,}123 \cdot 10^{-4}$	$-2{,}339 \cdot 10^{-1}$	$1{,}699 \cdot 10^{-1}$	$-1{,}884 \cdot 10^{-4}$	$-3{,}925 \cdot 10^{-1}$	$2{,}162 \cdot 10^{-1}$
$e_{24}\xi_2$	$-1{,}584 \cdot 10^{-4}$	$-9{,}903 \cdot 10^{-2}$	$3{,}646 \cdot 10^{-2}$	$-1{,}371 \cdot 10^{-4}$	$-8{,}569 \cdot 10^{-2}$	$3{,}263 \cdot 10^{-2}$
$e_{24}\xi_3$	$1{,}417 \cdot 10^{-4}$	$2{,}952 \cdot 10^{-1}$	$-1{,}900 \cdot 10^{-1}$	$1{,}919 \cdot 10^{-4}$	$3{,}998 \cdot 10^{-1}$	$-2{,}180 \cdot 10^{-1}$
$e_{24}\xi_4$	$1{,}290 \cdot 10^{-4}$	$8{,}062 \cdot 10^{-2}$	$-3{,}103 \cdot 10^{-2}$	$1{,}336 \cdot 10^{-4}$	$8{,}351 \cdot 10^{-2}$	$-3{,}195 \cdot 10^{-2}$
$e_{25}\xi_1$	$-7{,}937 \cdot 10^{-5}$	$-1{,}654 \cdot 10^{-1}$	$1{,}568 \cdot 10^{-1}$	$-1{,}663 \cdot 10^{-4}$	$-3{,}464 \cdot 10^{-1}$	$2{,}051 \cdot 10^{-1}$
$e_{25}\xi_2$	$-2{,}763 \cdot 10^{-5}$	$-1{,}727 \cdot 10^{-2}$	$6{,}687 \cdot 10^{-3}$	$-1{,}783 \cdot 10^{-5}$	$-1{,}115 \cdot 10^{-2}$	$4{,}251 \cdot 10^{-3}$
$e_{25}\xi_3$	$-7{,}245 \cdot 10^{-5}$	$-1{,}509 \cdot 10^{-1}$	$1{,}527 \cdot 10^{-1}$	$-1{,}200 \cdot 10^{-5}$	$-2{,}499 \cdot 10^{-2}$	$3{,}273 \cdot 10^{-2}$
$e_{25}\xi_4$	$1{,}794 \cdot 10^{-4}$	$1{,}122 \cdot 10^{-1}$	$-3{,}966 \cdot 10^{-2}$	$1{,}961 \cdot 10^{-4}$	$1{,}226 \cdot 10^{-1}$	$-4{,}179 \cdot 10^{-2}$
$e_{26}\xi_1$	$3{,}728 \cdot 10^{-4}$	$7{,}767 \cdot 10^{-1}$	$-3{,}435 \cdot 10^{-1}$	$3{,}691 \cdot 10^{-4}$	$7{,}690 \cdot 10^{-1}$	$-3{,}400 \cdot 10^{-1}$
$e_{26}\xi_2$	$-4{,}784 \cdot 10^{-6}$	$-2{,}990 \cdot 10^{-3}$	$1{,}111 \cdot 10^{-3}$	$-6{,}338 \cdot 10^{-6}$	$-3{,}961 \cdot 10^{-3}$	$1{,}477 \cdot 10^{-3}$
$e_{26}\xi_3$	$-2{,}434 \cdot 10^{-4}$	$-5{,}072 \cdot 10^{-1}$	$2{,}473 \cdot 10^{-1}$	$-2{,}418 \cdot 10^{-4}$	$-5{,}038 \cdot 10^{-1}$	$2{,}463 \cdot 10^{-1}$
$e_{26}\xi_4$	$-1{,}246 \cdot 10^{-4}$	$-7{,}786 \cdot 10^{-2}$	$3{,}013 \cdot 10^{-2}$	$-1{,}210 \cdot 10^{-4}$	$-7{,}560 \cdot 10^{-2}$	$2{,}937 \cdot 10^{-2}$
$e_{27}\xi_1$	$4{,}626 \cdot 10^{-4}$	$5{,}507 \cdot 10^{-1}$	$-2{,}604 \cdot 10^{-1}$	$5{,}483 \cdot 10^{-4}$	$6{,}527 \cdot 10^{-1}$	$-2{,}938 \cdot 10^{-1}$
$e_{27}\xi_2$	$-2{,}425 \cdot 10^{-5}$	$-1{,}516 \cdot 10^{-2}$	$1{,}022 \cdot 10^{-2}$	$-3{,}213 \cdot 10^{-5}$	$-2{,}008 \cdot 10^{-2}$	$1{,}369 \cdot 10^{-2}$
$e_{27}\xi_3$	$-2{,}563 \cdot 10^{-4}$	$-3{,}051 \cdot 10^{-1}$	$1{,}933 \cdot 10^{-1}$	$-3{,}299 \cdot 10^{-4}$	$-3{,}928 \cdot 10^{-1}$	$2{,}163 \cdot 10^{-1}$
$e_{27}\xi_4$	$-1{,}820 \cdot 10^{-4}$	$-1{,}138 \cdot 10^{-1}$	$7{,}003 \cdot 10^{-2}$	$-1{,}862 \cdot 10^{-4}$	$-1{,}164 \cdot 10^{-1}$	$7{,}099 \cdot 10^{-2}$
$e_{28}\xi_1$	$-1{,}205 \cdot 10^{-3}$	$-4{,}636 \cdot 10^{-1}$	$4{,}025 \cdot 10^{-1}$	$-1{,}212 \cdot 10^{-3}$	$-4{,}661 \cdot 10^{-1}$	$4{,}048 \cdot 10^{-1}$
$e_{28}\xi_2$	$1{,}119 \cdot 10^{-3}$	$1{,}244$	$-4{,}325$	$1{,}124 \cdot 10^{-3}$	$1{,}249$	$-4{,}367$
$e_{28}\xi_3$	$1{,}473 \cdot 10^{-5}$	$5{,}666 \cdot 10^{-3}$	$-4{,}786 \cdot 10^{-3}$	$1{,}454 \cdot 10^{-5}$	$5{,}592 \cdot 10^{-3}$	$-4{,}724 \cdot 10^{-3}$
$e_{28}\xi_4$	$7{,}125 \cdot 10^{-5}$	$7{,}916 \cdot 10^{-2}$	$-1{,}926 \cdot 10^{-1}$	$7{,}309 \cdot 10^{-5}$	$8{,}121 \cdot 10^{-2}$	$-1{,}975 \cdot 10^{-1}$

Table A.1: Flux tube element outputs ... *cont*

Element Region	$I_{(\mathrm{ph})} = \begin{bmatrix} -10 & 20 & -10 \end{bmatrix}^{\mathrm{T}}$					
	$x = 0\,\mathrm{mm}$			$x = 1\,\mathrm{mm}$		
	Φ [Wb]	B [T]	$\mathcal{F}$ [A]	Φ [Wb]	B [T]	$\mathcal{F}$ [A]
$e_{29}k_1$	$-3{,}840 \cdot 10^{-5}$	$-3{,}840 \cdot 10^{-2}$	$3{,}238 \cdot 10^{-2}$	$-5{,}566 \cdot 10^{-5}$	$-5{,}566 \cdot 10^{-2}$	$4{,}689 \cdot 10^{-2}$
$e_{29}k_2$	$1{,}156 \cdot 10^{-3}$	$1{,}284$	$-1{,}793$	$1{,}178 \cdot 10^{-3}$	$1{,}309$	$-1{,}883$
$e_{29}k_3$	$2{,}094 \cdot 10^{-6}$	$2{,}094 \cdot 10^{-3}$	$-1{,}770 \cdot 10^{-3}$	$2{,}010 \cdot 10^{-6}$	$2{,}010 \cdot 10^{-3}$	$-1{,}698 \cdot 10^{-3}$
$e_{29}k_4$	$-1{,}119 \cdot 10^{-3}$	$-1{,}244$	$1{,}664$	$-1{,}124 \cdot 10^{-3}$	$-1{,}249$	$1{,}680$
$e_{30}k_1$	$1{,}193 \cdot 10^{-3}$	$4{,}589 \cdot 10^{-1}$	$-3{,}982 \cdot 10^{-1}$	$1{,}218 \cdot 10^{-3}$	$4{,}685 \cdot 10^{-1}$	$-4{,}071 \cdot 10^{-1}$
$e_{30}k_2$	$-4{,}112 \cdot 10^{-5}$	$-4{,}568 \cdot 10^{-2}$	$1{,}112 \cdot 10^{-1}$	$-4{,}291 \cdot 10^{-5}$	$-4{,}767 \cdot 10^{-2}$	$1{,}161 \cdot 10^{-1}$
$e_{30}k_3$	$3{,}571 \cdot 10^{-6}$	$1{,}374 \cdot 10^{-3}$	$-1{,}161 \cdot 10^{-3}$	$2{,}690 \cdot 10^{-6}$	$1{,}035 \cdot 10^{-3}$	$-8{,}743 \cdot 10^{-4}$
$e_{30}k_4$	$-1{,}156 \cdot 10^{-3}$	$-1{,}284$	$4{,}661$	$-1{,}178 \cdot 10^{-3}$	$-1{,}309$	$4{,}896$

Table A.1: Flux tube element outputs ... *cont*

Element Region	$I_{(\mathrm{ph})} = \begin{bmatrix} -10 & 20 & -10 \end{bmatrix}^{\mathrm{T}}$					
	$x = 2\,\mathrm{mm}$			$x = 3\,\mathrm{mm}$		
	Φ [Wb]	B [T]	$\mathcal{F}$ [A]	Φ [Wb]	B [T]	$\mathcal{F}$ [A]
e_1k_1	$-1{,}471 \cdot 10^{-6}$	$-1{,}751 \cdot 10^{-3}$	$1{,}349 \cdot 10^{-3}$	$-1{,}624 \cdot 10^{-6}$	$-1{,}933 \cdot 10^{-3}$	$1{,}490 \cdot 10^{-3}$
e_1k_2	$-7{,}496 \cdot 10^{-5}$	$-7{,}496 \cdot 10^{-2}$	$5{,}102 \cdot 10^{-2}$	$-5{,}949 \cdot 10^{-5}$	$-5{,}949 \cdot 10^{-2}$	$4{,}130 \cdot 10^{-2}$
e_1k_3	$7{,}824 \cdot 10^{-5}$	$9{,}314 \cdot 10^{-2}$	$-7{,}259 \cdot 10^{-2}$	$6{,}310 \cdot 10^{-5}$	$7{,}512 \cdot 10^{-2}$	$-6{,}085 \cdot 10^{-2}$
e_1k_4	$-1{,}801 \cdot 10^{-6}$	$-1{,}801 \cdot 10^{-3}$	$1{,}165 \cdot 10^{-3}$	$-1{,}986 \cdot 10^{-6}$	$-1{,}986 \cdot 10^{-3}$	$1{,}286 \cdot 10^{-3}$
e_2k_1	$-7{,}639 \cdot 10^{-7}$	$-1{,}061 \cdot 10^{-3}$	$8{,}151 \cdot 10^{-4}$	$-8{,}503 \cdot 10^{-7}$	$-1{,}181 \cdot 10^{-3}$	$9{,}077 \cdot 10^{-4}$
e_2k_2	$-1{,}424 \cdot 10^{-4}$	$-1{,}424 \cdot 10^{-1}$	$6{,}728 \cdot 10^{-2}$	$-1{,}185 \cdot 10^{-4}$	$-1{,}185 \cdot 10^{-1}$	$6{,}150 \cdot 10^{-2}$
e_2k_3	$6{,}818 \cdot 10^{-5}$	$9{,}469 \cdot 10^{-2}$	$-7{,}350 \cdot 10^{-2}$	$5{,}987 \cdot 10^{-5}$	$8{,}316 \cdot 10^{-2}$	$-6{,}634 \cdot 10^{-2}$
e_2k_4	$7{,}496 \cdot 10^{-5}$	$7{,}496 \cdot 10^{-2}$	$-4{,}373 \cdot 10^{-2}$	$5{,}949 \cdot 10^{-5}$	$5{,}949 \cdot 10^{-2}$	$-3{,}540 \cdot 10^{-2}$
e_3k_1	$-4{,}530 \cdot 10^{-7}$	$-9{,}437 \cdot 10^{-4}$	$7{,}247 \cdot 10^{-4}$	$-5{,}074 \cdot 10^{-7}$	$-1{,}057 \cdot 10^{-3}$	$8{,}121 \cdot 10^{-4}$
e_3k_2	$-2{,}507 \cdot 10^{-4}$	$-2{,}507 \cdot 10^{-1}$	$5{,}243 \cdot 10^{-2}$	$-2{,}141 \cdot 10^{-4}$	$-2{,}141 \cdot 10^{-1}$	$4{,}961 \cdot 10^{-2}$
e_3k_3	$1{,}088 \cdot 10^{-4}$	$2{,}266 \cdot 10^{-1}$	$-1{,}051 \cdot 10^{-1}$	$9{,}613 \cdot 10^{-5}$	$2{,}003 \cdot 10^{-1}$	$-1{,}018 \cdot 10^{-1}$
e_3k_4	$1{,}424 \cdot 10^{-4}$	$1{,}424 \cdot 10^{-1}$	$-4{,}486 \cdot 10^{-2}$	$1{,}185 \cdot 10^{-4}$	$1{,}185 \cdot 10^{-1}$	$-4{,}100 \cdot 10^{-2}$
e_4k_1	$-6{,}436 \cdot 10^{-7}$	$-8{,}938 \cdot 10^{-4}$	$6{,}862 \cdot 10^{-4}$	$-7{,}241 \cdot 10^{-7}$	$-1{,}006 \cdot 10^{-3}$	$7{,}725 \cdot 10^{-4}$
e_4k_2	$-4{,}374 \cdot 10^{-4}$	$-4{,}374 \cdot 10^{-1}$	$1{,}024 \cdot 10^{-1}$	$-3{,}914 \cdot 10^{-4}$	$-3{,}914 \cdot 10^{-1}$	$9{,}717 \cdot 10^{-2}$
e_4k_3	$1{,}873 \cdot 10^{-4}$	$2{,}601 \cdot 10^{-1}$	$-1{,}111 \cdot 10^{-1}$	$1{,}779 \cdot 10^{-4}$	$2{,}471 \cdot 10^{-1}$	$-1{,}085 \cdot 10^{-1}$
e_4k_4	$2{,}507 \cdot 10^{-4}$	$2{,}507 \cdot 10^{-1}$	$-7{,}864 \cdot 10^{-2}$	$2{,}141 \cdot 10^{-4}$	$2{,}141 \cdot 10^{-1}$	$-7{,}441 \cdot 10^{-2}$
e_5k_1	$-4{,}189 \cdot 10^{-7}$	$-8{,}728 \cdot 10^{-4}$	$6{,}700 \cdot 10^{-4}$	$-4{,}743 \cdot 10^{-7}$	$-9{,}880 \cdot 10^{-4}$	$7{,}588 \cdot 10^{-4}$
e_5k_2	$-7{,}004 \cdot 10^{-4}$	$-7{,}004 \cdot 10^{-1}$	$9{,}341 \cdot 10^{-2}$	$-6{,}606 \cdot 10^{-4}$	$-6{,}606 \cdot 10^{-1}$	$8{,}896 \cdot 10^{-2}$
e_5k_3	$2{,}635 \cdot 10^{-4}$	$5{,}489 \cdot 10^{-1}$	$-1{,}624 \cdot 10^{-1}$	$2{,}697 \cdot 10^{-4}$	$5{,}618 \cdot 10^{-1}$	$-1{,}649 \cdot 10^{-1}$
e_5k_4	$4{,}374 \cdot 10^{-4}$	$4{,}374 \cdot 10^{-1}$	$-6{,}824 \cdot 10^{-2}$	$3{,}914 \cdot 10^{-4}$	$3{,}914 \cdot 10^{-1}$	$-6{,}478 \cdot 10^{-2}$
e_6k_1	$-6{,}134 \cdot 10^{-7}$	$-8{,}520 \cdot 10^{-4}$	$6{,}540 \cdot 10^{-4}$	$-7{,}029 \cdot 10^{-7}$	$-9{,}762 \cdot 10^{-4}$	$7{,}497 \cdot 10^{-4}$
e_6k_2	$-6{,}998 \cdot 10^{-4}$	$-6{,}998 \cdot 10^{-1}$	$1{,}400 \cdot 10^{-1}$	$-6{,}599 \cdot 10^{-4}$	$-6{,}599 \cdot 10^{-1}$	$1{,}333 \cdot 10^{-1}$
e_6k_3	$8{,}415 \cdot 10^{-9}$	$1{,}169 \cdot 10^{-5}$	$-8{,}942 \cdot 10^{-6}$	$1{,}110 \cdot 10^{-8}$	$1{,}542 \cdot 10^{-5}$	$-1{,}179 \cdot 10^{-5}$
e_6k_4	$7{,}004 \cdot 10^{-4}$	$7{,}004 \cdot 10^{-1}$	$-1{,}401 \cdot 10^{-1}$	$6{,}606 \cdot 10^{-4}$	$6{,}606 \cdot 10^{-1}$	$-1{,}334 \cdot 10^{-1}$
e_7k_1	$-4{,}120 \cdot 10^{-7}$	$-8{,}583 \cdot 10^{-4}$	$6{,}588 \cdot 10^{-4}$	$-4{,}780 \cdot 10^{-7}$	$-9{,}959 \cdot 10^{-4}$	$7{,}649 \cdot 10^{-4}$
e_7k_2	$-5{,}456 \cdot 10^{-4}$	$-5{,}456 \cdot 10^{-1}$	$7{,}766 \cdot 10^{-2}$	$-5{,}273 \cdot 10^{-4}$	$-5{,}273 \cdot 10^{-1}$	$7{,}600 \cdot 10^{-2}$
e_7k_3	$-1{,}538 \cdot 10^{-4}$	$-3{,}205 \cdot 10^{-1}$	$1{,}238 \cdot 10^{-1}$	$-1{,}320 \cdot 10^{-4}$	$-2{,}751 \cdot 10^{-1}$	$1{,}143 \cdot 10^{-1}$
e_7k_4	$6{,}998 \cdot 10^{-4}$	$6{,}998 \cdot 10^{-1}$	$-9{,}334 \cdot 10^{-2}$	$6{,}599 \cdot 10^{-4}$	$6{,}599 \cdot 10^{-1}$	$-8{,}889 \cdot 10^{-2}$
e_8k_1	$-6{,}606 \cdot 10^{-7}$	$-9{,}176 \cdot 10^{-4}$	$7{,}045 \cdot 10^{-4}$	$-7{,}717 \cdot 10^{-7}$	$-1{,}072 \cdot 10^{-3}$	$8{,}235 \cdot 10^{-4}$
e_8k_2	$-3{,}938 \cdot 10^{-4}$	$-3{,}938 \cdot 10^{-1}$	$9{,}743 \cdot 10^{-2}$	$-4{,}009 \cdot 10^{-4}$	$-4{,}009 \cdot 10^{-1}$	$9{,}820 \cdot 10^{-2}$
e_8k_3	$-1{,}511 \cdot 10^{-4}$	$-2{,}099 \cdot 10^{-1}$	$1{,}028 \cdot 10^{-1}$	$-1{,}256 \cdot 10^{-4}$	$-1{,}745 \cdot 10^{-1}$	$9{,}921 \cdot 10^{-2}$
e_8k_4	$5{,}456 \cdot 10^{-4}$	$5{,}456 \cdot 10^{-1}$	$-1{,}165 \cdot 10^{-1}$	$5{,}273 \cdot 10^{-4}$	$5{,}273 \cdot 10^{-1}$	$-1{,}140 \cdot 10^{-1}$
e_9k_1	$-4{,}924 \cdot 10^{-7}$	$-1{,}026 \cdot 10^{-3}$	$7{,}880 \cdot 10^{-4}$	$-5{,}790 \cdot 10^{-7}$	$-1{,}206 \cdot 10^{-3}$	$9{,}272 \cdot 10^{-4}$
e_9k_2	$-2{,}969 \cdot 10^{-4}$	$-2{,}969 \cdot 10^{-1}$	$5{,}717 \cdot 10^{-2}$	$-3{,}141 \cdot 10^{-4}$	$-3{,}141 \cdot 10^{-1}$	$5{,}883 \cdot 10^{-2}$
e_9k_3	$-9{,}636 \cdot 10^{-5}$	$-2{,}008 \cdot 10^{-1}$	$1{,}018 \cdot 10^{-1}$	$-8{,}628 \cdot 10^{-5}$	$-1{,}797 \cdot 10^{-1}$	$9{,}979 \cdot 10^{-2}$
e_9k_4	$3{,}938 \cdot 10^{-4}$	$3{,}938 \cdot 10^{-1}$	$-6{,}496 \cdot 10^{-2}$	$4{,}009 \cdot 10^{-4}$	$4{,}009 \cdot 10^{-1}$	$-6{,}547 \cdot 10^{-2}$

Table A.1: Flux tube element outputs ... *cont*

Element Region	$I_{(\mathrm{ph})} = \begin{bmatrix} -10 & 20 & -10 \end{bmatrix}^{\mathrm{T}}$					
	$x = 2\,\mathrm{mm}$			$x = 3\,\mathrm{mm}$		
	Φ [Wb]	B [T]	$\mathcal{F}$ [A]	Φ [Wb]	B [T]	$\mathcal{F}$ [A]
$\varrho_{10}\xi_1$	$-8{,}905 \cdot 10^{-7}$	$-1{,}237 \cdot 10^{-3}$	$9{,}508 \cdot 10^{-4}$	$-1{,}056 \cdot 10^{-6}$	$-1{,}467 \cdot 10^{-3}$	$1{,}129 \cdot 10^{-3}$
$\varrho_{10}\xi_2$	$-1{,}897 \cdot 10^{-4}$	$-1{,}897 \cdot 10^{-1}$	$7{,}255 \cdot 10^{-2}$	$-2{,}082 \cdot 10^{-4}$	$-2{,}082 \cdot 10^{-1}$	$7{,}390 \cdot 10^{-2}$
$\varrho_{10}\xi_3$	$-1{,}063 \cdot 10^{-4}$	$-1{,}477 \cdot 10^{-1}$	$9{,}475 \cdot 10^{-2}$	$-1{,}048 \cdot 10^{-4}$	$-1{,}456 \cdot 10^{-1}$	$9{,}425 \cdot 10^{-2}$
$\varrho_{10}\xi_4$	$2{,}969 \cdot 10^{-4}$	$2{,}969 \cdot 10^{-1}$	$-8{,}575 \cdot 10^{-2}$	$3{,}141 \cdot 10^{-4}$	$3{,}141 \cdot 10^{-1}$	$-8{,}825 \cdot 10^{-2}$
$\varrho_{11}\xi_1$	$-2{,}049 \cdot 10^{-6}$	$-2{,}439 \cdot 10^{-3}$	$1{,}883 \cdot 10^{-3}$	$-2{,}468 \cdot 10^{-6}$	$-2{,}938 \cdot 10^{-3}$	$2{,}273 \cdot 10^{-3}$
$\varrho_{11}\xi_2$	$-3{,}586 \cdot 10^{-6}$	$-3{,}586 \cdot 10^{-3}$	$2{,}336 \cdot 10^{-3}$	$-4{,}446 \cdot 10^{-6}$	$-4{,}446 \cdot 10^{-3}$	$2{,}905 \cdot 10^{-3}$
$\varrho_{11}\xi_3$	$-1{,}841 \cdot 10^{-4}$	$-2{,}191 \cdot 10^{-1}$	$1{,}040 \cdot 10^{-1}$	$-2{,}013 \cdot 10^{-4}$	$-2{,}396 \cdot 10^{-1}$	$1{,}072 \cdot 10^{-1}$
$\varrho_{11}\xi_4$	$1{,}897 \cdot 10^{-4}$	$1{,}897 \cdot 10^{-1}$	$-8{,}464 \cdot 10^{-2}$	$2{,}082 \cdot 10^{-4}$	$2{,}082 \cdot 10^{-1}$	$-8{,}621 \cdot 10^{-2}$
$\varrho_{12}\xi_1$	$-7{,}824 \cdot 10^{-5}$	$-9{,}314 \cdot 10^{-2}$	$1{,}161 \cdot 10^{-1}$	$-6{,}310 \cdot 10^{-5}$	$-7{,}512 \cdot 10^{-2}$	$9{,}736 \cdot 10^{-2}$
$\varrho_{12}\xi_2$	$-1{,}165 \cdot 10^{-4}$	$-7{,}283 \cdot 10^{-2}$	$4{,}974 \cdot 10^{-2}$	$-7{,}704 \cdot 10^{-5}$	$-4{,}815 \cdot 10^{-2}$	$3{,}362 \cdot 10^{-2}$
$\varrho_{12}\xi_3$	$1{,}969 \cdot 10^{-4}$	$2{,}344 \cdot 10^{-1}$	$-1{,}701 \cdot 10^{-1}$	$1{,}425 \cdot 10^{-4}$	$1{,}697 \cdot 10^{-1}$	$-1{,}578 \cdot 10^{-1}$
$\varrho_{12}\xi_4$	$-2{,}165 \cdot 10^{-6}$	$-1{,}353 \cdot 10^{-3}$	$8{,}743 \cdot 10^{-4}$	$-2{,}402 \cdot 10^{-6}$	$-1{,}501 \cdot 10^{-3}$	$9{,}706 \cdot 10^{-4}$
$\varrho_{13}\xi_1$	$-6{,}818 \cdot 10^{-5}$	$-9{,}469 \cdot 10^{-2}$	$1{,}176 \cdot 10^{-1}$	$-5{,}987 \cdot 10^{-5}$	$-8{,}316 \cdot 10^{-2}$	$1{,}061 \cdot 10^{-1}$
$\varrho_{13}\xi_2$	$-4{,}863 \cdot 10^{-5}$	$-3{,}040 \cdot 10^{-2}$	$1{,}804 \cdot 10^{-2}$	$-1{,}740 \cdot 10^{-5}$	$-1{,}087 \cdot 10^{-2}$	$6{,}216 \cdot 10^{-3}$
$\varrho_{13}\xi_3$	$2{,}930 \cdot 10^{-7}$	$4{,}070 \cdot 10^{-4}$	$-4{,}990 \cdot 10^{-4}$	$2{,}344 \cdot 10^{-7}$	$3{,}255 \cdot 10^{-4}$	$-3{,}989 \cdot 10^{-4}$
$\varrho_{13}\xi_4$	$1{,}165 \cdot 10^{-4}$	$7{,}283 \cdot 10^{-2}$	$-4{,}263 \cdot 10^{-2}$	$7{,}704 \cdot 10^{-5}$	$4{,}815 \cdot 10^{-2}$	$-2{,}881 \cdot 10^{-2}$
$\varrho_{14}\xi_1$	$-1{,}088 \cdot 10^{-4}$	$-2{,}266 \cdot 10^{-1}$	$1{,}681 \cdot 10^{-1}$	$-9{,}613 \cdot 10^{-5}$	$-2{,}003 \cdot 10^{-1}$	$1{,}628 \cdot 10^{-1}$
$\varrho_{14}\xi_2$	$-2{,}467 \cdot 10^{-4}$	$-1{,}542 \cdot 10^{-1}$	$4{,}614 \cdot 10^{-2}$	$-2{,}031 \cdot 10^{-4}$	$-1{,}269 \cdot 10^{-1}$	$4{,}257 \cdot 10^{-2}$
$\varrho_{14}\xi_3$	$3{,}068 \cdot 10^{-4}$	$6{,}392 \cdot 10^{-1}$	$-2{,}891 \cdot 10^{-1}$	$2{,}818 \cdot 10^{-4}$	$5{,}871 \cdot 10^{-1}$	$-2{,}718 \cdot 10^{-1}$
$\varrho_{14}\xi_4$	$4{,}863 \cdot 10^{-5}$	$3{,}040 \cdot 10^{-2}$	$-1{,}203 \cdot 10^{-2}$	$1{,}740 \cdot 10^{-5}$	$1{,}087 \cdot 10^{-2}$	$-4{,}144 \cdot 10^{-3}$
$\varrho_{15}\xi_1$	$-1{,}873 \cdot 10^{-4}$	$-2{,}601 \cdot 10^{-1}$	$1{,}778 \cdot 10^{-1}$	$-1{,}779 \cdot 10^{-4}$	$-2{,}471 \cdot 10^{-1}$	$1{,}737 \cdot 10^{-1}$
$\varrho_{15}\xi_2$	$-5{,}974 \cdot 10^{-5}$	$-3{,}734 \cdot 10^{-2}$	$2{,}229 \cdot 10^{-2}$	$-2{,}548 \cdot 10^{-5}$	$-1{,}592 \cdot 10^{-2}$	$9{,}222 \cdot 10^{-3}$
$\varrho_{15}\xi_3$	$3{,}574 \cdot 10^{-7}$	$4{,}964 \cdot 10^{-4}$	$-6{,}088 \cdot 10^{-4}$	$3{,}606 \cdot 10^{-7}$	$5{,}009 \cdot 10^{-4}$	$-6{,}143 \cdot 10^{-4}$
$\varrho_{15}\xi_4$	$2{,}467 \cdot 10^{-4}$	$1{,}542 \cdot 10^{-1}$	$-6{,}921 \cdot 10^{-2}$	$2{,}031 \cdot 10^{-4}$	$1{,}269 \cdot 10^{-1}$	$-6{,}385 \cdot 10^{-2}$
$\varrho_{16}\xi_1$	$-2{,}635 \cdot 10^{-4}$	$-5{,}489 \cdot 10^{-1}$	$2{,}599 \cdot 10^{-1}$	$-2{,}697 \cdot 10^{-4}$	$-5{,}618 \cdot 10^{-1}$	$2{,}639 \cdot 10^{-1}$
$\varrho_{16}\xi_2$	$-4{,}221 \cdot 10^{-5}$	$-2{,}638 \cdot 10^{-2}$	$1{,}039 \cdot 10^{-2}$	$-4{,}217 \cdot 10^{-5}$	$-2{,}636 \cdot 10^{-2}$	$1{,}038 \cdot 10^{-2}$
$\varrho_{16}\xi_3$	$2{,}460 \cdot 10^{-4}$	$5{,}124 \cdot 10^{-1}$	$-2{,}489 \cdot 10^{-1}$	$2{,}864 \cdot 10^{-4}$	$5{,}966 \cdot 10^{-1}$	$-2{,}749 \cdot 10^{-1}$
$\varrho_{16}\xi_4$	$5{,}974 \cdot 10^{-5}$	$3{,}734 \cdot 10^{-2}$	$-1{,}486 \cdot 10^{-2}$	$2{,}548 \cdot 10^{-5}$	$1{,}592 \cdot 10^{-2}$	$-6{,}148 \cdot 10^{-3}$
$\varrho_{17}\xi_1$	$1{,}538 \cdot 10^{-4}$	$3{,}205 \cdot 10^{-1}$	$-1{,}980 \cdot 10^{-1}$	$1{,}320 \cdot 10^{-4}$	$2{,}751 \cdot 10^{-1}$	$-1{,}829 \cdot 10^{-1}$
$\varrho_{17}\xi_2$	$-4{,}555 \cdot 10^{-4}$	$-2{,}847 \cdot 10^{-1}$	$5{,}588 \cdot 10^{-2}$	$-5{,}292 \cdot 10^{-4}$	$-3{,}307 \cdot 10^{-1}$	$6{,}029 \cdot 10^{-2}$
$\varrho_{17}\xi_3$	$2{,}593 \cdot 10^{-4}$	$5{,}402 \cdot 10^{-1}$	$-2{,}572 \cdot 10^{-1}$	$3{,}548 \cdot 10^{-4}$	$7{,}392 \cdot 10^{-1}$	$-3{,}271 \cdot 10^{-1}$
$\varrho_{17}\xi_4$	$4{,}233 \cdot 10^{-5}$	$2{,}646 \cdot 10^{-2}$	$-1{,}042 \cdot 10^{-2}$	$4{,}233 \cdot 10^{-5}$	$2{,}646 \cdot 10^{-2}$	$-1{,}042 \cdot 10^{-2}$
$\varrho_{18}\xi_1$	$1{,}511 \cdot 10^{-4}$	$2{,}099 \cdot 10^{-1}$	$-1{,}645 \cdot 10^{-1}$	$1{,}256 \cdot 10^{-4}$	$1{,}745 \cdot 10^{-1}$	$-1{,}587 \cdot 10^{-1}$
$\varrho_{18}\xi_2$	$-6{,}064 \cdot 10^{-4}$	$-3{,}790 \cdot 10^{-1}$	$9{,}587 \cdot 10^{-2}$	$-6{,}547 \cdot 10^{-4}$	$-4{,}092 \cdot 10^{-1}$	$9{,}911 \cdot 10^{-2}$
$\varrho_{18}\xi_3$	$-1{,}924 \cdot 10^{-7}$	$-2{,}673 \cdot 10^{-4}$	$3{,}275 \cdot 10^{-4}$	$-1{,}239 \cdot 10^{-7}$	$-1{,}720 \cdot 10^{-4}$	$2{,}107 \cdot 10^{-4}$
$\varrho_{18}\xi_4$	$4{,}555 \cdot 10^{-4}$	$2{,}847 \cdot 10^{-1}$	$-8{,}383 \cdot 10^{-2}$	$5{,}292 \cdot 10^{-4}$	$3{,}307 \cdot 10^{-1}$	$-9{,}044 \cdot 10^{-2}$
$\varrho_{19}\xi_1$	$9{,}636 \cdot 10^{-5}$	$2{,}008 \cdot 10^{-1}$	$-1{,}629 \cdot 10^{-1}$	$8{,}628 \cdot 10^{-5}$	$1{,}797 \cdot 10^{-1}$	$-1{,}597 \cdot 10^{-1}$
$\varrho_{19}\xi_2$	$-3{,}478 \cdot 10^{-4}$	$-2{,}174 \cdot 10^{-1}$	$4{,}981 \cdot 10^{-2}$	$-4{,}120 \cdot 10^{-4}$	$-2{,}575 \cdot 10^{-1}$	$5{,}308 \cdot 10^{-2}$
$\varrho_{19}\xi_3$	$-3{,}549 \cdot 10^{-4}$	$-7{,}395 \cdot 10^{-1}$	$3{,}272 \cdot 10^{-1}$	$-3{,}290 \cdot 10^{-4}$	$-6{,}854 \cdot 10^{-1}$	$3{,}056 \cdot 10^{-1}$
$\varrho_{19}\xi_4$	$6{,}064 \cdot 10^{-4}$	$3{,}790 \cdot 10^{-1}$	$-6{,}391 \cdot 10^{-2}$	$6{,}547 \cdot 10^{-4}$	$4{,}092 \cdot 10^{-1}$	$-6{,}607 \cdot 10^{-2}$
$\varrho_{20}\xi_1$	$1{,}063 \cdot 10^{-4}$	$1{,}477 \cdot 10^{-1}$	$-1{,}516 \cdot 10^{-1}$	$1{,}048 \cdot 10^{-4}$	$1{,}456 \cdot 10^{-1}$	$-1{,}508 \cdot 10^{-1}$
$\varrho_{20}\xi_2$	$-4{,}537 \cdot 10^{-4}$	$-2{,}836 \cdot 10^{-1}$	$8{,}366 \cdot 10^{-2}$	$-5{,}164 \cdot 10^{-4}$	$-3{,}228 \cdot 10^{-1}$	$8{,}942 \cdot 10^{-2}$
$\varrho_{20}\xi_3$	$-4{,}035 \cdot 10^{-7}$	$-5{,}604 \cdot 10^{-4}$	$6{,}875 \cdot 10^{-4}$	$-4{,}083 \cdot 10^{-7}$	$-5{,}670 \cdot 10^{-4}$	$6{,}956 \cdot 10^{-4}$
$\varrho_{20}\xi_4$	$3{,}478 \cdot 10^{-4}$	$2{,}174 \cdot 10^{-1}$	$-7{,}471 \cdot 10^{-2}$	$4{,}120 \cdot 10^{-4}$	$2{,}575 \cdot 10^{-1}$	$-7{,}961 \cdot 10^{-2}$
$\varrho_{21}\xi_1$	$1{,}841 \cdot 10^{-4}$	$2{,}191 \cdot 10^{-1}$	$-1{,}664 \cdot 10^{-1}$	$2{,}013 \cdot 10^{-4}$	$2{,}396 \cdot 10^{-1}$	$-1{,}715 \cdot 10^{-1}$
$\varrho_{21}\xi_2$	$-6{,}958 \cdot 10^{-6}$	$-4{,}349 \cdot 10^{-3}$	$2{,}841 \cdot 10^{-3}$	$-9{,}196 \cdot 10^{-6}$	$-5{,}747 \cdot 10^{-3}$	$3{,}773 \cdot 10^{-3}$
$\varrho_{21}\xi_3$	$-6{,}309 \cdot 10^{-4}$	$-7{,}510 \cdot 10^{-1}$	$3{,}321 \cdot 10^{-1}$	$-7{,}085 \cdot 10^{-4}$	$-8{,}435 \cdot 10^{-1}$	$3{,}760 \cdot 10^{-1}$
$\varrho_{21}\xi_4$	$4{,}537 \cdot 10^{-4}$	$2{,}836 \cdot 10^{-1}$	$-9{,}760 \cdot 10^{-2}$	$5{,}164 \cdot 10^{-4}$	$3{,}228 \cdot 10^{-1}$	$-1{,}043 \cdot 10^{-1}$
$\varrho_{22}\xi_1$	$-1{,}969 \cdot 10^{-4}$	$-2{,}344 \cdot 10^{-1}$	$1{,}701 \cdot 10^{-1}$	$-1{,}425 \cdot 10^{-4}$	$-1{,}697 \cdot 10^{-1}$	$1{,}578 \cdot 10^{-1}$
$\varrho_{22}\xi_2$	$1{,}068 \cdot 10^{-4}$	$6{,}676 \cdot 10^{-2}$	$-4{,}599 \cdot 10^{-2}$	$8{,}895 \cdot 10^{-5}$	$5{,}559 \cdot 10^{-2}$	$-3{,}870 \cdot 10^{-2}$
$\varrho_{22}\xi_3$	$9{,}138 \cdot 10^{-5}$	$1{,}088 \cdot 10^{-1}$	$-1{,}297 \cdot 10^{-1}$	$5{,}642 \cdot 10^{-5}$	$6{,}717 \cdot 10^{-2}$	$-8{,}809 \cdot 10^{-2}$
$\varrho_{22}\xi_4$	$-1{,}270 \cdot 10^{-6}$	$-7{,}937 \cdot 10^{-4}$	$5{,}116 \cdot 10^{-4}$	$-2{,}829 \cdot 10^{-6}$	$-1{,}768 \cdot 10^{-3}$	$1{,}144 \cdot 10^{-3}$
$\varrho_{23}\xi_1$	$-3{,}068 \cdot 10^{-4}$	$-6{,}392 \cdot 10^{-1}$	$2{,}891 \cdot 10^{-1}$	$-2{,}818 \cdot 10^{-4}$	$-5{,}871 \cdot 10^{-1}$	$2{,}718 \cdot 10^{-1}$
$\varrho_{23}\xi_2$	$4{,}593 \cdot 10^{-5}$	$2{,}870 \cdot 10^{-2}$	$-1{,}134 \cdot 10^{-2}$	$4{,}603 \cdot 10^{-5}$	$2{,}877 \cdot 10^{-2}$	$-1{,}136 \cdot 10^{-2}$
$\varrho_{23}\xi_3$	$2{,}292 \cdot 10^{-4}$	$4{,}774 \cdot 10^{-1}$	$-2{,}386 \cdot 10^{-1}$	$2{,}178 \cdot 10^{-4}$	$4{,}538 \cdot 10^{-1}$	$-2{,}319 \cdot 10^{-1}$
$\varrho_{23}\xi_4$	$3{,}173 \cdot 10^{-5}$	$1{,}983 \cdot 10^{-2}$	$-7{,}721 \cdot 10^{-3}$	$1{,}795 \cdot 10^{-5}$	$1{,}122 \cdot 10^{-2}$	$-4{,}278 \cdot 10^{-3}$

Table A.1: Flux tube element outputs ... *cont*

Element Region	$I_{(\mathrm{ph})} = \begin{bmatrix} -10 & 20 & -10 \end{bmatrix}^{\mathrm{T}}$					
	$x = 2\,\mathrm{mm}$			$x = 3\,\mathrm{mm}$		
	Φ [Wb]	B [T]	$\mathcal{F}$ [A]	Φ [Wb]	B [T]	$\mathcal{F}$ [A]
$\mathfrak{e}_{24}\mathfrak{k}_1$	$-2{,}460 \cdot 10^{-4}$	$-5{,}124 \cdot 10^{-1}$	$2{,}489 \cdot 10^{-1}$	$-2{,}864 \cdot 10^{-4}$	$-5{,}966 \cdot 10^{-1}$	$2{,}749 \cdot 10^{-1}$
$\mathfrak{e}_{24}\mathfrak{k}_2$	$-1{,}161 \cdot 10^{-4}$	$-7{,}255 \cdot 10^{-2}$	$2{,}833 \cdot 10^{-2}$	$-9{,}717 \cdot 10^{-5}$	$-6{,}073 \cdot 10^{-2}$	$2{,}407 \cdot 10^{-2}$
$\mathfrak{e}_{24}\mathfrak{k}_3$	$2{,}257 \cdot 10^{-4}$	$4{,}703 \cdot 10^{-1}$	$-2{,}365 \cdot 10^{-1}$	$2{,}462 \cdot 10^{-4}$	$5{,}130 \cdot 10^{-1}$	$-2{,}490 \cdot 10^{-1}$
$\mathfrak{e}_{24}\mathfrak{k}_4$	$1{,}363 \cdot 10^{-4}$	$8{,}520 \cdot 10^{-2}$	$-3{,}248 \cdot 10^{-2}$	$1{,}373 \cdot 10^{-4}$	$8{,}582 \cdot 10^{-2}$	$-3{,}267 \cdot 10^{-2}$
$\mathfrak{e}_{25}\mathfrak{k}_1$	$-2{,}593 \cdot 10^{-4}$	$-5{,}402 \cdot 10^{-1}$	$2{,}572 \cdot 10^{-1}$	$-3{,}548 \cdot 10^{-4}$	$-7{,}392 \cdot 10^{-1}$	$3{,}271 \cdot 10^{-1}$
$\mathfrak{e}_{25}\mathfrak{k}_2$	$-1{,}652 \cdot 10^{-6}$	$-1{,}033 \cdot 10^{-3}$	$3{,}808 \cdot 10^{-4}$	$1{,}835 \cdot 10^{-5}$	$1{,}147 \cdot 10^{-2}$	$-4{,}379 \cdot 10^{-3}$
$\mathfrak{e}_{25}\mathfrak{k}_3$	$4{,}426 \cdot 10^{-5}$	$9{,}221 \cdot 10^{-2}$	$-1{,}152 \cdot 10^{-1}$	$9{,}802 \cdot 10^{-5}$	$2{,}042 \cdot 10^{-1}$	$-1{,}635 \cdot 10^{-1}$
$\mathfrak{e}_{25}\mathfrak{k}_4$	$2{,}167 \cdot 10^{-4}$	$1{,}354 \cdot 10^{-1}$	$-4{,}392 \cdot 10^{-2}$	$2{,}384 \cdot 10^{-4}$	$1{,}490 \cdot 10^{-1}$	$-4{,}562 \cdot 10^{-2}$
$\mathfrak{e}_{26}\mathfrak{k}_1$	$3{,}549 \cdot 10^{-4}$	$7{,}395 \cdot 10^{-1}$	$-3{,}272 \cdot 10^{-1}$	$3{,}290 \cdot 10^{-4}$	$6{,}854 \cdot 10^{-1}$	$-3{,}056 \cdot 10^{-1}$
$\mathfrak{e}_{26}\mathfrak{k}_2$	$-7{,}293 \cdot 10^{-6}$	$-4{,}558 \cdot 10^{-3}$	$1{,}703 \cdot 10^{-3}$	$-7{,}450 \cdot 10^{-6}$	$-4{,}656 \cdot 10^{-3}$	$1{,}740 \cdot 10^{-3}$
$\mathfrak{e}_{26}\mathfrak{k}_3$	$-2{,}369 \cdot 10^{-4}$	$-4{,}935 \cdot 10^{-1}$	$2{,}433 \cdot 10^{-1}$	$-2{,}258 \cdot 10^{-4}$	$-4{,}705 \cdot 10^{-1}$	$2{,}366 \cdot 10^{-1}$
$\mathfrak{e}_{26}\mathfrak{k}_4$	$-1{,}108 \cdot 10^{-4}$	$-6{,}924 \cdot 10^{-2}$	$2{,}717 \cdot 10^{-2}$	$-9{,}569 \cdot 10^{-5}$	$-5{,}981 \cdot 10^{-2}$	$2{,}372 \cdot 10^{-2}$
$\mathfrak{e}_{27}\mathfrak{k}_1$	$6{,}309 \cdot 10^{-4}$	$7{,}510 \cdot 10^{-1}$	$-3{,}321 \cdot 10^{-1}$	$7{,}085 \cdot 10^{-4}$	$8{,}435 \cdot 10^{-1}$	$-3{,}760 \cdot 10^{-1}$
$\mathfrak{e}_{27}\mathfrak{k}_2$	$-5{,}067 \cdot 10^{-5}$	$-3{,}167 \cdot 10^{-2}$	$2{,}196 \cdot 10^{-2}$	$-7{,}740 \cdot 10^{-5}$	$-4{,}837 \cdot 10^{-2}$	$3{,}377 \cdot 10^{-2}$
$\mathfrak{e}_{27}\mathfrak{k}_3$	$-3{,}916 \cdot 10^{-4}$	$-4{,}662 \cdot 10^{-1}$	$2{,}354 \cdot 10^{-1}$	$-4{,}416 \cdot 10^{-4}$	$-5{,}257 \cdot 10^{-1}$	$2{,}528 \cdot 10^{-1}$
$\mathfrak{e}_{27}\mathfrak{k}_4$	$-1{,}886 \cdot 10^{-4}$	$-1{,}178 \cdot 10^{-1}$	$7{,}152 \cdot 10^{-2}$	$-1{,}895 \cdot 10^{-4}$	$-1{,}185 \cdot 10^{-1}$	$7{,}174 \cdot 10^{-2}$
$\mathfrak{e}_{28}\mathfrak{k}_1$	$-1{,}222 \cdot 10^{-3}$	$-4{,}700 \cdot 10^{-1}$	$4{,}085 \cdot 10^{-1}$	$-1{,}235 \cdot 10^{-3}$	$-4{,}749 \cdot 10^{-1}$	$4{,}130 \cdot 10^{-1}$
$\mathfrak{e}_{28}\mathfrak{k}_2$	$1{,}133 \cdot 10^{-3}$	$1{,}259$	$-4{,}443$	$1{,}143 \cdot 10^{-3}$	$1{,}270$	$-4{,}540$
$\mathfrak{e}_{28}\mathfrak{k}_3$	$1{,}449 \cdot 10^{-5}$	$5{,}573 \cdot 10^{-3}$	$-4{,}708 \cdot 10^{-3}$	$1{,}471 \cdot 10^{-5}$	$5{,}658 \cdot 10^{-3}$	$-4{,}780 \cdot 10^{-3}$
$\mathfrak{e}_{28}\mathfrak{k}_4$	$7{,}481 \cdot 10^{-5}$	$8{,}312 \cdot 10^{-2}$	$-2{,}022 \cdot 10^{-1}$	$7{,}682 \cdot 10^{-5}$	$8{,}536 \cdot 10^{-2}$	$-2{,}076 \cdot 10^{-1}$
$\mathfrak{e}_{29}\mathfrak{k}_1$	$-6{,}956 \cdot 10^{-5}$	$-6{,}956 \cdot 10^{-2}$	$5{,}858 \cdot 10^{-2}$	$-7{,}892 \cdot 10^{-5}$	$-7{,}892 \cdot 10^{-2}$	$6{,}645 \cdot 10^{-2}$
$\mathfrak{e}_{29}\mathfrak{k}_2$	$1{,}200 \cdot 10^{-3}$	$1{,}334$	$-1{,}985$	$1{,}220 \cdot 10^{-3}$	$1{,}356$	$-2{,}087$
$\mathfrak{e}_{29}\mathfrak{k}_3$	$1{,}920 \cdot 10^{-6}$	$1{,}920 \cdot 10^{-3}$	$-1{,}622 \cdot 10^{-3}$	$1{,}853 \cdot 10^{-6}$	$1{,}853 \cdot 10^{-3}$	$-1{,}565 \cdot 10^{-3}$
$\mathfrak{e}_{29}\mathfrak{k}_4$	$-1{,}133 \cdot 10^{-3}$	$-1{,}259$	$1{,}709$	$-1{,}143 \cdot 10^{-3}$	$-1{,}270$	$1{,}746$
$\mathfrak{e}_{30}\mathfrak{k}_1$	$1{,}246 \cdot 10^{-3}$	$4{,}791 \cdot 10^{-1}$	$-4{,}169 \cdot 10^{-1}$	$1{,}272 \cdot 10^{-3}$	$4{,}893 \cdot 10^{-1}$	$-4{,}266 \cdot 10^{-1}$
$\mathfrak{e}_{30}\mathfrak{k}_2$	$-4{,}683 \cdot 10^{-5}$	$-5{,}203 \cdot 10^{-2}$	$1{,}266 \cdot 10^{-1}$	$-5{,}224 \cdot 10^{-5}$	$-5{,}804 \cdot 10^{-2}$	$1{,}413 \cdot 10^{-1}$
$\mathfrak{e}_{30}\mathfrak{k}_3$	$1{,}519 \cdot 10^{-6}$	$5{,}842 \cdot 10^{-4}$	$-4{,}937 \cdot 10^{-4}$	$2{,}289 \cdot 10^{-7}$	$8{,}803 \cdot 10^{-5}$	$-7{,}440 \cdot 10^{-5}$
$\mathfrak{e}_{30}\mathfrak{k}_4$	$-1{,}200 \cdot 10^{-3}$	$-1{,}334$	$5{,}162$	$-1{,}220 \cdot 10^{-3}$	$-1{,}356$	$5{,}426$

Table A.1: Flux tube element outputs ... *cont*

Element Region	$I_{(\mathrm{ph})} = \begin{bmatrix} -10 & 20 & -10 \end{bmatrix}^{\mathrm{T}}$					
	$x = 4\,\mathrm{mm}$			$x = 5\,\mathrm{mm}$		
	Φ [Wb]	B [T]	$\mathcal{F}$ [A]	Φ [Wb]	B [T]	$\mathcal{F}$ [A]
$\mathfrak{e}_{1}\mathfrak{k}_1$	$-1{,}855 \cdot 10^{-6}$	$-2{,}208 \cdot 10^{-3}$	$1{,}704 \cdot 10^{-3}$	$-2{,}185 \cdot 10^{-6}$	$-2{,}601 \cdot 10^{-3}$	$2{,}010 \cdot 10^{-3}$
$\mathfrak{e}_{1}\mathfrak{k}_2$	$-4{,}705 \cdot 10^{-5}$	$-4{,}705 \cdot 10^{-2}$	$3{,}286 \cdot 10^{-2}$	$-3{,}657 \cdot 10^{-5}$	$-3{,}657 \cdot 10^{-2}$	$2{,}547 \cdot 10^{-2}$
$\mathfrak{e}_{1}\mathfrak{k}_3$	$5{,}117 \cdot 10^{-5}$	$6{,}092 \cdot 10^{-2}$	$-5{,}028 \cdot 10^{-2}$	$4{,}142 \cdot 10^{-5}$	$4{,}931 \cdot 10^{-2}$	$-4{,}098 \cdot 10^{-2}$
$\mathfrak{e}_{1}\mathfrak{k}_4$	$-2{,}262 \cdot 10^{-6}$	$-2{,}262 \cdot 10^{-3}$	$1{,}467 \cdot 10^{-3}$	$-2{,}663 \cdot 10^{-6}$	$-2{,}663 \cdot 10^{-3}$	$1{,}729 \cdot 10^{-3}$
$\mathfrak{e}_{2}\mathfrak{k}_1$	$-9{,}792 \cdot 10^{-7}$	$-1{,}360 \cdot 10^{-3}$	$1{,}046 \cdot 10^{-3}$	$-1{,}161 \cdot 10^{-6}$	$-1{,}613 \cdot 10^{-3}$	$1{,}242 \cdot 10^{-3}$
$\mathfrak{e}_{2}\mathfrak{k}_2$	$-9{,}877 \cdot 10^{-5}$	$-9{,}877 \cdot 10^{-2}$	$5{,}459 \cdot 10^{-2}$	$-8{,}039 \cdot 10^{-5}$	$-8{,}039 \cdot 10^{-2}$	$4{,}643 \cdot 10^{-2}$
$\mathfrak{e}_{2}\mathfrak{k}_3$	$5{,}270 \cdot 10^{-5}$	$7{,}319 \cdot 10^{-2}$	$-5{,}947 \cdot 10^{-2}$	$4{,}497 \cdot 10^{-5}$	$6{,}246 \cdot 10^{-2}$	$-5{,}148 \cdot 10^{-2}$
$\mathfrak{e}_{2}\mathfrak{k}_4$	$4{,}705 \cdot 10^{-5}$	$4{,}705 \cdot 10^{-2}$	$-2{,}816 \cdot 10^{-2}$	$3{,}657 \cdot 10^{-5}$	$3{,}657 \cdot 10^{-2}$	$-2{,}183 \cdot 10^{-2}$
$\mathfrak{e}_{3}\mathfrak{k}_1$	$-5{,}887 \cdot 10^{-7}$	$-1{,}226 \cdot 10^{-3}$	$9{,}428 \cdot 10^{-4}$	$-7{,}024 \cdot 10^{-7}$	$-1{,}463 \cdot 10^{-3}$	$1{,}126 \cdot 10^{-3}$
$\mathfrak{e}_{3}\mathfrak{k}_2$	$-1{,}716 \cdot 10^{-4}$	$-1{,}716 \cdot 10^{-1}$	$4{,}745 \cdot 10^{-2}$	$-1{,}369 \cdot 10^{-4}$	$-1{,}369 \cdot 10^{-1}$	$4{,}413 \cdot 10^{-2}$
$\mathfrak{e}_{3}\mathfrak{k}_3$	$7{,}340 \cdot 10^{-5}$	$1{,}529 \cdot 10^{-1}$	$-9{,}587 \cdot 10^{-2}$	$5{,}720 \cdot 10^{-5}$	$1{,}192 \cdot 10^{-1}$	$-8{,}569 \cdot 10^{-2}$
$\mathfrak{e}_{3}\mathfrak{k}_4$	$9{,}877 \cdot 10^{-5}$	$9{,}877 \cdot 10^{-2}$	$-3{,}639 \cdot 10^{-2}$	$8{,}039 \cdot 10^{-5}$	$8{,}039 \cdot 10^{-2}$	$-3{,}095 \cdot 10^{-2}$
$\mathfrak{e}_{4}\mathfrak{k}_1$	$-8{,}432 \cdot 10^{-7}$	$-1{,}171 \cdot 10^{-3}$	$9{,}001 \cdot 10^{-4}$	$-1{,}010 \cdot 10^{-6}$	$-1{,}403 \cdot 10^{-3}$	$1{,}079 \cdot 10^{-3}$
$\mathfrak{e}_{4}\mathfrak{k}_2$	$-3{,}363 \cdot 10^{-4}$	$-3{,}363 \cdot 10^{-1}$	$9{,}111 \cdot 10^{-2}$	$-2{,}752 \cdot 10^{-4}$	$-2{,}752 \cdot 10^{-1}$	$8{,}232 \cdot 10^{-2}$
$\mathfrak{e}_{4}\mathfrak{k}_3$	$1{,}655 \cdot 10^{-4}$	$2{,}299 \cdot 10^{-1}$	$-1{,}056 \cdot 10^{-1}$	$1{,}393 \cdot 10^{-4}$	$1{,}935 \cdot 10^{-1}$	$-1{,}011 \cdot 10^{-1}$
$\mathfrak{e}_{4}\mathfrak{k}_4$	$1{,}716 \cdot 10^{-4}$	$1{,}716 \cdot 10^{-1}$	$-7{,}118 \cdot 10^{-2}$	$1{,}369 \cdot 10^{-4}$	$1{,}369 \cdot 10^{-1}$	$-6{,}619 \cdot 10^{-2}$

Table A.1: Flux tube element outputs ... *cont*

Element Region	$I_{(\mathrm{ph})} = \begin{bmatrix} -10 & 20 & -10 \end{bmatrix}^{\mathrm{T}}$					
	$x = 4\,\mathrm{mm}$			$x = 5\,\mathrm{mm}$		
	Φ [Wb]	B [T]	$\mathcal{F}$ [A]	Φ [Wb]	B [T]	$\mathcal{F}$ [A]
$\varrho_5\varkappa_1$	$-5{,}557 \cdot 10^{-7}$	$-1{,}158 \cdot 10^{-3}$	$8{,}897 \cdot 10^{-4}$	$-6{,}699 \cdot 10^{-7}$	$-1{,}396 \cdot 10^{-3}$	$1{,}074 \cdot 10^{-3}$
$\varrho_5\varkappa_2$	$-6{,}037 \cdot 10^{-4}$	$-6{,}037 \cdot 10^{-1}$	$8{,}316 \cdot 10^{-2}$	$-5{,}305 \cdot 10^{-4}$	$-5{,}305 \cdot 10^{-1}$	$7{,}629 \cdot 10^{-2}$
$\varrho_5\varkappa_3$	$2{,}680 \cdot 10^{-4}$	$5{,}582 \cdot 10^{-1}$	$-1{,}642 \cdot 10^{-1}$	$2{,}560 \cdot 10^{-4}$	$5{,}333 \cdot 10^{-1}$	$-1{,}595 \cdot 10^{-1}$
$\varrho_5\varkappa_4$	$3{,}363 \cdot 10^{-4}$	$3{,}363 \cdot 10^{-1}$	$-6{,}074 \cdot 10^{-2}$	$2{,}752 \cdot 10^{-4}$	$2{,}752 \cdot 10^{-1}$	$-5{,}488 \cdot 10^{-2}$
$\varrho_6\varkappa_1$	$-8{,}339 \cdot 10^{-7}$	$-1{,}158 \cdot 10^{-3}$	$8{,}901 \cdot 10^{-4}$	$-1{,}016 \cdot 10^{-6}$	$-1{,}411 \cdot 10^{-3}$	$1{,}086 \cdot 10^{-3}$
$\varrho_6\varkappa_2$	$-6{,}028 \cdot 10^{-4}$	$-6{,}028 \cdot 10^{-1}$	$1{,}246 \cdot 10^{-1}$	$-5{,}295 \cdot 10^{-4}$	$-5{,}295 \cdot 10^{-1}$	$1{,}143 \cdot 10^{-1}$
$\varrho_6\varkappa_3$	$1{,}366 \cdot 10^{-8}$	$1{,}897 \cdot 10^{-5}$	$-1{,}451 \cdot 10^{-5}$	$1{,}608 \cdot 10^{-8}$	$2{,}233 \cdot 10^{-5}$	$-1{,}709 \cdot 10^{-5}$
$\varrho_6\varkappa_4$	$6{,}037 \cdot 10^{-4}$	$6{,}037 \cdot 10^{-1}$	$-1{,}247 \cdot 10^{-1}$	$5{,}305 \cdot 10^{-4}$	$5{,}305 \cdot 10^{-1}$	$-1{,}144 \cdot 10^{-1}$
$\varrho_7\varkappa_1$	$-5{,}745 \cdot 10^{-7}$	$-1{,}197 \cdot 10^{-3}$	$9{,}199 \cdot 10^{-4}$	$-7{,}077 \cdot 10^{-7}$	$-1{,}474 \cdot 10^{-3}$	$1{,}135 \cdot 10^{-3}$
$\varrho_7\varkappa_2$	$-5{,}006 \cdot 10^{-4}$	$-5{,}006 \cdot 10^{-1}$	$7{,}362 \cdot 10^{-2}$	$-4{,}676 \cdot 10^{-4}$	$-4{,}676 \cdot 10^{-1}$	$7{,}074 \cdot 10^{-2}$
$\varrho_7\varkappa_3$	$-1{,}016 \cdot 10^{-4}$	$-2{,}117 \cdot 10^{-1}$	$1{,}030 \cdot 10^{-1}$	$-6{,}123 \cdot 10^{-5}$	$-1{,}276 \cdot 10^{-1}$	$8{,}891 \cdot 10^{-2}$
$\varrho_7\varkappa_4$	$6{,}028 \cdot 10^{-4}$	$6{,}028 \cdot 10^{-1}$	$-8{,}308 \cdot 10^{-2}$	$5{,}295 \cdot 10^{-4}$	$5{,}295 \cdot 10^{-1}$	$-7{,}620 \cdot 10^{-2}$
$\varrho_8\varkappa_1$	$-9{,}334 \cdot 10^{-7}$	$-1{,}296 \cdot 10^{-3}$	$9{,}969 \cdot 10^{-4}$	$-1{,}157 \cdot 10^{-6}$	$-1{,}606 \cdot 10^{-3}$	$1{,}237 \cdot 10^{-3}$
$\varrho_8\varkappa_2$	$-3{,}980 \cdot 10^{-4}$	$-3{,}980 \cdot 10^{-1}$	$9{,}789 \cdot 10^{-2}$	$-3{,}837 \cdot 10^{-4}$	$-3{,}837 \cdot 10^{-1}$	$9{,}637 \cdot 10^{-2}$
$\varrho_8\varkappa_3$	$-1{,}017 \cdot 10^{-4}$	$-1{,}412 \cdot 10^{-1}$	$9{,}315 \cdot 10^{-2}$	$-8{,}270 \cdot 10^{-5}$	$-1{,}149 \cdot 10^{-1}$	$8{,}385 \cdot 10^{-2}$
$\varrho_8\varkappa_4$	$5{,}006 \cdot 10^{-4}$	$5{,}006 \cdot 10^{-1}$	$-1{,}104 \cdot 10^{-1}$	$4{,}676 \cdot 10^{-4}$	$4{,}676 \cdot 10^{-1}$	$-1{,}061 \cdot 10^{-1}$
$\varrho_9\varkappa_1$	$-7{,}052 \cdot 10^{-7}$	$-1{,}469 \cdot 10^{-3}$	$1{,}131 \cdot 10^{-3}$	$-8{,}795 \cdot 10^{-7}$	$-1{,}832 \cdot 10^{-3}$	$1{,}412 \cdot 10^{-3}$
$\varrho_9\varkappa_2$	$-3{,}241 \cdot 10^{-4}$	$-3{,}241 \cdot 10^{-1}$	$5{,}973 \cdot 10^{-2}$	$-3{,}216 \cdot 10^{-4}$	$-3{,}216 \cdot 10^{-1}$	$5{,}951 \cdot 10^{-2}$
$\varrho_9\varkappa_3$	$-7{,}316 \cdot 10^{-5}$	$-1{,}524 \cdot 10^{-1}$	$9{,}577 \cdot 10^{-2}$	$-6{,}122 \cdot 10^{-5}$	$-1{,}275 \cdot 10^{-1}$	$8{,}890 \cdot 10^{-2}$
$\varrho_9\varkappa_4$	$3{,}980 \cdot 10^{-4}$	$3{,}980 \cdot 10^{-1}$	$-6{,}526 \cdot 10^{-2}$	$3{,}837 \cdot 10^{-4}$	$3{,}837 \cdot 10^{-1}$	$-6{,}425 \cdot 10^{-2}$
$\varrho_{10}\varkappa_1$	$-1{,}297 \cdot 10^{-6}$	$-1{,}801 \cdot 10^{-3}$	$1{,}388 \cdot 10^{-3}$	$-1{,}627 \cdot 10^{-6}$	$-2{,}260 \cdot 10^{-3}$	$1{,}744 \cdot 10^{-3}$
$\varrho_{10}\varkappa_2$	$-2{,}202 \cdot 10^{-4}$	$-2{,}202 \cdot 10^{-1}$	$7{,}499 \cdot 10^{-2}$	$-2{,}245 \cdot 10^{-4}$	$-2{,}245 \cdot 10^{-1}$	$7{,}542 \cdot 10^{-2}$
$\varrho_{10}\varkappa_3$	$-1{,}026 \cdot 10^{-4}$	$-1{,}425 \cdot 10^{-1}$	$9{,}349 \cdot 10^{-2}$	$-9{,}555 \cdot 10^{-5}$	$-1{,}327 \cdot 10^{-1}$	$9{,}065 \cdot 10^{-2}$
$\varrho_{10}\varkappa_4$	$3{,}241 \cdot 10^{-4}$	$3{,}241 \cdot 10^{-1}$	$-8{,}960 \cdot 10^{-2}$	$3{,}216 \cdot 10^{-4}$	$3{,}216 \cdot 10^{-1}$	$-8{,}927 \cdot 10^{-2}$
$\varrho_{11}\varkappa_1$	$-3{,}077 \cdot 10^{-6}$	$-3{,}663 \cdot 10^{-3}$	$2{,}842 \cdot 10^{-3}$	$-3{,}914 \cdot 10^{-6}$	$-4{,}660 \cdot 10^{-3}$	$3{,}628 \cdot 10^{-3}$
$\varrho_{11}\varkappa_2$	$-5{,}685 \cdot 10^{-6}$	$-5{,}685 \cdot 10^{-3}$	$3{,}731 \cdot 10^{-3}$	$-7{,}378 \cdot 10^{-6}$	$-7{,}378 \cdot 10^{-3}$	$4{,}869 \cdot 10^{-3}$
$\varrho_{11}\varkappa_3$	$-2{,}115 \cdot 10^{-4}$	$-2{,}518 \cdot 10^{-1}$	$1{,}094 \cdot 10^{-1}$	$-2{,}132 \cdot 10^{-4}$	$-2{,}538 \cdot 10^{-1}$	$1{,}098 \cdot 10^{-1}$
$\varrho_{11}\varkappa_4$	$2{,}202 \cdot 10^{-4}$	$2{,}202 \cdot 10^{-1}$	$-8{,}749 \cdot 10^{-2}$	$2{,}245 \cdot 10^{-4}$	$2{,}245 \cdot 10^{-1}$	$-8{,}799 \cdot 10^{-2}$
$\varrho_{12}\varkappa_1$	$-5{,}117 \cdot 10^{-5}$	$-6{,}092 \cdot 10^{-2}$	$8{,}045 \cdot 10^{-2}$	$-4{,}142 \cdot 10^{-5}$	$-4{,}931 \cdot 10^{-2}$	$6{,}556 \cdot 10^{-2}$
$\varrho_{12}\varkappa_2$	$-4{,}625 \cdot 10^{-5}$	$-2{,}891 \cdot 10^{-2}$	$1{,}998 \cdot 10^{-2}$	$-2{,}549 \cdot 10^{-5}$	$-1{,}593 \cdot 10^{-2}$	$1{,}076 \cdot 10^{-2}$
$\varrho_{12}\varkappa_3$	$1{,}001 \cdot 10^{-4}$	$1{,}192 \cdot 10^{-1}$	$-1{,}371 \cdot 10^{-1}$	$7{,}009 \cdot 10^{-5}$	$8{,}344 \cdot 10^{-2}$	$-1{,}064 \cdot 10^{-1}$
$\varrho_{12}\varkappa_4$	$-2{,}725 \cdot 10^{-6}$	$-1{,}703 \cdot 10^{-3}$	$1{,}102 \cdot 10^{-3}$	$-3{,}186 \cdot 10^{-6}$	$-1{,}991 \cdot 10^{-3}$	$1{,}289 \cdot 10^{-3}$
$\varrho_{13}\varkappa_1$	$-5{,}270 \cdot 10^{-5}$	$-7{,}319 \cdot 10^{-2}$	$9{,}516 \cdot 10^{-2}$	$-4{,}497 \cdot 10^{-5}$	$-6{,}246 \cdot 10^{-2}$	$8{,}237 \cdot 10^{-2}$
$\varrho_{13}\varkappa_2$	$6{,}277 \cdot 10^{-6}$	$3{,}923 \cdot 10^{-3}$	$-2{,}193 \cdot 10^{-3}$	$1{,}938 \cdot 10^{-5}$	$1{,}211 \cdot 10^{-2}$	$-6{,}948 \cdot 10^{-3}$
$\varrho_{13}\varkappa_3$	$1{,}691 \cdot 10^{-7}$	$2{,}349 \cdot 10^{-4}$	$-2{,}877 \cdot 10^{-4}$	$1{,}078 \cdot 10^{-7}$	$1{,}498 \cdot 10^{-4}$	$-1{,}834 \cdot 10^{-4}$
$\varrho_{13}\varkappa_4$	$4{,}625 \cdot 10^{-5}$	$2{,}891 \cdot 10^{-2}$	$-1{,}713 \cdot 10^{-2}$	$2{,}549 \cdot 10^{-5}$	$1{,}593 \cdot 10^{-2}$	$-9{,}226 \cdot 10^{-3}$
$\varrho_{14}\varkappa_1$	$-7{,}340 \cdot 10^{-5}$	$-1{,}529 \cdot 10^{-1}$	$1{,}534 \cdot 10^{-1}$	$-5{,}720 \cdot 10^{-5}$	$-1{,}192 \cdot 10^{-1}$	$1{,}371 \cdot 10^{-1}$
$\varrho_{14}\varkappa_2$	$-1{,}640 \cdot 10^{-4}$	$-1{,}025 \cdot 10^{-1}$	$3{,}737 \cdot 10^{-2}$	$-1{,}149 \cdot 10^{-4}$	$-7{,}184 \cdot 10^{-2}$	$2{,}808 \cdot 10^{-2}$
$\varrho_{14}\varkappa_3$	$2{,}437 \cdot 10^{-4}$	$5{,}077 \cdot 10^{-1}$	$-2{,}475 \cdot 10^{-1}$	$1{,}915 \cdot 10^{-4}$	$3{,}990 \cdot 10^{-1}$	$-2{,}178 \cdot 10^{-1}$
$\varrho_{14}\varkappa_4$	$-6{,}277 \cdot 10^{-6}$	$-3{,}923 \cdot 10^{-3}$	$1{,}462 \cdot 10^{-3}$	$-1{,}938 \cdot 10^{-5}$	$-1{,}211 \cdot 10^{-2}$	$4{,}632 \cdot 10^{-3}$
$\varrho_{15}\varkappa_1$	$-1{,}655 \cdot 10^{-4}$	$-2{,}299 \cdot 10^{-1}$	$1{,}689 \cdot 10^{-1}$	$-1{,}393 \cdot 10^{-4}$	$-1{,}935 \cdot 10^{-1}$	$1{,}618 \cdot 10^{-1}$
$\varrho_{15}\varkappa_2$	$1{,}144 \cdot 10^{-6}$	$7{,}152 \cdot 10^{-4}$	$-3{,}950 \cdot 10^{-4}$	$2{,}404 \cdot 10^{-5}$	$1{,}502 \cdot 10^{-2}$	$-8{,}682 \cdot 10^{-3}$
$\varrho_{15}\varkappa_3$	$3{,}564 \cdot 10^{-7}$	$4{,}950 \cdot 10^{-4}$	$-6{,}071 \cdot 10^{-4}$	$3{,}447 \cdot 10^{-7}$	$4{,}787 \cdot 10^{-4}$	$-5{,}871 \cdot 10^{-4}$
$\varrho_{15}\varkappa_4$	$1{,}640 \cdot 10^{-4}$	$1{,}025 \cdot 10^{-1}$	$-5{,}605 \cdot 10^{-2}$	$1{,}149 \cdot 10^{-4}$	$7{,}184 \cdot 10^{-2}$	$-4{,}212 \cdot 10^{-2}$
$\varrho_{16}\varkappa_1$	$-2{,}680 \cdot 10^{-4}$	$-5{,}582 \cdot 10^{-1}$	$2{,}628 \cdot 10^{-1}$	$-2{,}560 \cdot 10^{-4}$	$-5{,}333 \cdot 10^{-1}$	$2{,}551 \cdot 10^{-1}$
$\varrho_{16}\varkappa_2$	$-4{,}212 \cdot 10^{-5}$	$-2{,}633 \cdot 10^{-2}$	$1{,}036 \cdot 10^{-2}$	$-4{,}206 \cdot 10^{-5}$	$-2{,}629 \cdot 10^{-2}$	$1{,}035 \cdot 10^{-2}$
$\varrho_{16}\varkappa_3$	$3{,}112 \cdot 10^{-4}$	$6{,}484 \cdot 10^{-1}$	$-2{,}922 \cdot 10^{-1}$	$3{,}221 \cdot 10^{-4}$	$6{,}710 \cdot 10^{-1}$	$-3{,}003 \cdot 10^{-1}$
$\varrho_{16}\varkappa_4$	$-1{,}144 \cdot 10^{-6}$	$-7{,}152 \cdot 10^{-4}$	$2{,}634 \cdot 10^{-4}$	$-2{,}404 \cdot 10^{-5}$	$-1{,}502 \cdot 10^{-2}$	$5{,}788 \cdot 10^{-3}$
$\varrho_{17}\varkappa_1$	$1{,}016 \cdot 10^{-4}$	$2{,}117 \cdot 10^{-1}$	$-1{,}649 \cdot 10^{-1}$	$6{,}123 \cdot 10^{-5}$	$1{,}276 \cdot 10^{-1}$	$-1{,}422 \cdot 10^{-1}$
$\varrho_{17}\varkappa_2$	$-5{,}930 \cdot 10^{-4}$	$-3{,}706 \cdot 10^{-1}$	$6{,}332 \cdot 10^{-2}$	$-6{,}418 \cdot 10^{-4}$	$-4{,}011 \cdot 10^{-1}$	$6{,}548 \cdot 10^{-2}$
$\varrho_{17}\varkappa_3$	$4{,}490 \cdot 10^{-4}$	$9{,}355 \cdot 10^{-1}$	$-4{,}311 \cdot 10^{-1}$	$5{,}383 \cdot 10^{-4}$	$1{,}121$	$-6{,}071 \cdot 10^{-1}$
$\varrho_{17}\varkappa_4$	$4{,}232 \cdot 10^{-5}$	$2{,}645 \cdot 10^{-2}$	$-1{,}042 \cdot 10^{-2}$	$4{,}230 \cdot 10^{-5}$	$2{,}644 \cdot 10^{-2}$	$-1{,}041 \cdot 10^{-2}$
$\varrho_{18}\varkappa_1$	$1{,}017 \cdot 10^{-4}$	$1{,}412 \cdot 10^{-1}$	$-1{,}490 \cdot 10^{-1}$	$8{,}270 \cdot 10^{-5}$	$1{,}149 \cdot 10^{-1}$	$-1{,}342 \cdot 10^{-1}$
$\varrho_{18}\varkappa_2$	$-6{,}946 \cdot 10^{-4}$	$-4{,}342 \cdot 10^{-1}$	$1{,}020 \cdot 10^{-1}$	$-7{,}245 \cdot 10^{-4}$	$-4{,}528 \cdot 10^{-1}$	$1{,}042 \cdot 10^{-1}$
$\varrho_{18}\varkappa_3$	$-4{,}336 \cdot 10^{-8}$	$-6{,}022 \cdot 10^{-5}$	$7{,}373 \cdot 10^{-5}$	$4{,}459 \cdot 10^{-8}$	$6{,}193 \cdot 10^{-5}$	$-7{,}582 \cdot 10^{-5}$
$\varrho_{18}\varkappa_4$	$5{,}930 \cdot 10^{-4}$	$3{,}706 \cdot 10^{-1}$	$-9{,}498 \cdot 10^{-2}$	$6{,}418 \cdot 10^{-4}$	$4{,}011 \cdot 10^{-1}$	$-9{,}822 \cdot 10^{-2}$

Table A.1: Flux tube element outputs ... *cont*

Element Region	$I_{(\mathrm{ph})} = \begin{bmatrix} -10 & 20 & -10 \end{bmatrix}^{\mathrm{T}}$					
	$x = 4\,\mathrm{mm}$			$x = 5\,\mathrm{mm}$		
	Φ [Wb]	B [T]	$\mathcal{F}$ [A]	Φ [Wb]	B [T]	$\mathcal{F}$ [A]
$e_{19}s_1$	$7{,}316 \cdot 10^{-5}$	$1{,}524 \cdot 10^{-1}$	$-1{,}532 \cdot 10^{-1}$	$6{,}122 \cdot 10^{-5}$	$1{,}275 \cdot 10^{-1}$	$-1{,}422 \cdot 10^{-1}$
$e_{19}s_2$	$-4{,}780 \cdot 10^{-4}$	$-2{,}988 \cdot 10^{-1}$	$5{,}735 \cdot 10^{-2}$	$-5{,}498 \cdot 10^{-4}$	$-3{,}436 \cdot 10^{-1}$	$6{,}132 \cdot 10^{-2}$
$e_{19}s_3$	$-2{,}898 \cdot 10^{-4}$	$-6{,}037 \cdot 10^{-1}$	$2{,}772 \cdot 10^{-1}$	$-2{,}360 \cdot 10^{-4}$	$-4{,}916 \cdot 10^{-1}$	$2{,}427 \cdot 10^{-1}$
$e_{19}s_4$	$6{,}946 \cdot 10^{-4}$	$4{,}342 \cdot 10^{-1}$	$-6{,}798 \cdot 10^{-2}$	$7{,}245 \cdot 10^{-4}$	$4{,}528 \cdot 10^{-1}$	$-6{,}950 \cdot 10^{-2}$
$e_{20}s_1$	$1{,}026 \cdot 10^{-4}$	$1{,}425 \cdot 10^{-1}$	$-1{,}496 \cdot 10^{-1}$	$9{,}555 \cdot 10^{-5}$	$1{,}327 \cdot 10^{-1}$	$-1{,}450 \cdot 10^{-1}$
$e_{20}s_2$	$-5{,}802 \cdot 10^{-4}$	$-3{,}626 \cdot 10^{-1}$	$9{,}412 \cdot 10^{-2}$	$-6{,}449 \cdot 10^{-4}$	$-4{,}031 \cdot 10^{-1}$	$9{,}843 \cdot 10^{-2}$
$e_{20}s_3$	$-4{,}097 \cdot 10^{-7}$	$-5{,}690 \cdot 10^{-4}$	$6{,}981 \cdot 10^{-4}$	$-4{,}086 \cdot 10^{-7}$	$-5{,}675 \cdot 10^{-4}$	$6{,}962 \cdot 10^{-4}$
$e_{20}s_4$	$4{,}780 \cdot 10^{-4}$	$2{,}988 \cdot 10^{-1}$	$-8{,}603 \cdot 10^{-2}$	$5{,}498 \cdot 10^{-4}$	$3{,}436 \cdot 10^{-1}$	$-9{,}199 \cdot 10^{-2}$
$e_{21}s_1$	$2{,}115 \cdot 10^{-4}$	$2{,}518 \cdot 10^{-1}$	$-1{,}751 \cdot 10^{-1}$	$2{,}132 \cdot 10^{-4}$	$2{,}538 \cdot 10^{-1}$	$-1{,}757 \cdot 10^{-1}$
$e_{21}s_2$	$-1{,}240 \cdot 10^{-5}$	$-7{,}751 \cdot 10^{-3}$	$5{,}121 \cdot 10^{-3}$	$-1{,}674 \cdot 10^{-5}$	$-1{,}046 \cdot 10^{-2}$	$6{,}970 \cdot 10^{-3}$
$e_{21}s_3$	$-7{,}793 \cdot 10^{-4}$	$-9{,}277 \cdot 10^{-1}$	$4{,}258 \cdot 10^{-1}$	$-8{,}413 \cdot 10^{-4}$	$-1{,}002$	$4{,}813 \cdot 10^{-1}$
$e_{21}s_4$	$5{,}802 \cdot 10^{-4}$	$3{,}626 \cdot 10^{-1}$	$-1{,}098 \cdot 10^{-1}$	$6{,}449 \cdot 10^{-4}$	$4{,}031 \cdot 10^{-1}$	$-1{,}148 \cdot 10^{-1}$
$e_{22}s_1$	$-1{,}001 \cdot 10^{-4}$	$-1{,}192 \cdot 10^{-1}$	$1{,}371 \cdot 10^{-1}$	$-7{,}009 \cdot 10^{-5}$	$-8{,}344 \cdot 10^{-2}$	$1{,}064 \cdot 10^{-1}$
$e_{22}s_2$	$7{,}127 \cdot 10^{-5}$	$4{,}454 \cdot 10^{-2}$	$-3{,}110 \cdot 10^{-2}$	$5{,}701 \cdot 10^{-5}$	$3{,}563 \cdot 10^{-2}$	$-2{,}479 \cdot 10^{-2}$
$e_{22}s_3$	$3{,}283 \cdot 10^{-5}$	$3{,}908 \cdot 10^{-2}$	$-5{,}190 \cdot 10^{-2}$	$1{,}815 \cdot 10^{-5}$	$2{,}161 \cdot 10^{-2}$	$-2{,}815 \cdot 10^{-2}$
$e_{22}s_4$	$-3{,}954 \cdot 10^{-6}$	$-2{,}471 \cdot 10^{-3}$	$1{,}603 \cdot 10^{-3}$	$-5{,}066 \cdot 10^{-6}$	$-3{,}167 \cdot 10^{-3}$	$2{,}060 \cdot 10^{-3}$
$e_{23}s_1$	$-2{,}437 \cdot 10^{-4}$	$-5{,}077 \cdot 10^{-1}$	$2{,}475 \cdot 10^{-1}$	$-1{,}915 \cdot 10^{-4}$	$-3{,}990 \cdot 10^{-1}$	$2{,}178 \cdot 10^{-1}$
$e_{23}s_2$	$4{,}456 \cdot 10^{-5}$	$2{,}785 \cdot 10^{-2}$	$-1{,}099 \cdot 10^{-2}$	$4{,}116 \cdot 10^{-5}$	$2{,}573 \cdot 10^{-2}$	$-1{,}012 \cdot 10^{-2}$
$e_{23}s_3$	$1{,}977 \cdot 10^{-4}$	$4{,}119 \cdot 10^{-1}$	$-2{,}209 \cdot 10^{-1}$	$1{,}663 \cdot 10^{-4}$	$3{,}466 \cdot 10^{-1}$	$-2{,}052 \cdot 10^{-1}$
$e_{23}s_4$	$1{,}425 \cdot 10^{-6}$	$8{,}909 \cdot 10^{-4}$	$-3{,}283 \cdot 10^{-4}$	$-1{,}598 \cdot 10^{-5}$	$-9{,}986 \cdot 10^{-3}$	$3{,}796 \cdot 10^{-3}$
$e_{24}s_1$	$-3{,}112 \cdot 10^{-4}$	$-6{,}484 \cdot 10^{-1}$	$2{,}922 \cdot 10^{-1}$	$-3{,}221 \cdot 10^{-4}$	$-6{,}710 \cdot 10^{-1}$	$3{,}003 \cdot 10^{-1}$
$e_{24}s_2$	$-8{,}211 \cdot 10^{-5}$	$-5{,}132 \cdot 10^{-2}$	$2{,}046 \cdot 10^{-2}$	$-7{,}262 \cdot 10^{-5}$	$-4{,}539 \cdot 10^{-2}$	$1{,}811 \cdot 10^{-2}$
$e_{24}s_3$	$2{,}565 \cdot 10^{-4}$	$5{,}345 \cdot 10^{-1}$	$-2{,}555 \cdot 10^{-1}$	$2{,}598 \cdot 10^{-4}$	$5{,}412 \cdot 10^{-1}$	$-2{,}575 \cdot 10^{-1}$
$e_{24}s_4$	$1{,}368 \cdot 10^{-4}$	$8{,}549 \cdot 10^{-2}$	$-3{,}257 \cdot 10^{-2}$	$1{,}349 \cdot 10^{-4}$	$8{,}432 \cdot 10^{-2}$	$-3{,}221 \cdot 10^{-2}$
$e_{25}s_1$	$-4{,}490 \cdot 10^{-4}$	$-9{,}355 \cdot 10^{-1}$	$4{,}311 \cdot 10^{-1}$	$-5{,}383 \cdot 10^{-4}$	$-1{,}121$	$6{,}071 \cdot 10^{-1}$
$e_{25}s_2$	$3{,}959 \cdot 10^{-5}$	$2{,}474 \cdot 10^{-2}$	$-9{,}719 \cdot 10^{-3}$	$5{,}946 \cdot 10^{-5}$	$3{,}716 \cdot 10^{-2}$	$-1{,}479 \cdot 10^{-2}$
$e_{25}s_3$	$1{,}509 \cdot 10^{-4}$	$3{,}144 \cdot 10^{-1}$	$-1{,}962 \cdot 10^{-1}$	$2{,}046 \cdot 10^{-4}$	$4{,}263 \cdot 10^{-1}$	$-2{,}246 \cdot 10^{-1}$
$e_{25}s_4$	$2{,}585 \cdot 10^{-4}$	$1{,}616 \cdot 10^{-1}$	$-4{,}677 \cdot 10^{-2}$	$2{,}742 \cdot 10^{-4}$	$1{,}714 \cdot 10^{-1}$	$-4{,}744 \cdot 10^{-2}$
$e_{26}s_1$	$2{,}898 \cdot 10^{-4}$	$6{,}037 \cdot 10^{-1}$	$-2{,}772 \cdot 10^{-1}$	$2{,}360 \cdot 10^{-4}$	$4{,}916 \cdot 10^{-1}$	$-2{,}427 \cdot 10^{-1}$
$e_{26}s_2$	$-6{,}605 \cdot 10^{-6}$	$-4{,}128 \cdot 10^{-3}$	$1{,}540 \cdot 10^{-3}$	$-4{,}555 \cdot 10^{-6}$	$-2{,}847 \cdot 10^{-3}$	$1{,}057 \cdot 10^{-3}$
$e_{26}s_3$	$-2{,}059 \cdot 10^{-4}$	$-4{,}290 \cdot 10^{-1}$	$2{,}253 \cdot 10^{-1}$	$-1{,}743 \cdot 10^{-4}$	$-3{,}631 \cdot 10^{-1}$	$2{,}093 \cdot 10^{-1}$
$e_{26}s_4$	$-7{,}728 \cdot 10^{-5}$	$-4{,}830 \cdot 10^{-2}$	$1{,}927 \cdot 10^{-2}$	$-5{,}716 \cdot 10^{-5}$	$-3{,}573 \cdot 10^{-2}$	$1{,}421 \cdot 10^{-2}$
$e_{27}s_1$	$7{,}793 \cdot 10^{-4}$	$9{,}277 \cdot 10^{-1}$	$-4{,}258 \cdot 10^{-1}$	$8{,}413 \cdot 10^{-4}$	$1{,}002$	$-4{,}813 \cdot 10^{-1}$
$e_{27}s_2$	$-1{,}098 \cdot 10^{-4}$	$-6{,}864 \cdot 10^{-2}$	$4{,}717 \cdot 10^{-2}$	$-1{,}455 \cdot 10^{-4}$	$-9{,}092 \cdot 10^{-2}$	$5{,}985 \cdot 10^{-2}$
$e_{27}s_3$	$-4{,}799 \cdot 10^{-4}$	$-5{,}713 \cdot 10^{-1}$	$2{,}668 \cdot 10^{-1}$	$-5{,}068 \cdot 10^{-4}$	$-6{,}033 \cdot 10^{-1}$	$2{,}771 \cdot 10^{-1}$
$e_{27}s_4$	$-1{,}896 \cdot 10^{-4}$	$-1{,}185 \cdot 10^{-1}$	$7{,}174 \cdot 10^{-2}$	$-1{,}891 \cdot 10^{-4}$	$-1{,}182 \cdot 10^{-1}$	$7{,}164 \cdot 10^{-2}$
$e_{28}s_1$	$-1{,}249 \cdot 10^{-3}$	$-4{,}805 \cdot 10^{-1}$	$4{,}183 \cdot 10^{-1}$	$-1{,}264 \cdot 10^{-3}$	$-4{,}863 \cdot 10^{-1}$	$4{,}238 \cdot 10^{-1}$
$e_{28}s_2$	$1{,}154 \cdot 10^{-3}$	$1{,}283$	$-4{,}648$	$1{,}165 \cdot 10^{-3}$	$1{,}294$	$-4{,}753$
$e_{28}s_3$	$1{,}533 \cdot 10^{-5}$	$5{,}895 \cdot 10^{-3}$	$-4{,}979 \cdot 10^{-3}$	$1{,}645 \cdot 10^{-5}$	$6{,}329 \cdot 10^{-3}$	$-5{,}346 \cdot 10^{-3}$
$e_{28}s_4$	$7{,}956 \cdot 10^{-5}$	$8{,}841 \cdot 10^{-2}$	$-2{,}150 \cdot 10^{-1}$	$8{,}345 \cdot 10^{-5}$	$9{,}273 \cdot 10^{-2}$	$-2{,}255 \cdot 10^{-1}$
$e_{29}s_1$	$-8{,}256 \cdot 10^{-5}$	$-8{,}256 \cdot 10^{-2}$	$6{,}951 \cdot 10^{-2}$	$-7{,}928 \cdot 10^{-5}$	$-7{,}928 \cdot 10^{-2}$	$6{,}675 \cdot 10^{-2}$
$e_{29}s_2$	$1{,}235 \cdot 10^{-3}$	$1{,}372$	$-2{,}171$	$1{,}242 \cdot 10^{-3}$	$1{,}380$	$-2{,}214$
$e_{29}s_3$	$1{,}833 \cdot 10^{-6}$	$1{,}833 \cdot 10^{-3}$	$-1{,}549 \cdot 10^{-3}$	$1{,}886 \cdot 10^{-6}$	$1{,}886 \cdot 10^{-3}$	$-1{,}594 \cdot 10^{-3}$
$e_{29}s_4$	$-1{,}154 \cdot 10^{-3}$	$-1{,}283$	$1{,}788$	$-1{,}165 \cdot 10^{-3}$	$-1{,}294$	$1{,}828$
$e_{30}s_1$	$1{,}295 \cdot 10^{-3}$	$4{,}979 \cdot 10^{-1}$	$-4{,}347 \cdot 10^{-1}$	$1{,}309 \cdot 10^{-3}$	$5{,}034 \cdot 10^{-1}$	$-4{,}399 \cdot 10^{-1}$
$e_{30}s_2$	$-5{,}850 \cdot 10^{-5}$	$-6{,}500 \cdot 10^{-2}$	$1{,}582 \cdot 10^{-1}$	$-6{,}498 \cdot 10^{-5}$	$-7{,}220 \cdot 10^{-2}$	$1{,}756 \cdot 10^{-1}$
$e_{30}s_3$	$-1{,}007 \cdot 10^{-6}$	$-3{,}873 \cdot 10^{-4}$	$3{,}273 \cdot 10^{-4}$	$-2{,}011 \cdot 10^{-6}$	$-7{,}733 \cdot 10^{-4}$	$6{,}535 \cdot 10^{-4}$
$e_{30}s_4$	$-1{,}235 \cdot 10^{-3}$	$-1{,}372$	$5{,}646$	$-1{,}242 \cdot 10^{-3}$	$-1{,}380$	$5{,}757$

Table A.1: Flux tube element outputs ... *cont*

Element Region	$I_{(\mathrm{ph})} = \left[-10\ -10\ 20\right]^{\mathrm{T}}$					
	$x = 0\,\mathrm{mm}$			$x = 1\,\mathrm{mm}$		
	Φ [Wb]	B [T]	$\mathcal{F}$ [A]	Φ [Wb]	B [T]	$\mathcal{F}$ [A]
$\varrho_1\kappa_1$	$3{,}079 \cdot 10^{-6}$	$3{,}665 \cdot 10^{-3}$	$-2{,}843 \cdot 10^{-3}$	$2{,}937 \cdot 10^{-6}$	$3{,}496 \cdot 10^{-3}$	$-2{,}711 \cdot 10^{-3}$
$\varrho_1\kappa_2$	$-1{,}734 \cdot 10^{-4}$	$-1{,}734 \cdot 10^{-1}$	$8{,}322 \cdot 10^{-2}$	$-1{,}476 \cdot 10^{-4}$	$-1{,}476 \cdot 10^{-1}$	$7{,}957 \cdot 10^{-2}$
$\varrho_1\kappa_3$	$1{,}655 \cdot 10^{-4}$	$1{,}970 \cdot 10^{-1}$	$-1{,}015 \cdot 10^{-1}$	$1{,}401 \cdot 10^{-4}$	$1{,}668 \cdot 10^{-1}$	$-9{,}823 \cdot 10^{-2}$
$\varrho_1\kappa_4$	$4{,}805 \cdot 10^{-6}$	$4{,}805 \cdot 10^{-3}$	$-3{,}144 \cdot 10^{-3}$	$4{,}511 \cdot 10^{-6}$	$4{,}511 \cdot 10^{-3}$	$-2{,}948 \cdot 10^{-3}$
$\varrho_2\kappa_1$	$1{,}414 \cdot 10^{-6}$	$1{,}964 \cdot 10^{-3}$	$-1{,}514 \cdot 10^{-3}$	$1{,}360 \cdot 10^{-6}$	$1{,}890 \cdot 10^{-3}$	$-1{,}456 \cdot 10^{-3}$
$\varrho_2\kappa_2$	$-3{,}113 \cdot 10^{-4}$	$-3{,}113 \cdot 10^{-1}$	$8{,}786 \cdot 10^{-2}$	$-2{,}706 \cdot 10^{-4}$	$-2{,}706 \cdot 10^{-1}$	$8{,}160 \cdot 10^{-2}$
$\varrho_2\kappa_3$	$1{,}365 \cdot 10^{-4}$	$1{,}896 \cdot 10^{-1}$	$-1{,}008 \cdot 10^{-1}$	$1{,}216 \cdot 10^{-4}$	$1{,}689 \cdot 10^{-1}$	$-9{,}852 \cdot 10^{-2}$
$\varrho_2\kappa_4$	$1{,}734 \cdot 10^{-4}$	$1{,}734 \cdot 10^{-1}$	$-7{,}133 \cdot 10^{-2}$	$1{,}476 \cdot 10^{-4}$	$1{,}476 \cdot 10^{-1}$	$-6{,}820 \cdot 10^{-2}$
$\varrho_3\kappa_1$	$7{,}968 \cdot 10^{-7}$	$1{,}660 \cdot 10^{-3}$	$-1{,}278 \cdot 10^{-3}$	$7{,}681 \cdot 10^{-7}$	$1{,}600 \cdot 10^{-3}$	$-1{,}232 \cdot 10^{-3}$
$\varrho_3\kappa_2$	$-4{,}614 \cdot 10^{-4}$	$-4{,}614 \cdot 10^{-1}$	$7{,}021 \cdot 10^{-2}$	$-4{,}272 \cdot 10^{-4}$	$-4{,}272 \cdot 10^{-1}$	$6{,}743 \cdot 10^{-2}$
$\varrho_3\kappa_3$	$1{,}493 \cdot 10^{-4}$	$3{,}110 \cdot 10^{-1}$	$-1{,}220 \cdot 10^{-1}$	$1{,}558 \cdot 10^{-4}$	$3{,}246 \cdot 10^{-1}$	$-1{,}245 \cdot 10^{-1}$
$\varrho_3\kappa_4$	$3{,}113 \cdot 10^{-4}$	$3{,}113 \cdot 10^{-1}$	$-5{,}858 \cdot 10^{-2}$	$2{,}706 \cdot 10^{-4}$	$2{,}706 \cdot 10^{-1}$	$-5{,}440 \cdot 10^{-2}$
$\varrho_4\kappa_1$	$1{,}084 \cdot 10^{-6}$	$1{,}506 \cdot 10^{-3}$	$-1{,}159 \cdot 10^{-3}$	$1{,}048 \cdot 10^{-6}$	$1{,}455 \cdot 10^{-3}$	$-1{,}120 \cdot 10^{-3}$
$\varrho_4\kappa_2$	$-7{,}212 \cdot 10^{-4}$	$-7{,}212 \cdot 10^{-1}$	$1{,}438 \cdot 10^{-1}$	$-6{,}999 \cdot 10^{-4}$	$-6{,}999 \cdot 10^{-1}$	$1{,}400 \cdot 10^{-1}$
$\varrho_4\kappa_3$	$2{,}587 \cdot 10^{-4}$	$3{,}593 \cdot 10^{-1}$	$-1{,}302 \cdot 10^{-1}$	$2{,}717 \cdot 10^{-4}$	$3{,}774 \cdot 10^{-1}$	$-1{,}329 \cdot 10^{-1}$
$\varrho_4\kappa_4$	$4{,}614 \cdot 10^{-4}$	$4{,}614 \cdot 10^{-1}$	$-1{,}053 \cdot 10^{-1}$	$4{,}272 \cdot 10^{-4}$	$4{,}272 \cdot 10^{-1}$	$-1{,}012 \cdot 10^{-1}$
$\varrho_5\kappa_1$	$6{,}834 \cdot 10^{-7}$	$1{,}424 \cdot 10^{-3}$	$-1{,}095 \cdot 10^{-3}$	$6{,}623 \cdot 10^{-7}$	$1{,}380 \cdot 10^{-3}$	$-1{,}061 \cdot 10^{-3}$
$\varrho_5\kappa_2$	$-1{,}018 \cdot 10^{-3}$	$-1{,}018$	$1{,}487 \cdot 10^{-1}$	$-1{,}005 \cdot 10^{-3}$	$-1{,}005$	$1{,}452 \cdot 10^{-1}$
$\varrho_5\kappa_3$	$2{,}963 \cdot 10^{-4}$	$6{,}174 \cdot 10^{-1}$	$-1{,}761 \cdot 10^{-1}$	$3{,}041 \cdot 10^{-4}$	$6{,}336 \cdot 10^{-1}$	$-1{,}795 \cdot 10^{-1}$
$\varrho_5\kappa_4$	$7{,}212 \cdot 10^{-4}$	$7{,}212 \cdot 10^{-1}$	$-9{,}588 \cdot 10^{-2}$	$6{,}999 \cdot 10^{-4}$	$6{,}999 \cdot 10^{-1}$	$-9{,}335 \cdot 10^{-2}$
$\varrho_6\kappa_1$	$1{,}050 \cdot 10^{-6}$	$1{,}458 \cdot 10^{-3}$	$-1{,}122 \cdot 10^{-3}$	$1{,}019 \cdot 10^{-6}$	$1{,}416 \cdot 10^{-3}$	$-1{,}089 \cdot 10^{-3}$
$\varrho_6\kappa_2$	$-1{,}019 \cdot 10^{-3}$	$-1{,}019$	$2{,}234 \cdot 10^{-1}$	$-1{,}006 \cdot 10^{-3}$	$-1{,}006$	$2{,}182 \cdot 10^{-1}$
$\varrho_6\kappa_3$	$-8{,}776 \cdot 10^{-9}$	$-1{,}219 \cdot 10^{-5}$	$9{,}325 \cdot 10^{-6}$	$-5{,}190 \cdot 10^{-9}$	$-7{,}208 \cdot 10^{-6}$	$5{,}514 \cdot 10^{-6}$
$\varrho_6\kappa_4$	$1{,}018 \cdot 10^{-3}$	$1{,}018$	$-2{,}230 \cdot 10^{-1}$	$1{,}005 \cdot 10^{-3}$	$1{,}005$	$-2{,}178 \cdot 10^{-1}$
$\varrho_7\kappa_1$	$7{,}367 \cdot 10^{-7}$	$1{,}535 \cdot 10^{-3}$	$-1{,}181 \cdot 10^{-3}$	$7{,}161 \cdot 10^{-7}$	$1{,}492 \cdot 10^{-3}$	$-1{,}148 \cdot 10^{-3}$
$\varrho_7\kappa_2$	$-6{,}355 \cdot 10^{-4}$	$-6{,}355 \cdot 10^{-1}$	$8{,}634 \cdot 10^{-2}$	$-6{,}488 \cdot 10^{-4}$	$-6{,}488 \cdot 10^{-1}$	$8{,}772 \cdot 10^{-2}$
$\varrho_7\kappa_3$	$-3{,}845 \cdot 10^{-4}$	$-8{,}010 \cdot 10^{-1}$	$2{,}218 \cdot 10^{-1}$	$-3{,}576 \cdot 10^{-4}$	$-7{,}450 \cdot 10^{-1}$	$2{,}060 \cdot 10^{-1}$
$\varrho_7\kappa_4$	$1{,}019 \cdot 10^{-3}$	$1{,}019$	$-1{,}490 \cdot 10^{-1}$	$1{,}006 \cdot 10^{-3}$	$1{,}006$	$-1{,}454 \cdot 10^{-1}$
$\varrho_8\kappa_1$	$1{,}142 \cdot 10^{-6}$	$1{,}586 \cdot 10^{-3}$	$-1{,}221 \cdot 10^{-3}$	$1{,}115 \cdot 10^{-6}$	$1{,}548 \cdot 10^{-3}$	$-1{,}192 \cdot 10^{-3}$
$\varrho_8\kappa_2$	$-3{,}349 \cdot 10^{-4}$	$-3{,}349 \cdot 10^{-1}$	$9{,}095 \cdot 10^{-2}$	$-3{,}609 \cdot 10^{-4}$	$-3{,}609 \cdot 10^{-1}$	$9{,}394 \cdot 10^{-2}$
$\varrho_8\kappa_3$	$-3{,}017 \cdot 10^{-4}$	$-4{,}191 \cdot 10^{-1}$	$1{,}392 \cdot 10^{-1}$	$-2{,}890 \cdot 10^{-4}$	$-4{,}013 \cdot 10^{-1}$	$1{,}365 \cdot 10^{-1}$
$\varrho_8\kappa_4$	$6{,}355 \cdot 10^{-4}$	$6{,}355 \cdot 10^{-1}$	$-1{,}295 \cdot 10^{-1}$	$6{,}488 \cdot 10^{-4}$	$6{,}488 \cdot 10^{-1}$	$-1{,}316 \cdot 10^{-1}$
$\varrho_9\kappa_1$	$8{,}160 \cdot 10^{-7}$	$1{,}700 \cdot 10^{-3}$	$-1{,}309 \cdot 10^{-3}$	$7{,}979 \cdot 10^{-7}$	$1{,}662 \cdot 10^{-3}$	$-1{,}280 \cdot 10^{-3}$
$\varrho_9\kappa_2$	$-1{,}718 \cdot 10^{-4}$	$-1{,}718 \cdot 10^{-1}$	$4{,}747 \cdot 10^{-2}$	$-2{,}067 \cdot 10^{-4}$	$-2{,}067 \cdot 10^{-1}$	$4{,}918 \cdot 10^{-2}$
$\varrho_9\kappa_3$	$-1{,}639 \cdot 10^{-4}$	$-3{,}414 \cdot 10^{-1}$	$1{,}274 \cdot 10^{-1}$	$-1{,}550 \cdot 10^{-4}$	$-3{,}230 \cdot 10^{-1}$	$1{,}242 \cdot 10^{-1}$
$\varrho_9\kappa_4$	$3{,}349 \cdot 10^{-4}$	$3{,}349 \cdot 10^{-1}$	$-6{,}063 \cdot 10^{-2}$	$3{,}609 \cdot 10^{-4}$	$3{,}609 \cdot 10^{-1}$	$-6{,}263 \cdot 10^{-2}$
$\varrho_{10}\kappa_1$	$1{,}395 \cdot 10^{-6}$	$1{,}937 \cdot 10^{-3}$	$-1{,}493 \cdot 10^{-3}$	$1{,}365 \cdot 10^{-6}$	$1{,}896 \cdot 10^{-3}$	$-1{,}462 \cdot 10^{-3}$
$\varrho_{10}\kappa_2$	$-8{,}471 \cdot 10^{-5}$	$-8{,}471 \cdot 10^{-2}$	$4{,}849 \cdot 10^{-2}$	$-1{,}075 \cdot 10^{-4}$	$-1{,}075 \cdot 10^{-1}$	$5{,}790 \cdot 10^{-2}$
$\varrho_{10}\kappa_3$	$-8{,}851 \cdot 10^{-5}$	$-1{,}229 \cdot 10^{-1}$	$8{,}720 \cdot 10^{-2}$	$-1{,}005 \cdot 10^{-4}$	$-1{,}397 \cdot 10^{-1}$	$9{,}272 \cdot 10^{-2}$
$\varrho_{10}\kappa_4$	$1{,}718 \cdot 10^{-4}$	$1{,}718 \cdot 10^{-1}$	$-7{,}120 \cdot 10^{-2}$	$2{,}067 \cdot 10^{-4}$	$2{,}067 \cdot 10^{-1}$	$-7{,}377 \cdot 10^{-2}$
$\varrho_{11}\kappa_1$	$2{,}816 \cdot 10^{-6}$	$3{,}353 \cdot 10^{-3}$	$-2{,}598 \cdot 10^{-3}$	$2{,}765 \cdot 10^{-6}$	$3{,}291 \cdot 10^{-3}$	$-2{,}550 \cdot 10^{-3}$
$\varrho_{11}\kappa_2$	$3{,}773 \cdot 10^{-6}$	$3{,}773 \cdot 10^{-3}$	$-2{,}460 \cdot 10^{-3}$	$3{,}688 \cdot 10^{-6}$	$3{,}688 \cdot 10^{-3}$	$-2{,}404 \cdot 10^{-3}$
$\varrho_{11}\kappa_3$	$-9{,}130 \cdot 10^{-5}$	$-1{,}087 \cdot 10^{-1}$	$8{,}099 \cdot 10^{-2}$	$-1{,}140 \cdot 10^{-4}$	$-1{,}357 \cdot 10^{-1}$	$9{,}157 \cdot 10^{-2}$
$\varrho_{11}\kappa_4$	$8{,}471 \cdot 10^{-5}$	$8{,}471 \cdot 10^{-2}$	$-5{,}657 \cdot 10^{-2}$	$1{,}075 \cdot 10^{-4}$	$1{,}075 \cdot 10^{-1}$	$-6{,}755 \cdot 10^{-2}$
$\varrho_{12}\kappa_1$	$-1{,}655 \cdot 10^{-4}$	$-1{,}970 \cdot 10^{-1}$	$1{,}623 \cdot 10^{-1}$	$-1{,}401 \cdot 10^{-4}$	$-1{,}668 \cdot 10^{-1}$	$1{,}572 \cdot 10^{-1}$
$\varrho_{12}\kappa_2$	$-2{,}948 \cdot 10^{-4}$	$-1{,}842 \cdot 10^{-1}$	$8{,}420 \cdot 10^{-2}$	$-2{,}329 \cdot 10^{-4}$	$-1{,}455 \cdot 10^{-1}$	$7{,}916 \cdot 10^{-2}$
$\varrho_{12}\kappa_3$	$4{,}524 \cdot 10^{-4}$	$5{,}385 \cdot 10^{-1}$	$-2{,}567 \cdot 10^{-1}$	$3{,}658 \cdot 10^{-4}$	$4{,}355 \cdot 10^{-1}$	$-2{,}270 \cdot 10^{-1}$
$\varrho_{12}\kappa_4$	$7{,}891 \cdot 10^{-6}$	$4{,}932 \cdot 10^{-3}$	$-3{,}228 \cdot 10^{-3}$	$7{,}181 \cdot 10^{-6}$	$4{,}488 \cdot 10^{-3}$	$-2{,}933 \cdot 10^{-3}$
$\varrho_{13}\kappa_1$	$-1{,}365 \cdot 10^{-4}$	$-1{,}896 \cdot 10^{-1}$	$1{,}612 \cdot 10^{-1}$	$-1{,}216 \cdot 10^{-4}$	$-1{,}689 \cdot 10^{-1}$	$1{,}576 \cdot 10^{-1}$
$\varrho_{13}\kappa_2$	$-1{,}587 \cdot 10^{-4}$	$-9{,}920 \cdot 10^{-2}$	$5{,}476 \cdot 10^{-2}$	$-1{,}117 \cdot 10^{-4}$	$-6{,}979 \cdot 10^{-2}$	$4{,}104 \cdot 10^{-2}$
$\varrho_{13}\kappa_3$	$4{,}514 \cdot 10^{-7}$	$6{,}269 \cdot 10^{-4}$	$-7{,}692 \cdot 10^{-4}$	$4{,}334 \cdot 10^{-7}$	$6{,}019 \cdot 10^{-4}$	$-7{,}385 \cdot 10^{-4}$
$\varrho_{13}\kappa_4$	$2{,}948 \cdot 10^{-4}$	$1{,}842 \cdot 10^{-1}$	$-7{,}217 \cdot 10^{-2}$	$2{,}329 \cdot 10^{-4}$	$1{,}455 \cdot 10^{-1}$	$-6{,}786 \cdot 10^{-2}$
$\varrho_{14}\kappa_1$	$-1{,}493 \cdot 10^{-4}$	$-3{,}110 \cdot 10^{-1}$	$1{,}952 \cdot 10^{-1}$	$-1{,}558 \cdot 10^{-4}$	$-3{,}246 \cdot 10^{-1}$	$1{,}992 \cdot 10^{-1}$
$\varrho_{14}\kappa_2$	$-5{,}561 \cdot 10^{-4}$	$-3{,}475 \cdot 10^{-1}$	$6{,}163 \cdot 10^{-2}$	$-5{,}002 \cdot 10^{-4}$	$-3{,}126 \cdot 10^{-1}$	$5{,}870 \cdot 10^{-2}$
$\varrho_{14}\kappa_3$	$5{,}466 \cdot 10^{-4}$	$1{,}139$	$-6{,}316 \cdot 10^{-1}$	$5{,}443 \cdot 10^{-4}$	$1{,}134$	$-6{,}247 \cdot 10^{-1}$
$\varrho_{14}\kappa_4$	$1{,}587 \cdot 10^{-4}$	$9{,}920 \cdot 10^{-2}$	$-3{,}651 \cdot 10^{-2}$	$1{,}117 \cdot 10^{-4}$	$6{,}979 \cdot 10^{-2}$	$-2{,}736 \cdot 10^{-2}$

Table A.1: Flux tube element outputs ... *cont*

Element Region	$I_{(\mathrm{ph})} = \begin{bmatrix} -10 & -10 & 20 \end{bmatrix}^{\mathrm{T}}$					
	$x = 0\,\mathrm{mm}$			$x = 1\,\mathrm{mm}$		
	Φ [Wb]	B [T]	$\mathcal{F}$ [A]	Φ [Wb]	B [T]	$\mathcal{F}$ [A]
$e_{15}s_1$	$-2{,}587 \cdot 10^{-4}$	$-3{,}593 \cdot 10^{-1}$	$2{,}084 \cdot 10^{-1}$	$-2{,}717 \cdot 10^{-4}$	$-3{,}774 \cdot 10^{-1}$	$2{,}127 \cdot 10^{-1}$
$e_{15}s_2$	$-2{,}977 \cdot 10^{-4}$	$-1{,}861 \cdot 10^{-1}$	$7{,}230 \cdot 10^{-2}$	$-2{,}289 \cdot 10^{-4}$	$-1{,}431 \cdot 10^{-1}$	$6{,}741 \cdot 10^{-2}$
$e_{15}s_3$	$3{,}597 \cdot 10^{-7}$	$4{,}996 \cdot 10^{-4}$	$-6{,}127 \cdot 10^{-4}$	$3{,}795 \cdot 10^{-7}$	$5{,}270 \cdot 10^{-4}$	$-6{,}465 \cdot 10^{-4}$
$e_{15}s_4$	$5{,}561 \cdot 10^{-4}$	$3{,}475 \cdot 10^{-1}$	$-9{,}244 \cdot 10^{-2}$	$5{,}002 \cdot 10^{-4}$	$3{,}126 \cdot 10^{-1}$	$-8{,}805 \cdot 10^{-2}$
$e_{16}s_1$	$-2{,}963 \cdot 10^{-4}$	$-6{,}174 \cdot 10^{-1}$	$2{,}817 \cdot 10^{-1}$	$-3{,}041 \cdot 10^{-4}$	$-6{,}336 \cdot 10^{-1}$	$2{,}871 \cdot 10^{-1}$
$e_{16}s_2$	$-4{,}242 \cdot 10^{-5}$	$-2{,}651 \cdot 10^{-2}$	$1{,}044 \cdot 10^{-2}$	$-4{,}238 \cdot 10^{-5}$	$-2{,}649 \cdot 10^{-2}$	$1{,}043 \cdot 10^{-2}$
$e_{16}s_3$	$4{,}103 \cdot 10^{-5}$	$8{,}549 \cdot 10^{-2}$	$-1{,}086 \cdot 10^{-1}$	$1{,}176 \cdot 10^{-4}$	$2{,}450 \cdot 10^{-1}$	$-1{,}730 \cdot 10^{-1}$
$e_{16}s_4$	$2{,}977 \cdot 10^{-4}$	$1{,}861 \cdot 10^{-1}$	$-4{,}820 \cdot 10^{-2}$	$2{,}289 \cdot 10^{-4}$	$1{,}431 \cdot 10^{-1}$	$-4{,}494 \cdot 10^{-2}$
$e_{17}s_1$	$3{,}845 \cdot 10^{-4}$	$8{,}010 \cdot 10^{-1}$	$-3{,}549 \cdot 10^{-1}$	$3{,}576 \cdot 10^{-4}$	$7{,}450 \cdot 10^{-1}$	$-3{,}296 \cdot 10^{-1}$
$e_{17}s_2$	$-1{,}889 \cdot 10^{-6}$	$-1{,}181 \cdot 10^{-3}$	$4{,}356 \cdot 10^{-4}$	$-6{,}194 \cdot 10^{-5}$	$-3{,}871 \cdot 10^{-2}$	$1{,}542 \cdot 10^{-2}$
$e_{17}s_3$	$-4{,}249 \cdot 10^{-4}$	$-8{,}853 \cdot 10^{-1}$	$3{,}992 \cdot 10^{-1}$	$-3{,}380 \cdot 10^{-4}$	$-7{,}042 \cdot 10^{-1}$	$3{,}129 \cdot 10^{-1}$
$e_{17}s_4$	$4{,}236 \cdot 10^{-5}$	$2{,}647 \cdot 10^{-2}$	$-1{,}043 \cdot 10^{-2}$	$4{,}237 \cdot 10^{-5}$	$2{,}648 \cdot 10^{-2}$	$-1{,}043 \cdot 10^{-2}$
$e_{18}s_1$	$3{,}017 \cdot 10^{-4}$	$4{,}191 \cdot 10^{-1}$	$-2{,}227 \cdot 10^{-1}$	$2{,}890 \cdot 10^{-4}$	$4{,}013 \cdot 10^{-1}$	$-2{,}183 \cdot 10^{-1}$
$e_{18}s_2$	$-3{,}032 \cdot 10^{-4}$	$-1{,}895 \cdot 10^{-1}$	$7{,}254 \cdot 10^{-2}$	$-3{,}505 \cdot 10^{-4}$	$-2{,}191 \cdot 10^{-1}$	$7{,}487 \cdot 10^{-2}$
$e_{18}s_3$	$-4{,}403 \cdot 10^{-7}$	$-6{,}116 \cdot 10^{-4}$	$7{,}504 \cdot 10^{-4}$	$-4{,}087 \cdot 10^{-7}$	$-5{,}677 \cdot 10^{-4}$	$6{,}964 \cdot 10^{-4}$
$e_{18}s_4$	$1{,}889 \cdot 10^{-6}$	$1{,}181 \cdot 10^{-3}$	$-6{,}534 \cdot 10^{-4}$	$6{,}194 \cdot 10^{-5}$	$3{,}871 \cdot 10^{-2}$	$-2{,}313 \cdot 10^{-2}$
$e_{19}s_1$	$1{,}639 \cdot 10^{-4}$	$3{,}414 \cdot 10^{-1}$	$-2{,}038 \cdot 10^{-1}$	$1{,}550 \cdot 10^{-4}$	$3{,}230 \cdot 10^{-1}$	$-1{,}988 \cdot 10^{-1}$
$e_{19}s_2$	$-2{,}351 \cdot 10^{-5}$	$-1{,}469 \cdot 10^{-2}$	$5{,}657 \cdot 10^{-3}$	$-6{,}583 \cdot 10^{-5}$	$-4{,}115 \cdot 10^{-2}$	$1{,}641 \cdot 10^{-2}$
$e_{19}s_3$	$-4{,}435 \cdot 10^{-4}$	$-9{,}241 \cdot 10^{-1}$	$4{,}233 \cdot 10^{-1}$	$-4{,}397 \cdot 10^{-4}$	$-9{,}161 \cdot 10^{-1}$	$4{,}181 \cdot 10^{-1}$
$e_{19}s_4$	$3{,}032 \cdot 10^{-4}$	$1{,}895 \cdot 10^{-1}$	$-4{,}836 \cdot 10^{-2}$	$3{,}505 \cdot 10^{-4}$	$2{,}191 \cdot 10^{-1}$	$-4{,}992 \cdot 10^{-2}$
$e_{20}s_1$	$8{,}851 \cdot 10^{-5}$	$1{,}229 \cdot 10^{-1}$	$-1{,}395 \cdot 10^{-1}$	$1{,}005 \cdot 10^{-4}$	$1{,}397 \cdot 10^{-1}$	$-1{,}483 \cdot 10^{-1}$
$e_{20}s_2$	$-1{,}117 \cdot 10^{-4}$	$-6{,}979 \cdot 10^{-2}$	$4{,}104 \cdot 10^{-2}$	$-1{,}660 \cdot 10^{-4}$	$-1{,}038 \cdot 10^{-1}$	$5{,}652 \cdot 10^{-2}$
$e_{20}s_3$	$-3{,}683 \cdot 10^{-7}$	$-5{,}116 \cdot 10^{-4}$	$6{,}275 \cdot 10^{-4}$	$-3{,}798 \cdot 10^{-7}$	$-5{,}275 \cdot 10^{-4}$	$6{,}470 \cdot 10^{-4}$
$e_{20}s_4$	$2{,}351 \cdot 10^{-5}$	$1{,}469 \cdot 10^{-2}$	$-8{,}485 \cdot 10^{-3}$	$6{,}583 \cdot 10^{-5}$	$4{,}115 \cdot 10^{-2}$	$-2{,}461 \cdot 10^{-2}$
$e_{21}s_1$	$9{,}130 \cdot 10^{-5}$	$1{,}087 \cdot 10^{-1}$	$-1{,}296 \cdot 10^{-1}$	$1{,}140 \cdot 10^{-4}$	$1{,}357 \cdot 10^{-1}$	$-1{,}465 \cdot 10^{-1}$
$e_{21}s_2$	$5{,}052 \cdot 10^{-6}$	$3{,}158 \cdot 10^{-3}$	$-2{,}054 \cdot 10^{-3}$	$4{,}811 \cdot 10^{-6}$	$3{,}007 \cdot 10^{-3}$	$-1{,}955 \cdot 10^{-3}$
$e_{21}s_3$	$-2{,}080 \cdot 10^{-4}$	$-2{,}476 \cdot 10^{-1}$	$1{,}738 \cdot 10^{-1}$	$-2{,}848 \cdot 10^{-4}$	$-3{,}390 \cdot 10^{-1}$	$2{,}032 \cdot 10^{-1}$
$e_{21}s_4$	$1{,}117 \cdot 10^{-4}$	$6{,}979 \cdot 10^{-2}$	$-4{,}788 \cdot 10^{-2}$	$1{,}660 \cdot 10^{-4}$	$1{,}038 \cdot 10^{-1}$	$-6{,}594 \cdot 10^{-2}$
$e_{22}s_1$	$-4{,}524 \cdot 10^{-4}$	$-5{,}385 \cdot 10^{-1}$	$2{,}567 \cdot 10^{-1}$	$-3{,}658 \cdot 10^{-4}$	$-4{,}355 \cdot 10^{-1}$	$2{,}270 \cdot 10^{-1}$
$e_{22}s_2$	$1{,}477 \cdot 10^{-4}$	$9{,}229 \cdot 10^{-2}$	$-6{,}055 \cdot 10^{-2}$	$1{,}387 \cdot 10^{-4}$	$8{,}666 \cdot 10^{-2}$	$-5{,}763 \cdot 10^{-2}$
$e_{22}s_3$	$2{,}710 \cdot 10^{-4}$	$3{,}226 \cdot 10^{-1}$	$-1{,}987 \cdot 10^{-1}$	$1{,}997 \cdot 10^{-4}$	$2{,}377 \cdot 10^{-1}$	$-1{,}710 \cdot 10^{-1}$
$e_{22}s_4$	$3{,}375 \cdot 10^{-5}$	$2{,}109 \cdot 10^{-2}$	$-1{,}441 \cdot 10^{-2}$	$2{,}753 \cdot 10^{-5}$	$1{,}720 \cdot 10^{-2}$	$-1{,}166 \cdot 10^{-2}$
$e_{23}s_1$	$-5{,}466 \cdot 10^{-4}$	$-1{,}139$	$6{,}316 \cdot 10^{-1}$	$-5{,}443 \cdot 10^{-4}$	$-1{,}134$	$6{,}247 \cdot 10^{-1}$
$e_{23}s_2$	$1{,}813 \cdot 10^{-4}$	$1{,}133 \cdot 10^{-1}$	$-3{,}992 \cdot 10^{-2}$	$1{,}834 \cdot 10^{-4}$	$1{,}146 \cdot 10^{-1}$	$-4{,}019 \cdot 10^{-2}$
$e_{23}s_3$	$3{,}037 \cdot 10^{-4}$	$6{,}327 \cdot 10^{-1}$	$-2{,}868 \cdot 10^{-1}$	$3{,}023 \cdot 10^{-4}$	$6{,}297 \cdot 10^{-1}$	$-2{,}858 \cdot 10^{-1}$
$e_{23}s_4$	$6{,}161 \cdot 10^{-5}$	$3{,}851 \cdot 10^{-2}$	$-1{,}534 \cdot 10^{-2}$	$5{,}873 \cdot 10^{-5}$	$3{,}671 \cdot 10^{-2}$	$-1{,}461 \cdot 10^{-2}$
$e_{24}s_1$	$-4{,}103 \cdot 10^{-5}$	$-8{,}549 \cdot 10^{-2}$	$1{,}086 \cdot 10^{-1}$	$-1{,}176 \cdot 10^{-4}$	$-2{,}450 \cdot 10^{-1}$	$1{,}730 \cdot 10^{-1}$
$e_{24}s_2$	$-5{,}315 \cdot 10^{-5}$	$-3{,}322 \cdot 10^{-2}$	$1{,}318 \cdot 10^{-2}$	$-3{,}169 \cdot 10^{-5}$	$-1{,}981 \cdot 10^{-2}$	$7{,}712 \cdot 10^{-3}$
$e_{24}s_3$	$1{,}002 \cdot 10^{-4}$	$2{,}088 \cdot 10^{-1}$	$-1{,}643 \cdot 10^{-1}$	$1{,}505 \cdot 10^{-4}$	$3{,}135 \cdot 10^{-1}$	$-1{,}959 \cdot 10^{-1}$
$e_{24}s_4$	$-6{,}049 \cdot 10^{-6}$	$-3{,}780 \cdot 10^{-3}$	$1{,}408 \cdot 10^{-3}$	$-1{,}196 \cdot 10^{-6}$	$-7{,}477 \cdot 10^{-4}$	$2{,}754 \cdot 10^{-4}$
$e_{25}s_1$	$4{,}249 \cdot 10^{-4}$	$8{,}853 \cdot 10^{-1}$	$-3{,}992 \cdot 10^{-1}$	$3{,}380 \cdot 10^{-4}$	$7{,}042 \cdot 10^{-1}$	$-3{,}129 \cdot 10^{-1}$
$e_{25}s_2$	$-1{,}967 \cdot 10^{-4}$	$-1{,}229 \cdot 10^{-1}$	$4{,}185 \cdot 10^{-2}$	$-1{,}868 \cdot 10^{-4}$	$-1{,}168 \cdot 10^{-1}$	$4{,}065 \cdot 10^{-2}$
$e_{25}s_3$	$-2{,}397 \cdot 10^{-4}$	$-4{,}994 \cdot 10^{-1}$	$2{,}450 \cdot 10^{-1}$	$-1{,}794 \cdot 10^{-4}$	$-3{,}737 \cdot 10^{-1}$	$2{,}118 \cdot 10^{-1}$
$e_{25}s_4$	$1{,}140 \cdot 10^{-5}$	$7{,}128 \cdot 10^{-3}$	$-2{,}686 \cdot 10^{-3}$	$2{,}819 \cdot 10^{-5}$	$1{,}762 \cdot 10^{-2}$	$-6{,}828 \cdot 10^{-3}$
$e_{26}s_1$	$4{,}435 \cdot 10^{-4}$	$9{,}241 \cdot 10^{-1}$	$-4{,}233 \cdot 10^{-1}$	$4{,}397 \cdot 10^{-4}$	$9{,}161 \cdot 10^{-1}$	$-4{,}181 \cdot 10^{-1}$
$e_{26}s_2$	$-1{,}400 \cdot 10^{-4}$	$-8{,}751 \cdot 10^{-2}$	$3{,}319 \cdot 10^{-2}$	$-1{,}414 \cdot 10^{-4}$	$-8{,}840 \cdot 10^{-2}$	$3{,}345 \cdot 10^{-2}$
$e_{26}s_3$	$-2{,}846 \cdot 10^{-4}$	$-5{,}928 \cdot 10^{-1}$	$2{,}737 \cdot 10^{-1}$	$-2{,}830 \cdot 10^{-4}$	$-5{,}895 \cdot 10^{-1}$	$2{,}726 \cdot 10^{-1}$
$e_{26}s_4$	$-1{,}897 \cdot 10^{-5}$	$-1{,}186 \cdot 10^{-2}$	$4{,}531 \cdot 10^{-3}$	$-1{,}530 \cdot 10^{-5}$	$-9{,}565 \cdot 10^{-3}$	$3{,}631 \cdot 10^{-3}$
$e_{27}s_1$	$2{,}080 \cdot 10^{-4}$	$2{,}476 \cdot 10^{-1}$	$-1{,}738 \cdot 10^{-1}$	$2{,}848 \cdot 10^{-4}$	$3{,}390 \cdot 10^{-1}$	$-2{,}032 \cdot 10^{-1}$
$e_{27}s_2$	$5{,}469 \cdot 10^{-6}$	$3{,}418 \cdot 10^{-3}$	$-2{,}225 \cdot 10^{-3}$	$6{,}414 \cdot 10^{-7}$	$4{,}009 \cdot 10^{-4}$	$-2{,}580 \cdot 10^{-4}$
$e_{27}s_3$	$-1{,}702 \cdot 10^{-4}$	$-2{,}026 \cdot 10^{-1}$	$1{,}632 \cdot 10^{-1}$	$-2{,}382 \cdot 10^{-4}$	$-2{,}835 \cdot 10^{-1}$	$1{,}859 \cdot 10^{-1}$
$e_{27}s_4$	$-4{,}330 \cdot 10^{-5}$	$-2{,}706 \cdot 10^{-2}$	$1{,}866 \cdot 10^{-2}$	$-4{,}728 \cdot 10^{-5}$	$-2{,}955 \cdot 10^{-2}$	$2{,}044 \cdot 10^{-2}$
$e_{28}s_1$	$-1{,}303 \cdot 10^{-3}$	$-5{,}013 \cdot 10^{-1}$	$4{,}379 \cdot 10^{-1}$	$-1{,}281 \cdot 10^{-3}$	$-4{,}927 \cdot 10^{-1}$	$4{,}297 \cdot 10^{-1}$
$e_{28}s_2$	$1{,}289 \cdot 10^{-3}$	$1{,}432$	$-6{,}716$	$1{,}268 \cdot 10^{-3}$	$1{,}408$	$-6{,}229$
$e_{28}s_3$	$-1{,}206 \cdot 10^{-5}$	$-4{,}638 \cdot 10^{-3}$	$3{,}918 \cdot 10^{-3}$	$-1{,}311 \cdot 10^{-5}$	$-5{,}041 \cdot 10^{-3}$	$4{,}259 \cdot 10^{-3}$
$e_{28}s_4$	$2{,}627 \cdot 10^{-5}$	$2{,}919 \cdot 10^{-2}$	$-7{,}113 \cdot 10^{-2}$	$2{,}640 \cdot 10^{-5}$	$2{,}933 \cdot 10^{-2}$	$-7{,}147 \cdot 10^{-2}$

Table A.1: Flux tube element outputs ... *cont*

Element Region	$I_{(\mathrm{ph})} = \begin{bmatrix} -10 & -10 & 20 \end{bmatrix}^{\mathrm{T}}$					
	$x = 0\,\mathrm{mm}$			$x = 1\,\mathrm{mm}$		
	Φ [Wb]	B [T]	$\mathcal{F}$ [A]	Φ [Wb]	B [T]	$\mathcal{F}$ [A]
$e_{29}k_1$	$7{,}671 \cdot 10^{-5}$	$7{,}671 \cdot 10^{-2}$	$-6{,}459 \cdot 10^{-2}$	$7{,}746 \cdot 10^{-5}$	$7{,}746 \cdot 10^{-2}$	$-6{,}523 \cdot 10^{-2}$
$e_{29}k_2$	$1{,}217 \cdot 10^{-3}$	$1{,}352$	$-2{,}068$	$1{,}195 \cdot 10^{-3}$	$1{,}327$	$-1{,}958$
$e_{29}k_3$	$-4{,}286 \cdot 10^{-6}$	$-4{,}286 \cdot 10^{-3}$	$3{,}621 \cdot 10^{-3}$	$-4{,}373 \cdot 10^{-6}$	$-4{,}373 \cdot 10^{-3}$	$3{,}694 \cdot 10^{-3}$
$e_{29}k_4$	$-1{,}289 \cdot 10^{-3}$	$-1{,}432$	$2{,}583$	$-1{,}268 \cdot 10^{-3}$	$-1{,}408$	$2{,}396$
$e_{30}k_1$	$1{,}327 \cdot 10^{-3}$	$5{,}105 \cdot 10^{-1}$	$-4{,}466 \cdot 10^{-1}$	$1{,}306 \cdot 10^{-3}$	$5{,}021 \cdot 10^{-1}$	$-4{,}387 \cdot 10^{-1}$
$e_{30}k_2$	$-8{,}585 \cdot 10^{-5}$	$-9{,}539 \cdot 10^{-2}$	$2{,}320 \cdot 10^{-1}$	$-8{,}634 \cdot 10^{-5}$	$-9{,}593 \cdot 10^{-2}$	$2{,}333 \cdot 10^{-1}$
$e_{30}k_3$	$-2{,}454 \cdot 10^{-5}$	$-9{,}440 \cdot 10^{-3}$	$7{,}972 \cdot 10^{-3}$	$-2{,}468 \cdot 10^{-5}$	$-9{,}492 \cdot 10^{-3}$	$8{,}016 \cdot 10^{-3}$
$e_{30}k_4$	$-1{,}217 \cdot 10^{-3}$	$-1{,}352$	$5{,}378$	$-1{,}195 \cdot 10^{-3}$	$-1{,}327$	$5{,}091$

Table A.1: Flux tube element outputs ... *cont*

Element Region	$I_{(\mathrm{ph})} = \begin{bmatrix} -10 & -10 & 20 \end{bmatrix}^{\mathrm{T}}$					
	$x = 2\,\mathrm{mm}$			$x = 3\,\mathrm{mm}$		
	Φ [Wb]	B [T]	$\mathcal{F}$ [A]	Φ [Wb]	B [T]	$\mathcal{F}$ [A]
e_1k_1	$2{,}788 \cdot 10^{-6}$	$3{,}319 \cdot 10^{-3}$	$-2{,}572 \cdot 10^{-3}$	$2{,}605 \cdot 10^{-6}$	$3{,}102 \cdot 10^{-3}$	$-2{,}401 \cdot 10^{-3}$
e_1k_2	$-1{,}227 \cdot 10^{-4}$	$-1{,}227 \cdot 10^{-1}$	$7{,}317 \cdot 10^{-2}$	$-1{,}013 \cdot 10^{-4}$	$-1{,}013 \cdot 10^{-1}$	$6{,}486 \cdot 10^{-2}$
e_1k_3	$1{,}157 \cdot 10^{-4}$	$1{,}377 \cdot 10^{-1}$	$-9{,}217 \cdot 10^{-2}$	$9{,}477 \cdot 10^{-5}$	$1{,}128 \cdot 10^{-1}$	$-8{,}293 \cdot 10^{-2}$
e_1k_4	$4{,}234 \cdot 10^{-6}$	$4{,}234 \cdot 10^{-3}$	$-2{,}764 \cdot 10^{-3}$	$3{,}935 \cdot 10^{-6}$	$3{,}935 \cdot 10^{-3}$	$-2{,}567 \cdot 10^{-3}$
e_2k_1	$1{,}297 \cdot 10^{-6}$	$1{,}801 \cdot 10^{-3}$	$-1{,}388 \cdot 10^{-3}$	$1{,}211 \cdot 10^{-6}$	$1{,}681 \cdot 10^{-3}$	$-1{,}295 \cdot 10^{-3}$
e_2k_2	$-2{,}296 \cdot 10^{-4}$	$-2{,}296 \cdot 10^{-1}$	$7{,}598 \cdot 10^{-2}$	$-1{,}928 \cdot 10^{-4}$	$-1{,}928 \cdot 10^{-1}$	$7{,}276 \cdot 10^{-2}$
e_2k_3	$1{,}056 \cdot 10^{-4}$	$1{,}467 \cdot 10^{-1}$	$-9{,}451 \cdot 10^{-2}$	$9{,}027 \cdot 10^{-5}$	$1{,}254 \cdot 10^{-1}$	$-8{,}812 \cdot 10^{-2}$
e_2k_4	$1{,}227 \cdot 10^{-4}$	$1{,}227 \cdot 10^{-1}$	$-6{,}272 \cdot 10^{-2}$	$1{,}013 \cdot 10^{-4}$	$1{,}013 \cdot 10^{-1}$	$-5{,}559 \cdot 10^{-2}$
e_3k_1	$7{,}331 \cdot 10^{-7}$	$1{,}527 \cdot 10^{-3}$	$-1{,}176 \cdot 10^{-3}$	$6{,}848 \cdot 10^{-7}$	$1{,}427 \cdot 10^{-3}$	$-1{,}098 \cdot 10^{-3}$
e_3k_2	$-3{,}873 \cdot 10^{-4}$	$-3{,}873 \cdot 10^{-1}$	$6{,}450 \cdot 10^{-2}$	$-3{,}458 \cdot 10^{-4}$	$-3{,}458 \cdot 10^{-1}$	$6{,}150 \cdot 10^{-2}$
e_3k_3	$1{,}569 \cdot 10^{-4}$	$3{,}269 \cdot 10^{-1}$	$-1{,}249 \cdot 10^{-1}$	$1{,}523 \cdot 10^{-4}$	$3{,}174 \cdot 10^{-1}$	$-1{,}232 \cdot 10^{-1}$
e_3k_4	$2{,}296 \cdot 10^{-4}$	$2{,}296 \cdot 10^{-1}$	$-5{,}065 \cdot 10^{-2}$	$1{,}928 \cdot 10^{-4}$	$1{,}928 \cdot 10^{-1}$	$-4{,}851 \cdot 10^{-2}$
e_4k_1	$1{,}002 \cdot 10^{-6}$	$1{,}391 \cdot 10^{-3}$	$-1{,}070 \cdot 10^{-3}$	$9{,}352 \cdot 10^{-7}$	$1{,}299 \cdot 10^{-3}$	$-9{,}988 \cdot 10^{-4}$
e_4k_2	$-6{,}631 \cdot 10^{-4}$	$-6{,}631 \cdot 10^{-1}$	$1{,}339 \cdot 10^{-1}$	$-6{,}134 \cdot 10^{-4}$	$-6{,}134 \cdot 10^{-1}$	$1{,}262 \cdot 10^{-1}$
e_4k_3	$2{,}748 \cdot 10^{-4}$	$3{,}817 \cdot 10^{-1}$	$-1{,}335 \cdot 10^{-1}$	$2{,}667 \cdot 10^{-4}$	$3{,}704 \cdot 10^{-1}$	$-1{,}319 \cdot 10^{-1}$
e_4k_4	$3{,}873 \cdot 10^{-4}$	$3{,}873 \cdot 10^{-1}$	$-9{,}674 \cdot 10^{-2}$	$3{,}458 \cdot 10^{-4}$	$3{,}458 \cdot 10^{-1}$	$-9{,}224 \cdot 10^{-2}$
e_5k_1	$6{,}339 \cdot 10^{-7}$	$1{,}321 \cdot 10^{-3}$	$-1{,}016 \cdot 10^{-3}$	$5{,}912 \cdot 10^{-7}$	$1{,}232 \cdot 10^{-3}$	$-9{,}468 \cdot 10^{-4}$
e_5k_2	$-9{,}728 \cdot 10^{-4}$	$-9{,}728 \cdot 10^{-1}$	$1{,}374 \cdot 10^{-1}$	$-9{,}232 \cdot 10^{-4}$	$-9{,}232 \cdot 10^{-1}$	$1{,}268 \cdot 10^{-1}$
e_5k_3	$3{,}091 \cdot 10^{-4}$	$6{,}439 \cdot 10^{-1}$	$-1{,}817 \cdot 10^{-1}$	$3{,}092 \cdot 10^{-4}$	$6{,}441 \cdot 10^{-1}$	$-1{,}817 \cdot 10^{-1}$
e_5k_4	$6{,}631 \cdot 10^{-4}$	$6{,}631 \cdot 10^{-1}$	$-8{,}923 \cdot 10^{-2}$	$6{,}134 \cdot 10^{-4}$	$6{,}134 \cdot 10^{-1}$	$-8{,}412 \cdot 10^{-2}$
e_6k_1	$9{,}745 \cdot 10^{-7}$	$1{,}354 \cdot 10^{-3}$	$-1{,}041 \cdot 10^{-3}$	$9{,}053 \cdot 10^{-7}$	$1{,}257 \cdot 10^{-3}$	$-9{,}667 \cdot 10^{-4}$
e_6k_2	$-9{,}737 \cdot 10^{-4}$	$-9{,}737 \cdot 10^{-1}$	$2{,}065 \cdot 10^{-1}$	$-9{,}241 \cdot 10^{-4}$	$-9{,}241 \cdot 10^{-1}$	$1{,}905 \cdot 10^{-1}$
e_6k_3	$-1{,}291 \cdot 10^{-9}$	$-1{,}793 \cdot 10^{-6}$	$1{,}371 \cdot 10^{-6}$	$2{,}220 \cdot 10^{-9}$	$3{,}083 \cdot 10^{-6}$	$-2{,}359 \cdot 10^{-6}$
e_6k_4	$9{,}728 \cdot 10^{-4}$	$9{,}728 \cdot 10^{-1}$	$-2{,}062 \cdot 10^{-1}$	$9{,}232 \cdot 10^{-4}$	$9{,}232 \cdot 10^{-1}$	$-1{,}903 \cdot 10^{-1}$
e_7k_1	$6{,}831 \cdot 10^{-7}$	$1{,}423 \cdot 10^{-3}$	$-1{,}095 \cdot 10^{-3}$	$6{,}310 \cdot 10^{-7}$	$1{,}315 \cdot 10^{-3}$	$-1{,}011 \cdot 10^{-3}$
e_7k_2	$-6{,}509 \cdot 10^{-4}$	$-6{,}509 \cdot 10^{-1}$	$8{,}794 \cdot 10^{-2}$	$-6{,}390 \cdot 10^{-4}$	$-6{,}390 \cdot 10^{-1}$	$8{,}670 \cdot 10^{-2}$
e_7k_3	$-3{,}236 \cdot 10^{-4}$	$-6{,}741 \cdot 10^{-1}$	$1{,}884 \cdot 10^{-1}$	$-2{,}858 \cdot 10^{-4}$	$-5{,}953 \cdot 10^{-1}$	$1{,}716 \cdot 10^{-1}$
e_7k_4	$9{,}737 \cdot 10^{-4}$	$9{,}737 \cdot 10^{-1}$	$-1{,}377 \cdot 10^{-1}$	$9{,}241 \cdot 10^{-4}$	$9{,}241 \cdot 10^{-1}$	$-1{,}270 \cdot 10^{-1}$
e_8k_1	$1{,}066 \cdot 10^{-6}$	$1{,}480 \cdot 10^{-3}$	$-1{,}139 \cdot 10^{-3}$	$9{,}834 \cdot 10^{-7}$	$1{,}366 \cdot 10^{-3}$	$-1{,}051 \cdot 10^{-3}$
e_8k_2	$-3{,}840 \cdot 10^{-4}$	$-3{,}840 \cdot 10^{-1}$	$9{,}640 \cdot 10^{-2}$	$-3{,}987 \cdot 10^{-4}$	$-3{,}987 \cdot 10^{-1}$	$9{,}796 \cdot 10^{-2}$
e_8k_3	$-2{,}679 \cdot 10^{-4}$	$-3{,}721 \cdot 10^{-1}$	$1{,}321 \cdot 10^{-1}$	$-2{,}412 \cdot 10^{-4}$	$-3{,}351 \cdot 10^{-1}$	$1{,}263 \cdot 10^{-1}$
e_8k_4	$6{,}509 \cdot 10^{-4}$	$6{,}509 \cdot 10^{-1}$	$-1{,}319 \cdot 10^{-1}$	$6{,}390 \cdot 10^{-4}$	$6{,}390 \cdot 10^{-1}$	$-1{,}300 \cdot 10^{-1}$
e_9k_1	$7{,}628 \cdot 10^{-7}$	$1{,}589 \cdot 10^{-3}$	$-1{,}223 \cdot 10^{-3}$	$7{,}021 \cdot 10^{-7}$	$1{,}463 \cdot 10^{-3}$	$-1{,}126 \cdot 10^{-3}$
e_9k_2	$-2{,}400 \cdot 10^{-4}$	$-2{,}400 \cdot 10^{-1}$	$5{,}148 \cdot 10^{-2}$	$-2{,}657 \cdot 10^{-4}$	$-2{,}657 \cdot 10^{-1}$	$5{,}389 \cdot 10^{-2}$
e_9k_3	$-1{,}448 \cdot 10^{-4}$	$-3{,}016 \cdot 10^{-1}$	$1{,}201 \cdot 10^{-1}$	$-1{,}337 \cdot 10^{-4}$	$-2{,}786 \cdot 10^{-1}$	$1{,}151 \cdot 10^{-1}$
e_9k_4	$3{,}840 \cdot 10^{-4}$	$3{,}840 \cdot 10^{-1}$	$-6{,}427 \cdot 10^{-2}$	$3{,}987 \cdot 10^{-4}$	$3{,}987 \cdot 10^{-1}$	$-6{,}531 \cdot 10^{-2}$

Table A.1: Flux tube element outputs ... *cont*

Element Region	$I_{(\mathrm{ph})} = \begin{bmatrix} -10 & -10 & 20 \end{bmatrix}^{\mathrm{T}}$					
	$x = 2\,\mathrm{mm}$			$x = 3\,\mathrm{mm}$		
	Φ [Wb]	B [T]	$\mathcal{F}$ [A]	Φ [Wb]	B [T]	$\mathcal{F}$ [A]
$e_{10}s_1$	$1{,}305 \cdot 10^{-6}$	$1{,}812 \cdot 10^{-3}$	$-1{,}396 \cdot 10^{-3}$	$1{,}196 \cdot 10^{-6}$	$1{,}661 \cdot 10^{-3}$	$-1{,}279 \cdot 10^{-3}$
$e_{10}s_2$	$-1{,}300 \cdot 10^{-4}$	$-1{,}300 \cdot 10^{-1}$	$6{,}463 \cdot 10^{-2}$	$-1{,}486 \cdot 10^{-4}$	$-1{,}486 \cdot 10^{-1}$	$6{,}837 \cdot 10^{-2}$
$e_{10}s_3$	$-1{,}113 \cdot 10^{-4}$	$-1{,}545 \cdot 10^{-1}$	$9{,}619 \cdot 10^{-2}$	$-1{,}183 \cdot 10^{-4}$	$-1{,}642 \cdot 10^{-1}$	$9{,}785 \cdot 10^{-2}$
$e_{10}s_4$	$2{,}400 \cdot 10^{-4}$	$2{,}400 \cdot 10^{-1}$	$-7{,}722 \cdot 10^{-2}$	$2{,}657 \cdot 10^{-4}$	$2{,}657 \cdot 10^{-1}$	$-8{,}084 \cdot 10^{-2}$
$e_{11}s_1$	$2{,}628 \cdot 10^{-6}$	$3{,}129 \cdot 10^{-3}$	$-2{,}422 \cdot 10^{-3}$	$2{,}365 \cdot 10^{-6}$	$2{,}816 \cdot 10^{-3}$	$-2{,}178 \cdot 10^{-3}$
$e_{11}s_2$	$3{,}417 \cdot 10^{-6}$	$3{,}417 \cdot 10^{-3}$	$-2{,}225 \cdot 10^{-3}$	$2{,}882 \cdot 10^{-6}$	$2{,}882 \cdot 10^{-3}$	$-1{,}873 \cdot 10^{-3}$
$e_{11}s_3$	$-1{,}361 \cdot 10^{-4}$	$-1{,}620 \cdot 10^{-1}$	$9{,}751 \cdot 10^{-2}$	$-1{,}539 \cdot 10^{-4}$	$-1{,}832 \cdot 10^{-1}$	$1{,}001 \cdot 10^{-1}$
$e_{11}s_4$	$1{,}300 \cdot 10^{-4}$	$1{,}300 \cdot 10^{-1}$	$-7{,}541 \cdot 10^{-2}$	$1{,}486 \cdot 10^{-4}$	$1{,}486 \cdot 10^{-1}$	$-7{,}977 \cdot 10^{-2}$
$e_{12}s_1$	$-1{,}157 \cdot 10^{-4}$	$-1{,}377 \cdot 10^{-1}$	$1{,}475 \cdot 10^{-1}$	$-9{,}477 \cdot 10^{-5}$	$-1{,}128 \cdot 10^{-1}$	$1{,}327 \cdot 10^{-1}$
$e_{12}s_2$	$-1{,}815 \cdot 10^{-4}$	$-1{,}134 \cdot 10^{-1}$	$6{,}990 \cdot 10^{-2}$	$-1{,}386 \cdot 10^{-4}$	$-8{,}661 \cdot 10^{-2}$	$5{,}760 \cdot 10^{-2}$
$e_{12}s_3$	$2{,}906 \cdot 10^{-4}$	$3{,}459 \cdot 10^{-1}$	$-2{,}050 \cdot 10^{-1}$	$2{,}273 \cdot 10^{-4}$	$2{,}706 \cdot 10^{-1}$	$-1{,}813 \cdot 10^{-1}$
$e_{12}s_4$	$6{,}586 \cdot 10^{-6}$	$4{,}116 \cdot 10^{-3}$	$-2{,}687 \cdot 10^{-3}$	$6{,}038 \cdot 10^{-6}$	$3{,}774 \cdot 10^{-3}$	$-2{,}460 \cdot 10^{-3}$
$e_{13}s_1$	$-1{,}056 \cdot 10^{-4}$	$-1{,}467 \cdot 10^{-1}$	$1{,}512 \cdot 10^{-1}$	$-9{,}027 \cdot 10^{-5}$	$-1{,}254 \cdot 10^{-1}$	$1{,}410 \cdot 10^{-1}$
$e_{13}s_2$	$-7{,}625 \cdot 10^{-5}$	$-4{,}766 \cdot 10^{-2}$	$2{,}852 \cdot 10^{-2}$	$-4{,}863 \cdot 10^{-5}$	$-3{,}039 \cdot 10^{-2}$	$1{,}804 \cdot 10^{-2}$
$e_{13}s_3$	$3{,}860 \cdot 10^{-7}$	$5{,}361 \cdot 10^{-4}$	$-6{,}576 \cdot 10^{-4}$	$3{,}191 \cdot 10^{-7}$	$4{,}431 \cdot 10^{-4}$	$-5{,}434 \cdot 10^{-4}$
$e_{13}s_4$	$1{,}815 \cdot 10^{-4}$	$1{,}134 \cdot 10^{-1}$	$-5{,}991 \cdot 10^{-2}$	$1{,}386 \cdot 10^{-4}$	$8{,}661 \cdot 10^{-2}$	$-4{,}937 \cdot 10^{-2}$
$e_{14}s_1$	$-1{,}569 \cdot 10^{-4}$	$-3{,}269 \cdot 10^{-1}$	$1{,}999 \cdot 10^{-1}$	$-1{,}523 \cdot 10^{-4}$	$-3{,}174 \cdot 10^{-1}$	$1{,}971 \cdot 10^{-1}$
$e_{14}s_2$	$-4{,}504 \cdot 10^{-4}$	$-2{,}815 \cdot 10^{-1}$	$5{,}555 \cdot 10^{-2}$	$-4{,}016 \cdot 10^{-4}$	$-2{,}510 \cdot 10^{-1}$	$5{,}246 \cdot 10^{-2}$
$e_{14}s_3$	$5{,}310 \cdot 10^{-4}$	$1{,}106$	$-5{,}877 \cdot 10^{-1}$	$5{,}053 \cdot 10^{-4}$	$1{,}053$	$-5{,}281 \cdot 10^{-1}$
$e_{14}s_4$	$7{,}625 \cdot 10^{-5}$	$4{,}766 \cdot 10^{-2}$	$-1{,}902 \cdot 10^{-2}$	$4{,}863 \cdot 10^{-5}$	$3{,}039 \cdot 10^{-2}$	$-1{,}203 \cdot 10^{-2}$
$e_{15}s_1$	$-2{,}748 \cdot 10^{-4}$	$-3{,}817 \cdot 10^{-1}$	$2{,}137 \cdot 10^{-1}$	$-2{,}667 \cdot 10^{-4}$	$-3{,}704 \cdot 10^{-1}$	$2{,}110 \cdot 10^{-1}$
$e_{15}s_2$	$-1{,}760 \cdot 10^{-4}$	$-1{,}100 \cdot 10^{-1}$	$5{,}875 \cdot 10^{-2}$	$-1{,}353 \cdot 10^{-4}$	$-8{,}455 \cdot 10^{-2}$	$4{,}842 \cdot 10^{-2}$
$e_{15}s_3$	$3{,}863 \cdot 10^{-7}$	$5{,}365 \cdot 10^{-4}$	$-6{,}581 \cdot 10^{-4}$	$3{,}833 \cdot 10^{-7}$	$5{,}323 \cdot 10^{-4}$	$-6{,}530 \cdot 10^{-4}$
$e_{15}s_4$	$4{,}504 \cdot 10^{-4}$	$2{,}815 \cdot 10^{-1}$	$-8{,}332 \cdot 10^{-2}$	$4{,}016 \cdot 10^{-4}$	$2{,}510 \cdot 10^{-1}$	$-7{,}868 \cdot 10^{-2}$
$e_{16}s_1$	$-3{,}091 \cdot 10^{-4}$	$-6{,}439 \cdot 10^{-1}$	$2{,}907 \cdot 10^{-1}$	$-3{,}092 \cdot 10^{-4}$	$-6{,}441 \cdot 10^{-1}$	$2{,}908 \cdot 10^{-1}$
$e_{16}s_2$	$-4{,}233 \cdot 10^{-5}$	$-2{,}646 \cdot 10^{-2}$	$1{,}042 \cdot 10^{-2}$	$-4{,}228 \cdot 10^{-5}$	$-2{,}642 \cdot 10^{-2}$	$1{,}041 \cdot 10^{-2}$
$e_{16}s_3$	$1{,}754 \cdot 10^{-4}$	$3{,}655 \cdot 10^{-1}$	$-2{,}098 \cdot 10^{-1}$	$2{,}162 \cdot 10^{-4}$	$4{,}504 \cdot 10^{-1}$	$-2{,}310 \cdot 10^{-1}$
$e_{16}s_4$	$1{,}760 \cdot 10^{-4}$	$1{,}100 \cdot 10^{-1}$	$-3{,}917 \cdot 10^{-2}$	$1{,}353 \cdot 10^{-4}$	$8{,}455 \cdot 10^{-2}$	$-3{,}228 \cdot 10^{-2}$
$e_{17}s_1$	$3{,}236 \cdot 10^{-4}$	$6{,}741 \cdot 10^{-1}$	$-3{,}014 \cdot 10^{-1}$	$2{,}858 \cdot 10^{-4}$	$5{,}953 \cdot 10^{-1}$	$-2{,}745 \cdot 10^{-1}$
$e_{17}s_2$	$-1{,}213 \cdot 10^{-4}$	$-7{,}578 \cdot 10^{-2}$	$2{,}943 \cdot 10^{-2}$	$-1{,}796 \cdot 10^{-4}$	$-1{,}122 \cdot 10^{-1}$	$3{,}968 \cdot 10^{-2}$
$e_{17}s_3$	$-2{,}447 \cdot 10^{-4}$	$-5{,}097 \cdot 10^{-1}$	$2{,}481 \cdot 10^{-1}$	$-1{,}486 \cdot 10^{-4}$	$-3{,}095 \cdot 10^{-1}$	$1{,}947 \cdot 10^{-1}$
$e_{17}s_4$	$4{,}236 \cdot 10^{-5}$	$2{,}647 \cdot 10^{-2}$	$-1{,}043 \cdot 10^{-2}$	$4{,}235 \cdot 10^{-5}$	$2{,}647 \cdot 10^{-2}$	$-1{,}042 \cdot 10^{-2}$
$e_{18}s_1$	$2{,}679 \cdot 10^{-4}$	$3{,}721 \cdot 10^{-1}$	$-2{,}114 \cdot 10^{-1}$	$2{,}412 \cdot 10^{-4}$	$3{,}351 \cdot 10^{-1}$	$-2{,}022 \cdot 10^{-1}$
$e_{18}s_2$	$-3{,}888 \cdot 10^{-4}$	$-2{,}430 \cdot 10^{-1}$	$7{,}760 \cdot 10^{-2}$	$-4{,}205 \cdot 10^{-4}$	$-2{,}628 \cdot 10^{-1}$	$8{,}041 \cdot 10^{-2}$
$e_{18}s_3$	$-3{,}551 \cdot 10^{-7}$	$-4{,}932 \cdot 10^{-4}$	$6{,}049 \cdot 10^{-4}$	$-2{,}871 \cdot 10^{-7}$	$-3{,}987 \cdot 10^{-4}$	$4{,}888 \cdot 10^{-4}$
$e_{18}s_4$	$1{,}213 \cdot 10^{-4}$	$7{,}578 \cdot 10^{-2}$	$-4{,}415 \cdot 10^{-2}$	$1{,}796 \cdot 10^{-4}$	$1{,}122 \cdot 10^{-1}$	$-5{,}952 \cdot 10^{-2}$
$e_{19}s_1$	$1{,}448 \cdot 10^{-4}$	$3{,}016 \cdot 10^{-1}$	$-1{,}921 \cdot 10^{-1}$	$1{,}337 \cdot 10^{-4}$	$2{,}786 \cdot 10^{-1}$	$-1{,}841 \cdot 10^{-1}$
$e_{19}s_2$	$-1{,}083 \cdot 10^{-4}$	$-6{,}772 \cdot 10^{-2}$	$2{,}662 \cdot 10^{-2}$	$-1{,}555 \cdot 10^{-4}$	$-9{,}717 \cdot 10^{-2}$	$3{,}597 \cdot 10^{-2}$
$e_{19}s_3$	$-4{,}253 \cdot 10^{-4}$	$-8{,}859 \cdot 10^{-1}$	$3{,}996 \cdot 10^{-1}$	$-3{,}988 \cdot 10^{-4}$	$-8{,}308 \cdot 10^{-1}$	$3{,}695 \cdot 10^{-1}$
$e_{19}s_4$	$3{,}888 \cdot 10^{-4}$	$2{,}430 \cdot 10^{-1}$	$-5{,}174 \cdot 10^{-2}$	$4{,}205 \cdot 10^{-4}$	$2{,}628 \cdot 10^{-1}$	$-5{,}360 \cdot 10^{-2}$
$e_{20}s_1$	$1{,}113 \cdot 10^{-4}$	$1{,}545 \cdot 10^{-1}$	$-1{,}539 \cdot 10^{-1}$	$1{,}183 \cdot 10^{-4}$	$1{,}642 \cdot 10^{-1}$	$-1{,}566 \cdot 10^{-1}$
$e_{20}s_2$	$-2{,}192 \cdot 10^{-4}$	$-1{,}370 \cdot 10^{-1}$	$6{,}622 \cdot 10^{-2}$	$-2{,}734 \cdot 10^{-4}$	$-1{,}708 \cdot 10^{-1}$	$7{,}111 \cdot 10^{-2}$
$e_{20}s_3$	$-3{,}839 \cdot 10^{-7}$	$-5{,}332 \cdot 10^{-4}$	$6{,}541 \cdot 10^{-4}$	$-3{,}828 \cdot 10^{-7}$	$-5{,}317 \cdot 10^{-4}$	$6{,}521 \cdot 10^{-4}$
$e_{20}s_4$	$1{,}083 \cdot 10^{-4}$	$6{,}772 \cdot 10^{-2}$	$-3{,}994 \cdot 10^{-2}$	$1{,}555 \cdot 10^{-4}$	$9{,}717 \cdot 10^{-2}$	$-5{,}395 \cdot 10^{-2}$
$e_{21}s_1$	$1{,}361 \cdot 10^{-4}$	$1{,}620 \cdot 10^{-1}$	$-1{,}560 \cdot 10^{-1}$	$1{,}539 \cdot 10^{-4}$	$1{,}832 \cdot 10^{-1}$	$-1{,}602 \cdot 10^{-1}$
$e_{21}s_2$	$4{,}031 \cdot 10^{-6}$	$2{,}520 \cdot 10^{-3}$	$-1{,}635 \cdot 10^{-3}$	$2{,}533 \cdot 10^{-6}$	$1{,}583 \cdot 10^{-3}$	$-1{,}024 \cdot 10^{-3}$
$e_{21}s_3$	$-3{,}593 \cdot 10^{-4}$	$-4{,}278 \cdot 10^{-1}$	$2{,}249 \cdot 10^{-1}$	$-4{,}298 \cdot 10^{-4}$	$-5{,}116 \cdot 10^{-1}$	$2{,}486 \cdot 10^{-1}$
$e_{21}s_4$	$2{,}192 \cdot 10^{-4}$	$1{,}370 \cdot 10^{-1}$	$-7{,}725 \cdot 10^{-2}$	$2{,}734 \cdot 10^{-4}$	$1{,}708 \cdot 10^{-1}$	$-8{,}296 \cdot 10^{-2}$
$e_{22}s_1$	$-2{,}906 \cdot 10^{-4}$	$-3{,}459 \cdot 10^{-1}$	$2{,}050 \cdot 10^{-1}$	$-2{,}273 \cdot 10^{-4}$	$-2{,}706 \cdot 10^{-1}$	$1{,}813 \cdot 10^{-1}$
$e_{22}s_2$	$1{,}230 \cdot 10^{-4}$	$7{,}685 \cdot 10^{-2}$	$-5{,}213 \cdot 10^{-2}$	$1{,}039 \cdot 10^{-4}$	$6{,}494 \cdot 10^{-2}$	$-4{,}484 \cdot 10^{-2}$
$e_{22}s_3$	$1{,}447 \cdot 10^{-4}$	$1{,}722 \cdot 10^{-1}$	$-1{,}583 \cdot 10^{-1}$	$1{,}038 \cdot 10^{-4}$	$1{,}235 \cdot 10^{-1}$	$-1{,}399 \cdot 10^{-1}$
$e_{22}s_4$	$2{,}298 \cdot 10^{-5}$	$1{,}436 \cdot 10^{-2}$	$-9{,}668 \cdot 10^{-3}$	$1{,}965 \cdot 10^{-5}$	$1{,}228 \cdot 10^{-2}$	$-8{,}224 \cdot 10^{-3}$
$e_{23}s_1$	$-5{,}310 \cdot 10^{-4}$	$-1{,}106$	$5{,}877 \cdot 10^{-1}$	$-5{,}053 \cdot 10^{-4}$	$-1{,}053$	$5{,}281 \cdot 10^{-1}$
$e_{23}s_2$	$1{,}849 \cdot 10^{-4}$	$1{,}155 \cdot 10^{-1}$	$-4{,}039 \cdot 10^{-2}$	$1{,}853 \cdot 10^{-4}$	$1{,}158 \cdot 10^{-1}$	$-4{,}045 \cdot 10^{-2}$
$e_{23}s_3$	$2{,}970 \cdot 10^{-4}$	$6{,}188 \cdot 10^{-1}$	$-2{,}822 \cdot 10^{-1}$	$2{,}853 \cdot 10^{-4}$	$5{,}943 \cdot 10^{-1}$	$-2{,}742 \cdot 10^{-1}$
$e_{23}s_4$	$4{,}916 \cdot 10^{-5}$	$3{,}072 \cdot 10^{-2}$	$-1{,}216 \cdot 10^{-2}$	$3{,}473 \cdot 10^{-5}$	$2{,}171 \cdot 10^{-2}$	$-8{,}483 \cdot 10^{-3}$

Table A.1: Flux tube element outputs ... *cont*

Element Region	$I_{(\mathrm{ph})} = \left[-10\ -10\ 20\right]^{\mathrm{T}}$					
	$x = 2\,\mathrm{mm}$			$x = 3\,\mathrm{mm}$		
	Φ [Wb]	B [T]	$\mathcal{F}$ [A]	Φ [Wb]	B [T]	$\mathcal{F}$ [A]
$\mathrm{e}_{24}\mathrm{k}_1$	$-1{,}754 \cdot 10^{-4}$	$-3{,}655 \cdot 10^{-1}$	$2{,}098 \cdot 10^{-1}$	$-2{,}162 \cdot 10^{-4}$	$-4{,}504 \cdot 10^{-1}$	$2{,}310 \cdot 10^{-1}$
$\mathrm{e}_{24}\mathrm{k}_2$	$-1{,}058 \cdot 10^{-5}$	$-6{,}615 \cdot 10^{-3}$	$2{,}488 \cdot 10^{-3}$	$8{,}408 \cdot 10^{-6}$	$5{,}255 \cdot 10^{-3}$	$-1{,}968 \cdot 10^{-3}$
$\mathrm{e}_{24}\mathrm{k}_3$	$1{,}844 \cdot 10^{-4}$	$3{,}842 \cdot 10^{-1}$	$-2{,}143 \cdot 10^{-1}$	$2{,}052 \cdot 10^{-4}$	$4{,}274 \cdot 10^{-1}$	$-2{,}249 \cdot 10^{-1}$
$\mathrm{e}_{24}\mathrm{k}_4$	$1{,}597 \cdot 10^{-6}$	$9{,}981 \cdot 10^{-4}$	$-3{,}680 \cdot 10^{-4}$	$2{,}595 \cdot 10^{-6}$	$1{,}622 \cdot 10^{-3}$	$-5{,}994 \cdot 10^{-4}$
$\mathrm{e}_{25}\mathrm{k}_1$	$2{,}447 \cdot 10^{-4}$	$5{,}097 \cdot 10^{-1}$	$-2{,}481 \cdot 10^{-1}$	$1{,}486 \cdot 10^{-4}$	$3{,}095 \cdot 10^{-1}$	$-1{,}947 \cdot 10^{-1}$
$\mathrm{e}_{25}\mathrm{k}_2$	$-1{,}703 \cdot 10^{-4}$	$-1{,}064 \cdot 10^{-1}$	$3{,}834 \cdot 10^{-2}$	$-1{,}498 \cdot 10^{-4}$	$-9{,}365 \cdot 10^{-2}$	$3{,}499 \cdot 10^{-2}$
$\mathrm{e}_{25}\mathrm{k}_3$	$-1{,}231 \cdot 10^{-4}$	$-2{,}565 \cdot 10^{-1}$	$1{,}766 \cdot 10^{-1}$	$-6{,}920 \cdot 10^{-5}$	$-1{,}442 \cdot 10^{-1}$	$1{,}502 \cdot 10^{-1}$
$\mathrm{e}_{25}\mathrm{k}_4$	$4{,}878 \cdot 10^{-5}$	$3{,}049 \cdot 10^{-2}$	$-1{,}207 \cdot 10^{-2}$	$7{,}049 \cdot 10^{-5}$	$4{,}405 \cdot 10^{-2}$	$-1{,}758 \cdot 10^{-2}$
$\mathrm{e}_{26}\mathrm{k}_1$	$4{,}253 \cdot 10^{-4}$	$8{,}859 \cdot 10^{-1}$	$-3{,}996 \cdot 10^{-1}$	$3{,}988 \cdot 10^{-4}$	$8{,}308 \cdot 10^{-1}$	$-3{,}695 \cdot 10^{-1}$
$\mathrm{e}_{26}\mathrm{k}_2$	$-1{,}423 \cdot 10^{-4}$	$-8{,}893 \cdot 10^{-2}$	$3{,}362 \cdot 10^{-2}$	$-1{,}424 \cdot 10^{-4}$	$-8{,}898 \cdot 10^{-2}$	$3{,}363 \cdot 10^{-2}$
$\mathrm{e}_{26}\mathrm{k}_3$	$-2{,}779 \cdot 10^{-4}$	$-5{,}790 \cdot 10^{-1}$	$2{,}693 \cdot 10^{-1}$	$-2{,}666 \cdot 10^{-4}$	$-5{,}554 \cdot 10^{-1}$	$2{,}619 \cdot 10^{-1}$
$\mathrm{e}_{26}\mathrm{k}_4$	$-5{,}047 \cdot 10^{-6}$	$-3{,}154 \cdot 10^{-3}$	$1{,}172 \cdot 10^{-3}$	$1{,}018 \cdot 10^{-5}$	$6{,}361 \cdot 10^{-3}$	$-2{,}391 \cdot 10^{-3}$
$\mathrm{e}_{27}\mathrm{k}_1$	$3{,}593 \cdot 10^{-4}$	$4{,}278 \cdot 10^{-1}$	$-2{,}249 \cdot 10^{-1}$	$4{,}298 \cdot 10^{-4}$	$5{,}116 \cdot 10^{-1}$	$-2{,}486 \cdot 10^{-1}$
$\mathrm{e}_{27}\mathrm{k}_2$	$-1{,}440 \cdot 10^{-5}$	$-8{,}998 \cdot 10^{-3}$	$5{,}968 \cdot 10^{-3}$	$-3{,}738 \cdot 10^{-5}$	$-2{,}337 \cdot 10^{-2}$	$1{,}602 \cdot 10^{-2}$
$\mathrm{e}_{27}\mathrm{k}_3$	$-2{,}955 \cdot 10^{-4}$	$-3{,}517 \cdot 10^{-1}$	$2{,}065 \cdot 10^{-1}$	$-3{,}420 \cdot 10^{-4}$	$-4{,}072 \cdot 10^{-1}$	$2{,}197 \cdot 10^{-1}$
$\mathrm{e}_{27}\mathrm{k}_4$	$-4{,}950 \cdot 10^{-5}$	$-3{,}094 \cdot 10^{-2}$	$2{,}144 \cdot 10^{-2}$	$-5{,}035 \cdot 10^{-5}$	$-3{,}147 \cdot 10^{-2}$	$2{,}182 \cdot 10^{-2}$
$\mathrm{e}_{28}\mathrm{k}_1$	$-1{,}258 \cdot 10^{-3}$	$-4{,}838 \cdot 10^{-1}$	$4{,}214 \cdot 10^{-1}$	$-1{,}234 \cdot 10^{-3}$	$-4{,}747 \cdot 10^{-1}$	$4{,}128 \cdot 10^{-1}$
$\mathrm{e}_{28}\mathrm{k}_2$	$1{,}245 \cdot 10^{-3}$	$1{,}383$	$-5{,}808$	$1{,}221 \cdot 10^{-3}$	$1{,}356$	$-5{,}431$
$\mathrm{e}_{28}\mathrm{k}_3$	$-1{,}394 \cdot 10^{-5}$	$-5{,}361 \cdot 10^{-3}$	$4{,}529 \cdot 10^{-3}$	$-1{,}445 \cdot 10^{-5}$	$-5{,}559 \cdot 10^{-3}$	$4{,}696 \cdot 10^{-3}$
$\mathrm{e}_{28}\mathrm{k}_4$	$2{,}688 \cdot 10^{-5}$	$2{,}987 \cdot 10^{-2}$	$-7{,}278 \cdot 10^{-2}$	$2{,}800 \cdot 10^{-5}$	$3{,}111 \cdot 10^{-2}$	$-7{,}579 \cdot 10^{-2}$
$\mathrm{e}_{29}\mathrm{k}_1$	$7{,}411 \cdot 10^{-5}$	$7{,}411 \cdot 10^{-2}$	$-6{,}241 \cdot 10^{-2}$	$6{,}788 \cdot 10^{-5}$	$6{,}788 \cdot 10^{-2}$	$-5{,}716 \cdot 10^{-2}$
$\mathrm{e}_{29}\mathrm{k}_2$	$1{,}175 \cdot 10^{-3}$	$1{,}306$	$-1{,}873$	$1{,}157 \cdot 10^{-3}$	$1{,}286$	$-1{,}799$
$\mathrm{e}_{29}\mathrm{k}_3$	$-4{,}470 \cdot 10^{-6}$	$-4{,}470 \cdot 10^{-3}$	$3{,}777 \cdot 10^{-3}$	$-4{,}552 \cdot 10^{-6}$	$-4{,}552 \cdot 10^{-3}$	$3{,}846 \cdot 10^{-3}$
$\mathrm{e}_{29}\mathrm{k}_4$	$-1{,}245 \cdot 10^{-3}$	$-1{,}383$	$2{,}234$	$-1{,}221 \cdot 10^{-3}$	$-1{,}356$	$2{,}089$
$\mathrm{e}_{30}\mathrm{k}_1$	$1{,}289 \cdot 10^{-3}$	$4{,}957 \cdot 10^{-1}$	$-4{,}326 \cdot 10^{-1}$	$1{,}274 \cdot 10^{-3}$	$4{,}901 \cdot 10^{-1}$	$-4{,}273 \cdot 10^{-1}$
$\mathrm{e}_{30}\mathrm{k}_2$	$-8{,}822 \cdot 10^{-5}$	$-9{,}803 \cdot 10^{-2}$	$2{,}384 \cdot 10^{-1}$	$-9{,}119 \cdot 10^{-5}$	$-1{,}013 \cdot 10^{-1}$	$2{,}464 \cdot 10^{-1}$
$\mathrm{e}_{30}\mathrm{k}_3$	$-2{,}513 \cdot 10^{-5}$	$-9{,}666 \cdot 10^{-3}$	$8{,}163 \cdot 10^{-3}$	$-2{,}576 \cdot 10^{-5}$	$-9{,}906 \cdot 10^{-3}$	$8{,}366 \cdot 10^{-3}$
$\mathrm{e}_{30}\mathrm{k}_4$	$-1{,}175 \cdot 10^{-3}$	$-1{,}306$	$4{,}869$	$-1{,}157 \cdot 10^{-3}$	$-1{,}286$	$4{,}678$

Table A.1: Flux tube element outputs ... *cont*

Element Region	$I_{(\mathrm{ph})} = \left[-10\ -10\ 20\right]^{\mathrm{T}}$					
	$x = 4\,\mathrm{mm}$			$x = 5\,\mathrm{mm}$		
	Φ [Wb]	B [T]	$\mathcal{F}$ [A]	Φ [Wb]	B [T]	$\mathcal{F}$ [A]
$\mathrm{e}_{1}\mathrm{k}_1$	$2{,}363 \cdot 10^{-6}$	$2{,}814 \cdot 10^{-3}$	$-2{,}176 \cdot 10^{-3}$	$2{,}038 \cdot 10^{-6}$	$2{,}426 \cdot 10^{-3}$	$-1{,}873 \cdot 10^{-3}$
$\mathrm{e}_{1}\mathrm{k}_2$	$-8{,}408 \cdot 10^{-5}$	$-8{,}408 \cdot 10^{-2}$	$5{,}623 \cdot 10^{-2}$	$-7{,}093 \cdot 10^{-5}$	$-7{,}093 \cdot 10^{-2}$	$4{,}858 \cdot 10^{-2}$
$\mathrm{e}_{1}\mathrm{k}_3$	$7{,}814 \cdot 10^{-5}$	$9{,}302 \cdot 10^{-2}$	$-7{,}252 \cdot 10^{-2}$	$6{,}575 \cdot 10^{-5}$	$7{,}827 \cdot 10^{-2}$	$-6{,}305 \cdot 10^{-2}$
$\mathrm{e}_{1}\mathrm{k}_4$	$3{,}582 \cdot 10^{-6}$	$3{,}582 \cdot 10^{-3}$	$-2{,}333 \cdot 10^{-3}$	$3{,}140 \cdot 10^{-6}$	$3{,}140 \cdot 10^{-3}$	$-2{,}042 \cdot 10^{-3}$
$\mathrm{e}_{2}\mathrm{k}_1$	$1{,}090 \cdot 10^{-6}$	$1{,}514 \cdot 10^{-3}$	$-1{,}165 \cdot 10^{-3}$	$9{,}248 \cdot 10^{-7}$	$1{,}284 \cdot 10^{-3}$	$-9{,}876 \cdot 10^{-4}$
$\mathrm{e}_{2}\mathrm{k}_2$	$-1{,}629 \cdot 10^{-4}$	$-1{,}629 \cdot 10^{-1}$	$7{,}031 \cdot 10^{-2}$	$-1{,}398 \cdot 10^{-4}$	$-1{,}398 \cdot 10^{-1}$	$6{,}678 \cdot 10^{-2}$
$\mathrm{e}_{2}\mathrm{k}_3$	$7{,}772 \cdot 10^{-5}$	$1{,}080 \cdot 10^{-1}$	$-8{,}063 \cdot 10^{-2}$	$6{,}794 \cdot 10^{-5}$	$9{,}436 \cdot 10^{-2}$	$-7{,}331 \cdot 10^{-2}$
$\mathrm{e}_{2}\mathrm{k}_4$	$8{,}408 \cdot 10^{-5}$	$8{,}408 \cdot 10^{-2}$	$-4{,}820 \cdot 10^{-2}$	$7{,}093 \cdot 10^{-5}$	$7{,}093 \cdot 10^{-2}$	$-4{,}164 \cdot 10^{-2}$
$\mathrm{e}_{3}\mathrm{k}_1$	$6{,}154 \cdot 10^{-7}$	$1{,}282 \cdot 10^{-3}$	$-9{,}858 \cdot 10^{-4}$	$5{,}177 \cdot 10^{-7}$	$1{,}078 \cdot 10^{-3}$	$-8{,}286 \cdot 10^{-4}$
$\mathrm{e}_{3}\mathrm{k}_2$	$-3{,}070 \cdot 10^{-4}$	$-3{,}070 \cdot 10^{-1}$	$5{,}817 \cdot 10^{-2}$	$-2{,}710 \cdot 10^{-4}$	$-2{,}710 \cdot 10^{-1}$	$5{,}445 \cdot 10^{-2}$
$\mathrm{e}_{3}\mathrm{k}_3$	$1{,}435 \cdot 10^{-4}$	$2{,}989 \cdot 10^{-1}$	$-1{,}195 \cdot 10^{-1}$	$1{,}307 \cdot 10^{-4}$	$2{,}723 \cdot 10^{-1}$	$-1{,}137 \cdot 10^{-1}$
$\mathrm{e}_{3}\mathrm{k}_4$	$1{,}629 \cdot 10^{-4}$	$1{,}629 \cdot 10^{-1}$	$-4{,}687 \cdot 10^{-2}$	$1{,}398 \cdot 10^{-4}$	$1{,}398 \cdot 10^{-1}$	$-4{,}452 \cdot 10^{-2}$
$\mathrm{e}_{4}\mathrm{k}_1$	$8{,}373 \cdot 10^{-7}$	$1{,}163 \cdot 10^{-3}$	$-8{,}937 \cdot 10^{-4}$	$6{,}977 \cdot 10^{-7}$	$9{,}690 \cdot 10^{-4}$	$-7{,}441 \cdot 10^{-4}$
$\mathrm{e}_{4}\mathrm{k}_2$	$-5{,}542 \cdot 10^{-4}$	$-5{,}542 \cdot 10^{-1}$	$1{,}177 \cdot 10^{-1}$	$-4{,}882 \cdot 10^{-4}$	$-4{,}882 \cdot 10^{-1}$	$1{,}088 \cdot 10^{-1}$
$\mathrm{e}_{4}\mathrm{k}_3$	$2{,}464 \cdot 10^{-4}$	$3{,}422 \cdot 10^{-1}$	$-1{,}275 \cdot 10^{-1}$	$2{,}165 \cdot 10^{-4}$	$3{,}007 \cdot 10^{-1}$	$-1{,}199 \cdot 10^{-1}$
$\mathrm{e}_{4}\mathrm{k}_4$	$3{,}070 \cdot 10^{-4}$	$3{,}070 \cdot 10^{-1}$	$-8{,}725 \cdot 10^{-2}$	$2{,}710 \cdot 10^{-4}$	$2{,}710 \cdot 10^{-1}$	$-8{,}167 \cdot 10^{-2}$

Table A.1: Flux tube element outputs ... *cont*

Element Region	$I_{(\mathrm{ph})} = \begin{bmatrix} -10 & -10 & 20 \end{bmatrix}^{\mathrm{T}}$					
	$x = 4\,\mathrm{mm}$			$x = 5\,\mathrm{mm}$		
	Φ [Wb]	B [T]	$\mathcal{F}$ [A]	Φ [Wb]	B [T]	$\mathcal{F}$ [A]
$\varrho_5\kappa_1$	$5{,}271 \cdot 10^{-7}$	$1{,}098 \cdot 10^{-3}$	$-8{,}437 \cdot 10^{-4}$	$4{,}345 \cdot 10^{-7}$	$9{,}053 \cdot 10^{-4}$	$-6{,}950 \cdot 10^{-4}$
$\varrho_5\kappa_2$	$-8{,}568 \cdot 10^{-4}$	$-8{,}568 \cdot 10^{-1}$	$1{,}149 \cdot 10^{-1}$	$-7{,}747 \cdot 10^{-4}$	$-7{,}747 \cdot 10^{-1}$	$1{,}028 \cdot 10^{-1}$
$\varrho_5\kappa_3$	$3{,}021 \cdot 10^{-4}$	$6{,}293 \cdot 10^{-1}$	$-1{,}786 \cdot 10^{-1}$	$2{,}860 \cdot 10^{-4}$	$5{,}958 \cdot 10^{-1}$	$-1{,}716 \cdot 10^{-1}$
$\varrho_5\kappa_4$	$5{,}542 \cdot 10^{-4}$	$5{,}542 \cdot 10^{-1}$	$-7{,}846 \cdot 10^{-2}$	$4{,}882 \cdot 10^{-4}$	$4{,}882 \cdot 10^{-1}$	$-7{,}252 \cdot 10^{-2}$
$\varrho_6\kappa_1$	$8{,}015 \cdot 10^{-7}$	$1{,}113 \cdot 10^{-3}$	$-8{,}554 \cdot 10^{-4}$	$6{,}529 \cdot 10^{-7}$	$9{,}067 \cdot 10^{-4}$	$-6{,}962 \cdot 10^{-4}$
$\varrho_6\kappa_2$	$-8{,}576 \cdot 10^{-4}$	$-8{,}576 \cdot 10^{-1}$	$1{,}726 \cdot 10^{-1}$	$-7{,}753 \cdot 10^{-4}$	$-7{,}753 \cdot 10^{-1}$	$1{,}543 \cdot 10^{-1}$
$\varrho_6\kappa_3$	$5{,}004 \cdot 10^{-9}$	$6{,}950 \cdot 10^{-6}$	$-5{,}317 \cdot 10^{-6}$	$7{,}271 \cdot 10^{-9}$	$1{,}010 \cdot 10^{-5}$	$-7{,}726 \cdot 10^{-6}$
$\varrho_6\kappa_4$	$8{,}568 \cdot 10^{-4}$	$8{,}568 \cdot 10^{-1}$	$-1{,}724 \cdot 10^{-1}$	$7{,}747 \cdot 10^{-4}$	$7{,}747 \cdot 10^{-1}$	$-1{,}542 \cdot 10^{-1}$
$\varrho_7\kappa_1$	$5{,}538 \cdot 10^{-7}$	$1{,}154 \cdot 10^{-3}$	$-8{,}867 \cdot 10^{-4}$	$4{,}447 \cdot 10^{-7}$	$9{,}264 \cdot 10^{-4}$	$-7{,}113 \cdot 10^{-4}$
$\varrho_7\kappa_2$	$-6{,}112 \cdot 10^{-4}$	$-6{,}112 \cdot 10^{-1}$	$8{,}390 \cdot 10^{-2}$	$-5{,}680 \cdot 10^{-4}$	$-5{,}680 \cdot 10^{-1}$	$7{,}974 \cdot 10^{-2}$
$\varrho_7\kappa_3$	$-2{,}470 \cdot 10^{-4}$	$-5{,}146 \cdot 10^{-1}$	$1{,}559 \cdot 10^{-1}$	$-2{,}078 \cdot 10^{-4}$	$-4{,}329 \cdot 10^{-1}$	$1{,}414 \cdot 10^{-1}$
$\varrho_7\kappa_4$	$8{,}576 \cdot 10^{-4}$	$8{,}576 \cdot 10^{-1}$	$-1{,}151 \cdot 10^{-1}$	$7{,}753 \cdot 10^{-4}$	$7{,}753 \cdot 10^{-1}$	$-1{,}029 \cdot 10^{-1}$
$\varrho_8\kappa_1$	$8{,}580 \cdot 10^{-7}$	$1{,}192 \cdot 10^{-3}$	$-9{,}160 \cdot 10^{-4}$	$6{,}785 \cdot 10^{-7}$	$9{,}424 \cdot 10^{-4}$	$-7{,}236 \cdot 10^{-4}$
$\varrho_8\kappa_2$	$-3{,}987 \cdot 10^{-4}$	$-3{,}987 \cdot 10^{-1}$	$9{,}796 \cdot 10^{-2}$	$-3{,}825 \cdot 10^{-4}$	$-3{,}825 \cdot 10^{-1}$	$9{,}624 \cdot 10^{-2}$
$\varrho_8\kappa_3$	$-2{,}133 \cdot 10^{-4}$	$-2{,}963 \cdot 10^{-1}$	$1{,}190 \cdot 10^{-1}$	$-1{,}861 \cdot 10^{-4}$	$-2{,}585 \cdot 10^{-1}$	$1{,}108 \cdot 10^{-1}$
$\varrho_8\kappa_4$	$6{,}112 \cdot 10^{-4}$	$6{,}112 \cdot 10^{-1}$	$-1{,}258 \cdot 10^{-1}$	$5{,}680 \cdot 10^{-4}$	$5{,}680 \cdot 10^{-1}$	$-1{,}196 \cdot 10^{-1}$
$\varrho_9\kappa_1$	$6{,}076 \cdot 10^{-7}$	$1{,}266 \cdot 10^{-3}$	$-9{,}733 \cdot 10^{-4}$	$4{,}706 \cdot 10^{-7}$	$9{,}803 \cdot 10^{-4}$	$-7{,}529 \cdot 10^{-4}$
$\varrho_9\kappa_2$	$-2{,}783 \cdot 10^{-4}$	$-2{,}783 \cdot 10^{-1}$	$5{,}521 \cdot 10^{-2}$	$-2{,}782 \cdot 10^{-4}$	$-2{,}782 \cdot 10^{-1}$	$5{,}519 \cdot 10^{-2}$
$\varrho_9\kappa_3$	$-1{,}210 \cdot 10^{-4}$	$-2{,}520 \cdot 10^{-1}$	$1{,}095 \cdot 10^{-1}$	$-1{,}048 \cdot 10^{-4}$	$-2{,}183 \cdot 10^{-1}$	$1{,}039 \cdot 10^{-1}$
$\varrho_9\kappa_4$	$3{,}987 \cdot 10^{-4}$	$3{,}987 \cdot 10^{-1}$	$-6{,}531 \cdot 10^{-2}$	$3{,}825 \cdot 10^{-4}$	$3{,}825 \cdot 10^{-1}$	$-6{,}416 \cdot 10^{-2}$
$\varrho_{10}\kappa_1$	$1{,}022 \cdot 10^{-6}$	$1{,}420 \cdot 10^{-3}$	$-1{,}093 \cdot 10^{-3}$	$7{,}667 \cdot 10^{-7}$	$1{,}065 \cdot 10^{-3}$	$-8{,}180 \cdot 10^{-4}$
$\varrho_{10}\kappa_2$	$-1{,}599 \cdot 10^{-4}$	$-1{,}599 \cdot 10^{-1}$	$6{,}995 \cdot 10^{-2}$	$-1{,}669 \cdot 10^{-4}$	$-1{,}669 \cdot 10^{-1}$	$7{,}073 \cdot 10^{-2}$
$\varrho_{10}\kappa_3$	$-1{,}195 \cdot 10^{-4}$	$-1{,}660 \cdot 10^{-1}$	$9{,}811 \cdot 10^{-2}$	$-1{,}120 \cdot 10^{-4}$	$-1{,}556 \cdot 10^{-1}$	$9{,}640 \cdot 10^{-2}$
$\varrho_{10}\kappa_4$	$2{,}783 \cdot 10^{-4}$	$2{,}783 \cdot 10^{-1}$	$-8{,}282 \cdot 10^{-2}$	$2{,}782 \cdot 10^{-4}$	$2{,}782 \cdot 10^{-1}$	$-8{,}279 \cdot 10^{-2}$
$\varrho_{11}\kappa_1$	$1{,}937 \cdot 10^{-6}$	$2{,}306 \cdot 10^{-3}$	$-1{,}780 \cdot 10^{-3}$	$1{,}304 \cdot 10^{-6}$	$1{,}552 \cdot 10^{-3}$	$-1{,}195 \cdot 10^{-3}$
$\varrho_{11}\kappa_2$	$2{,}007 \cdot 10^{-6}$	$2{,}007 \cdot 10^{-3}$	$-1{,}300 \cdot 10^{-3}$	$7{,}144 \cdot 10^{-7}$	$7{,}144 \cdot 10^{-4}$	$-4{,}604 \cdot 10^{-4}$
$\varrho_{11}\kappa_3$	$-1{,}638 \cdot 10^{-4}$	$-1{,}950 \cdot 10^{-1}$	$1{,}013 \cdot 10^{-1}$	$-1{,}689 \cdot 10^{-4}$	$-2{,}011 \cdot 10^{-1}$	$1{,}019 \cdot 10^{-1}$
$\varrho_{11}\kappa_4$	$1{,}599 \cdot 10^{-4}$	$1{,}599 \cdot 10^{-1}$	$-8{,}161 \cdot 10^{-2}$	$1{,}669 \cdot 10^{-4}$	$1{,}669 \cdot 10^{-1}$	$-8{,}252 \cdot 10^{-2}$
$\varrho_{12}\kappa_1$	$-7{,}814 \cdot 10^{-5}$	$-9{,}302 \cdot 10^{-2}$	$1{,}160 \cdot 10^{-1}$	$-6{,}575 \cdot 10^{-5}$	$-7{,}827 \cdot 10^{-2}$	$1{,}009 \cdot 10^{-1}$
$\varrho_{12}\kappa_2$	$-1{,}040 \cdot 10^{-4}$	$-6{,}501 \cdot 10^{-2}$	$4{,}488 \cdot 10^{-2}$	$-7{,}842 \cdot 10^{-5}$	$-4{,}901 \cdot 10^{-2}$	$3{,}421 \cdot 10^{-2}$
$\varrho_{12}\kappa_3$	$1{,}767 \cdot 10^{-4}$	$2{,}103 \cdot 10^{-1}$	$-1{,}646 \cdot 10^{-1}$	$1{,}393 \cdot 10^{-4}$	$1{,}659 \cdot 10^{-1}$	$-1{,}570 \cdot 10^{-1}$
$\varrho_{12}\kappa_4$	$5{,}471 \cdot 10^{-6}$	$3{,}420 \cdot 10^{-3}$	$-2{,}226 \cdot 10^{-3}$	$4{,}824 \cdot 10^{-6}$	$3{,}015 \cdot 10^{-3}$	$-1{,}960 \cdot 10^{-3}$
$\varrho_{13}\kappa_1$	$-7{,}772 \cdot 10^{-5}$	$-1{,}080 \cdot 10^{-1}$	$1{,}290 \cdot 10^{-1}$	$-6{,}794 \cdot 10^{-5}$	$-9{,}436 \cdot 10^{-2}$	$1{,}173 \cdot 10^{-1}$
$\varrho_{13}\kappa_2$	$-2{,}653 \cdot 10^{-5}$	$-1{,}658 \cdot 10^{-2}$	$9{,}618 \cdot 10^{-3}$	$-1{,}065 \cdot 10^{-5}$	$-6{,}658 \cdot 10^{-3}$	$3{,}757 \cdot 10^{-3}$
$\varrho_{13}\kappa_3$	$2{,}453 \cdot 10^{-7}$	$3{,}408 \cdot 10^{-4}$	$-4{,}177 \cdot 10^{-4}$	$1{,}773 \cdot 10^{-7}$	$2{,}463 \cdot 10^{-4}$	$-3{,}017 \cdot 10^{-4}$
$\varrho_{13}\kappa_4$	$1{,}040 \cdot 10^{-4}$	$6{,}501 \cdot 10^{-2}$	$-3{,}847 \cdot 10^{-2}$	$7{,}842 \cdot 10^{-5}$	$4{,}901 \cdot 10^{-2}$	$-2{,}933 \cdot 10^{-2}$
$\varrho_{14}\kappa_1$	$-1{,}435 \cdot 10^{-4}$	$-2{,}989 \cdot 10^{-1}$	$1{,}912 \cdot 10^{-1}$	$-1{,}307 \cdot 10^{-4}$	$-2{,}723 \cdot 10^{-1}$	$1{,}819 \cdot 10^{-1}$
$\varrho_{14}\kappa_2$	$-3{,}488 \cdot 10^{-4}$	$-2{,}180 \cdot 10^{-1}$	$4{,}985 \cdot 10^{-2}$	$-2{,}912 \cdot 10^{-4}$	$-1{,}820 \cdot 10^{-1}$	$4{,}801 \cdot 10^{-2}$
$\varrho_{14}\kappa_3$	$4{,}658 \cdot 10^{-4}$	$9{,}704 \cdot 10^{-1}$	$-4{,}564 \cdot 10^{-1}$	$4{,}112 \cdot 10^{-4}$	$8{,}567 \cdot 10^{-1}$	$-3{,}831 \cdot 10^{-1}$
$\varrho_{14}\kappa_4$	$2{,}653 \cdot 10^{-5}$	$1{,}658 \cdot 10^{-2}$	$-6{,}412 \cdot 10^{-3}$	$1{,}065 \cdot 10^{-5}$	$6{,}658 \cdot 10^{-3}$	$-2{,}505 \cdot 10^{-3}$
$\varrho_{15}\kappa_1$	$-2{,}464 \cdot 10^{-4}$	$-3{,}422 \cdot 10^{-1}$	$2{,}040 \cdot 10^{-1}$	$-2{,}165 \cdot 10^{-4}$	$-3{,}007 \cdot 10^{-1}$	$1{,}918 \cdot 10^{-1}$
$\varrho_{15}\kappa_2$	$-1{,}028 \cdot 10^{-4}$	$-6{,}428 \cdot 10^{-2}$	$3{,}807 \cdot 10^{-2}$	$-7{,}501 \cdot 10^{-5}$	$-4{,}688 \cdot 10^{-2}$	$2{,}806 \cdot 10^{-2}$
$\varrho_{15}\kappa_3$	$3{,}739 \cdot 10^{-7}$	$5{,}193 \cdot 10^{-4}$	$-6{,}369 \cdot 10^{-4}$	$3{,}603 \cdot 10^{-7}$	$5{,}005 \cdot 10^{-4}$	$-6{,}138 \cdot 10^{-4}$
$\varrho_{15}\kappa_4$	$3{,}488 \cdot 10^{-4}$	$2{,}180 \cdot 10^{-1}$	$-7{,}477 \cdot 10^{-2}$	$2{,}912 \cdot 10^{-4}$	$1{,}820 \cdot 10^{-1}$	$-7{,}201 \cdot 10^{-2}$
$\varrho_{16}\kappa_1$	$-3{,}021 \cdot 10^{-4}$	$-6{,}293 \cdot 10^{-1}$	$2{,}857 \cdot 10^{-1}$	$-2{,}860 \cdot 10^{-4}$	$-5{,}958 \cdot 10^{-1}$	$2{,}746 \cdot 10^{-1}$
$\varrho_{16}\kappa_2$	$-4{,}222 \cdot 10^{-5}$	$-2{,}639 \cdot 10^{-2}$	$1{,}039 \cdot 10^{-2}$	$-4{,}214 \cdot 10^{-5}$	$-2{,}634 \cdot 10^{-2}$	$1{,}037 \cdot 10^{-2}$
$\varrho_{16}\kappa_3$	$2{,}415 \cdot 10^{-4}$	$5{,}030 \cdot 10^{-1}$	$-2{,}461 \cdot 10^{-1}$	$2{,}531 \cdot 10^{-4}$	$5{,}273 \cdot 10^{-1}$	$-2{,}533 \cdot 10^{-1}$
$\varrho_{16}\kappa_4$	$1{,}028 \cdot 10^{-4}$	$6{,}428 \cdot 10^{-2}$	$-2{,}538 \cdot 10^{-2}$	$7{,}501 \cdot 10^{-5}$	$4{,}688 \cdot 10^{-2}$	$-1{,}871 \cdot 10^{-2}$
$\varrho_{17}\kappa_1$	$2{,}470 \cdot 10^{-4}$	$5{,}146 \cdot 10^{-1}$	$-2{,}495 \cdot 10^{-1}$	$2{,}078 \cdot 10^{-4}$	$4{,}329 \cdot 10^{-1}$	$-2{,}263 \cdot 10^{-1}$
$\varrho_{17}\kappa_2$	$-2{,}357 \cdot 10^{-4}$	$-1{,}473 \cdot 10^{-1}$	$4{,}544 \cdot 10^{-2}$	$-2{,}863 \cdot 10^{-4}$	$-1{,}790 \cdot 10^{-1}$	$4{,}786 \cdot 10^{-2}$
$\varrho_{17}\kappa_3$	$-5{,}357 \cdot 10^{-5}$	$-1{,}116 \cdot 10^{-1}$	$1{,}318 \cdot 10^{-1}$	$3{,}625 \cdot 10^{-5}$	$7{,}552 \cdot 10^{-2}$	$-9{,}781 \cdot 10^{-2}$
$\varrho_{17}\kappa_4$	$4{,}232 \cdot 10^{-5}$	$2{,}645 \cdot 10^{-2}$	$-1{,}042 \cdot 10^{-2}$	$4{,}228 \cdot 10^{-5}$	$2{,}643 \cdot 10^{-2}$	$-1{,}041 \cdot 10^{-2}$
$\varrho_{18}\kappa_1$	$2{,}133 \cdot 10^{-4}$	$2{,}963 \cdot 10^{-1}$	$-1{,}903 \cdot 10^{-1}$	$1{,}861 \cdot 10^{-4}$	$2{,}585 \cdot 10^{-1}$	$-1{,}773 \cdot 10^{-1}$
$\varrho_{18}\kappa_2$	$-4{,}489 \cdot 10^{-4}$	$-2{,}805 \cdot 10^{-1}$	$8{,}317 \cdot 10^{-2}$	$-4{,}724 \cdot 10^{-4}$	$-2{,}952 \cdot 10^{-1}$	$8{,}549 \cdot 10^{-2}$
$\varrho_{18}\kappa_3$	$-2{,}101 \cdot 10^{-7}$	$-2{,}919 \cdot 10^{-4}$	$3{,}577 \cdot 10^{-4}$	$-1{,}153 \cdot 10^{-7}$	$-1{,}602 \cdot 10^{-4}$	$1{,}962 \cdot 10^{-4}$
$\varrho_{18}\kappa_4$	$2{,}357 \cdot 10^{-4}$	$1{,}473 \cdot 10^{-1}$	$-6{,}816 \cdot 10^{-2}$	$2{,}863 \cdot 10^{-4}$	$1{,}790 \cdot 10^{-1}$	$-7{,}179 \cdot 10^{-2}$

Table A.1: Flux tube element outputs ... *cont*

Element Region	$I_{(\mathrm{ph})} = \begin{bmatrix} -10 & -10 & 20 \end{bmatrix}^{\mathrm{T}}$					
	$x = 4\,\mathrm{mm}$			$x = 5\,\mathrm{mm}$		
	Φ [Wb]	B [T]	$\mathcal{F}$ [A]	Φ [Wb]	B [T]	$\mathcal{F}$ [A]
$e_{19}s_1$	$1{,}210 \cdot 10^{-4}$	$2{,}520 \cdot 10^{-1}$	$-1{,}752 \cdot 10^{-1}$	$1{,}048 \cdot 10^{-4}$	$2{,}183 \cdot 10^{-1}$	$-1{,}662 \cdot 10^{-1}$
$e_{19}s_2$	$-2{,}110 \cdot 10^{-4}$	$-1{,}319 \cdot 10^{-1}$	$4{,}338 \cdot 10^{-2}$	$-2{,}731 \cdot 10^{-4}$	$-1{,}707 \cdot 10^{-1}$	$4{,}740 \cdot 10^{-2}$
$e_{19}s_3$	$-3{,}589 \cdot 10^{-4}$	$-7{,}476 \cdot 10^{-1}$	$3{,}307 \cdot 10^{-1}$	$-3{,}040 \cdot 10^{-4}$	$-6{,}334 \cdot 10^{-1}$	$2{,}871 \cdot 10^{-1}$
$e_{19}s_4$	$4{,}489 \cdot 10^{-4}$	$2{,}805 \cdot 10^{-1}$	$-5{,}545 \cdot 10^{-2}$	$4{,}724 \cdot 10^{-4}$	$2{,}952 \cdot 10^{-1}$	$-5{,}699 \cdot 10^{-2}$
$e_{20}s_1$	$1{,}195 \cdot 10^{-4}$	$1{,}660 \cdot 10^{-1}$	$-1{,}570 \cdot 10^{-1}$	$1{,}120 \cdot 10^{-4}$	$1{,}556 \cdot 10^{-1}$	$-1{,}542 \cdot 10^{-1}$
$e_{20}s_2$	$-3{,}301 \cdot 10^{-4}$	$-2{,}063 \cdot 10^{-1}$	$7{,}374 \cdot 10^{-2}$	$-3{,}848 \cdot 10^{-4}$	$-2{,}405 \cdot 10^{-1}$	$7{,}728 \cdot 10^{-2}$
$e_{20}s_3$	$-3{,}778 \cdot 10^{-7}$	$-5{,}248 \cdot 10^{-4}$	$6{,}437 \cdot 10^{-4}$	$-3{,}709 \cdot 10^{-7}$	$-5{,}151 \cdot 10^{-4}$	$6{,}318 \cdot 10^{-4}$
$e_{20}s_4$	$2{,}110 \cdot 10^{-4}$	$1{,}319 \cdot 10^{-1}$	$-6{,}507 \cdot 10^{-2}$	$2{,}731 \cdot 10^{-4}$	$1{,}707 \cdot 10^{-1}$	$-7{,}110 \cdot 10^{-2}$
$e_{21}s_1$	$1{,}638 \cdot 10^{-4}$	$1{,}950 \cdot 10^{-1}$	$-1{,}620 \cdot 10^{-1}$	$1{,}689 \cdot 10^{-4}$	$2{,}011 \cdot 10^{-1}$	$-1{,}630 \cdot 10^{-1}$
$e_{21}s_2$	$1{,}396 \cdot 10^{-7}$	$8{,}724 \cdot 10^{-5}$	$-5{,}608 \cdot 10^{-5}$	$-3{,}328 \cdot 10^{-6}$	$-2{,}080 \cdot 10^{-3}$	$1{,}347 \cdot 10^{-3}$
$e_{21}s_3$	$-4{,}941 \cdot 10^{-4}$	$-5{,}882 \cdot 10^{-1}$	$2{,}722 \cdot 10^{-1}$	$-5{,}504 \cdot 10^{-4}$	$-6{,}552 \cdot 10^{-1}$	$2{,}946 \cdot 10^{-1}$
$e_{21}s_4$	$3{,}301 \cdot 10^{-4}$	$2{,}063 \cdot 10^{-1}$	$-8{,}603 \cdot 10^{-2}$	$3{,}848 \cdot 10^{-4}$	$2{,}405 \cdot 10^{-1}$	$-9{,}016 \cdot 10^{-2}$
$e_{22}s_1$	$-1{,}767 \cdot 10^{-4}$	$-2{,}103 \cdot 10^{-1}$	$1{,}646 \cdot 10^{-1}$	$-1{,}393 \cdot 10^{-4}$	$-1{,}659 \cdot 10^{-1}$	$1{,}570 \cdot 10^{-1}$
$e_{22}s_2$	$8{,}484 \cdot 10^{-5}$	$5{,}303 \cdot 10^{-2}$	$-3{,}697 \cdot 10^{-2}$	$6{,}912 \cdot 10^{-5}$	$4{,}320 \cdot 10^{-2}$	$-3{,}016 \cdot 10^{-2}$
$e_{22}s_3$	$7{,}476 \cdot 10^{-5}$	$8{,}900 \cdot 10^{-2}$	$-1{,}121 \cdot 10^{-1}$	$5{,}545 \cdot 10^{-5}$	$6{,}601 \cdot 10^{-2}$	$-8{,}670 \cdot 10^{-2}$
$e_{22}s_4$	$1{,}707 \cdot 10^{-5}$	$1{,}067 \cdot 10^{-2}$	$-7{,}112 \cdot 10^{-3}$	$1{,}477 \cdot 10^{-5}$	$9{,}234 \cdot 10^{-3}$	$-6{,}129 \cdot 10^{-3}$
$e_{23}s_1$	$-4{,}658 \cdot 10^{-4}$	$-9{,}704 \cdot 10^{-1}$	$4{,}564 \cdot 10^{-1}$	$-4{,}112 \cdot 10^{-4}$	$-8{,}567 \cdot 10^{-1}$	$3{,}831 \cdot 10^{-1}$
$e_{23}s_2$	$1{,}842 \cdot 10^{-4}$	$1{,}151 \cdot 10^{-1}$	$-4{,}030 \cdot 10^{-2}$	$1{,}809 \cdot 10^{-4}$	$1{,}130 \cdot 10^{-1}$	$-3{,}986 \cdot 10^{-2}$
$e_{23}s_3$	$2{,}644 \cdot 10^{-4}$	$5{,}508 \cdot 10^{-1}$	$-2{,}605 \cdot 10^{-1}$	$2{,}317 \cdot 10^{-4}$	$4{,}827 \cdot 10^{-1}$	$-2{,}401 \cdot 10^{-1}$
$e_{23}s_4$	$1{,}729 \cdot 10^{-5}$	$1{,}081 \cdot 10^{-2}$	$-4{,}117 \cdot 10^{-3}$	$-1{,}332 \cdot 10^{-6}$	$-8{,}325 \cdot 10^{-4}$	$3{,}067 \cdot 10^{-4}$
$e_{24}s_1$	$-2{,}415 \cdot 10^{-4}$	$-5{,}030 \cdot 10^{-1}$	$2{,}461 \cdot 10^{-1}$	$-2{,}531 \cdot 10^{-4}$	$-5{,}273 \cdot 10^{-1}$	$2{,}533 \cdot 10^{-1}$
$e_{24}s_2$	$2{,}355 \cdot 10^{-5}$	$1{,}472 \cdot 10^{-2}$	$-5{,}666 \cdot 10^{-3}$	$3{,}323 \cdot 10^{-5}$	$2{,}077 \cdot 10^{-2}$	$-8{,}101 \cdot 10^{-3}$
$e_{24}s_3$	$2{,}158 \cdot 10^{-4}$	$4{,}497 \cdot 10^{-1}$	$-2{,}308 \cdot 10^{-1}$	$2{,}196 \cdot 10^{-4}$	$4{,}575 \cdot 10^{-1}$	$-2{,}329 \cdot 10^{-1}$
$e_{24}s_4$	$2{,}067 \cdot 10^{-6}$	$1{,}292 \cdot 10^{-3}$	$-4{,}768 \cdot 10^{-4}$	$2{,}936 \cdot 10^{-7}$	$1{,}835 \cdot 10^{-4}$	$-6{,}743 \cdot 10^{-5}$
$e_{25}s_1$	$5{,}357 \cdot 10^{-5}$	$1{,}116 \cdot 10^{-1}$	$-1{,}318 \cdot 10^{-1}$	$-3{,}625 \cdot 10^{-5}$	$-7{,}552 \cdot 10^{-2}$	$9{,}781 \cdot 10^{-2}$
$e_{25}s_2$	$-1{,}282 \cdot 10^{-4}$	$-8{,}013 \cdot 10^{-2}$	$3{,}087 \cdot 10^{-2}$	$-1{,}083 \cdot 10^{-4}$	$-6{,}766 \cdot 10^{-2}$	$2{,}660 \cdot 10^{-2}$
$e_{25}s_3$	$-1{,}591 \cdot 10^{-5}$	$-3{,}315 \cdot 10^{-2}$	$4{,}385 \cdot 10^{-2}$	$3{,}840 \cdot 10^{-5}$	$8{,}000 \cdot 10^{-2}$	$-1{,}028 \cdot 10^{-1}$
$e_{25}s_4$	$9{,}056 \cdot 10^{-5}$	$5{,}660 \cdot 10^{-2}$	$-2{,}250 \cdot 10^{-2}$	$1{,}061 \cdot 10^{-4}$	$6{,}632 \cdot 10^{-2}$	$-2{,}612 \cdot 10^{-2}$
$e_{26}s_1$	$3{,}589 \cdot 10^{-4}$	$7{,}476 \cdot 10^{-1}$	$-3{,}307 \cdot 10^{-1}$	$3{,}040 \cdot 10^{-4}$	$6{,}334 \cdot 10^{-1}$	$-2{,}871 \cdot 10^{-1}$
$e_{26}s_2$	$-1{,}414 \cdot 10^{-4}$	$-8{,}837 \cdot 10^{-2}$	$3{,}345 \cdot 10^{-2}$	$-1{,}391 \cdot 10^{-4}$	$-8{,}696 \cdot 10^{-2}$	$3{,}302 \cdot 10^{-2}$
$e_{26}s_3$	$-2{,}462 \cdot 10^{-4}$	$-5{,}130 \cdot 10^{-1}$	$2{,}491 \cdot 10^{-1}$	$-2{,}141 \cdot 10^{-4}$	$-4{,}460 \cdot 10^{-1}$	$2{,}298 \cdot 10^{-1}$
$e_{26}s_4$	$2{,}877 \cdot 10^{-5}$	$1{,}798 \cdot 10^{-2}$	$-6{,}975 \cdot 10^{-3}$	$4{,}916 \cdot 10^{-5}$	$3{,}073 \cdot 10^{-2}$	$-1{,}216 \cdot 10^{-2}$
$e_{27}s_1$	$4{,}941 \cdot 10^{-4}$	$5{,}882 \cdot 10^{-1}$	$-2{,}722 \cdot 10^{-1}$	$5{,}504 \cdot 10^{-4}$	$6{,}552 \cdot 10^{-1}$	$-2{,}946 \cdot 10^{-1}$
$e_{27}s_2$	$-6{,}606 \cdot 10^{-5}$	$-4{,}129 \cdot 10^{-2}$	$2{,}881 \cdot 10^{-2}$	$-9{,}816 \cdot 10^{-5}$	$-6{,}135 \cdot 10^{-2}$	$4{,}252 \cdot 10^{-2}$
$e_{27}s_3$	$-3{,}778 \cdot 10^{-4}$	$-4{,}497 \cdot 10^{-1}$	$2{,}308 \cdot 10^{-1}$	$-4{,}026 \cdot 10^{-4}$	$-4{,}793 \cdot 10^{-1}$	$2{,}392 \cdot 10^{-1}$
$e_{27}s_4$	$-5{,}025 \cdot 10^{-5}$	$-3{,}141 \cdot 10^{-2}$	$2{,}177 \cdot 10^{-2}$	$-4{,}959 \cdot 10^{-5}$	$-3{,}100 \cdot 10^{-2}$	$2{,}148 \cdot 10^{-2}$
$e_{28}s_1$	$-1{,}209 \cdot 10^{-3}$	$-4{,}650 \cdot 10^{-1}$	$4{,}039 \cdot 10^{-1}$	$-1{,}182 \cdot 10^{-3}$	$-4{,}548 \cdot 10^{-1}$	$3{,}943 \cdot 10^{-1}$
$e_{28}s_2$	$1{,}194 \cdot 10^{-3}$	$1{,}326$	$-5{,}080$	$1{,}163 \cdot 10^{-3}$	$1{,}293$	$-4{,}740$
$e_{28}s_3$	$-1{,}455 \cdot 10^{-5}$	$-5{,}597 \cdot 10^{-3}$	$4{,}728 \cdot 10^{-3}$	$-1{,}414 \cdot 10^{-5}$	$-5{,}440 \cdot 10^{-3}$	$4{,}596 \cdot 10^{-3}$
$e_{28}s_4$	$3{,}000 \cdot 10^{-5}$	$3{,}333 \cdot 10^{-2}$	$-8{,}120 \cdot 10^{-2}$	$3{,}314 \cdot 10^{-5}$	$3{,}682 \cdot 10^{-2}$	$-8{,}968 \cdot 10^{-2}$
$e_{29}s_1$	$6{,}001 \cdot 10^{-5}$	$6{,}001 \cdot 10^{-2}$	$-5{,}055 \cdot 10^{-2}$	$5{,}176 \cdot 10^{-5}$	$5{,}176 \cdot 10^{-2}$	$-4{,}361 \cdot 10^{-2}$
$e_{29}s_2$	$1{,}138 \cdot 10^{-3}$	$1{,}265$	$-1{,}728$	$1{,}116 \cdot 10^{-3}$	$1{,}240$	$-1{,}653$
$e_{29}s_3$	$-4{,}592 \cdot 10^{-6}$	$-4{,}592 \cdot 10^{-3}$	$3{,}879 \cdot 10^{-3}$	$-4{,}564 \cdot 10^{-6}$	$-4{,}564 \cdot 10^{-3}$	$3{,}856 \cdot 10^{-3}$
$e_{29}s_4$	$-1{,}194 \cdot 10^{-3}$	$-1{,}326$	$1{,}954$	$-1{,}163 \cdot 10^{-3}$	$-1{,}293$	$1{,}823$
$e_{30}s_1$	$1{,}260 \cdot 10^{-3}$	$4{,}844 \cdot 10^{-1}$	$-4{,}220 \cdot 10^{-1}$	$1{,}242 \cdot 10^{-3}$	$4{,}778 \cdot 10^{-1}$	$-4{,}157 \cdot 10^{-1}$
$e_{30}s_2$	$-9{,}490 \cdot 10^{-5}$	$-1{,}054 \cdot 10^{-1}$	$2{,}564 \cdot 10^{-1}$	$-9{,}903 \cdot 10^{-5}$	$-1{,}100 \cdot 10^{-1}$	$2{,}676 \cdot 10^{-1}$
$e_{30}s_3$	$-2{,}641 \cdot 10^{-5}$	$-1{,}016 \cdot 10^{-2}$	$8{,}579 \cdot 10^{-3}$	$-2{,}696 \cdot 10^{-5}$	$-1{,}037 \cdot 10^{-2}$	$8{,}757 \cdot 10^{-3}$
$e_{30}s_4$	$-1{,}138 \cdot 10^{-3}$	$-1{,}265$	$4{,}494$	$-1{,}116 \cdot 10^{-3}$	$-1{,}240$	$4{,}298$

Table A.2: Source outputs

Source Boundary	$I_{(\mathrm{ph})} = [\,20\ -10\ -10\,]^{\mathrm{T}}$					
	$x = 0\,\mathrm{mm}$		$x = 1\,\mathrm{mm}$		$x = 2\,\mathrm{mm}$	
	Φ [Wb]	H [A/m]	Φ [Wb]	H [A/m]	Φ [Wb]	H [A/m]
ζ_1	$-1{,}300 \cdot 10^{-3}$	$1{,}290 \cdot 10^{4}$	$-1{,}322 \cdot 10^{-3}$	$1{,}168 \cdot 10^{4}$	$-1{,}334 \cdot 10^{-3}$	$8{,}641 \cdot 10^{3}$
ζ_2	$-7{,}894 \cdot 10^{-5}$	$2{,}222 \cdot 10^{5}$	$-7{,}507 \cdot 10^{-5}$	$2{,}371 \cdot 10^{5}$	$-7{,}457 \cdot 10^{-5}$	$2{,}562 \cdot 10^{5}$
ζ_3	$1{,}431 \cdot 10^{-3}$	$0{,}000$	$1{,}450 \cdot 10^{-3}$	$0{,}000$	$1{,}460 \cdot 10^{-3}$	$0{,}000$
ζ_4	$-5{,}210 \cdot 10^{-5}$	$-3{,}077 \cdot 10^{5}$	$-5{,}256 \cdot 10^{-5}$	$-3{,}167 \cdot 10^{5}$	$-5{,}170 \cdot 10^{-5}$	$-3{,}121 \cdot 10^{5}$
ζ_5	$1{,}281 \cdot 10^{-3}$	$3{,}670 \cdot 10^{2}$	$1{,}282 \cdot 10^{-3}$	$-4{,}359 \cdot 10^{2}$	$1{,}286 \cdot 10^{-3}$	$8{,}051 \cdot 10^{2}$
ζ_6	$6{,}073 \cdot 10^{-5}$	$-2{,}623 \cdot 10^{5}$	$5{,}905 \cdot 10^{-5}$	$-2{,}660 \cdot 10^{5}$	$5{,}688 \cdot 10^{-5}$	$-2{,}720 \cdot 10^{5}$
ζ_7	$-1{,}419 \cdot 10^{-3}$	$0{,}000$	$-1{,}421 \cdot 10^{-3}$	$0{,}000$	$-1{,}423 \cdot 10^{-3}$	$0{,}000$
ζ_8	$7{,}733 \cdot 10^{-5}$	$2{,}802 \cdot 10^{5}$	$7{,}944 \cdot 10^{-5}$	$2{,}801 \cdot 10^{5}$	$7{,}961 \cdot 10^{-5}$	$2{,}761 \cdot 10^{5}$

Table A.2: Source outputs *... cont*

Source Boundary	$I_{(\mathrm{ph})} = [\,20\ -10\ -10\,]^{\mathrm{T}}$					
	$x = 3\,\mathrm{mm}$		$x = 4\,\mathrm{mm}$		$x = 5\,\mathrm{mm}$	
	Φ [Wb]	H [A/m]	Φ [Wb]	H [A/m]	Φ [Wb]	H [A/m]
ζ_1	$-1{,}336 \cdot 10^{-3}$	$4{,}744 \cdot 10^{3}$	$-1{,}330 \cdot 10^{-3}$	$8{,}339 \cdot 10^{2}$	$-1{,}316 \cdot 10^{-3}$	$-2{,}298 \cdot 10^{3}$
ζ_2	$-7{,}600 \cdot 10^{-5}$	$2{,}754 \cdot 10^{5}$	$-7{,}802 \cdot 10^{-5}$	$2{,}918 \cdot 10^{5}$	$-7{,}932 \cdot 10^{-5}$	$3{,}029 \cdot 10^{5}$
ζ_3	$1{,}463 \cdot 10^{-3}$	$0{,}000$	$1{,}459 \cdot 10^{-3}$	$0{,}000$	$1{,}447 \cdot 10^{-3}$	$0{,}000$
ζ_4	$-5{,}057 \cdot 10^{-5}$	$-2{,}990 \cdot 10^{5}$	$-5{,}020 \cdot 10^{-5}$	$-2{,}827 \cdot 10^{5}$	$-5{,}162 \cdot 10^{-5}$	$-2{,}686 \cdot 10^{5}$
ζ_5	$1{,}290 \cdot 10^{-3}$	$3{,}483 \cdot 10^{3}$	$1{,}289 \cdot 10^{-3}$	$7{,}012 \cdot 10^{3}$	$1{,}279 \cdot 10^{-3}$	$1{,}080 \cdot 10^{4}$
ζ_6	$5{,}451 \cdot 10^{-5}$	$-2{,}808 \cdot 10^{5}$	$5{,}215 \cdot 10^{-5}$	$-2{,}934 \cdot 10^{5}$	$5{,}000 \cdot 10^{-5}$	$-3{,}110 \cdot 10^{5}$
ζ_7	$-1{,}423 \cdot 10^{-3}$	$0{,}000$	$-1{,}419 \cdot 10^{-3}$	$0{,}000$	$-1{,}407 \cdot 10^{-3}$	$0{,}000$
ζ_8	$7{,}883 \cdot 10^{-5}$	$2{,}687 \cdot 10^{5}$	$7{,}807 \cdot 10^{-5}$	$2{,}591 \cdot 10^{5}$	$7{,}828 \cdot 10^{-5}$	$2{,}483 \cdot 10^{5}$

Table A.2: Source outputs *... cont*

Source Boundary	$I_{(\mathrm{ph})} = [\,-10\ 20\ -10\,]^{\mathrm{T}}$					
	$x = 0\,\mathrm{mm}$		$x = 1\,\mathrm{mm}$		$x = 2\,\mathrm{mm}$	
	Φ [Wb]	H [A/m]	Φ [Wb]	H [A/m]	Φ [Wb]	H [A/m]
ζ_1	$-1{,}067 \cdot 10^{-3}$	$4{,}524 \cdot 10^{3}$	$-1{,}073 \cdot 10^{-3}$	$7{,}057 \cdot 10^{3}$	$-1{,}083 \cdot 10^{-3}$	$9{,}687 \cdot 10^{3}$
ζ_2	$-8{,}429 \cdot 10^{-5}$	$2{,}959 \cdot 10^{5}$	$-8{,}389 \cdot 10^{-5}$	$2{,}850 \cdot 10^{5}$	$-8{,}476 \cdot 10^{-5}$	$2{,}703 \cdot 10^{5}$
ζ_3	$1{,}205 \cdot 10^{-3}$	$0{,}000$	$1{,}212 \cdot 10^{-3}$	$0{,}000$	$1{,}222 \cdot 10^{-3}$	$0{,}000$
ζ_4	$-5{,}356 \cdot 10^{-5}$	$-3{,}103 \cdot 10^{5}$	$-5{,}501 \cdot 10^{-5}$	$-3{,}242 \cdot 10^{5}$	$-5{,}443 \cdot 10^{-5}$	$-3{,}311 \cdot 10^{5}$
ζ_5	$1{,}048 \cdot 10^{-3}$	$-7{,}935 \cdot 10^{3}$	$1{,}076 \cdot 10^{-3}$	$-1{,}058 \cdot 10^{4}$	$1{,}107 \cdot 10^{-3}$	$-1{,}029 \cdot 10^{4}$
ζ_6	$6{,}223 \cdot 10^{-5}$	$-2{,}647 \cdot 10^{5}$	$6{,}022 \cdot 10^{-5}$	$-2{,}647 \cdot 10^{5}$	$5{,}788 \cdot 10^{-5}$	$-2{,}682 \cdot 10^{5}$
ζ_7	$-1{,}193 \cdot 10^{-3}$	$0{,}000$	$-1{,}218 \cdot 10^{-3}$	$0{,}000$	$-1{,}246 \cdot 10^{-3}$	$0{,}000$
ζ_8	$8{,}285 \cdot 10^{-5}$	$3{,}546 \cdot 10^{5}$	$8{,}172 \cdot 10^{-5}$	$3{,}661 \cdot 10^{5}$	$8{,}034 \cdot 10^{-5}$	$3{,}672 \cdot 10^{5}$

Table A.2: Source outputs ... *cont*

Source Boundary	$I_{(\mathrm{ph})} = [\,-10\ 20\ -10\,]^{\mathrm{T}}$					
	$x = 3\,\mathrm{mm}$		$x = 4\,\mathrm{mm}$		$x = 5\,\mathrm{mm}$	
	Φ [Wb]	H [A/m]	Φ [Wb]	H [A/m]	Φ [Wb]	H [A/m]
ζ_1	$-1{,}096 \cdot 10^{-3}$	$1{,}228 \cdot 10^{4}$	$-1{,}112 \cdot 10^{-3}$	$1{,}469 \cdot 10^{4}$	$-1{,}130 \cdot 10^{-3}$	$1{,}680 \cdot 10^{4}$
ζ_2	$-8{,}593 \cdot 10^{-5}$	$2{,}542 \cdot 10^{5}$	$-8{,}644 \cdot 10^{-5}$	$2{,}390 \cdot 10^{5}$	$-8{,}532 \cdot 10^{-5}$	$2{,}271 \cdot 10^{5}$
ζ_3	$1{,}235 \cdot 10^{-3}$	$0{,}000$	$1{,}249 \cdot 10^{-3}$	$0{,}000$	$1{,}264 \cdot 10^{-3}$	$0{,}000$
ζ_4	$-5{,}265 \cdot 10^{-5}$	$-3{,}341 \cdot 10^{5}$	$-5{,}050 \cdot 10^{-5}$	$-3{,}364 \cdot 10^{5}$	$-4{,}880 \cdot 10^{-5}$	$-3{,}412 \cdot 10^{5}$
ζ_5	$1{,}138 \cdot 10^{-3}$	$-7{,}943 \cdot 10^{3}$	$1{,}163 \cdot 10^{-3}$	$-4{,}397 \cdot 10^{3}$	$1{,}180 \cdot 10^{-3}$	$-5{,}195 \cdot 10^{2}$
ζ_6	$5{,}541 \cdot 10^{-5}$	$-2{,}759 \cdot 10^{5}$	$5{,}299 \cdot 10^{-5}$	$-2{,}884 \cdot 10^{5}$	$5{,}081 \cdot 10^{-5}$	$-3{,}061 \cdot 10^{5}$
ζ_7	$-1{,}272 \cdot 10^{-3}$	$0{,}000$	$-1{,}295 \cdot 10^{-3}$	$0{,}000$	$-1{,}309 \cdot 10^{-3}$	$0{,}000$
ζ_8	$7{,}903 \cdot 10^{-5}$	$3{,}608 \cdot 10^{5}$	$7{,}815 \cdot 10^{-5}$	$3{,}501 \cdot 10^{5}$	$7{,}804 \cdot 10^{-5}$	$3{,}380 \cdot 10^{5}$

Table A.2: Source outputs ... *cont*

Source Boundary	$I_{(\mathrm{ph})} = [\,-10\ -10\ 20\,]^{\mathrm{T}}$					
	$x = 0\,\mathrm{mm}$		$x = 1\,\mathrm{mm}$		$x = 2\,\mathrm{mm}$	
	Φ [Wb]	H [A/m]	Φ [Wb]	H [A/m]	Φ [Wb]	H [A/m]
ζ_1	$-1{,}159 \cdot 10^{-3}$	$-1{,}051 \cdot 10^{4}$	$-1{,}135 \cdot 10^{-3}$	$-9{,}281 \cdot 10^{3}$	$-1{,}112 \cdot 10^{-3}$	$-8{,}674 \cdot 10^{3}$
ζ_2	$-8{,}006 \cdot 10^{-5}$	$3{,}495 \cdot 10^{5}$	$-7{,}894 \cdot 10^{-5}$	$3{,}507 \cdot 10^{5}$	$-7{,}929 \cdot 10^{-5}$	$3{,}535 \cdot 10^{5}$
ζ_3	$1{,}303 \cdot 10^{-3}$	$0{,}000$	$1{,}281 \cdot 10^{-3}$	$0{,}000$	$1{,}258 \cdot 10^{-3}$	$0{,}000$
ζ_4	$-6{,}482 \cdot 10^{-5}$	$-2{,}467 \cdot 10^{5}$	$-6{,}681 \cdot 10^{-5}$	$-2{,}605 \cdot 10^{5}$	$-6{,}645 \cdot 10^{-5}$	$-2{,}677 \cdot 10^{5}$
ζ_5	$1{,}196 \cdot 10^{-3}$	$1{,}549 \cdot 10^{4}$	$1{,}172 \cdot 10^{-3}$	$1{,}319 \cdot 10^{4}$	$1{,}156 \cdot 10^{-3}$	$1{,}205 \cdot 10^{4}$
ζ_6	$4{,}986 \cdot 10^{-5}$	$-3{,}236 \cdot 10^{5}$	$4{,}926 \cdot 10^{-5}$	$-3{,}262 \cdot 10^{5}$	$4{,}821 \cdot 10^{-5}$	$-3{,}286 \cdot 10^{5}$
ζ_7	$-1{,}327 \cdot 10^{-3}$	$0{,}000$	$-1{,}306 \cdot 10^{-3}$	$0{,}000$	$-1{,}289 \cdot 10^{-3}$	$0{,}000$
ζ_8	$8{,}166 \cdot 10^{-5}$	$2{,}258 \cdot 10^{5}$	$8{,}422 \cdot 10^{-5}$	$2{,}367 \cdot 10^{5}$	$8{,}493 \cdot 10^{-5}$	$2{,}481 \cdot 10^{5}$

Table A.2: Source outputs ... *cont*

Source Boundary	$I_{(\mathrm{ph})} = [\,-10\ -10\ 20\,]^{\mathrm{T}}$					
	$x = 3\,\mathrm{mm}$		$x = 4\,\mathrm{mm}$		$x = 5\,\mathrm{mm}$	
	Φ [Wb]	H [A/m]	Φ [Wb]	H [A/m]	Φ [Wb]	H [A/m]
ζ_1	$-1{,}089 \cdot 10^{-3}$	$-8{,}316 \cdot 10^{3}$	$-1{,}064 \cdot 10^{-3}$	$-7{,}840 \cdot 10^{3}$	$-1{,}038 \cdot 10^{-3}$	$-6{,}884 \cdot 10^{3}$
ζ_2	$-8{,}049 \cdot 10^{-5}$	$3{,}562 \cdot 10^{5}$	$-8{,}189 \cdot 10^{-5}$	$3{,}572 \cdot 10^{5}$	$-8{,}285 \cdot 10^{-5}$	$3{,}548 \cdot 10^{5}$
ζ_3	$1{,}234 \cdot 10^{-3}$	$0{,}000$	$1{,}209 \cdot 10^{-3}$	$0{,}000$	$1{,}182 \cdot 10^{-3}$	$0{,}000$
ζ_4	$-6{,}476 \cdot 10^{-5}$	$-2{,}714 \cdot 10^{5}$	$-6{,}273 \cdot 10^{-5}$	$-2{,}744 \cdot 10^{5}$	$-6{,}139 \cdot 10^{-5}$	$-2{,}795 \cdot 10^{5}$
ζ_5	$1{,}143 \cdot 10^{-3}$	$1{,}184 \cdot 10^{4}$	$1{,}131 \cdot 10^{-3}$	$1{,}235 \cdot 10^{4}$	$1{,}115 \cdot 10^{-3}$	$1{,}336 \cdot 10^{4}$
ζ_6	$4{,}685 \cdot 10^{-5}$	$-3{,}325 \cdot 10^{5}$	$4{,}532 \cdot 10^{-5}$	$-3{,}398 \cdot 10^{5}$	$4{,}378 \cdot 10^{-5}$	$-3{,}524 \cdot 10^{5}$
ζ_7	$-1{,}274 \cdot 10^{-3}$	$0{,}000$	$-1{,}260 \cdot 10^{-3}$	$0{,}000$	$-1{,}242 \cdot 10^{-3}$	$0{,}000$
ζ_8	$8{,}448 \cdot 10^{-5}$	$2{,}589 \cdot 10^{5}$	$8{,}358 \cdot 10^{-5}$	$2{,}680 \cdot 10^{5}$	$8{,}293 \cdot 10^{-5}$	$2{,}742 \cdot 10^{5}$

Table A.3: Flux linkages

λ [Wb]	$I_{(\mathrm{ph})} = [\,20\ -10\ -10\,]^{\mathrm{T}}$					
Phase	$x = 0\,\mathrm{mm}$	$x = 1\,\mathrm{mm}$	$x = 2\,\mathrm{mm}$	$x = 3\,\mathrm{mm}$	$x = 4\,\mathrm{mm}$	$x = 5\,\mathrm{mm}$
1	$1{,}976 \cdot 10^{-2}$	$2{,}075 \cdot 10^{-2}$	$2{,}125 \cdot 10^{-2}$	$2{,}134 \cdot 10^{-2}$	$2{,}104 \cdot 10^{-2}$	$2{,}037 \cdot 10^{-2}$
2	$-1{,}555 \cdot 10^{-2}$	$-1{,}412 \cdot 10^{-2}$	$-1{,}241 \cdot 10^{-2}$	$-1{,}050 \cdot 10^{-2}$	$-8{,}431 \cdot 10^{-3}$	$-6{,}236 \cdot 10^{-3}$
3	$-2{,}548 \cdot 10^{-3}$	$-4{,}953 \cdot 10^{-3}$	$-7{,}153 \cdot 10^{-3}$	$-9{,}143 \cdot 10^{-3}$	$-1{,}090 \cdot 10^{-2}$	$-1{,}241 \cdot 10^{-2}$

Table A.3: Flux linkages *... cont*

λ [Wb]	$I_{(\mathrm{ph})} = [\,-10\ 20\ -10\,]^{\mathrm{T}}$					
Phase	$x = 0\,\mathrm{mm}$	$x = 1\,\mathrm{mm}$	$x = 2\,\mathrm{mm}$	$x = 3\,\mathrm{mm}$	$x = 4\,\mathrm{mm}$	$x = 5\,\mathrm{mm}$
1	$6{,}193 \cdot 10^{-3}$	$7{,}307 \cdot 10^{-3}$	$7{,}977 \cdot 10^{-3}$	$8{,}208 \cdot 10^{-3}$	$8{,}009 \cdot 10^{-3}$	$7{,}390 \cdot 10^{-3}$
2	$-5{,}655 \cdot 10^{-3}$	$-4{,}295 \cdot 10^{-3}$	$-2{,}686 \cdot 10^{-3}$	$-8{,}618 \cdot 10^{-4}$	$1{,}142 \cdot 10^{-3}$	$3{,}291 \cdot 10^{-3}$
3	$-2{,}569 \cdot 10^{-3}$	$-5{,}017 \cdot 10^{-3}$	$-7{,}277 \cdot 10^{-3}$	$-9{,}318 \cdot 10^{-3}$	$-1{,}111 \cdot 10^{-2}$	$-1{,}261 \cdot 10^{-2}$

Table A.3: Flux linkages *... cont*

λ [Wb]	$I_{(\mathrm{ph})} = [\,-10\ -10\ 20\,]^{\mathrm{T}}$					
Phase	$x = 0\,\mathrm{mm}$	$x = 1\,\mathrm{mm}$	$x = 2\,\mathrm{mm}$	$x = 3\,\mathrm{mm}$	$x = 4\,\mathrm{mm}$	$x = 5\,\mathrm{mm}$
1	$8{,}499 \cdot 10^{-3}$	$9{,}614 \cdot 10^{-3}$	$1{,}028 \cdot 10^{-2}$	$1{,}051 \cdot 10^{-2}$	$1{,}029 \cdot 10^{-2}$	$9{,}651 \cdot 10^{-3}$
2	$-1{,}337 \cdot 10^{-2}$	$-1{,}200 \cdot 10^{-2}$	$-1{,}038 \cdot 10^{-2}$	$-8{,}543 \cdot 10^{-3}$	$-6{,}517 \cdot 10^{-3}$	$-4{,}344 \cdot 10^{-3}$
3	$5{,}147 \cdot 10^{-3}$	$2{,}693 \cdot 10^{-3}$	$4{,}228 \cdot 10^{-4}$	$-1{,}631 \cdot 10^{-3}$	$-3{,}437 \cdot 10^{-3}$	$-4{,}961 \cdot 10^{-3}$

Table A.4: Force

F [N]	$I_{(\mathrm{ph})} = [\,20\ -10\ -10\,]^{\mathrm{T}}\,\mathrm{A}$					
	$x = 0\,\mathrm{mm}$	$x = 1\,\mathrm{mm}$	$x = 2\,\mathrm{mm}$	$x = 3\,\mathrm{mm}$	$x = 4\,\mathrm{mm}$	$x = 5\,\mathrm{mm}$
Tangential force	26,77	24,34	15,35	2,24	−12,61	−26,93
Normal force	−438,71	−446,60	−452,59	−455,22	−452,49	−442,49

Table A.4: Force *... cont*

F [N]	$I_{(\mathrm{ph})} = [\,-10\ 20\ -10\,]^{\mathrm{T}}\,\mathrm{A}$					
	$x = 0\,\mathrm{mm}$	$x = 1\,\mathrm{mm}$	$x = 2\,\mathrm{mm}$	$x = 3\,\mathrm{mm}$	$x = 4\,\mathrm{mm}$	$x = 5\,\mathrm{mm}$
Tangential force	25,44	35,24	40,60	42,05	40,33	36,32
Normal force	−255,49	−266,72	−282,70	−300,87	−318,49	−332,70

Table A.4: Force ... *cont*

F [N]	$I_{(\mathrm{ph})} = [\,-10\ -10\ 20\,]^{\mathrm{T}}$ A					
	$x = 0$ mm	$x = 1$ mm	$x = 2$ mm	$x = 3$ mm	$x = 4$ mm	$x = 5$ mm
Tangential force	−52,03	−46,76	−43,25	−41,02	−39,68	−38,90
Normal force	−347,29	−328,19	−312,66	−299,04	−285,73	−271,16

Table A.5: Percentage rms errors

% rms Error	$I_{(\mathrm{ph})} = [\,20\ -10\ -10\,]^{\mathrm{T}}$ A					
	$x = 0$ mm					
	$\Phi_{\underset{\sim}{\epsilon}}$	$\Phi_{\underset{\sim}{\zeta}}$	$H_{\underset{\sim}{\zeta}}$	$\lambda_{(\underset{\sim}{\mathrm{ph}})}$	F(tangent)	F(normal)
B-H curves	0,34	0,20	1,23	0,09	25,46	10,41
$\mu r_{\underset{\sim}{\chi}_1} = 7185$, $\mu r_{\underset{\sim}{\chi}_2} = 2119$	0,14	0,06	1,27	0,05	25,63	10,83
$\mu r_{\underset{\sim}{\chi}_1}, \mu r_{\underset{\sim}{\chi}_2} = 100$	1,86	0,23	1,87	2,15	22,59	12,79
$\mu r_{\underset{\sim}{\chi}_1}, \mu r_{\underset{\sim}{\chi}_2} = 50$	3,14	0,55	2,73	3,75	19,85	14,08
$\mu r_{\underset{\sim}{\chi}_1}, \mu r_{\underset{\sim}{\chi}_2} = 10$	7,53	3,38	5,82	8,14	4,97	20,26

Table A.5: Percentage rms errors ... *cont*

% rms Error	$I_{(\mathrm{ph})} = [\,20\ -10\ -10\,]^{\mathrm{T}}$ A					
	$x = 1$ mm					
	$\Phi_{\underset{\sim}{\epsilon}}$	$\Phi_{\underset{\sim}{\zeta}}$	$H_{\underset{\sim}{\zeta}}$	$\lambda_{(\underset{\sim}{\mathrm{ph}})}$	F(tangent)	F(normal)
B-H curves	0,49	0,30	3,49	0,31	22,22	8,95
$\mu r_{\underset{\sim}{\chi}_1} = 7185$, $\mu r_{\underset{\sim}{\chi}_2} = 2119$	0,29	0,12	3,04	0,20	22,04	9,85
$\mu r_{\underset{\sim}{\chi}_1}, \mu r_{\underset{\sim}{\chi}_2} = 100$	1,95	0,28	2,95	2,45	18,40	11,71
$\mu r_{\underset{\sim}{\chi}_1}, \mu r_{\underset{\sim}{\chi}_2} = 50$	3,25	0,54	3,49	4,14	15,45	12,91
$\mu r_{\underset{\sim}{\chi}_1}, \mu r_{\underset{\sim}{\chi}_2} = 10$	7,71	3,29	6,39	8,94	3,44	18,23

Table A.5: Percentage rms errors ... *cont*

% rms Error	$I_{(\mathrm{ph})} = [\,20\ -10\ -10\,]^{\mathrm{T}}$ A					
	$x = 2$ mm					
	$\Phi_{\underset{\sim}{\epsilon}}$	$\Phi_{\underset{\sim}{\zeta}}$	$H_{\underset{\sim}{\zeta}}$	$\lambda_{(\underset{\sim}{\mathrm{ph}})}$	F(tangent)	F(normal)
B-H curves	0,77	0,57	1,77	0,99	25,30	7,36
$\mu r_{\underset{\sim}{\chi}_1} = 7185$, $\mu r_{\underset{\sim}{\chi}_2} = 2119$	0,08	0,04	1,22	0,03	26,08	8,82
$\mu r_{\underset{\sim}{\chi}_1}, \mu r_{\underset{\sim}{\chi}_2} = 100$	1,90	0,23	2,49	2,35	20,09	10,89
$\mu r_{\underset{\sim}{\chi}_1}, \mu r_{\underset{\sim}{\chi}_2} = 50$	3,23	0,48	3,45	4,12	15,95	12,28
$\mu r_{\underset{\sim}{\chi}_1}, \mu r_{\underset{\sim}{\chi}_2} = 10$	7,88	3,21	6,79	9,34	0,37	18,22

Table A.5: Percentage rms errors ... *cont*

% rms Error	$I_{(\underset{\sim}{\text{ph}})} = \left[20\ -10\ -10\right]^{\mathrm{T}}$ A					
	$x = 3$ mm					
	$\Phi_{\underset{\sim}{\epsilon}}$	$\Phi_{\underset{\sim}{\zeta}}$	$H_{\underset{\sim}{\zeta}}$	$\lambda_{(\underset{\sim}{\text{ph}})}$	F(tangent)	F(normal)
B-H curves	1,11	0,82	1,76	1,59	11,90	6,14
$\mu r_{\underset{\sim}{\chi}_1} = 7185$, $\mu r_{\underset{\sim}{\chi}_2} = 2119$	0,14	0,13	0,80	0,09	37,16	7,97
$\mu r_{\underset{\sim}{\chi}_1}, \mu r_{\underset{\sim}{\chi}_2} = 100$	1,88	0,19	1,90	2,32	11,54	10,40
$\mu r_{\underset{\sim}{\chi}_1}, \mu r_{\underset{\sim}{\chi}_2} = 50$	3,24	0,42	2,88	4,16	4,21	12,08
$\mu r_{\underset{\sim}{\chi}_1}, \mu r_{\underset{\sim}{\chi}_2} = 10$	8,06	3,07	6,32	9,86	29,26	19,16

Table A.5: Percentage rms errors ... *cont*

% rms Error	$I_{(\underset{\sim}{\text{ph}})} = \left[20\ -10\ -10\right]^{\mathrm{T}}$ A					
	$x = 4$ mm					
	$\Phi_{\underset{\sim}{\epsilon}}$	$\Phi_{\underset{\sim}{\zeta}}$	$H_{\underset{\sim}{\zeta}}$	$\lambda_{(\underset{\sim}{\text{ph}})}$	F(tangent)	F(normal)
B-H curves	1,26	0,88	1,10	1,89	36,41	6,24
$\mu r_{\underset{\sim}{\chi}_1} = 7185$, $\mu r_{\underset{\sim}{\chi}_2} = 2119$	0,14	0,10	0,56	0,03	29,84	8,27
$\mu r_{\underset{\sim}{\chi}_1}, \mu r_{\underset{\sim}{\chi}_2} = 100$	1,93	0,23	1,91	2,52	41,42	11,09
$\mu r_{\underset{\sim}{\chi}_1}, \mu r_{\underset{\sim}{\chi}_2} = 50$	3,31	0,43	2,91	4,44	61,23	13,08
$\mu r_{\underset{\sim}{\chi}_1}, \mu r_{\underset{\sim}{\chi}_2} = 10$	8,28	2,94	6,38	10,51	849,02	21,33

Table A.5: Percentage rms errors ... *cont*

% rms Error	$I_{(\underset{\sim}{\text{ph}})} = \left[20\ -10\ -10\right]^{\mathrm{T}}$ A					
	$x = 5$ mm					
	$\Phi_{\underset{\sim}{\epsilon}}$	$\Phi_{\underset{\sim}{\zeta}}$	$H_{\underset{\sim}{\zeta}}$	$\lambda_{(\underset{\sim}{\text{ph}})}$	F(tangent)	F(normal)
B-H curves	1,23	0,65	2,03	1,87	34,17	6,86
$\mu r_{\underset{\sim}{\chi}_1} = 7185$, $\mu r_{\underset{\sim}{\chi}_2} = 2119$	0,36	0,15	1,05	0,25	29,67	8,84
$\mu r_{\underset{\sim}{\chi}_1}, \mu r_{\underset{\sim}{\chi}_2} = 100$	2,06	0,47	1,41	2,83	33,28	11,91
$\mu r_{\underset{\sim}{\chi}_1}, \mu r_{\underset{\sim}{\chi}_2} = 50$	3,44	0,61	2,44	4,80	37,44	14,05
$\mu r_{\underset{\sim}{\chi}_1}, \mu r_{\underset{\sim}{\chi}_2} = 10$	8,45	2,62	6,09	11,05	71,54	22,43

Table A.5: Percentage rms errors ... *cont*

% rms Error	$I_{(\underset{\sim}{\text{ph}})} = \left[-10\ 20\ -10\right]^{\mathrm{T}}$ A					
	$x = 0$ mm					
	$\Phi_{\underset{\sim}{\epsilon}}$	$\Phi_{\underset{\sim}{\zeta}}$	$H_{\underset{\sim}{\zeta}}$	$\lambda_{(\underset{\sim}{\text{ph}})}$	F(tangent)	F(normal)
B-H curves	0,14	0,08	1,12	0,10	28,96	18,73
$\mu r_{\underset{\sim}{\chi}_1} = 7185$, $\mu r_{\underset{\sim}{\chi}_2} = 2119$	0,13	0,06	1,12	0,07	28,98	18,88
$\mu r_{\underset{\sim}{\chi}_1}, \mu r_{\underset{\sim}{\chi}_2} = 100$	1,59	0,54	1,88	4,69	25,62	24,84
$\mu r_{\underset{\sim}{\chi}_1}, \mu r_{\underset{\sim}{\chi}_2} = 50$	2,54	0,63	2,54	7,72	22,64	28,94
$\mu r_{\underset{\sim}{\chi}_1}, \mu r_{\underset{\sim}{\chi}_2} = 10$	6,11	2,34	4,54	17,14	6,97	46,23

Table A.5: Percentage rms errors ... *cont*

% rms Error	$I_{(\underset{\sim}{\text{ph}})} = \left[-10\ 20\ -10\right]^{\mathrm{T}}$ A					
	$x = 1$ mm					
	$\Phi_{\underset{\sim}{\epsilon}}$	$\Phi_{\underset{\sim}{\zeta}}$	$H_{\underset{\sim}{\zeta}}$	$\lambda_{(\underset{\sim}{\text{ph}})}$	F(tangent)	F(normal)
B-H curves	0,35	0,05	2,55	0,50	28,05	16,28
$\mu r_{\underset{\sim}{\chi}_1} = 7185$, $\mu r_{\underset{\sim}{\chi}_2} = 2119$	0,35	0,08	2,49	0,54	28,09	16,44
$\mu r_{\underset{\sim}{\chi}_1}, \mu r_{\underset{\sim}{\chi}_2} = 100$	1,80	0,63	1,79	5,19	25,02	21,99
$\mu r_{\underset{\sim}{\chi}_1}, \mu r_{\underset{\sim}{\chi}_2} = 50$	2,81	0,76	2,05	8,35	22,42	25,76
$\mu r_{\underset{\sim}{\chi}_1}, \mu r_{\underset{\sim}{\chi}_2} = 10$	6,48	2,28	4,44	18,11	12,34	40,72

Table A.5: Percentage rms errors ... *cont*

% rms Error	$I_{(\underset{\sim}{\text{ph}})} = \left[-10\ 20\ -10\right]^{\mathrm{T}}$ A					
	$x = 2$ mm					
	$\Phi_{\underset{\sim}{\epsilon}}$	$\Phi_{\underset{\sim}{\zeta}}$	$H_{\underset{\sim}{\zeta}}$	$\lambda_{(\underset{\sim}{\text{ph}})}$	F(tangent)	F(normal)
B-H curves	0,12	0,06	1,14	0,05	29,54	14,44
$\mu r_{\underset{\sim}{\chi}_1} = 7185$, $\mu r_{\underset{\sim}{\chi}_2} = 2119$	0,10	0,05	1,10	0,10	29,58	14,61
$\mu r_{\underset{\sim}{\chi}_1}, \mu r_{\underset{\sim}{\chi}_2} = 100$	1,77	0,66	1,84	4,51	26,63	20,22
$\mu r_{\underset{\sim}{\chi}_1}, \mu r_{\underset{\sim}{\chi}_2} = 50$	2,88	0,82	2,62	7,55	24,10	24,13
$\mu r_{\underset{\sim}{\chi}_1}, \mu r_{\underset{\sim}{\chi}_2} = 10$	6,81	2,19	5,34	17,23	14,47	39,86

Table A.5: Percentage rms errors ... *cont*

% rms Error	$I_{(\underset{\sim}{\text{ph}})} = \left[-10\ 20\ -10\right]^{\mathrm{T}}$ A					
	$x = 3$ mm					
	$\Phi_{\underset{\sim}{\epsilon}}$	$\Phi_{\underset{\sim}{\zeta}}$	$H_{\underset{\sim}{\zeta}}$	$\lambda_{(\underset{\sim}{\text{ph}})}$	F(tangent)	F(normal)
B-H curves	0,15	0,13	0,99	0,28	29,86	13,16
$\mu r_{\underset{\sim}{\chi}_1} = 7185$, $\mu r_{\underset{\sim}{\chi}_2} = 2119$	0,12	0,09	0,92	0,20	29,91	13,34
$\mu r_{\underset{\sim}{\chi}_1}, \mu r_{\underset{\sim}{\chi}_2} = 100$	1,79	0,67	1,33	4,05	27,11	19,01
$\mu r_{\underset{\sim}{\chi}_1}, \mu r_{\underset{\sim}{\chi}_2} = 50$	3,00	0,89	2,19	7,01	24,59	23,05
$\mu r_{\underset{\sim}{\chi}_1}, \mu r_{\underset{\sim}{\chi}_2} = 10$	7,20	2,04	5,14	16,59	13,52	39,64

Table A.5: Percentage rms errors ... *cont*

% rms Error	$I_{(\underset{\sim}{\text{ph}})} = \left[-10\ 20\ -10\right]^{\mathrm{T}}$ A					
	$x = 4$ mm					
	$\Phi_{\underset{\sim}{\epsilon}}$	$\Phi_{\underset{\sim}{\zeta}}$	$H_{\underset{\sim}{\zeta}}$	$\lambda_{(\underset{\sim}{\text{ph}})}$	F(tangent)	F(normal)
B-H curves	0,15	0,14	0,47	0,08	29,90	12,89
$\mu r_{\underset{\sim}{\chi}_1} = 7185$, $\mu r_{\underset{\sim}{\chi}_2} = 2119$	0,14	0,09	0,48	0,08	29,98	13,08
$\mu r_{\underset{\sim}{\chi}_1}, \mu r_{\underset{\sim}{\chi}_2} = 100$	1,94	0,73	1,84	4,08	27,58	18,64
$\mu r_{\underset{\sim}{\chi}_1}, \mu r_{\underset{\sim}{\chi}_2} = 50$	3,24	0,99	2,77	6,91	25,26	22,61
$\mu r_{\underset{\sim}{\chi}_1}, \mu r_{\underset{\sim}{\chi}_2} = 10$	7,71	1,88	5,76	16,06	13,86	39,13

Table A.5: Percentage rms errors ... *cont*

% rms Error	$I_{(\underset{\sim}{\text{ph}})} = \left[-10\ 20\ -10\right]^{\mathrm{T}}$ A					
	$x = 5$ mm					
	$\Phi_{\underset{\sim}{\epsilon}}$	$\Phi_{\underset{\sim}{\zeta}}$	$H_{\underset{\sim}{\zeta}}$	$\lambda_{(\underset{\sim}{\text{ph}})}$	F(tangent)	F(normal)
B-H curves	0,38	0,10	0,88	0,33	30,21	12,06
$\mu r_{\underset{\sim}{\chi}_1} = 7185$, $\mu r_{\underset{\sim}{\chi}_2} = 2119$	0,39	0,15	0,81	0,40	30,32	12,24
$\mu r_{\underset{\sim}{\chi}_1}, \mu r_{\underset{\sim}{\chi}_2} = 100$	2,21	0,98	1,39	4,17	27,86	17,36
$\mu r_{\underset{\sim}{\chi}_1}, \mu r_{\underset{\sim}{\chi}_2} = 50$	3,56	1,29	2,41	6,81	25,31	20,96
$\mu r_{\underset{\sim}{\chi}_1}, \mu r_{\underset{\sim}{\chi}_2} = 10$	8,21	1,67	5,73	15,23	11,14	35,19

Table A.5: Percentage rms errors ... *cont*

% rms Error	$I_{(\underset{\sim}{\text{ph}})} = \left[-10\ -10\ 20\right]^{\mathrm{T}}$ A					
	$x = 0$ mm					
	$\Phi_{\underset{\sim}{\epsilon}}$	$\Phi_{\underset{\sim}{\zeta}}$	$H_{\underset{\sim}{\zeta}}$	$\lambda_{(\underset{\sim}{\text{ph}})}$	F(tangent)	F(normal)
B-H curves	0,15	0,11	1,01	0,11	30,30	12,88
$\mu r_{\underset{\sim}{\chi}_1} = 7185$, $\mu r_{\underset{\sim}{\chi}_2} = 2119$	0,10	0,06	1,02	0,05	30,32	13,14
$\mu r_{\underset{\sim}{\chi}_1}, \mu r_{\underset{\sim}{\chi}_2} = 100$	1,56	0,29	1,63	2,89	28,15	16,68
$\mu r_{\underset{\sim}{\chi}_1}, \mu r_{\underset{\sim}{\chi}_2} = 50$	2,58	0,38	2,41	4,85	26,36	19,00
$\mu r_{\underset{\sim}{\chi}_1}, \mu r_{\underset{\sim}{\chi}_2} = 10$	6,29	2,78	5,26	10,87	19,43	28,27

Table A.5: Percentage rms errors ... *cont*

% rms Error	$I_{(\underset{\sim}{\text{ph}})} = \left[-10\ -10\ 20\right]^{\mathrm{T}}$ A					
	$x = 1$ mm					
	$\Phi_{\underset{\sim}{\epsilon}}$	$\Phi_{\underset{\sim}{\zeta}}$	$H_{\underset{\sim}{\zeta}}$	$\lambda_{(\underset{\sim}{\text{ph}})}$	F(tangent)	F(normal)
B-H curves	0,33	0,10	2,49	0,27	30,47	13,92
$\mu r_{\underset{\sim}{\chi}_1} = 7185$, $\mu r_{\underset{\sim}{\chi}_2} = 2119$	0,32	0,09	2,38	0,31	30,48	14,15
$\mu r_{\underset{\sim}{\chi}_1}, \mu r_{\underset{\sim}{\chi}_2} = 100$	1,59	0,30	1,92	3,18	28,47	17,80
$\mu r_{\underset{\sim}{\chi}_1}, \mu r_{\underset{\sim}{\chi}_2} = 50$	2,52	0,37	2,38	5,15	26,68	20,16
$\mu r_{\underset{\sim}{\chi}_1}, \mu r_{\underset{\sim}{\chi}_2} = 10$	6,07	2,96	5,42	10,81	17,57	28,98

Table A.5: Percentage rms errors ... *cont*

% rms Error	$I_{(\underset{\sim}{\text{ph}})} = \left[-10\ -10\ 20\right]^{\mathrm{T}}$ A					
	$x = 2$ mm					
	$\Phi_{\underset{\sim}{\epsilon}}$	$\Phi_{\underset{\sim}{\zeta}}$	$H_{\underset{\sim}{\zeta}}$	$\lambda_{(\underset{\sim}{\text{ph}})}$	F(tangent)	F(normal)
B-H curves	0,13	0,07	0,97	0,03	27,48	14,51
$\mu r_{\underset{\sim}{\chi}_1} = 7185$, $\mu r_{\underset{\sim}{\chi}_2} = 2119$	0,09	0,05	0,92	0,07	27,48	14,72
$\mu r_{\underset{\sim}{\chi}_1}, \mu r_{\underset{\sim}{\chi}_2} = 100$	1,49	0,28	1,64	3,23	25,84	18,88
$\mu r_{\underset{\sim}{\chi}_1}, \mu r_{\underset{\sim}{\chi}_2} = 50$	2,41	0,35	2,45	5,31	24,36	21,67
$\mu r_{\underset{\sim}{\chi}_1}, \mu r_{\underset{\sim}{\chi}_2} = 10$	5,96	3,12	5,64	10,64	16,22	32,39

Table A.5: Percentage rms errors ... *cont*

% rms Error	$I_{(\underset{\sim}{\text{ph}})} = \left[-10\ -10\ 20\right]^{\mathrm{T}}$ A					
	$x = 3$ mm					
	$\Phi_{\underset{\sim}{\epsilon}}$	$\Phi_{\underset{\sim}{\zeta}}$	$H_{\underset{\sim}{\zeta}}$	$\lambda_{(\underset{\sim}{\text{ph}})}$	F(tangent)	F(normal)
B-H curves	0,19	0,16	0,85	0,26	26,28	14,17
$\mu r_{\underset{\sim}{\chi}_1} = 7185$, $\mu r_{\underset{\sim}{\chi}_2} = 2119$	0,15	0,12	0,77	0,20	26,27	14,35
$\mu r_{\underset{\sim}{\chi}_1}, \mu r_{\underset{\sim}{\chi}_2} = 100$	1,43	0,24	1,22	3,20	24,87	18,96
$\mu r_{\underset{\sim}{\chi}_1}, \mu r_{\underset{\sim}{\chi}_2} = 50$	2,34	0,32	1,98	5,39	23,75	22,15
$\mu r_{\underset{\sim}{\chi}_1}, \mu r_{\underset{\sim}{\chi}_2} = 10$	5,93	3,18	5,00	10,00	18,49	35,16

Table A.5: Percentage rms errors ... *cont*

% rms Error	$I_{(\underset{\sim}{\text{ph}})} = \left[-10\ -10\ 20\right]^{\mathrm{T}}$ A					
	$x = 4$ mm					
	$\Phi_{\underset{\sim}{\epsilon}}$	$\Phi_{\underset{\sim}{\zeta}}$	$H_{\underset{\sim}{\zeta}}$	$\lambda_{(\underset{\sim}{\text{ph}})}$	F(tangent)	F(normal)
B-H curves	0,16	0,15	0,47	0,09	28,19	14,53
$\mu r_{\underset{\sim}{\chi}_1} = 7185$, $\mu r_{\underset{\sim}{\chi}_2} = 2119$	0,15	0,11	0,48	0,04	28,17	14,70
$\mu r_{\underset{\sim}{\chi}_1}, \mu r_{\underset{\sim}{\chi}_2} = 100$	1,47	0,22	1,57	3,56	26,66	19,55
$\mu r_{\underset{\sim}{\chi}_1}, \mu r_{\underset{\sim}{\chi}_2} = 50$	2,38	0,27	2,33	5,88	25,58	22,96
$\mu r_{\underset{\sim}{\chi}_1}, \mu r_{\underset{\sim}{\chi}_2} = 10$	6,04	3,20	5,09	9,45	22,31	37,66

Table A.5: Percentage rms errors ... *cont*

% rms Error	$I_{(\underset{\sim}{\text{ph}})} = \left[-10\ -10\ 20\right]^{\mathrm{T}}$ A					
	$x = 5$ mm					
	$\Phi_{\underset{\sim}{\epsilon}}$	$\Phi_{\underset{\sim}{\zeta}}$	$H_{\underset{\sim}{\zeta}}$	$\lambda_{(\underset{\sim}{\text{ph}})}$	F(tangent)	F(normal)
B-H curves	0,37	0,08	0,94	0,42	30,30	15,28
$\mu r_{\underset{\sim}{\chi}_1} = 7185$, $\mu r_{\underset{\sim}{\chi}_2} = 2119$	0,38	0,12	0,89	0,47	30,28	15,43
$\mu r_{\underset{\sim}{\chi}_1}, \mu r_{\underset{\sim}{\chi}_2} = 100$	1,61	0,43	0,98	4,24	29,08	20,15
$\mu r_{\underset{\sim}{\chi}_1}, \mu r_{\underset{\sim}{\chi}_2} = 50$	2,50	0,43	1,74	6,69	28,49	23,41
$\mu r_{\underset{\sim}{\chi}_1}, \mu r_{\underset{\sim}{\chi}_2} = 10$	6,14	2,95	4,61	9,59	29,50	37,21

A.3 Schwarz-Christoffel conformal mapping

A.3.1 Overview

As discussed in section 3.1.2, although it is more accurate and practical to use FEM to obtain the precomputed parameter sets for the hybrid method, for simple geometries it is feasible to obtain values for these parameters using a conformal mapping approach. This is achieved by calculating a 'rectified' Schwarz-Christoffel mapping that transforms a rectangular region to the geometry of the space surrounding the highly-permeable materials represented by MECs (refer to background section 2.1.1). This is useful because, for a particular component of the boundary flux, the MECs are "seen" to be infinitely permeable and thus the lines of flux intersect perpendicularly with all of the boundaries. The mutual permeances and source boundary fluxes are then obtained using the height-to-width ratio of corresponding rectangular regions in the rectified domain. This conformal mapping approach does, however, require the desired angle for each vertex in the rectified domain to be chosen and it is sometimes necessary to include vertices at critical points where a change in the direction of flux is expected. This poses a problem for automating the process and hence limits the method's usefulness.

Nevertheless, to demonstrate the procedure, several mutual permeances and normalised source boundary fluxes are calculated for the worked example of section 3.2 and compared to the values obtained by FEM. The calculations are for the reaction plate centred over the stator ($x = 0$) and the mappings are calculated using the free Schwarz-Christoffel toolbox for MATLAB® [57].

As shown in figure A.3, the geometry of the highly-permeable regions in the example problem is specified in the complex plane as a sequence of vertices. Since the Schwarz-Christoffel transformation must map the rectified domain to a closed region, it is necessary to truncate any open boundaries at a distance that is sufficiently far away. The rule of thumb provided by Chen and Konrad [145] is applied here, whereby the distance from the centre of the problem to the truncated outer boundary is chosen to be five times the distance from the centre to the outside of the regions of interest. The formation of this outer boundary is depicted in figure A.4.

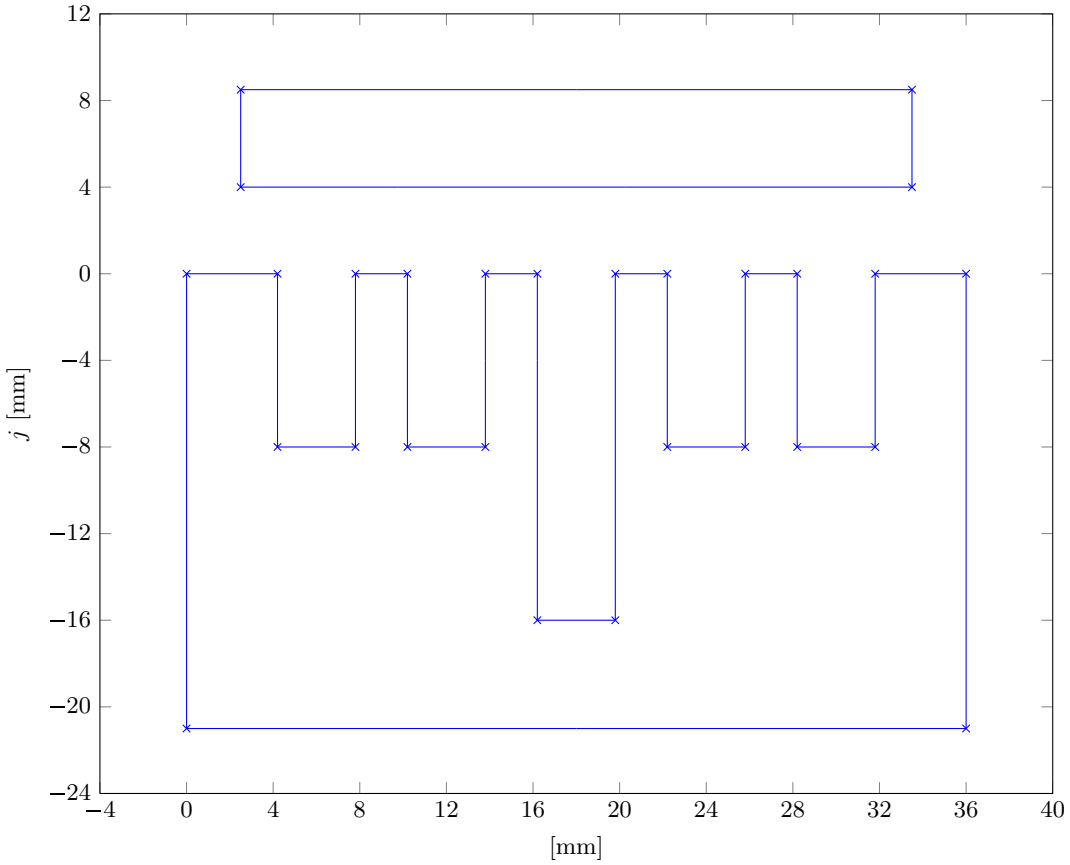

Figure A.3: Geometry of the highly-permeable regions in the complex plane

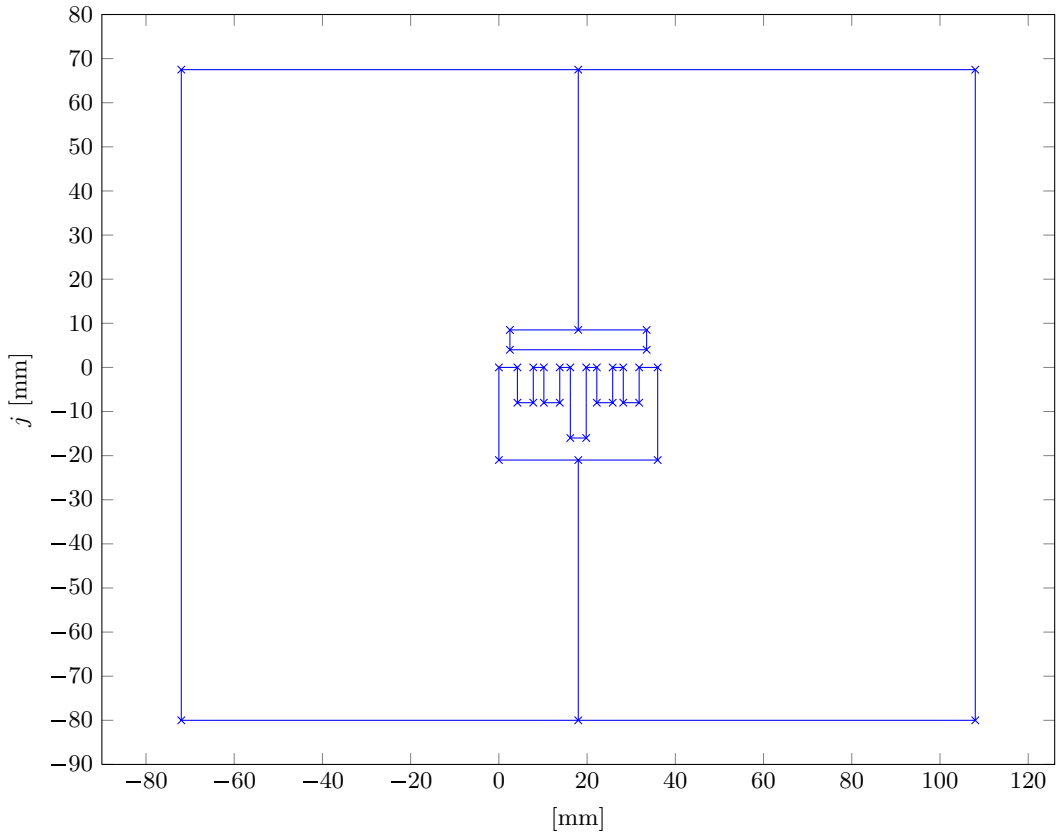

Figure A.4: Truncation of open boundary with a rectangular outer boundary

A.3.2 Mutual permeances

The calculation of several mutual permeances is demonstrated for the mmf of element 24, region 3 of the worked example of section 3.2. The MATLAB® script to perform this task is provided as code listings A.39–A.45.

Figure A.5 shows the vertices that are specified as points in the complex plane. Note that a walk along the path connecting the vertices in sequence outlines a closed region. Vertices 10 and 13 are included to demarcate region 3 of element 24. Furthermore, vertices 37 and 38 are required to specify critical points where there is a change in the direction of the flux through the boundary. The positions of these vertices on the boundary need to be adjusted until the resulting magnetic potentials at all of the points along this boundary are equal, since the bounded region is infinitely permeable. This is achieved by adjusting the positions of the two vertices until the prevertices (vertices in the rectified domain) for this boundary are vertically aligned, having the same real component in the complex plane.

The calculation of a suitable conformal mapping requires an input of the desired angle at each prevertex, specified as a multiple of π rad. Figure A.6 shows the resulting prevertices in the complex plane. For clarity, the numbering for closely-spaced/overlapping prevertices have been omitted. Also, any extra vertices, potentially added by the algorithm to maintain prevertex cross-ratios and prevent numerical ill-conditioning in calculating the mapping, are removed.

Once the appropriate mapping has been calculated, horizontal lines in the rectified domain map to the actual flux lines and vertical lines map to equipotential contours. Hence, the flux distribution shown in figure A.7 is obtained by plotting the transformation of horizontal lines that are equally spaced over the rectified domain. This flux distribution in the air-gap very closely matches that obtained by FEM (shown in figure 3.12). However, an exception is along the two boundaries of the active element region (10–11 & 12–13), where a Dirichlet boundary condition for the scalar potential is imposed, as opposed to the correct condition (in terms of magnetic vector potential) that $\frac{\partial}{\partial \vec{A}} \hat{\boldsymbol{n}} = -\mu \vec{\boldsymbol{J}}$. In essence, it is assumed that no leakage flux flows through the source boundaries themselves, which is inaccurate.

Each mutual permeance is calculated as the ratio of the width to length of the relevant region in the rectified domain, multiplied by the permeability of free space.

Code listing A.39: Mutual permeances—define geometry (`exampleSCpermeances.m`)

```
%% Problem depth
d = 0.2;

%% Airgap geometry
p_v(1)  = -21j;
p_v(2)  = 0;
p_v(3)  = 4.2;
p_v(4)  = 4.2-8j;
p_v(5)  = 7.8-8j;
p_v(6)  = 7.8;
p_v(7)  = 4.2+6;
p_v(8)  = 4.2+6-8j;
p_v(9)  = 7.8+6-8j;
p_v(10) = 7.8+6-4j;
p_v(11) = 7.8+6;
p_v(12) = 4.2+2*6;
p_v(13) = 4.2+2*6-4j;
p_v(14) = 4.2+2*6-8j;
p_v(15) = 4.2+2*6-16j;
p_v(16) = 7.8+2*6-16j;
p_v(17) = 7.8+2*6-8j;
p_v(18) = 7.8+2*6;
p_v(19) = 4.2+3*6;
p_v(20) = 4.2+3*6-8j;
p_v(21) = 7.8+3*6-8j;
p_v(22) = 7.8+3*6;
p_v(23) = 4.2+4*6;
p_v(24) = 4.2+4*6-8j;
p_v(25) = 7.8+4*6-8j;
p_v(26) = 7.8+4*6;
p_v(27) = 7.8+4*6+4.2;
p_v(28) = 7.8+4*6+4.2-21j;
p_v(29) = 36/2-21j;
p_v(30) = 36/2-21j-59j; %outer boundary (bottom)
p_v(31) = 36+72-21j-59j; %outer boundary (bottom)
p_v(32) = 36+72+8.5j+59j; %outer boundary (top)
p_v(33) = 36/2+8.5j+59j; %outer boundary (top)
p_v(34) = 36/2+8.5j;
p_v(35) = 36-2.5+8.5j;
p_v(36) = 36-2.5+4j;
p_v(37) = 36-2.5-13.24+4j; %adjust
p_v(38) = 36-2.5-23.76+4j; %adjust
p_v(39) = 2.5+4j;
p_v(40) = 2.5+8.5j;
p_v(41) = 36/2+8.5j;
p_v(42) = 36/2+8.5j+59j; %outer boundary (top)
p_v(43) = -72+8.5j+59j; %outer boundary (top)
p_v(44) = -72-21j-59j; %outer boundary (bottom)
p_v(45) = 36/2-21j-59j; %outer boundary (bottom)
p_v(46) = 36/2-21j;

figure; plot(polygon(p_v),'x');
```

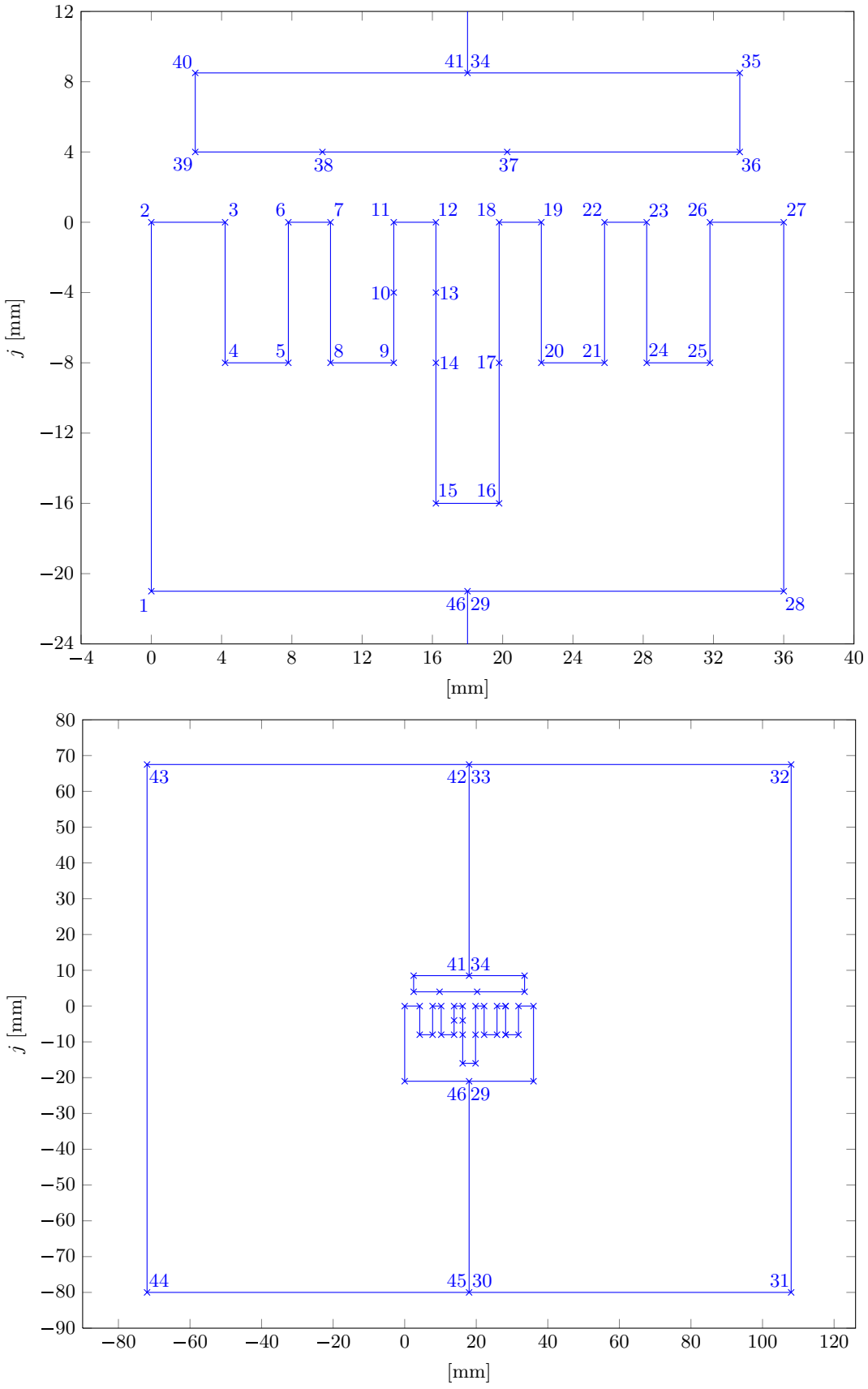

Figure A.5: Mutual permeances—geometry in the complex plane

Code listing A.40: Mutual permeances—calculate mapping (`exampleSCpermeances.m`)

```
53 %% Required angles in rectified domain (normalised as multiple of pi)
54 theta_pv(1)  = 1;
55 theta_pv(2)  = 1;
56 theta_pv(3)  = 1;
57 theta_pv(4)  = 1;
58 theta_pv(5)  = 1;
59 theta_pv(6)  = 1;
60 theta_pv(7)  = 1;
61 theta_pv(8)  = 1;
62 theta_pv(9)  = 1;
63 theta_pv(10) = 0.5;
64 theta_pv(11) = 0.5;
65 theta_pv(12) = 0.5;
66 theta_pv(13) = 0.5;
67 theta_pv(14) = 1;
68 theta_pv(15) = 1;
69 theta_pv(16) = 1;
70 theta_pv(17) = 1;
71 theta_pv(18) = 1;
72 theta_pv(19) = 1;
73 theta_pv(20) = 1;
74 theta_pv(21) = 1;
75 theta_pv(22) = 1;
76 theta_pv(23) = 1;
77 theta_pv(24) = 1;
78 theta_pv(25) = 1;
79 theta_pv(26) = 1;
80 theta_pv(27) = 1;
81 theta_pv(28) = 1;
82 theta_pv(29) = 0.5;
83 theta_pv(30) = 1;
84 theta_pv(31) = 1;
85 theta_pv(32) = 1;
86 theta_pv(33) = 1;
87 theta_pv(34) = 0.5;
88 theta_pv(35) = 1;
89 theta_pv(36) = 1;
90 theta_pv(37) = 2;
91 theta_pv(38) = 2;
92 theta_pv(39) = 1;
93 theta_pv(40) = 1;
94 theta_pv(41) = 0.5;
95 theta_pv(42) = 1;
96 theta_pv(43) = 1;
97 theta_pv(44) = 1;
98 theta_pv(45) = 1;
99 theta_pv(46) = 0.5;
100
101 %% Calculate map
102 map = crrectmap(polygon(p_v), theta_pv, scmapopt('tolerance',1e-12));
```

Code listing A.41: Mutual permeances—prevertices (`exampleSCpermeances.m`)

```
%% Vertices in rectified domain (prevertices)
p_pv = prevertex(map);
% Eliminate vertices added to maintain prevertex crossratios
poly_rect = polygon(map);
p_pv = p_pv(ismember(poly_rect.vertex,p_v));
figure; plot(p_pv,'x');
text(real(p_pv),imag(p_pv),cellstr(num2str((1:length(p_pv))')),...
  'VerticalAlignment','bottom','HorizontalAlignment','right');
```

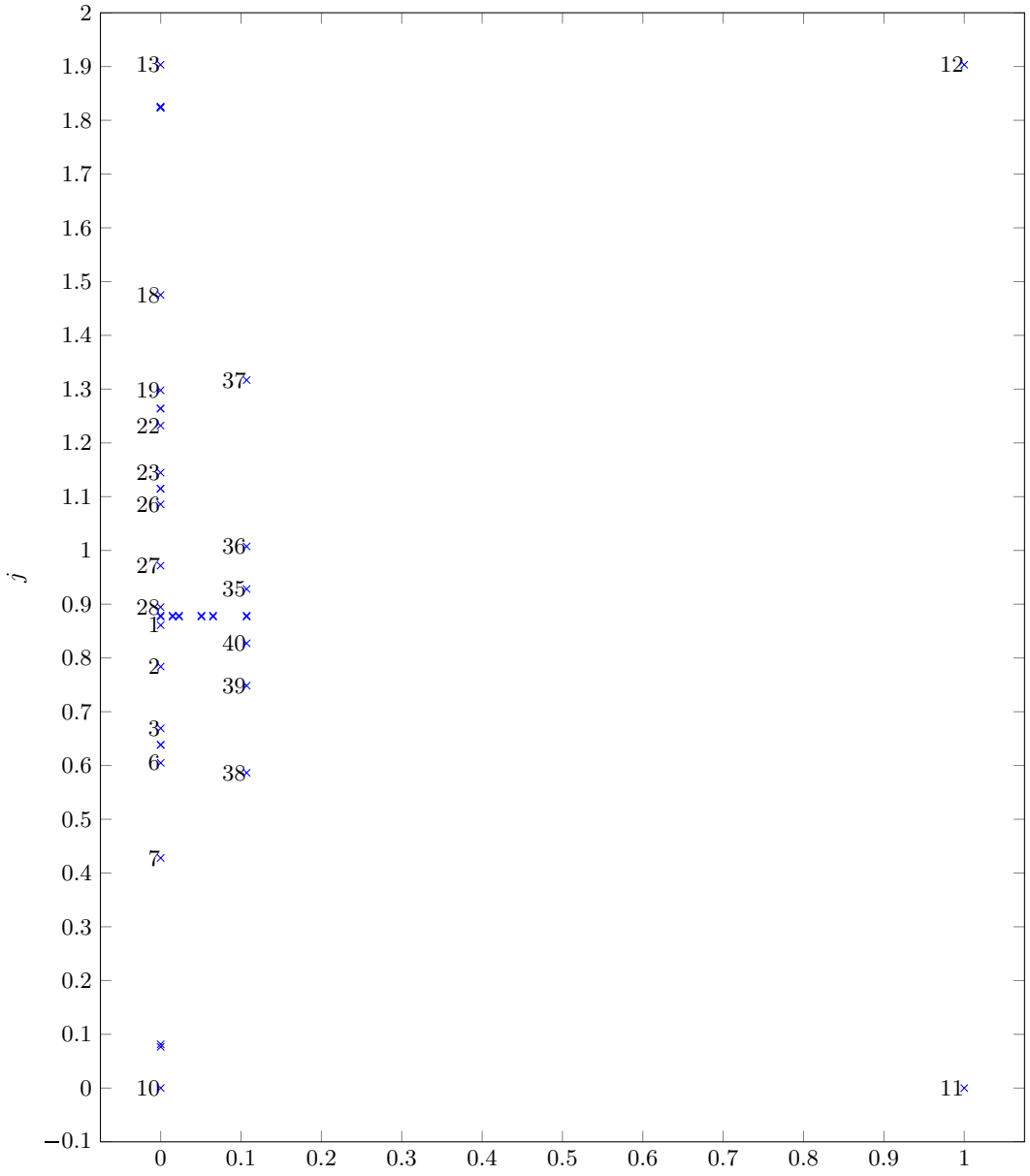

Figure A.6: Mutual permeances—prevertices in the complex plane

Code listing A.42: Mutual permeances—flux distribution (`exampleSCpermeances.m`)

```
%% Contour plot to show flux lines
figure; plot(map,[],min(imag(p_pv)):(max(imag(p_pv))-...
  min(imag(p_pv)))/100:max(imag(p_pv)));
% Cross-hatch region of interest
crosshatch_poly(real([p_v(10) p_v(11) p_v(12) p_v(13)]),...
  imag([p_v(10) p_v(11) p_v(12) p_v(13)]),...
  45,0.5,'edgewidth',0,'linewidth',0.5,'linecolor','g','hold',1);
crosshatch_poly(real([p_v(10) p_v(11) p_v(12) p_v(13)]),...
  imag([p_v(10) p_v(11) p_v(12) p_v(13)]),...
  -45,0.5,'edgewidth',0,'linewidth',0.5,'linecolor','g','hold',1);
```

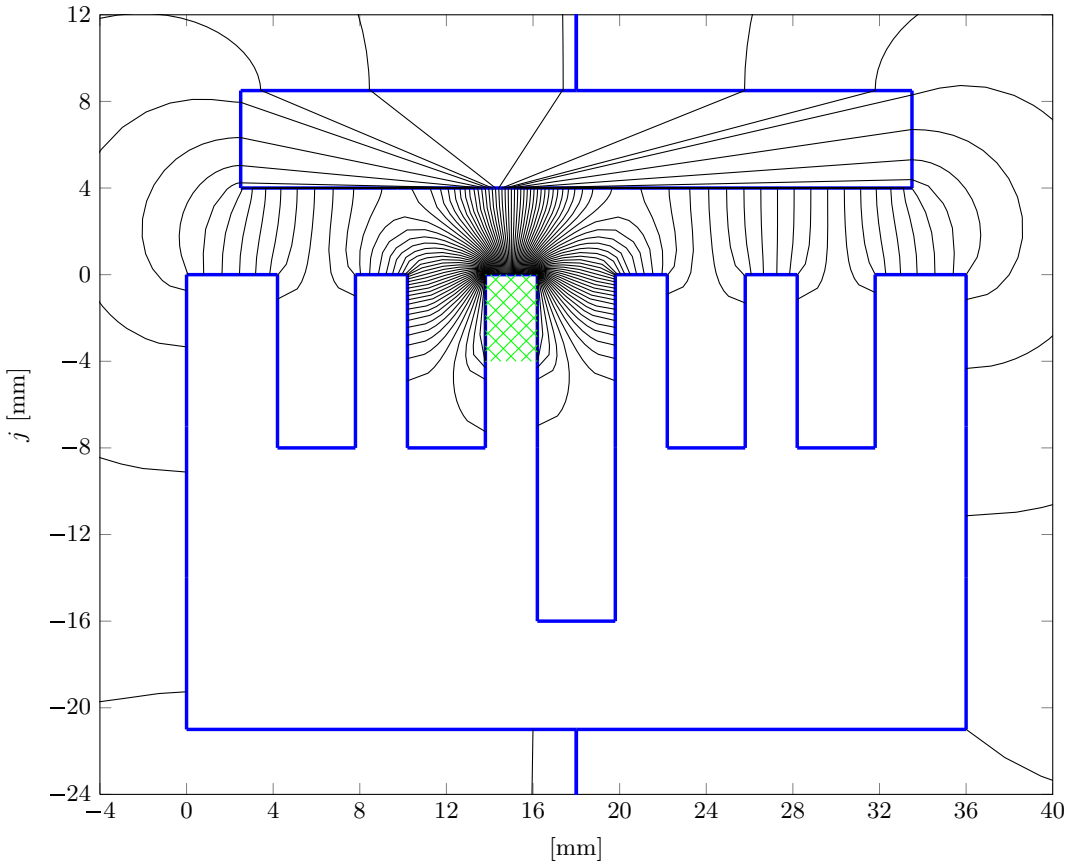

Figure A.7: Mutual permeances—contour plot showing flux lines for $\mathcal{F}_{\underset{\sim}{e}_{24}\underset{\sim}{\kappa}_3}$

Code listing A.43: Mutual permeances—calculate $\mathcal{G}_{\underset{\sim}{\epsilon}_{30}\underset{\sim}{e}_{24}\underset{\sim}{\kappa}_3}$ (`exampleSCpermeances.m`)

```
121 crosshatch_poly(real([p_pv(10) p_pv(11) p_pv(12) p_pv(13)]),...
122   imag([p_pv(10) p_pv(11) p_pv(12) p_pv(13)]),...
123   45,0.03,'edgewidth',0,'linewidth',0.5,'linecolor','g','hold',1);
124 crosshatch_poly(real([p_pv(10) p_pv(11) p_pv(12) p_pv(13)]),...
125   imag([p_pv(10) p_pv(11) p_pv(12) p_pv(13)]),...
126   -45,0.03,'edgewidth',0,'linewidth',0.5,'linecolor','g','hold',1);

127 calG_epsilon30_e24_kappa3 = d*imag(p_pv(13)-p_pv(10))*(4*pi*1e-7)/...
128   real(p_pv(11)-p_pv(10));
```

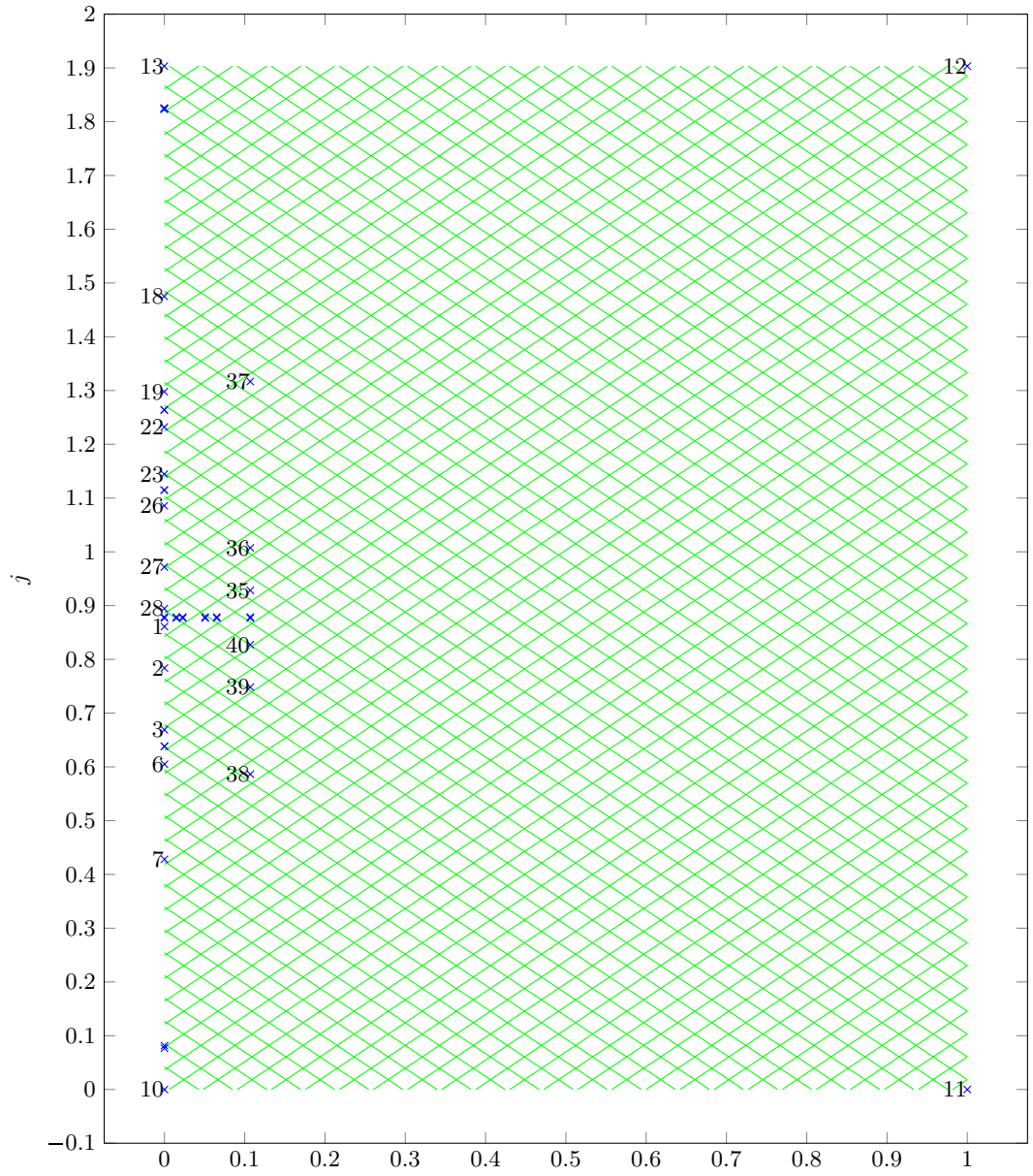

Figure A.8: Mutual permeances—region used to calculate $\mathcal{G}_{\underset{\sim}{\epsilon}_{30}\underset{\sim}{e}_{24}\underset{\sim}{\kappa}_3}$ ($\underset{\sim}{\epsilon}_{30} \triangleq \underset{\sim}{e}_{24}\underset{\sim}{\kappa}_3$)

Code listing A.44: Mutual permeances—calculate $\mathcal{G}_{\underset{\sim}{\epsilon}_{36}\underset{\sim}{e}_{24}\underset{\sim}{\kappa}_3}$ (`exampleSCpermeances.m`)

```
129 crosshatch_poly(real([p_pv(10) p_pv(11) p_pv(12) p_pv(13)]),...
130   imag([p_pv(23) p_pv(23) p_pv(22) p_pv(22)]),...
131   45,0.03,'edgewidth',0,'linewidth',0.5,'linecolor','g','hold',1);
132 crosshatch_poly(real([p_pv(10) p_pv(11) p_pv(12) p_pv(13)]),...
133   imag([p_pv(23) p_pv(23) p_pv(22) p_pv(22)]),...
134   -45,0.03,'edgewidth',0,'linewidth',0.5,'linecolor','g','hold',1);

135 calG_epsilon36_e24_kappa3 = d*imag(p_pv(23)-p_pv(22))*(4*pi*1e-7)/...
136   real(p_pv(11)-p_pv(10));
```

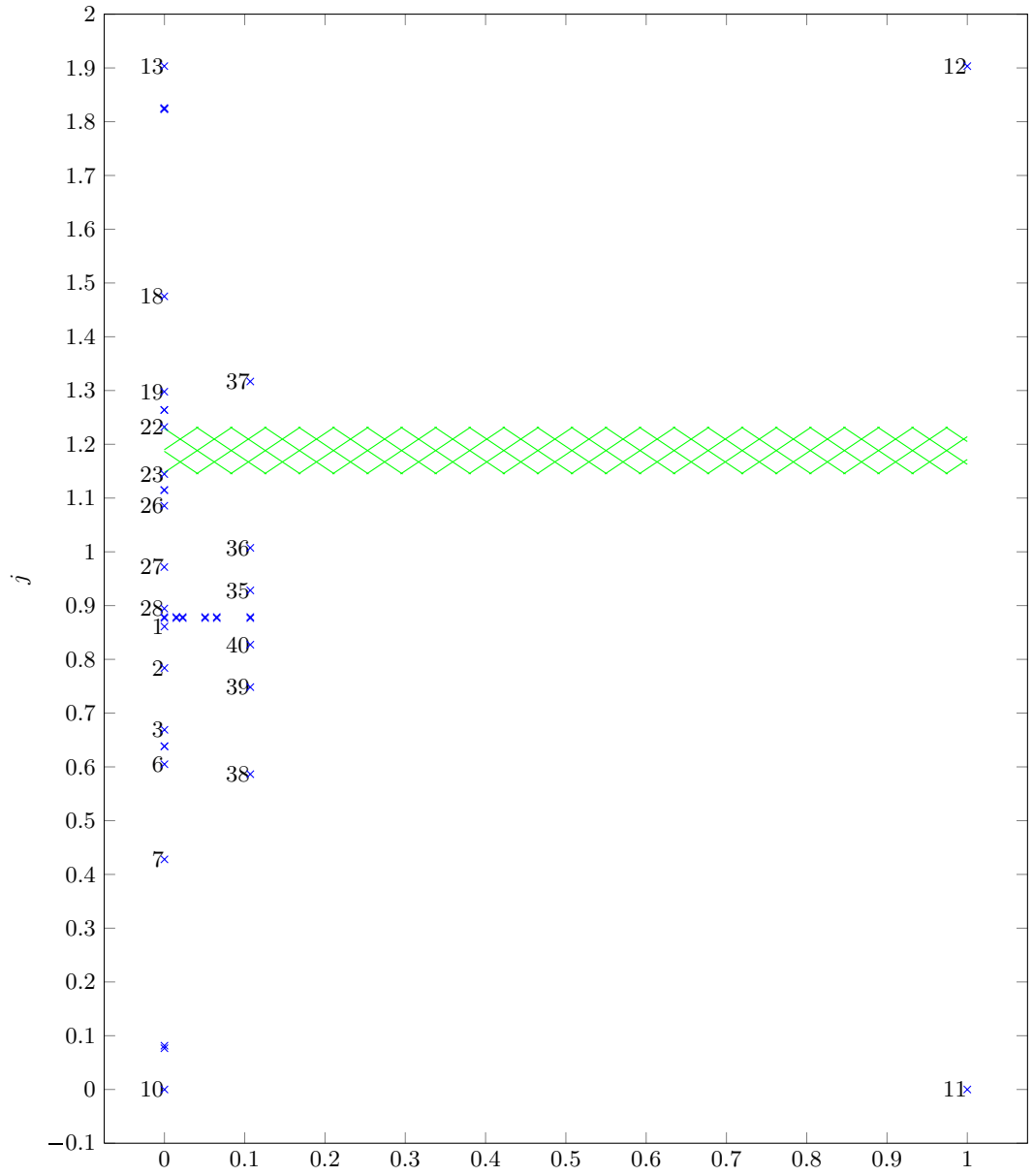

Figure A.9: Mutual permeances—region used to calculate $\mathcal{G}_{\underset{\sim}{\epsilon}_{36}\underset{\sim}{e}_{24}\underset{\sim}{\kappa}_3}$ ($\underset{\sim}{\epsilon}_{36} \triangleq \underset{\sim}{e}_{26}\underset{\sim}{\kappa}_3$)

Code listing A.45: Mutual permeances—calculate $\mathcal{G}_{\underset{\sim}{\epsilon}_{46}\underset{\sim}{e}_{24}\underset{\sim}{\kappa}_3}$ (`exampleSCpermeances.m`)

```
crosshatch_poly(real([p_pv(10) p_pv(11) p_pv(12) p_pv(13)]),...
  imag([p_pv(36) p_pv(36) p_pv(37) p_pv(37)]),...
  45,0.03,'edgewidth',0,'linewidth',0.5,'linecolor','g','hold',1);
crosshatch_poly(real([p_pv(10) p_pv(11) p_pv(12) p_pv(13)]),...
  imag([p_pv(36) p_pv(36) p_pv(37) p_pv(37)]),...
  -45,0.03,'edgewidth',0,'linewidth',0.5,'linecolor','g','hold',1);

calG_epsilon46_e24_kappa3 = d*imag(p_pv(37)-p_pv(36))*(4*pi*1e-7)/...
  real(p_pv(11)-p_pv(10));
```

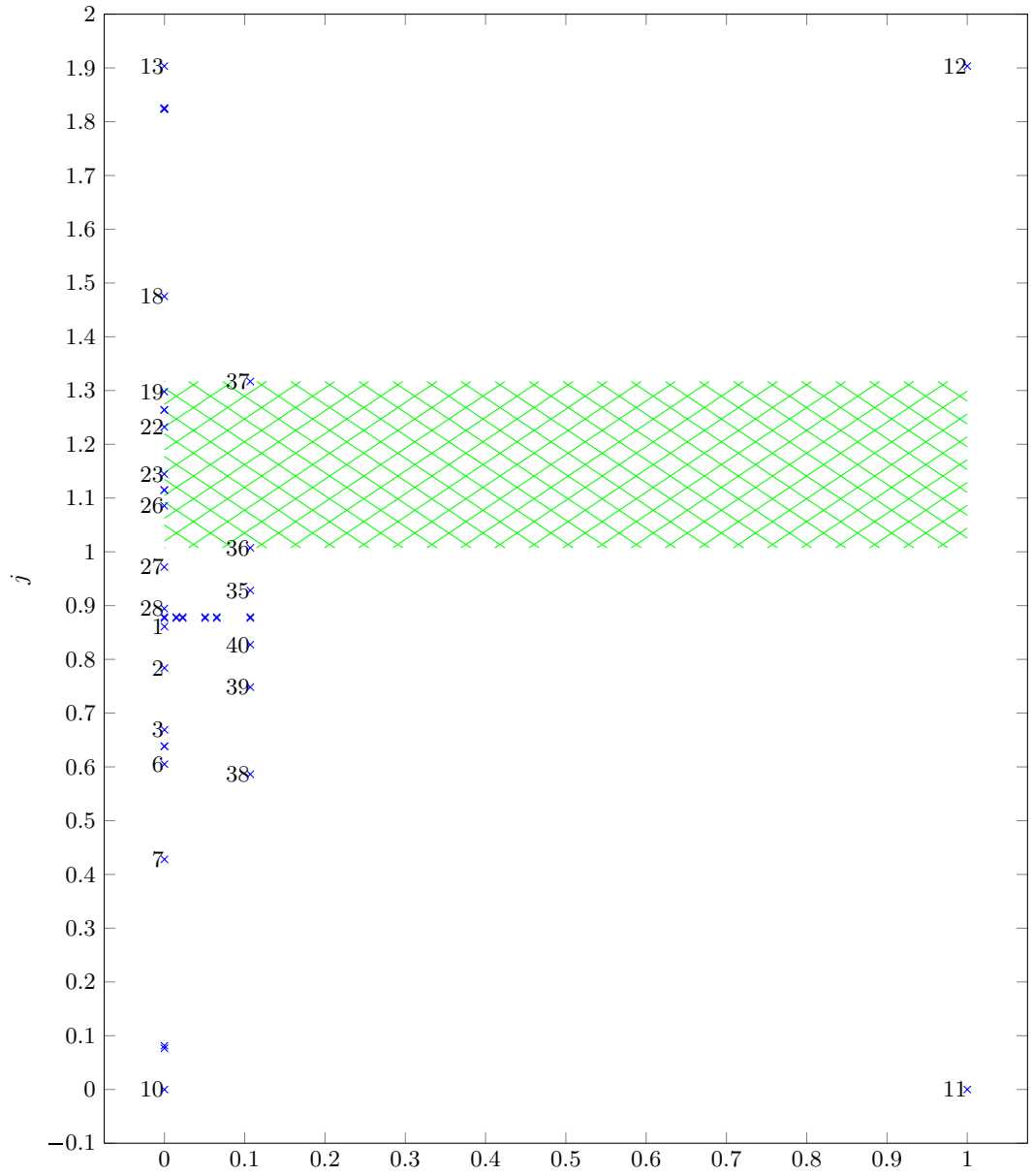

Figure A.10: Mutual permeances—region used to calculate $\mathcal{G}_{\underset{\sim}{\epsilon}_{46}\underset{\sim}{e}_{24}\underset{\sim}{\kappa}_3}$ ($\underset{\sim}{\epsilon}_{46} \triangleq \underset{\sim}{e}_{30}\underset{\sim}{\kappa}_1$)

Table A.6 provides a comparison of the values obtained by the conformal mapping method and those obtained using FEM. The evident inaccuracy is due to the implied boundary condition for the source mmf's boundaries, as discussed. Thus, the errors would be reduced with a subdivision of the flux tube elements, yielding shorter element boundaries.

Table A.6: Comparison of mutual permeances calculated by FEM and the conformal mapping method

	Schwarz-Christoffel Mapping	Finite Element Method	Error
$\mathcal{G}_{\epsilon_{30}\epsilon_{24}\kappa_3}$	$4{,}784 \cdot 10^{-7}$ Wb/A	$2{,}894 \cdot 10^{-7}$ Wb/A	65,3 %
$\mathcal{G}_{\epsilon_{36}\epsilon_{24}\kappa_3}$	$-2{,}202 \cdot 10^{-8}$ Wb/A	$-2{,}590 \cdot 10^{-8}$ Wb/A	−15,0 %
$\mathcal{G}_{\epsilon_{46}\epsilon_{24}\kappa_3}$	$7{,}776 \cdot 10^{-8}$ Wb/A	$9{,}077 \cdot 10^{-8}$ Wb/A	−14,3 %

A.3.3 Source boundary flux

As with the mutual permeances, the calculation of several source boundary flux values is demonstrated for the worked example of section 3.2, where the left-hand permanent magnet is the chosen magnetic source. The corresponding MATLAB® script is provided as code listings A.46–A.52.

Figure A.11 shows the specified vertices in the complex plane. As with when calculating the mutual permeances, vertices 3 and 12 are included to specify critical points where the flux through the boundary changes direction. The positions of these vertices on the boundary need to be adjusted until the resulting magnetic potentials at all of the points along that boundary are equal. This is achieved when the prevertices for this boundary are vertically aligned (having the same real component in the complex plane). The permanent magnet is represented by the two folded paths, 37–38–39 and 40–41–42, over which the magnet's mmf is distributed.

The resulting prevertices in the complex plane are shown in figure A.12. Again, the numbering of closely-spaced/overlapping prevertices has been omitted for clarity and any extra vertices, added by the algorithm to maintain prevertex cross-ratios and prevent numerical ill-conditioning in calculating the mapping, have been removed.

Figure A.13 is a contour plot showing the resulting flux distribution in the air-gap, which closely matches that obtained by FEM (shown in figure 3.15).

Code listing A.46: Source boundary flux—define geometry (`exampleSCsourcePM.m`)

```
%% Problem depth
d = 0.2;

%% Airgap geometry
p_v(1)  = -21j;
p_v(2)  = 0;
p_v(3)  = 1.02; %adjust
p_v(4)  = 4.2;
p_v(5)  = 4.2-8j;
p_v(6)  = 7.8-8j;
p_v(7)  = 7.8;
p_v(8)  = 4.2+6;
p_v(9)  = 4.2+6-8j;
p_v(10) = 7.8+6-8j;
p_v(11) = 7.8+6;
p_v(12) = 4.2+2*6-0.115; %adjust
p_v(13) = 4.2+2*6;
p_v(14) = 4.2+2*6-8j;
p_v(15) = 4.2+2*6-16j;
p_v(16) = 7.8+2*6-16j;
p_v(17) = 7.8+2*6-8j;
p_v(18) = 7.8+2*6;
p_v(19) = 4.2+3*6;
p_v(20) = 4.2+3*6-8j;
p_v(21) = 7.8+3*6-8j;
p_v(22) = 7.8+3*6;
p_v(23) = 4.2+4*6;
p_v(24) = 4.2+4*6-8j;
p_v(25) = 7.8+4*6-8j;
p_v(26) = 7.8+4*6;
p_v(27) = 7.8+4*6+4.2;
p_v(28) = 7.8+4*6+4.2-21j;
p_v(29) = 36/2-21j;
p_v(30) = 36/2-21j-59j; %outer boundary (bottom)
p_v(31) = 36+72-21j-59j; %outer boundary (bottom)
p_v(32) = 36+72+8.5j+59j; %outer boundary (top)
p_v(33) = 36/2+8.5j+59j; %outer boundary (top)
p_v(34) = 36/2+8.5j;
p_v(35) = 36-2.5+8.5j;
p_v(36) = 36-2.5+4j;
p_v(37) = 36-2.5-18+4j;
p_v(38) = 36-2.5-18+2.5j;
p_v(39) = 36-2.5-18+4j;
p_v(40) = 2.5+4j;
p_v(41) = 2.5+2.5j;
p_v(42) = 2.5+4j;
p_v(43) = 2.5+8.5j;
p_v(44) = 36/2+8.5j;
p_v(45) = 36/2+8.5j+59j; %outer boundary (top)
p_v(46) = -72+8.5j+59j; %outer boundary (top)
p_v(47) = -72-21j-59j; %outer boundary (bottom)
p_v(48) = 36/2-21j-59j; %outer boundary (bottom)
p_v(49) = 36/2-21j;
```

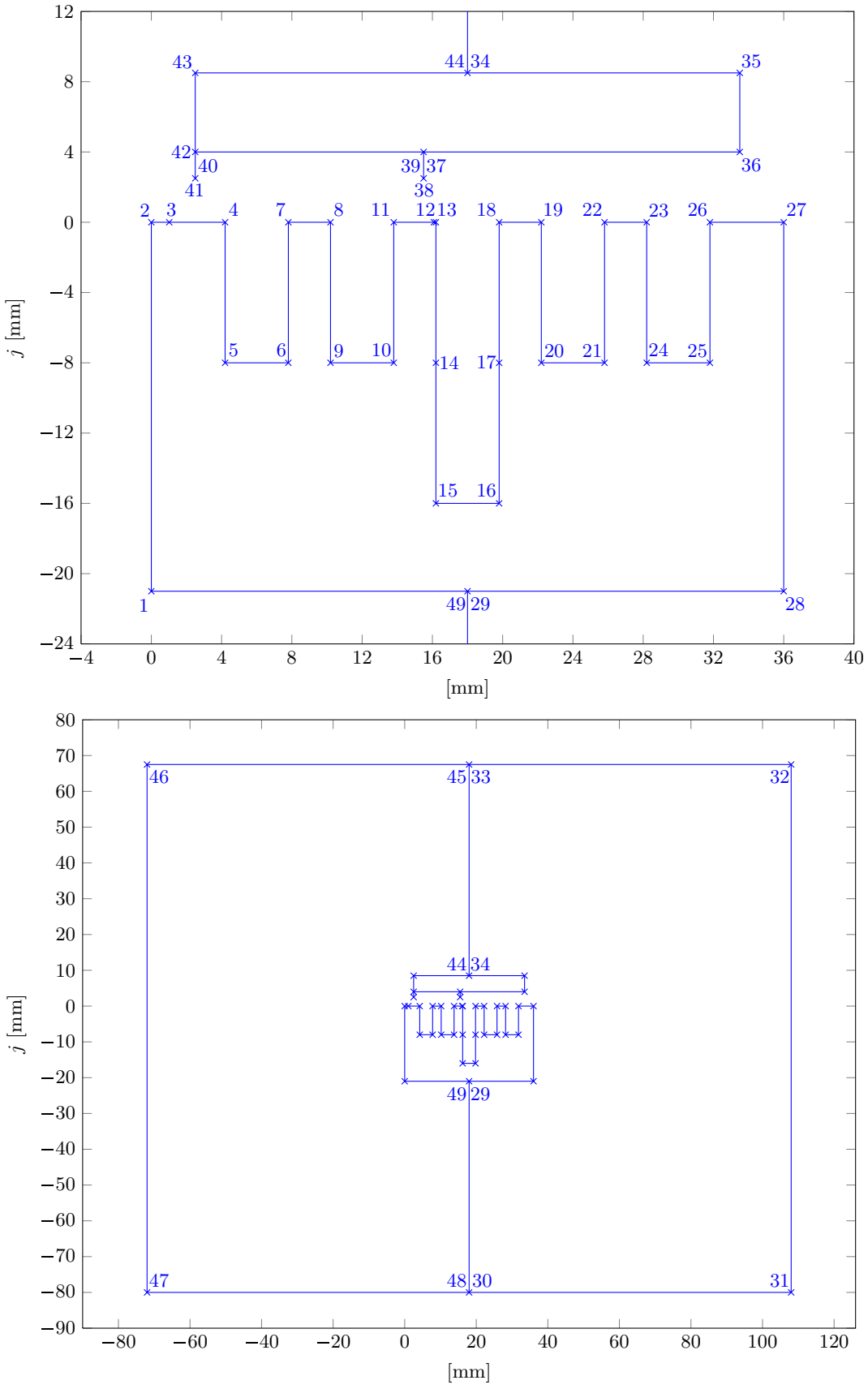

Figure A.11: Source boundary flux—geometry in the complex plane

Code listing A.47: Source boundary flux—calculate mapping (`exampleSCsourcePM.m`)

```
%% Required angles in rectified domain (normalised as multiple of pi)
theta_pv(1)  = 1;
theta_pv(2)  = 1;
theta_pv(3)  = 2;
theta_pv(4)  = 1;
theta_pv(5)  = 1;
theta_pv(6)  = 1;
theta_pv(7)  = 1;
theta_pv(8)  = 1;
theta_pv(9)  = 1;
theta_pv(10) = 1;
theta_pv(11) = 1;
theta_pv(12) = 2;
theta_pv(13) = 1;
theta_pv(14) = 1;
theta_pv(15) = 1;
theta_pv(16) = 1;
theta_pv(17) = 1;
theta_pv(18) = 1;
theta_pv(19) = 1;
theta_pv(20) = 1;
theta_pv(21) = 1;
theta_pv(22) = 1;
theta_pv(23) = 1;
theta_pv(24) = 1;
theta_pv(25) = 1;
theta_pv(26) = 1;
theta_pv(27) = 1;
theta_pv(28) = 1;
theta_pv(29) = 0.5;
theta_pv(30) = 1;
theta_pv(31) = 1;
theta_pv(32) = 1;
theta_pv(33) = 1;
theta_pv(34) = 0.5;
theta_pv(35) = 1;
theta_pv(36) = 1;
theta_pv(37) = 0.5;
theta_pv(38) = 1;
theta_pv(39) = 0.5;
theta_pv(40) = 0.5;
theta_pv(41) = 1;
theta_pv(42) = 0.5;
theta_pv(43) = 1;
theta_pv(44) = 0.5;
theta_pv(45) = 1;
theta_pv(46) = 1;
theta_pv(47) = 1;
theta_pv(48) = 1;
theta_pv(49) = 0.5;

%% Calculate map
map = crrectmap(polygon(p_v), theta_pv, scmapopt('tolerance',1e-12));
```

Code listing A.48: Source boundary flux—prevertices (`exampleSCsourcePM.m`)

```
%% Vertices in rectified domain (prevertices)
p_pv = prevertex(map);
% Eliminate vertices added to maintain prevertex crossratios
poly_rect = polygon(map);
p_pv = p_pv(ismember(poly_rect.vertex,p_v));
figure; plot(p_pv,'x');
text(real(p_pv),imag(p_pv),cellstr(num2str((1:length(p_pv))')),...
  'VerticalAlignment','bottom','HorizontalAlignment','right');
```

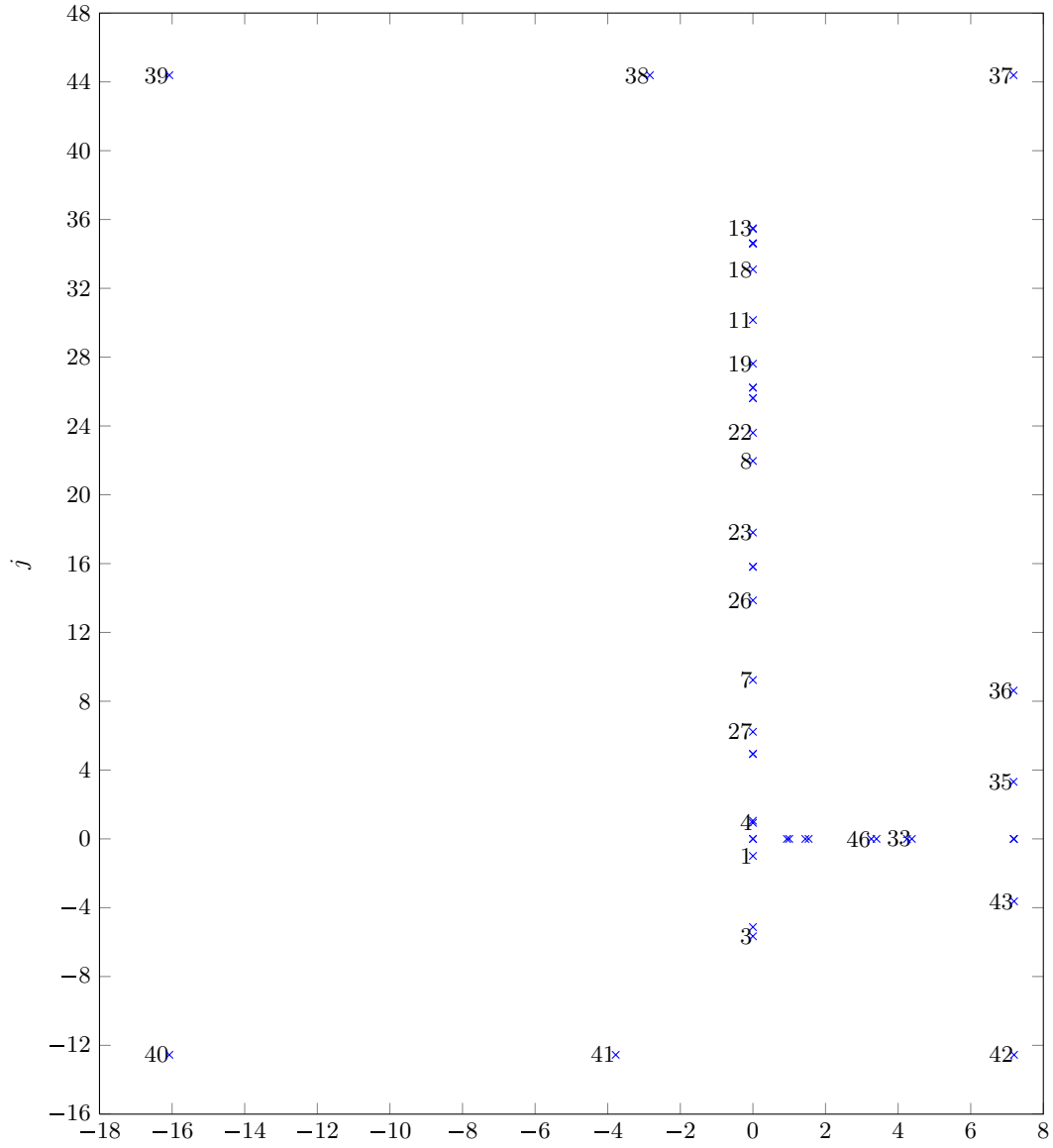

Figure A.12: Source boundary flux—prevertices in the complex plane

Code listing A.49: Source boundary flux—flux distribution (`exampleSCsourcePM.m`)

```
%% Contour plot to show flux lines
figure; plot(map,[],min(imag(p_pv)):(max(imag(p_pv))-...
  min(imag(p_pv)))/100:max(imag(p_pv)));
% Cross-hatch region of interest
crosshatch_poly(real([p_v(38) p_v(39) p_v(40) p_v(41)]),...
  imag([p_v(38) p_v(39) p_v(40) p_v(41)]),...
  45,0.5,'edgewidth',0,'linewidth',0.5,'linecolor','g','hold',1);
crosshatch_poly(real([p_v(38) p_v(39) p_v(40) p_v(41)]),...
  imag([p_v(38) p_v(39) p_v(40) p_v(41)]),...
  -45,0.5,'edgewidth',0,'linewidth',0.5,'linecolor','g','hold',1);
```

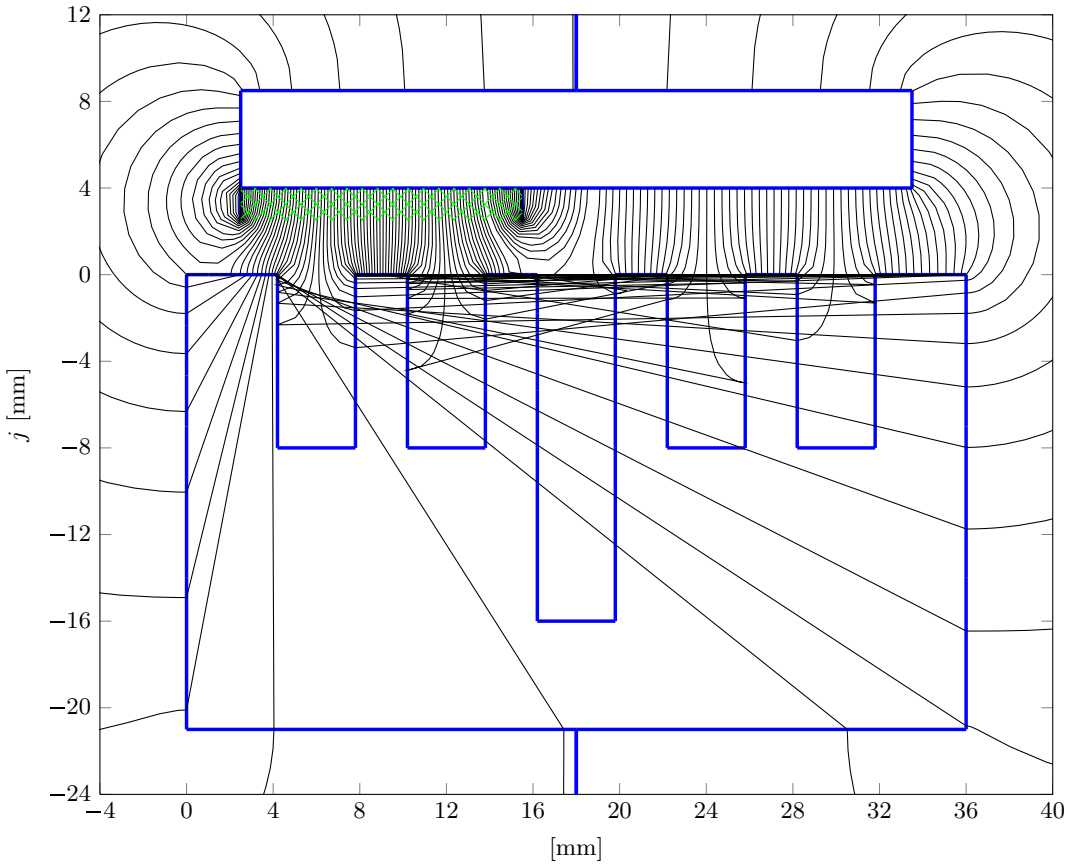

Figure A.13: Source boundary flux—contour plot showing flux lines for $\mathcal{F}_{(\underset{\sim}{\mathcal{F}0})_7}$

Code listing A.50: Source boundary flux—calculate $\Phi_{\underset{\sim}{\epsilon}_{36}(\underset{\sim}{\mathcal{F}0})_7}$ (`exampleSCsourcePM.m`)

```
125 crosshatch_poly(real([p_pv(40) p_pv(42) p_pv(37) p_pv(39)]),...
126   imag([p_pv(23) p_pv(23) p_pv(22) p_pv(22)]),...
127   45,1,'edgewidth',0,'linewidth',0.5,'linecolor','g','hold',1);
128 crosshatch_poly(real([p_pv(40) p_pv(42) p_pv(37) p_pv(39)]),...
129   imag([p_pv(23) p_pv(23) p_pv(22) p_pv(22)]),...
130   -45,1,'edgewidth',0,'linewidth',0.5,'linecolor','g','hold',1);

131 calF = 979e3*1.5e-3;
132 Phi_epsilon36_calF7 = calF*d*imag(p_pv(23)-p_pv(22))*(4*pi*1e-7)/...
133   real(p_pv(42)-p_pv(40));
```

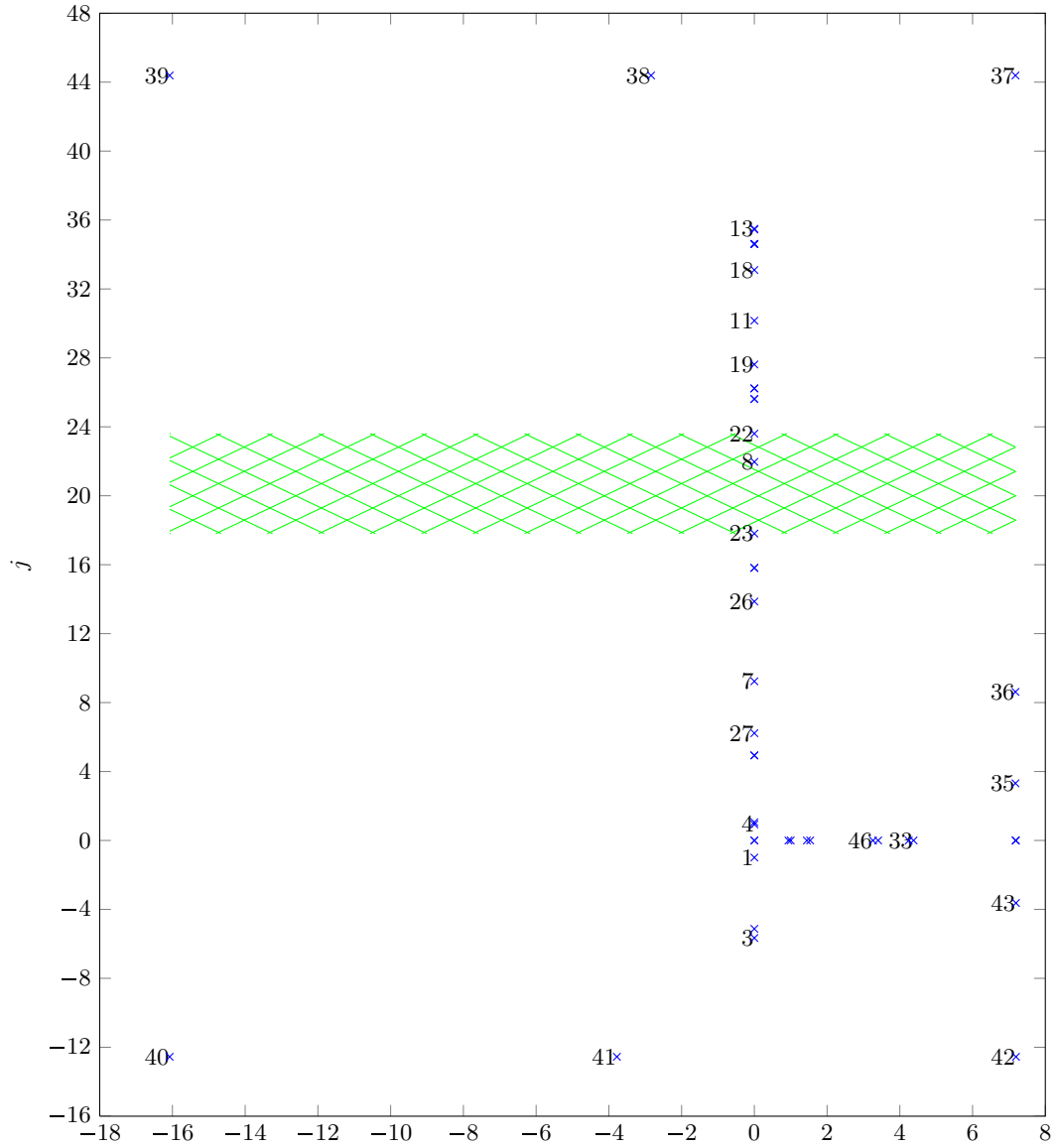

Figure A.14: Source boundary flux—region used to calculate $\Phi_{\underset{\sim}{\epsilon}_{36}(\underset{\sim}{\mathcal{F}0})_7}$ ($\epsilon_{36} \triangleq \underset{\sim}{\epsilon}_{26}\kappa_3$)

Code listing A.51: Source boundary flux—calculate $\Phi_{\underset{\sim}{\epsilon}_{41}(\underset{\sim}{\mathcal{F}}0)_7}$ (exampleSCsourcePM.m)

```
crosshatch_poly(real([p_pv(40) p_pv(42) p_pv(37) p_pv(39)]),...
  imag([p_pv(40) p_pv(42) p_pv(37) p_pv(39)]),...
  45,1,'edgewidth',0,'linewidth',0.5,'linecolor','g','hold',1);
crosshatch_poly(real([p_pv(40) p_pv(42) p_pv(37) p_pv(39)]),...
  imag([p_pv(40) p_pv(42) p_pv(37) p_pv(39)]),...
  -45,1,'edgewidth',0,'linewidth',0.5,'linecolor','g','hold',1);

calF = 979e3*1.5e-3;
Phi_epsilon41_calF7 = calF*d*imag(p_pv(40)-p_pv(39))*(4*pi*1e-7)/...
  real(p_pv(42)-p_pv(40));
```

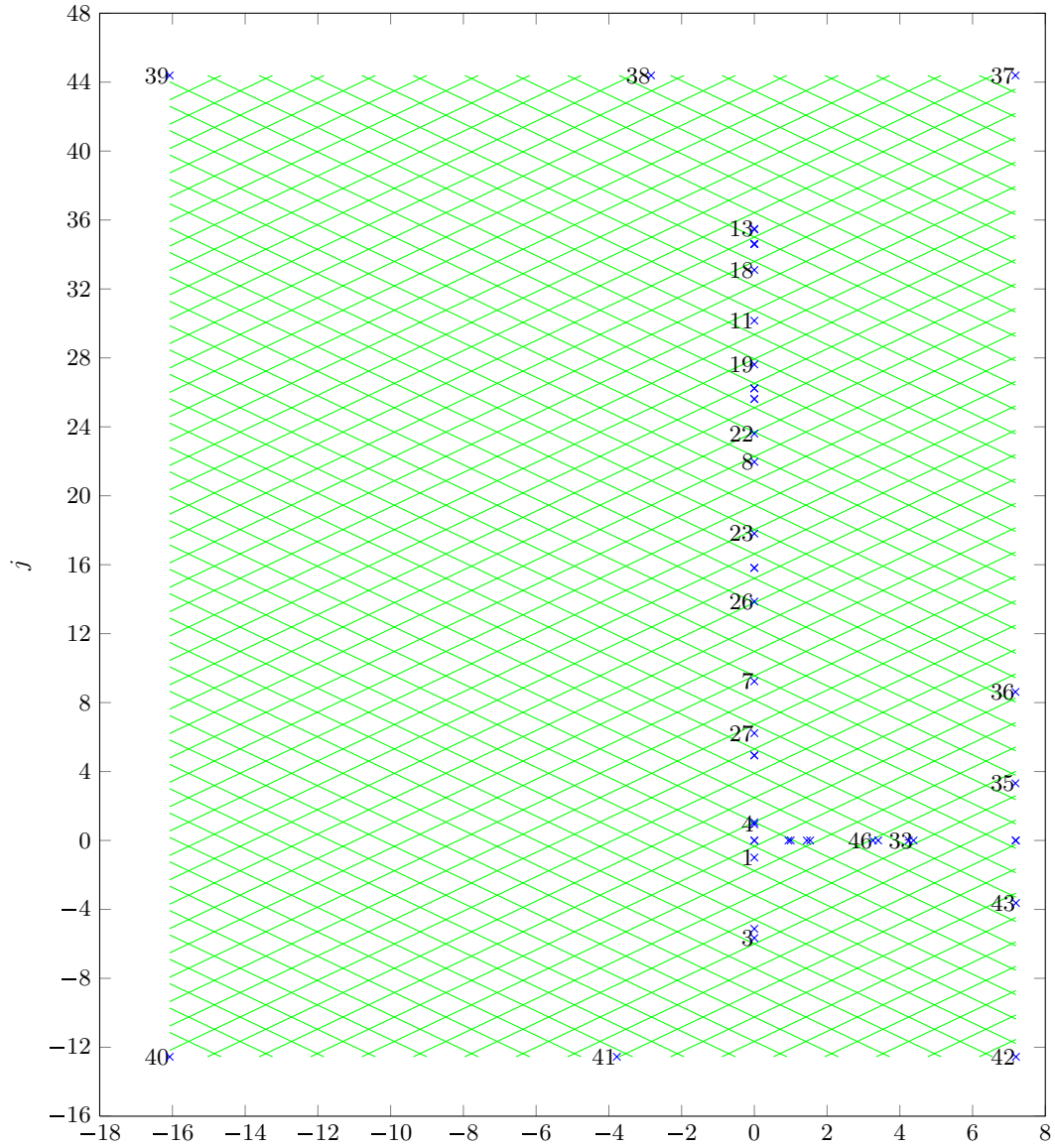

Figure A.15: Source boundary flux—region used to calculate $\Phi_{\underset{\sim}{\epsilon}_{41}(\underset{\sim}{\mathcal{F}}0)_7}$ ($\epsilon_{41} \triangleq \underset{\sim}{\epsilon}_{28}\kappa_1$)

Code listing A.52: Source boundary flux—calculate $\Phi_{\underset{\sim}{\epsilon}_{47}(\underset{\sim}{\mathcal{F}}0)_7}$ (`exampleSCsourcePM.m`)

```
143 crosshatch_poly(real([p_pv(40) p_pv(42) p_pv(37) p_pv(39)]),...
144   imag([p_pv(36) p_pv(36) p_pv(35) p_pv(35)]),...
145   45,1,'edgewidth',0,'linewidth',0.5,'linecolor','g','hold',1);
146 crosshatch_poly(real([p_pv(40) p_pv(42) p_pv(37) p_pv(39)]),...
147   imag([p_pv(36) p_pv(36) p_pv(35) p_pv(35)]),...
148   -45,1,'edgewidth',0,'linewidth',0.5,'linecolor','g','hold',1);

149 calF = 979e3*1.5e-3;
150 Phi_epsilon47_calF7 = calF*d*imag(p_pv(36)-p_pv(35))*(4*pi*1e-7)/...
151   real(p_pv(42)-p_pv(40));
```

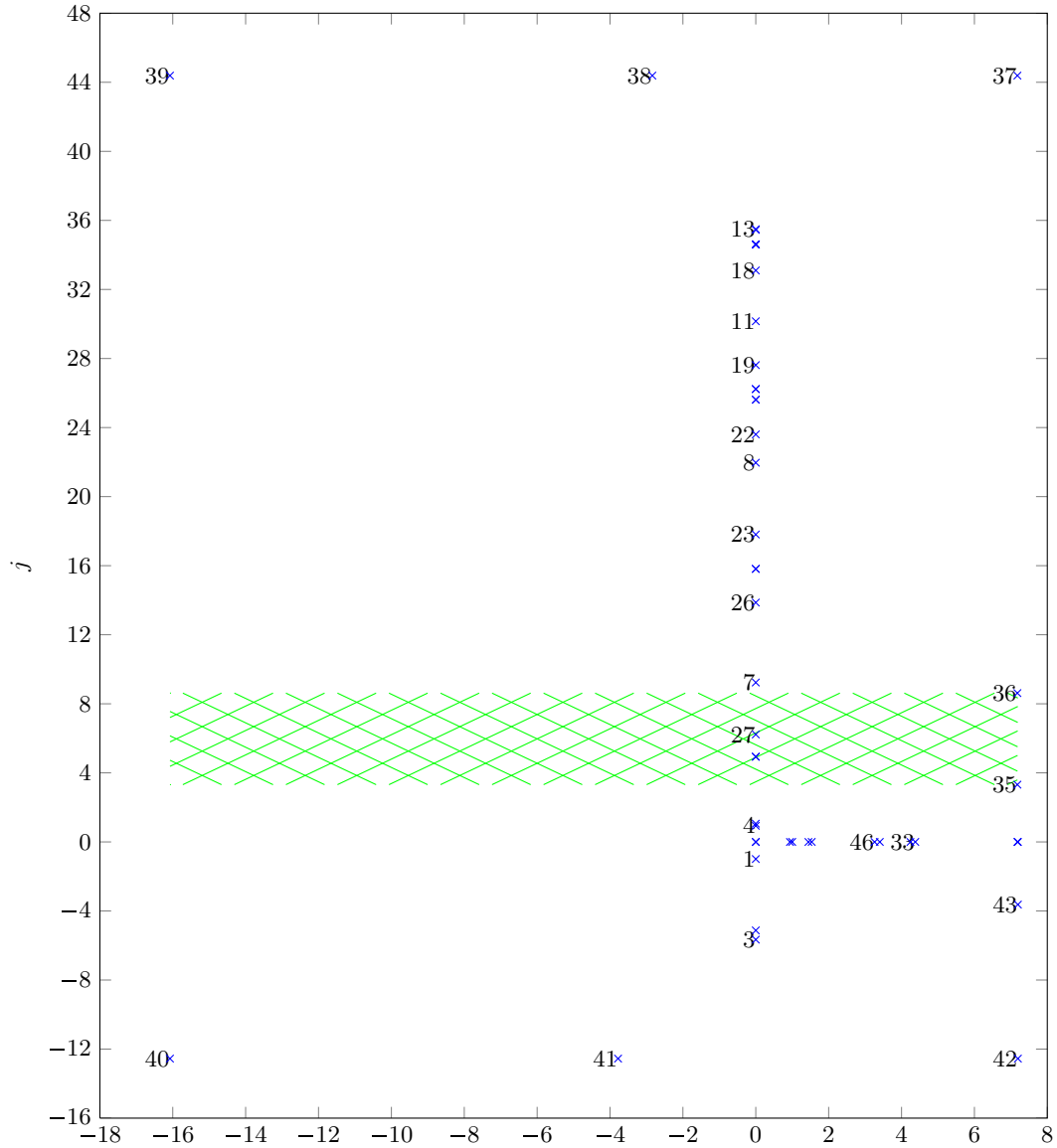

Figure A.16: Source boundary flux—region used to calculate $\Phi_{\underset{\sim}{\epsilon}_{47}(\underset{\sim}{\mathcal{F}}0)_7}$ ($\epsilon_{47} \triangleq \underset{\sim}{\epsilon}_{30}\kappa_2$)

Table A.7 shows that the values obtained by the conformal mapping method closely match those obtained using FEM.

Table A.7: Comparison of source boundary fluxes calculated by FEM and the conformal mapping method

	Schwarz-Christoffel Mapping	Finite Element Method	Error
$\Phi_{\underset{\sim}{\epsilon}_{36}(\underset{\sim}{\mathcal{F}}0)_7}$	$-9{,}197 \cdot 10^{-5}$ Wb	$-9{,}296 \cdot 10^{-5}$ Wb	$-1{,}1\,\%$
$\Phi_{\underset{\sim}{\epsilon}_{41}(\underset{\sim}{\mathcal{F}}0)_7}$	$-9{,}031 \cdot 10^{-4}$ Wb	$-9{,}506 \cdot 10^{-4}$ Wb	$-5{,}0\,\%$
$\Phi_{\underset{\sim}{\epsilon}_{47}(\underset{\sim}{\mathcal{F}}0)_7}$	$8{,}412 \cdot 10^{-5}$ Wb	$8{,}400 \cdot 10^{-5}$ Wb	$0{,}2\,\%$

Appendix B

Motor Dynamic Model

This appendix provides the detailed mathematical derivations for the dynamic model of a segmented LSMs based on a space-vector approach and includes all related custom Simulink® subsystems and MATLAB® functions.

B.1 Power-invariant $\alpha/\beta/0$ transformation

Under the assumption that the neutral point of a three-phase winding is isolated, the phase currents must sum to zero by Kirchhoff's Current Law. This is expressed in (B.1). Furthermore, the sum of line voltages is zero, as expressed in (B.2). The neutral (star point) of the three-phase windings is chosen as the zero voltage reference. Owing to the redundancy implied by (B.1) and (B.2), the voltages and currents of the three-phase winding are fully described by any two components of line voltage and any two components of line current.

$$I_{\mathrm{a}} + I_{\mathrm{b}} + I_{\mathrm{c}} = 0 \tag{B.1}$$

$$V_{(\mathrm{ab})} + V_{(\mathrm{bc})} + V_{(\mathrm{ca})} = 0 \tag{B.2}$$

$$\because \qquad (V_{\mathrm{a}} - V_{\mathrm{b}}) + (V_{\mathrm{b}} - V_{\mathrm{c}}) + (V_{\mathrm{c}} - V_{\mathrm{a}}) = 0$$

Considering that the α-axis is aligned with phase 'a' and that the β-axis is in space quadrature with it, the three-phase currents and corresponding mmf can be resolved

into α and β components using (B.1). The resulting components are (B.3a) and (B.3b), where c_1 is an arbitrary scaling factor.

$$\begin{aligned} I_\alpha &= c_1 \left(I_\mathrm{a} \cos(0) + I_\mathrm{b} \cos(2\pi/3) + I_\mathrm{c} \cos(4\pi/3)\right) \\ &= c_1 \left(I_\mathrm{a} - \frac{1}{2} I_\mathrm{b} - \frac{1}{2}(-I_\mathrm{a} - I_\mathrm{b})\right) \\ &= c_1 \frac{3}{2} I_\mathrm{a} \end{aligned} \tag{B.3a}$$

$$\begin{aligned} I_\beta &= c_1 \left(I_\mathrm{a} \sin(0) + I_\mathrm{b} \sin(2\pi/3) + I_\mathrm{c} \sin(4\pi/3)\right) \\ &= c_1 \left(0 + \frac{\sqrt{3}}{2} I_\mathrm{b} - \frac{\sqrt{3}}{2}(-I_\mathrm{a} - I_\mathrm{b})\right) \\ &= c_1 \left(\frac{\sqrt{3}}{2} I_\mathrm{a} + \sqrt{3} I_\mathrm{b}\right) \end{aligned} \tag{B.3b}$$

Similarly, the phase voltages can be resolved into α and β components as shown in (B.4a) and (B.4b). However, unlike for the phase currents, the phase voltages do not necessarily sum to zero and so it is not possible to substitute for V_c in terms of V_a and V_b. Thus, a zero-sequence voltage component must be introduced to obtain an invertible transformation.

$$\begin{aligned} V_\alpha &= c_1 \left(V_\mathrm{a} \cos(0) + V_\mathrm{b} \cos(2\pi/3) + V_\mathrm{c} \cos(4\pi/3)\right) \\ &= c_1 \left(V_\mathrm{a} - \frac{1}{2} V_\mathrm{b} - \frac{1}{2} V_\mathrm{c}\right) \end{aligned} \tag{B.4a}$$

$$\begin{aligned} V_\beta &= c_1 \left(V_\mathrm{a} \sin(0) + V_\mathrm{b} \sin(2\pi/3) + V_\mathrm{c} \sin(4\pi/3)\right) \\ &= c_1 \left(\frac{\sqrt{3}}{2} V_\mathrm{b} - \frac{\sqrt{3}}{2} V_\mathrm{c}\right) \end{aligned} \tag{B.4b}$$

The zero-sequence voltage component, V_0, is chosen to be at a potential central to the three phase voltages, as given by (B.5), where c_2 is an arbitrary scaling factor.

$$\begin{aligned} V_{(\mathrm{a}0)} + V_{(\mathrm{b}0)} + V_{(\mathrm{c}0)} &= 0 \\ \therefore \qquad (V_\mathrm{a} - c_2 V_0) + (V_\mathrm{b} - c_2 V_0) + (V_\mathrm{c} - c_2 V_0) &= 0 \\ \therefore \qquad V_0 &= \frac{1}{3c_2} \left(V_\mathrm{a} + V_\mathrm{b} + V_\mathrm{c}\right) \end{aligned} \tag{B.5}$$

As shown in (B.6), the value of c_1 can be chosen to yield power invariance between the three-phase and two-phase reference frames.

$$
\begin{aligned}
V_\alpha I_\alpha + V_\beta I_\beta + V_0 I_0 &= V_\mathrm{a} I_\mathrm{a} + V_\mathrm{b} I_\mathrm{b} + V_\mathrm{c} I_\mathrm{c} \\
\therefore \quad \left(c_1\left(V_\mathrm{a} - \frac{1}{2}V_\mathrm{b} - \frac{1}{2}V_\mathrm{c}\right)\right)&\left(c_1\frac{3}{2}I_\mathrm{a}\right) + \\
\left(c_1\left(\frac{\sqrt{3}}{2}V_\mathrm{b} - \frac{\sqrt{3}}{2}V_\mathrm{c}\right)\right)&\left(c_1\left(\frac{\sqrt{3}}{2}I_\mathrm{a} + \frac{2\sqrt{3}}{2}I_\mathrm{b}\right)\right) + \\
&\left(\frac{1}{3c_2}\left(V_\mathrm{a} + V_\mathrm{b} + V_\mathrm{c}\right)\right)(0) = V_\mathrm{a} I_\mathrm{a} + V_\mathrm{b} I_\mathrm{b} + V_\mathrm{c} I_\mathrm{c} \\
\therefore \quad c_1^2\frac{3}{2}&\left(V_\mathrm{a} I_\mathrm{a} - \frac{1}{2}V_\mathrm{b} I_\mathrm{a} - \frac{1}{2}V_\mathrm{c} I_\mathrm{a}\right) + \\
c_1^2\frac{3}{2}&\left(\frac{1}{2}V_\mathrm{b} I_\mathrm{a} + V_\mathrm{b} I_\mathrm{b} - \frac{1}{2}V_\mathrm{c} I_\mathrm{a} - V_\mathrm{c} I_\mathrm{b}\right) = V_\mathrm{a} I_\mathrm{a} + V_\mathrm{b} I_\mathrm{b} + V_\mathrm{c} I_\mathrm{c} \\
\therefore \quad c_1^2\frac{3}{2}&\left(V_\mathrm{a} I_\mathrm{a} + V_\mathrm{b} I_\mathrm{b} + V_\mathrm{c}\left(-I_\mathrm{a} - I_\mathrm{b}\right)\right) = V_\mathrm{a} I_\mathrm{a} + V_\mathrm{b} I_\mathrm{b} + V_\mathrm{c} I_\mathrm{c} \\
\therefore \quad c_1^2\frac{3}{2}&\left(V_\mathrm{a} I_\mathrm{a} + V_\mathrm{b} I_\mathrm{b} + V_\mathrm{c} I_\mathrm{c}\right) = V_\mathrm{a} I_\mathrm{a} + V_\mathrm{b} I_\mathrm{b} + V_\mathrm{c} I_\mathrm{c} \\
\therefore \quad c_1 &= \sqrt{\frac{2}{3}}
\end{aligned}
\tag{B.6}
$$

Similarly, c_2 is chosen to ensure power invariance without the assumption that the zero-sequence component of the current is zero. (B.7) shows that the requirement for this is that $\mathbf{T}_{(33)}^{-1} = \mathbf{T}_{(33)}^{\mathrm{T}}$ so that $\left(\mathbf{T}_{(33)}^{-1}\right)^{\mathrm{T}}\mathbf{T}_{(33)}^{-1} = \mathbf{T}_{(33)}\mathbf{T}_{(33)}^{-1} = \mathbf{I}$. This means that the transformation matrix must be orthogonal, which is achieved by choosing $c_2 = \frac{1}{\sqrt{3}}$.

$$
\begin{aligned}
\boldsymbol{V}_{(\mathrm{abc})}^{\mathrm{T}}\boldsymbol{I}_{(\mathrm{abc})} &= \left(\mathbf{T}_{(33)}^{-1}\boldsymbol{V}_{(\alpha\beta 0)}\right)^{\mathrm{T}}\left(\mathbf{T}_{(33)}^{-1}\boldsymbol{I}_{(\alpha\beta 0)}\right) \\
&= \boldsymbol{V}_{(\alpha\beta 0)}^{\mathrm{T}}\left(\mathbf{T}_{(33)}^{-1}\right)^{\mathrm{T}}\mathbf{T}_{(33)}^{-1}\boldsymbol{I}_{(\alpha\beta 0)} \\
&= \boldsymbol{V}_{(\alpha\beta 0)}^{\mathrm{T}}\boldsymbol{I}_{(\alpha\beta 0)}
\end{aligned}
\tag{B.7}
$$

Expressed in matrix form, the resulting transformations from the three-phase currents and voltages to quantities in the $\alpha/\beta/0$ frame are given by (B.8) and (B.9), respectively. Code listings B.1 and B.2 are the implementation of (B.8) and (B.9) as MATLAB® functions and figure B.1 is the inverse of (B.8), as a Simulink® subsystem.

$$\begin{bmatrix} I_\alpha \\ I_\beta \end{bmatrix} = \begin{bmatrix} \sqrt{\frac{3}{2}} & 0 \\ \frac{1}{\sqrt{2}} & \sqrt{2} \end{bmatrix} \begin{bmatrix} I_\mathrm{a} \\ I_\mathrm{b} \end{bmatrix} \tag{B.8}$$

Code listing B.1: Transform from a/b/c to α/β (`T_32.m`)

```
function output = T_32
%  Transformation matrix for three-phase currents to alpha/beta
%  reference frame

output = [sqrt(3/2)  0;
          1/sqrt(2)  sqrt(2) ];
```

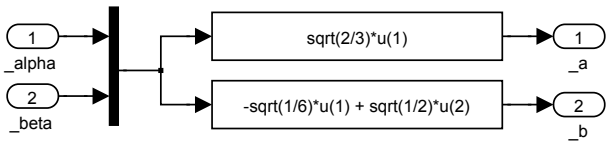

Figure B.1: Subsystem `lsm/dq/Transforms/inv T_32`

$$\begin{bmatrix} V_\alpha \\ V_\beta \\ V_0 \end{bmatrix} = \sqrt{\frac{2}{3}} \begin{bmatrix} 1 & -\frac{1}{2} & -\frac{1}{2} \\ 0 & \frac{\sqrt{3}}{2} & -\frac{\sqrt{3}}{2} \\ \frac{1}{\sqrt{2}} & \frac{1}{\sqrt{2}} & \frac{1}{\sqrt{2}} \end{bmatrix} \begin{bmatrix} V_\mathrm{a} \\ V_\mathrm{b} \\ V_\mathrm{c} \end{bmatrix} \tag{B.9}$$

Code listing B.2: Transform from a/b/c to $\alpha/\beta/0$ (`T_33.m`)

```
function output = T_33
%  Transformation matrix from three-phase quantities to alpha/beta/0
%  reference frame

output = sqrt(2/3)*[1            -1/2          -1/2;
                    0            sqrt(3)/2     -sqrt(3)/2;
                    1/sqrt(2)    1/sqrt(2)     1/sqrt(2)    ];
```

Note that, in order to obtain the actual mmf and air-gap flux from quantities in the $\alpha/\beta/0$ frame, it is necessary to scale by $\frac{1}{c_1} = \sqrt{\frac{3}{2}}$ because the air-gap mmf

is proportional to the current and the air-gap flux is proportional to the induced voltage [85].

The transformation of the line voltages to the stationary frame is derived in (B.11) by combining the relationship between the line and phase voltages given by (B.10) with (B.9) and the redundancy of (B.2). Code listings B.3 and B.2 and figure B.3 are the relevant MATLAB® and Simulink® implementations.

$$\begin{bmatrix} V_{(\mathrm{ab})} \\ V_{(\mathrm{bc})} \\ V_{(\mathrm{ca})} \end{bmatrix} = \begin{bmatrix} 1 & -1 & 0 \\ 0 & 1 & -1 \\ -1 & 0 & 1 \end{bmatrix} \begin{bmatrix} V_{\mathrm{a}} \\ V_{\mathrm{b}} \\ V_{\mathrm{c}} \end{bmatrix} \tag{B.10}$$

$$\begin{bmatrix} V_{\mathrm{ab}} \\ V_{\mathrm{bc}} \\ V_{\mathrm{ca}} \end{bmatrix} = \begin{bmatrix} 1 & -1 & 0 \\ 0 & 1 & -1 \\ -1 & 0 & 1 \end{bmatrix} \mathbf{T}_{(33)}^{-1} \begin{bmatrix} V_{\alpha} \\ V_{\beta} \\ V_{0} \end{bmatrix}$$

$$\therefore \quad \begin{bmatrix} V_{\mathrm{ab}} \\ V_{\mathrm{bc}} \\ V_{\mathrm{ca}} \end{bmatrix} = \begin{bmatrix} \frac{\sqrt{6}}{2} & -\frac{1}{\sqrt{2}} & 0 \\ 0 & \sqrt{2} & 0 \\ -\frac{\sqrt{6}}{2} & -\frac{1}{\sqrt{2}} & 0 \end{bmatrix} \begin{bmatrix} V_{\alpha} \\ V_{\beta} \\ V_{0} \end{bmatrix}$$

$$\therefore \quad \begin{bmatrix} V_{\mathrm{ab}} \\ V_{\mathrm{bc}} \end{bmatrix} = \begin{bmatrix} \frac{\sqrt{6}}{2} & -\frac{1}{\sqrt{2}} \\ 0 & \sqrt{2} \end{bmatrix} \begin{bmatrix} V_{\alpha} \\ V_{\beta} \end{bmatrix}$$

$$\therefore \quad \begin{bmatrix} V_{\alpha} \\ V_{\beta} \end{bmatrix} = \begin{bmatrix} \frac{\sqrt{6}}{2} & -\frac{1}{\sqrt{2}} \\ 0 & \sqrt{2} \end{bmatrix}^{-1} \begin{bmatrix} V_{\mathrm{ab}} \\ V_{\mathrm{bc}} \end{bmatrix}$$

$$\therefore \quad \begin{bmatrix} V_{\alpha} \\ V_{\beta} \end{bmatrix} = \begin{bmatrix} \sqrt{\frac{2}{3}} & \frac{1}{\sqrt{6}} \\ 0 & \frac{1}{\sqrt{2}} \end{bmatrix} \begin{bmatrix} V_{\mathrm{ab}} \\ V_{\mathrm{bc}} \end{bmatrix} \tag{B.11}$$

Code listing B.3: Transform from ab/bc to α/β (`T_22.m`)

```
function output = T_22
%  Transformation matrix for three-phase line voltages to alpha/beta
%  reference frame

output = [sqrt(2/3)  1/sqrt(6);
          0          1/sqrt(2) ];
```

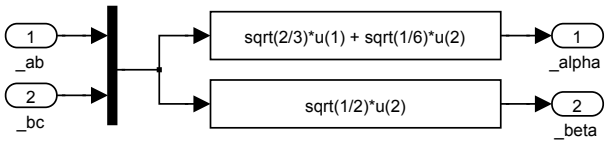

Figure B.2: Subsystem `lsm/dq/Transforms/T_22`

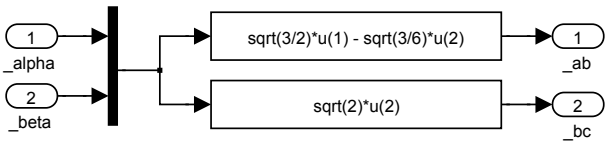

Figure B.3: Subsystem `lsm/dq/Transforms/inv T_22`

B.2 Transformation between α/β and d/q frames

Code listing B.4 and figures B.4 and B.5 are the MATLAB® and Simulink® implementations of the transformation between the stationary and moving reference frames.

Code listing B.4: Transform from α/β/0 to d/q/0 (`T_3r.m`)

```
1 function output = T_3r(theta)
2 %  Transformation matrix from alpha/beta/0 quantities to the d/q/0
3 %  reference frame
4
5 output = [cos(theta)      sin(theta)      0;
6           -sin(theta)     cos(theta)      0;
7           0               0               1 ];
```

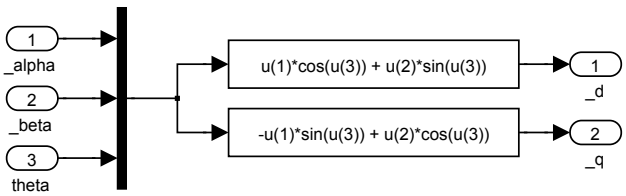

Figure B.4: Subsystem `lsm/dq/Transforms/T_2r`

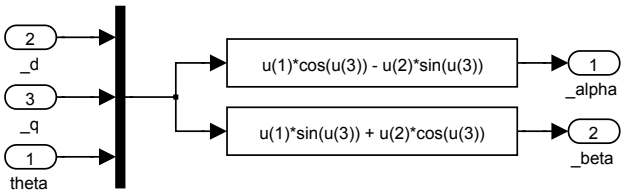

Figure B.5: Subsystem `lsm/dq/Transforms/inv T_2r`

B.3 d/q Motor equations

B.3.1 Electrical

Noting that the back-emf is equal to the rate of change of flux linkage, by Ohm's Law the relationship between the phase voltages and phase currents is given by (B.12).

$$\begin{bmatrix} V_\mathrm{a} \\ V_\mathrm{b} \\ V_\mathrm{c} \end{bmatrix} = \begin{bmatrix} R_\mathrm{a} & 0 & 0 \\ 0 & R_\mathrm{b} & 0 \\ 0 & 0 & R_\mathrm{c} \end{bmatrix} \begin{bmatrix} I_\mathrm{a} \\ I_\mathrm{b} \\ I_\mathrm{c} \end{bmatrix} + \begin{bmatrix} \dot{\lambda}_\mathrm{a} \\ \dot{\lambda}_\mathrm{b} \\ \dot{\lambda}_\mathrm{c} \end{bmatrix} \tag{B.12}$$

The stator equation, relating the electrical quantities in the α/β reference frame, is then obtained from (B.12) by substituting for the transformed currents using (B.8) and multiplying through by $\mathbf{T}_{(33)}$ to give (B.13).

$$\begin{bmatrix} V_\mathrm{a} \\ V_\mathrm{b} \\ V_\mathrm{c} \end{bmatrix} = \begin{bmatrix} R_\mathrm{a} & 0 & 0 \\ 0 & R_\mathrm{b} & 0 \\ 0 & 0 & R_\mathrm{c} \end{bmatrix} \begin{bmatrix} I_\mathrm{a} \\ I_\mathrm{b} \\ I_\mathrm{c} \end{bmatrix} + \begin{bmatrix} \dot{\lambda}_\mathrm{a} \\ \dot{\lambda}_\mathrm{b} \\ \dot{\lambda}_\mathrm{c} \end{bmatrix}$$

$$\therefore \quad \mathbf{T}_{(33)} \begin{bmatrix} V_\mathrm{a} \\ V_\mathrm{b} \\ V_\mathrm{c} \end{bmatrix} = \mathbf{T}_{(33)} \begin{bmatrix} R_\mathrm{a} & 0 & 0 \\ 0 & R_\mathrm{b} & 0 \\ 0 & 0 & R_\mathrm{c} \end{bmatrix} \mathbf{T}_{(33)}^{-1} \begin{bmatrix} I_\alpha \\ I_\beta \\ I_0 \end{bmatrix} + \frac{\mathrm{d}}{\mathrm{d}t} \left(\mathbf{T}_{(33)} \begin{bmatrix} \lambda_\mathrm{a} \\ \lambda_\mathrm{b} \\ \lambda_\mathrm{c} \end{bmatrix} \right)$$

$$\therefore \quad \begin{bmatrix} V_\alpha \\ V_\beta \\ V_0 \end{bmatrix} = \mathbf{T}_{(33)} \begin{bmatrix} R_\mathrm{a} & 0 & 0 \\ 0 & R_\mathrm{b} & 0 \\ 0 & 0 & R_\mathrm{c} \end{bmatrix} \mathbf{T}_{(33)}^{-1} \begin{bmatrix} I_\alpha \\ I_\beta \\ 0 \end{bmatrix} + \begin{bmatrix} \dot{\lambda}_\alpha \\ \dot{\lambda}_\beta \\ \dot{\lambda}_0 \end{bmatrix} \tag{B.13}$$

If the winding resistance is assumed to be equal for all three phases, (B.13) simplifies to (B.14).

$$\begin{bmatrix} V_\alpha \\ V_\beta \\ V_0 \end{bmatrix} = \mathbf{T}_{(33)} R \begin{bmatrix} 1 & 0 & 0 \\ 0 & 1 & 0 \\ 0 & 0 & 1 \end{bmatrix} \mathbf{T}_{(33)}^{-1} \begin{bmatrix} I_\alpha \\ I_\beta \\ 0 \end{bmatrix} + \begin{bmatrix} \dot{\lambda}_\alpha \\ \dot{\lambda}_\beta \\ \dot{\lambda}_0 \end{bmatrix}$$

$$\therefore \quad \begin{bmatrix} V_\alpha \\ V_\beta \\ V_0 \end{bmatrix} = R \begin{bmatrix} I_\alpha \\ I_\beta \\ 0 \end{bmatrix} + \begin{bmatrix} \dot{\lambda}_\alpha \\ \dot{\lambda}_\beta \\ \dot{\lambda}_0 \end{bmatrix} \tag{B.14}$$

Multiplying through (B.14) by $\mathbf{T}_{(3r)}(\theta)$, substituting for the flux linkages using $\mathbf{T}_{(3r)}^{-1}(\theta)$ and applying the product rule for differentiation, yields (B.15).

$$\mathbf{T}_{(3r)}(\theta) \begin{bmatrix} V_\alpha \\ V_\beta \\ V_0 \end{bmatrix} = \mathbf{T}_{(3r)}(\theta) R \begin{bmatrix} I_\alpha \\ I_\beta \\ 0 \end{bmatrix} + \mathbf{T}_{(3r)}(\theta) \frac{\mathrm{d}}{\mathrm{d}t} \begin{bmatrix} \lambda_\alpha \\ \lambda_\beta \\ \lambda_0 \end{bmatrix}$$

$$\therefore \quad \begin{bmatrix} V_\mathrm{d} \\ V_\mathrm{q} \\ V_0 \end{bmatrix} = R \begin{bmatrix} I_\mathrm{d} \\ I_\mathrm{q} \\ 0 \end{bmatrix} + \mathbf{T}_{(3r)}(\theta) \frac{\mathrm{d}}{\mathrm{d}t} \left(\mathbf{T}_{(3r)}^{-1}(\theta) \begin{bmatrix} \lambda_\mathrm{d} \\ \lambda_\mathrm{q} \\ \lambda_0 \end{bmatrix} \right)$$

$$\therefore \quad \begin{bmatrix} V_\mathrm{d} \\ V_\mathrm{q} \\ V_0 \end{bmatrix} = R \begin{bmatrix} I_\mathrm{d} \\ I_\mathrm{q} \\ 0 \end{bmatrix} + \mathbf{T}_{(3r)}(\theta) \left(\mathbf{T}_{(3r)}^{-1}(\theta) \frac{\mathrm{d}}{\mathrm{d}t} \begin{bmatrix} \lambda_\mathrm{d} \\ \lambda_\mathrm{q} \\ \lambda_0 \end{bmatrix} + \frac{\mathrm{d}}{\mathrm{d}t} \left(\mathbf{T}_{(3r)}^{-1}(\theta) \right) \begin{bmatrix} \lambda_\mathrm{d} \\ \lambda_\mathrm{q} \\ \lambda_0 \end{bmatrix} \right)$$

$$\therefore \quad \begin{bmatrix} V_\mathrm{d} \\ V_\mathrm{q} \\ V_0 \end{bmatrix} = R \begin{bmatrix} I_\mathrm{d} \\ I_\mathrm{q} \\ 0 \end{bmatrix} + \begin{bmatrix} \dot{\lambda}_\mathrm{d} \\ \dot{\lambda}_\mathrm{q} \\ \dot{\lambda}_0 \end{bmatrix} + \mathbf{T}_{(3r)}(\theta) \frac{\mathrm{d}}{\mathrm{d}t} \left(\mathbf{T}_{(3r)}^{-1}(\theta) \right) \begin{bmatrix} \lambda_\mathrm{d} \\ \lambda_\mathrm{q} \\ \lambda_0 \end{bmatrix} \tag{B.15}$$

The time derivative in (B.15) is simplified in (B.16), using the chain rule to express the time derivative as a angular displacement derivative multiplied by the rate of change of the angular displacement with time (ω).

$$
\begin{aligned}
\mathbf{T}_{(3r)}(\theta)\frac{\mathrm{d}}{\mathrm{d}t}\left(\mathbf{T}^{-1}_{(3r)}(\theta)\right) &= \mathbf{T}_{(3r)}(\theta)\frac{\mathrm{d}}{\mathrm{d}\theta}\left(\mathbf{T}^{-1}_{(3r)}(\theta)\right)\frac{\mathrm{d}\theta}{\mathrm{d}t} \\
&= \begin{bmatrix} \cos(\theta) & \sin(\theta) & 0 \\ -\sin(\theta) & \cos(\theta) & 0 \\ 0 & 0 & 1 \end{bmatrix} \frac{\mathrm{d}}{\mathrm{d}\theta} \begin{bmatrix} \cos(\theta) & -\sin(\theta) & 0 \\ \sin(\theta) & \cos(\theta) & 0 \\ 0 & 0 & 1 \end{bmatrix} \frac{\mathrm{d}\theta}{\mathrm{d}t} \\
&= \begin{bmatrix} \cos(\theta) & \sin(\theta) & 0 \\ -\sin(\theta) & \cos(\theta) & 0 \\ 0 & 0 & 1 \end{bmatrix} \begin{bmatrix} -\sin(\theta) & -\cos(\theta) & 0 \\ \cos(\theta) & -\sin(\theta) & 0 \\ 0 & 0 & 0 \end{bmatrix} \frac{\mathrm{d}\theta}{\mathrm{d}t} \\
&= \begin{bmatrix} 0 & -\left(\cos^2(\theta)+\sin^2(\theta)\right) & 0 \\ \sin^2(\theta)+\cos^2(\theta) & 0 & 0 \\ 0 & 0 & 0 \end{bmatrix} \frac{\mathrm{d}\theta}{\mathrm{d}t} \\
&= \begin{bmatrix} 0 & -1 & 0 \\ 1 & 0 & 0 \\ 0 & 0 & 0 \end{bmatrix} \omega
\end{aligned}
\tag{B.16}
$$

Substituting (B.16) into (B.15) yields (B.17), the resulting stator electrical matrix equation in the d/q reference frame. Note that the induced emf is in two components—one due to the time variation of the flux linkage and the other due to the speed, ω, of the d/q reference frame / reaction plate.

$$
\begin{bmatrix} V_\mathrm{d} \\ V_\mathrm{q} \\ V_0 \end{bmatrix} = R \begin{bmatrix} I_\mathrm{d} \\ I_\mathrm{q} \\ 0 \end{bmatrix} + \begin{bmatrix} \dot{\lambda}_\mathrm{d} \\ \dot{\lambda}_\mathrm{q} \\ \dot{\lambda}_0 \end{bmatrix} + \omega \begin{bmatrix} 0 & -1 & 0 \\ 1 & 0 & 0 \\ 0 & 0 & 0 \end{bmatrix} \begin{bmatrix} \lambda_\mathrm{d} \\ \lambda_\mathrm{q} \\ \lambda_0 \end{bmatrix} \tag{B.17}
$$

The Simulink® implementation of the electrical matrix equation (B.17) is included as figure B.6. The two flux linkage states, λ_d and λ_q are initialised with initial values of $\lambda_{\mathrm{d(t0)}}$ and $\lambda_{\mathrm{q(t0)}}$, respectively.

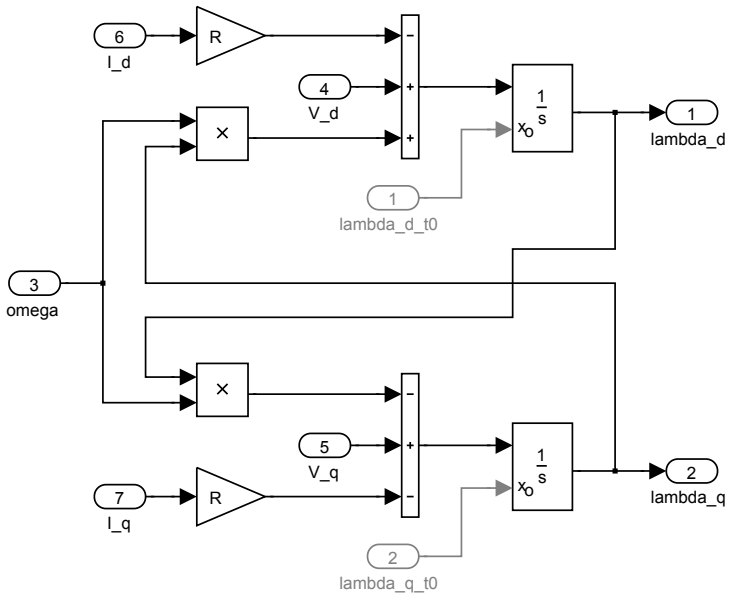

Figure B.6: Subsystem `lsm/dq/Electrical`

B.3.2 Inductances and flux linkages

Equation (B.18) derives the transformation between inductances and PM flux linkages in the a/b/c frame and the d/q/0 frame. Code listings B.6 and B.7 are MATLAB® functions to calculate a stator section's d/q/0 inductances and PM flux linkages from its a/b/c inductances and flux linkages, respectively. These values are calculated over a range of discrete relative positions of the reaction plate to the section, which correspond to angular displacements calculated by the function included as code listing B.5.

Code listing B.5: Calculate set of angular displacements (`calc_theta_x.m`)

```
1 function theta_x = calc_theta_x(x_rs_x,x_alpha,tau)
2 %  Calculate angular displacement between array of d-axis positions and
3 %  the alpha-axis, given an array of relative reaction plate positions
4
5 x_d_x = x_rs_x + tau/2;
6 theta_x = (x_d_x-x_alpha)*pi/tau;
7 theta_x = atan2(sin(theta_x),cos(theta_x)); %Wrap angle
```

$$
\begin{aligned}
&\begin{bmatrix}\lambda_{\mathrm{a}}\\ \lambda_{\mathrm{b}}\\ \lambda_{\mathrm{c}}\end{bmatrix} = \boldsymbol{L}_{(\mathrm{abc})}(x)\begin{bmatrix}I_{\mathrm{a}}\\ I_{\mathrm{b}}\\ I_{\mathrm{c}}\end{bmatrix} + \begin{bmatrix}\lambda_{\mathrm{ma}}(x)\\ \lambda_{\mathrm{mb}}(x)\\ \lambda_{\mathrm{mc}}(x)\end{bmatrix}\\
\therefore\quad &\begin{bmatrix}\lambda_{\mathrm{a}}\\ \lambda_{\mathrm{b}}\\ \lambda_{\mathrm{c}}\end{bmatrix} = \boldsymbol{L}_{(\mathrm{abc})}(x)\mathbf{T}_{(33)}^{-1}\begin{bmatrix}I_{\alpha}\\ I_{\beta}\\ I_{0}\end{bmatrix} + \begin{bmatrix}\lambda_{\mathrm{ma}}(x)\\ \lambda_{\mathrm{mb}}(x)\\ \lambda_{\mathrm{mc}}(x)\end{bmatrix}\\
\therefore\quad \mathbf{T}_{(33)}&\begin{bmatrix}\lambda_{\mathrm{a}}\\ \lambda_{\mathrm{b}}\\ \lambda_{\mathrm{c}}\end{bmatrix} = \mathbf{T}_{(33)}\boldsymbol{L}_{(\mathrm{abc})}(x)\mathbf{T}_{(33)}^{-1}\begin{bmatrix}I_{\alpha}\\ I_{\beta}\\ 0\end{bmatrix} + \mathbf{T}_{(33)}\begin{bmatrix}\lambda_{\mathrm{ma}}(x)\\ \lambda_{\mathrm{mb}}(x)\\ \lambda_{\mathrm{mc}}(x)\end{bmatrix}\\
\therefore\quad &\begin{bmatrix}\lambda_{\alpha}\\ \lambda_{\beta}\\ \lambda_{0}\end{bmatrix} = \mathbf{T}_{(33)}\boldsymbol{L}_{(\mathrm{abc})}(x)\mathbf{T}_{(33)}^{-1}\begin{bmatrix}I_{\alpha}\\ I_{\beta}\\ 0\end{bmatrix} + \mathbf{T}_{(33)}\begin{bmatrix}\lambda_{\mathrm{ma}}(x)\\ \lambda_{\mathrm{mb}}(x)\\ \lambda_{\mathrm{mc}}(x)\end{bmatrix}\\
\therefore\quad \mathbf{T}_{(3\mathrm{r})}(\theta)&\begin{bmatrix}\lambda_{\alpha}\\ \lambda_{\beta}\\ \lambda_{0}\end{bmatrix} = \mathbf{T}_{(3\mathrm{r})}(\theta)\mathbf{T}_{(33)}\boldsymbol{L}_{(\mathrm{abc})}(x)\mathbf{T}_{(33)}^{-1}\mathbf{T}_{(3\mathrm{r})}^{-1}(\theta)\begin{bmatrix}I_{\mathrm{d}}\\ I_{\mathrm{q}}\\ 0\end{bmatrix} + \mathbf{T}_{(3\mathrm{r})}(\theta)\mathbf{T}_{(33)}\begin{bmatrix}\lambda_{\mathrm{ma}}(x)\\ \lambda_{\mathrm{mb}}(x)\\ \lambda_{\mathrm{mc}}(x)\end{bmatrix}\\
\therefore\quad &\begin{bmatrix}\lambda_{\mathrm{d}}\\ \lambda_{\mathrm{q}}\\ \lambda_{0}\end{bmatrix} = \begin{bmatrix}L_{(\mathrm{dd})}(x) & L_{(\mathrm{dq})}(x) & L_{(\mathrm{d0})}(x)\\ L_{(\mathrm{qd})}(x) & L_{(\mathrm{qq})}(x) & L_{(\mathrm{q0})}(x)\\ L_{(0\mathrm{d})}(x) & L_{(0\mathrm{q})}(x) & L_{(00)}(x)\end{bmatrix}\begin{bmatrix}I_{\mathrm{d}}\\ I_{\mathrm{q}}\\ 0\end{bmatrix} + \begin{bmatrix}\lambda_{\mathrm{md}}(x)\\ \lambda_{\mathrm{mq}}(x)\\ \lambda_{\mathrm{m0}}(x)\end{bmatrix}
\end{aligned}
\tag{B.18}
$$

Code listing B.6: Calculate set of d/q/0 inductances (`calc_L_dq0_x.m`)

```
function L_dq0_x = calc_L_dq0_x(theta_x,L_abc_x)
%  Transform set of a/b/c inductance matrices to the d/q/0 frame

N_x = numel(theta_x);
L_dq0_x = zeros(3,3,N_x); %Preallocate output
for idx_x = 1:N_x
  L_dq0_x(:,:,idx_x) = T_3r(theta_x(idx_x))*T_33*...
    L_abc_x(:,:,idx_x)/T_33/T_3r(theta_x(idx_x));
end
```

Code listing B.7: Calculate set of d/q/0 PM flux linkages (`calc_lambda_m_dq0_x.m`)

```
function lambda_m_dq0_x = calc_lambda_m_dq0_x(theta_x,lambda_m_abc_x)
%  Transform set of a/b/c PM flux linkage matrices to the d/q/0 frame

N_x = numel(theta_x);
lambda_m_dq0_x = zeros(3,1,N_x); %Preallocate output
for idx_x = 1:N_x
  lambda_m_dq0_x(:,:,idx_x) = T_3r(theta_x(idx_x))*...
    T_33*lambda_m_abc_x(:,:,idx_x);
end
```

An advantage of using the d/q reference frame is that it can usually be assumed that the PM flux linkage is entirely in the d-axis and that the mutual inductances, $L_{(\mathrm{dq})}$ and $L_{(\mathrm{qd})}$, are zero (i.e. no cross-coupling of d and q-axis flux linkage). The full flux linkage Simulink® model is included as figure B.7 and a reduced model as figure B.8.

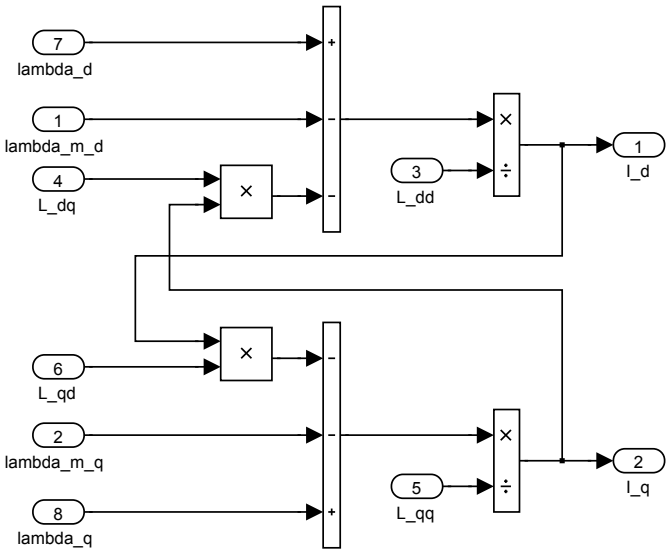

Figure B.7: Subsystem `lsm/dq/Motor Model/Flux Linkage`

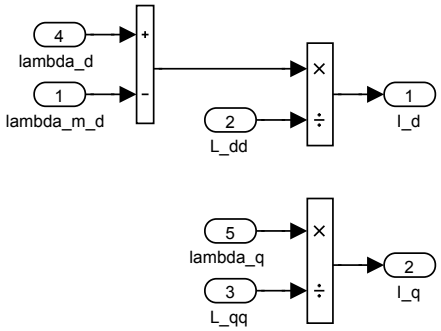

Figure B.8: Subsystem `lsm/dq/Motor Model (reduced)/Flux Linkage`

B.3.3 Power and electromagnetic force

The power invariance between the stationary and moving reference frames is demonstrated in (B.19).

$$\begin{aligned} P_{(\text{in})} &= V_\alpha I_\alpha + V_\beta I_\beta \\ &= \left(V_\text{d}\cos(\theta) - V_\text{q}\sin(\theta)\right)\left(I_\text{d}\cos(\theta) - I_\text{q}\sin(\theta)\right) \\ &\quad + \left(V_\text{d}\sin(\theta) + V_\text{q}\cos(\theta)\right)\left(I_\text{d}\sin(\theta) + I_\text{q}\cos(\theta)\right) \\ &= V_\text{d}I_\text{d}\left(\cos^2(\theta) + \sin^2(\theta)\right) + V_\text{q}I_\text{q}\left(\sin^2(\theta) + \cos^2(\theta)\right) \\ &= V_\text{d}I_\text{d} + V_\text{q}I_\text{q} \end{aligned} \tag{B.19}$$

The Simulink® subsystem to calculate the electromagnetic force in the d/q frame is included as figure B.9.

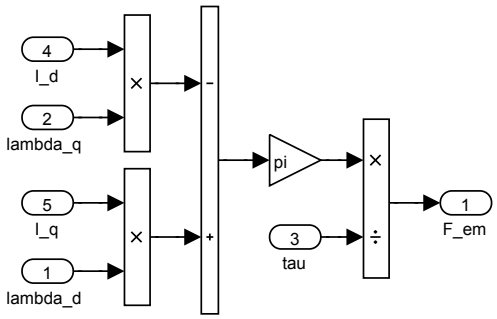

Figure B.9: Subsystem `lsm/dq/EM Force`

B.3.4 Complete d/q motor model

The Simulink® implementation of the full d/q motor model is given as figure B.10 and, with the simplified but less accurate flux linkage calculation, as figure B.11.

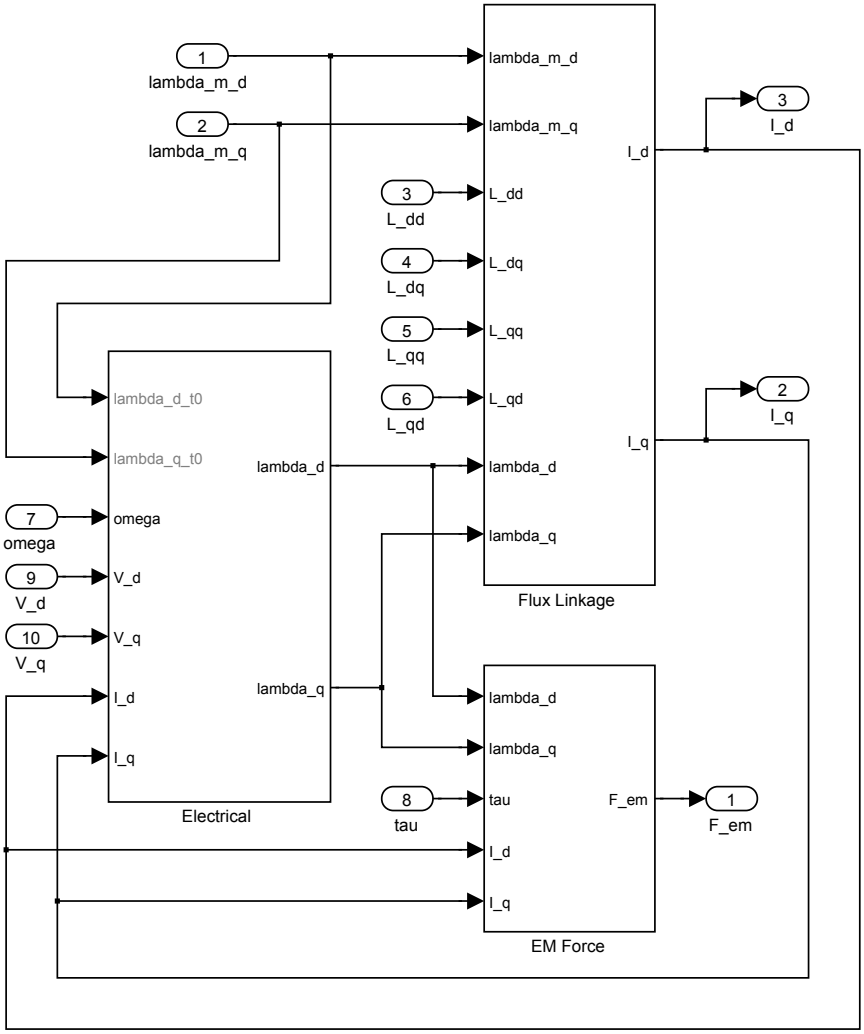

Figure B.10: Subsystem `lsm/dq/Motor Model`

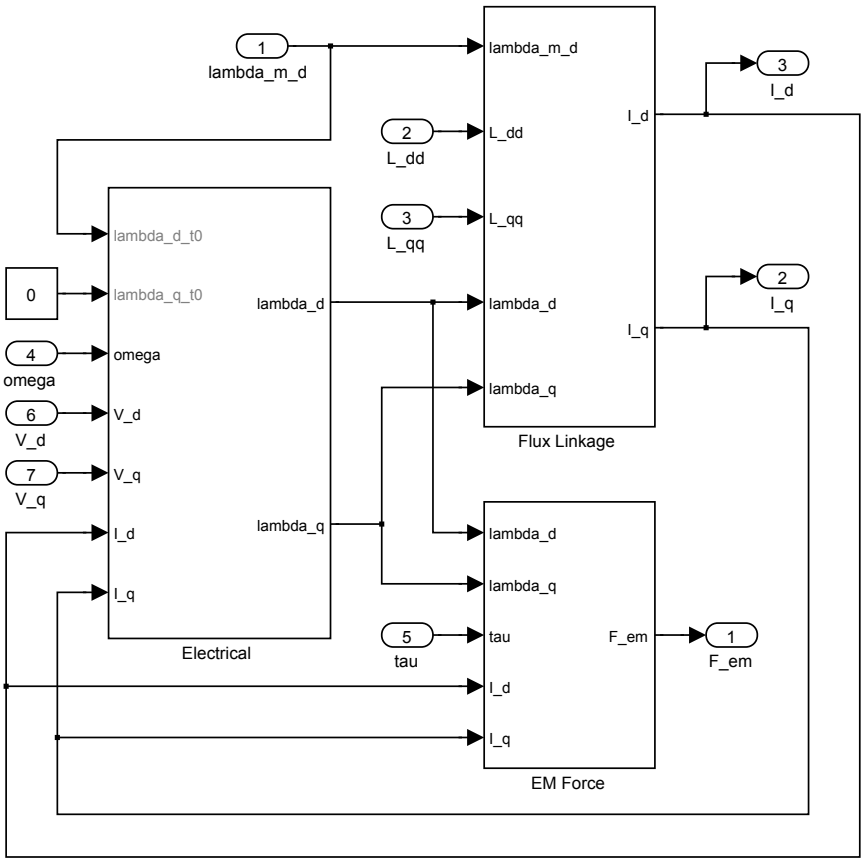

Figure B.11: Subsystem `lsm/dq/Motor Model (reduced)`

B.4 Relative displacements

Figure B.12 shows how the relative positions of the reaction plate and each stator section are defined for the simulation model. The position of the i^{th} stator section is specified in absolute space by giving its starting position, $x_{\mathrm{s}_i(\mathrm{start})}$ and its length, l_{s_i}. The reference position for that particular stator section is then chosen to be the position of its centre, x_{s_i}. The position of the α-axis is obtained from the stator section's reference position and $x_{(\alpha\mathrm{s})}$ is the relative position of any one of the α axes (since each stator section typically has more than one pole pair). Similarly, the centre of the reaction plate, x_{r} is used as its reference position, where the relative position (offset) of any one of the d axes, $x_{(\mathrm{dr})}$ is specified. The simulation model thus calculates the relative displacement between the d and α axes and hence the angular displacement, $\theta_{(\mathrm{d}\alpha)} = \theta$, at each time step.

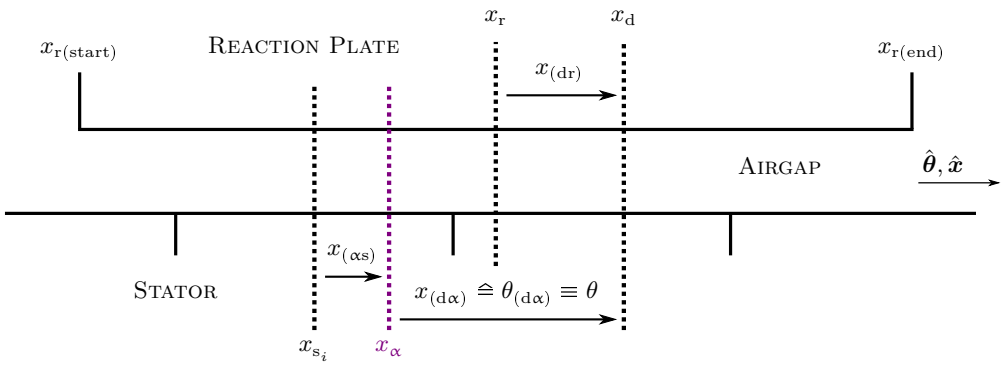

Figure B.12: Relative displacement of reaction plate to stator

B.5 Stator section model

The Simulink® block diagram used to model each stator section is shown in figure B.13 (figure B.14 if simplified flux linkage model is used). The model interfaces to the SimPowerSystems blockset by measuring the line voltages and enforcing the calculated currents at each time instant. The block also interfaces to the SimScape blockset for the simulation of the mechanical dynamics by using an 'Ideal Force Source' that acts on the connected reaction plate block.

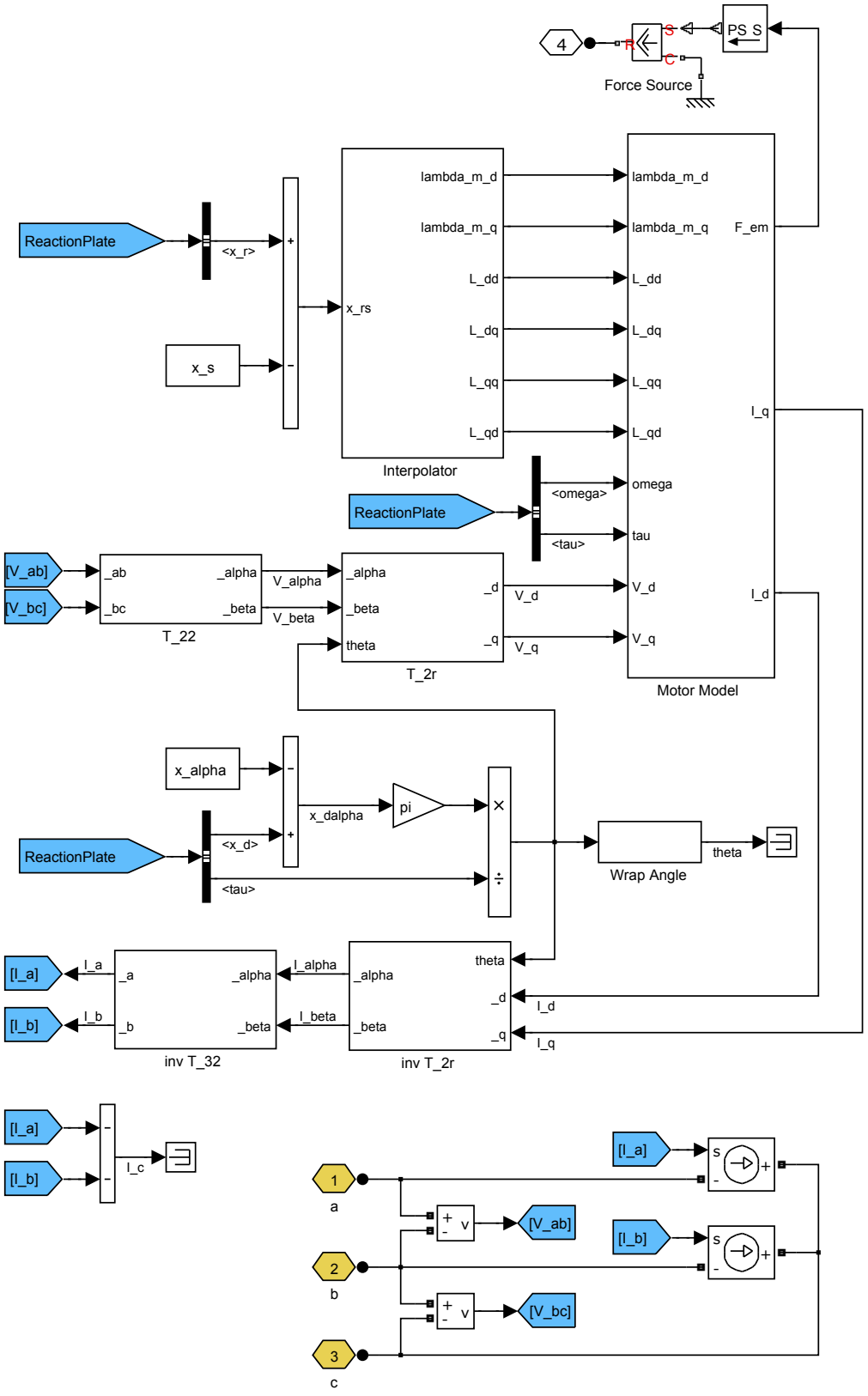

Figure B.13: Subsystem `lsm/Stator Section/Full`

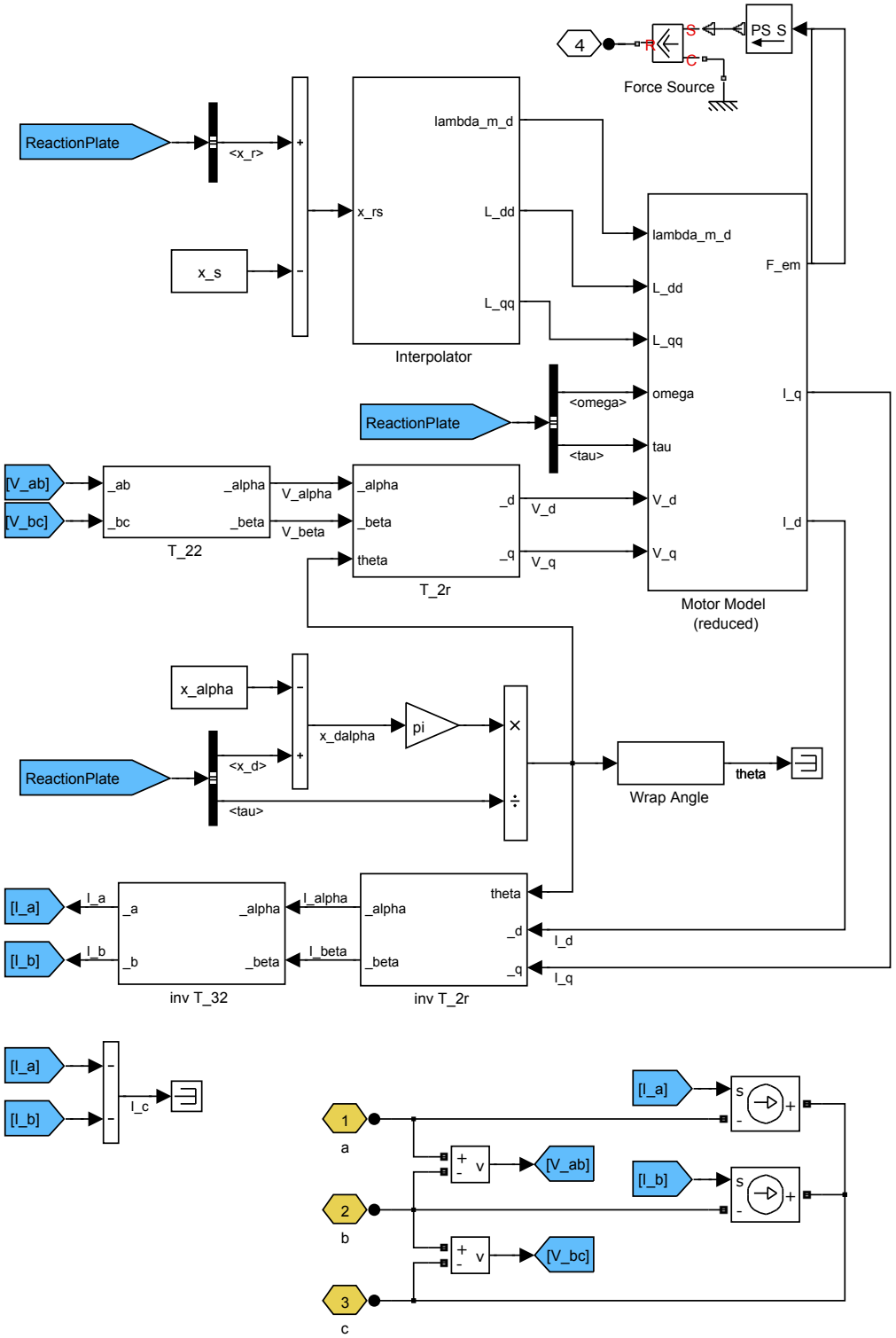

Figure B.14: Subsystem `lsm/Stator Section/Reduced`

B.5.1 Interpolation of inductances and flux linkages

The interpolator subsystem shown in figure B.15 is used to obtain continuous values of the flux linkages and inductances by interpolation across a set of predetermined values for N_{x} displacements of the reaction plate relative to the stator section. A pre-lookup block is used for computational efficiency because the inductance and flux linkage arrays correspond to the same displacement array, $\boldsymbol{x}_{(\mathrm{rs})\underset{\sim}{\mathrm{x}}}$. The interpolator subsystem shown in figure B.16 suffices for the reduced motor model implementation. The 'Lookup Table' blocks perform simple linear interpolation and are set to not extrapolate (output clips to the end values).

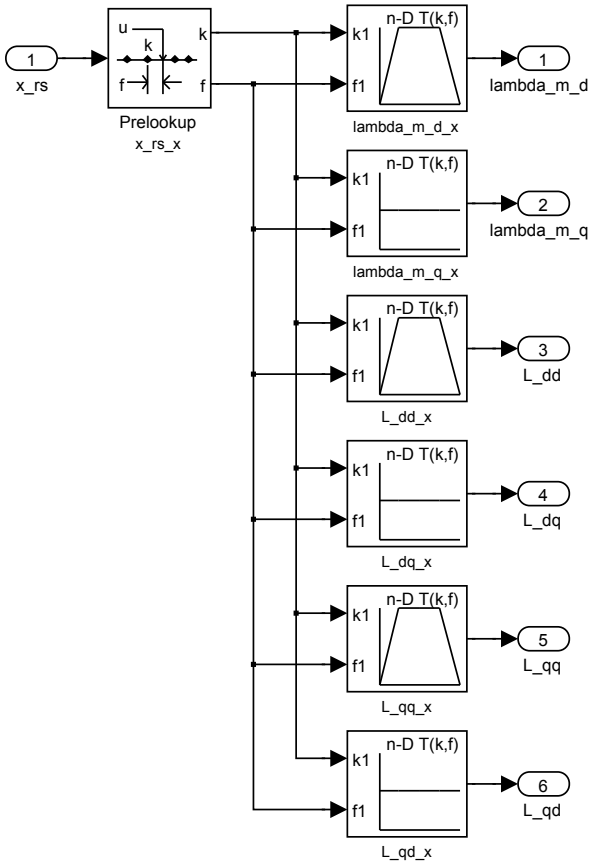

Figure B.15: Subsystem `lsm/Stator Section/Full/Interpolator`

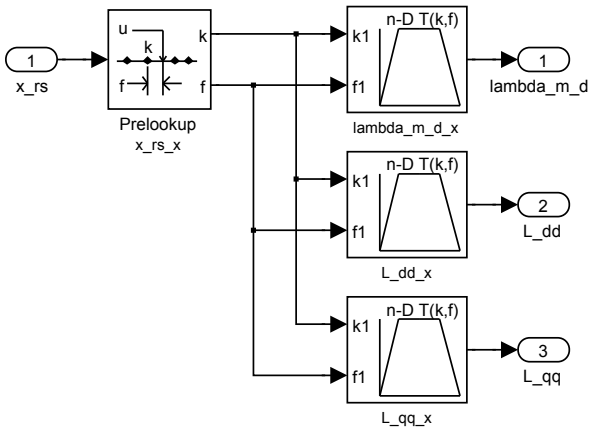

Figure B.16: Subsystem `lsm/Stator Section/Reduced/Interpolator`

B.5.2 Wrapping of angular displacement, θ

Although it is not necessary to wrap the angular displacement between the moving and stationary reference frames, θ, for the d/q transformation blocks, it is useful to have the possibility to monitor an angular displacement value that is wrapped within the standard interval $[-\pi, \pi]$. The subsystem shown in figure B.17 achieves this.

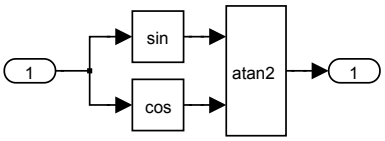

Figure B.17: Subsystem `lsm/dq/Wrap Angle`

B.6 Reaction plate model

The SimScape blockset is used to model the mechanical dynamics of the linear motor. Two variations are implemented, as shown in figures B.18 and B.19—one with simple viscous damping (friction force is directly proportional to the speed) and one with a nonlinear Stribeck friction model (viscous friction component, speed-independent Coulomb friction component and an additional Stribeck friction force resisting breakaway at zero speed). As shown, both implementations allow for the reaction plate weight to be included in the model if the motor is orientated vertically.

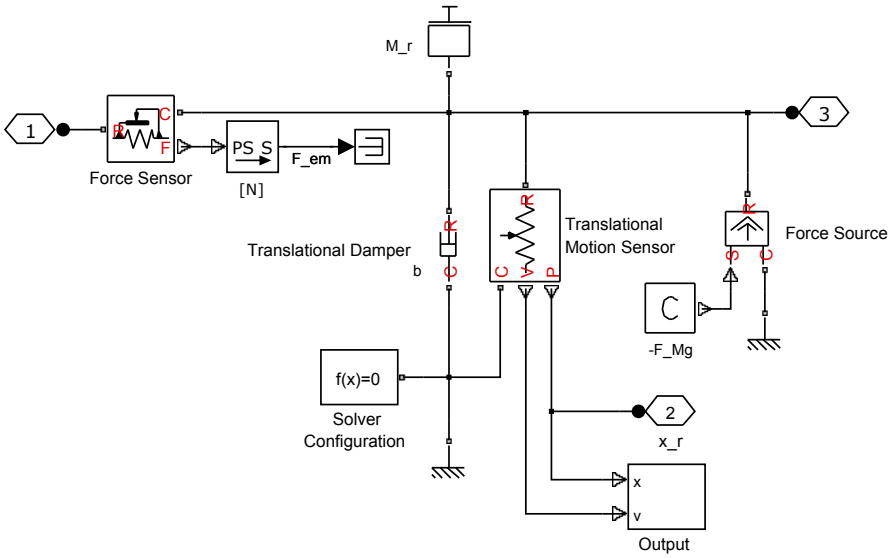

Figure B.18: Subsystem `lsm/Reaction Plate/Viscous Friction`

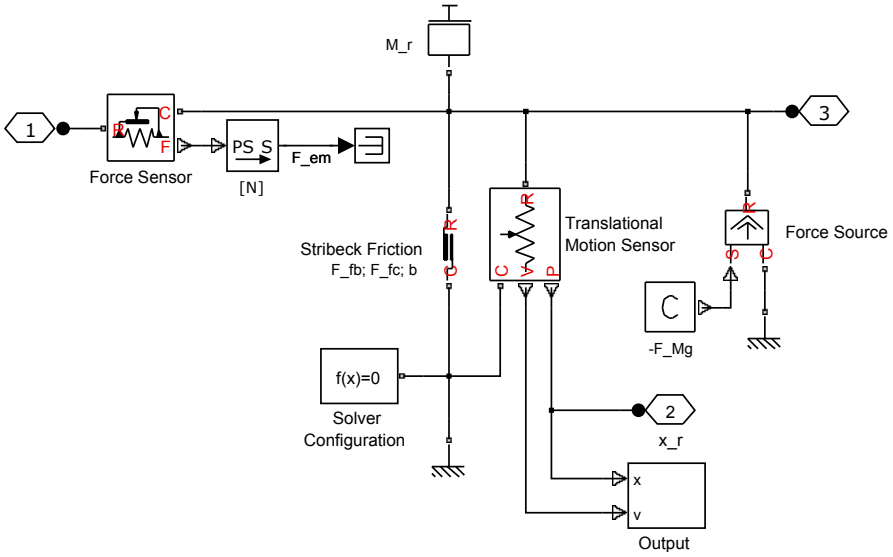

Figure B.19: Subsystem `lsm/Reaction Plate/Stribeck Friction`

Both implementations share an 'Output' block, shown in figure B.20, that conveys the relevant signals to the d/q motor model.

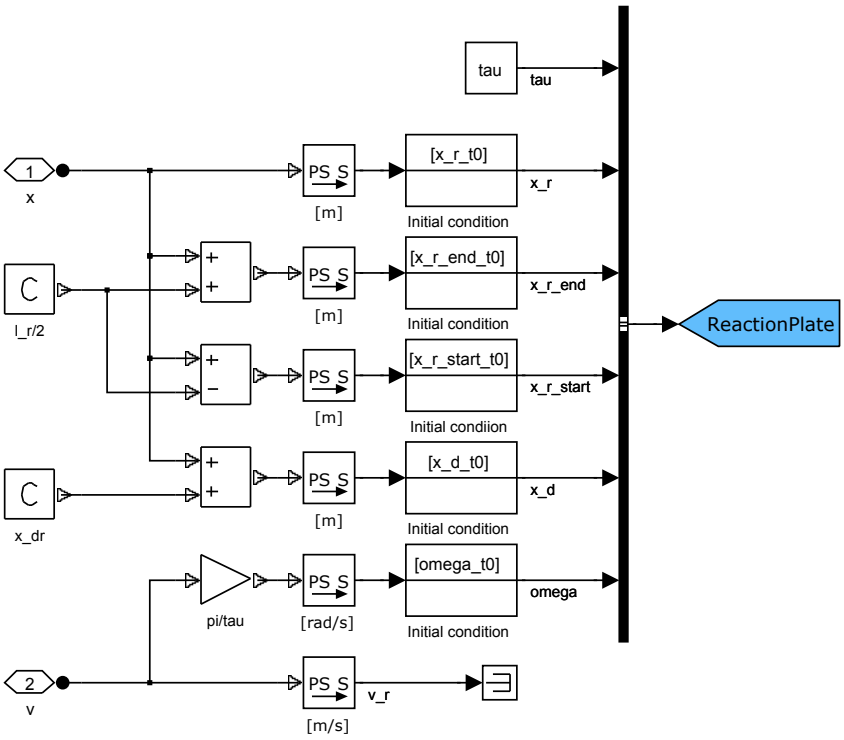

Figure B.20: Subsystem `lsm/Reaction Plate/Output`

B.6.1 Load force

An arbitrary load force can be applied to the reaction plate via a signal to the 'Load' block, shown in figure B.21.

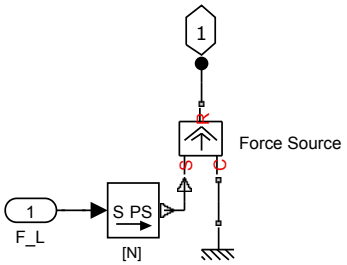

Figure B.21: Subsystem `lsm/Load`

Appendix C

Prototype Construction

This appendix details the materials, equipment and construction aspects of the prototype segmented-stator linear permanent magnet motor used to demonstrate the novel control strategy.

C.1 Motor

C.1.1 Stator sections

Core

Transvaal Electric Motors (Pty) Ltd manufactured the stator sections (their ref: motor type 14870). The individual 0,5 mm stator laminations were laser cut and stacked to form the stator section cores (according to the drawing given in figure C.1). The overall dimensions for each core are 288 mm × 186 mm × 50 mm. Each lamination was cut from low-loss non-oriented fully-processed SURA® steel (EN 10106 grade M250-50A) [147].

Although expensive, laser cutting the laminations rather than punching them allowed for a custom slot design without incurring very high tooling costs.

End caps

To protect the winding overhangs and to provide a means to mount the stator sections, stainless steel end caps were machined to "sandwich" the lamination stack. The chosen AISI 304L grade stainless steel has an austenitic crystal lattice structure and

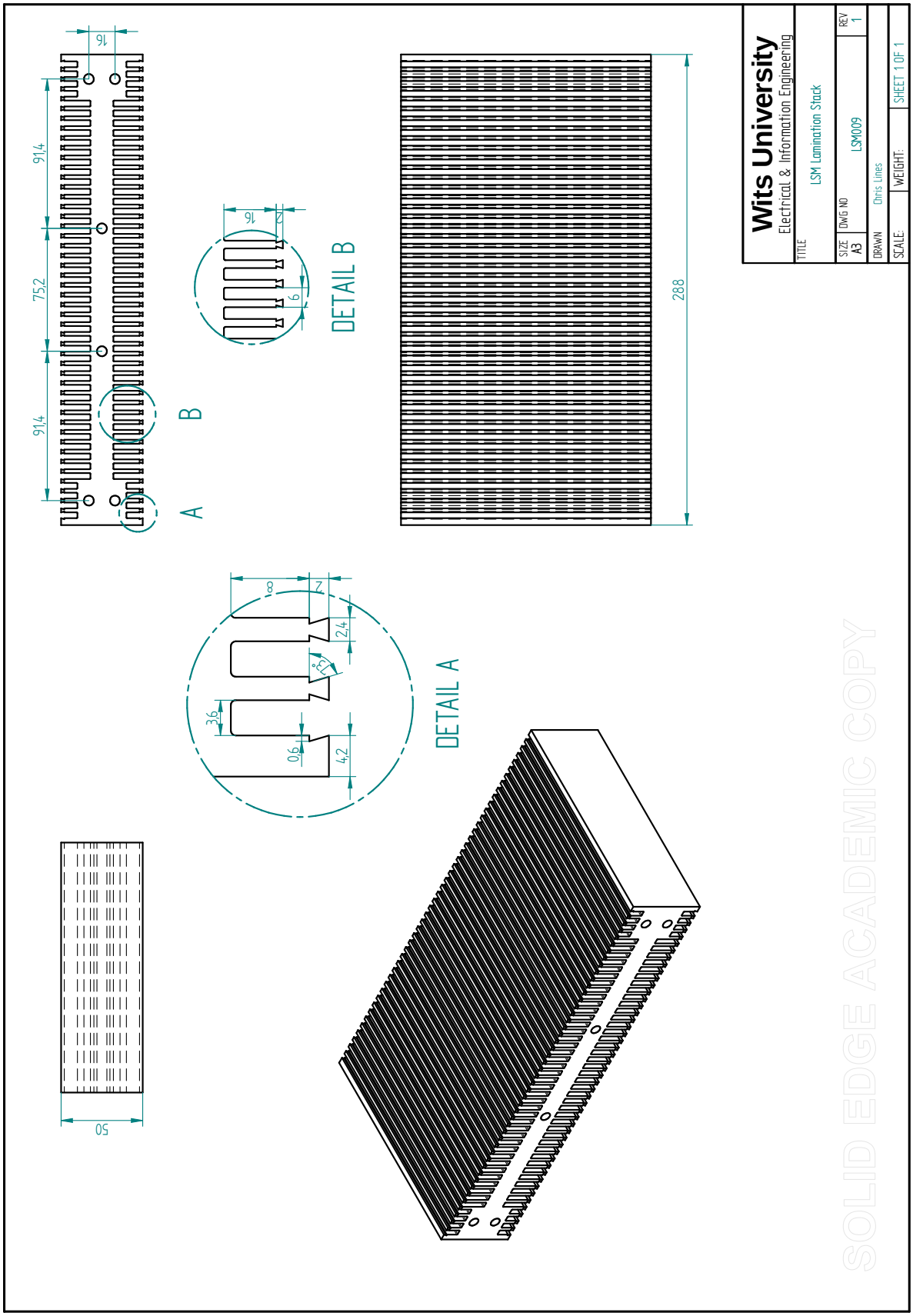

Figure C.1: LSM stator section lamination stack

is essentially non-magnetic [148]. M6 threaded rods and nuts are used to secure these end caps and the laminations. Drawings of the end caps are provided in figures C.2 and C.3. Three slots are machined along each end cap to reduce weight and potential eddy current losses (even though the stainless steel has a relatively high resistivity of 72 μΩ·cm [148]).

The end cap on the one side (end cap 2) allows for more space to accommodate the inter-coil connections and connections to the six external leads for each end of each phase winding. These external leads exit via the additional holes at both ends.

Windings

The hand-wound "mush" windings are formed with 0,95 mm diameter copper wire. The wire is insulated with a Grade 2, Class H enamel that can withstand a maximum operating temperature of 180 °C. Furthermore, Nomex® slot liners were used that also comply with the NEMA/IEC Class H temperature tolerance specification.

Slot wedges are used to keep the windings in place and because they are magnetic slot wedges, the open slots appear magnetically to be more like semi-closed slots. This reduces slot harmonics in the air-gap field [149]. (Magnetic slot wedges comprise powdered iron uniformly distributed within a suitable plastic or glass-fibre epoxy mix.)

Overhang covers

To protect the winding overhangs, 1 mm stainless steel covers (detailed in figures C.4 and C.5) were secured to the stator section end caps with M3 countersunk screws.

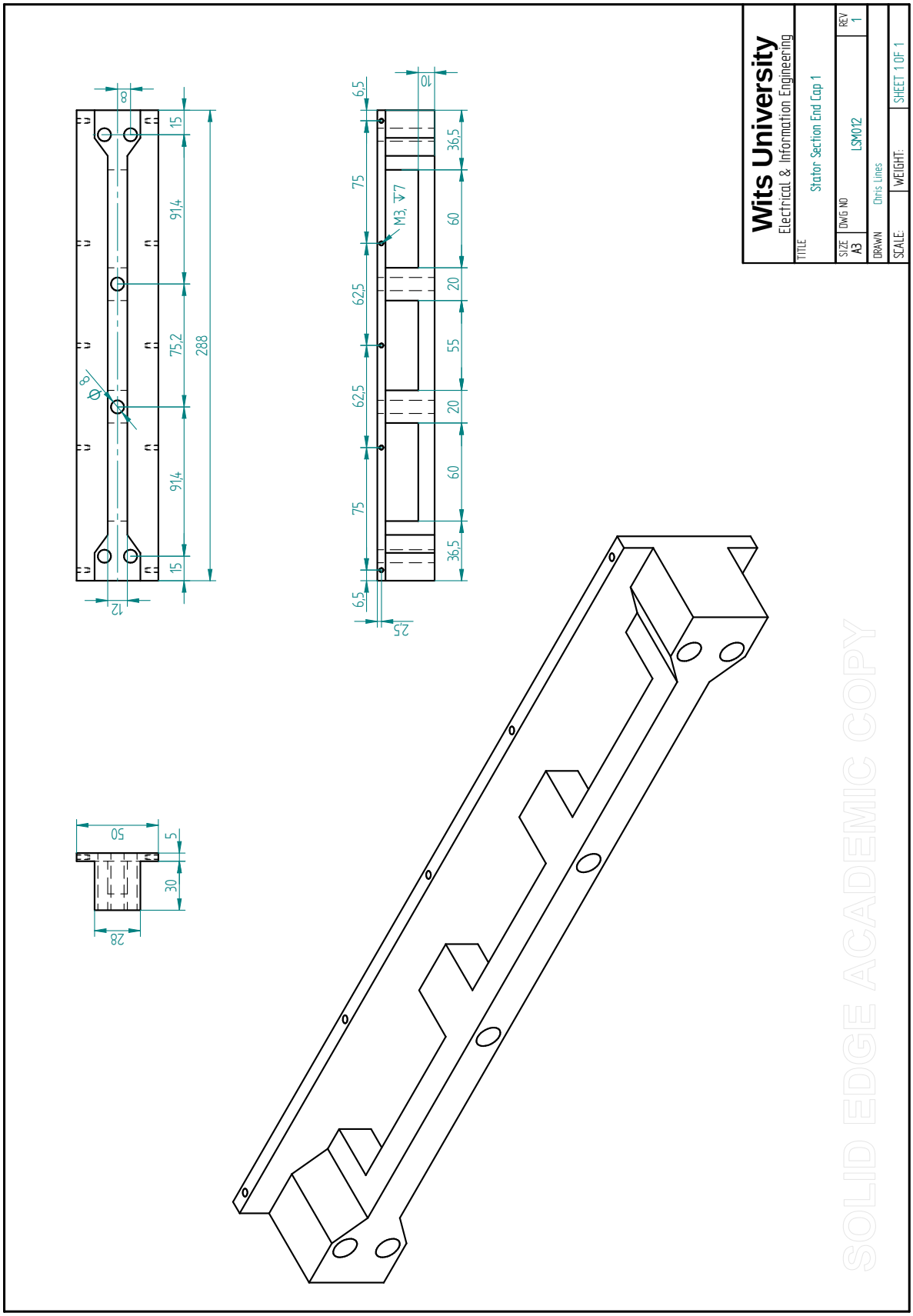

Figure C.2: LSM stator section end cap 1

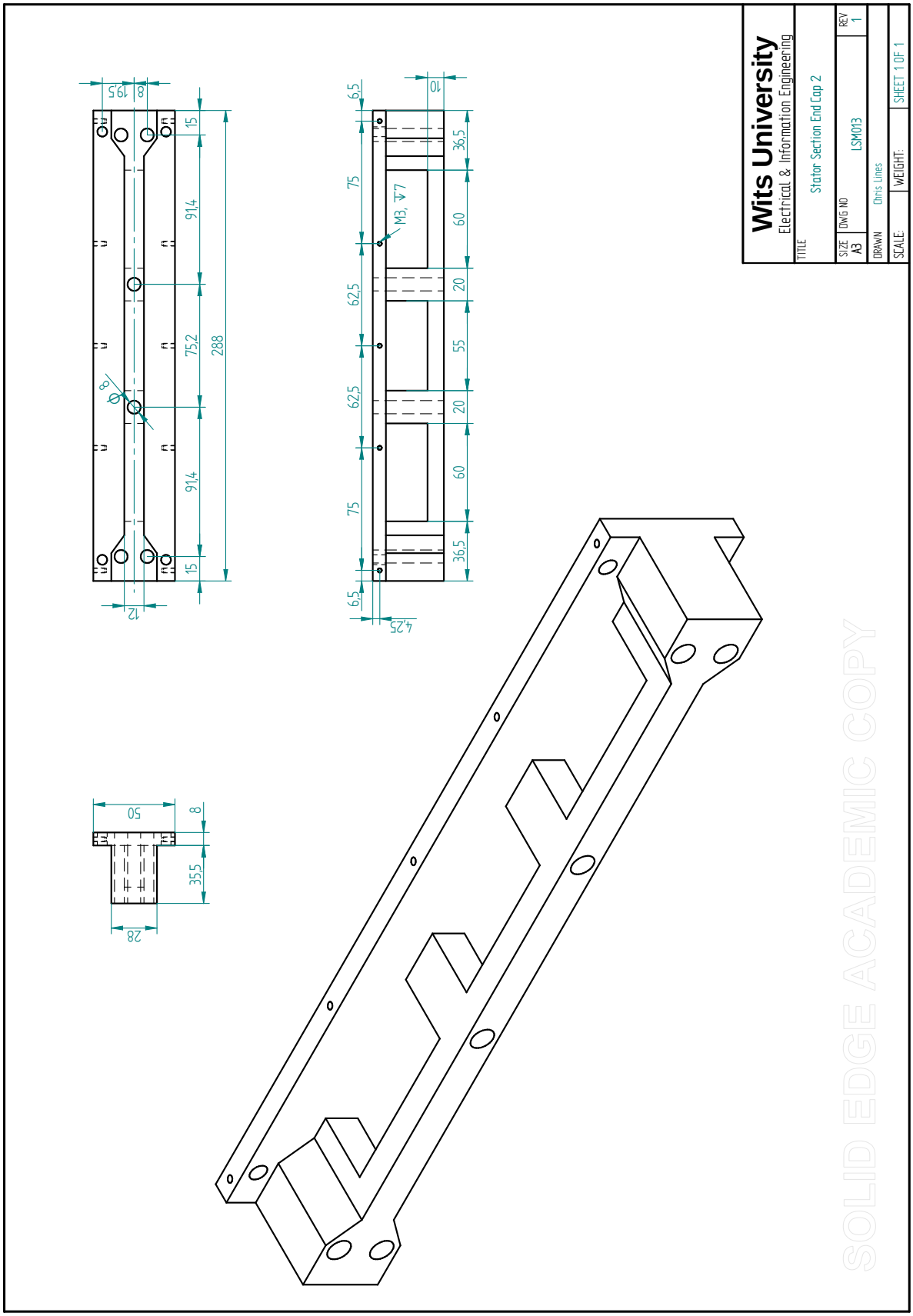

Figure C.3: LSM stator section end cap 2

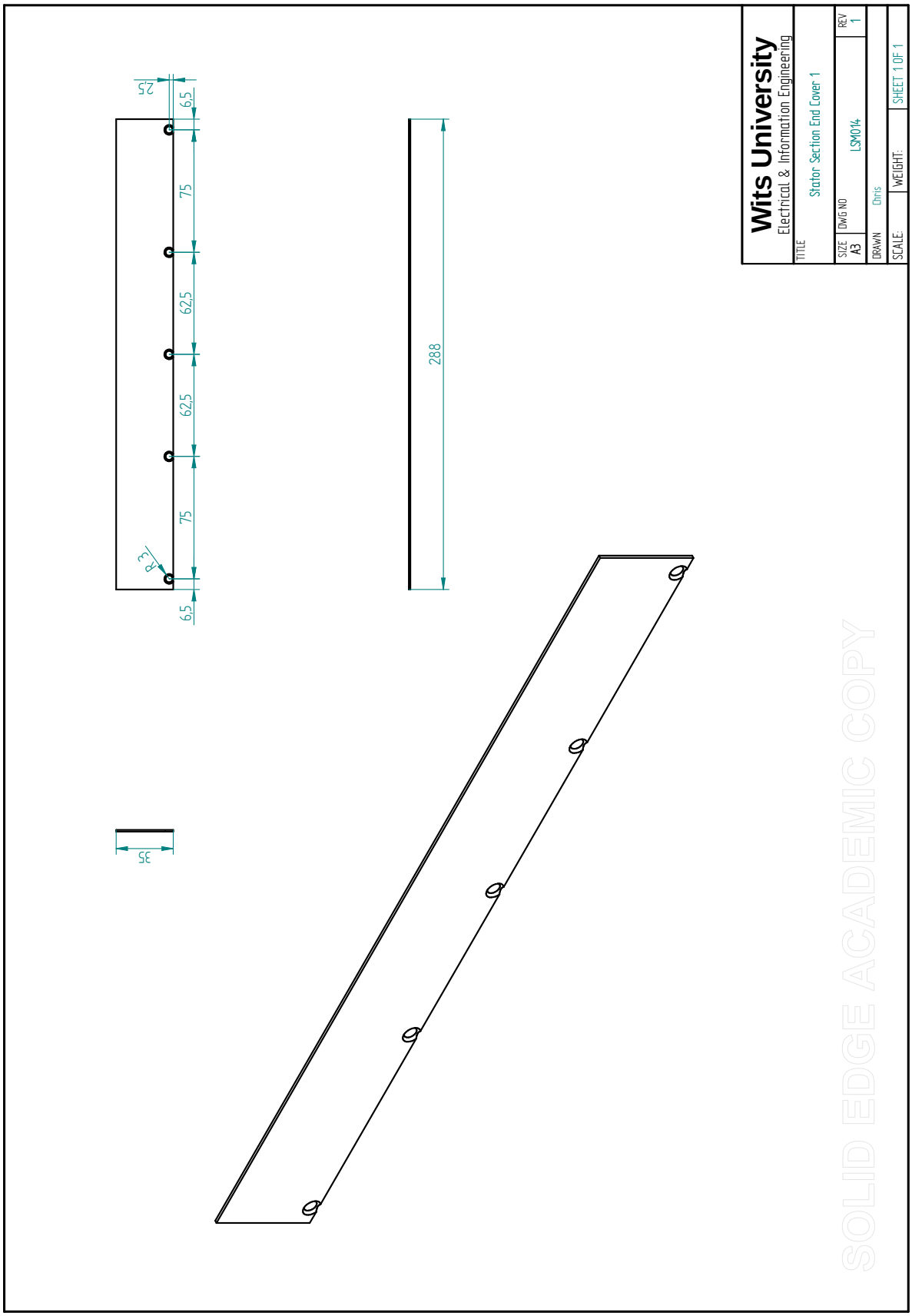

Figure C.4: LSM stator section winding overhang cover 1

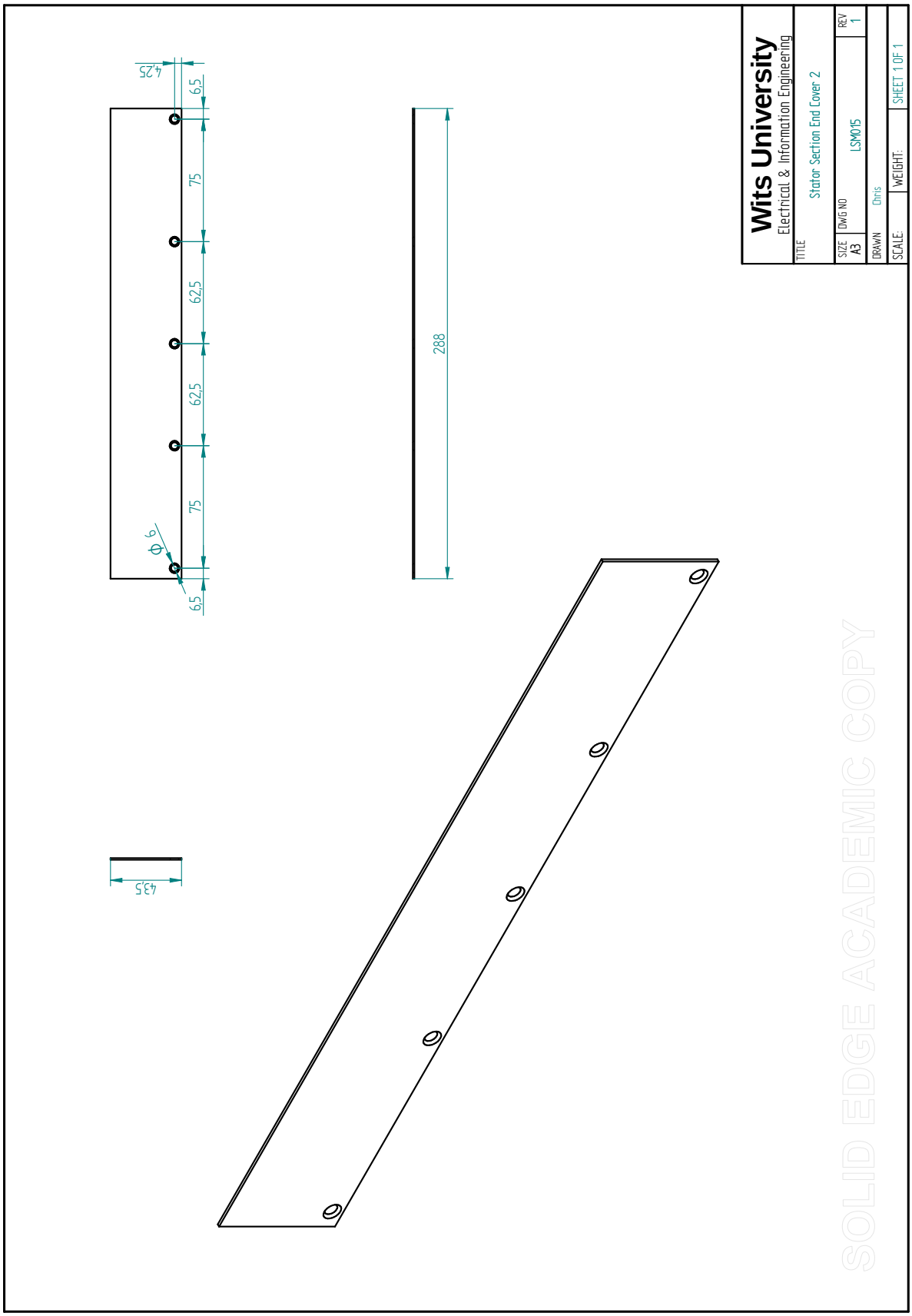

Figure C.5: LSM stator section winding overhang cover 2

Complete stator section

Once assembled and wound, each stator section was insulated with an epoxy resin by vacuum pressure impregnation (VPI) to form a solid, mechanically-robust stator "brick" that is resistant to moisture and most chemical contaminants. The VPI process is a vacuum cycle followed by high positive pressure that forces the resin into all voids of the wound stator [50]. Afterwards, the outer surfaces of the stator sections were cleaned of all excess epoxy using a Dremel® rotary grinder. Photographs of a finished stator section are included as figure C.6.

C.1.2 Stator assembly

It was necessary to find a means of mounting the stator sections in alignment and providing a track for the reaction plate to travel along with a constant air-gap. The solution was to use two stainless steel 'z'-section rails, as detailed in figures C.7 and C.8. They simultaneously keep the stator sections in place (with locating holes matched to the M6 nuts on the threaded rods of the stator sections) and provide flat, continuous surfaces for the reaction plate rollers to travel along.

The rails were manufactured by bending 6 mm 304L stainless steel plate. A benefit of the bending process is that 304L stainless steel becomes marginally work-hardened [148]. However, it was observed that the severe bending stress also caused the material to became slightly ferromagnetic along the bends. Fortunately the bends are far enough away from the air-gap field that this effect doesn't tangibly influence the motor's operation. To prevent those holes very close to the bends from "pulling" during the bending process, their centre positions were marked with the cutting laser before bending and then the holes were manually drilled through afterwards.

To verify that 6 mm-thick stainless steel would be structurally sufficient, given the high attractive force between the reaction plate and the stator sections, the worst-case deflection of the lip was approximated. Also, the maximum bending stress under loading was calculated to ensure that the lips would not yield and permanently distort.

Under the conservative assumption that each roller exerts a point load on the very edge of the lip and that the rollers are spaced far enough apart to be considered individually, the deflection for the longer of the two lips is calculated using the

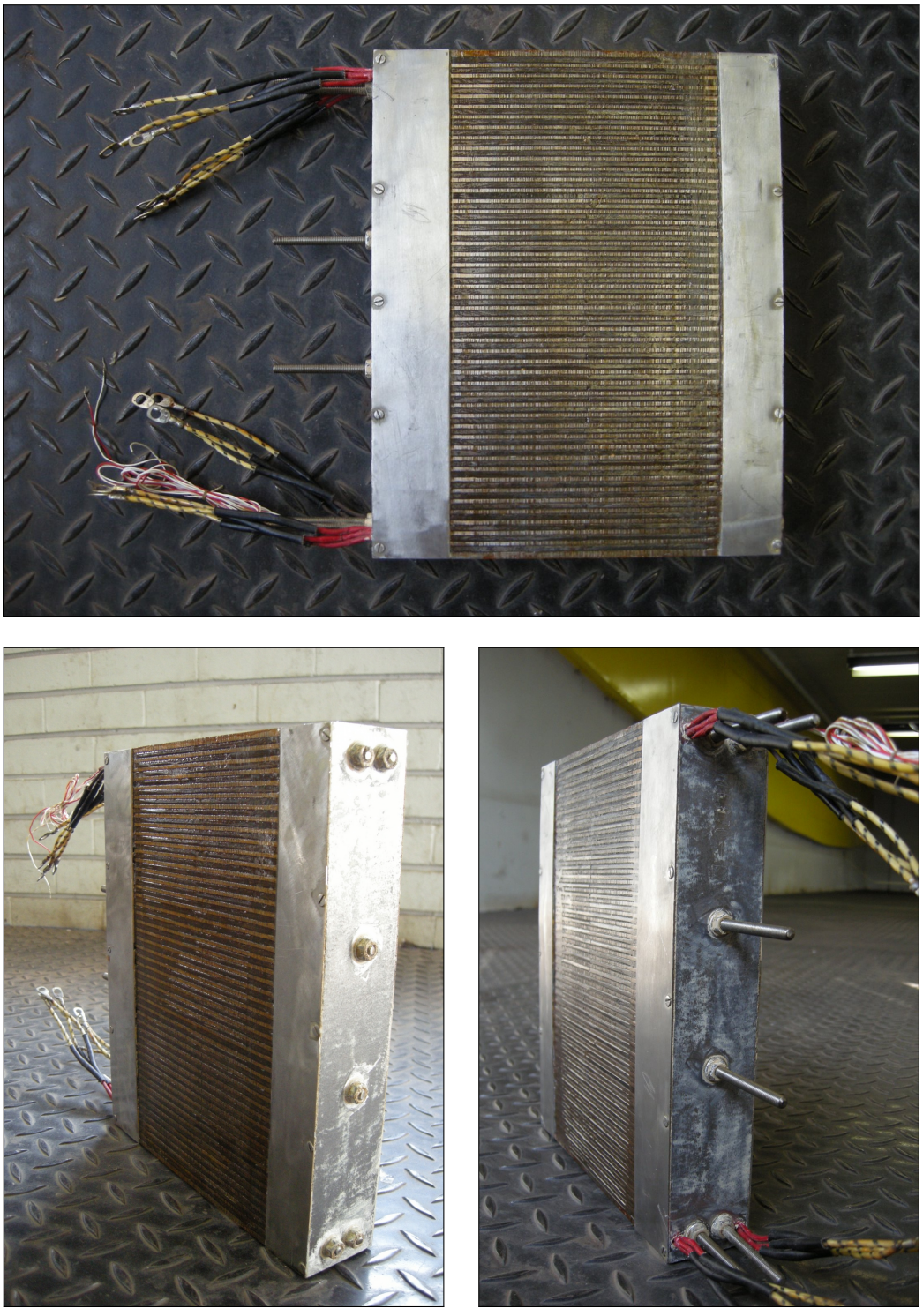

Figure C.6: VPI-insulated stator section after cleaning

formula for a loaded cantilever beam, given by (C.1) [150].

$$x_{\mathrm{z}} = \frac{F_{\mathrm{z}} l_{\mathrm{x}}^3}{3E\mathcal{I}_{\mathrm{yy}}} \tag{C.1}$$

where

x_{z} = deflection in $\hat{\boldsymbol{z}}$ direction

F_{z} = force in $\hat{\boldsymbol{z}}$ direction

l_{x} = length of cantilever in $\hat{\boldsymbol{x}}$ direction

E = Young's modulus

$\mathcal{I}$ = area-moment-of-inertia about the $\hat{\boldsymbol{y}}$ axis

To calculate an appropriate area-moment-of-inertia, it is assumed that the load from each roller is only carried by a rectangular region of the lip (twice as wide as the lip distance) [150]. The area-moment-of-inertia for a rectangular cross-section is thus given by (C.2).

$$\mathcal{I}_{\mathrm{yy}} = \frac{1}{12} w_{\mathrm{y}} d_{\mathrm{z}}^3 \tag{C.2}$$

where

w_{y} = width of cross-section

d_{z} = depth of cross-section

The Young's modulus of 304L stainless steel is 193 GPa [148] and the maximum expected force per roller is taken to be 800 N (refer to section 6.2.1). Therefore, the predicted deflection is only 33 µm for the wider lip, as calculated in (C.3).

$$\begin{aligned} x_{\mathrm{z}} &= \frac{12 F_{\mathrm{z}} l_{\mathrm{x}}^3}{3E w_{\mathrm{y}} d_{\mathrm{z}}^3} \\ &= \frac{12(800)(29{,}5 \cdot 10^{-3})^3}{3(193 \cdot 10^9)(2 \times 29{,}5 \cdot 10^{-3})(6 \cdot 10^{-3})^3} \\ &= 33 \cdot 10^{-6} \end{aligned} \tag{C.3}$$

The corresponding maximum bending stress, σ, is calculated in (C.4) to be 67 MPa. l_{z} is the distance from the neutral surface and thus equal to half of the lip thickness.

$$\begin{aligned}\sigma &= \frac{F_z l_x l_z}{\mathcal{I}_{yy}} \\ &= \frac{12(800)(29{,}5 \cdot 10^{-3})(3 \cdot 10^{-3})}{(2 \times 29{,}5 \cdot 10^{-3})(6 \cdot 10^{-3})^3} \\ &= 67 \cdot 10^6 \end{aligned} \tag{C.4}$$

Since the calculated maximum stress is well below the yield stress for 304L stainless steel (290 MPa [148]), the sections won't permanently distort under the expected loading.

The rails are secured with M8 bolts to the mild steel base plates on the underside of the assembly. Figure C.9 details these base plates. The spacing of the base plates was chosen to match that of the motor test beds in the GENMIN Laboratories at the University.

As shown in figure C.10, the base plates were initially secured to the one 'z'-section rail and the stator sections were then inserted against the rail and supported vertically using temporary spacers.

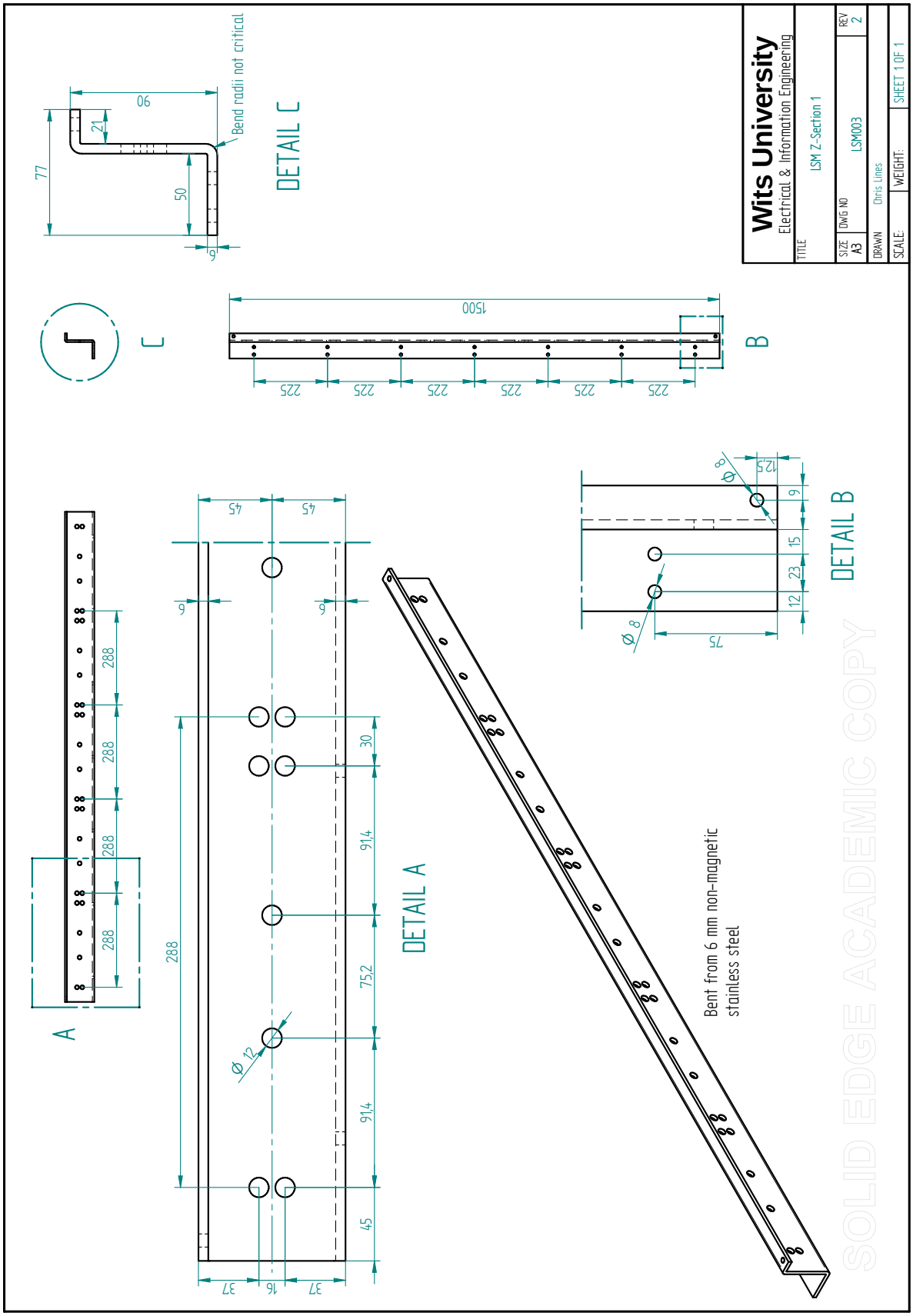

Figure C.7: LSM rail 1

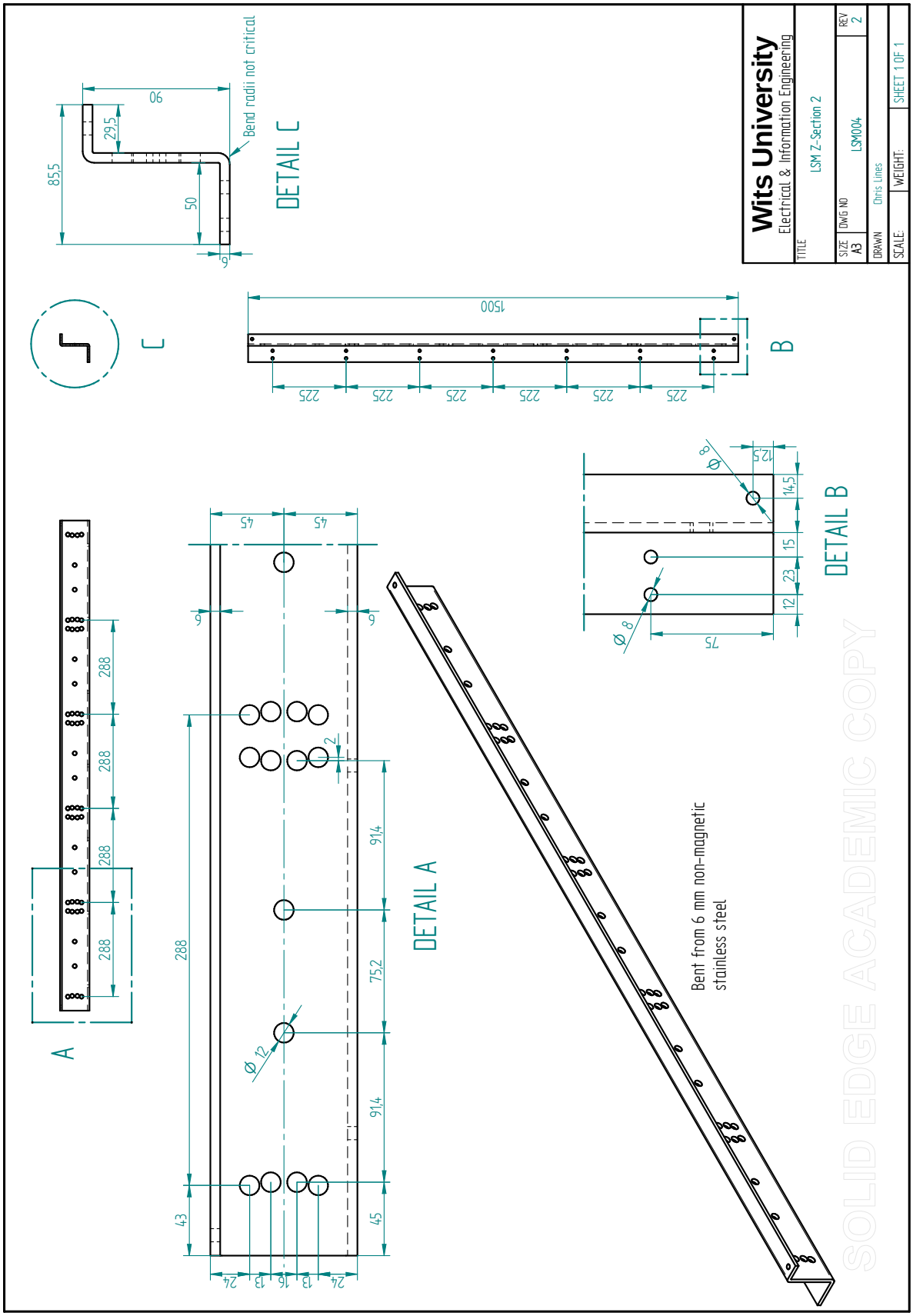

Figure C.8: LSM rail 2

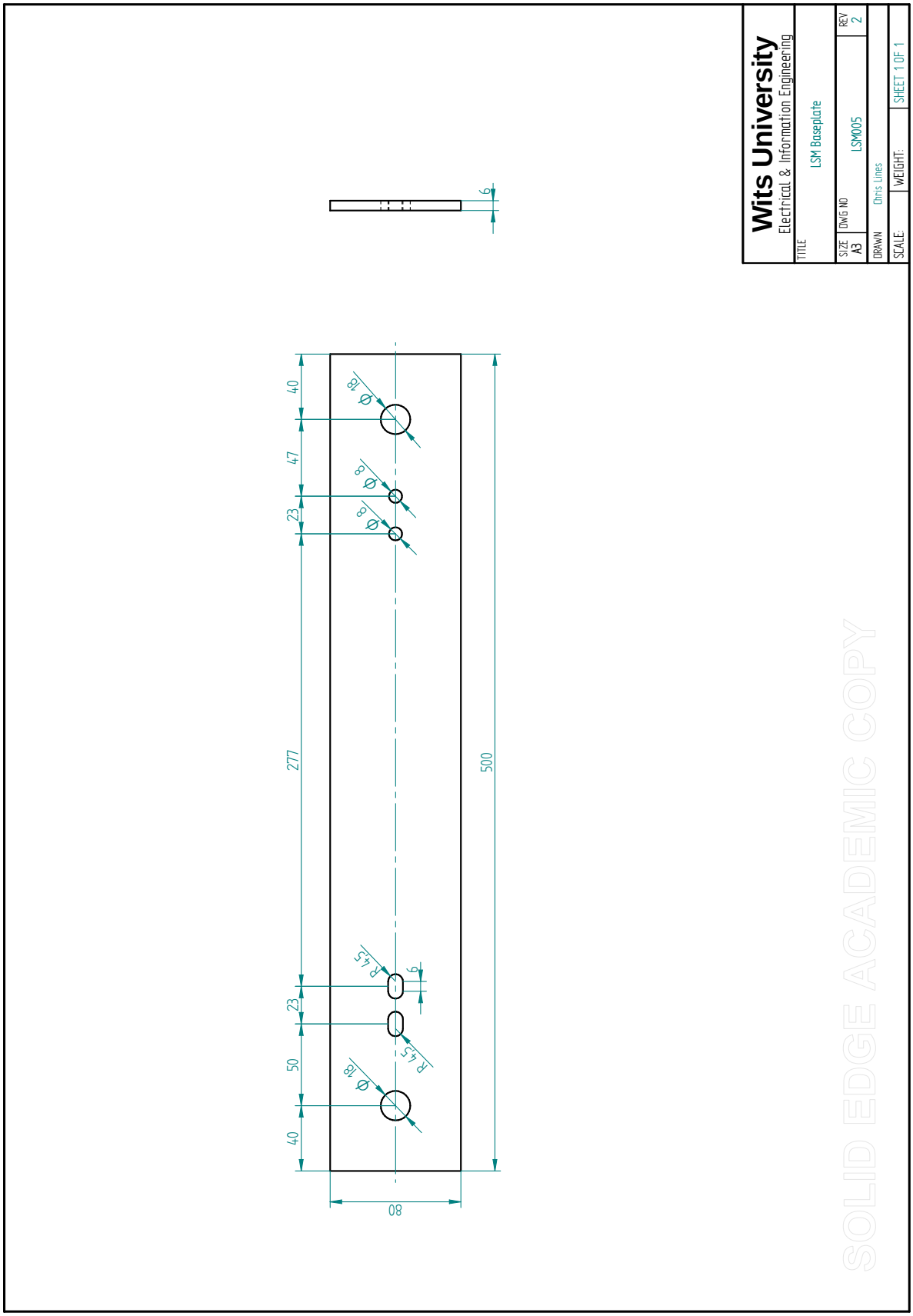

Figure C.9: LSM base plates

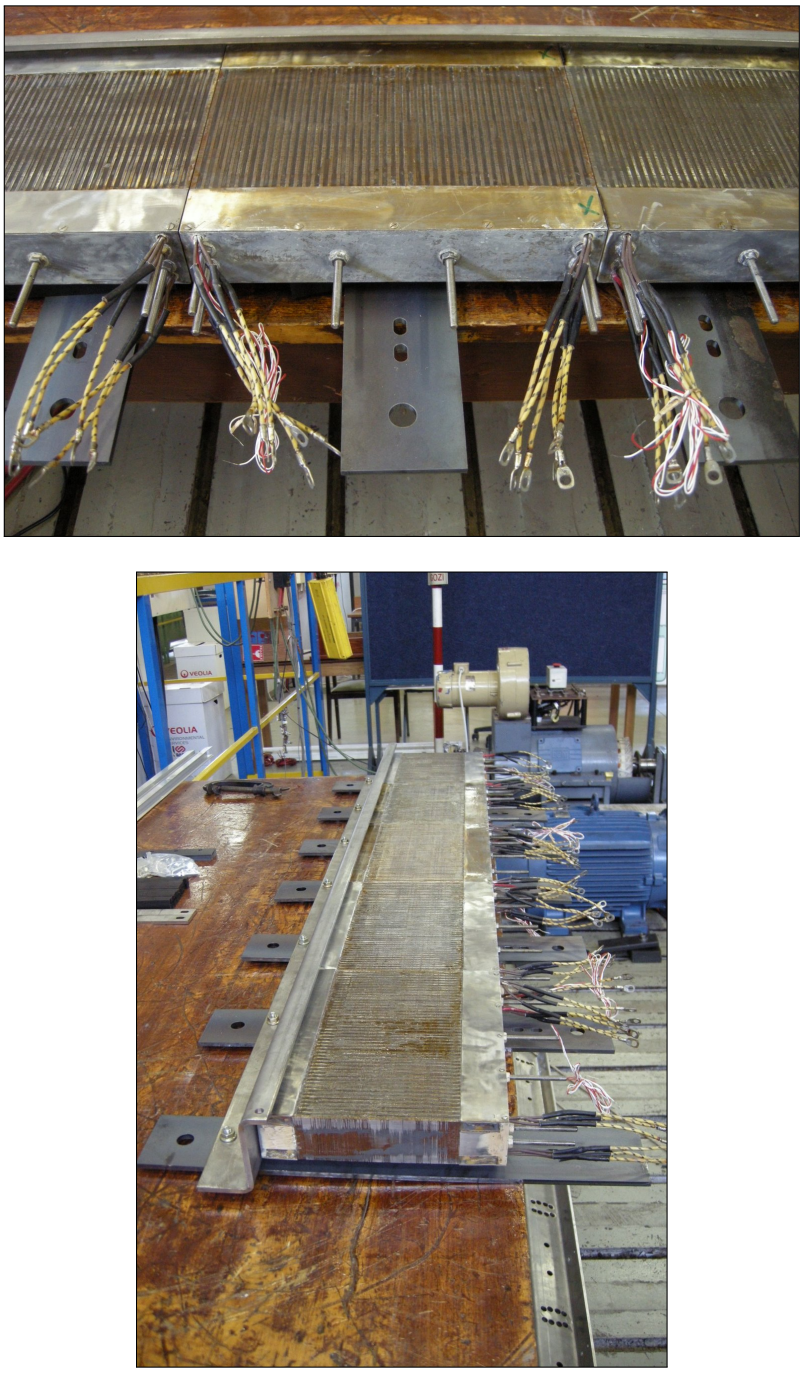

Figure C.10: Aligning the stator sections against the first rail

Once all of the stator sections were aligned and located along the first rail, the second rail was positioned. Care was taken to pass the motor coil and temperature sensor wires through the appropriate holes undamaged and the rail was temporarily clamped in place, as shown in figure C.11.

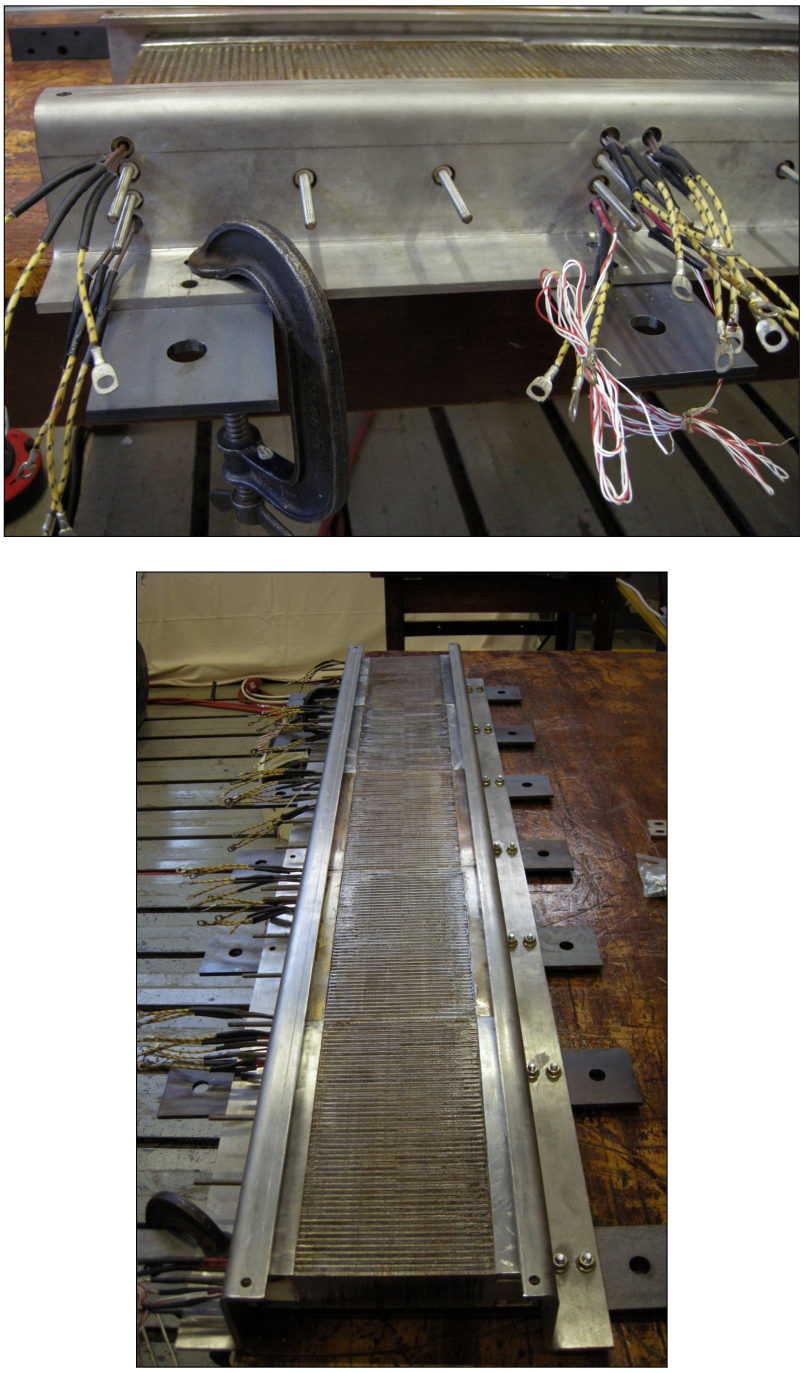

Figure C.11: Fastening the stator sections between the two rails

The two rails were then aligned to be parallel (whilst firmly clamping the stator sections together) before tightening the final bolts through the second rail and the slotted holes in the base plates. Lastly, a second set of M6 nuts were tightened over the protruding threaded rods of the stator sections to prevent any possible lateral movement of the stator sections within the two rails.

As shown in figure C.12, terminal boxes were constructed for each stator section to provide convenient screw terminals for each of the phases and to connect the three-phase windings in a star configuration.

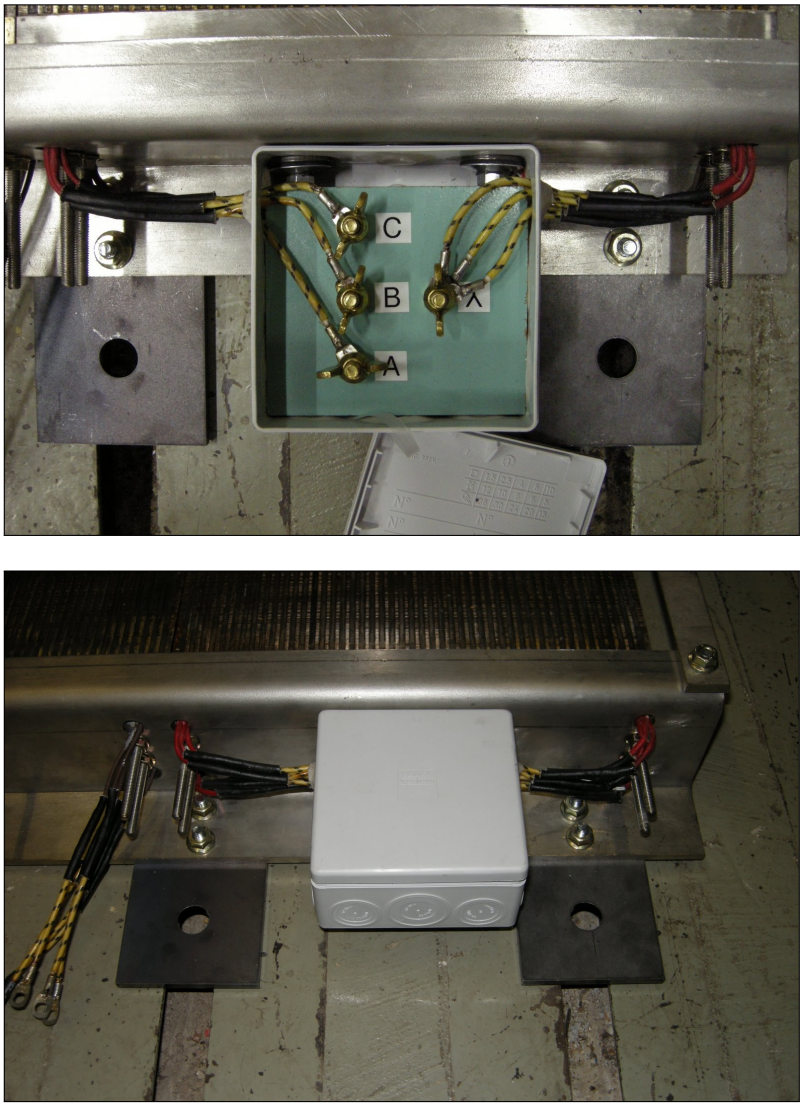

Figure C.12: Stator section terminal boxes

Finally, end stops were secured to the top of the track at each end using M8 bolts. These end stops (detailed in figure C.14 and photographed in figure C.13) also provide mounting points for the coded rail for the Stahltronic® position sensor (see section C.5.3) and act as additional structural members to strengthen the track.

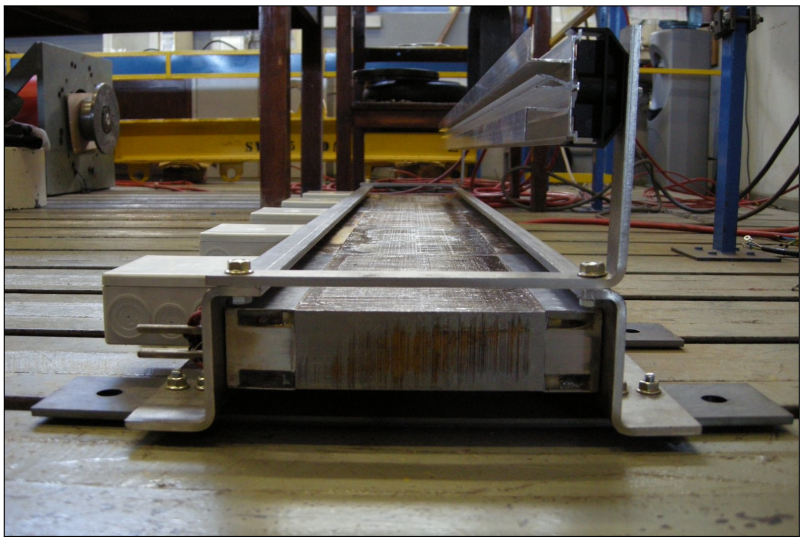

Figure C.13: Stator track with end-stops in place

The fully-assembled stator and track was aligned with the test bed slots (as shown in figure C.15 and bolted down using shims, as necessary, to mount it level.

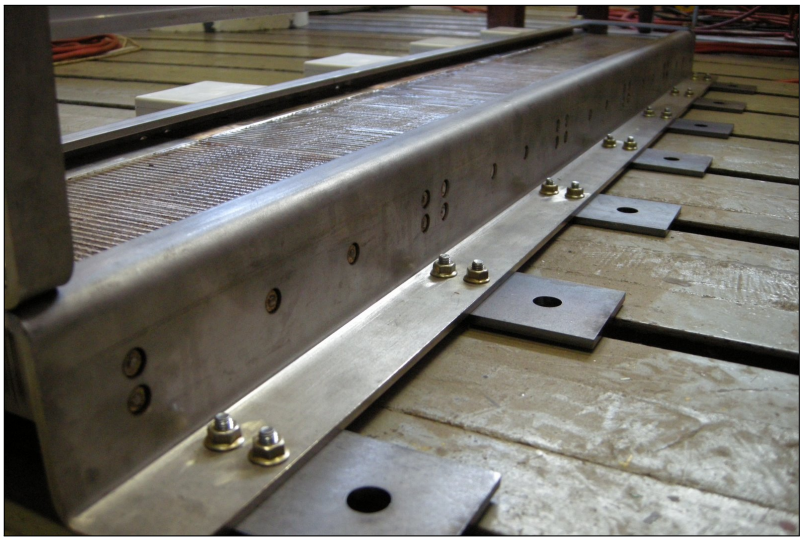

Figure C.15: Stator in position to be bolted to the test bed

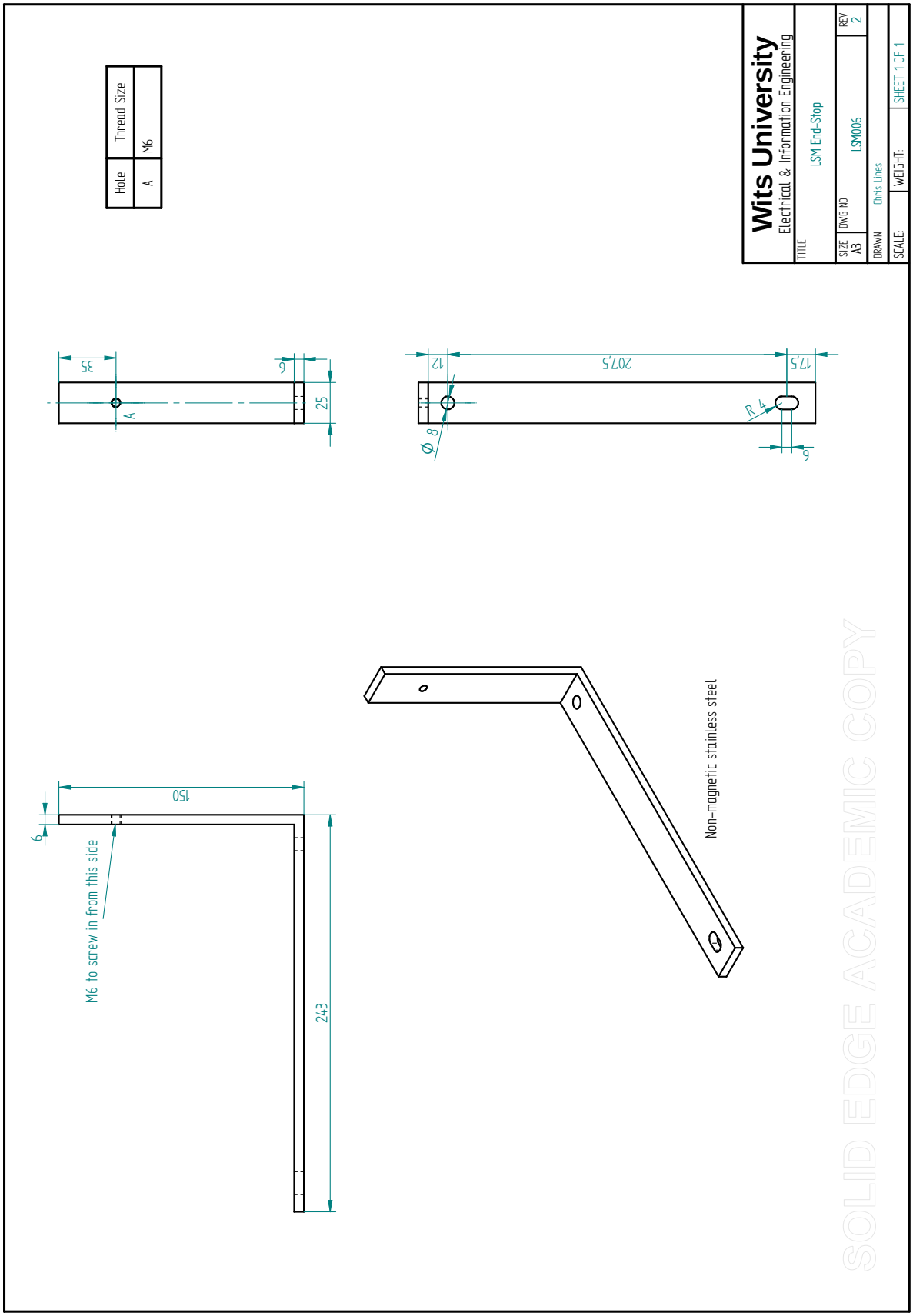

Figure C.14: LSM end brackets

C.1.3 Reaction plate

Back iron

16 mm 300WA rolled steel plate is used as the reaction plate back-iron. Its dimensions are detailed in the drawing provided as figure C.16. Unfortunately, as supplied, the plate was not within acceptable tolerances for this application and so needed to be milled flat, in-house. The final tolerance achieved was within 0,1 mm but the back-iron thickness was consequently reduced to 15,8 mm.

Permanent magnets

Sintered NdFeB permanent magnets form the magnetic poles of the reaction plate. They are manufactured with a nickel plating to protect against corrosion. To be more manageable during assembly, is was decided to construct each magnetic pole as a row of 6 smaller magnets (with dimensions as detailed in figure C.17). Grade 45H magnets are used, which implies that they have a maximum energy product of 45 Mega Gauss Oersted ($\approx$350 kJ/m^3) and are rated for high-temperature use (up to 120 °C).

Spacers

Cuboid nylon spacers (as detailed in figure C.18) were machined to keep the rows of magnets in register and to also eliminate the possibility of the magnets accidentally coming in direct contact with, and attaching themselves to, other metal surfaces (either during assembly or if the rollers were to fail, etc.)

Side and end covers

To contain the magnets and spacers, side and end covers are bolted to the sides of the back-iron using M8 bolts. The side covers (detailed in figure C.19) also have holes to accommodate the rollers and each spacer is secured between the side covers with an M6 nylon countersunk screw at each end. Since the side covers also serve to provide bearing surfaces to keep the reaction plate located within the two rails, the covers are manufactured from Vesconite™, a specialised thermoplastic made from internally lubricated polymers designed for bush and bearing applications [151]. The end covers (detailed in figure C.20) also cater for eye-bolts to be secured to each end of the reaction plate providing a way to attach a rope to the motor and load it.

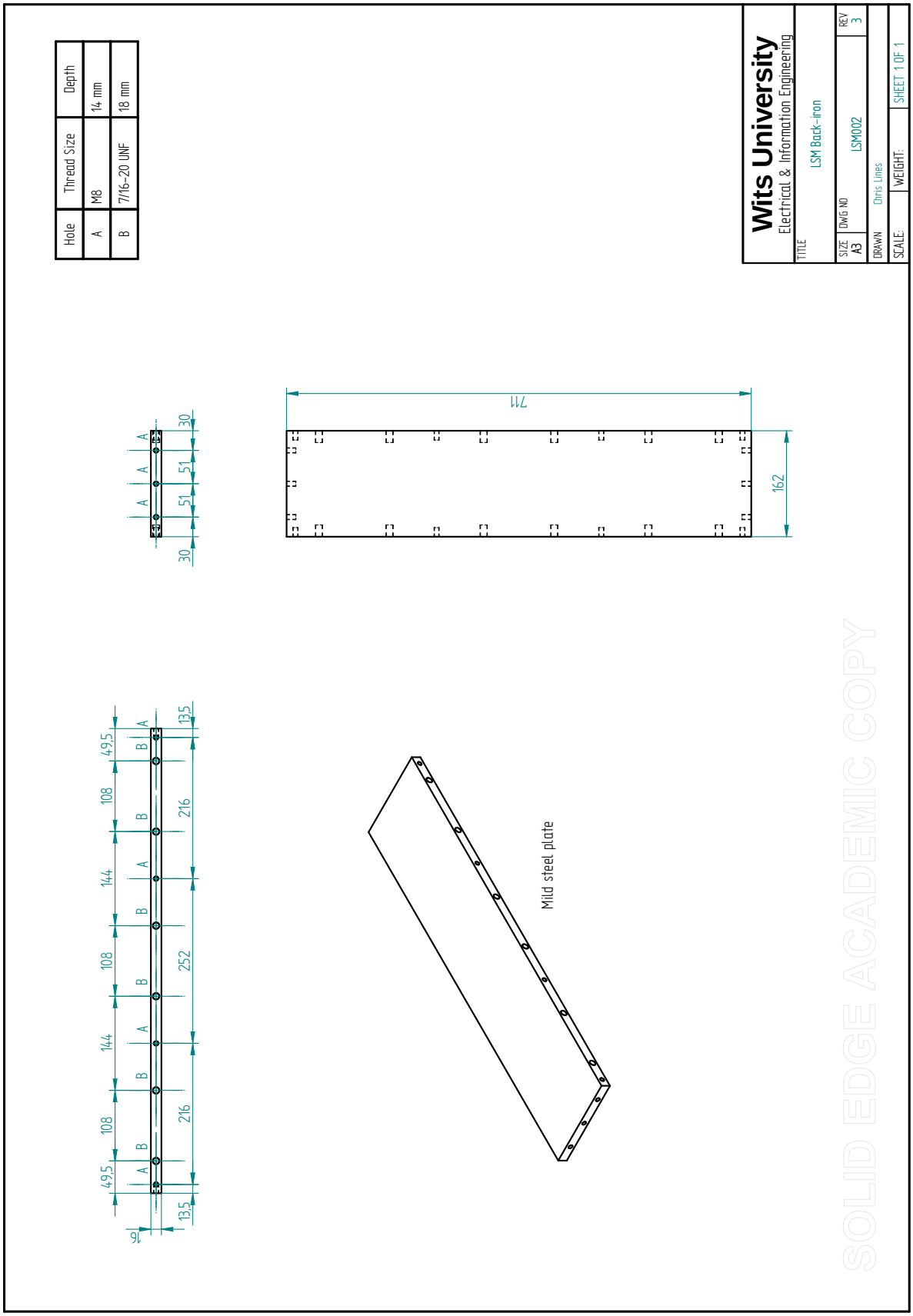

Figure C.16: LSM reaction plate back-iron

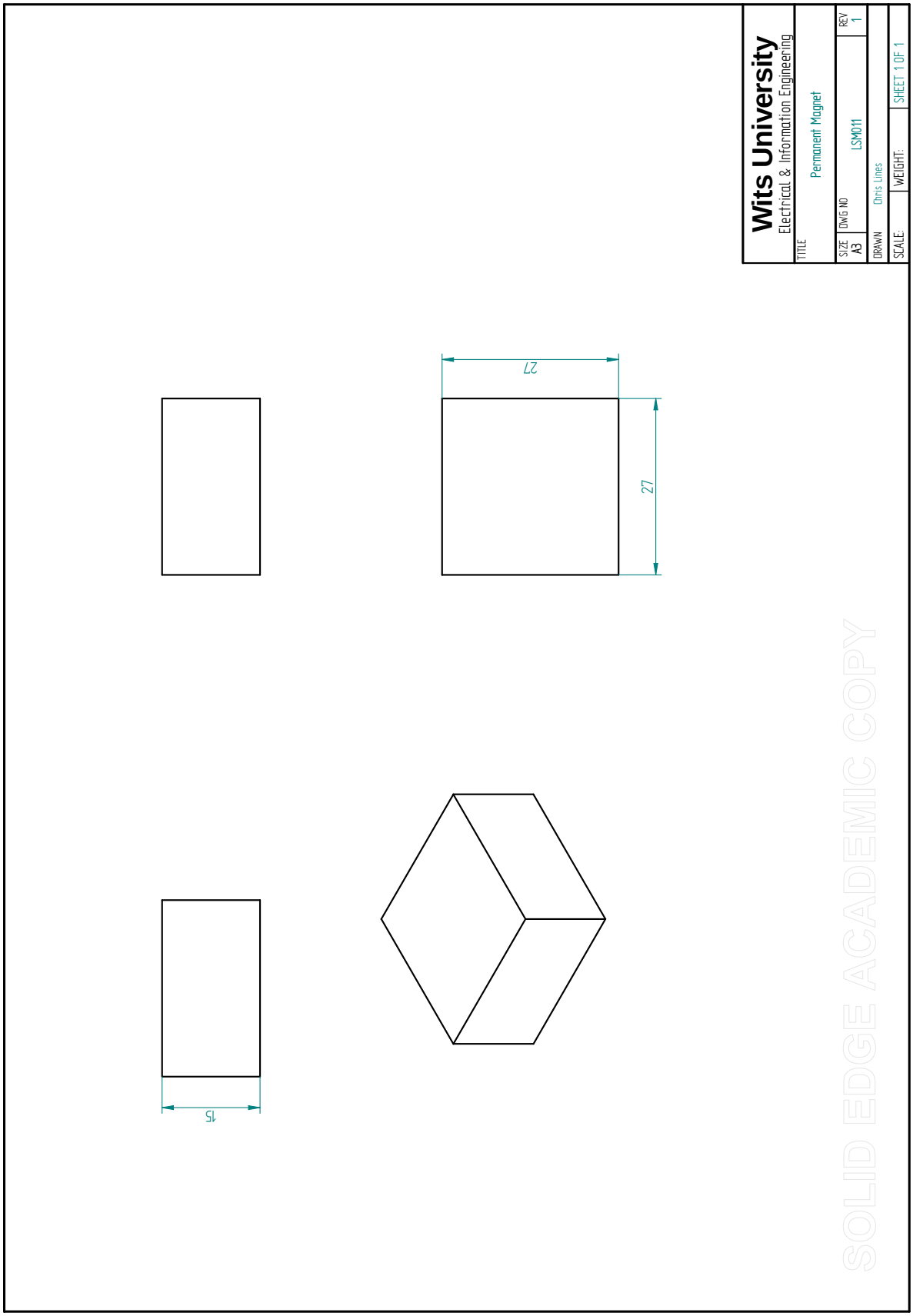

Figure C.17: LSM reaction plate permanent magnets

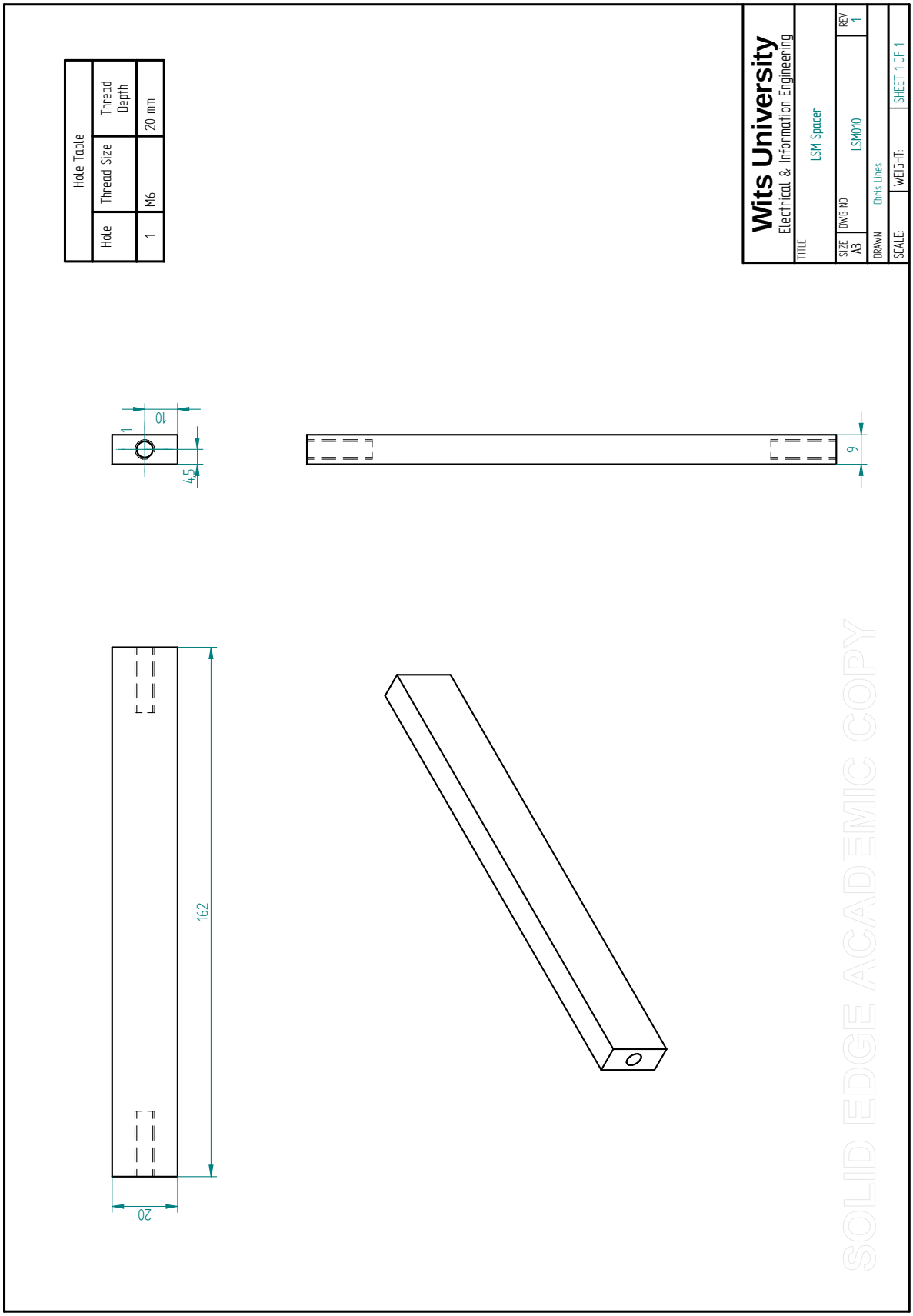

Figure C.18: LSM reaction plate spacers

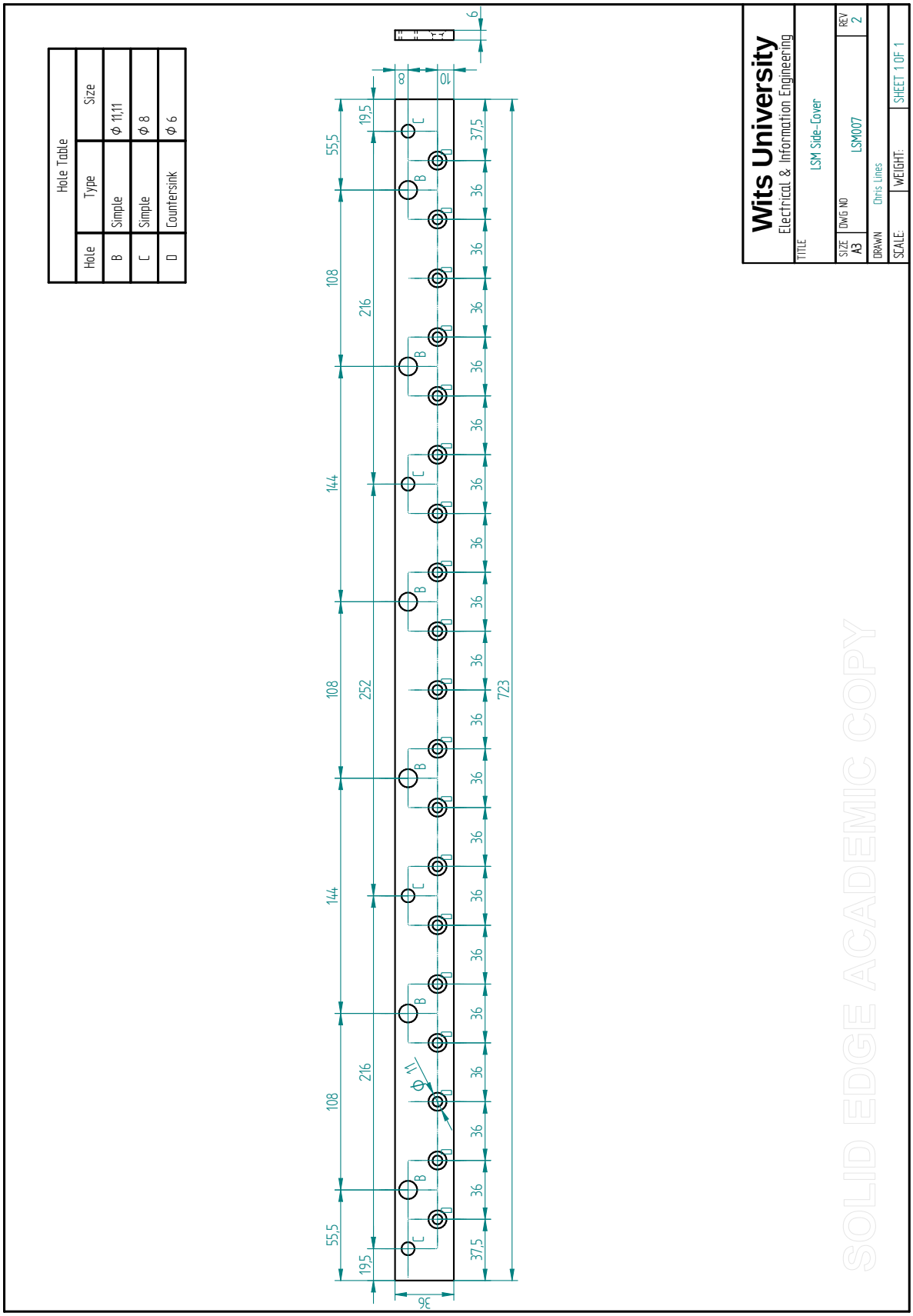

Figure C.19: LSM reaction plate side covers

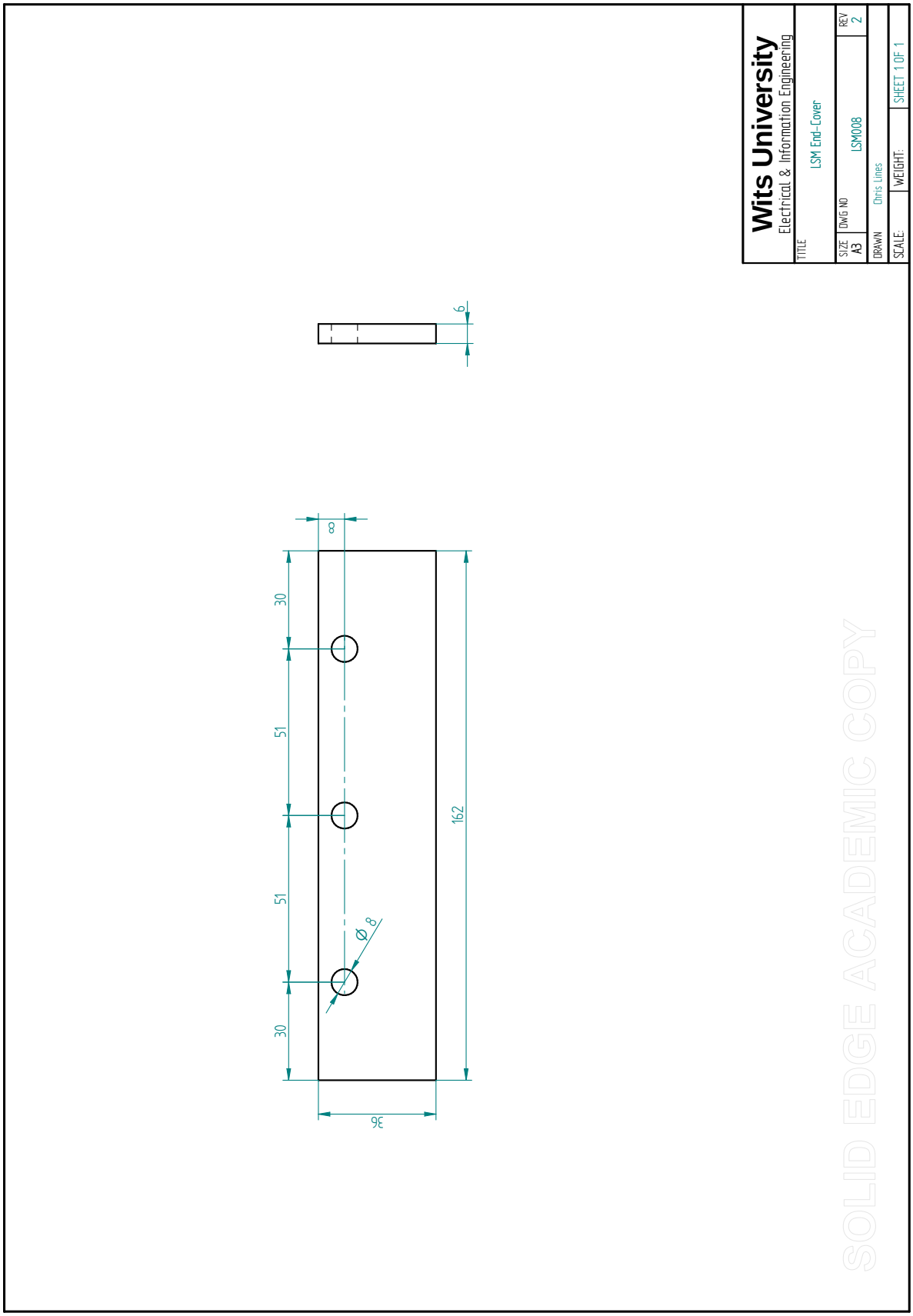

Figure C.20: LSM reaction plate end covers

Rollers

1-inch-diameter RBC Bearings long life cam followers are used to maintain the air-gap between the reaction plate and stator assembly and to achieve a low-friction guidance mechanism. The calculated maximum force per roller is only 800 N (as determined in section 6.2.1), which is well below the maximum allowed load of 1400 lbf (= 6,2 kN) [152].

Since it is impossible to eliminate all possible misalignment, the track surface is periodically lubricated with silicon oil to prevent excessive wear to the centre thrust rings of the rollers.

Assembly

To begin with, the desired magnet and spacer positions were precisely marked out on the back-iron using 'marking blue' and a scriber. Next, as shown in figure C.21, the side covers and two spacers were secured to check that everything aligned correctly.

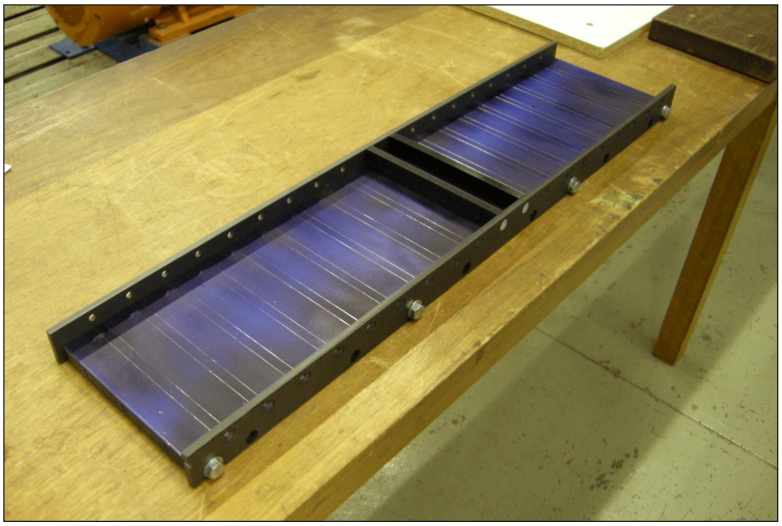

Figure C.21: Back-iron with side covers and two spacers

In order to position the magnets, the one side cover was temporarily removed and, as shown in figure C.22, pieces of wood were clamped in place to cover the surrounding back-iron. This was to avoid any chance of the magnets attaching themselves to other magnets or the back-iron in the wrong location. A piece of wood was also clamped over the top of the two adjacent nylon spacers to form a narrow slot to slide

Figure C.22: Back-iron with protective pieces of wood

Figure C.23: Back-iron with first row of magnets

the magnets into. This was necessary because, when placing subsequent magnets, they had a tendency to try and flip over before attaching to the back-iron because of their like magnetic poles repelling.

The magnets even repel each other in their final locations but the friction force (due to their high attractive force towards the back-iron) is what keeps them in place. In fact, as can be seen in figure C.23, when placing the first row of magnets, this attractive force was not sufficient for the magnets to stay right next to each other. It was only once the second row of magnets was added that the friction force was sufficiently high to keep them all in place.

Figure C.24: Procedure to add each subsequent row of magnets

Figure C.25: How each magnet was tapped towards the back-iron and then along to its final position

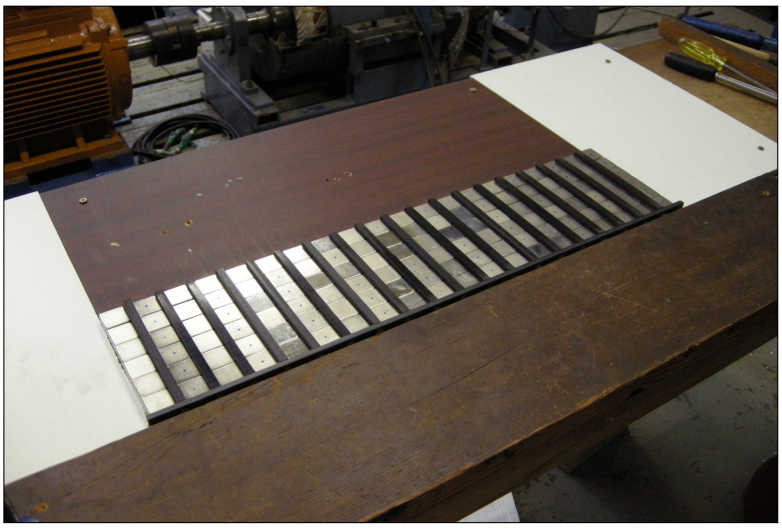

Figure C.26: Back-iron with all magnets in place

Figures C.24 and C.25 show how each subsequent row of magnets was added. The north pole of each magnet was first determined using a Gauss meter and marked with a blue dot. Then, the magnet was placed with the correct orientation within the channel formed by the pieces of wood. It was then gently tapped towards the back-iron until it was drawn onto and attached itself to the back-iron and then further tapped along the back-iron to its final position. Figure C.26 shows the reaction plate with all the magnets in place.

Next, the remaining side cover and end covers were secured to the back-iron and to the spacers. Lastly, the cam followers were screwed into the back-iron with lubricated threads and torqued to the maximum specified clamping torque of 12 N·m ($\approx$ 100 in·lbf). A photograph of the complete reaction plate is provided as figure C.27.

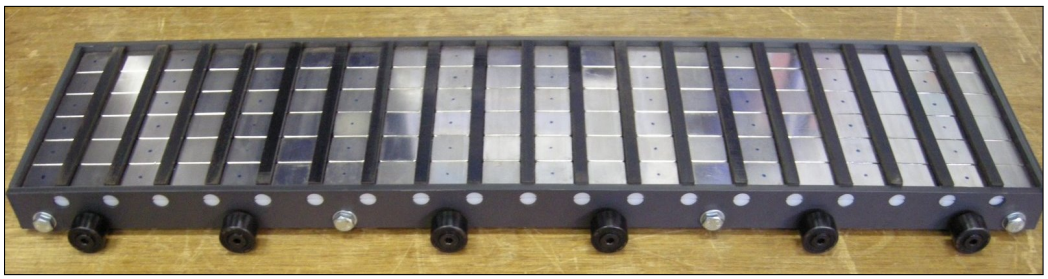

Figure C.27: Fully-assembled reaction plate

Table C.1 gives magnetic field strength readings obtained with a Gauss-meter probe placed in the centre of each magnet for the first few poles of the reaction plate. It demonstrates the consistency of the resulting magnetic field.

Table C.1: Measured magnetic field strength over a portion of the reaction plate [Gauss ($= 1 \cdot 10^{-4}$ T)]

560	-608	586	-609	616	-606	···
537	-608	581	-606	588	-603	···
540	-600	582	-598	581	-589	···
537	-605	581	-586	582	-588	···
526	-616	586	-588	586	-604	···
564	-630	593	-593	608	-626	···

Placing the reaction plate on the track

Figure C.28 shows how the assembled reaction plate was placed on the track using a crane. Firstly, the stator surface was protected with a strip of 3 mm plyboard. Then, the reaction plate was lifted using the crane (with due care to keep the magnets sufficiently far away from the metal shackles, etc.) and positioned, hanging vertically, over the track. The reaction plate was then lowered until the two eye-bolts on its one end were resting on the stator. It was then slowly lowered into place within the rails, pivoting on the eye-bolts until the rollers came in contact with the rails. A drawing showing an end-on view of the entire motor assembly is provided in figure C.29.

Figure C.28: Reaction plate being placed on the track using a crane

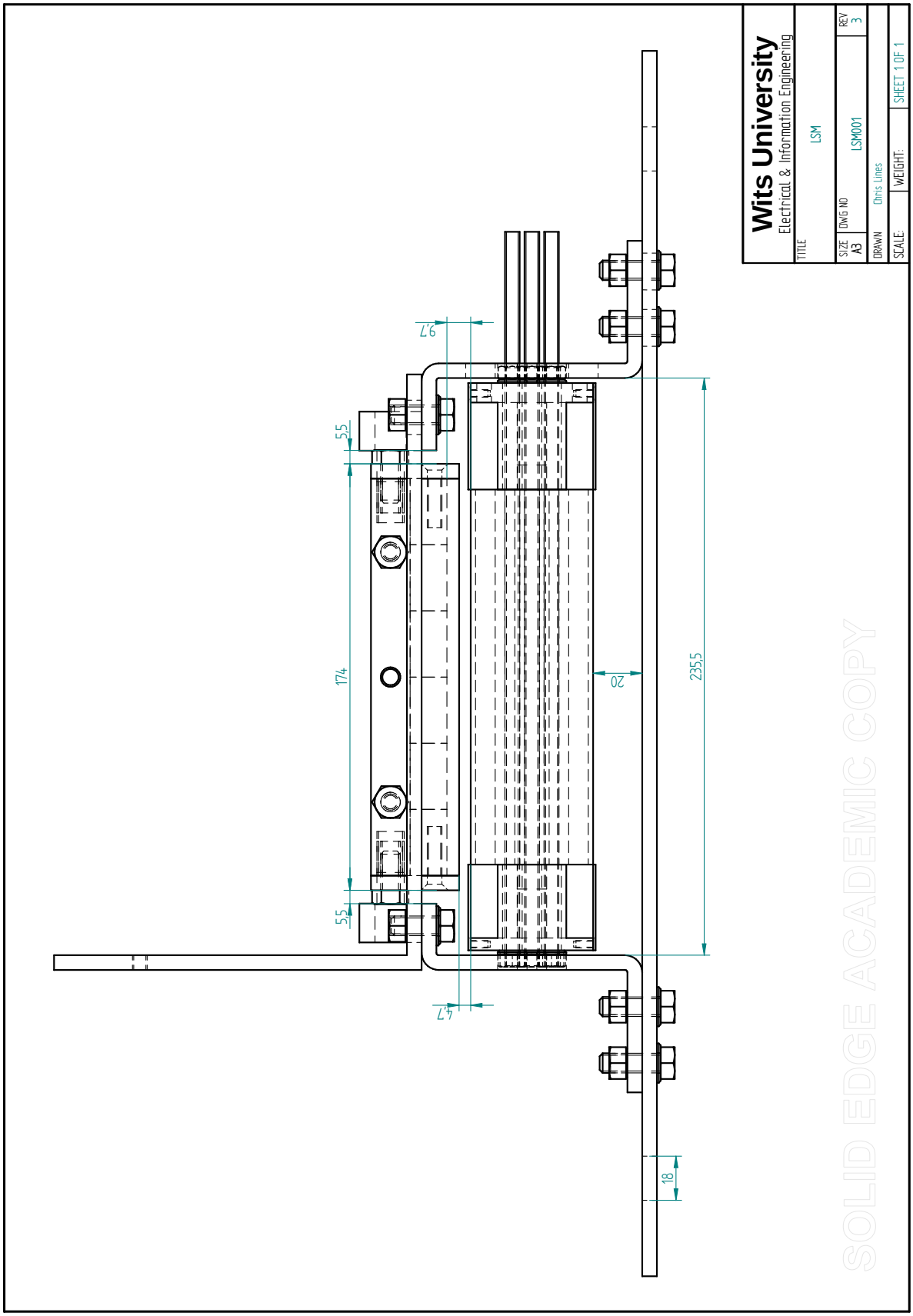

Figure C.29: LSM assembly (end view)

C.2 Inverter and interfacing circuitry

C.2.1 Inverter

A SEMIKRON® SEMITOP Stack (SKS 21F B6U+E1CIF+B6CI 12 V12) three-phase inverter is used. It comprises a three-phase rectifier, dc-link capacitor bank, a two-level three-phase IGBT inverter, IGBT chopper for an external brake resistor and Hall-effect current sensors for two of the phases. It is an ideal research hardware platform because it gives complete flexibility in terms of the inverter switching, yet handles the complexity of correctly driving the IGBT gates and provides the necessary protection (interlocks ensure that the top and bottom legs of a particular phase are not switched on simultaneously, etc.). Photographs of the unit are shown in figure C.30.

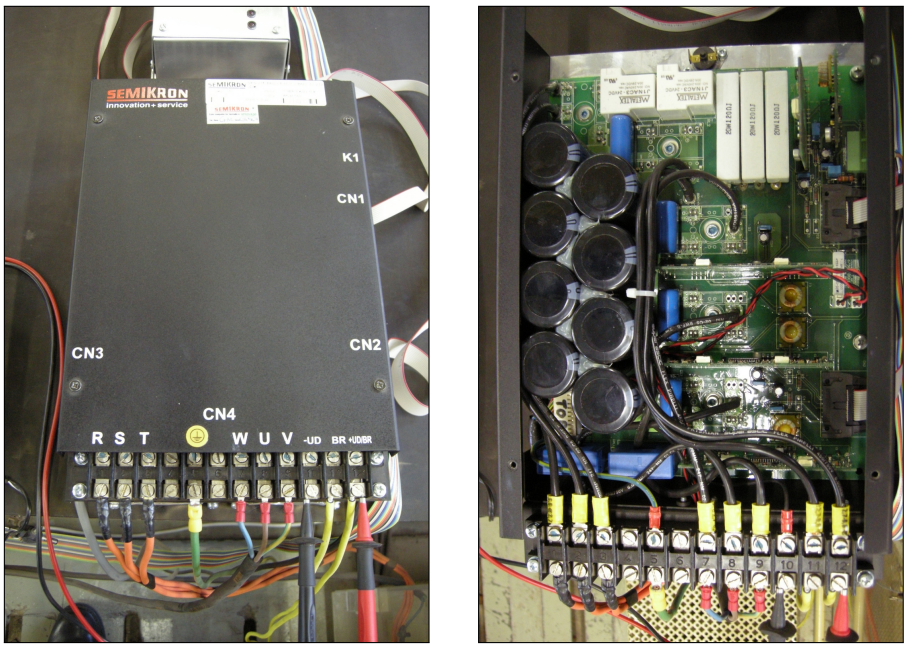

(a) closed **(b)** with cover removed

Figure C.30: SEMISTACK inverter unit

The supply voltage to the three-phase rectifier (and hence the DC bus voltage) is controlled using a variac. A 56 Ω 'brake resistor' is also connected to prevent the DC bus voltage from climbing under regenerative operation. The 'brake resistor' is switched in across the DC bus capacitance using an IGBT, as necessary, because power cannot flow back through the rectification bridge to the supply. Figure C.31 is a photograph of the variac and resistor.

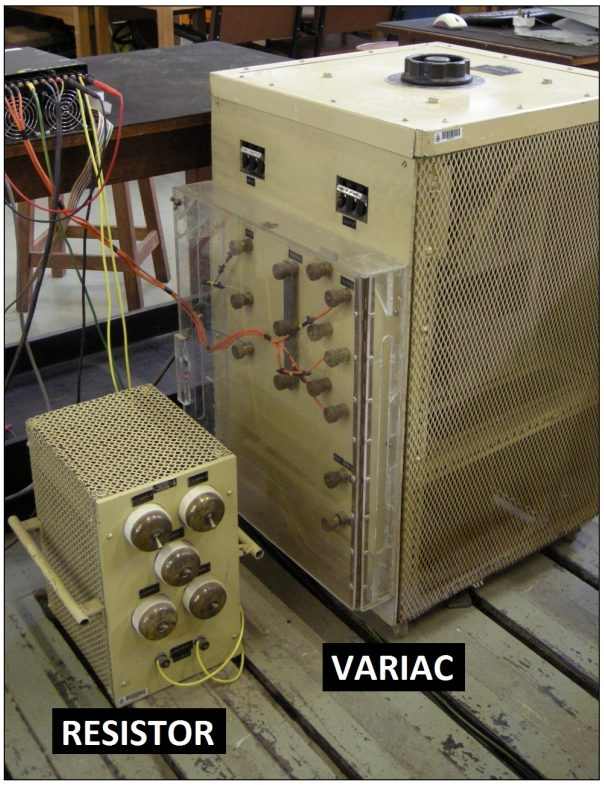

Figure C.31: Three-phase variac and brake resistor

C.2.2 Interfacing circuitry

A custom interface circuit was used between the SEMIKRON SEMISTACK and the dSPACE® DS1104 real-time controller board. It was designed and built by Mikail Ansari, an MSc (Eng) candidate at the University. This circuitry is required because dSPACE is only compatible with TTL voltage levels (0 V to 5 V), whereas the SEMISTACK uses CMOS voltage levels (0 V to 15 V). In addition to level-shifting, the circuit provides galvanic isolation and a latching emergency override mode to turn off all of the IGBT gate signals, regardless of the dSPACE outputs. The circuit allows dSPACE to set the 6 IGBT gate signals (3 top and 3 bottom legs of the inverter bridge) from its designated space-vector PWM outputs and monitor whether the SEMISTACK has detected an error condition via a digital input. Furthermore, it allows a dSPACE digital output to switch in a brake resistor to control the dc bus voltage under regenerative braking. The interface circuit was designed to be suitable for a range of SEMIKRON® SEMISTACK products and thus provides two sets of connectors to match either of the two possible SEMISTACK configurations.

Figure C.33 is a photograph of the interface circuit (mounted in an aluminium

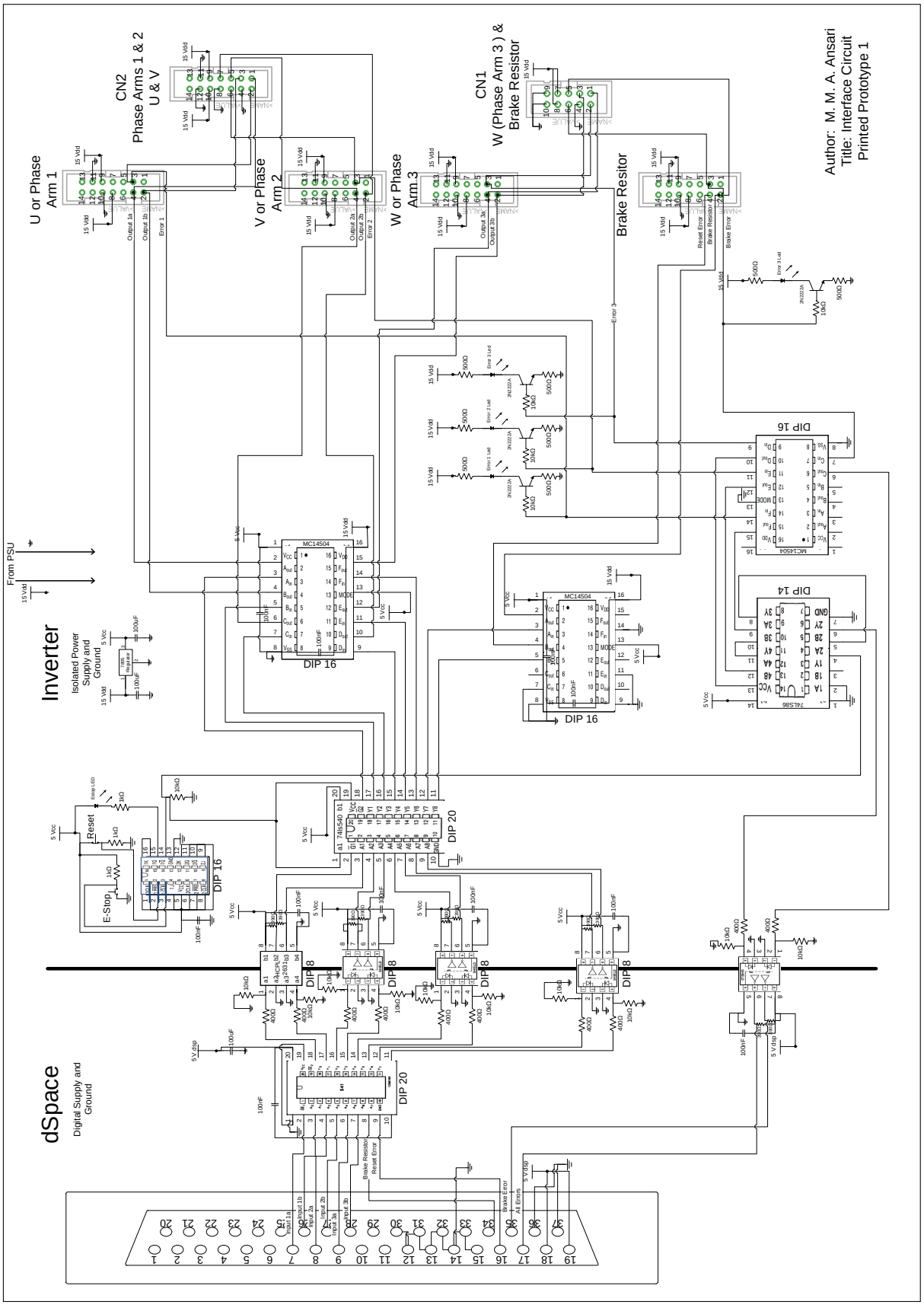

Figure C.32: SEMISTACK / dSPACE interface circuit

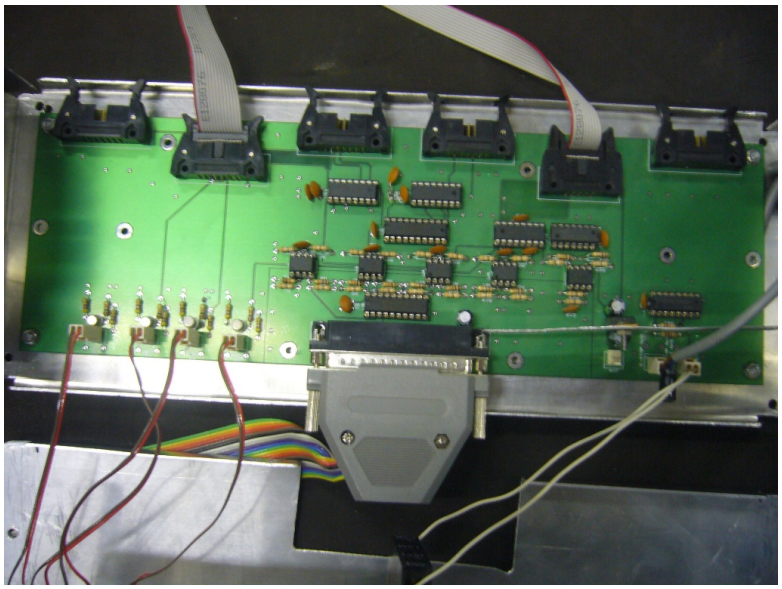

Figure C.33: SEMISTACK / dSPACE interface circuit

housing) and figure C.32 is the circuit schematic. The output transition times are in the order of 100 ns [153], which does not place a significant limitation on the minimum PWM duty cycle, considering that the chosen PWM period is 100 µs (10 kHz). The small propagation delay is of no consequence since it does not affect the resulting PWM duty cycle.

C.3 Solid-state contactors and interfacing circuitry

C.3.1 Contactors

POWER-IO™ DDA-6V75 solid-state contactors are used. They have a peak blocking voltage of 1200 V, built-in I^2T fuses, overtemperature auto-shutdown, oversized thyristors for high inrush capability and are DC activated [154]. These 75 A units are grossly overrated for the prototype application. However, they were spare from a previous application and so readily available. A photograph of one of the contactors is shown in figure C.34. A built-in snubber restricts the voltage rise-time to below 1000 V/µs and hence ensures that false triggering of the thyristors does not occur.

Figure C.34: POWER-IO™ DDA-6V75 solid-state contactor

As shown in figure C.35, the ten contactors (two for each stator section) were mounted on DIN rails within a cabinet. Figure C.36 is the corresponding wiring diagram.

Figure C.35: Solid-state contactors housed within cabinet

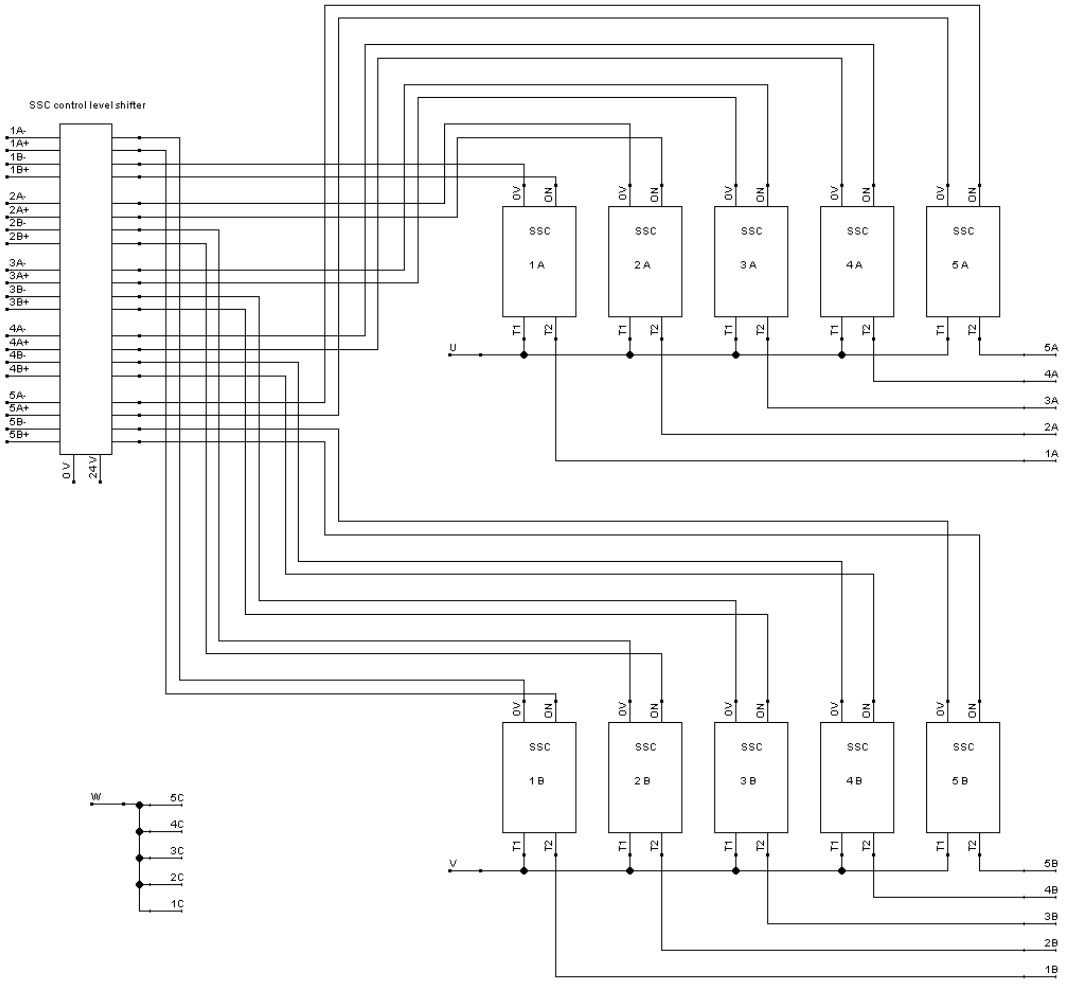

Figure C.36: Solid-state contactor wiring

C.3.2 Interfacing circuitry

ICL6776 dual-driver ICs are used as a buffering stage between the dSPACE digital outputs and the contactor control inputs. They are necessary to source the required current per contactor input of 6 mA to 9 mA [154]. The 24 V supply is regulated down to 15 V so that it is within the ICL6776's allowable range. Pull-up resistors are used on the input side to ensure that the outputs to the contactors remain low (off) if the inputs are disconnected or dSPACE is off. The required transistor-transistor logic (TTL) 'high' reference is created using a 4,7 V Zener diode.

The circuit diagram is included as figure C.37 and the Veroboard layout as figure C.38. Figure C.39 is a photograph of the circuit, as built.

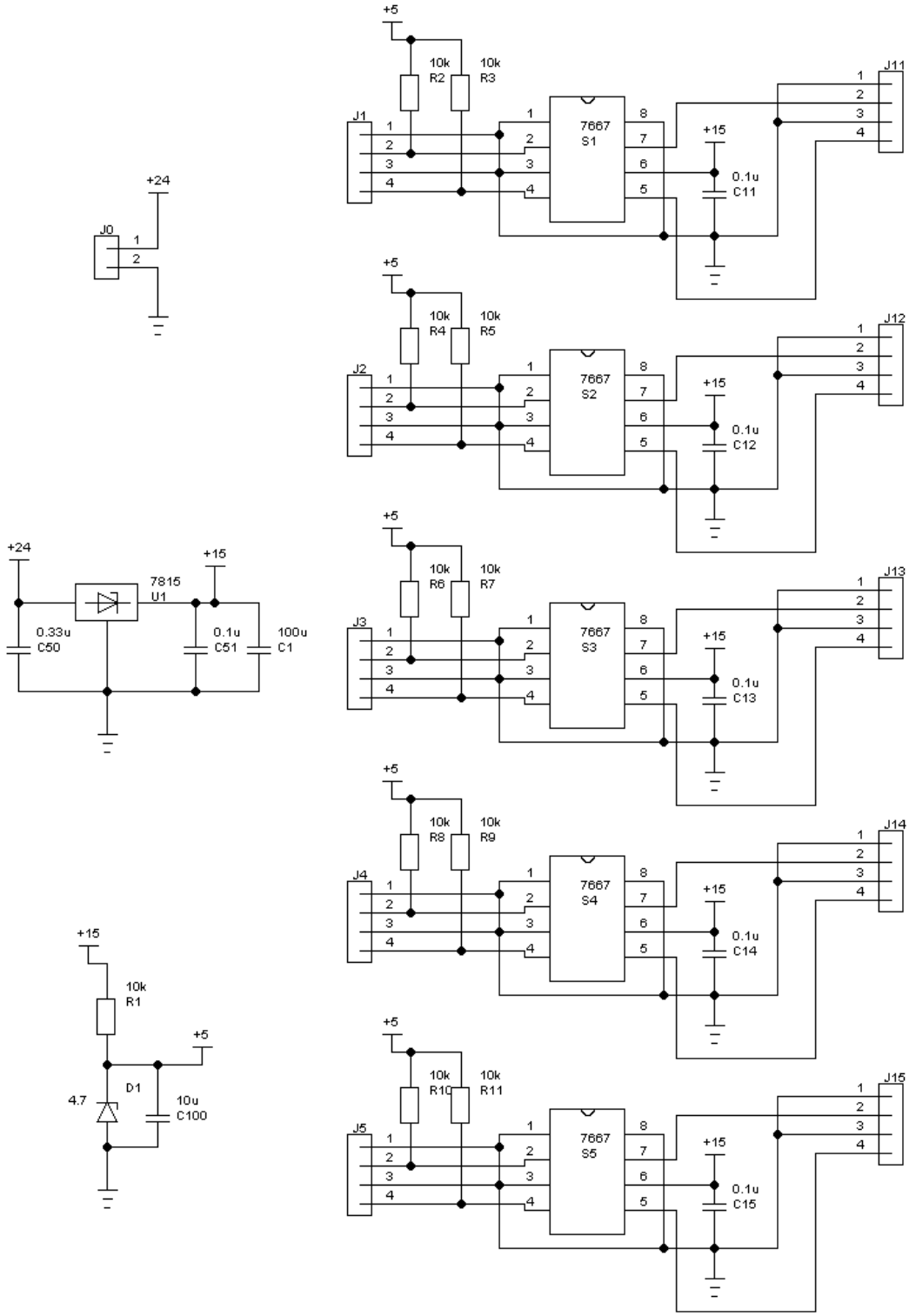

Figure C.37: Solid-state contactor interface circuit

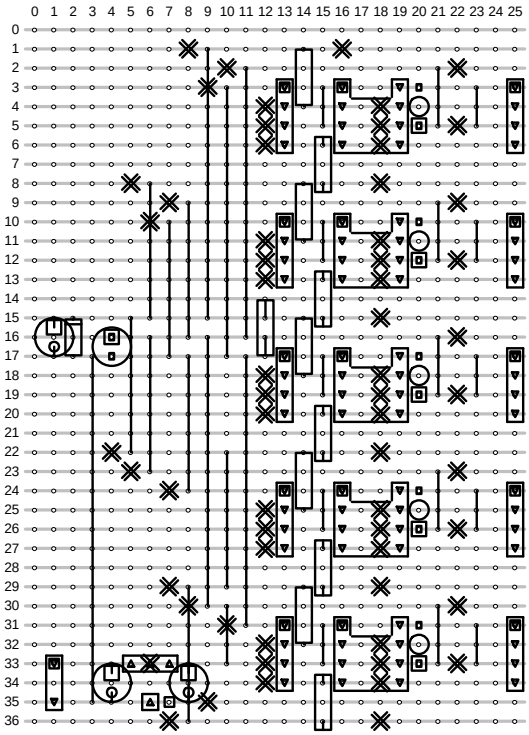

Figure C.38: Veroboard layout of solid-state contactor interface circuit

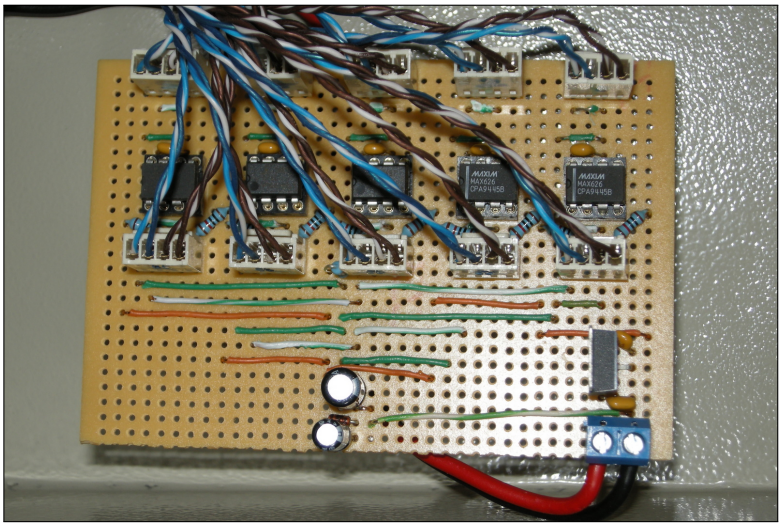

Figure C.39: Solid-state contactor interface circuit

C.4 Auxiliary switchgear and wiring

The SEMISTACK inverter is connected to its three-phase supply and the 220 V supply is turned on using a primary contactor (three phases and an additional normally-open contact). As shown in the wiring diagram, included as figure C.40, the primary contactor is turned on with a rotary switch but its coil is also connected in series with one of the normally-closed terminals of the push-button emergency stop (e-stop). Thus, if the e-stop button is depressed, it releases. The e-stop button also provides two other normally-closed contacts – one to provide an emergency signal to dDSPACE ('ES1') and one to provide an emergency signal to the inverter interfacing circuitry ('ES2'). The primary contactor also signals its state to dSPACE via a normally-closed connector (signal 'OFF'). Figure C.41a is a photograph of the primary contactor.

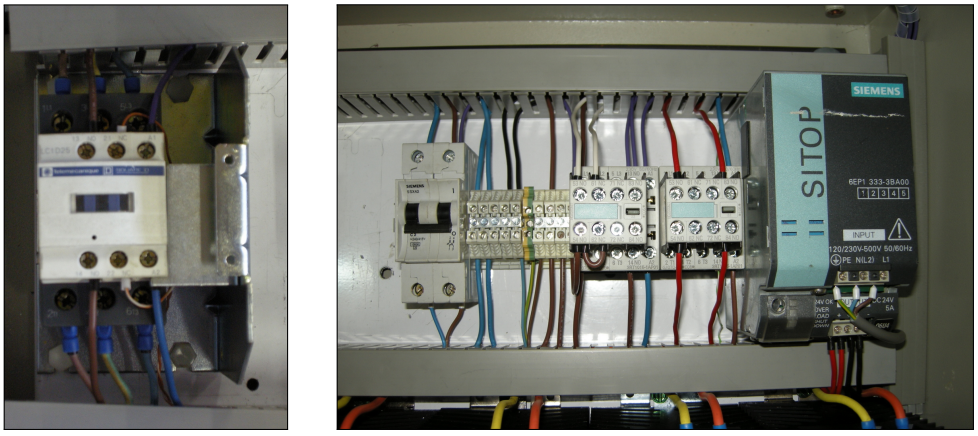

(a) Primary contactor **(b)** Secondary contactors and 24 V power supply

Figure C.41: Auxiliary switchgear

A second contactor is connected to two illuminated push-buttons (green and red) and wired in a self-latching configuration. When the contactor is 'off', the red button illuminates and, when the green button is pushed, the contactor latches 'on' and the green light illuminates. If the red button is pushed, the contactor releases. When the contactor is 'on', it powers the coil of a third contactor to close three normally-open contacts – one to provide dDSPACE with an 'ON' signal and two to provide a 24 V supply to the solid-state contactor interfacing circuits and the inverter. The two secondary contactors and 24 V power supply are shown in figure C.41b and figure C.42 shows the connections to the e-stop and illuminated buttons on the back of the cabinet door.

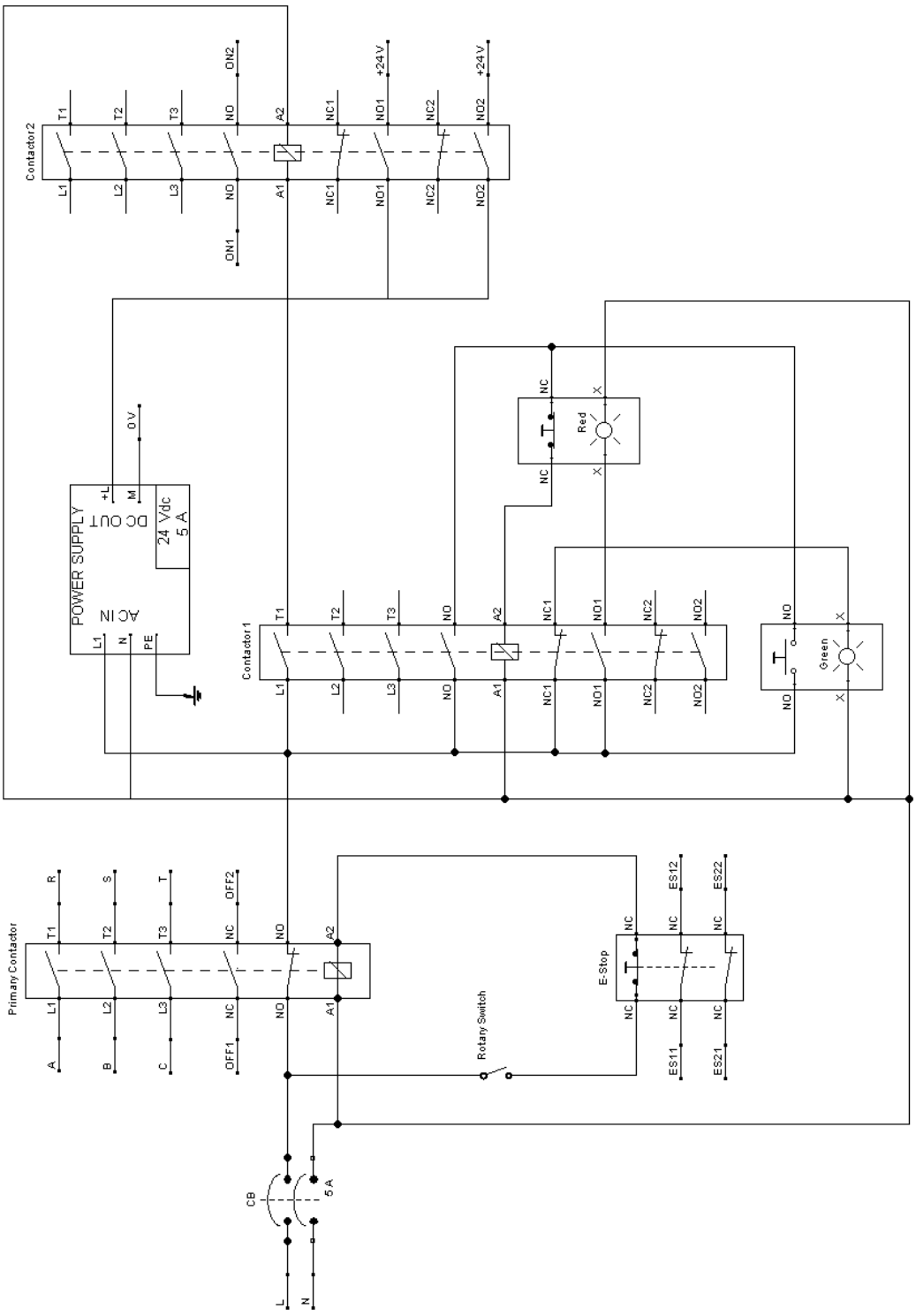

Figure C.40: Auxiliary switchgear and wiring

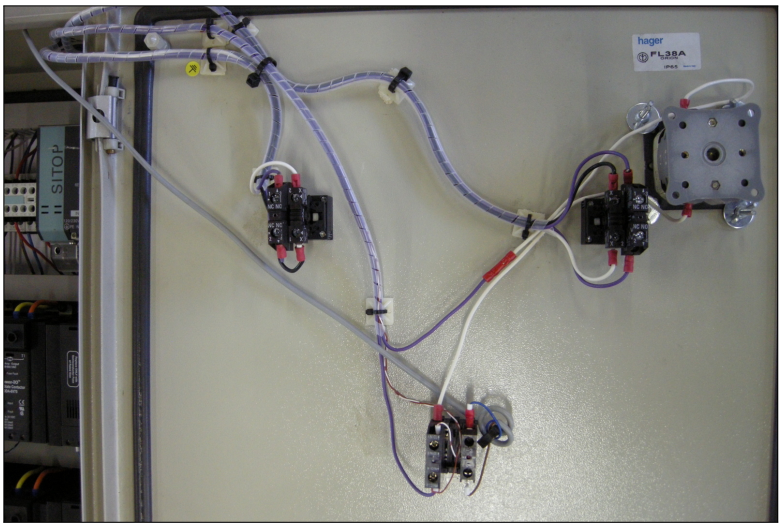

Figure C.42: Back of cabinet door

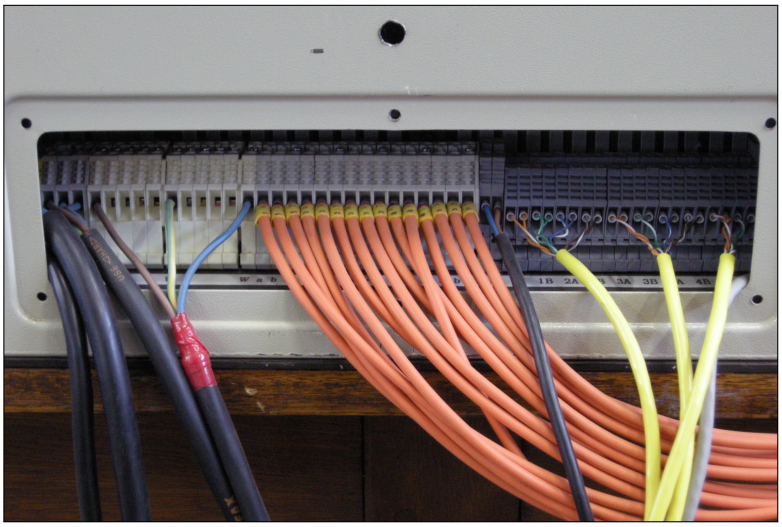

Figure C.43: Cabinet terminals

The three contactors, 24 V power supply and illuminated push buttons are fed with a 220 V ac supply that is protected with a 5 A circuit breaker. All of the auxiliary switchgear and the 24 V power supply unit are housed in a cabinet, together with the solid-state motor contactors. Figure C.43 is a photograph showing how all of the connections to the components housed in the cabinet are made through terminal blocks, mounted at the one end of the cabinet.

C.5 Measurement

C.5.1 Inverter DC bus voltage

The SEMISTACK's dc bus voltage is measured using an ELDITEST Electronic GE8115 differential voltage probe providing a 100:1 scaled output, with a bandwidth of 20 MHz and accuracy of ±3 %. The probe output is connected to dSPACE's analogue input ADC7.

C.5.2 Stator currents

The SEMIKRON SEMISTACK comes packaged with two LEM® LA 55-P close-loop current transducers to allow for a measurement of the phase a and phase b output currents. It is only necessary to measure two of the three phase currents since the three phase currents must sum to zero because there are no other return paths for the current. Since the transducers are current sources, it is still necessary to connect an appropriate measurement/shunt resistor to each of their outputs to obtain a corresponding voltage signal. As per the LEM datasheet [155], a measuring/shunt resistance of 150 Ω is chosen as it is a common value resistor that will provide the highest allowable voltage signal for currents up to 50 A with a ±15 V supply.

To measure the currents in each of the stator sections, as well as the total current, additional LA 55-P transducers are used. Since two transducers are required for each of the five stator sections, in addition to the pair for the total current, it is necessary to sample 12 analogue signals. This presented a problem because the dSPACE controller card only has 8 analogue inputs. In fact, the dSPACE card only has 5 independent analogue-to-digital converters—4 15-bit ADCs and one 16-bit ADC, which can be multiplexed to sample 4 inputs [156]. Thus, an additional layer of multiplexing needed to be implemented. A custom circuit was consequently designed and built, containing the additional LA 55-P LEMs for the stator section current measurements, regulated ±15 V supplies for the LEMs and 2 triple 2-channel analogue multiplexers (MC14053B/CD4053) to provide 6 analogue outputs with a digital input to select which of the two banks of LEMs to connect to these outputs. The circuit diagram is provided in figure C.44 and the Veroboard layout is shown in figure C.45. The ±15 V supply for the LEMs needed to be regulated down to 8 V & −9 V for the multiplexers' supply to be within the specified absolute maximum

of 18 V. Also, an ICL7667 driver chip is used to buffer and level-shift the control inputs to the 2-channel multiplexers from the TTL 'bank select' signal from dSPACE. 100 nF decoupling capacitors are placed locally at all the component supply pins to reduce noise.

Since the current measurements are sampled, it is important to implement anti-alias filters to ensure that the signals do not contain frequency components above the Nyquist frequency. As derived in (C.5), placing a capacitor in parallel with the shunt resistance for a current source results in a voltage signal that is first-order low-pass filtered. The cut-off frequency, $\frac{1}{RC}$, is thus chosen to be higher than the required current measurement bandwidth and lower than the Nyquist frequency (half the sampling frequency). Because the measurement bandwidth of the LEMs is at least 200 kHz [155], the signals would otherwise need to be sampled above 400 kHz to ensure no aliasing. 1 µF capacitors are used for a chosen cut-off frequency of approximately 1 kHz. Since the natural electrical bandwidth of the stator sections is only $\frac{R}{L} \approx 300\,\text{rad/s} \approx 47\,\text{Hz}$, the additional filtering is somewhat unnecessary. However, it is effective in reducing any induced high frequency noise.

$$\begin{aligned} I &= I_{(\text{resistor})} + I_{(\text{capacitor})} \\ &= \frac{V}{R} + C\dot{V} \\ \therefore \qquad I(s) &= \frac{V(s)}{R} + CsV(s) \\ \therefore \qquad \frac{V(s)}{I(s)} &= \frac{R}{RCs+1} \end{aligned} \tag{C.5}$$

The accurately-measured shut resistances for each of the LEMs are listed in table C.2. Also, the mapping of the current measurement signals to dSPACE is provided in table C.3. Lastly, photographs of the resulting measurement and multiplexing circuitry are included as figure C.46.

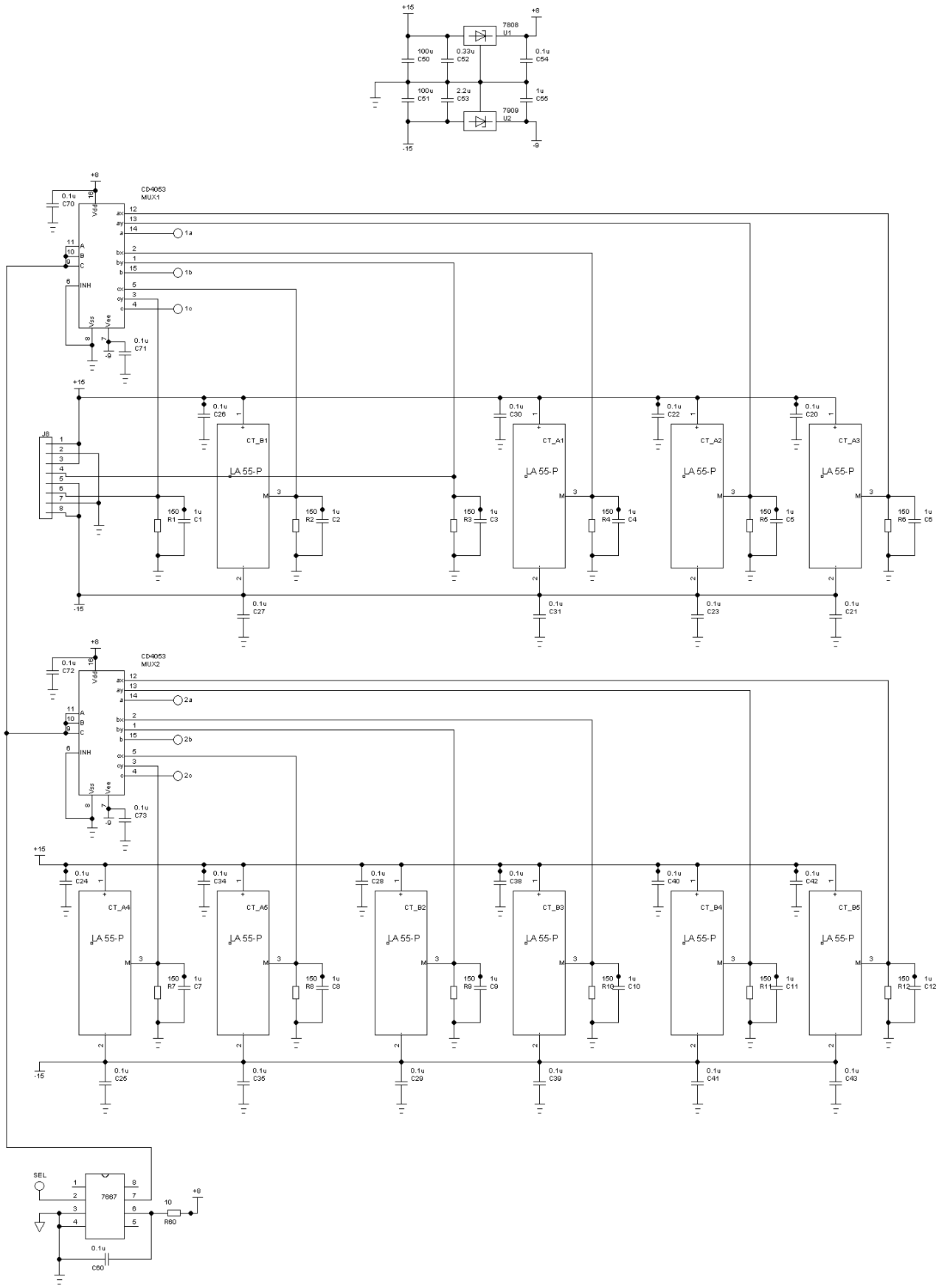

Figure C.44: Current measurement and multiplexer circuit

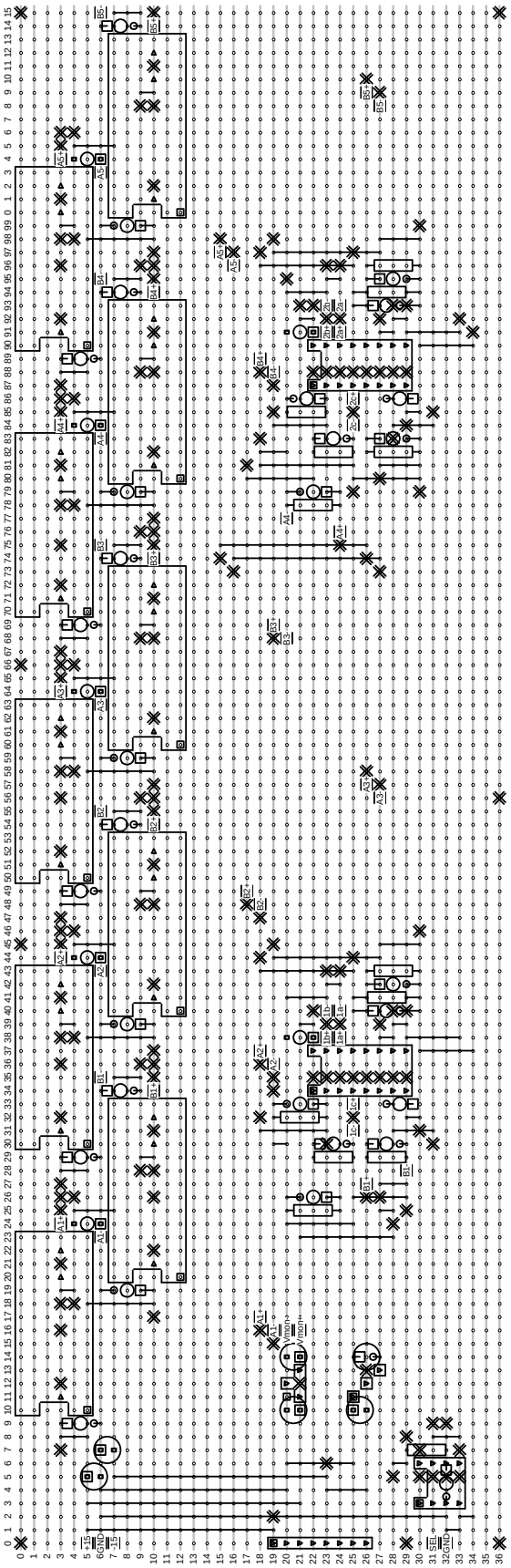

Figure C.45: Veroboard layout for current measurement and multiplexer circuit

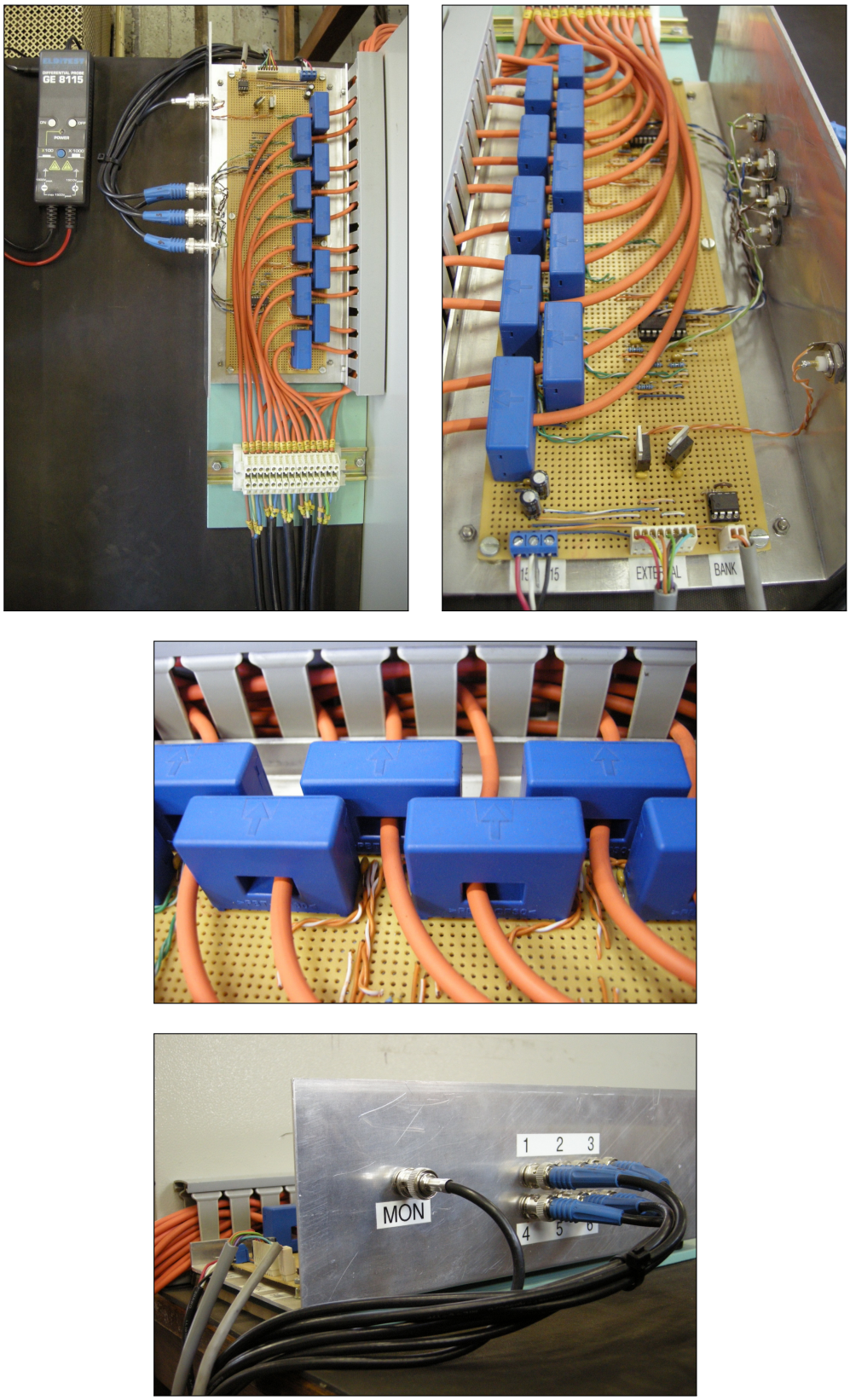

Figure C.46: Current measurement and multiplexing circuit

Table C.2: Measured LEM shunt resistances (using 4-wire ohmmeter)

LEM	Shunt Resistance [Ω]
A1	150.4
B1	149.3
A2	150.7
B2	150.3
A3	149.6
B3	150.4
A4	149.6
B4	149.7
A5	149.8
B5	150.4
A6	149.6
B6	150.3

Table C.3: Mapping of measured current signals from LEMs to dSPACE

Signal	Circuit BNC	Bank	dSPACE ADC Ch
A1	2	0	5
B1	3	0	6
A2	1	1	1
B2	5	1	2
A3	1	0	1
B3	5	0	2
A4	6	1	3
B4	4	1	4
A5	6	0	3
B5	4	0	4
A6	3	1	6
B6	2	1	5

C.5.3 Reaction plate position

To measure the position of the reaction plate, a Stahltronic WCS2 absolute position encoder is used. It is a system designed for the material handing industry and consists of a reading head unit that travels along a stationary coded rail. The reading head is attached to the reaction plate using a custom aluminium bracket. There are 1200 codes per metre, yielding a resolution of 0,833 mm and the particular reading head unit used has an RS485 interface operating at 19,2 kBaud [157].

Figure C.47 shows a photograph of the linear encoder reading head.

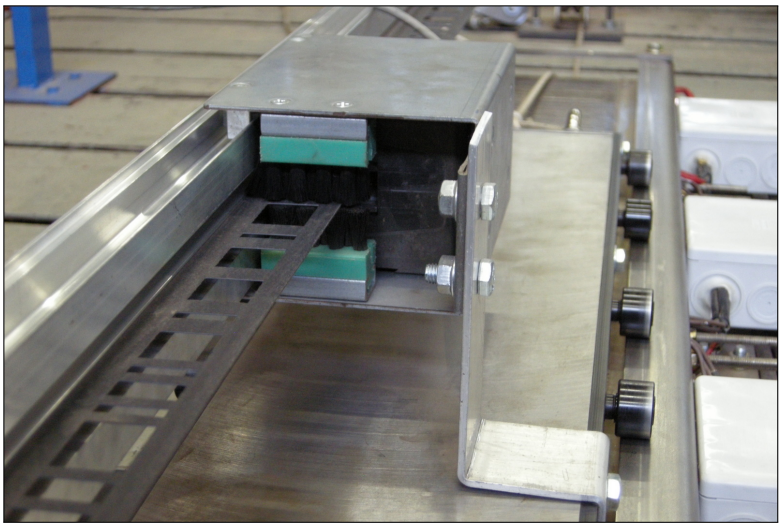

Figure C.47: Stahltronic WCS2 reading head and coded rail

The interfacing of the position reading head to dSPACE is detailed in figure C.48. Although it is recommended that shielded twisted-pair cable is used for the RS485 interface [157], given the short distance between the reading head and the control system, a readily-available length of CAT5 Ethernet cable was used instead. By default, dSPACE's UART is configured as an RS422 transceiver and so to use it as RS485 transceiver, it is necessary to connect together the 'RXD' and 'TXD' signals [156].

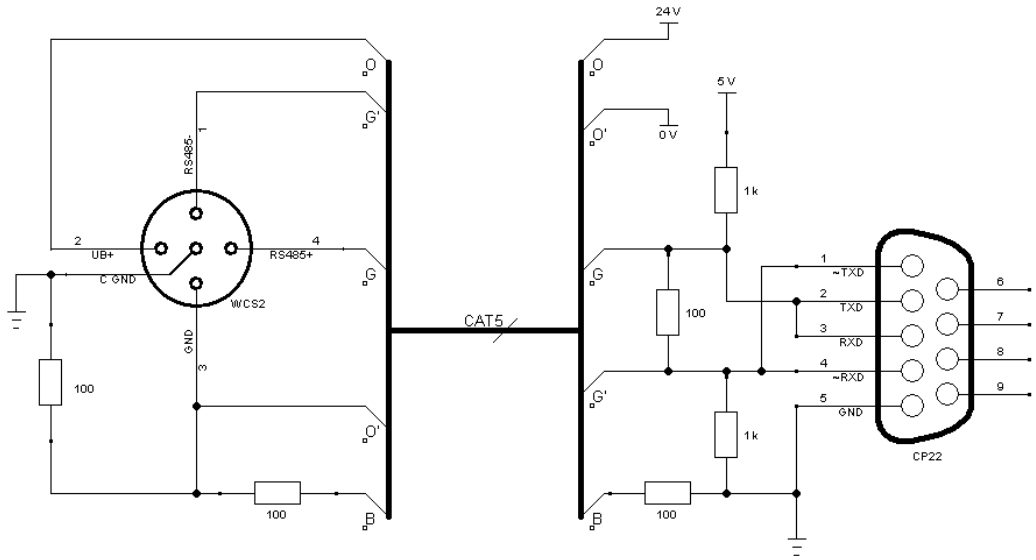

Figure C.48: Stahltronic WCS2 position encoder wiring

dSPACE does not provide line termination, hence a 100 Ω termination resistor is used to match the characteristic impedance of the CAT5 twisted-pair. In addition, to avoid undefined conditions (when there is no active transmitter on the RS485 network) 1 kΩ pull-up and pull-down resistors are used. Lastly, to limit potentially high ground currents, 100 Ω series resistors are used between the signal and power ground lines, as recommended by dSPACE [156].

C.6 Overall setup and interconnections

Figure C.50 is a wiring diagram showing the interconnections between the various components of the prototype system. The connections to the dSPACE ADC inputs are made using coaxial cable with BNC connectors and the digital IO signals are connected using the twisted pairs of CAT5 cables. A photograph of the connections to dSPACE is included as figure C.49.

Photographs of the complete segmented LSM are included as figure C.51 and figure C.52 shows how a pulley arrangement is used to load the motor with a hanging weight (constant force).

Lastly, figure C.53 is a top view of the computer workstation, switchgear cabinet and associated control circuitry.

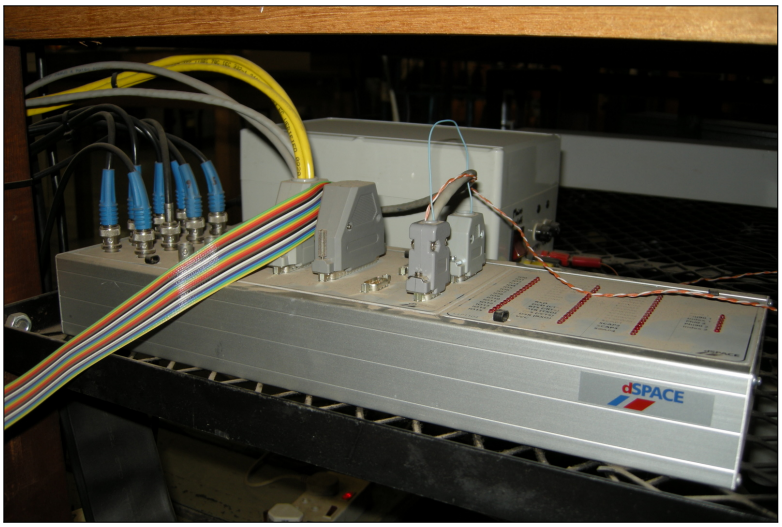

Figure C.49: dSPACE break-out connection box

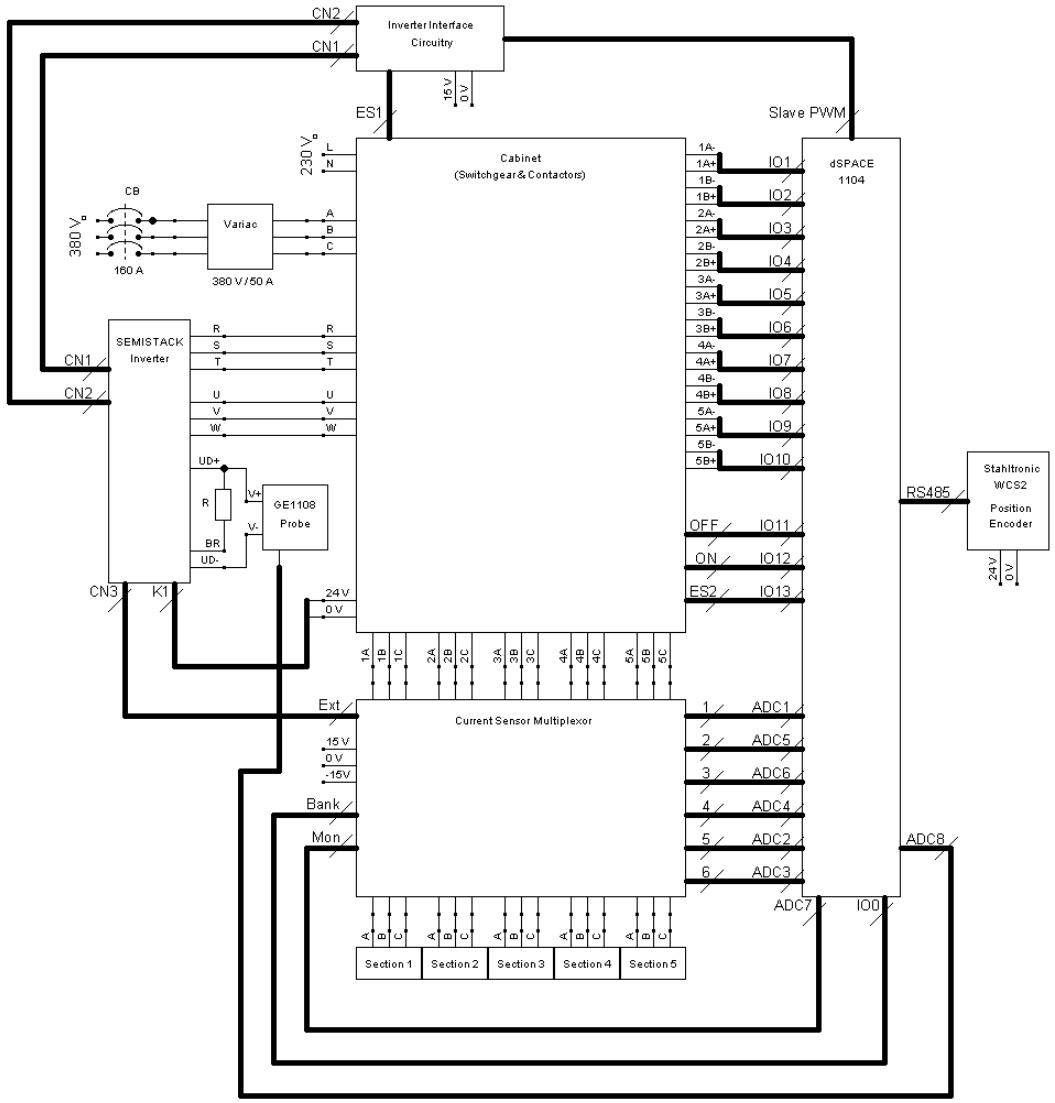

Figure C.50: Component interconnections

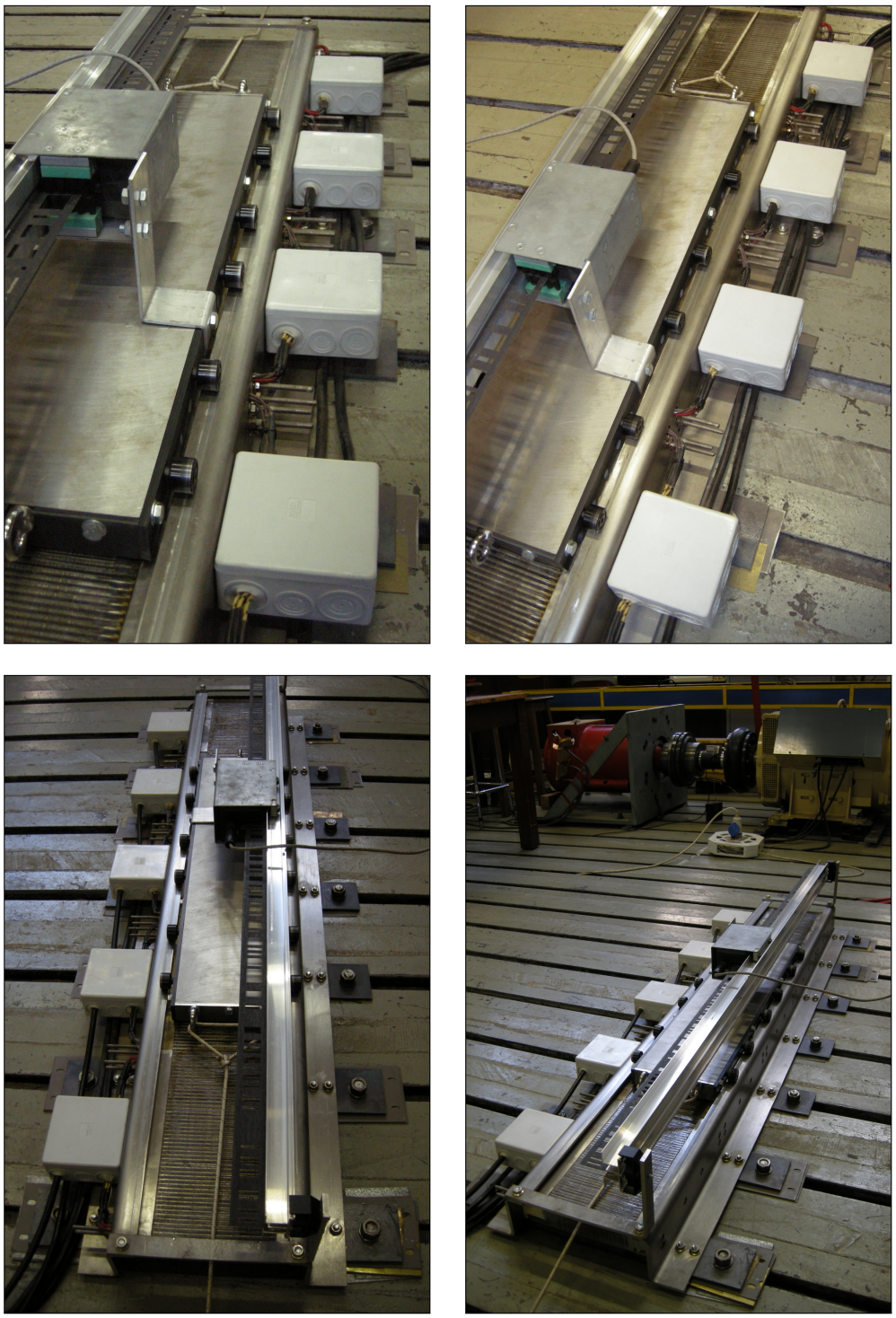

Figure C.51: Complete linear synchronous motor

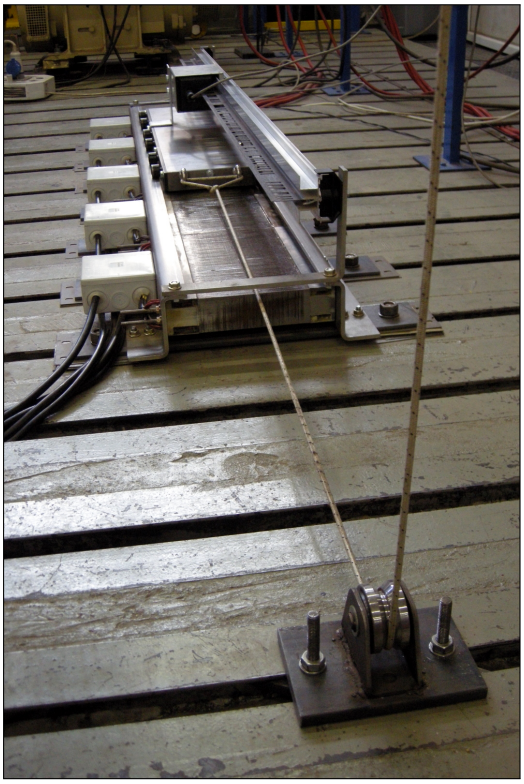

Figure C.52: Pulley arrangement used to load motor

Figure C.53: LSM control setup

Appendix D

Prototype Characterisation and Modelling

This appendix provides supporting material for the characterisation and modelling of the prototype segmented LSM, including the relevant MATLAB® scripts and Simulink® subsystems.

D.1 Motor

D.1.1 FEMM model

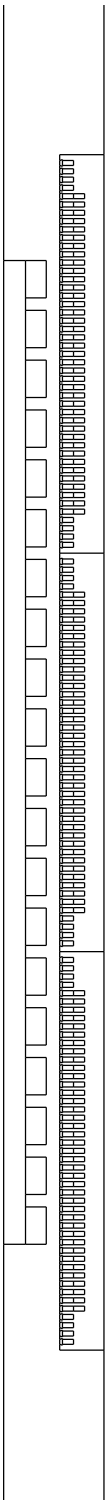

Figure D.1: FEMM model geometry `lsm.fem`

D.1.2 Electromagnetic force

Code listing D.1: Obtain $\hat{\boldsymbol{x}}$ and $\hat{\boldsymbol{y}}$ forces using FEMM (`fem_F_xy_x.m`)

```
function F_xy_x = fem_F_xy_x(x_rs_x,I_abc)
%  Obtain forces for particular phase currents and a range of
%  relative reaction plate positions using FEMM

openfemm;
opendocument('lsm.fem');
main_maximize;
mi_saveas('tmp.fem');

% Apply phase currents
mi_modifycircprop('A2',1,I_abc(1));
mi_modifycircprop('B2',1,I_abc(2));
mi_modifycircprop('C2',1,I_abc(3));

N_x = numel(x_rs_x);
F_xy_x = zeros(2,N_x); %Preallocate output
x_rs_delta_x = diff([0; x_rs_x]);

for idx_x = 1:N_x
  % Move reaction plate to position
  mi_selectgroup(2);
  mi_movetranslate2(x_rs_delta_x(idx_x)*1e3,0,4);
  % Get force
  mi_analyze;
  mi_loadsolution;
  mo_seteditmode('area');
  mo_clearblock();
  mo_groupselectblock(2);
  F_xy_x(1,idx_x) = mo_blockintegral(18);
  F_xy_x(2,idx_x) = mo_blockintegral(19);
  mo_close;
end
closefemm;
delete tmp.*;
```

D.1.3 Position of α-axis

Code listing D.2: Calculate α-axis offset using FEMM (`fem_x_alpha.m`)

```
function x_alpha = fem_x_alpha
%  Calculate alpha-axis offset from stator section edge using FEMM

openfemm;
opendocument('lsm.fem');
main_maximize;
mi_saveas('tmp.fem');

%Remove PM flux contribution (set Hc = 0)
mi_modifymaterial('NdFeB 45H',3,0);

% Apply alpha-axis mmf
mi_modifycircprop('A2',1,1);
mi_modifycircprop('B2',1,-0.5);
mi_modifycircprop('C2',1,-0.5);

% Solve
mi_analyze;
mi_loadsolution;

% Draw contour along middle stator section's boundary with airgap
mo_addcontour(-144,0);
mo_addcontour(144,0);

%Export normal component of flux density
mo_makeplot(2,2^10,'lsm.txt',1);

mo_close;
closefemm;
delete tmp.*;

lsm = importdata('lsm.txt');
delete lsm.txt;

tau = 36e-3;
T = (lsm(2,1)-lsm(1,1))*1e-3;
N = numel(lsm(:,2));
Y = fft(-lsm(:,2));  %Flux density from reaction plate's perspective

x_alpha = mod(-tau/pi*(interp1(1/(2*T)*linspace(0,1,1+N/2),...
    unwrap(angle(Y(1:(1+N/2)))),1/(2*tau),'spline')),2*tau);
```

D.1.4 Flux linkage and inductances

Code listing D.3: Obtain a/b/c inductances using FEMM (`fem_L_abc_x.m`)

```
function L_abc_x = fem_L_abc_x(x_rs_x)
%  Obtain a/b/c inductance matrix for a set of relative reaction
%  plate positions using FEMM

openfemm;
opendocument('lsm.fem');
main_maximize;
mi_saveas('tmp.fem');

%Remove PM flux
mi_modifymaterial('NdFeB 45H',3,0);

N_x = numel(x_rs_x);
L_abc_x = zeros(3,3,N_x); %Preallocate output
x_rs_delta_x = diff([0; x_rs_x]);

for idx_x = 1:N_x
  %Move reaction plate to position
  mi_selectgroup(2);
  mi_movetranslate2(x_rs_delta_x(idx_x)*1e3,0,4);
  %Get inductances for phase a
  mi_modifycircprop('A2',1,1);
  mi_analyze;
  mi_loadsolution;
  A = mo_getcircuitproperties('A2');
  L_abc_x(1,1,idx_x) = A(3);
  B = mo_getcircuitproperties('B2');
  L_abc_x(2,1,idx_x) = B(3);
  C = mo_getcircuitproperties('C2');
  L_abc_x(3,1,idx_x) = C(3);
  mo_close;
  mi_modifycircprop('A2',1,0);
  %Get inductances for phase b
  mi_modifycircprop('B2',1,1);
  mi_analyze;
  mi_loadsolution;
  A = mo_getcircuitproperties('A2');
  L_abc_x(1,2,idx_x) = A(3);
  B = mo_getcircuitproperties('B2');
  L_abc_x(2,2,idx_x) = B(3);
  C = mo_getcircuitproperties('C2');
  L_abc_x(3,2,idx_x) = C(3);
  mo_close;
  mi_modifycircprop('B2',1,0);
  %Get inductances for phase c
  mi_modifycircprop('C2',1,1);
```

Code listing D.3: Obtain a/b/c inductances using FEMM (`fem_L_abc_x.m`) *... cont*

```
41    mi_analyze;
42    mi_loadsolution;
43    A = mo_getcircuitproperties('A2');
44    L_abc_x(1,3,idx_x) = A(3);
45    B = mo_getcircuitproperties('B2');
46    L_abc_x(2,3,idx_x) = B(3);
47    C = mo_getcircuitproperties('C2');
48    L_abc_x(3,3,idx_x) = C(3);
49    mo_close;
50    mi_modifycircprop('C2',1,0);
51  end
52  closefemm;
53  delete tmp.*;
```

Code listing D.4: Obtain a/b/c PM flux linkage using FEMM (`fem_lambda_m_abc_x.m`)

```
1   function lambda_m_abc_x = fem_lambda_m_abc_x(x_rs_x)
2   %  Calculate a/b/c PM flux linkages for a set of relative reaction
3   %  plate positions
4
5   openfemm;
6   opendocument('lsm.fem');
7   main_maximize;
8   mi_saveas('tmp.fem');
9
10  N_x = numel(x_rs_x);
11  lambda_m_abc_x = zeros(3,1,N_x);
12  x_rs_delta_x = diff([0; x_rs_x]);
13
14  for idx_x = 1:N_x
15    %Move reaction plate to position
16    mi_selectgroup(2);
17    mi_movetranslate2(x_rs_delta_x(idx_x),0,4);
18    %Get flux linkages
19    mi_analyze;
20    mi_loadsolution;
21    A = mo_getcircuitproperties('A2');
22    lambda_m_abc_x(1,1,idx_x) = A(3);
23    B = mo_getcircuitproperties('B2');
24    lambda_m_abc_x(2,1,idx_x) = B(3);
25    C = mo_getcircuitproperties('C2');
26    lambda_m_abc_x(3,1,idx_x) = C(3);
27    mo_close;
28  end
29
30  closefemm;
31  delete tmp.*;
```

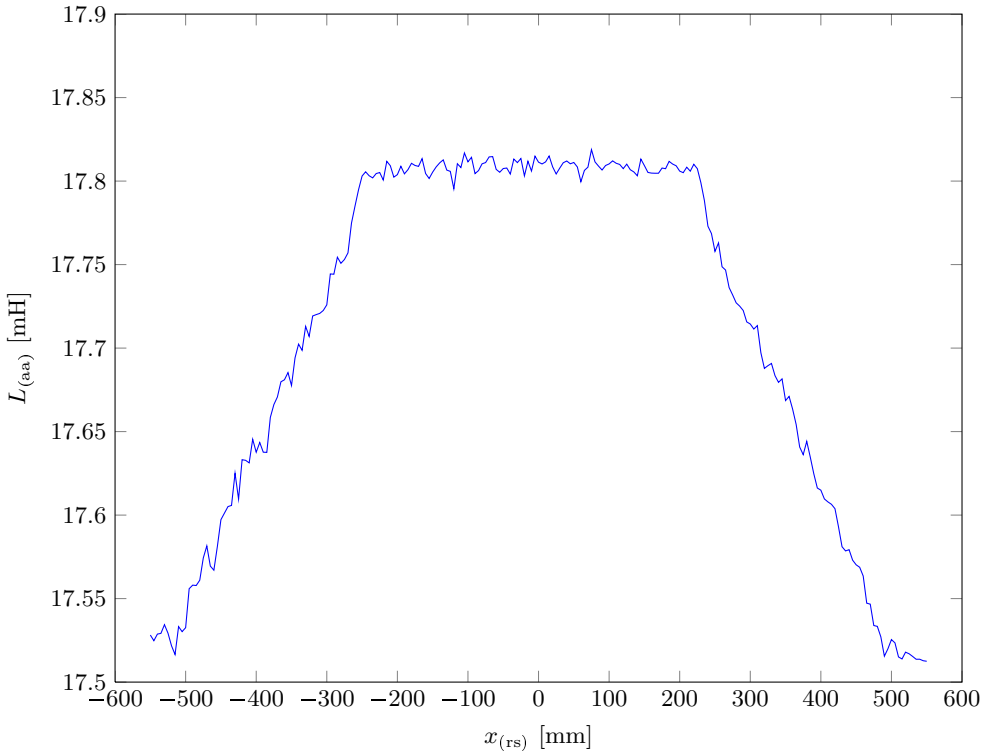

Figure D.2: $L_{(aa)}$ versus relative position of reaction plate

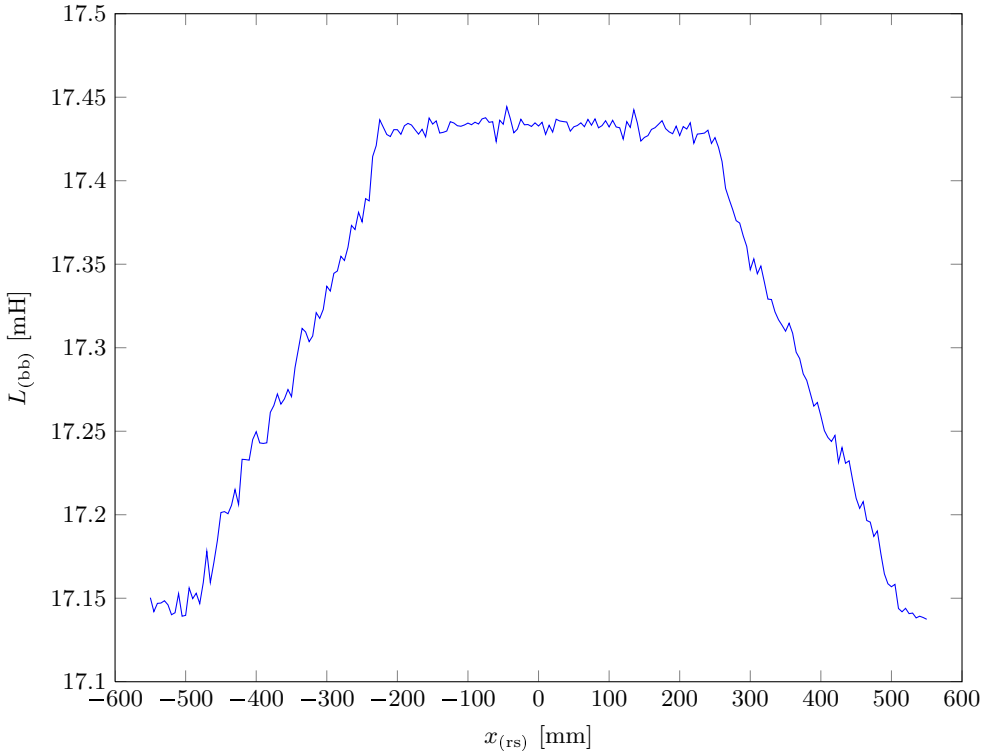

Figure D.3: $L_{(bb)}$ versus relative position of reaction plate

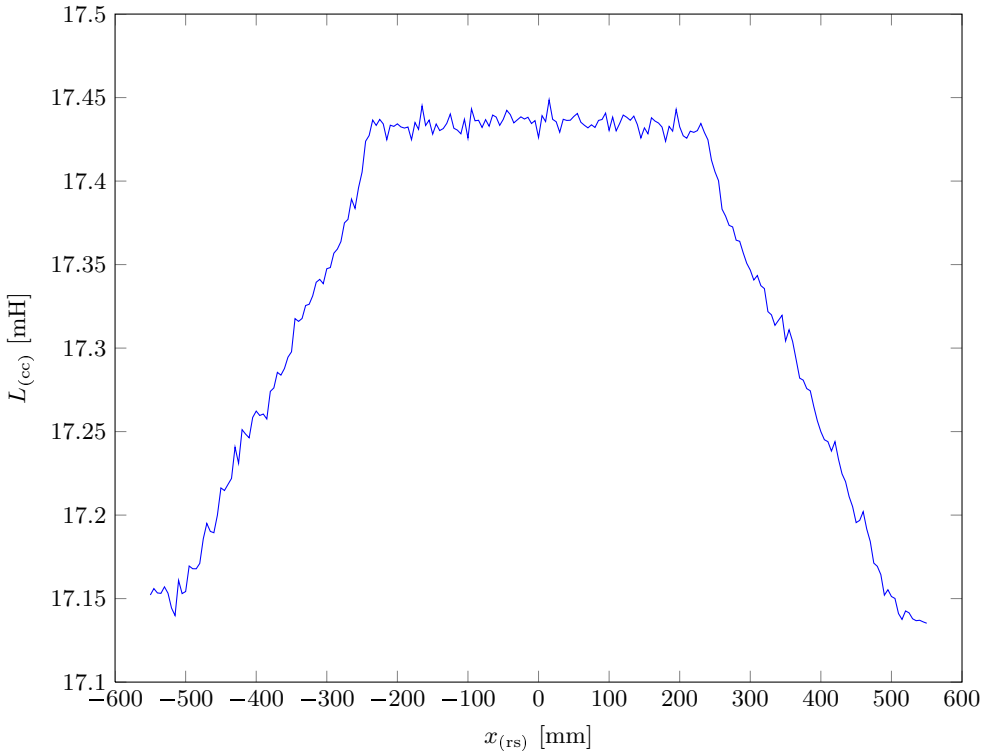

Figure D.4: $L_{(cc)}$ versus relative position of reaction plate

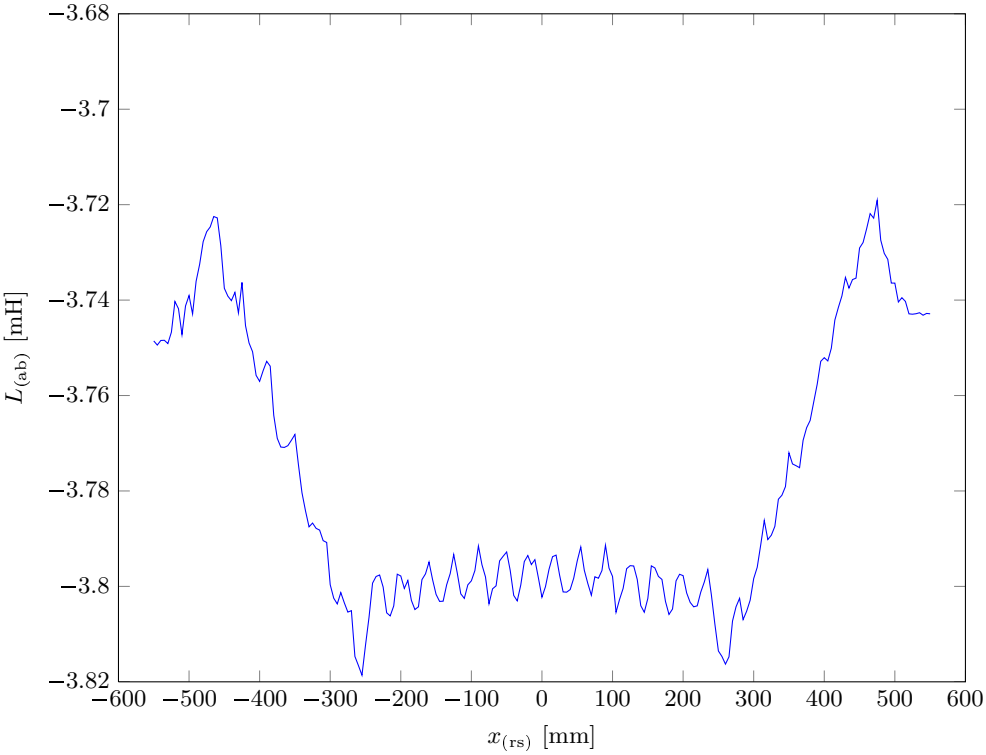

Figure D.5: $L_{(ab)}$ versus relative position of reaction plate

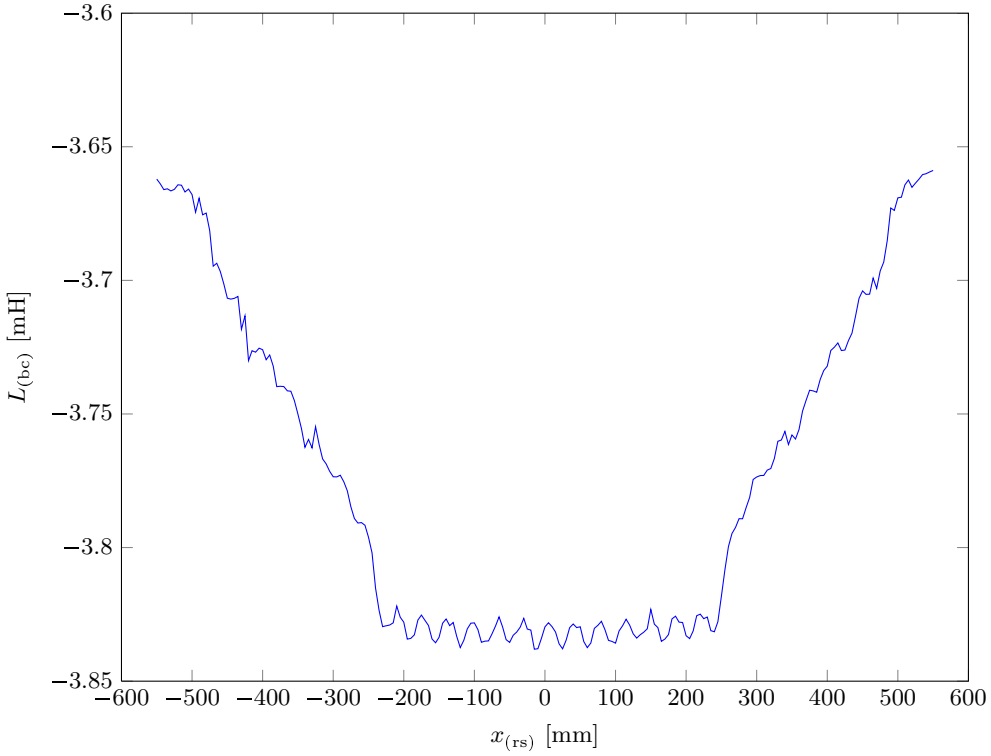

Figure D.6: $L_{(\mathrm{bc})}$ versus relative position of reaction plate

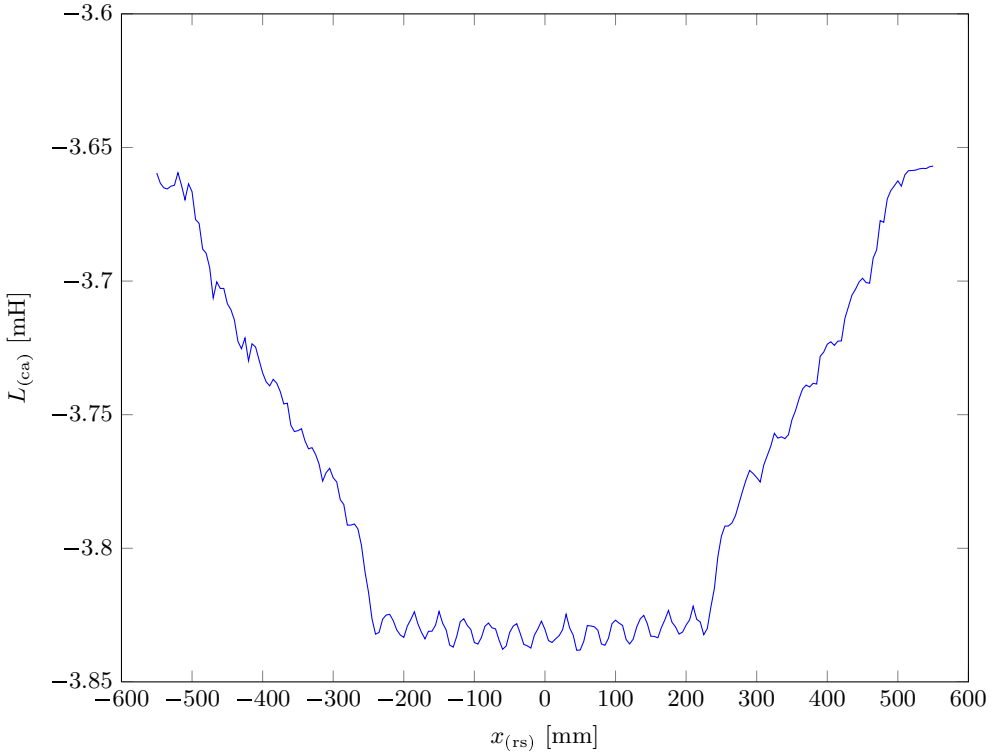

Figure D.7: $L_{(\mathrm{ca})}$ versus relative position of reaction plate

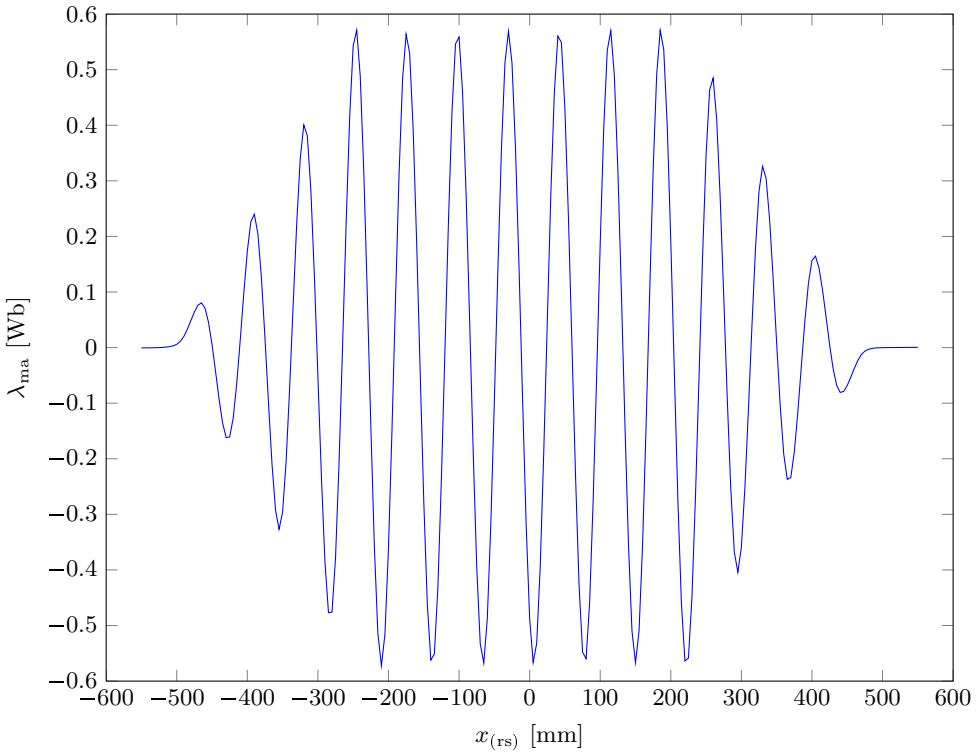

Figure D.8: λ_{ma} versus relative position of reaction plate

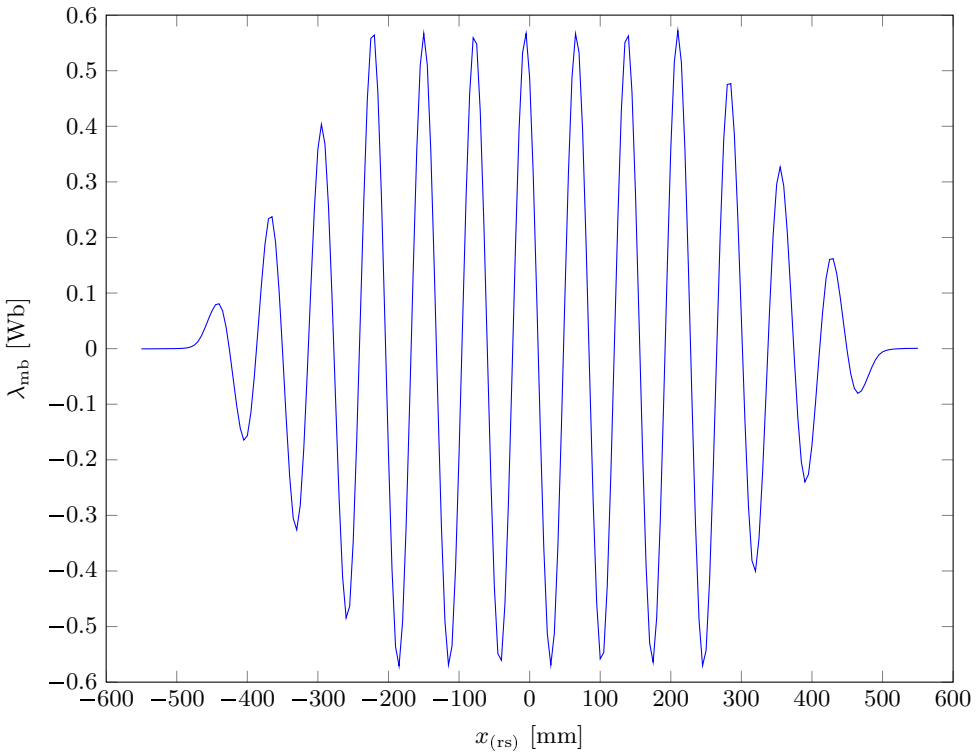

Figure D.9: λ_{mb} versus relative position of reaction plate

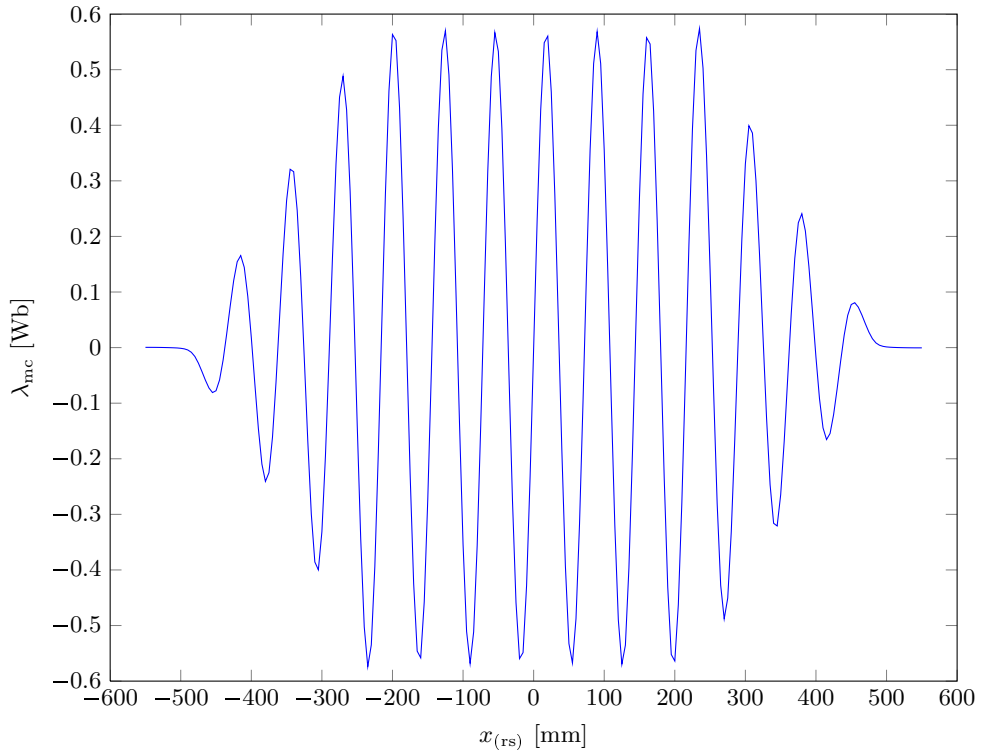

Figure D.10: λ_{mc} versus relative position of reaction plate

Code listing D.5: Calculate θ for a set of reaction plate positions (`calc_theta_x.m`)

```
function theta_x = calc_theta_x(x_rs_x,x_alpha,tau)
%  Calculate angular displacement between array of d-axis positions and
%  the alpha-axis, given an array of relative reaction plate positions

x_d_x = x_rs_x + tau/2;
theta_x = (x_d_x-x_alpha)*pi/tau;
theta_x = atan2(sin(theta_x),cos(theta_x)); %Wrap angle
```

Code listing D.6: Calculate d/q/0 inductances (`calc_L_dq0_x.m`)

```
function L_dq0_x = calc_L_dq0_x(theta_x,L_abc_x)
%  Transform set of a/b/c inductance matrices to the d/q/0 frame

N_x = numel(theta_x);
L_dq0_x = zeros(3,3,N_x); %Preallocate output
for idx_x = 1:N_x
  L_dq0_x(:,:,idx_x) = T_3r(theta_x(idx_x))*T_33*...
    L_abc_x(:,:,idx_x)/T_33/T_3r(theta_x(idx_x));
end
```

Code listing D.7: Calculate d/q/0 flux linkages (`calc_lambda_m_dq0_x.m`)

```
function lambda_m_dq0_x = calc_lambda_m_dq0_x(theta_x,lambda_m_abc_x)
%  Transform set of a/b/c PM flux linkage matrices to the d/q/0 frame

N_x = numel(theta_x);
lambda_m_dq0_x = zeros(3,1,N_x); %Preallocate output
for idx_x = 1:N_x
  lambda_m_dq0_x(:,:,idx_x) = T_3r(theta_x(idx_x))*...
    T_33*lambda_m_abc_x(:,:,idx_x);
end
```

D.2 Feeding efficiency and reaction plate utilisation

Code listing D.8: Calculate reaction plate utilisation (`calc_eta_r.m`)

```
function eta_r = calc_eta_r(N_p_s,N_p_r)
%  Calculate reaction plate utilisation

eta_r = ( rem(N_p_r,N_p_s)*floor(N_p_r/N_p_s) + ...
  (N_p_s-rem(N_p_r,N_p_s))*(floor(N_p_r/N_p_s)-1) ) / N_p_r;
```

Code listing D.9: Calculate stator feeding efficiency (`calc_eta_s.m`)

```
function eta_s = calc_eta_s(N_p_s,N_p_r)
%  Calculate stator feeding efficiency

eta_s = (rem(N_p_r,N_p_s)*N_p_r)/((floor(N_p_r/N_p_s)+2)*N_p_s^2) +...
  ((N_p_s-rem(N_p_r,N_p_s))*N_p_r)/((floor(N_p_r/N_p_s)+1)*N_p_s^2);
```

D.3 Inverter

Since dSPACE provides a space-vector pulse-width modulated (PWM) interface that, in turn, provides the correct IGBT gate signals for the three-phase inverter, the 'Inverter' simulation model is designed to use the same interface for consistency. Therefore, the effective terminal voltage is calculated from the space-vector sector and the proportions of the total switching period for which the two bordering voltage vectors are applied.

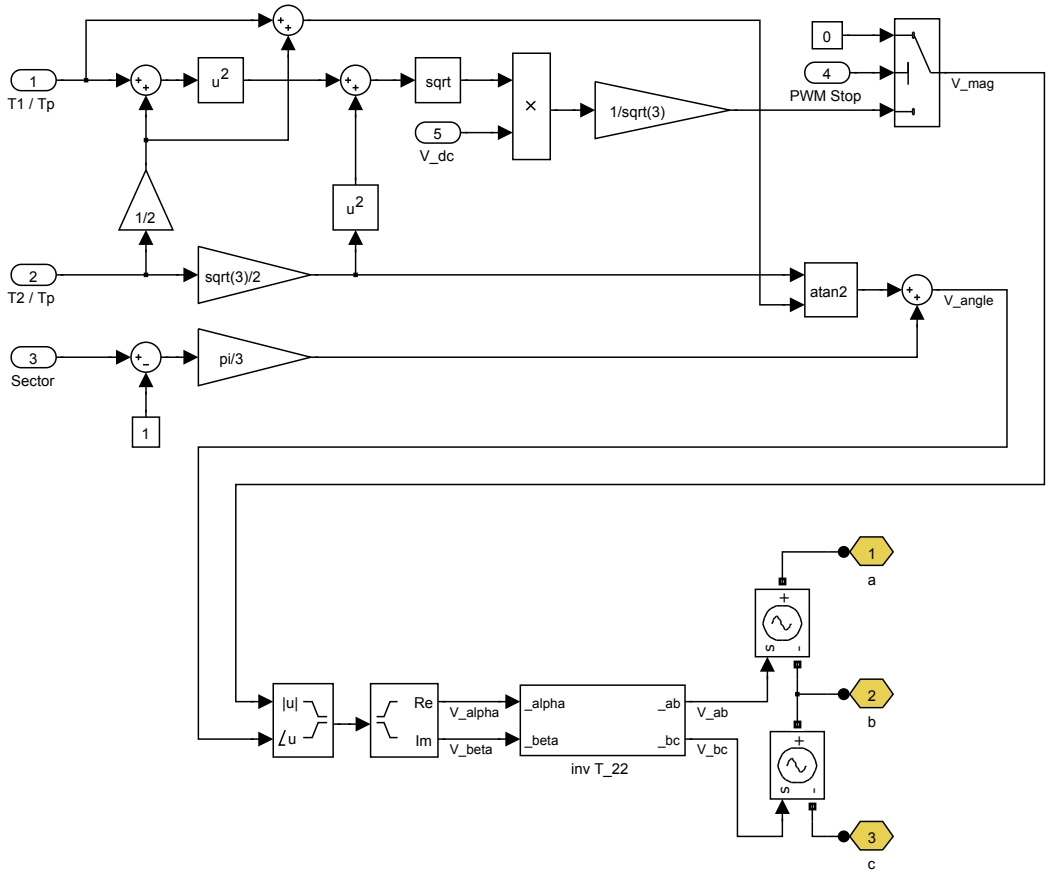

Figure D.11: Subsystem `lsmProto/Inverter`

D.4 Solid state contactors

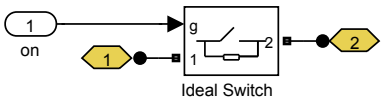

Figure D.12: Subsystem `lsmProto/Contactor/Ideal Switch`

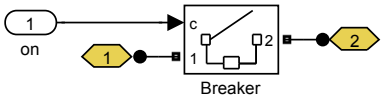

Figure D.13: Subsystem `lsmProto/Contactor/Breaker`

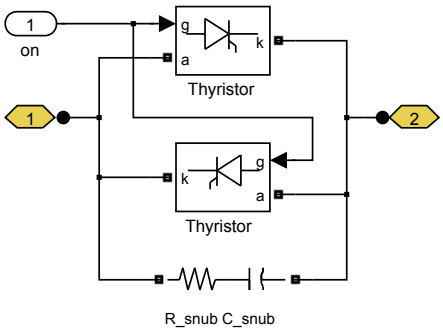

Figure D.14: Subsystem `lsmProto/Contactor/AP SCC`

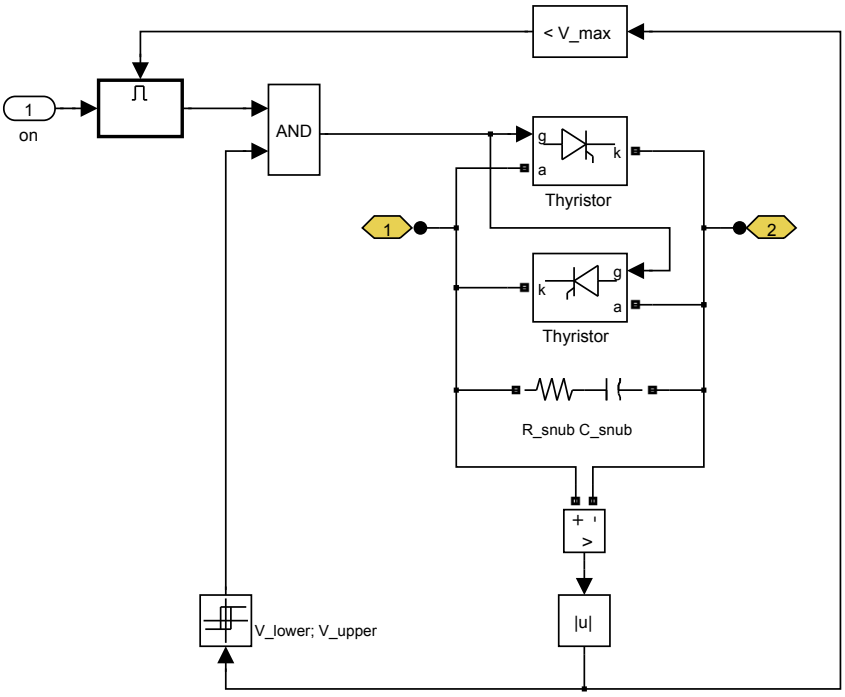

Figure D.15: Subsystem `lsmProto/Contactor/AP SCC 2`

Table D.1: Measured SSC turn-on threshold voltages

Contactor	Voltage [V]	Contactor	Voltage [V]
1A	14	1B	13
2A	16	2B	14
3A	17	3B	14
4A	15	4B	13
5A	15	5B	14

D.5 Stator current measurement

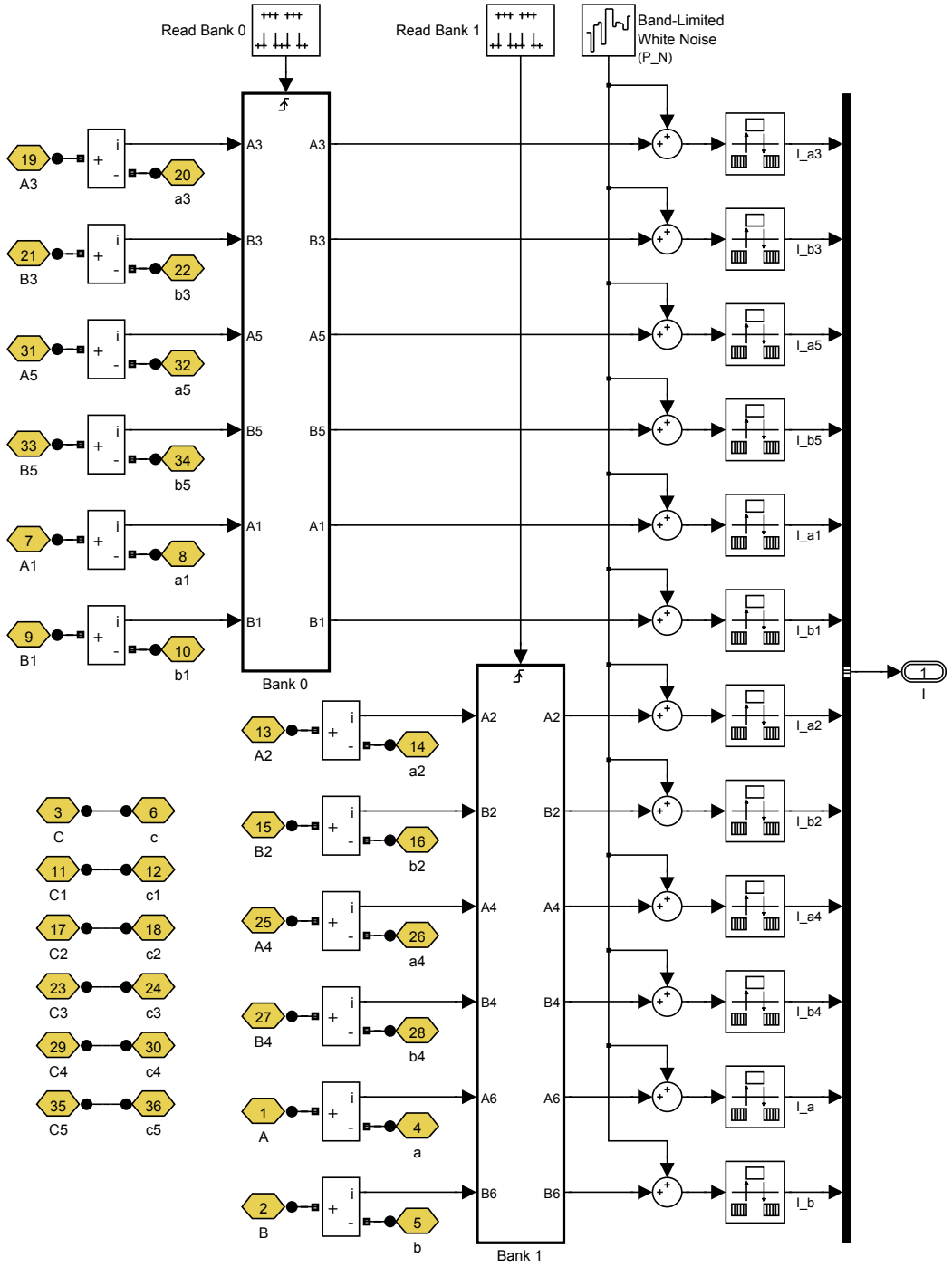

Figure D.16: Subsystem `lsmProto/Current Sensors/Unlimited Bandwidth`

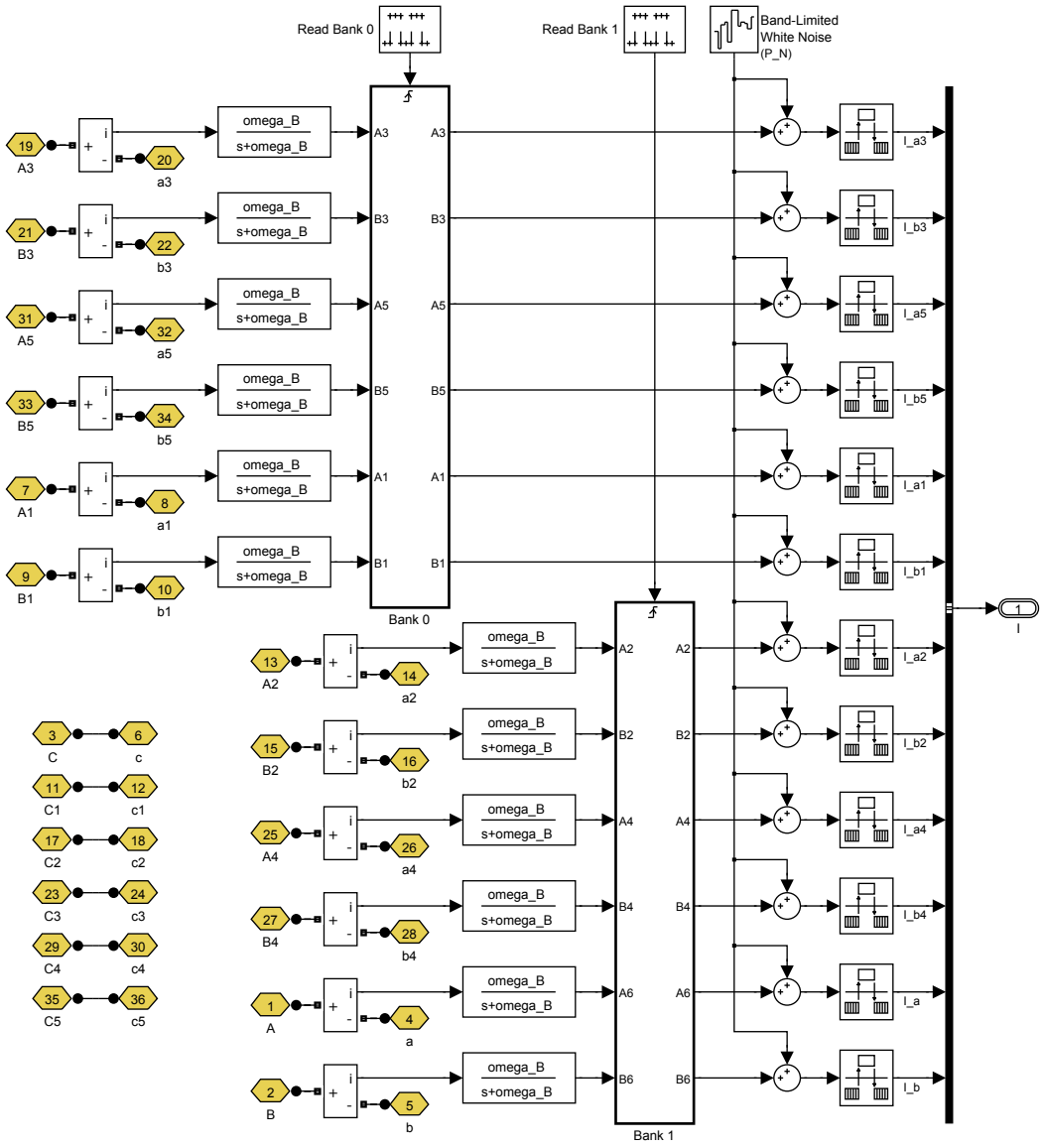

Figure D.17: Subsystem `lsmProto/Current Sensors/Limited Bandwidth`

D.6 Reaction plate position measurement

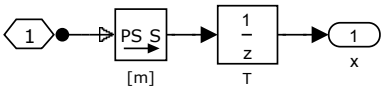

Figure D.18: Subsystem `lsmProto/Position Sensor/Simple`

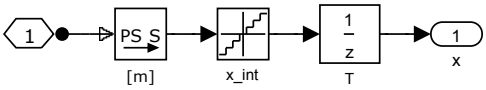

Figure D.19: Subsystem `lsmProto/Position Sensor/Quantisation`

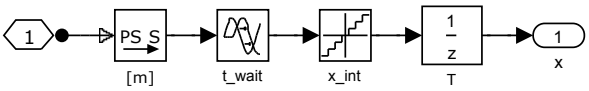

Figure D.20: Subsystem `lsmProto/Position Sensor/Quantisation and Delay`

Appendix E

Prototype Controller

This appendix details the prototype controller blocks not included in chapter 6 and the design of the feedback control loops in the frequency domain.

E.1 Controller blocks

E.1.1 Background tasks

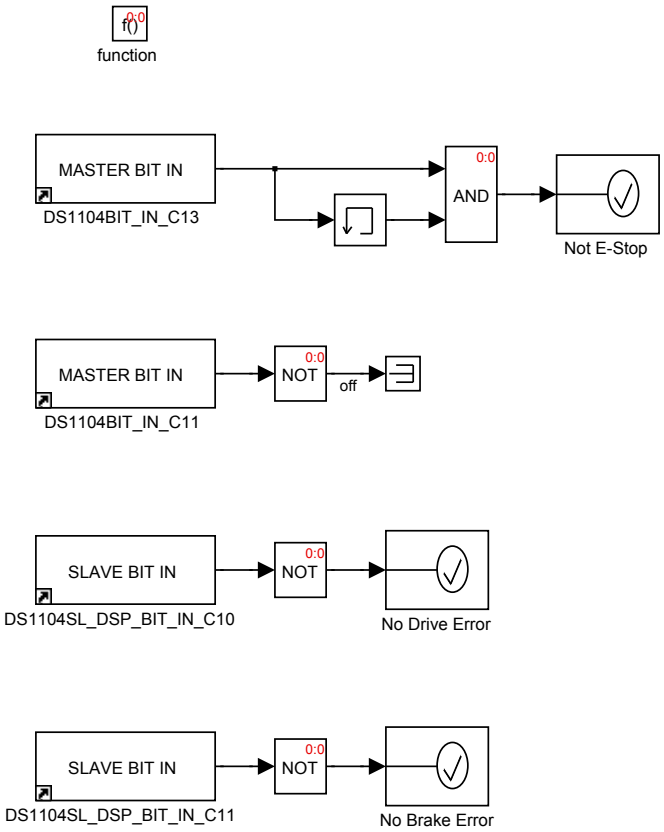

Figure E.1: Subsystem `lsmDSPACE/Monitor`

E.1.2 DC bus voltage control

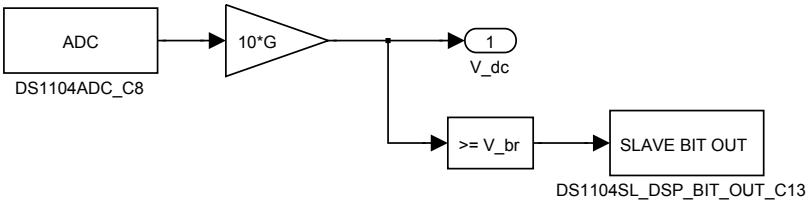

Figure E.2: Subsystem `lsmProtoHw/DC Bus Control`

E.1.3 Solid-state contactor actuation

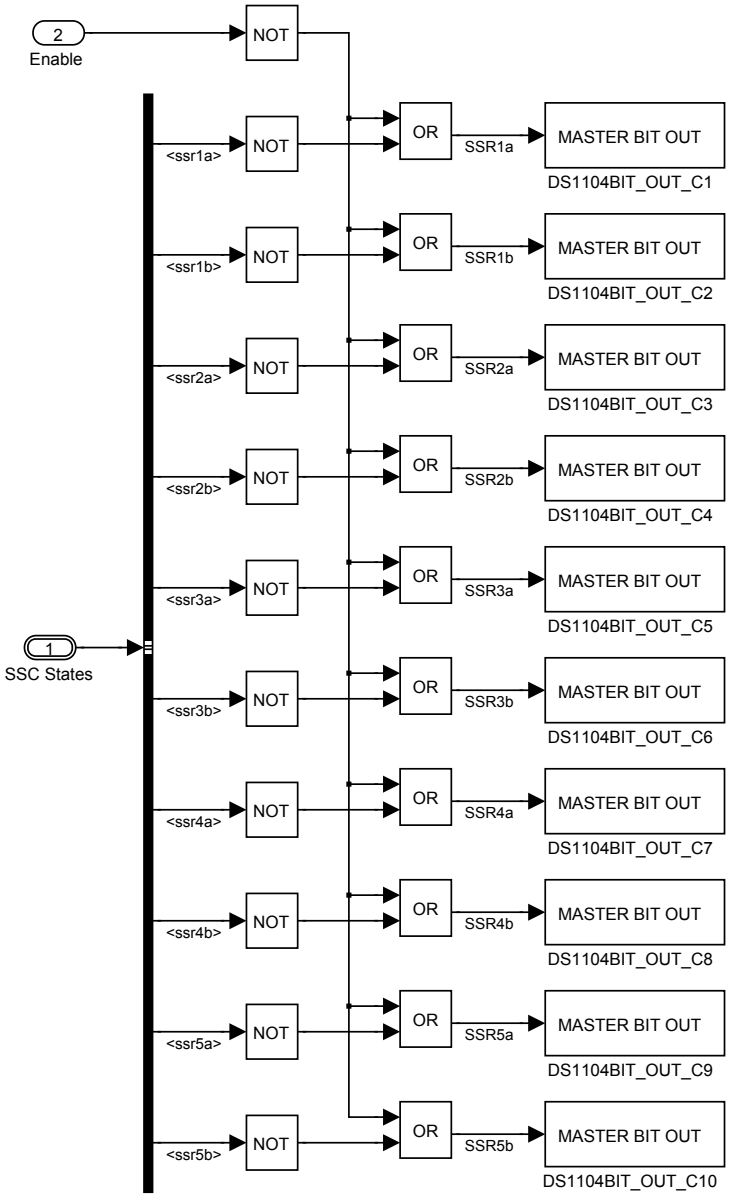

Figure E.3: Subsystem `lsmProtoHw/Solid-state Contactors`

E.1.4 Stator current measurement

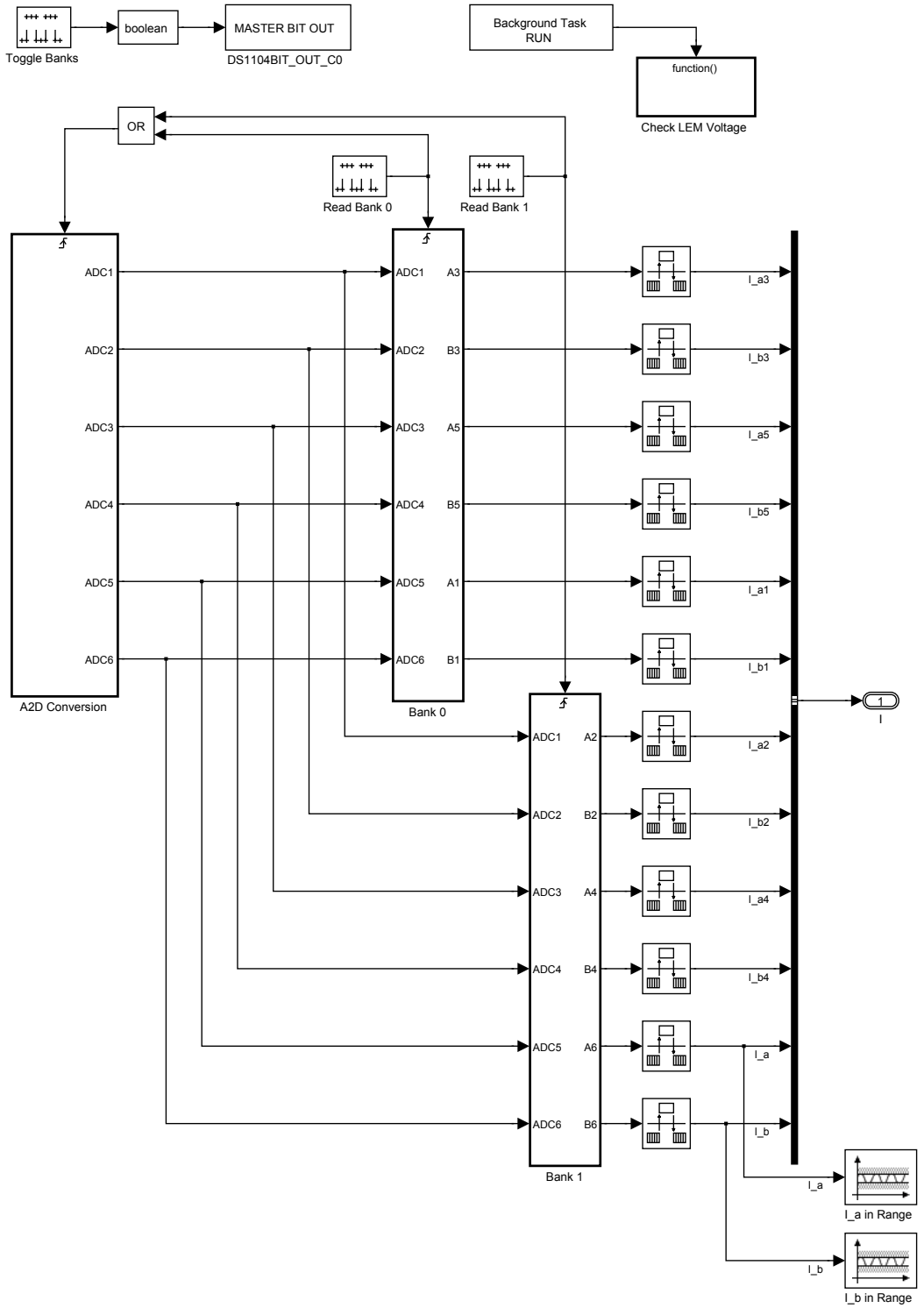

Figure E.4: Subsystem `lsmProtoHw/Current Sensors`

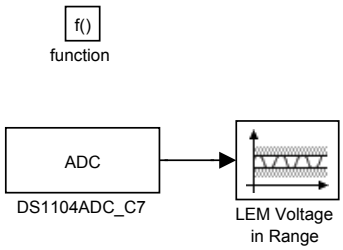

Figure E.5: Subsystem `lsmProtoHw/Current Sensors/Check LEM Voltage`

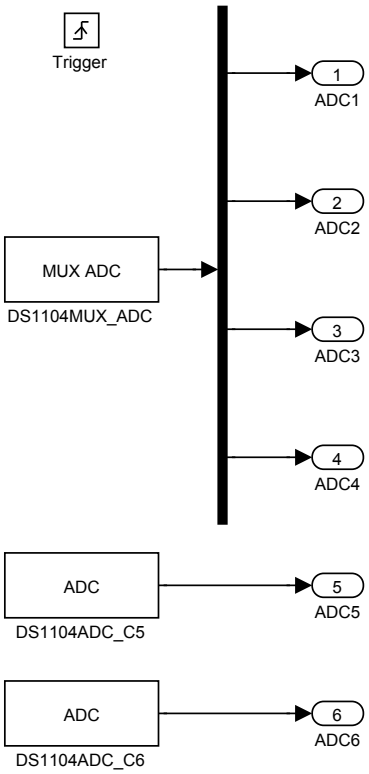

Figure E.6: Subsystem `lsmProtoHw/Current Sensors/A2D Conversion`

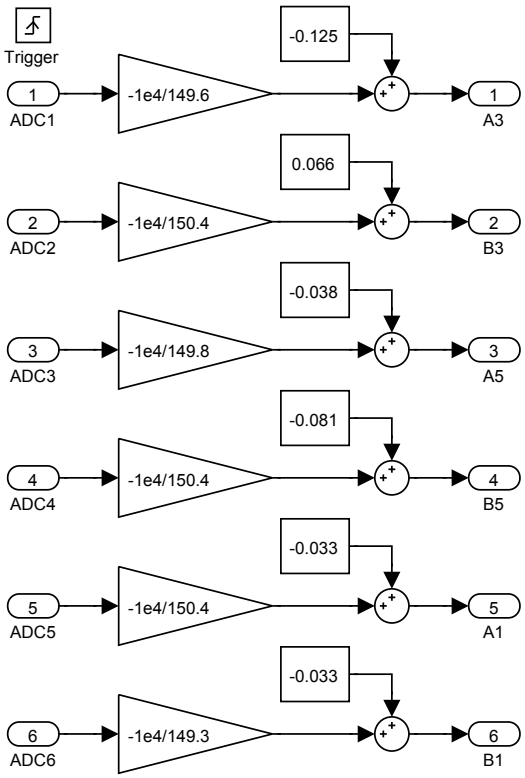

Figure E.7: Subsystem `lsmProtoHw/Current Sensors/Bank 0`

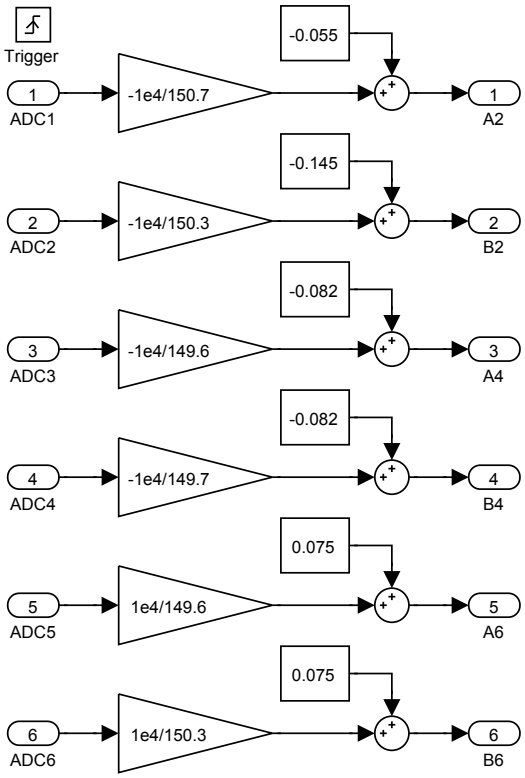

Figure E.8: Subsystem `lsmProtoHw/Current Sensors/Bank 1`

E.1.5 Reaction plate position measurement

The Stahltronic WCS2 reading head uses 'Data protocol 3' with no parity bit and a rate of 19,2 kBaud [157]. The dSPACE UART is thus configured to use 8 data bits, no parity bit and 1 stop bit, as required. Since the reading head address 'A1A0' is zero and the diagnosis bit, 'F0', functionality is obsolete, the position reading is requested with a byte having only its 7^{th} bit set (or decimal value of $2^7 = 128$).

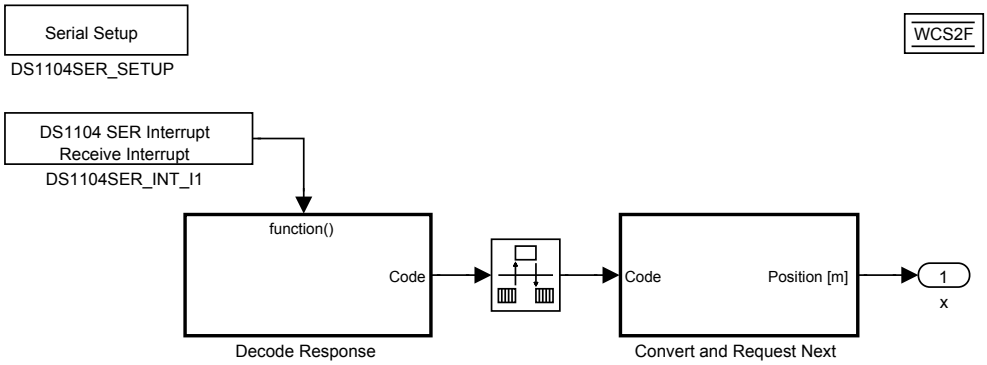

Figure E.9: Subsystem `lsmProtoHw/Stahl WCS2`

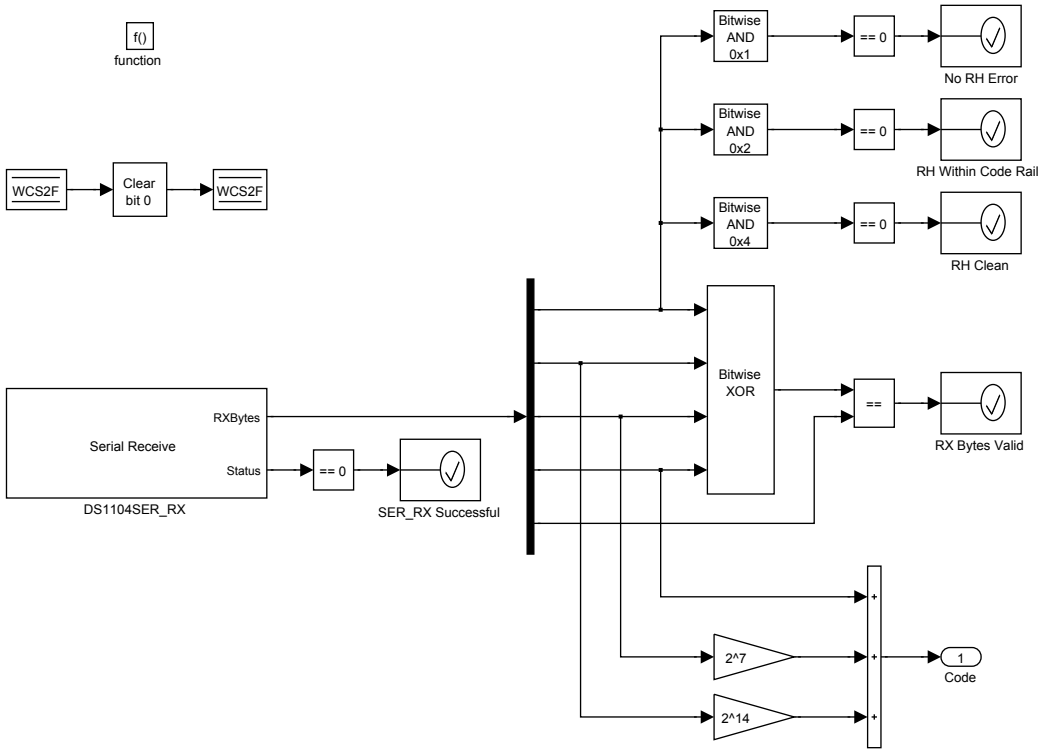

Figure E.10: Subsystem `lsmProtoHw/Stahl WCS2/Decode Response`

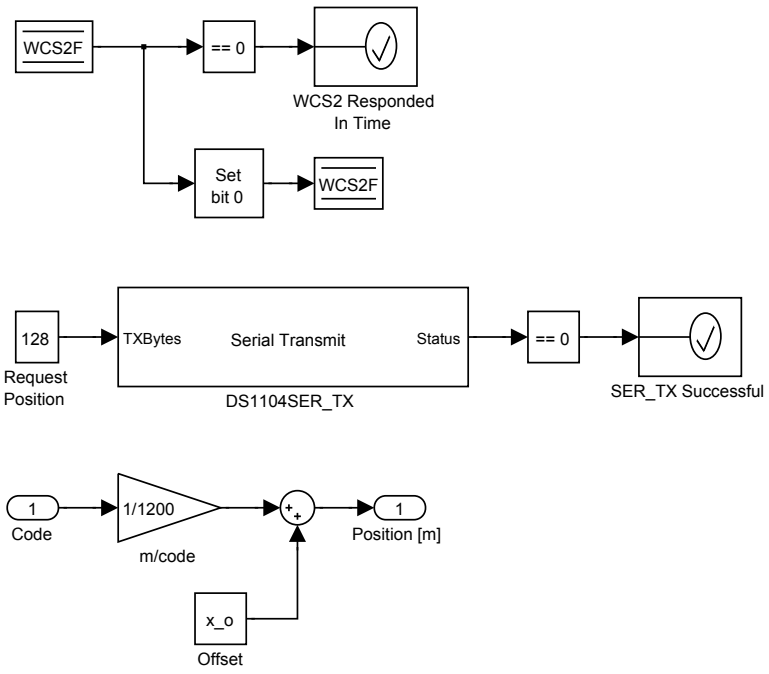

Figure E.11: Subsystem `lsmProtoHw/Stahl WCS2/Convert and Request Next`

E.1.6 Position trajectory generator

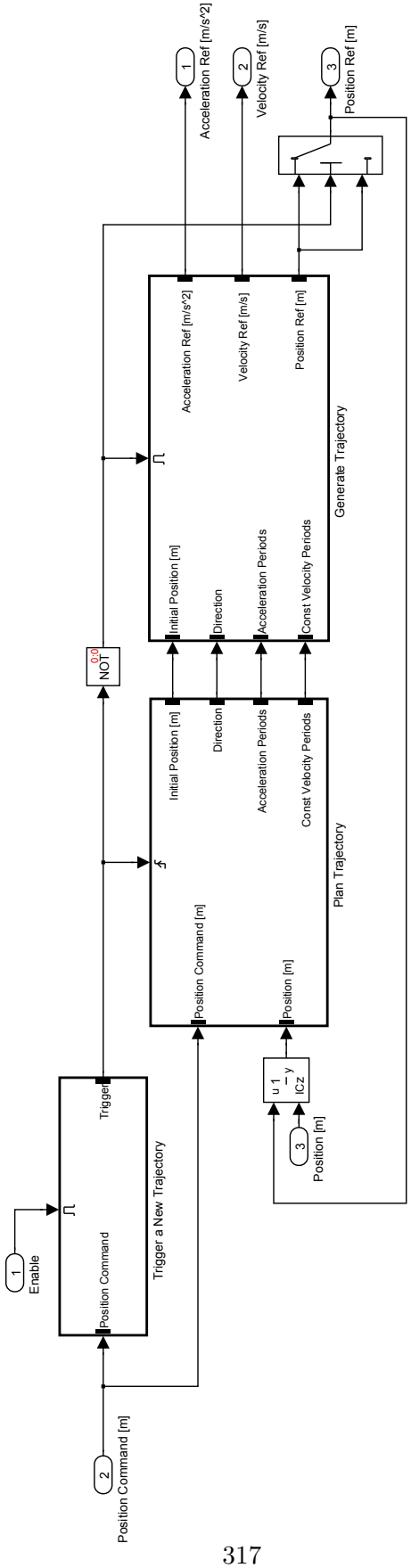

Figure E.12: Subsystem `lsmController/Trajectory Generator`

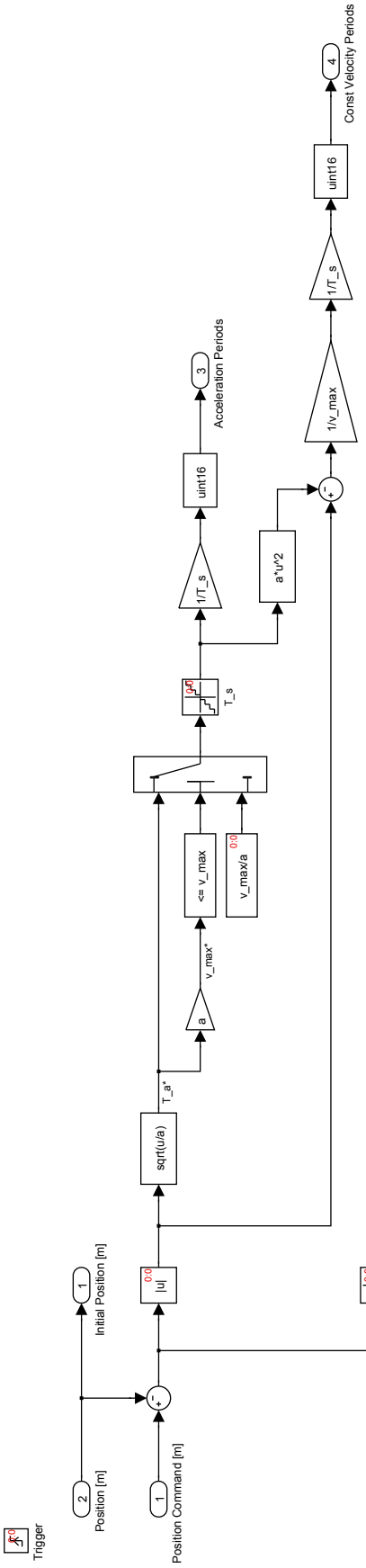

Figure E.13: Subsystem `lsmController/Trajectory Generator/Plan Trajectory`

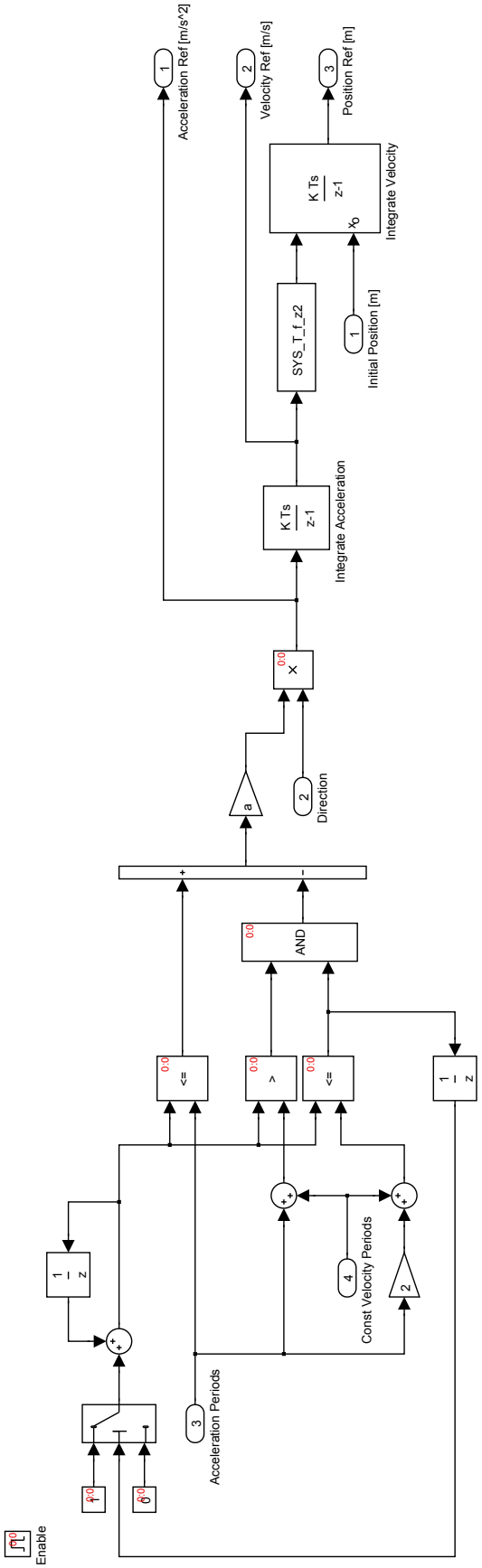

Figure E.14: Subsystem `lsmController/Trajectory Generator/Generate Trajectory`

E.1.7 Force feedforward compensation

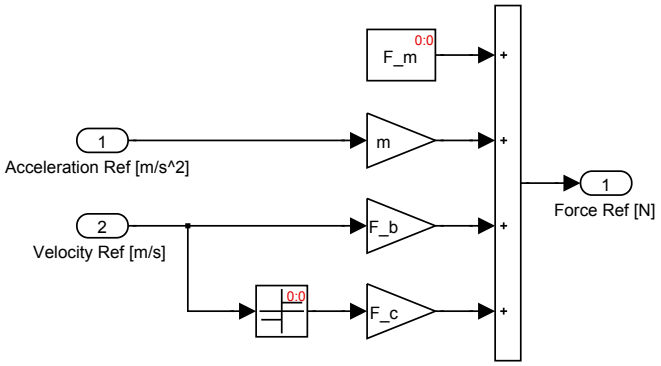

Figure E.15: Subsystem `lsmController/Force Feedforward`

E.1.8 Motor vector controller

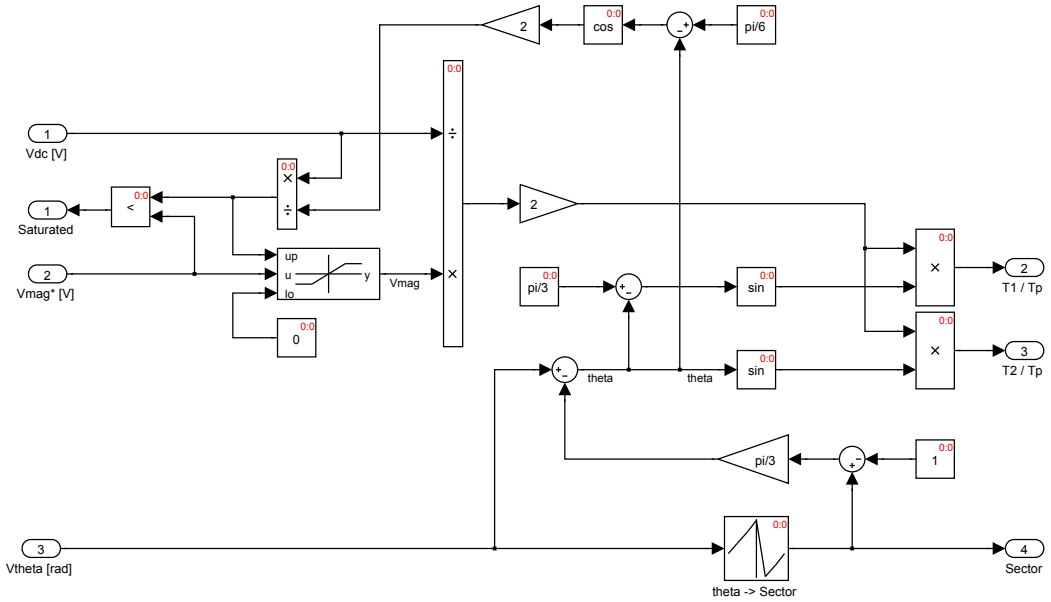

Figure E.16: Subsystem `lsmController/Motor Drive/FOC/mod-arg to SVM`

E.1.9 Force the solid-state contactors to turn on

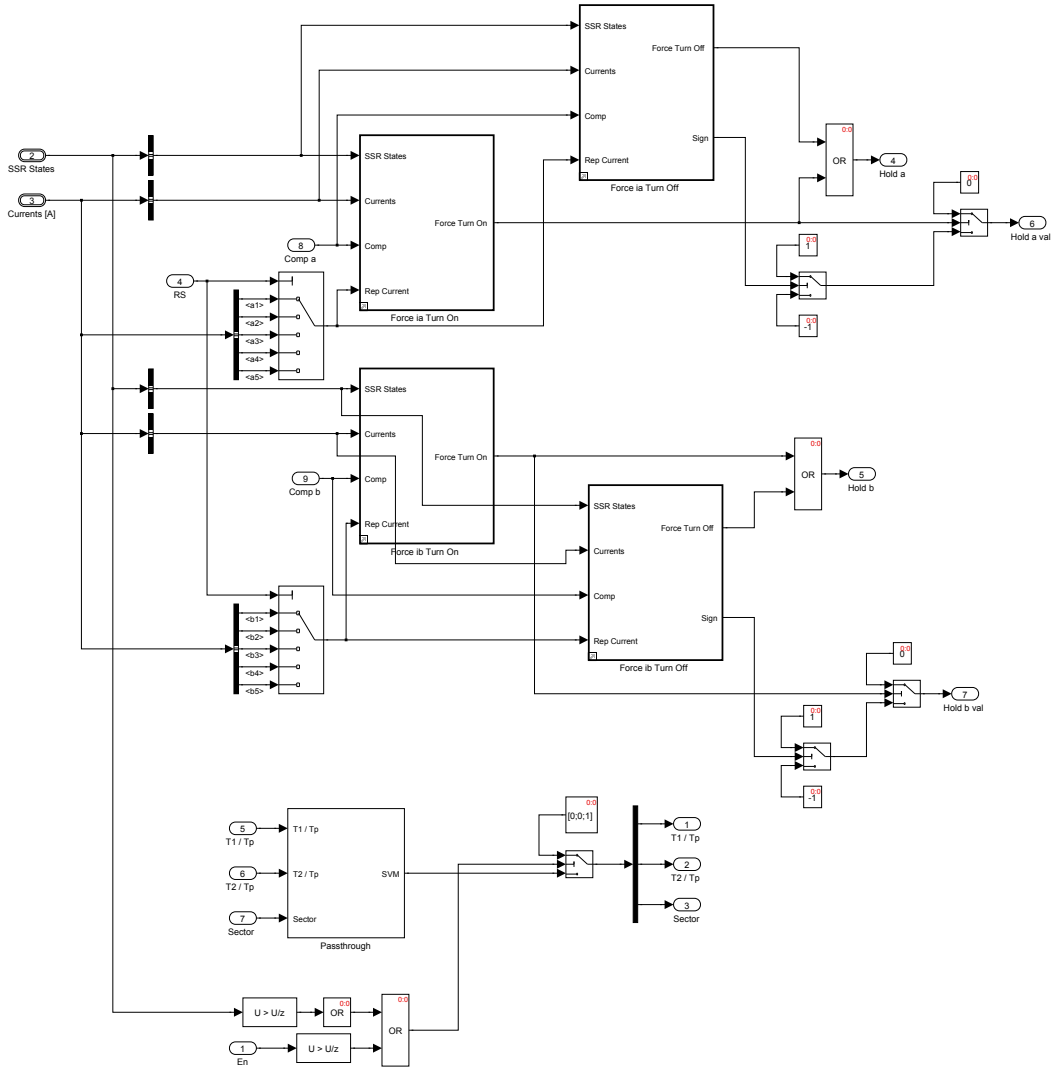

Figure E.17: Subsystem `lsmController/Ensure SSRs turn on`

E.2 Design of feedback control loops

Code listing E.1: Design of feedback control loops (`lsmControlDesign.m`)

```
T_s_c = 1/600;
T_s_p = 1/200;
T_r = 620e-6;

s = tf('s');
z_c = tf('z',T_s_c);
z_p = tf('z',T_s_p);

%% Current Control
T_I = L_s_q/R_s;
K = 10^(-6.5/20)*omega_b_P_c*R_s*T_I;

% Discrete PI with anti-windup
SYS_G_c_I1_z = K*(T_I+T_s_c/2)/T_I;
SYS_G_c_I2_z = T_s_c/(T_I+T_s_c/2)*...
    ss(1/(z_c-(T_I-T_s_c/2)/(T_I+T_s_c/2)));
SYS_G_c_I_z = series(SYS_G_c_I1_z,feedback(1,SYS_G_c_I2_z,+1));

figure; nichols(SYS_G_c_I_z*SYS_PH_c_z); ngrid;

SYS_G_c_F_z = c2d(ss(1/(s^2/300^2+s/300+1)),T_s_c,'prewarp',300);
zpk(SYS_G_c_F_z);
figure; bode(SYS_G_c_F_z);

SYS_G_c_z = series(SYS_G_c_F_z,SYS_G_c_I_z);

% Introduce a sample period delay at controller output
% for computation time
SYS_G_c_z = SYS_G_c_z/z_c;

figure; nichols(SYS_G_c_z*SYS_PH_c_z); ngrid;
figure; ngrid; hold on;
for n = 1:numel(SYS__PH_c_z)
    nichols(SYS_G_c_z*SYS__PH_c_z{n});
end

% |L(jw)| to check for wobbles
figure; bode(SYS_G_c_z*SYS_PH_c_z);
figure; hold on;
for n = 1:numel(SYS__PH_c_z)
    bode(SYS_G_c_z*SYS__PH_c_z{n});
end

% Sensitivity transfer function
SYS_S_c_z = 1/(1+series(SYS_G_c_z,SYS_PH_c_z));
figure; bode(SYS_S_c_z);
```

Code listing E.1: Design of feedback control loops (`lsmControlDesign.m`) *... cont*

```
% Closed-loop transfer function
SYS_T_c_z = feedback(series(SYS_G_c_z,SYS_PH_c_z),1);
for n = 1:numel(SYS__PH_c_z)
    SYS__T_c_z{n} = feedback(series(SYS_G_c_z,SYS__PH_c_z{n}),1);
end

omega_b_T_c = bandwidth(SYS_T_c_z);

figure; bode(SYS_P_c/freqresp(SYS_P_c,0)); hold on; bode(SYS_T_c_z);

figure; step(SYS_P_c/freqresp(SYS_P_c,0)); hold on; step(SYS_T_c_z);
figure; hold on;
for n = 1:numel(SYS__T_c_z)
    step(SYS__T_c_z{n});
end

% Plot plant input for step in reference
figure; step(feedback(SYS_G_c_z,SYS_PH_c_z));

%% Force Control
SYS_G_f_z = tau/pi/Psi_r_d;

SYS_T_f_z = SYS_G_f_z*SYS_T_c_z*SYS_P_f;
SYS__T_f_z = [];
for i = 1:numel(SYS__T_c_z)
    for j = 1:numel(SYS__P_f)
        SYS__T_f_z{end+1} = SYS_G_f_z*SYS__T_c_z{i}*SYS__P_f{j};
    end
end

SYS_T_f_z2 = d2d(minreal(delay2z(SYS_T_f_z)/z_c^2),T_s_p);

figure; nichols(SYS_PH_p_z); ngrid;
figure; ngrid; hold on;
for n = 1:numel(SYS__PH_p_z)
    nichols(SYS__PH_p_z{n});
end

figure; bode(SYS_PH_p_z);
figure; hold on;
for n = 1:numel(SYS__PH_p_z)
    bode(SYS__PH_p_z{n});
end

%%
SYS_G_p_z = 10^(72/20)*c2d(ss((s/7+1)/(s^2/100^2+2*0.4*s/100+1)),...
    T_s_p,'prewarp',100);
zpk(SYS_G_p_z)

%%
figure; nichols(SYS_G_p_z*SYS_PH_p_z); ngrid;
figure; ngrid; hold on;
```

Code listing E.1: Design of feedback control loops (`lsmControlDesign.m`) *... cont*

```
100 for n = 1:numel(SYS__PH_p_z)
101     nichols(SYS_G_p_z*SYS__PH_p_z{n});
102 end
103
104 % |L(jw)| to check for wobbles
105 figure; bode(SYS_G_p_z*SYS_PH_p_z);
106 figure; hold on;
107 for n = 1:numel(SYS__PH_p_z)
108     bode(SYS_G_p_z*SYS__PH_p_z{n});
109 end
110
111 %%
112 % Closed-loop transfer function
113 SYS_T_p_z = feedback(series(SYS_G_p_z,SYS_PH_p_z),1);
114 for n = 1:numel(SYS__PH_p_z)
115     SYS__T_p_z{n} = feedback(series(SYS_G_p_z,SYS__PH_p_z{n}),1);
116 end
117
118 omega_b_T_p = bandwidth(SYS_T_p_z);
119
120 figure; bode(SYS_T_p_z);
121 figure; hold on;
122 for n = 1:numel(SYS__T_p_z)
123     bode(SYS__T_p_z{n});
124 end
125
126 SYS_F_p_z = c2d(ss(1/(s/5.5+1)),T_s_p,'prewarp',5.5);
127 figure; bode(SYS_F_p_z*SYS_T_p_z);
128
129 figure; step(SYS_F_p_z*SYS_T_p_z);
130 figure; hold on;
131 for n = 1:numel(SYS__T_p_z)
132     step(SYS__T_p_z{n});
133 end
```

References

[1] T Ishii, "Elevators for skyscrapers," *IEEE Spectrum*, vol. 31, no 9, pp 42–46, Sep 1994.

[2] H J Kim, I Muraoka, S Torii, M Watada and D Ebihara, "The Study of the Control System for Ropeless Elevator with Vertical Linear Synchronous Motor," in proc. of *International Symposium on Linear Drives for Industry Applications (LDIA)*, 1995, pp 69–72.

[3] V C Gore, R J Cruise and C F Landy, "Considerations for an integrated transport system using linear synchronous motors for ultra-deep level mining," in proc. of *IEEE International Electric Machines and Drives Conference (IEMDC)*, Seattle, 1999, pp 568–570.

[4] M Platen and G Kenneberger, "Controller design for a linear drive of a hoisting system," in proc. of *25th Annual Conference of the IEEE Industrial Electronics Society (IECON)*, vol. 3, San Jose, 1999, pp 1477–1480.

[5] A W van Zyl, "Design, Construction and Evaluation of a Modified Tubular Linear Synchronous Motor," PhD thesis, University of the Witwatersrand, Johannesburg, 2006.

[6] Y W Zhu and Y H Cho, "Structure selection of permanent magnet linear synchronous motor for ropeless elevator system," *14th Biennial IEEE Conference on Electromagnetic Field Computation*, vol. 37, no 5, May 2010.

[7] K Toida, T Honda, M Watada, S Torii and D Ebihara, "The positioning control with velocity feed-forward for the rope-less elevator using linear synchronous motor," in proc. of *IEEE International Electric Machines and Drives Conference Record*, 1997.

[8] N Bodika, "Modeling of a Permanent Magnet Linear Synchronous Motor Under Regenerative Braking," Masters dissertation, University of the Witwatersrand, 2004.

[9] S Y Jung, J S Chun and H K Jung, "Performance evaluation of slotless permanent magnet linear synchronous motor energized by partially excited primary current," *IEEE Transactions on Magnetics*, vol. 37, no 5, pp 3757–3761, 2001.

[10] M S Kwak and S K Sul, "A New Method of Partial Excitation for Dual Moving Magnet Linear Synchronous Motor," *IEEE Transactions on Industry Applications*, vol. 40, no 2, pp 499–505, Mar 2004.

[11] C Lines, R Cruise, B Wigdorowitz and C Pritchard, "Suitability of various force control techniques for a modular-stator linear synchronous motor," in proc. of *Fifth International Symposium on Linear Drives for Industry Applications (LDIA)*, Kobe-Awaji, 2005.

[12] C Jiefan, W Chengyuan, Y Junyou and L Lifeng, "Analysis of direct thrust force control for permanent magnet linear synchronous motor," in proc. of *Fifth World Congress on Intelligent Control and Automation (WCICA)*, vol. 5. Hangzhou: IEEE, Jun 2004, pp 4418–4421.

[13] S Torii, N Izuno, M Watada and D Ebihara, "Optimum control scheme for the maximum efficiency drive of linear synchronous motor used for ropeless elevator," *Electrical Engineering in Japan*, vol. 155, no 3, pp 70–78, 2006.

[14] Q Hu, J Zhang, D Yu and J Cui, "Velocity Control for Rope-less Elevator Using Permanent Magnet Linear Synchronous Motor with Adaptive Fuzzy PID," *IEEE International Conference on Automation and Logistics*, pp 2361–2366, Aug 2007.

[15] T Sakamoto and Y Noma, "Guidelines for VSS Controller Design of LSM-driven Ropeless Elevator," in proc. of *IEEE International Symposium on Industrial Electronics*, Seoul, Korea, 2009, pp 1564–1568.

[16] D Patterson, A Monti, C Brice, R Dougal, R Pettus, S Dhulipala, D Kovuri and T Bertoncelli, "Design and Simulation of a Permanent-Magnet Electromagnetic Aircraft Launcher," *IEEE Transactions on Industry Applications*, vol. 41, no 2, pp 566–575, Mar 2005.

[17] A Monti, K Patel, D Patterson and R Dougal, "Modular control for electromagnetic aircraft launching system," in proc. of *34th Annual IEEE Power Electronics Specialists Conference (PESC)*, vol. 4, Columbia, Jun 2003, pp 1877–1882.

[18] K Yoshida, H Takami and A Fujii, "Smooth Section Crossing of Controlled-Repulsive PM LSM Vehicle by DTC Method Based on New Concept of Fictitious Section," *IEEE Transactions on Industrial Electronics*, vol. 51, no 4, pp 821–826, Aug 2004.

[19] R Leidhold and P Mutschler, "Speed Sensorless Control of a Long-Stator Linear Synchronous Motor Arranged in Multiple Segments," *IEEE Transactions on Industrial Electronics*, vol. 54, no 6, pp 3246–3254, Dec 2007.

[20] R B Oswald, "Investigation of Control Methods for Segmented Long Stator Linear Drives," PhD thesis, Technischen Universitaet Darmstadt, 2008.

[21] B M Perreault, "Optimizing Operation of Segmented Stator Linear Synchronous Motors," *Proceedings of the IEEE*, vol. 97, no 11, pp 1777–1785, 2009.

[22] L Li-Yi, H Jun-Jie, W Hong-Xing, L Peng, Z Zhe and L Xiao-Peng, "Section Crossing Drive With Fuzzy-PI Controller for the Long Stroke Electromagnetic Launcher," *IEEE Transactions on Magnetics*, vol. 45, no 1, pp 363–367, Jan 2009.

[23] J Batelaan, "A Linear Motor Design Provides Close and Secure Vehicle Separation of Many Transit Vehicles on a Guideway," *IEEE Transactions on Industrial Electronics*, vol. 54, no 3, pp 1778–1782, Jun 2007.

[24] B Gamble, D Cope and E Leung, "Design of a superconducting magnet system for Maglev applications," *IEEE Transactions on Appiled Superconductivity*, vol. 3, no 1, pp 434–437, Mar 1993.

[25] J Fujie and H Shibakawa, "Multiple feeder system of feeder sections for feeding ground coils of superconductive magnetically levitated railway," Patent US 5 361 707, 1994.

[26] Y J Kim, H Dohmeki and D Ebihara, "Optimal driving method of stationary discontinuous primary PM-LSM by open-loop control," *IEE Proceedings on Electric Power Applications*, vol. 153, no 4, p 585, 2006.

[27] C E Miller, A W van Zyl and C F Landy, "Modelling a permanent magnet linear synchronous motor for control purposes," in proc. of *6th Africon Conference in Africa*, vol. 2. IEEE, 2002, pp 671–674.

[28] X H Wang, H W Zhang and R S Kang, "Research on modeling and simulation of Permanent Magnet Linear Synchronous Motor for vertical transportation system," in proc. of *Chinese Control and Decision Conference*. Henan Jiaozuo: IEEE, Jun 2009, pp 3332–3336.

[29] G Gentile, A Ometto and N Rotondale, "Transient analysis of permanent magnet linear synchronous motors," in proc. of *European Conference on Power Electronics and Applications*. IEEE, 2005.

[30] H Polinder, J G Slootweg, M J Hoeijmakers and J C Compter, "Modeling of a linear PM machine including magnetic saturation and end effects: maximum force-to-current ratio," *IEEE Transactions on Industry Applications*, vol. 39, no 6, pp 1681–1688, Nov 2003.

[31] S Vaez-Zadeh and A Hassanpour Isfahani, "Enhanced Modeling of Linear Permanent-Magnet Synchronous Motors," *IEEE Transactions on Magnetics*, vol. 43, pp 33–39, 2007.

[32] B Sheikh-Ghalavand, S Vaez-Zadeh and A Hassanpour Isfahani, "An Improved Magnetic Equivalent Circuit Model for Iron-Core Linear Permanent-Magnet Synchronous Motors," *IEEE Transactions on Magnetics*, vol. 46, no 1, pp 112–120, Jan 2010.

[33] E Kazan and A Onat, "Modeling of Air Core Permanent-Magnet Linear Motors with a Simplified Nonlinear Magnetic Analysis," *IEEE Transactions on Magnetics*, vol. 47, no 6, pp 1753–1762, 2011.

[34] R Qu and T A Lipo, "Analysis and Modeling of Air-Gap and Zigzag Leakage Fluxes in a Surface-Mounted Permanent-Magnet Machine," *IEEE Transactions on Industry Applications*, vol. 40, no 1, pp 121–127, Jan 2004.

[35] I S Jung, J Hur and D S Hyun, "3-D analysis of permanent magnet linear synchronous motor with magnet arrangement using equivalent magnetic circuit network method," *IEEE Transactions on Magnetics*, vol. 35, no 5, pp 3736–3738, 1999.

[36] R Leidhold, R Benavides and P Mutschler, "Comparison of control oriented models for the Long-Stator Linear Synchronous Motor and their experimental validation," in proc. of *International Symposium on Power Electronics, Electrical Drives, Automation and Motion (SPEEDAM)*, Taormina, Italy, 2006, pp 457–462.

[37] R Leidhold and P Mutschler, "A Linear Synchronous-Motor Model for Evaluation of Sensorless Methods," in proc. of *IEEE International Symposium on Industrial Electronics*, vol. 3, 2006, pp 2467–2472.

[38] R Leidhold and P Mutschler, "Evaluation of sensorless methods for synchronous linear motors by using a magnetic equivalent circuit based model," in proc. of *IEEE International Electric Machines & Drives Conference*, vol. 1, Antalya, Turkey, 2007, pp 386–391.

[39] C R Lines, W A Cronjé and B Wigdorowitz, "Extended 2D magnetic equivalent circuit method," *COMPEL: The International Journal for Computation and Mathematics in Electrical and Electronic Engineering*, vol. 29, no 6, pp 1435 – 1443, 2010.

[40] C R Lines and W A Cronjé, "Extended Magnetic Equivalent Circuit Method That Accounts for Leakage Flux Using Schwarz-Christoffel Mapping and the Separation of MMF Sources," in proc. of *8th International Symposium on Electric and Magnetic Fields*, Mondovì, Italy, 2009.

[41] V Ostović, *Dynamics of saturated electric machines*. New York: Springer-Verlag, 1989.

[42] V Ostović, "A novel method for evaluation of transient states in saturated electric machines," *IEEE Transactions on Industry Applications*, vol. 25, no 1, pp 96–100, 1989.

[43] B Asghari and V Dinavahi, "Permeance Network Based Real-Time Induction Machine Model," in proc. of *International Conference on Power Systems Transients (IPST)*, Kyoto, Japan, 2009.

[44] H E Knoepfel, *Magnetic Fields*. John Wiley & Sons, Inc., 2000.

[45] M Andriollo, T Bertoncelli and A Di Gerlando, "A magnetic network approach to the transient analysis of synchronous machines," *COMPEL: The International Journal for Computation and Mathematics in Electrical and Electronic Engineering*, vol. 22, no 4, pp 953–968, 2003.

[46] H Roisse, M Hecquet and P Brochet, "Simulations of synchronous machines using a electric-magnetic coupled network model," *IEEE Transactions on Magnetics*, vol. 34, pp 3656–3659, 1998.

[47] J Perho, "Calculation of Equivalent Circuit of Cage-Induction Motor by Reluctance Network Method," PhD thesis, Helsinki University of Technology, 2002.

[48] B Bekkouche, A Chaouch and Y Mezari, "A Switched Reluctance Motors Analyse using Permeance Network Method," *International Journal of Applied Engineering Research*, vol. 1, no 2, pp 137–152, 2006.

[49] C B Rasmussen and E Ritchie, "Improved reluctance-mmf network for calculation of magnetic field distribution in surface-mounted permanent magnet motors," in proc. of *2nd International Symposium on Advanced Electromechanical Motion Systems*, 1997.

[50] J Pyrhönen, T Jokinen and V Hrabovcová, *Design of Rotating Electrical Machines*. Chichester, UK: John Wiley & Sons, Ltd, Dec 2008.

[51] G A Cividjian, A G Cividjian and N G Silvis-Cividjian, "Some formulas for two-dimensional permeances," *IEEE Transactions on Magnetics*, vol. 36, no 5 Part 2, pp 3754–3758, 2000.

[52] G A Cividjian and A G Cividjian, "Constriction and Corner Permeances for Finite Domains," *IEEE Transactions on Magnetics*, vol. 42, no 12, pp 3825–3831, 2006.

[53] A Balakrishnan, W T Joines and T G Wilson, "Air-gap reluctance and inductance calculations for magnetic circuits using a Schwarz-Christoffel transformation," *IEEE Transactions on Power Electronics*, vol. 12, no 4, pp 654–663, Jul 1997.

[54] M Marković, M Jufer and Y Perriard, "An exact formula for "Tooth-to-Tooth" permeance," *IEEE Transactions on Magnetics*, vol. 41, no 7, pp 2295–2299, Jul 2005.

[55] D C J Krop, E A Lomonova and A J A Vandenput, "Application of Schwarz-Christoffel Mapping to Permanent-Magnet Linear Motor Analysis," *IEEE Transactions on Magnetics*, vol. 44, no 3, pp 352–359, 2008.

[56] M Marković, M Jufer and Y Perriard, "Reducing the Cogging Torque in Brushless DC Motors by Using Conformal Mappings," *IEEE Transactions on Magnetics*, vol. 40, no 2, pp 451–455, Mar 2004.

[57] T A Driscoll, "Schwarz-Christoffel toolbox for MATLAB, version 2.41, 2009. Online: http://www.math.udel.edu/~driscoll/SC/

[58] T A Driscoll and L N Trefethen, *Schwarz-Christoffel Mapping*, series Cambridge Monographs on Applied and Computational Mathematics. Cambridge University Press, 2002.

[59] S J Salon, *Finite Element Analysis of Electrical Machines*, series The Kluwer International Series in Engineering and Computer Science. Boston: Kluwer Academic Publishers, 1995.

[60] V Thomée, "The finite difference versus the finite element method for the solution of boundary value problems," *Bulletin of the Australian Mathematical Society*, vol. 29, no 02, p 267, Apr 2009.

[61] J P Webb, "Edge elements and what they can do for you," *IEEE Transactions on Magnetics*, vol. 29, no 2, pp 1460–1465, Mar 1993.

[62] A Bossavit, "Edge elements for magnetostatics," *International Journal of Numerical Modelling*, vol. 9, no Figure 2, pp 19–34, 1996.

[63] D Meeker, "Finite Element Method Magnetics (FEMM), version 4.2," Computer Software, 2011. Online: http://www.femm.info

[64] D Meeker, "Finite Element Method Magnetics, Version 4.2," User's Manual, Oct, 2010.

[65] A Demenko and J K Sykulski, "Network equivalents of nodal and edge elements in electromagnetics," *IEEE Transactions on Magnetics*, vol. 38, no 2 Part 1, pp 1305–1308, 2002.

[66] A Demenko, L Nowak and W Szelag, "Reluctance network formed by means of edge element method," *IEEE Transactions on Magnetics*, vol. 34, no 5 Part 1, pp 2485–2488, 1998.

[67] C A Brebbia, J C F Telles and L C Wrobel, *Boundary Element Techniques*. Springer-Verlag, 1984.

[68] C Brebbia, "The boundary element method for electromagnetic problems," *Engineering Analysis with Boundary Elements*, vol. 4, no 4, pp 178–185, Dec 1987.

[69] M D Greenberg, *Application of Green's Functions in Science and Engineering*. New Jersey: Prentice Hall, 1971.

[70] J Lobry, "A new BEM technique for nonlinear 2D magnetostatics," *Engineering Analysis with Boundary Elements*, vol. 26, pp 795–801, 2002.

[71] A Canova, F Freschi, M Repetto and G Gruosso, "Coupling of finite formulation with integral techniques," *COMPEL: The International Journal for Computation and Mathematics in Electrical and Electronic Engineering*, vol. 27, no 1, pp 37–46, 2008.

[72] K Bill, "Development of the Boundary Element Method aimed at magnetic field computation of an induction motor," *Electrical Engineering (Archiv fur Elektrotechnik)*, vol. 72, no 5, pp 309–317, 1989.

[73] M Clemens and T Weiland, "Discrete Electromagnetism with the Finite Integration Technique," *Progress In Electromagnetics Research*, vol. 32, pp 65–87, 2001.

[74] G Albertier, Y Le Menach, J P Ducreux and F Piriou, "Consideration of the coupling of the magnetic and electric equations with Finite Integration Technique (FIT)," *The European Physical Journal Applied Physics*, vol. 30, no 1, pp 17–21, Mar 2005.

[75] J Korecki, Y Le Menach, J P Ducreux and F Piriou, "Numerical solutions in primal and dual meshes of magnetostatic problems solved with the finite integration technique," *COMPEL: The International Journal for Computation and Mathematics in Electrical and Electronic Engineering*, vol. 27, no 1, pp 47–55, 2008.

[76] A Demenko, J K Sykulski and R Wojciechowski, "On the Equivalence of Finite Element and Finite Integration Formulations," *IEEE Transactions on Magnetics*, vol. 46, no 8, pp 3169–3172, 2010.

[77] E Tonti, "Finite formulation of electromagnetic field," *IEEE Transactions on Magnetics*, vol. 38, no 2, pp 333–336, Mar 2002.

[78] A Canova, G Gruosso and M Repetto, "Integral methods for analysis and design of low-frequency conductive shields," *IEEE Transactions on Magnetics*, vol. 39, no 4, pp 2009–2017, Jul 2003.

[79] M Arehpanahi and J Milimonfared, "Analysis of Rotating Magnetic Device By Surface-Current Method," in proc. of *12th Biennial IEEE Conference on Electromagnetic Field Computation*, 2006, pp 84–84.

[80] M Andriollo, G Martinelli, A Morini and A Tortella, "Application of the surface-current method to the analysis of saturated electromagnetic devices," *COMPEL: The International Journal for Computation and Mathematics in Electrical and Electronic Engineering*, vol. 23, no 1, pp 328–347, 2004.

[81] M Arehpanahi and J Milimonfared, "Nonlinear Analysis of Magnetic Device By Finite Difference Surface-Current Method (FDSCM)," in proc. of *12th Biennial IEEE Conference on Electromagnetic Field Computation*, 2006.

[82] M Arehpanahi and J Milimonfared, "Electrical and Magnetic Circuit Coupling Using Surface Current Method," in proc. of *IEEE International Electric Machines & Drives Conference*, vol. 2, May 2007, pp 1587–1589.

[83] M Berlec, "An integral approach for 3D magnetostatic field calculation," *COMPEL: The International Journal for Computation and Mathematics in Electrical and Electronic Engineering*, vol. 17, no 1, pp 55–58, 1998.

[84] D Novotny and T Lipo, *Vector control and dynamics of ac drives*. New York: Oxford University Press, 1996.

[85] G Terörde, *Electrical Drives and Control Techniques*. Acco, 2004.

[86] J Chiasson, *Modeling and High-Performance Control of Electric Machines*, M E El-Hawary, Ed. John Wiley & Sons, Inc., 2005.

[87] S Vaez-Zadeh and E Jalali, "Combined vector control and direct torque control method for high performance induction motor drives," *Energy Conversion and Management*, vol. 48, no 12, pp 3095–3101, Dec 2007.

[88] M S Merzoug and F Naceri, "Comparison of Field-Oriented Control and Direct Torque Control for Permanent Magnet Synchronous Motor (PMSM)," *World Acaemy of Science, Engineering and Technology*, vol. 45, pp 299–304, 2008.

[89] R Souad and H Zeroug, "Comparison between direct torque control and vector control of a permanent magnet synchronous motor drive," in proc. of *13th International Power Electronics and Motion Control Conference*, no VC. IEEE, Sep 2008, pp 1209–1214.

[90] T D Batzel and K Y Lee, "Electric Propulsion With the Sensorless Permanent Magnet Synchronous Motor: Model and Approach," *IEEE Transactions on Energy Conversion*, vol. 20, no 4, pp 818–825, Dec 2005.

[91] P P Acarnley and J F Watson, "Review of position-sensorless operation of brushless permanent-magnet machines," *IEEE Transactions on Industrial Electronics*, vol. 53, no 2, pp 352–362, Apr 2006.

[92] M E Haque, L Zhong and M F Rahman, "A sensorless initial rotor position estimation scheme for a direct torque controlled interior permanent magnet synchronous motor drive," *IEEE Transactions on Power Electronics*, vol. 18, no 6, pp 1376–1383, Nov 2003.

[93] S Bolognani, M Zigliotto and M Zordan, "Extended-range PMSM sensorless speed drive based on stochastic filtering," *IEEE Transactions on Power Electronics*, vol. 16, no 1, pp 110–117, 2001.

[94] F Briz, M W Degner, P Garcia and R D Lorenz, "Comparison of Saliency-Based Sensorless Control Techniques for AC Machines," *IEEE Transactions on Industry Applications*, vol. 40, no 4, pp 1107–1115, Jul 2004.

[95] P B Schmidt, M L Gasperi, G Ray and A H Wijenayake, "Initial rotor angle detection of a nonsalient pole permanent magnet synchronous machine," in proc. of *Industry Applications Conference Thirty-Second IAS Annual Meeting*, vol. 1, 1997, pp 459–463.

[96] G Zhu, A Kaddouri, L A Dessaint and O Akhrif, "A nonlinear state observer for the sensorless control of a permanent-magnet AC machine," *IEEE Transactions on Industrial Electronics*, vol. 48, no 6, pp 1098–1108, 2001.

[97] M Eskola and H Tuusa, "Sensorless control of a permanent magnet synchronous motor-application to a hoist drive," in proc. of *33rd Annual IEEE Power Electronics Specialists Conference*, vol. 2, 2002, pp 967–972.

[98] M Leksell, L Harnefors and M Jansson, "Direct sensorless speed control of PM-motors-a simple and effective sensorless method," in proc. of *32nd Annual Power Electronics Specialists Conference*, vol. 2. IEEE, 2001, pp 805–810.

[99] E Robeischl and M Schroedl, "Optimized INFORM Measurement Sequence for Sensorless PM Synchronous Motor Drives With Respect to Minimum Current Distortion," *IEEE Transactions on Industry Applications*, vol. 40, no 2, pp 591–598, Mar 2004.

[100] D Paulus, P Landsmann and R Kennel, "Sensorless field-oriented control for permanent magnet synchronous machines with an arbitrary injection scheme and direct angle calculation," in proc. of *Symposium on Sensorless Control for Electrical Drives*, no 4, Birmingham, United Kingdom, Sep 2011, pp 41–46.

[101] I Hahn, "Differential magnetic anisotropy - prerequisite for rotor position detection of PM-synchronous machines with signal injection methods," in proc. of *Symposium on Sensorless Control for Electrical Drives*, Padova, Italy, Jul 2010, pp 40–49.

[102] M Linke, R Kennel and J Holtz, "Sensorless position control of permanent magnet synchronous machines without limitation at zero speed," *28th Annual Conference of the Industrial Electronics Society (IECON'02)*, pp 674–679, 2002.

[103] Q Ge, Y Li and L Kong, "A Comparative Study of FOC for Long Stator Linear Synchronous Motor Control," in proc. of *International Conference on Electrical Machines and Systems*, Seoul, Korea, 2007, pp 398–402.

[104] G S Buja and M P Kazmierkowski, "Direct Torque Control of PWM Inverter-Fed AC Motors—A Survey," *IEEE Transactions on Industrial Electronics*, vol. 51, no 4, pp 744–757, Aug 2004.

[105] J Faiz and S H Mohseni-Zonoozi, "A novel technique for estimation and control of stator flux of a salient-pole PMSM in DTC method based on MTPF," *IEEE Transactions on Industrial Electronics*, vol. 50, no 2, pp 262–271, Apr 2003.

[106] J Luukko, "Direct torque control of permanent magnet synchronous machines-analysis and implementation," PhD thesis, Lappeenranta University of Technology, Finland, 2000.

[107] L Tang, L Zhong, M F Rahman and Y Hu, "A Novel Direct Torque Controlled Interior Permanent Magnet Synchronous Machine Drive With Low Ripple in Flux and Torque and Fixed Switching Frequency," *IEEE Transactions on Power Electronics*, vol. 19, no 2, pp 346–354, Mar 2004.

[108] Y S Lai, W K Wang and Y C Chen, "Novel Switching Techniques for Reducing the Speed Ripple of AC Drives With Direct Torque Control," *IEEE Transactions on Industrial Electronics*, vol. 51, no 4, pp 768–775, Aug 2004.

[109] S Rafa, A Larabi, L Hocine and L Barazane, "Control Techniques for Permanent Magnet Synchronous Motor Drive," in proc. of *18th Mediterranean Conference on Control & Automation*, Morocco, 2010.

[110] J Cui, C Wang, J Yang and D Yu, "Research on force and direct thrust control for a pennanent magnet synchronous linear motor," in proc. of *30th Annual Conference of IEEE Industrial Electronics Society (IECON)*, Busan, Korea, 2004, pp 2269–2272.

[111] J F Cui, H M Wang, J Z Wan, G Mu and J Y Yang, "Thrust Force Control of Permanent Magnet Linear Synchronous Motor Based on Sliding Mode Variable Structure," in proc. of *IEEE International Conference on Control and Automation*, May 2007, pp 1698–1700.

[112] J Faiz, I Tabatabaei-Ardakani and S H Mohseni-Zoonozi, "Direct Force Control of Linear Permanent Magnet Synchronous Motors," in proc. of *Fifth International Symposium on Linear Drives for Industry Applications (LDIA)*, Kobe-Awaji, Japan, 2005, pp 124–127.

[113] G Lirong, Y Junyou and C Jiefan, "Direct Thrust Control Approach Using Adaptive Variable Structure for Permanent Magnet Linear Synchronous Motor," in proc. of *IEEE International Conference on Control and Automation*, May 2007, pp 2217–2220.

[114] P Mutschler, "Comparison of topologies for linear drives in industrial material handling and processing applications," in proc. of *7th Internatonal Conference on Power Electronics*. IEEE, Oct 2007, pp 1027–1032.

[115] T M Clark, "Position sensing and control of a linear synchronous motor," PhD thesis, Massachusetts Institute of Technology, 1995.

[116] R Benavides and P Mutschler, "Controlling a System of Linear Drives," in proc. of *36th Annual Power Electronics Specialists Conference*. IEEE, 2005, pp 1587–1593.

[117] R Hellinger, M Engel and J Nothhaft, "Propulsion System and Power Supply for TRANSRAPID Commercial Lines," in proc. of *17th International Conference on Magnetically Levitated Systems and Linear Drives (MAGLEV'02)*, Lausanne, 2002.

[118] U Henning, D Hoke and J Nothhaft, "Development and operation results of Transrapid propulsion system," in proc. of *18th International Conference on Magnetically Levitated Systems and Linear Drives (MAGLEV'04)*, Shanghai, 2004, pp 759–770.

[119] T G Habetler, R Naik and T A Nondahl, "Design and implementation of an inverter output LC filter used for dv/dt reduction," *IEEE Transactions on Power Electronics*, vol. 17, no 3, pp 327–331, May 2002.

[120] K Patel, S D D'Arco, A Monti, D Patterson and R Dougal, "Design and testing of a modular permanent magnets brushless linear drive," in proc. of *Twentieth Annual IEEE Applied Power Electronics Conference and Exposition*, vol. 1, no l, 2005, pp 1883–1888.

[121] A Pottharst, M Henke and H Grotstollen, "Power Supply Concept of the Longstator Linear Motor of the NBP-Test Track," in proc. of *Power Electronics and Motion Conference (PEMC)*, 2002.

[122] J P Gibson, "Power supply for the traveling-field winding of a synchronous linear motor," Patent US 4 361 095, 1982.

[123] M Engel and J Nothhaft, "Optimization of the Transrapid Propulsion System," in proc. of *19th International Conference on Magnetically Levitated Systems and Linear Drives (MAGLEV'06)*, Dresden, 2006.

[124] R Fischperer, "Arrangement having at least one long-stator linear motor, for operating magnetically levitated vehicles," Patent US 7 173 387, 2007.

[125] R Fischperer and J Maj, "Power supply system and method for linear stator motor," Patent US 5 302 884, 1994.

[126] R Fischperer, "Section switching process for railway systems with a long stator linear motor," Patent US 6 087 790, 2000.

[127] H Shigeeda, H Ohtsuki and S Koga, "Novel Feeding System for Maglev aiming at Cost Reduction," in proc. of *17th International Conference on Magnetically Levitated Systems and Linear Drives (MAGLEV'02)*, Lausanne, 2002.

[128] H Ikeda, S Kaga, Y Osada, K Ito, Y Mugiya and K Tutumi, "Development of power supply system for Yamanashi Maglev Test Line," in proc. of *Power Conversion Conference*, vol. 1. Nagaoka, Japan: IEEE, 1997, pp 37–41.

[129] Q Zhang, F Lin, X You and T Zheng, "A Novel Stator Section Crossing Method of Long Stator Linear Synchronous Motor for Maglev Vehicles," in proc. of *5th International Power Electronics and Motion Control Conference*. IEEE, Aug 2006.

[130] T Onuki, Y Kamiya, Y Kurimoto and M Yoshizawa, "A novel block feeding method in the single-sided linear induction motor with a short secondary member," *IEEE Transactions on Energy Conversion*, vol. 14, no 4, pp 1323–1328, 1999.

[131] B M Perreault, "Control Strategies for Linear Synchronous Motors," in proc. of *IEEE International Electric Machines & Drives Conference*, vol. 2, Antalya, Turkey, May 2007, pp 969–971.

[132] J Colton, D Patterson, J Hudgins and A Monti, "A Modular Linear Permanent-Magnet Machine with an FPGA-Based Controller," in proc. of *IEEE International Electric Machines & Drives Conference*, vol. 2, May 2007, pp 1757–1761.

[133] A Monti, K Patel, D Patterson, D Kovuri and R Dougal, "Hierarchichal Current Control Design For Electromagnetic Aircraft Launching System," in proc. of *European Power Electronics Conference*, Toulouse, France, Sep 2003.

[134] R Benavides and P Mutschler, "Compensation of Disturbances in Segmented Long Stator Linear Drives using Finite Element Models," in proc. of *International Symposium on Industrial Electronics (ISIE)*. IEEE, 2006, pp 5–9.

[135] R Benavides and P Mutschler, "Detent force compensation in segmented long stator permanent magnet linear drives using Finite Element Models," in proc. of *European Conference on Power Electronics and Applications*, no 1. IEEE, 2007.

[136] K Yoshida, A Fuji and H Takami, "Pass-through-section experiment in mass-reduced-mode of controlled-repulsive PM LSM Maglev vehicle by new DTC method," in proc. of *Proceedings of the Power Conversion Conference*, vol. 2. Osaka: IEEE, 2002, pp 867–872.

[137] R Leidhold and P Mutschler, "Sensorless position-control method based on magnetic saliencies for a Long-Stator Linear Synchronous-Motor," in proc. of *32nd Annual Conference on IEEE Industrial Electronics (IECON)*, 2006, pp 781–786.

[138] K Seki, M Watada, S Torii and D Ebihara, "Discontinuous arrangement of long stator linear synchronous motor for transportation system," *Second International Conference on Power Electronics and Drive Systems*, vol. 2, pp 697–702, 1997.

[139] K Suzuki, Y J Kim and H Dohmeki, "Proposal of the section change method of the stator block of the discontinuous stator permanent magnet type linear synchronous motor aimed at long-distance transportation," in proc. of *18th International Conference on Electrical Machines*. IEEE, 2008, pp 1–6.

[140] K Suzuki, Y J Kim and H Dohmeki, "Proposal of the long-distance transportation system in the factory using PM-LSM," in proc. of *International Conference on Electrical Machines and Systems*. IEEE, Nov 2009, pp 1–6.

[141] E P Furlani, *Permanent Magnet and Electromechanical Devices - Materials, Analysis, and Applications*. Academic Press, 2001.

[142] R Ramshaw and R Van Heeswijk, *Energy Conversion: Electric Motors and Generators*, series Electrical Engineering. Saunders College Publishing, 1990.

[143] B Adkins and R G Harley, *The General Theory of Alternating Current Machines*. London: Chapman and Hall Ltd., 1975.

[144] T W Kim, J Watanabe, S Sonoda and J Hirai, "New Initial Pole-Position Estimation of Surface PM-LSM Using Reference Currents," *IEEE Transactions on Industry Applications*, vol. 41, no 3, pp 817–824, May 2005.

[145] Q Chen and A Konrad, "A review of finite element open boundary techniques for static and quasi-static electromagnetic field problems," *IEEE Transactions on Magnetics*, vol. 33, no 1, pp 663–676, 1997.

[146] J Kirk, "Count Loops in a Graph," MATLAB source code, 2007. Online: http://www.mathworks.com/matlabcentral/fileexchange/10722

[147] "Typical data for SURA® M250-50A," Product information, 2008. Online: http://www.sura.se/

[148] F Cardarelli, *Materials Handbook*, 2nd ed. London: Springer London, 2008.

[149] R J Cruise and C F Landy, "Reduction of cogging forces in linear synchronous motors," in proc. of *5th Africon Conference in Africa*, vol. 2. Cape Town: IEEE, 1999, pp 623–626.

[150] V Lines, "BSc(Eng)(Civil) Pr Eng," Personal communication, Johannesburg, South Africa, 2010.

[151] "Vesconite," Product information. Online: http://www.vesconite.com/prod/vesconite.htm

[152] "RBC Bearings®," Product information. Online: http://www.rbcbearings.com/literature/pdfs/RBC-CF.pdf

[153] M Ansari, "MSc(Eng) candidate," Personal communication, Johannesburg, South Africa, 2010.

[154] POWER-IO, "Single phase, up to 50, 75, 100 amp, din rail contactor," Product information. Online: http://www.power-io.com/products/dda5075100.htm

[155] "LEM® Current Transducer LA 55-P," Product information. Online: http://www.lem.com/docs/products/la55-pe.pdf

[156] "dSPACE User Manual," Product information. Online: http://www.dspace.com/

[157] STAHL, "The STAHLTRONIC Position Encoding System WCS," Product information, 2003.